Methodology for the selection and optimization of energy converters for automotive powertrain applications

Wissam Bou Nader

![PSL Université Paris logo]

THÈSE DE DOCTORAT
DE L'UNIVERSITÉ PSL

Préparée à Mines ParisTech

Methodology for the Selection and Optimization of Energy Converters for Automotive Powertrain Applications

Méthodologie de Choix et d'Optimisation de Convertisseurs d'Energie pour les Applications Chaînes de Traction Automobile

Soutenue par
Wissam BOU NADER
Le 01 Février 2019

Ecole doctorale n° 621-ISMME
Ingénierie des systèmes, Matériaux, Mécanique, Energétique

Spécialité
Energétique et Génie des Procédés

![Mines ParisTech PSL logo]

Composition du jury :

Christine ROUSSELLE Prof. Dr, University of Orléans	*Présidente*
Predrag PEGA HRNJAK Prof. Dr, University of Illinois	*Rapporteur*
Vincent LEMORT Prof. Dr, University of Liège	*Rapporteur*
Rochdi TRIGUI Research Director, IFSTTAR	*Examinateur*
Clément DUMAND Dr, PSA Groupe	*Examinateur*
Charbel MANSOUR Assistat Prof. Dr, LAU	*Examinateur*
Maroun NEMER Research Director, Mines ParisTech	*Examinateur*
Dominique MARCHIO Prof. Dr, Mines ParisTech	*Directeur de thèse*

"Knowledge in not power. Knowledge is only potential power. It becomes power only when, and if, it is organized into definite plans of action, and directed to a definite end"

(Napoleon HILL)

Acknowledgement

Nomenclature

Symbol

A	Section area	m^2
C_b	Capacity of the battery	kW.h
C_p	Specific heat	$J.kg^{-1}.K^{-1}$
C_x	Coefficient of drag	-
DT	Temperature difference / Pinch	K
DP	Pressure drop	Pa
E, Ex	Exergy	$kJ.kg^{-1}$
f_r	Coefficient of the wheel friction	-
h	Specific enthalpy	$kJ.kg^{-1}$
h	Heat transfer coefficient	$W.m^{-2}.K^{-1}$
H	Height	m
H_v	Fuel heating value	$MJ.kg^{-1}$
i	Transmission ratio	-
I	Irreversibility	$kJ.kg^{-1}$
j	Colburn j-factor	-
k	Thermal conductivity	$W.m^{-1}.K^{-1}$
L	Length	m
Lv	Latent heat of vaporization	$kJ.kg^{-1}$
m	Mass flow rate	$Kg.s^{-1}$
M_v	Mass of the vehicle	Kg
P	Pressure	Pa
P_{aux}	Consumption of the auxiliaries	W
Q	Heat capacity	$kJ.kg^{-1}$
R_w	Radius of the wheels	m
s	Specific entropy	$kJ.kg^{-1}.K^{-1}$
S	Frontal area	m^2
T	Temperature	°C (K)
u	Control variable	-
V	volume	m^3
V	Velocity	$m.s^{-1}$
V_{oc}	Open-circuit voltage of the battery	V
U	Global heat transfer coefficient	$W.m^{-2}.K^{-1}$
W	Net specific work	$kJ.kg^{-1}$

Greek letters

η	Efficiency	%
Δ	Relative variation	%
τ	Turbine expansion ratio	-
ρ	Density	$Kg.m^{-3}$
ξ	Friction factor	-
δ	Thickness	mm
θ	Angle	°
λ	Thermal conductivity	$W.m^{-1}.K^{-1}$
π	Compressor pressure ratio	-

Abbreviations

AC	Alternative Current
AFC	Alkaline Fuel Cell
APU	Auxiliary Power Unit
ASE	Automotive Stirling Engine
ATDC	After Top Dead Centre
B	Battery
BMEP	Brake Mean Effective Pressure
BSFC	Brake Specific Fuel Consumption
BTDC	Before Top Dead Centre
C	Condenser
CC	Combustion Chamber
CCB	Combustion Chamber Blower
CO	Carbon monoxide
CVT	Continuous Variable Transmission
CCGT	Combined Cycle Gas Turbine
DC	Direct Current
DMFC	Direct Methanol Fuel Cell
DOE	Department Of Energy
DP	Dynamic Programming
E	Energy
EC	Energy converter
ECGT	External Combustion Gas Turbine
ECU	Electronic Control Unit
EECU	Engine Electronic Control Unit
EG	Electric Generator
EG	Exhaust Gases
EM	Electric Machine
EMS	Energy Management Strategy
EPA	Environmental Protection Agency
EREV	Extended Range Electric Vehicle
FC	Fuel Cell
FC	Fuel consumption
FCS	Fuel Cell System
FCV	Fuel Cell Vehicle
G	Gearbox
GHG	Greenhouse Gas
GT	Gas Turbine
GWP	Global Warming Potential
H2	Hydrogen
He	Helium
HEV	Hybrid electric Vehicle
HEX	Heat Exchanger
HSS	Hydrogen Storage System
ICE	Internal combustion Engine
IcRGT	Isothermal Compression Regenerative Gas Turbine
IcRIeGT	Isothermal Compression Regenerative Isothermal Expansion Gas Turbine
IcRReGT	Isothermal Compression Regenerative Reheat Gas Turbine
IRGT	Intercooling Regenerative Gas Turbine
IRReGT	Intercooling Regenerative Reheat Gas Turbine

LHV	Low Heating Value
MCFC	Molten Carbonate Fuel Cell
MGT	Micro Gas Turbine
NASA	National Aeronautics and Space Administration
NOx	Nitrogen Oxide
NSGA	Non-dominated Sorting Genetic Algorithm
NVH	Noise, Vibration and Harshness
OEM	Original Equipment Manufacturer
ORC	Organic Rankine Cycle
ODP	Ozone Depletion Potential
PC	Passenger car
PEMFC	Proton Exchange Membrane Fuel Cell
PHEV	Parallel Hybrid electric Vehicle
RDE	Real Driving Emission
RG	Reduction Gear
RGT	Regenerative Gas Turbine
SCE	Split Cycle Engine
SHEV	Series Hybrid Electric Vehicle
SI	Spark Ignition
SOC	State Of Charge
SRC	Steam Rankine Cycle
SUV	Sport Utility Vehicle
TA	ThermoAcoustic
TDC	Top Dead Center
TEG	ThermoElectric Generator
TIT	Turbine Inlet Temperature
UHC	Unburned Hydrocarbons
VCM	Vapor Cycle Machine
WHR	Waste Heat Recovery
WLTC	Worldwide Harmonized Light Vehicles Test Cycle

Non-dimensional numbers

$$Nu = \frac{h.D}{k}$$ Nusselt number

$$Pr = \frac{\mu.c_p}{k}$$ Prandtl number

$$Re = \frac{\rho.V.D}{\mu}$$ Reynolds number

CONTENTS

General introduction

Road transportation sector is amongst the fast-growing consumers of world oil and a source of greenhouse gas emissions, the most pressing factors of the current global environmental problems. Governments around the world are implementing policies to reduce oil consumption, climate-related emissions, and local air pollution. Several solutions have been offered by car manufacturers and stakeholders to reduce the environmental impact of road transportation.

Today, the Internal Combustion Engines (ICEs) continue to play an important role as a power source for automobiles and is expected to keep its leadership as a primary converter for many years to come. However, the ICE, compatible with conventional fuels such as gasoline, natural gas and gasoil, generates non-negligible amounts of carbon dioxide (CO_2) and is partly responsible of these greenhouse gas emissions. Therefore, according to an amended regulation, the average CO_2 fleet emissions for particular cars in Europe must be reduced to 95 g CO_2/km by the end of 2020 and to an indicative target range of around 70 g CO_2/km in 2025; which means an approximate 50 % reduction in comparison to the 2015 target value of 130 g CO_2/km. These numbers highlight the pressure on the automotive industry to innovate and push technological measures within every new vehicle to achieve these challenging targets; otherwise, high penalty payments are applied. Along with the introduction of such new targets, homologation procedures are either updated or created in order to reflect the vehicle usage in real life and avoid discrepancies between homologated values and what the driver is seeing in terms of fuel consumption, improving then realistically the air quality in the cities.

To reach these ambitious regulations targets, with the introduction of EURO6c regulation, associated to Worldwide Harmonized Light Vehicles Test cycle (WLTC) and Read Drive Emission (RDE) cycles, it is necessary to look for new technologies and powertrain innovations. A CO_2 emission reduction can be achieved by either improving the power train efficiency of the energy conversion and/or by reducing the vehicle energy demands. Beside the development of hybrid electric vehicles (HEV) or plug-in hybrid vehicles (PHEV), innovations in the ICEs are essential to maximize the overall efficiency of the powertrains. Therefore, several technologies were identified during the period up to 2020, including innovation in combustion, engine architecture, thermal management, ICE component electrifications, ICE waste heat recovery systems, among others.

However, while these technologies allow to achieve the desired reduction in CO_2 emissions, the potential of gain for after 2025, where the regulation will be more severe, is difficult to reach. In fact, the potential of the fuel efficiency gain is limited by the maximum theoretical efficiency of the ICE thermodynamic cycle performed. The ICE itself presents exergetic losses and its efficiency remains far from ideal engine efficiency, the Carnot engine. Also, adding these technologies to gain few efficiency points is at the expense of a cost that is becoming significant, which opens the opportunity for other energy converters to act as a replacement for the ICE.

Another key point to consider when using the ICE as primary converter, is its compatibility with different fuel types. ICE is compatible with conventional fuel, and the development of new energy vectors such as solid fuels, amoniac, or bio-fuels may jeopardize the operation of this machine.

Similarly, the homologation tests aim to reproduce the real vehicle consumption and emission and try to represent the driving mode. However, these cycles do not take into account the additional fuel consumption needed to ensure the thermal needs, (heating and cooling the vehicle cabin) which, under certain ambient conditions, could seriously impact the customer's consumption.

In addition, battery electric vehicle (BEV) promotion efforts across the world are increasingly diverse, with many governments and automakers pushing to promote awareness and sales of advanced electric-drive vehicles, as well as the necessary regulatory, charging infrastructure, and financial support. However, well-to-wheel CO_2 emissions of a BEV is not advantageous mainly in markets where the electricity production relies on dirty fossil fuels.

In this context, and in order to meet the future CO_2 requirements that are going to be set after 2025, PSA Groupe is investigating the potential of new energy converters, based on conventional thermodynamic cycles such as Stirling, Brayton, Gas Turbine, among others and not conventional machines such as fuel cells, thermoacoustic, thermoelectric generator, as primary energy converter in replacement of the ICE in automotive powertrain applications.

Therefore, this thesis work aims at investigating the new potential energy converters that could replace the ICE, and targets at developing a methodology of choice and optimization of energy converters for automotive applications, while considering the energy converters compatibility with fuel and powertrain, the vehicle power needs to be included in the traction power, in the cabin heating and cooling power and in the electric auxiliary power, as well as in vehicle integration constraints such as weight and size. This scientific approach for the automotive industry requires taking into account technological constraints such as materials, maximum temperatures, maximum pressures, and automotive constraints such as mass, volume, power density, noise, price among others. Therefore, a methodology for choice and optimization of energy converters for automotive applications is required.

Chapter 1 of this work is a review for the different energy converters for automotive powertrain applications. The different energy converters are classified as internal combustion machines, external combustion machines or electro-chemical machines. Then a literature review and performance assessment is realized for each energy converter and the state of the art of each energy converter in automotive powertrain application is presented. The advantages and disadvantages of each energy converter compared to the reference internal combustion engine are presented. The chapter ends up by a synthesis in which a classification of the different energy converters in term of powertrain compatibility, fuel compatibility among other criteria is done. This synthesis highlights the advantages and disadvantages of energy converters other than piston engines for the automotive sector. It also helps understand the technological barriers

that must be removed in order to improve the efficiency and the performance of these converters.

Based on this synthesis, the gas turbine energy converter is selected among the potential energy converters for future electrified powertrains. It presents many vehicle intrinsic benefits such as multi-fuel capability, compactness, reduced weight, cogeneration capability, reduced number of moving parts compared to the reference internal combustion engine. Therefore, this energy converter has been selected for the rest of the study.

In chapter 2, the overall methodology for selecting the best suited thermodynamic configuration of the gas turbine cycle and its optimization for a series hybrid electric vehicle is presented. An exergo-technological explicit selection method, based on exergy analysis and optimization under technological constraints is applied and the intercooled regenerative reheat gas turbine (IRReGT) thermodynamic configuration is prioritized among others identified through the methodology. The optimization main criterion was the thermodynamic efficiency which impacts directly the fuel consumption. A series hybrid electric vehicle model is developed and the identified gas turbine cycle is coupled to an electric generator and integrated as auxiliary power unit (APU) to recharge the battery of the vehicle once depleted. A methodology for accounting for the additional vehicle non-mechanical energetic needs on the WLTC is presented. Fuel consumption simulations were then performed on this modified WLTC using the dynamic programing global optimal control strategy. Results are compared to the same vehicle equipped by an ICE-APU.

Since the weight of the system impacts the vehicle energetic demands and consequently the fuel consumption, a pre-design of the different realistic gas turbine system identified is performed in chapter 3. Based on the thermodynamic optimization of efficiency and net specific work, the power to weight ratio of each gas turbine identified configuration is calculated by accounting for the weight of the different components that constitute the system. Then each GT-system is integrated in the SHEV vehicle developed in chapter 2 and simulations are performed using a bi-level optimization method to find the optimal operating parameters in terms of system net output power and the number of times the ON/OFF switch of the APU is toggled on the pareto curve.

In order to account for the fuel consumption penalty when considering the transient operation of the IRReGT system, a dynamic model of the IRReGT was developed in chapter 4. The model considers both the turbomachines and the heat exchangers dynamic behavior. A dynamic mechanical model was developed for the turbomachines including the compressors and the turbines. Moreover, a dynamic model was also developed for the regenerator heat exchanger. Simulations are performed while considering two different gas turbine startup strategies and the additional fuel consumption were compared to results found in chapter 3.

Finally, in chapter 5, different subsystems of the IRReGT system were tested. In this manuscript, only the turbine reheat subsystem was presented. Tests results were compared to the simulation theoretical results. The importance of the the turbine reheat process is then checked and confirmed.

State-of-art on energy converters for automotive powertrain applications
Chapter 1

-Bibliography study on energy converters
-performance in term of efficiency, power density
-Qualitative criteria (fuel and powertrain compatibility, noise, vibrations, ...)
-Qualitative criteria (weight, size, efficiency...)

Choice of energy converter

-State of art results
-PSA manufacturer decision

Identification of potentiel thermodynamic configurations and fuel consumption simulations
Chapter 2

-Exergo-technological methodology for identication of the suited configuration
-Integration in SHEV
-Fuel consumption simulation on WLTC modified cycle using a global optimal strategy

Pre-design and technoeconomic analysis of all identified configurations
Chapter 3

-Pre-design of identified system components
-Weight and size estimation
-Fuel consumption simulation using NSGA-DP (limiting the number of switching ON/OFF)

Dynamic modeling for the selected configuration
Chapter 4

-Selection of the best suited configuration
-Dynamic model of the system
-FC considering EC transient operation

Testing of subsystems of the selected energy converter
Chapter 5

-Testing of different subsystems including turbine reheat, intercooler compression and regenerator

WLTC optimization cycle accounting for all vehicle energetic needs
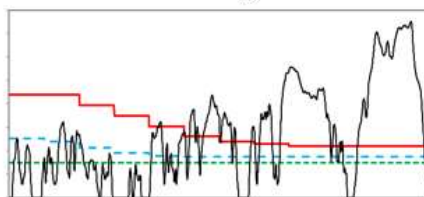
| Cabine heating | Electric Auxiliaries | Air Conditioning |

SHEV
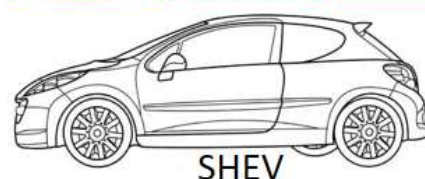
Fig. 0: Thesis general approach

Résumé chapitre 1

L'électrification des groupes motopropulseurs représente aujourd'hui la solution pour les constructeurs automobiles pour respecter les réglementations strictes imposées en matière de consommation et d'émissions de polluants, et de maintenir une autonomie comparable à celle des véhicules à chaîne de traction conventionnelle. La consommation de carburant de ces groupes motopropulseurs dépend en grande partie du rendement des convertisseurs d'énergie et de la stratégie de gestion de l'énergie déployée à bord. Une revue de la littérature montre une diminution des activités de développement sur les moteurs à combustion interne (ICE) comme convertisseur d'énergie primaire pour les véhicules. D'une part, ces convertisseurs présentent très peu de marge d'amélioration supplémentaire du rendement en raison des pertes d'énergie associées au cycle thermodynamique effectué, et d'autre part, ils n'ont pas la capacité d'utiliser plusieurs carburants, ce qui limite leur fonctionnement principalement aux combustibles liquides tels que l'essence et le diesel. Dans ce contexte, et afin de répondre aux exigences en matière de CO_2 pour l'après 2025, il est important d'étudier la possibilité de remplacer les moteurs à combustion interne par de nouveaux types de convertisseurs d'énergie.

Ce chapitre présente une revue des différents convertisseurs d'énergie thermodynamique et thermochimique pour les applications automobiles. Une étude bibliographique est d'abord effectuée pour chacun des convertisseurs d'énergie étudiés afin d'identifier les meilleures pratiques d'utilisation de ces convertisseurs dans les applications automobiles. Ensuite, une analyse est effectuée afin de comprendre le principe de fonctionnement de ces convertisseurs ainsi que d'identifier les paramètres de conception clés. Une évaluation technique des indicateurs clés de performance des convertisseurs est effectuée à l'aide de critères de performance quantitatifs et qualitatifs. Les critères quantitatifs évalués sont le rendement, le travail spécifique net, le rapport poids/puissance et le rapport taille/puissance, et les critères qualitatifs évalués sont la fiabilité, les aspects de maintenance, l'impact environnemental, le bruit et la maturité technologique dans les applications automobiles et autres applications industrielles. Enfin, les convertisseurs d'énergie sont classés en fonction de leur attractivité pour les constructeurs automobiles dans l'intégration dans de nouvelles architectures de groupes motopropulseurs électrifiés et de leur potentiel de développement pour atteindre les objectifs de consommation et d'émissions après 2025.

Chapter 1: A review on energy converters for automotive powertrain applications

1.1 Introduction

Various machines are dedicated to the conversion of fuel into mechanical or electrical energy. They are classified in the automotive applications under three different categories:

1. Internal combustion machines, such as internal combustion engines (ICEs), split cycle engines (SCE) and Gas Turbine systems (GT).
2. External combustion machines, such as Brayton or external combustion gas turbine (ECGT), Stirling, Vapor Cycle machines (VCM), Ericsson, Thermoacoustic (TA) and Thermo-electric generators (TEG).
3. Electrochemical energy converters such as fuel cell (FC) which exists in different types: Proton Exchange Membrane Fuel Cells (PEMFCs), Direct Methanol Fuel Cells (DMFCs), Solid Oxide Fuel Cells (SOFCs), Alkaline Fuel Cells (AFCs), Phosphoric Acid Fuel Cells (PAFCs) and the Molten Carbonate Fuel Cells (MCFCs).

Some of these machines have been commercialized at the beginning of the late century as vehicle prime movers. Among these machines the VCM, where production continued to the 1930's on steam cars [VM1, VM2]. Other machines have been also largely investigated as main energy converter instead of conventional piston ICE in automotive application. We can list for example: the gas turbine system [GT1], the Stirling machine [ST1-ST9], and recently the fuel cell [FC1-FC7].
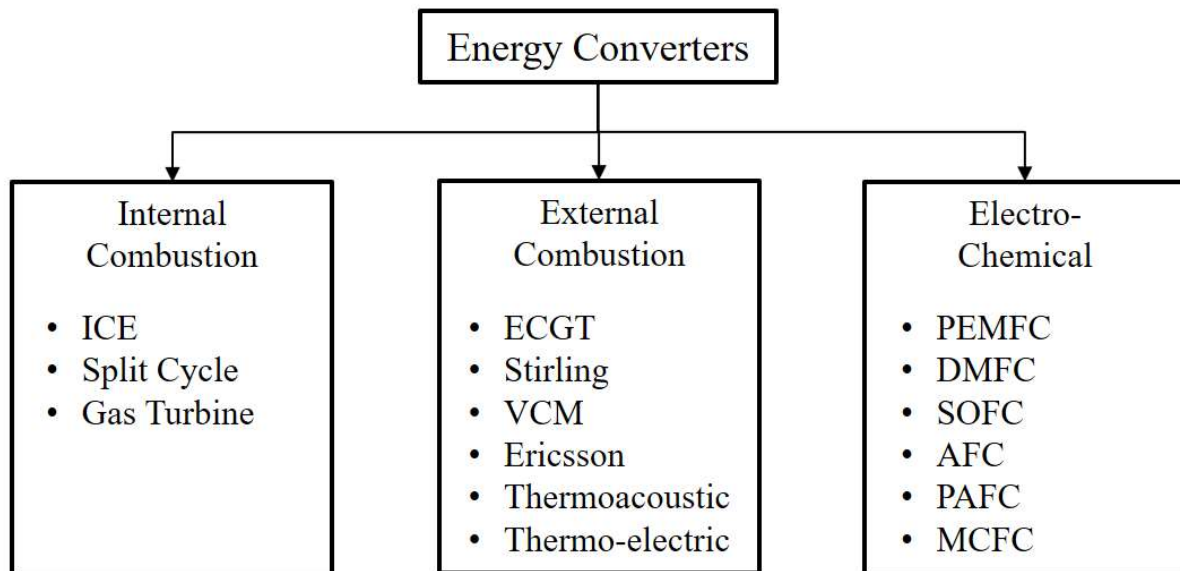
Fig. 1.1: Classification of different energy converters

1.2 ICE: the dominant prime mover in automotive powertrain applications

Nowadays, the ICE, which pioneered for more than decades the automotive industry by being the widely used prime mover, is still undergoing plenty of research and engineering developments in order to improve its performance at all levels. The recent turbocharged ICE presents high specific power, high power to weight ratio and high power to size ratio. Recently, turbocharged engines are the technology of choice in vehicles, due to their good efficiency, fast time response, affordable cost, as well as availability of production and logistic processes. These engines continue to play an important role as a prime mover for automobiles and are expected to keep their leadership as a primary converter where around 88% of vehicles are expected to be equipped with an ICE on the near to medium terms [IC1-IC3].
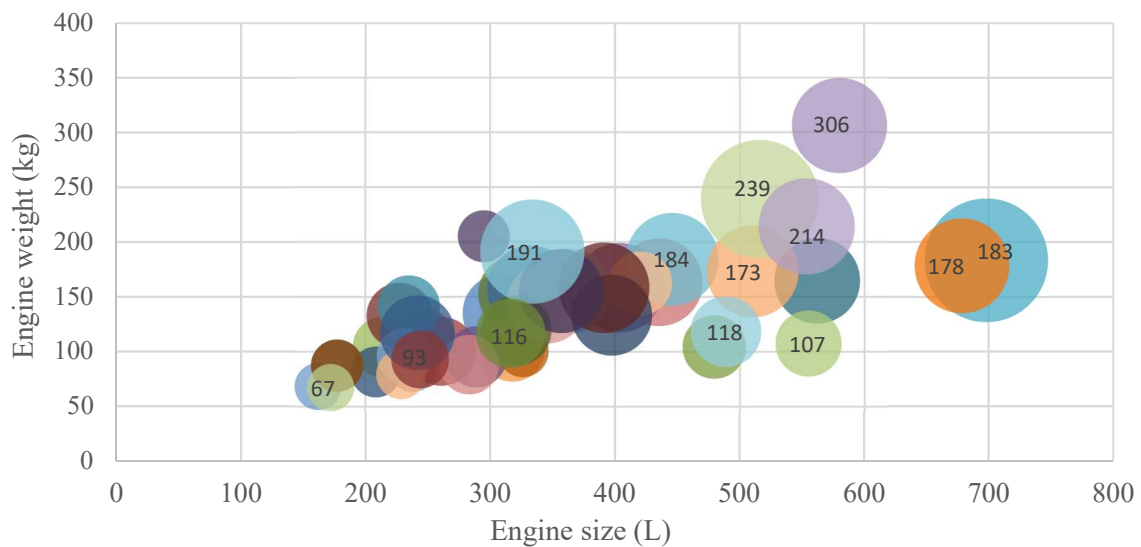
Fig.1.2: Automotive engine power (kW) function of engine's weight (kg) and size (L)
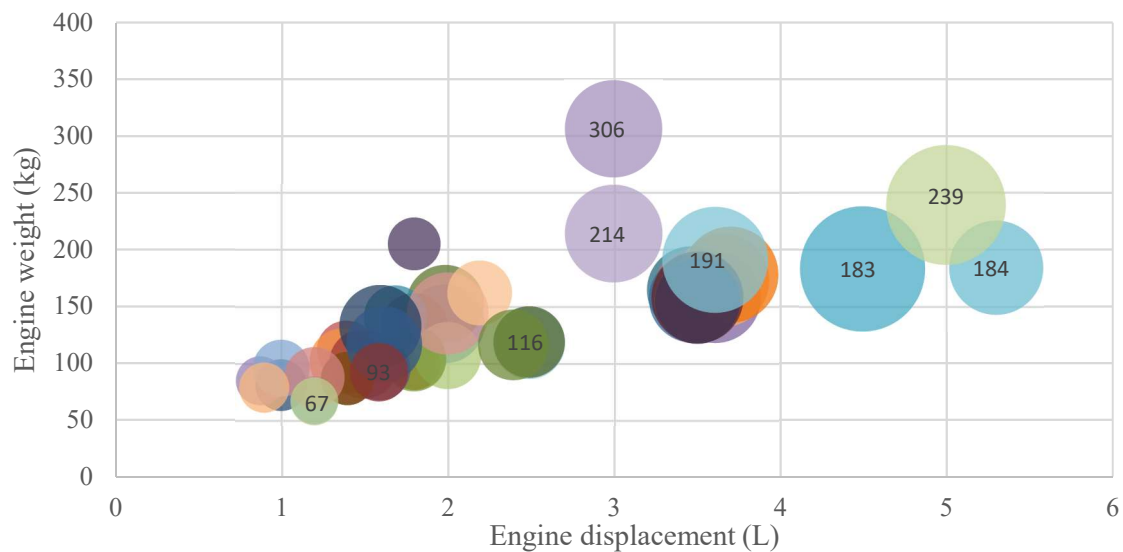
Fig.1.3: Automotive engine power (kW) function of engine's weight (kg) and displacement (L)

1.2.1 Regulating the GHG emissions from vehicles

Meanwhile, governments from around the world are implementing policies to reduce fuel consumption and climate-related emissions, as well as to improve air quality in urban areas. For instance, the European Union (EU) adopted a roadmap for reducing greenhouse gas emissions from the transportation sector by 60% in 2050 compared to emission levels of 1990 [IC4, IC5]. Therefore, the automotive industry needs to bundle their full innovation potential and stringently work for the achievement of the upcoming legislative requirements.

Accordingly, the market of electric vehicle (EV) is expanding, due to the benefit of zero CO_2 and pollutant tank-to-wheel emissions from these vehicles. However, EVs still suffer from mileage limitation, expensive battery cost, additional battery weight and limited charging infrastructure. In addition, the well-to-wheel CO_2 emissions of an EV can be as poor as that of conventional vehicles in countries with dirty electricity generation mixes [IC6].

Therefore, regulating the CO_2 emissions for the whole fleet of new passenger cars (PCs) is a key instrument to reduce emissions from road traffic. For instance, according to a recently amended regulation, the average CO_2 fleet emissions for passenger cars (PCs) in Europe must be reduced to 95 g CO_2/km by the end of 2020 and to around 70 g CO_2/km in 2025 [IC7]. These numbers highlight the pressure on the automotive industry to innovate and push technological measures within every new vehicle to achieve these challenging targets, otherwise, penalty payments are applied [IC8].
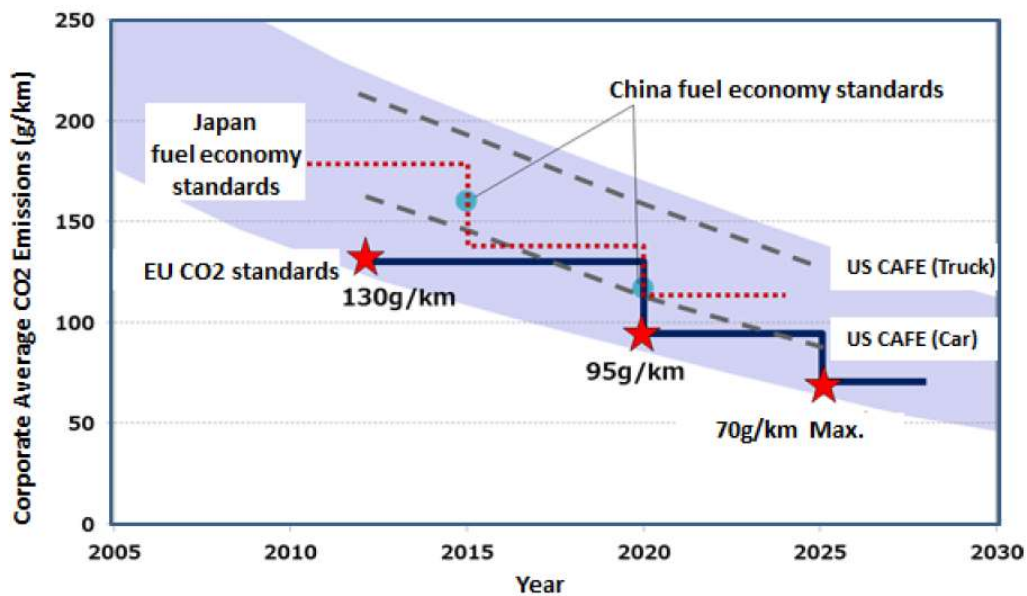
Fig.1.4: CO2 emissions regulations in the world [IC7]

With the recent introduction of new regulations test procedures such as the WLTP and the RDE cycles [IC9] in order to reflect the vehicle under real driving conditions, it is necessary to look for the development of new generations of ICE and advanced powertrains. In fact, CO_2 emission reduction can be achieved by either improving the powertrain efficiency or by reducing the vehicle energy demands. Research and development targets from the literature

shows that several technologies are identified to increase powertrain efficiency until 2025 [IC10], such as:

- Engine architecture: friction reduction [IC11, IC12], lubricating system [IC13, IC14], variable compression ratio and variable displacement [IC15-IC17], engine downsizing [IC18, IC19]
- Combustion: innovative combustion and downsizing [IC20, IC21], variable valve train [IC20], Cylinder Deactivation [IC21-IC23], homogenous charge compression ignition [IC24, IC25].
- Electrification of drive train and auxiliary consumers, as well as working on transmission, driving resistance and waste heat recovery (WHR) systems.
- Thermodynamic advanced cycles: Atkinson-Miller thermodynamic Cycles [IC26],
- Turbocharging [IC20, IC27]
- Thermal management [IC28],
- Hybrid powertrains including [IC29, IC30]
- Electrification of auxiliary consumers [IC31-IC33]
- New driving systems such as CVT and dual clutch transmission [IC34, IC35]

On the other hand, reducing the vehicle energy demand is done by improving the driving resistances, such as reducing the tires rolling-resistance and the vehicle aerodynamic, embedding lightweight materials in the chassis and components as well as optimizing the thermal energy needs for passengers' comfort. Current used thermal comfort technologies could dramatically increase the vehicle consumption under certain weather conditions [IC36].

1.2.2 ICE's fuel consumption savings potential

However, despite these innovations and technological developments on ICE, the potential of fuel consumption savings of ICE based powertrain is limited by the maximum theoretical efficiency of its thermodynamic cycle. The machine itself presents exergy losses [IC37, ICE38] and its efficiency is far from Carnot maximum theoretical efficiency. Therefore, the ICE has been the target of much controversy in regard to both its potential improvement and its possible replacement. While some significant increase in efficiency and pollutants reductions have recently been achieved by costly and complex technologies, substantial further improvements will be very difficult to attain. Today, it seems rather improbable that higher efficiency and acceptable pollution levels can ever be attained without a great deal of mechanical complexity and cost penalties. This matter is serious enough to interest automotive constructers in alternative propulsion systems.

Another disadvantage for the use of ICE as the vehicle prime mover, is its lack of use of multi-fuel, which limits it operation to some fuels, mainly liquid fuels such as gasoline and diesel [IC39]. Therefore, ICE cannot make any advantageous use from the new solid fuel energy vector that is gaining recent interest in the automotive industry.
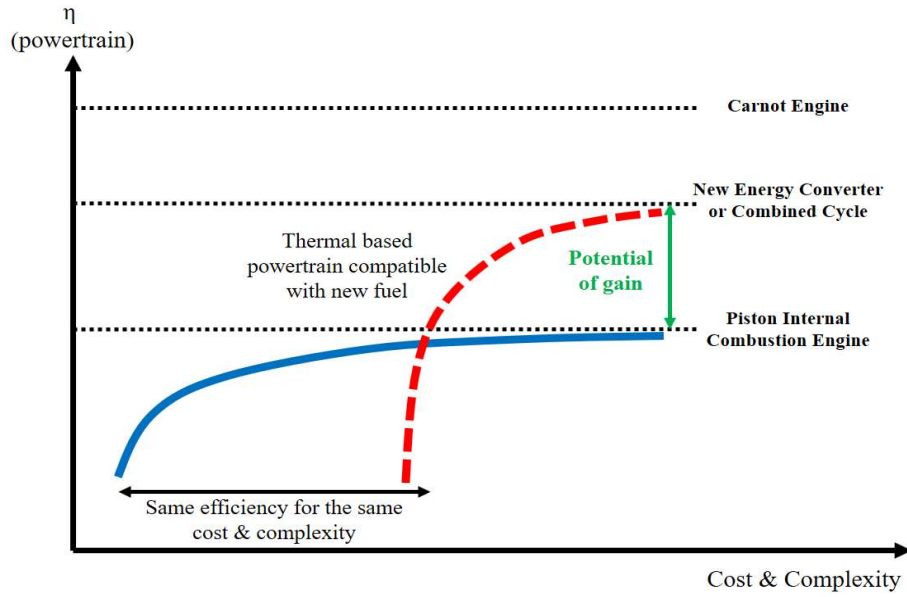
Fig.1.5: Illustration of the powertrain efficiency versus cost/complexity for ICE and other energy converters

1.3 Investigation of the potential use of new energy converters

In this context, and in order to meet the post 2025 CO2 requirements under the ongoing trend of hybrid electric powertrains development, it is important to investigate the potential applicability of new energy converters as a substitute to ICEs. This imposes on these new energy converters to meet the basic requirements imposed on prime movers in vehicle. Among these requirements, we can list: fuel efficient operation over a duty cycle, competitive manufacturing, affordable initial and life cycle cost, fast acceleration and time response, compatibility with new powertrains, reduced emission and noise levels, acceptable reliability and safety, acceptable volume and weight, cogeneration and multi-fuel capability.
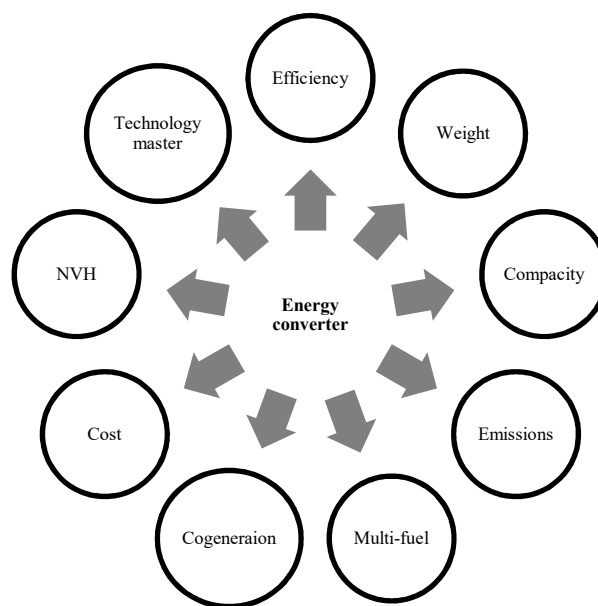
Fig.1.6: Automotive requirements for new energy converters

1.3.1 Research questions

The study of the literature shows that there have been many attempts in the past to replace the ICE by these energy converters. We can mention, Chrysler, Volkswagen, Fiat and Citroën studies on gas turbines [GT1-GT4], GM, Opel and Ford investigations on Stirling machines [ST1-ST7], and GM studies on steam vapor cycles [VM3]. So what were the obstacles against commercialization in series production cars? Similarly, other industries have much more efficient attractive machines such as the combined cycle gas turbine (CCGT) systems for power generation where efficiency can reach more than 60% on specific operating points compared to a maximum around 40% for ICE piston engines. What are the technological problematics that prevent their use in small scales in automotive vehicles?

Today, split cycle engines (SCE) offer high efficiency and good power density, with the advantage of many components and functional synergies with actual ICE. Also, The GT has very favorable specific power and energy efficiency characteristics and presents a forthcoming potential for improving modern vehicle efficiency and emissions with the benefit of fuel-use flexibility when compared to ICEVs. Furthermore, with the development of series hybrid architectures, which combines a thermal and an electric powertrain in a series energy flow arrangement, the GT operating point is easily controllable to operate on the best efficiency. On the other hand, external-combustion (EC) engines have received much recent attention because of their very low pollution characteristics among them, Stirling and Ericsson engines. Besides their very low pollution level, these engines are very quiet and have multi-fuel capability and good efficiency. Also the external combustion steam Vapor Cycle machines engine has, despite its limited efficiency, high specific power, and a multi-fuel capability. Finally, the Fuel cell systems today offer high efficiency despite the fact that they have limited specific power.

In order to highlight the advantages and drawbacks of different energy converters for vehicle powertrains, and to respond to the interrogated questions above, this chapter presents an overview on different energy converters as prime movers for automotive applications.

1.3.2 Review approach adopted in the manuscript

The approach adopted in this study is presented in figure 1.7 below. A bibliographical study is conducted first for each of the investigated energy converters in order to identify the best practices of use of these converters in automotive applications. Then, a design analysis is performed in order to understand the operating principle of the energy converter as well as the key design points and parameters is performed. The third step consists of a technical assessment of these converters, using quantitative and qualitative performance criteria. Among the quantitative criteria, we can mention the efficiency, the net specific work, the weight to power ratio and the size to power ratio. Among the qualitative criteria, the reliability, the maintenance aspects, the environmental impact, the noise and the technology master in automotive and no automotive industry are stand out. Finally, results are synthesized while considering the fuel use capability, the powertrain configuration compatibility including conventional, parallel hybrid and series hybrid as well as other automotive criteria and technical recommendation are proposed.
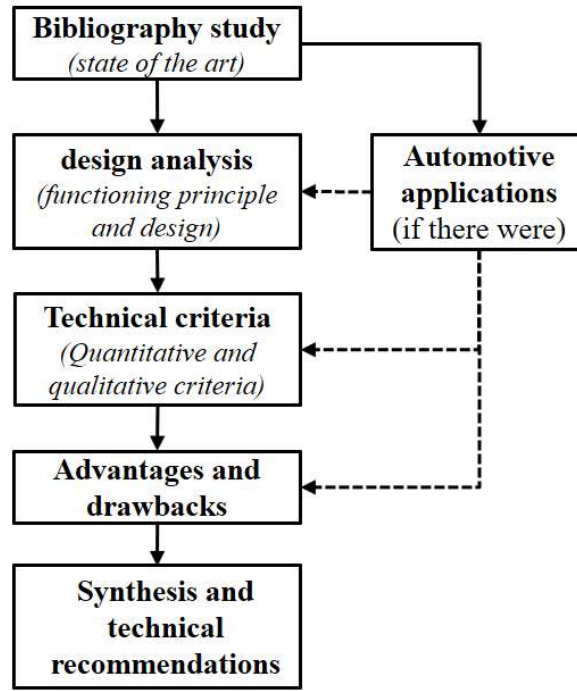
Fig.1.7: Approach of the study

Table 1.1: Internal Combustion Engine (ICE) for automotive powertrain applications

Characteristics	Value and Description
Efficiency range	35 to 38% (Gasoline engines) 38 to 42% (Diesel engines)
Power to weight ratio	400-600 W/kg (atmospheric) 800-1200 W/kg turbocharger
Power to size ratio	300 – 750 W/L
Fuel	Liquid and gaseous conventional fuels (Gasoline, Gasoil, Ethanol, Natural gas…)
Combustion process	Internal Combustion
Working fluid	Air
Emissions	Norm Euro 6 after-treatment emissions
Complexity/size	Moderate to high complexity integration - acceptable size
NVH	Moderate noise and vibration aspects
Controllability	Mastered controllability aspect
Maintainability	Good maintainability
Reliability	High reliability – validated for more than 180.000 km driving distance
Safety	High safety level
Powertrain compatibility	All powertrain architectures
Cogeneration capability	Ensure hot thermal need for vehicle cabin heating
Technical maturity	High technical maturity – Commercialized on automotive applications

1.4 Internal combustion engines

1.4.1   Split Cycle Engine

1.4.1.1 Literature review and performance assessment

The Split Cycle Engine (SCE) is an internal combustion engine based on the piston-connecting rod architecture where the intake and compression strokes are performed in one cylinder and the power/expansion and exhaust strokes in a second cylinder, as illustrated in figure 1.8. The compression and power cylinders are connected through a cross over passage that transport the compressed air into the power cylinder.

The SCE operates similar to two-stroke engines. It produces one power stroke for every revolution of the crankshaft. Therefore, the net power-to-weight ratio and the net power-to-size ratio are comparable to actual ICE [SC2].

Splitting between the engine strokes offers advantageous design flexibility compared to conventional ICE [SC3]. In fact, one of the advantages of performing the compression and the expansion in two different cylinders, is the possibility of increasing the power stroke cylinder volume and downsizing the compression cylinder [SC4], performing therefore more easily the Miller thermodynamic cycle. This concept offers also the advantage of optimizing the thermal management of each cylinder: A cooler compression to reduce the compression work and a hotter expansion to maximize the expansion work [SC5, SC6]. Note also the possibility to adapt the kinematic motion of each piston and the displacement as for an Atkinson ICE.

The thermodynamic operation of this concept is based on the Ericsson cycle when the compression and expansion strokes are isothermal, and it is based on the Joule thermodynamic cycle when these strokes are adiabatic, which makes the SCE gain advantage in terms of efficiency when compared to Otto, Diesel, Dual or Atkinson-Miller thermodynamic cycles actually performed on piston ICE.
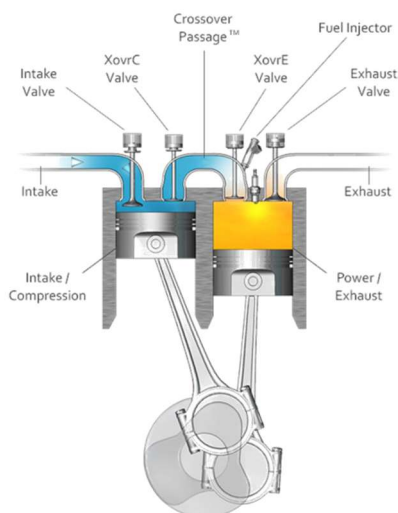
Fig.1.8: Split cycle engine concept [SCE1]   *Fig.1.9: Turbocharged Scuderi SCE concept with air storage tank [SCE23]*
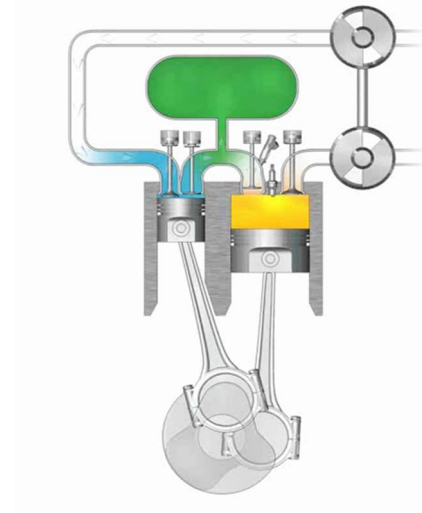
The split cycle concept preceded the Otto and Diesel engines, and dates back to 1891 when it was invented and produced for the first time by Backus Water Motor Company [SC7].

The power range of the first produced engines varied between 1/2 and 3 horsepower, with potential power increase up to 25 horsepower [SC8]. Several studies trace further developments on this concept back to 1910 [SC9], where different architectures and thermodynamic configurations were investigated [SC10-SC12].

Despite the several advantages of the SCE, the review of the literature attributed some drawbacks to this concept. Patil et al. [SC1] highlighted the poor SCE breathing as compared to the ICE, caused by the high-pressure gas trapped in the compression cylinder, which should have been re-expanded before another intake stroke occurs in the compression cylinder. This drawback leads to poor volumetric efficiency, which reduces the engine's capacity to pump air and presents potential work losses. Another drawback underlined by the authors is the low thermal efficiency of the SCE caused by firing the air fuel mixture before the piston reaches its top dead center. In fact, when the compressed air trapped in the crossover passage expands into the power cylinder while the power piston is in its upward stroke, the work done on the air in the compression cylinder is lost, and the engine performs the compression work twice leading to low thermal efficiency [SC1].

Additional technical difficulties must be addressed while operating the SCE. Scuderi company [SC13] showed that the valves timing has to be adapted for each engine operating point in order to maximize the corresponding volumetric efficiency. Scuderi reported that the cylinder head, the liner and the expansion piston temperatures have to be controlled in order to avoid the breakdown of the lubricating oil film and the risk of thermo-mechanical failure of these components. In fact, the cold air during the intake stroke never enters into the power cylinder to cool it down, as the case in conventional ICE; consequently, the average temperature in the power cylinder exceeds the melting temperature of the components material, in particular the cylinder head if made out of aluminum.

In addition to the mentioned control difficulties, extensive validation test procedures are required to ensure the reliability of SCE, since it was not fairly explored in commercial application yet. Therefore, the literature presents gaps in terms of information on the maintenance routine and the reliability of this machine.

1.4.1.2 State-of-the-art of split cycle engines in automotive powertrain applications

Although the SCE was not sufficiently explored in commercial applications, numerous studies have proposed the SCE as a substitute to the conventional ICE in automotive powertrain applications.

The Scuderi Group has extensively explored the use of SCE in powertrains. It presented in [SC1, SC14-SC16] an SCE model with high compression ratio ranging between 75:1 and 100:1. Gaikwad et al. present in [SC17] a detailed description of the operation and the thermodynamic processes of the Scuderi SCE. Several advancements are made to the proposed model compared to the theoretical SCE thermodynamic cycle presented in the previous section, such as firing

the air-fuel mixture after the top dead center, improving the design of the crossover passage valve, and increasing the turbulence in the power cylinder. These advancements resulted in an enhanced volumetric efficiency and thermal efficiency of the engine.

Numeral studies were later presented in the literature assessing the performance of the Scuderi SCE using CFD modeling and simulation. Patil et al. [SC1] compared the performance between a Scuderi SCE and a conventional spark ignition ICE of approximately same volume and for same amount of charge. The Scuderi SCE showed 5% improved indicative thermal efficiency and higher torque at low engine speed, which provided the SCE, 15 to 20% additional power compared to the reference conventional SI engine [SC1]. Scuderi Group explained in their patent [SC14] that the compression and expansion ratios, the top-dead-center pistons phasing, the crossover valve duration and the combustion duration are the key variables affecting the SCE performance and efficiency. Moreover, Scuderi revealed in later publications on methods to improve the part load efficiency of SCE [SC18, SC19]. Other such as Lam et al. proposed also in their study [SC20] a double compression expansion engine concept in order to further improve the SCE efficiency and its net specific power.

Scuderi in [SC21-SC25] also investigated other SCE configurations, namely an air hybrid SCE concept and a Miller turbocharged SCE cycle with air storage tank, illustrated in figure 1.9. SwRI simulations show in [SC26] that the Scuderi SCE consumes 25% less fuel than a comparable conventional ICE, and up to 36% with the hybrid configuration. The turbocharged SCE configuration allows decreasing the brake specific fuel consumption by 14% and increasing the brake mean effective pressure by 140% compared to the regular Scuderi SCE. In that case, the engine has been downsized by 29% thanks to adding a turbocharger, and it was capable of delivering a specific power of 135 hp/liter at 6,000 rpm. In addition to the consumption and performance improvements, the Scuderi SCE concept proved in [SC27] to reduce the NOx emissions by 80% as compared to an equivalent conventional ICE.

Dong et al. performed a thermodynamic analysis on split cycle with internal heat exchanger recuperator to recover the waste heat at the outlet of the expansion cylinder [SC28]. The authors propose a method to decrease the compression work through the injection of a controlled quantity of water in the compression cylinder, lowering therefore the gas temperature during compression. The detailed cycle simulation indicates up to 32% efficiency improvement compared to conventional diesel engine.

Several studies in the literature investigated the combustion process of SCE. Cameron et al. showed in their study [SC29] that the main combustion duration is very rapid for all tested conditions despite the late combustion phasing. This has the advantage of reducing the NOx during rapid expansion as well as reducing the detonation tendency compared to conventional spark ignition controlled combustion [SC22]. Caterpillar showed that Diesel SCE could be favorable to control diesel HCCI combustion and to limit the NOx emissions [SC30, SC31].

Tour Engine is developing an opposed split cycle engine [SC32-SC35], by coupling the two opposing cylinders of two GVX50 Honda engines with a single crossover valve which allows minimal dead space and superior thermal management. Motiv Engines presents similar SCE

configuration in [SC36], where 20% increase in efficiency are announced as compared to modern diesel engines. The engine achieves a high compression ratio of 56:1 leading to 30 MPa peak pressure.

Despite the numerous presented concepts of SCE, none reached the mass-production phase yet on passenger cars. The only commercially available SCE is the Ricardo split cycle isothermal compression engine with water injection and internal heat recovery developed with RWE Innogy [SC37-SC39], illustrated in figure 1.10. This model is available with a wide power range between 1 MW and 30 MW, it uses water injection during the compression stroke to achieve isothermal compression and higher efficiency of around 56%. It is currently mainly dedicated for heavy-duty applications, marine applications and power generation. An improved version of this model was presented in [SC5], substituting the water injection during compression by liquid nitrogen. A pilot simulation of this concept has predicted a thermal efficiency of 60% [SC6, SC40].
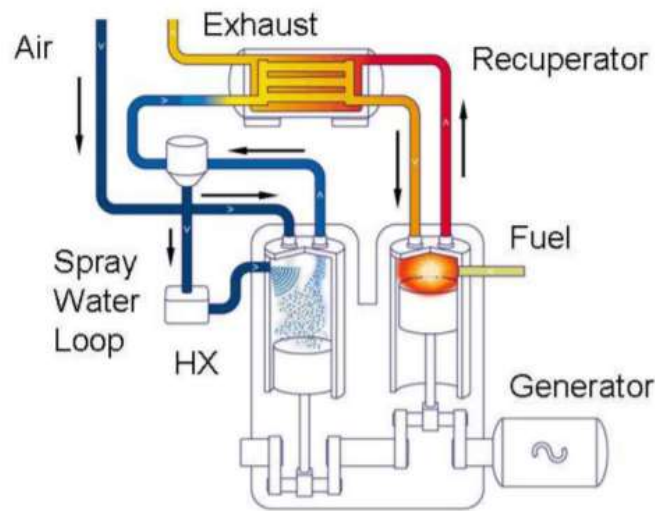
Fig.1.10: Ricardo split cycle isothermal compression engine with water injection and internal heat recovery. [SC38]

1.4.1.3 Synthesis on split cycle engine

Due to the high efficiency and the expertise of manufacturing piston reciprocating engines in the automotive industry, the SCE presents a potential energy converter for the next generation powertrains in order to meet the future CO2 and emissions regulation targets. This piston-cylinder-based machine offers higher efficiency, lower emissions and comparable power density to the conventional ICE. Moreover, it is compatible with liquid and gas fuels, and adaptable to conventional and electrified powertrains. In addition, alike ICE, the SCE is a cogeneration machine capable of covering the cabin thermal needs through the engine cooling system. Therefore, this type of piston-based engine with quasi-identical conventional architecture can limit the investment costs while relying on the acquired expertise for the engine development and validation. However, some technical issues such as the material resistance in the power cylinder and the valves controllability as well as additional validation tests under variable load driving conditions have to be overcame in order to ensure the machine's

reliability. Table 1.2 summarizes the advantages and drawback of SCE observed in the literature and table 1.3 synthesized the performance assessment.

Table 1.2. Advantages and drawbacks of the split cycle engine.

Advantages	· Engine design flexibility · Compatibility with existing engine equipment namely turbochargers and waste heat recovery systems · Higher torque at low engine speed and higher power performance compared to the basic ICE architecture · Higher volumetric, thermal and overall efficiencies · Reduced piston-cylinder friction by offsetting the cylinders · NOx emission reduction · Compatibility with all ICE fuels
Drawbacks	· Still under research investigation, none of the powertrain applications reached the mass production level yet · May require expansive material compared to conventional four stroke ICE, in order to resist to the high temperature in the power cylinder · Require valve controllability for different operating points · More expensive than conventional ICE due to the higher number of cylinders since two cylinders are required to complete the four strokes · May increases the engine cost

Table 1.3. Summary of split cycle engine performance criteria.

Characteristics	Value and Description
Efficiency range	40 – 43% without regenerator [SC1] Up to 45% with regenerator and more than 50% with regenerator and isothermal compression [SC38, SC41]
Net specific power	similar performance compared to ICE or 20% higher [SC26]
Power to weight ratio	250 – 900 W/kg(*)
Power to size ratio	275 – 650 W/L(*)
Fuel	Same as ICE fuels
Combustion process	Internal Combustion
Working fluid	Air
Emissions	Reduced emissions compared to ICE [SC27]
Complexity/size	Moderate to high complexity integration, comparable to ICE size
Noise and vibration	Moderate noise and vibration aspects
Controllability	Complex controllability for transient operation
Maintainability	Still under investigation
Reliability	Still under investigation
Safety	High safety level – same architecture components such ICE
Powertrain compatibility	Compatible with conventional and electrified powertrain architectures
Cogeneration capability	Ensure hot thermal need for vehicle cabin heating
Technical maturity	Medium technical maturity in automotive industry, still in R&D phase

*Based on ICE data and considering the additional weight and volume of components such as crossover and regenerator heat exchanger

1.4.2 Gas turbine

1.4.2.1 Literature review and performance assessment

Gas turbine (GT) energy converters are thermodynamic turbomachines that convert the thermal energy of the working fluid into useful mechanical energy, and generate torque on the turbine shaft.

The simple GT configuration operates according to the Brayton cycle [GT5], as illustrated in figure 1.11. It is composed of an upstream compressor coupled to a downstream turbine. The compressor increases the air pressure, before heat is added, either internally through a combustion chamber or externally through a heat exchanger in the case of an externally fired gas turbine [GT6]. The high temperature pressurized gases then expand in the turbine and produce a mechanical work that could be used in multipurpose operations, namely driving an electric generator to produce electricity [GT7, GT8], or propelling a blade for marine transportation [GT9, GT10], or producing thrust in aeronautical applications [GT11], or propelling a vehicle [GT1, GT12]. Gas turbine cycle can also be of open cycle type or closed cycle type. The open cycle internal combustion is the most common one, in which the combustion products are rejected to the ambient surrounding, whereas the closed cycle uses a heat exchanger to reject the heat to the ambient surrounding [GT13].
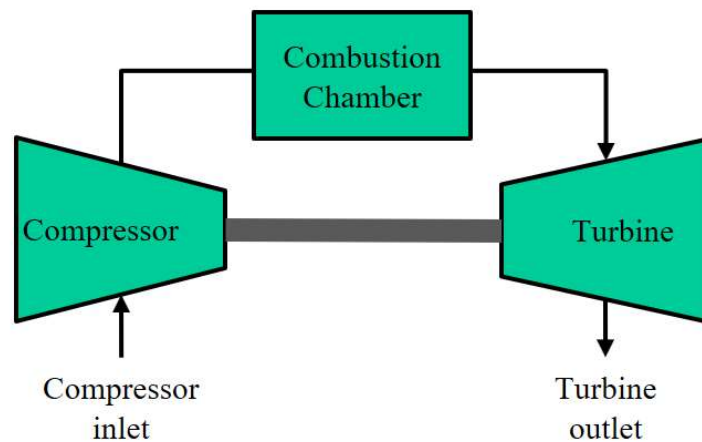
Fig.1.11: Simple Gas Turbine system configuration.

John Barber patented the first turbine system configuration in 1791 [GT14]. In 1903, Aegidus Elling built the first successful simple gas turbine system, using a six-stage radial compressor and a single-stage radial turbine, with a maximum turbine inlet temperature (TIT) of 400°C and a net output power of 8 kW [GT15, GT16]. In 1905, Stolze [GT17] installed the first ten axial compressor stages and fifteen axial turbine stages GT at Berlin-Weissensee power station [GT18, GT19]. His machine delivered a net power output of approximately 150 kW. During the same year, Hans Holzwart [GT20] introduced the constant-volume combustion chamber turbine. In 1906, Charles Lemale and Rene Armengaud developed a 400 horsepower GT designed by August Rateau with twenty-five stage centrifugal compressor, an intercooler and two-stage impulse design axial turbine [GT14]. The world first successfully commercial GT

system generating electric power was developed by BBC, and went into market first in Switzerland [GT21]. This GT system consisted of twenty-three stage axial compressor and a seven-stage axial turbine. It reached a TIT of 550°C and a compression ratio of 4.4, and it delivered 4000 kW net mechanical power and achieved an overall efficiency of 17.4%, with compressor and turbine overall efficiency of 85% and 88% respectively.

Since early developments in the gas turbine technology, the struggle was to achieve higher cycle efficiencies. The design efficiency of GT is mainly controlled by the operating temperatures of the cycle and the efficiency of the components [GT22, GT23]. Therefore, considerable efforts were devoted to increase the TIT from 788°C in the 1960's [GT24], to 1260°C in the 1990's and up to more than 1650°C nowadays [GT25-GT33]. These improvements are based on the development of high strength materials, high temperature coatings and improved blade-cooling methods, blade designs and aerodynamics.

Numerous studies in the literature explore the developments made to the other constituting components of the GT system. Whittle, Cheshire and Eckardt et al. presented respectively in [GT19, GT34, GT35] the early developments made to the two main compressor types used in GT systems: (1) the axial flow compressor and (2) the centrifugal compressor. Each type is used in a different application depending on the required specifications such as the frontal area, the weight, the efficiency and the cost [GT36]. Alike the compressor, there are two basic types of turbines, the radial flow type and the axial flow type. The radial turbine is more compact and can handle efficiently low mass flow rates [GT8], but it is normally less efficient than the axial flow turbine [GT37]. Therefore, it is used as aircrafts auxiliary power units [GT38] and for supercharged ICE [GT39]. Cohen et al. and Nagpurwala set up in [GT8] and [GT40] the main requirements for the design of the combustion chamber: high combustion efficiency, high reliability, low costs and no visible smoke. Several studies highlighted the different techniques considered nowadays to cope with nitrogen oxides emissions from combustion chambers, such as using the water or steam injection technique [GT41, GT42], the selective catalytic reduction, the SCONOX catalytic absorption system or the dry low NOx (DLE) technology [GT8, GT43-GT45]. Reduction of pressure loss in combustion chambers [GT47-GT49] and heat exchangers namely the regenerator [GT50] was also a major concern tackled in the literature, as it strongly affects the GT system efficiency [GT51]. Recent heat exchangers effectiveness exceeds 90% with a pressure drop less than 5% [GT49]. Rotary ceramic-matrix regenerators achieve heat transfer effectiveness between 93% and 98% with leakage below 4.5% and pressure-drop per stream between 1.8% and 5.4% [GT52, GT53]. Pathiranthna, Nada and Shah et al. [GT54-GT56] highlighted other pressure drop concerns in the GT system, mainly at the compressor inlet and the turbine outlet.

Beside the developments made to the components and their material, advanced gas turbine thermodynamic cycles have been examined [GT50, GT52], and several GT-system thermodynamic configurations are explored in the literature, as summarized in table 1.4.

Table 1.4: Synthesis on the different GT-system configurations explored in the literature.

GT system thermodynamic configuration	Insights
Combined GT cycle [GT58-GT64]	Combining a gas turbine cycle to steam Rankine cycle in order to achieve high efficiency and high power density.
GT with recuperator [GT7, GT65]	Increasing the efficiency by recovering thermal waste heat at turbine outlet at the expense of the net specific work
GT with intercooling [GT65-GT69]	Increasing the net specific work by reducing the compression work through an intercooled compression
Reheat GT cycle [GT19, GT70]	Increasing the net specific work by performing a turbine reheat cycle
Intercooled recuperated GT [GT22, GT71]	Increasing the cycle efficiency by increasing the net specific work and by recovering heat lost at turbine outlet
Intercooled recuperated reheat GT [GT11, GT72]	Increasing the cycle efficiency and the net specific work by both technics described above
Isothermal expansion GT [GT73]	High net specific work and efficiency by achieving an isothermal expansion through a combustion inside the turbine
Steam Injected Gas Turbine cycle (SIGT) [GT74-GT76]	Combined GT cycle where water is injected in various locations to increase the efficiency and the net specific work
Chemically Recuperated Gas Turbine (CRGT) [GT77-GT80]	Exhaust heat is recovered in a Heat Recovery Steam Generator (HRSG) in which the super-heater section is replaced by a Methane Steam Reformer (MSR)
Advanced Integrated Gasification Combined Cycle (IGCC) [GT81]	Use high pressure gasified to turn coal and other carbon based fuels into gas
Evaporative GT (EGT) [GT82], Humid Air Turbine (HAT) [GT83] and Cascaded Humidified Advanced Turbine (CHAT) [GT84]	Water is injected downstream the compressor (EGT) and at other locations (HAT, CHAT) in order to cool the air upstream the regenerator. The addition of water increases the turbine mass flow and power output, and reduces the temperature drop which increase the regenerator effectiveness
Gas turbine coupled to SOFC [GT85, GT86]	High efficiency (of more than 70%) can be achieved by combining the GT to the SOFC

1.4.2.2 State-of-the-art of gas turbine systems in automotive powertrain applications

Many attempts to substitute the conventional ICE in passenger vehicles with GT are explored in the literature [GT8, GT17, GT87]. Chrysler presented in the 1950's the first regenerative GT prime mover powertrain configuration [GT1], with radial compressor, illustrated in figure 1.12. Many improvements have followed in the subsequent generations of the concept, aiming mainly at improving the compressor and turbine efficiency, increasing the TIT and the regenerator effectiveness, development of new materials, variable geometry at the turbine nozzle and variable geometry compressor, water injection, material cost, leakage seals, production process.

GM, Fiat and Volkswagen introduced in the 1950's the GM Firebird prototype, the Fiat Turbina (200 hp GT [GT88]) and the SquareBack VW (75 hp GT [GT2]). Additional prototypes were developed for racing vehicles, such as the Rover-BRM [GT5] and the Lotus 600 hp GT Formula1 [GT-89]; and other prototypes for heavy trucks such as the Chevrolet Turbo Titan III [GT90] and the GMC Astro Gas Turbine truck [GT91].

All these GT vehicle models showed poor acceleration response and higher fuel consumption compared to internal combustion engine vehicles (ICEV). These drawbacks where mainly due

to operating the GT at high speed even at idle conditions, in addition to mechanically coupling the turbine to the vehicle driving load, which resulted in a low efficiency operating range of the GT-system. Despite the many technological advancements and improvements made on GTs, the acceleration lag and the poor fuel efficiency were still the main reasons hindering their deployment in conventional powertrains.
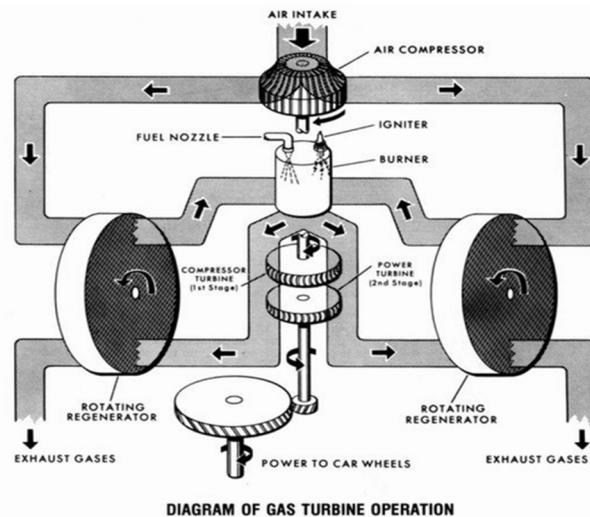
Fig.1.12: Chrysler regenerative gas turbine system for passenger vehicles [GT1].

A review of recent research and development programs of automotive manufacturers revealed new interests in GT for automotive applications, demonstrated in several vehicle concept cars. In 1995, Volvo presented its Environmental Concept Car (ECC) with GT as main energy converter, based on the Volvo 850 serial model [GT92]. In 1997, PSA investigated the GT on the Peugeot 406 with series hybrid electric powertrain architecture [GT4]. In 1998, GM introduced the EV-1 series hybrid vehicle that was adaptable to use either an ICE or a 40 kW GT as range extender driving a generator to recharge the batteries [GT93]. In 2006, GM presented the Ecojet Concept Car using a helicopter GT generating 650 hp maximum power and 790 Nm torque [GT3] and in 2009, Jaguar presented the C-X75 concept car that uses a pair of twin-shaft Capstone CTM-380 GT as range extender [GT94]. In the same year, ETV Motors investigated the potential of GT on a Toyota Prius, equipped with a micro GT, operating as a Range Extender [GT95]. In 2012, Pininfarina announces the development of a super Car equipped with a Diesel GT as a range extender [GT96]. The GT system is expected to extend the vehicle autonomy by 600 km, originally designed for 200 km all electric range. The vehicle will not require NOx after-treatment system since emissions will not exceed 0.05 g/km, which makes the vehicle pass the Euro 6 standards. Similar conclusion was derived by a study at the University of Rome, showing that GT emissions at optimal efficiency operation meet the Euro 6 emissions levels for CO, NOx and soot without the use of after-treatment systems [GT97]. TechRules announced the development of similar series-hybrid range-extender powertrain configuration for its high performance sports car [GT98], using a 96,000 RPM turbine mounted on air bearings with pneumatic positioning. The vehicle autonomy is expected to reach 1850 km with an average consumption of 4.8 L/100 km. The main drive behind developing series-hybrid range-extender configurations by all manufacturer for their GT systems was explained

by a study at Chalmers University of Technology, which highlighted the improved efficiency by operating GT at optimal efficiency point compared to an ICE [GT12], in addition to all the benefits derived from using an electric machine for the propulsion.

GT applications were also observed in heavy-duty prototypes. Volvo developed in 1990's both the Environmental Concept Truck (ECT) and the Environmental Concept Bus (ECB), two prototypes with hybrid propulsion system coupled to GT [GT99]. Wrightspeed unveiled the Fulcrum GT, a 80 kW two-stage compression regenerative GT [GT100], with a power to weight ratio of 750W/kg. It operates as range extender on electric powertrain truck. Walmart showcased the Walmart Advanced Vehicle Experience (WAVE), a range extender series hybrid tractor-trailer prototype, with a multi fuel capability Capstone GT [GT101].
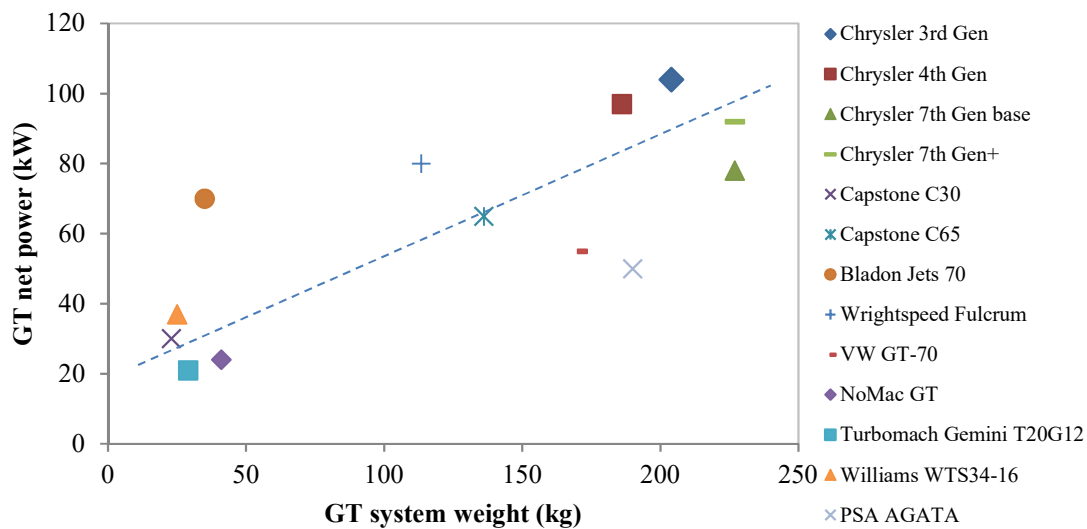
Fig.1.13: GT net power as function of the GT system weight for different GTs.

1.4.2.3 Synthesis on gas turbine systems

Different manufacturers explored the potential integration of GT in conventional powertrains since the 50's as a substitute to the ICE. The poor vehicle acceleration response and the high fuel consumption compared to ICE vehicles were among the main drawbacks, which prevented their commercialization.

Recent literature reflected a revived interest in GT application, in particular on series-hybrid electric vehicles, which combine the GT to an electric powertrain in a series energy-flow arrangement. Since the GT operation is cinematically decoupled from the vehicle speed, the operating point is easily controllable to run on the GT best efficiency point, which enhance the overall vehicle efficiency. The GT-system offers in addition other intrinsic benefits for vehicle powertrains such as the reduced number of moving parts, the vibration-free operation, the high durability and the absence of cooling and emissions after-treatment systems. All these benefits combined makes the GT a forthcoming potential for improving modern vehicle efficiency and emissions, with the benefit of fuel-use flexibility when compared to ICEVs. In addition, GT is a cogeneration machine, capable of covering the cabin thermal needs.

Table 1.5 summarizes the advantages and drawback of GT systems observed in the literature and table 1.6 synthesized the performance assessment.

Table 1.5: Advantages and drawbacks of the gas turbine system.

Advantages	· Multi-fuel capability · High efficiency at optimal operating load · Low emission of CO, NOx and particulate compared to ICE · Less number of moving part compared to ICE · Low maintenance cost and high durability · No need for cooling system as in ICE · Free vibration operation due to the absence of reciprocating components · Good cold start behavior · Improved power-to-weight ratio compared to ICE · No need for muffler when regenerator is used
Drawbacks	· Low efficiency under partial load operation, where partial load consists a considerable fraction of the driving pattern in automotive application · Acceleration lag challenges in conventional powertrain architecture · High rotational speed even at idle conditions: high consumption at idle · High impact of turbine downstream pressure on GT efficiency

Table 1.6: Summary of gas turbine systems performance criteria.

Characteristics	Value and Description
Efficiency range	20 – 30% simple GT 40 – 42% regenerative Intercooled GT 45 – 52% advanced GT
Power to weight ratio	450 – 1400 W/kg
Power to size ratio	225 – 900 W/L
Fuel	Liquid and gas fuels (gasoline, gasoil, ethanol, natural gas etc.)
Combustion process	Internal Combustion
Working fluid	Air
Emissions	Reduced emissions at source compared to ICE
Complexity/size	Low complexity integration
Noise and vibration	Low noise and vibration aspects
Controllability	Complex controllability for transient operation
Maintainability	Good maintainability aspect
Reliability	High reliability
Safety	High safety level
Powertrain compatibility	More suited for series and range extender powertrain architectures
Cogeneration capability	Ensure hot thermal need for vehicle cabin heating
Technical maturity	Good technical maturity for industrial applications, lacks maturity in automotive applications

1.5 External combustion engines

1.1.1 Stirling Engine

1.1.1.1 Literature review and performance assessment

Stirling engines are among air engines invented in the first half of the 19th century. The first machine was patented and built by Robert Stirling in 1816 (figure 1.14) in order to propose a better alternative for mechanical energy production than steam engines at the time, where many accidents with steam boiler occurred due to deficiency in material strength [ST1, ST2]. Stirling engine is an external combustion reversible machine, using a gas working fluid and mainly known for its "Regenerator" (a thermal energy storage device) [ST9].

Stirling engine is a multi-service machine which can produce work, heat and cold [ST10, ST11]. It also involves several engineering disciplines such as thermodynamics, heat transfer, metallurgy, fluid mechanics, mechanical structure, cinematic and dynamic of motions [ST4, ST11-ST12]. It is used today in many different industries and applications such as solar machines [ST14–ST20], submarine [ST21, ST22], residential use as micro-cogeneration [ST23-ST26], biomass applications [ST27, ST28], cold production [ST29], waste heat recovery system [ST30] and even investigated as range extender for electric vehicles [ST31].
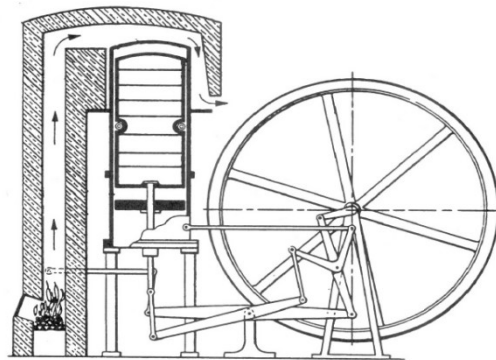
Fig.1.14: Draft of the Robert Stirling's engine patent, 1816 [ST8].

The Stirling machine's efficiency is directly affected by some physical operating parameters and by the thermodynamic system configurations, namely the temperature of the hot and cold energy sources, the heat exchangers design (geometry, size and material), the regenerator design (thermal conductivity, thermal inertia, architecture, mass, porosity and pressure drop), the engine architecture (pistons kinematic, law of volume, compression ratio, among others), the working fluid characteristics (heat capacity, diffusivity, density and viscosity) and the engine mechanical friction losses [ST32].

Material alloys are also among key factors to achieve high efficiency [ST33, ST34]. In fact, like all thermodynamic machines, Stirling engine efficiency increases by increasing the hot source temperature and by reducing the cold source temperature [ST35-ST39]. The limitation of maximum temperature is set up to prevent thermo-mechanical stress failure, mainly on the hot head component [ST40].

The regenerator plays an essential role in improving the efficiency by recovering internally part of the wasted energy and therefore reducing the thermal energy added to the cycle [ST41-ST43]. However, a high performance regenerator is subject to many criteria such as the thermal insulation in the axial direction, capability to operate at high temperature, low dead volume and low pressure drop [ST44]. Nonetheless, its design and size must be a compromise because it increases the dead volume which reduces the maximum cycle pressure and consequently the Stirling machine efficiency.

Another important point when considering the Stirling machine efficiency is the confined pressurized working fluid gas used. NASA demonstrated in [ST4] that the best efficiency can be achieved using Hydrogen as working fluid, followed by Helium, Argon and Nitrogen. Same results were shown by Finkelstein et al [ST45]. In fact, the highest efficiency is achieved with isothermal compression and expansion, which require quick heat diffusion, high thermal conductivity and low density working fluid. Low density and low dynamic viscosity are also required to decrease the viscous friction and to achieve higher rotational speed [ST2, ST46].

As for the engine architecture, Stirling machine can be found in many configurations: simple acting machines, double effects machines, double parallel crankshaft, and swash plate [ST47] among others. Simple acting machines can be devised in 3 types: The alpha type (α-type) where pistons are separated in two cylinders, the beta-type (β-type) where the displacer and the power piston are incorporated in the same cylinder and the gamma-type (γ-type) using two separate cylinders, one for the displacer and the other for the power piston [ST2, ST48]. The advantages of each configuration in term of efficiency, engine size, dead space, maintenance, power density, sealing system and others criteria have been assessed in the literature [ST49].

Finally, several Stirling-system options can be considered, combining a basic Stirling machine to a combustion chamber preheater or a heat recovery multi-stage Stirling in serial configuration for example [ST50]. The review of literature showed that several system configurations have been studied and performance were analyzed in many applications as described above [ST51-ST54]. Table 1.7 presents a summary on the related main developments and specifications.

Table 1.7: Synthesis on the different Stirling engine configurations explored in the literature.

Stirling engines development [ST29, ST55]						
Engine	Engine Type	Working fluid	Max pressure (Mpa)	Heater Wall T (K)	Max Power (kW)	Max Efficiency (%@RPM)
4-95 [ST56]	Double-acting	H2, He	15	993	43@4000	34@2000
Upgraded ModI [ST57]	Double acting	H2, He	15	1043	56.5@4000	35@1700
ModII [ST57]	Double acting	H2, He	15	1093	58@4000	38@1500
4-275R [ST58]	Double acting	H2, He	15	1033	85@2200	38@1200
NS03M [ST59, ST60]	Displacer crank	He	6.2	1059	3.81@1400	35.9
NS03T [ST61]	2 piston crank	He	6.4	1080	4.14@1300	32.6
NS30A [ST62, ST63]	swash plate	He	14.7	1017	30.4@1500	37.5
NS30S [ST64]	2-crank (U4)	He	15.5	1220	45.6@1800	37.2
V160F [ST65]	2 piston crank	H2, He	15	1023	15@2400	30@1000
STM4-120 [ST66, ST67]	Swash plate	H2, He	11	1023	24.5@1800	45.5/1800
SE20H [ST68]	Double-acting	H2, He	8	1073	30@1600	32.3@750

1.1.1.2 State-of-the-art of Stirling engines in automotive powertrain applications

Stirling machines for automotive applications in conventional powertrains have been largely investigated over years as the main energy converter instead of conventional internal combustion engines (ICE) [ST57, ST69-ST71]. The improved efficiency of this machine compared to ICE has attracted automotive constructers to develop many prototypes in the 1970's and 1980's [ST72, ST73]. In addition to its efficiency advantage, the Stirling engine offers other intrinsic benefits for vehicle powertrains such as silent operation, low vibration [ST71], simplicity in operation, absence of valves, and multi-fuel use capability [ST74, ST75].

Due to the large efforts invested by Philips in reducing the Stirling engine size per unit power by 125%, increasing the power per kilogram by 50% and improving the efficiency by 15% [ST8, ST76-ST78], the Stirling engine found its way to the automotive industry. Among the developments done for passenger vehicle applications, we can list the 4-98 and the 4-215 Ford engines [ST73, ST79], the P-40 engine produced by United Stirling Company, which was subject to several modifications and adapted later to applications other than automotive [ST69, ST80], the MODI [ST81, ST82], the upgraded MODI, the MODII [ST83, ST84] and the GPU-3 GM engine [ST72, ST85], which was adapted later for non-automotive applications [ST86].

Note that the MODI and MODII engines consist of a family of improved engines based on the P-40 USAB Stirling machine. MODI improvements consisted mainly on weight reduction and increasing the operation temperature from 720°C to 820°C [ST87]. The MODII, illustrated in figure 1.15, provided additional weight and size reduction by 40%, a 30% fuel economy [ST84] and a design with competitive manufacturing cost compared to gasoline and Diesel ICE at the time, in addition to the multi-fuel use ability [ST57, ST84].
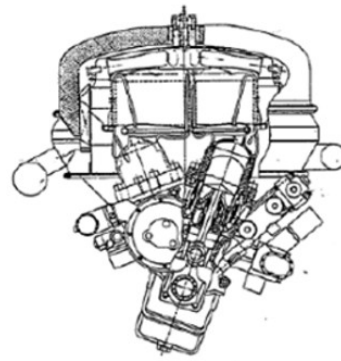
(a) P40 Stirling engine   *(b) MODII stirling engine*

Fig. 1.15: Automotive Stirling engines

Early Stirling vehicle models in the 70's and 80's on conventional powertrains showed better consumption and acceleration performance compared to ICE vehicles (ICEV). This was mainly due to the higher thermal efficiency of Stirling engines, and their high torque capabilities at low engine speed [ST57, ST83]. Among the vehicle prototypes, we can list the Ford Torino [ST88, ST89] equipped with the 4-215 DA Stirling engine, the Ford Pinto and the Ford Taunus, both equipped with the V4X31 engine [ST90] and the Chevrolet celebrity powered by the MODII

Stirling engine [ST84, ST91]. Note also that hybrid prototypes were also proposed such as the Stir-Lec, a series hybrid electric vehicle prototype based on the Opel Kadett and equipped with the P-40 Stirling engine for recharging the lead-acid batteries.

Another important advantage observed on Stirling engine vehicles is their low level of emissions [ST92-ST95]. The NASA demonstrated in [ST57] that the MODII engine shows better emissions of CO, NOx and soot as compared to petrol ICE at the time, due to the continuous combustion process.

1.1.1.3 Synthesis on Stirling engines

Different manufacturers have investigated the integration of Stirling engines in conventional powertrains over years in an attempt to cope with consumption and emissions reductions from vehicles. Early Stirling models for conventional powertrain vehicles showed adequate vehicle acceleration performance and improved fuel consumption compared to internal combustion engine vehicles (ICEV). However, despite the advantages and the many technological advancements made to the Stirling machine in terms of improving power to weight and size as illustrated in figures 1.16 and 1.17 [ST57, ST82, ST84], many reasons hindered their deployment in conventional powertrains. We can list: the leakage problematics, the higher cost compared to the ICE at time and the complex control during transient load [ST36-ST39, ST57].
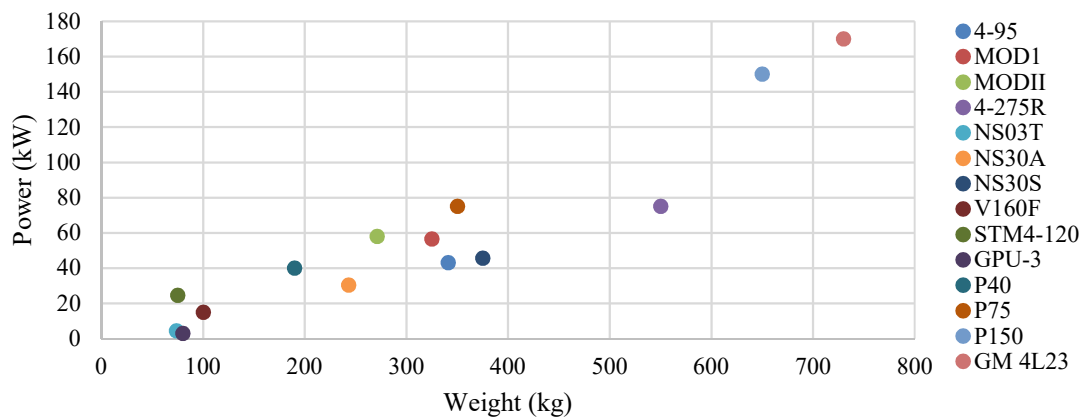
Fig. 1.16: Stirling engines power (kW) versus weight (kg).
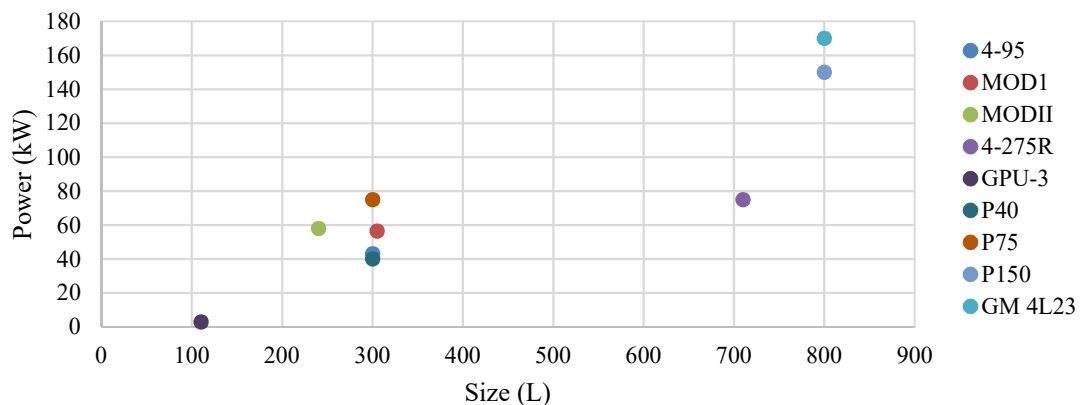
Fig. 1.17: Stirling engines power (kW) versus engine size (L).

Nowadays, the continuous technological advancement on magnetic coupling systems to completely seal the engine and avoid any working fluid leakages, in addition to the rising interest in using biofuels and reducing CO2 from vehicles, revived the interest in this machine. This is in particular for hybrid vehicle applications that require a quasi-steady engine operation, namely series and series-parallel hybrid powertrain configurations. This can reduce the engine control complexity, as the engine will operate on its optimal efficiency operating line.

Table 1.8 summarizes the advantages and drawback of Stirling engines observed in the literature and table 1.9 synthesized the performance assessment.

Table 1.8: Advantages and drawbacks of the Stirling machine.

Advantages	· Multi-fuel capability · High torque at low engine speed · Good thermal efficiency · No need for intake and exhaust valves · Low vibration and noise levels · Reliability of mechanical components · Low pollutant emissions due to the continuous combustion · Good technological maturity · Acceptable weight to power and size to power ratio
Drawbacks	· Sealing challenges · Difficulty to lubricate the mobile parts particularly in the hot side of the engine · Regenerator challenges (efficiency, dead volume, integration) · Complex system to control engine load (through working fluid gas pressure) · Hydrogen storage challenges · Maximum temperature (metallurgic limitation)

Table 1.9: Summary of Stirling engine performance criteria.

Characteristics	Value and Description
Efficiency range	34% to 42%
Power to weight ratio	225 – 350 W/kg
Power to size ratio	225 – 350 W/L
Fuel	Multi-fuel capability
Combustion process	External combustion
Working fluid	Hydrogen, Helium, Argon, Nitrogen
Emissions	Controlled at source through continuous combustion and EGR
Complexity/size	Moderate complexity integration
Noise and vibration	Low noise and vibration aspects
Controllability	Complex systems for transient load behavior
Maintainability	Moderate challenges related to working fluid leakage
Reliability	High reliability machine
Safety	Moderate to good safety level (depending on the used working fluid)
Powertrain compatibility	Compatible with all powertrain architectures
Technical maturity	Good technical maturity (in particular for non-automotive applications)

1.1.2 Vapor Cycle Machine

1.1.2.1 Literature review and performance assessment

Vapor cycle machines (VCM) also known as steam engines are external combustion engines that operate according to Rankine or Hirn thermodynamic cycles. A simple VCM configuration is illustrated in figure 1.18. It consists of (1) a Rankine cycle loop (RC) and (2) a combustion chamber loop (CC). The RC-loop consists of a pump, a heat exchanger (HEX) evaporator, an expansion machine and a condenser, whereas the CC-loop includes a combustion chamber blower (CCB) and a combustion chamber. The CCB is used to blow the air into the CC where the combustion takes place. The thermal heat generated is partly transferred to the RC through the HEX, which serves at the same time as heater, boiler and super-heater to the water circulating in the RC-loop. Then, the generated steam at the outlet of the evaporator expands in the expansion machine and generates mechanical work.
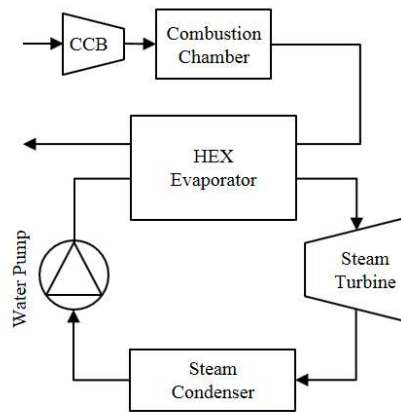
Fig. 1.18: Simple vapor cycle machine configuration.

The cycle efficiency of steam engines depends on the system physical operating parameters, such as the pressure, the temperature of the energy sources, the components efficiency, as well as the thermodynamic cycle configuration [VM4-VM6]. Water is used in these engines as it is among the best suitable working fluids for recovering heat from high temperature energy source, as used today in power generation machines [VM7-VM8].

Several expansion machines are used, such as steam radial and axial turbines, scroll machines [VM10], piston expander [VM11-VM16], among other types [VM17, VM18]. Three types of steam turbines are used, the axial flow turbine [VM19] the tangential flow turbine and the radial flow turbine. These machines present some advantages when compared to expansion machines. First, there is no direct contact between the moving and stationary parts outside the bearings, which means that there is no risk for lubricating oil infiltration in the working fluid. Therefore, steam at a higher temperature can be used, which is also needed to avoid condensation and drops impinging on the blades. The other advantage is the open volume architecture, which requires no intake and exhaust valves.

1.1.2.2 State-of-the-art of steam engines in automotive powertrain applications

The Cugnot Steam Trolley was the first steam vehicle constructed in 1769 in France [VM20, VM21]. Later, 20 kW steam-driven road tractors to pull passenger carriages were produced and used in France until the mid-nineteen thirties [VM22]. In the U.S, first models appeared in 1878 [VM23]. We can list the Model G steam touring car in 1907, the Doble Model C in 1917, the Besler Steam car in 1930 and the Ford Falcon steam car [VM24]. At that time, Steam cars and ICE cars were developed contemporaneously as engineers had gained 100 years of experience in steam engines for trains and heavy tractors. However, the steam cars left their place with time to the ICE cars because of their lower complexity and better response time.
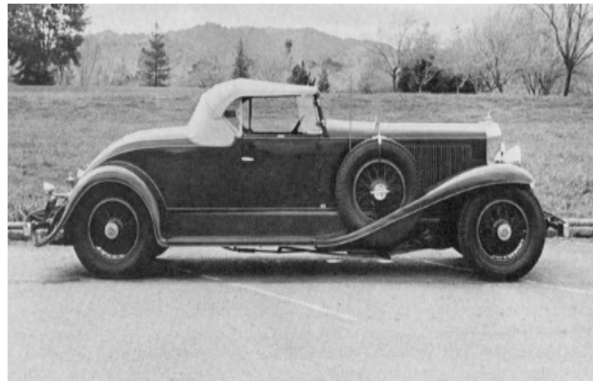
Fig. 1.19: 1924 Doble steam Car [VM24].

Many investigations found in 1960 that the reciprocating steam engine is a reasonable alternative to the ICE for automotive applications [VM25-VM28]. In 1969, GM presented the Chevelle SE 124 (figure 1.20), a steam car with a conventional powertrain, in an attempt to replace the ICE with cleaner energy converters for air quality issues. The vehicle was powered by four cylinders steam engine developing up to 50hp. The proposed steam engine presented several advantages such as the silent operation, the high torque at low engine speed and the capability to operate with variety of fuels; however, the project was abandoned by GM as the power unit was bulky and the cost was estimated 3 times that of piston engines even on a mass production scale. In addition, the system presented many technical challenges, such as the risk of water's freezing, the water's consumption across the condenser, the condenser size and the lubrication problematic that need filtration to prevent deposit formation that may contaminate the working fluid [VM23].

Following GM's work, NASA performed a parametric analysis for an 1815 kg steam-powered car of 130 kW with comparable performance to typical passenger car of the same weight [VM3]. The target of the study was to determine the size, weight and the required condenser fan power. The study demonstrated that for most operating conditions, the condenser fan power is quite low, around 0.7 kW. However, under peak-power or in hot day conditions, the condenser fan power increased drastically to around 37 kW, unless the condenser is four or five times larger than a conventional automobile radiator. The study showed also that the total steam propulsion system could be designed to weigh approximately the same as a conventional automobile propulsion system. The investigation on pollutant emissions showed interesting insights on emissions reductions of steam engines with a low temperature and a low pressure

continuous combustion. For instance, the CO was reduced by a factor of 1000, the unburned hydrocarbons by 10 and NOx by 30 compared to ICE at the time [VM3]. However, and similar to the GM conclusions on this engine, the unresolved related challenges such as the higher fuel consumption, the investment cost and the size of the components, have put an end to the steam vapor engine as main energy converter for conventional vehicle applications.
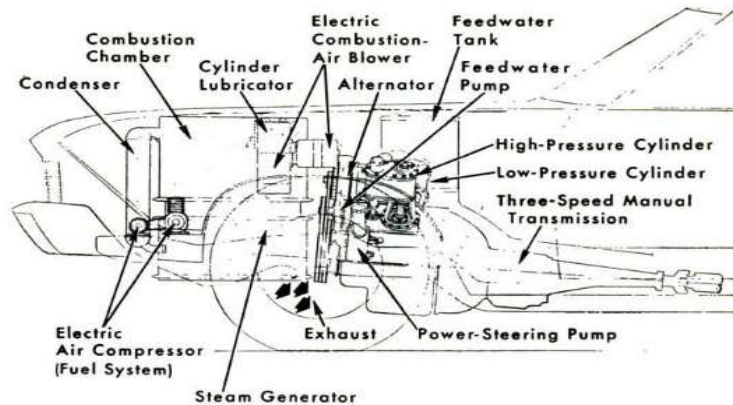
Fig. 1.20: Steam engine mounted on GM Chevelle SE car [VM23]

VCM regained importance recently in engine WHR applications from engine coolant and exhaust gas, due to the rising interest in reducing emissions [VM29-VM31]. Main developments are performed on steam Rankine cycles (SRC) and on Organic Rankine Cycle (ORC), depending on waste heat temperature [VM32-VM41].

The first steam Rankine WHR implemented prototype was on Honda in 2007 [VM42, VM43] followed by BMW in 2009 [VM44, VM45]. Honda showed an increase of the thermal efficiency by 3.8% when driving at constant speed of 100 km/h. On the other side, a fuel consumption gain of 3 to 5% was announced by BMW for vehicle velocity between 70 to 150 km/h. IFPEN announces a 1kW net mechanical power recovered at 130 km/h cruising speed and estimated a net gain of 2-3% [VM16, VM46] with Steam Rankine Cycle (SRC) on gasoline engine. All of these works, confirm the virtue of VCM in quasi-stable operation applications.

Always in the transportation sector, Rankine systems are largely investigated on heavy duty truck, such as Man [VM47], Volvo [VM48], Renault, Daimler trucks [VM49] and Hino [VM50]. Cummins developed in 2008, a complete on-board Rankine system and announced a fuel consumption saving up to 10% [VM51-VM53]. AVL Powertrain Engineering investigated the fuel economy benefit from recovering waste heat from a 10.8L HD truck diesel engine with Rankine system using ethanol as the working fluid [VM54, VM55]. Investigations show a fuel consumption potential saving between 5% to 10%.

1.1.2.3 Synthesis on vapor cycle machines

The Rankine-cycle reciprocating steam engine is one of the oldest heat machines that contributed to the evolution of humankind history. Study of the literature reveals the numerous investigations on the potential of steam engines as main power unit for automotive applications. This external combustion cogeneration machine with multi-fuel capability, and multi

powertrain compatibility, has a very favorable torque-speed curve. This important automotive characteristic can minimize or even eliminate the need for a transmission in the conventional or parallel hybrid electric powertrain. However, the total powertrain mass and size are higher than ICE powertrains for the same performance requirements such as during highway and maximum speed driving. Moreover, other drawbacks prevented its deployment in vehicle applications, summarized in table 1.10 and a synthesis on the performance assessment of vapor cycle machines observed in the literature is presented in table 1.11.

Table 1.10: Advantages and drawbacks of the vapor cycle machine.

Advantages	· Multi-fuel capability
	· Silent operation
	· Design flexibility
	· Reliability of mechanical components
	· Low pollutant emissions by controlling the choice of the fuel
Drawbacks	· Low efficiency compared to ICE
	· Water freezing challenges
	· Size and weight of the steam condenser
	· Water consumption from the condenser
	· Lubrication need filtration
	· Low specific weight and size power compared to conventional ICE
	· Metallurgic limitation

Table 1.11: Summary of performance criteria of vapor cycle machine.

Characteristics	Value and Description
Efficiency range	18 to 30%
Power to weight ratio	100-225W/kg
Power to size ratio	75-175W/L
Fuel	Multi-fuel capability
Combustion process	External combustion
Working fluid	Water, ethanol, organic fluid (R245fa, 1234yf…)
Emissions	Controlled through continuous combustion and EGR system
Complexity/size	High complexity integration – size of the machine
Noise and vibration	Low noise and vibration aspects – Silent operation
Controllability	Complex systems for a conventional powertrains
Maintainability	Technological problematics: air infiltration, corrosion and freezing when water used
Reliability	High reliability machine
Safety	Moderate to good safety level (depending on working fluid used)
Powertrain compatibility	Compatible with all powertrain architectures but more suitable for SHEV
Technical maturity	Good technical maturity (for non-automotive application)

1.1.3 Ericsson Engine

1.1.3.1 Literature review and performance assessment

Ericsson engines are among thermal air engines with monophasic gaseous working fluid and external heat supply, invented just directly after the steam vapor machine [ER1-ER3]. The first prototype date back to 1826, where Ericsson designed a two separated cylinders engine, one for air heating and another for cooling, without a regenerator. In 1833, Ericsson built a 3.7 kW machine with valves and recuperator, operating in a closed loop. The machine achieved a thermal efficiency of 8.7% [ER4]. Another engine has been built in 1851, with rotational speed between 30 and 50 RPM and delivered 2kW to 3kW [ER5-ER7]. In 1853, Ericsson invented an open loop 220kW marine engine, which was widely installed on American boats, and achieved an overall efficiency of 13.3% [ER1, ER8]. Between 1855 and 1860, around 3000 models of 600W Ericsson engine were sold in Europe and in the U.S. The reliability and the suitability of this machine for powertrain ranging from 1kW to dozen of kW were demonstrated. However, after experiencing a major boom in the 19th century, this energy converter has been left out with the invention of the ICE and the electric machines, whose technological impediments were much simpler to solve at that time [ER9].
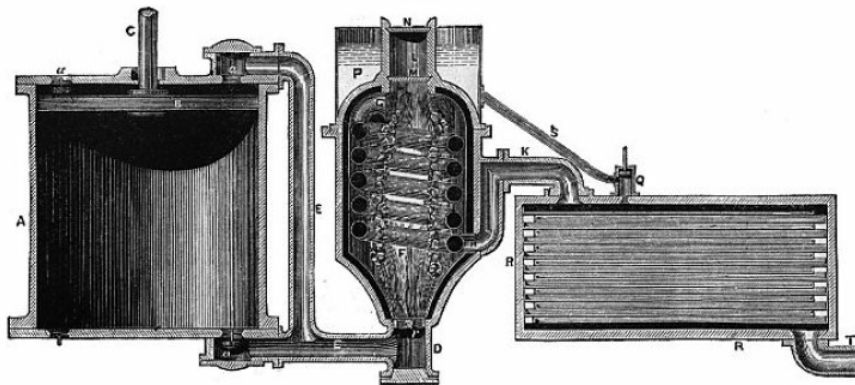
Fig. 1.21: First Ericsson engine [ER2]

Ericsson machine like all thermodynamic machines, operates by receiving heat from a hot source at high temperature and rejects heat to a cold source at lower temperature. Physical parameters such as the maximum temperature, the maximum pressure, the compression and expansion processes [ER9-ER11] as well as the system thermodynamic configurations, impact directly the machine performance in terms of efficiency and net specific work [ER12].

These machines can be found in both open-loop or closed-loop configurations. Ambient air is used as working fluid in open cycle machines, while Helium, Hydrogen, Argon or Nitrogen are the main gases used in closed cycles. In both configurations, a compression piston sucks the working fluid and compresses it to reach high pressure. A heater-regenerator recovers heat from the gas at the outlet of an expansion piston and heat the air upstream the heater. The choice of the engine configuration depends on technological and energy choices. The use of open loop allows using the exhaust gases for heating cogeneration or other processes. Open loop machines, with ambient air as cold sink are also designed to operate at lower pressure [ER13],

limiting therefore the leakage problems [ER14] found in Stirling machines, and reducing the system complexity [ER15].

It is worthy to mention that Ericsson's working fluid flows always in the same direction in a counter-flow recuperator, which leads in lower pressure drop and higher component efficiency compared to the regenerator found on the Stirling machines. In addition, Ericsson engine requires intake and exhaust valves so that compression and expansion volumes are isolated from the regenerator. Therefore, the regenerator presents lower complexity, and is not considered as dead volume that reduces the net specific work and the engine efficiency such in Stirling machines, where it is necessary to find a compromise between the regenerator minimum dead volume and the maximum heat exchanger surface [ER12]. On another hand, the use of valves solicited in each cycle reduce their reliability. These valves yield to additional pressure losses, higher noise level compared to Stirling and higher energy consumption.
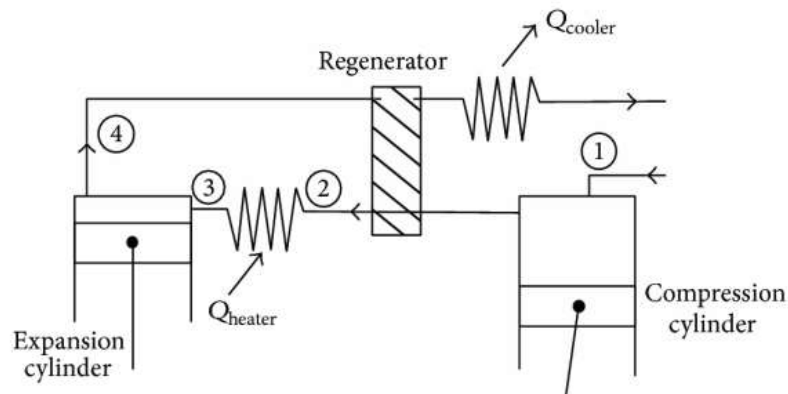
Fig. 1.22: Ericsson hot air engine with open cycle [ER38]

Note also that piston kinematic does not degrade the energy performance of the engine. This allows the use of simple kinematics, more attractive for automotive applications. Other compression and expansion machines and technologies [ER16] such as scroll machines [ER17, ER18 and free piston machines [ER19] were also tested.

Modularity of Ericsson engine is also an advantage. In fact, every component can be studied and optimized separately, and then considered in the operation of the machine [ER9].

1.1.3.2 State-of-the-art of Ericsson engines in automotive powertrain applications

The first spark ignition ICE, de Lenoir [ER20], was an Ericsson inspired engine, but the combustion chamber heat exchangers resistance was among the challenges to let this concept succeed. Today, there are no known industrial applications of Ericsson machines, and very few studies on Ericsson machine as energy converter instead of ICE for automotive application are found in the literature [ER21]. The majority of investigations of this concept, remains as scientific studies [ER22-ER29] with low technological maturity level and targeting mainly solar concentrator [ER30, ER31], biomass and micro-cogeneration systems [ER12, ER32-ER37].

Some scientific studies of Ericsson engine consider internal combustion machine as well as external combustion machines [ER39]. R. W. Moss et al [ER40] studied a multi-fuel internal combustion Ericsson engine, based on alternative piston architecture and delivering 5 kW of mechanical power and up to 8 kW of thermal power. Simulations showed that with 89% recuperator efficiency, a 33% of thermal efficiency can be achieved at 1000 RPM. Wojewoda and Z. Kazimierski [ER41] modeled a closed loop Ericsson engine using air as working fluid operating at a pressure of 90 bars and 3000 RPM, with maximum temperature between 800-1000°C. They show the impact of the engine configuration and the heat exchanger surface on the performance of the machine. M.A Bell et al. [ER42] performed theoretical studies on a V8 vehicle Ericsson engine, called RJC engine where a continuous combustion occurs in a combustor located outside the expansion piston. With 85% of recuperator efficiency and considering real functioning parameters, 50% of indicated efficiency can be achieved at maximum operating temperature of 1300K. Schlatter showed that continuous combustion process in Ericsson engines ensure low emissions of NOx, CO and unburned HC [ER43]. Warren and Bjerkle [ER44] show that an Ericsson machine based on Joule-Brayton cycle achieve 20% reduction in fuel consumption and pollutant emissions compared to conventional ICE with the advantages of multi-fuel capability engine. Femto-ST lab in collaboration with Assystem developed a variable displacement Ericsson engine prototype for micro cogeneration applications [ER45-ER47]. This variable displacement technology allows better efficiency for different engine power demands. Assystem engine produces 3.3 kW of electric power and 13 kW of thermal power.
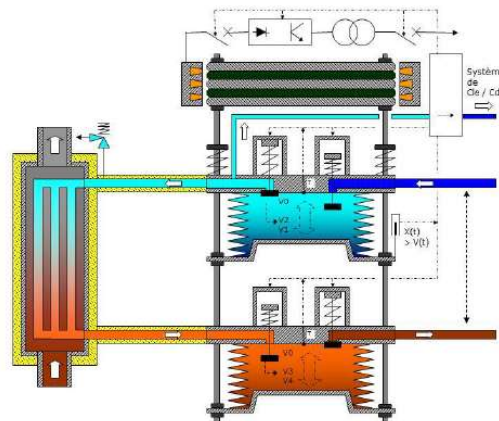
Fig. 1.23: Femto-st/Assystem variable displacement Ericsson machine [ER45]

1.1.3.3 Synthesis on Ericsson engines

Ericsson engine invented long time ago was a successful and reliable machine that was mainly used in marine applications. However, with the invention of internal combustion engines and electric machines, Ericsson engines developments stopped. Recently, numerous scientific investigations on the potential of Ericsson engines for power production are considered, due to the system modularity attractiveness, the reliability, the maximum thermodynamic efficiency, the multi-fuel capability and the system simplicity, mainly for open loop configuration using the ambient air as working fluid and cold sink. Efficient models to design these engines, including thermodynamics, fluid mechanics, heat exchanger, tribology and others scientific

disciplines are proposed. Numerous numerical simulations and experimental investigations show that acceptable efficiency can be reached. Similar to the Stirling machine, the Ericsson engine is compatible with all powertrain architectures including conventional and parallel hybrid. However, series hybrid powertrain remains the best suited configuration, due to the fact of reducing the system complexity, the controllability and the time response challenges. Advancements in metallurgy must be considered also in order to increase the Ericsson machine efficiency and power density.

Table 1.12 summarizes the advantages and drawbacks of Ericsson engines observed in the literature and table 1.13 synthesizes the performance assessment.

Table 1.12: Advantages and drawbacks of the Ericsson engine.

Advantages	· Modularity of the engine · Good efficiency · Low components cost · Capability to operate with different fuel types
Drawbacks	· Requires intake and exhaust valves which add more complexity · Metallurgic limitation · Response time – thermal inertia of the hot source · Low technological maturity · High power density requires high compression ratio and isothermal compression and expansion which are technically difficult to achieve

Table 1.13: Summary of Ericsson engine performance criteria.

Characteristics	Value and Description
Efficiency range	25-35% (realistic) / 45% (simulations)
Power to weight ratio	150 – 250 W/kg (*)
Power to size ratio	150 – 300 W/L (*)
Fuel	Multi-fuel capability
Combustion process	External combustion
Working fluid	Air (open loop) and monophasic gas (H2, He, Argon,…) (closed loop)
Emissions	Controlled at source through continuous combustion
Complexity/size	Moderate complexity integration
Noise and vibration	Low to Medium vibration and noise level
Controllability	Complex for a conventional powertrains control
Maintainability	Good maintainability
Reliability	Good reliability aspect
Safety	Good safety with air as working fluid
Powertrain compatibility	Compatible with all powertrain architectures. More suitable for SHEV
Technical maturity	Research level for cogeneration - No commercialized machines

*Based on ICE and split cycle weight and size power densities, and considering a maximum temperature of 1100°C.

1.1.4 Thermoacoustic Machine

1.1.4.1 Literature review and performance assessment

Thermoacoustic machines are among external combustion thermodynamic reversible machines that exchange energy as form of heat or power with external sources. These systems use monophasic gases as working medium and have no internal moving parts, which makes them a serious alternative technology to produce mechanical/electrical or cooling power reliable in a sustainable and environmentally friendly way.

The thermoacoustic effect was identified by glass blowers [TA1] long time ago, using a long cold tube producing monotone sound when heated on the far end. Scientific works begin with Higgins [TA2] and Rijke [TA3, TA4] and the theoretical explanation of the physical phenomenon came over a century later from Lord Rayleigh [TA5, TA6]. He concluded that a sound wave in a gas consists of coupled pressure, motion oscillations and temperature oscillations [TA7] and when the sound travels in small channels, oscillating heat also flows to and from the channel walls. The combination of all such oscillations produces a thermoacoustic wave characterized by its frequency, its amplitude and its wave length [TA7, TA8]. The acoustic power produced, depends on the pressure, the speed and the section of the tube where the wave propagates. Note that these interactions are too small to be obvious in the air with which we communicate every day. However, in pressurized gases, it can be harnessed to produce powerful engines, pulsating combustion [TA9], heat pumps, refrigerators [TA10, TA11], and mixture separators [TA12, TA13].

The combination of thermal heat and acoustic, gives the name of "thermoacoustics" by Rott [TA14-TA16] who developed the mathematical description of acoustic wave oscillations of a gas in a channel [TA17]. The wave propagation can be a stationary in which we have a wave reflexion, a progressive wave resonator in which we have a continuity without reflexion, or a hybrid acoustic wave resonator such the one developed by Swift – Backhaus [TA18].

It is noteworthy to mention that from a thermodynamic point of view, the thermoacoustic effect described by waves is in fact a variant of the Stirling reversible thermodynamic cycle [TA19, TA20], used for power generation and cold production [TA8, TA21]. While sound waves are simple and reliable, current thermoacoustic researchers are motivated in upgrading this technology for the energy industry. Many thermoacoustic versions of such engines were demonstrated by Yazaki [TA22], de Blok [TA23], Backhaus [TA24] and others.

A thermoacoustic machine is composed of a resonator, and an acoustic conversion device. The resonator consists of a tube, a hot heat exchanger, a cold heat exchanger and a stack or a regenerator. The acoustic conversion device transforms the acoustic power to mechanical or electrical power. The efficiency and performance of the thermoacoustic machine depend mainly on the performance of the resonator, the architecture of the resonator, the system architecture as well as the efficiency of the acousto-electric device.

As for the resonator, the efficiency depends on three main parameters: the working fluid on which will depend the acoustic pressure [TA25], the stack or regenerator which constitutes the center of the thermoacoustic phenomenon [TA26] [TA27] and the heat exchangers [TA27-TA31].
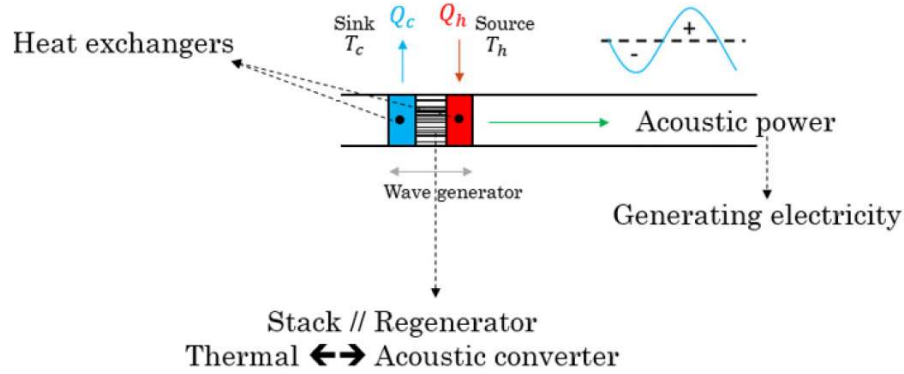
Fig. 1.24: Scheme of the wave generator in ta thermoacoustic resonator [TA31]

Regarding the resonator architecture, many were proposed in the literature with different power density and efficiency [TA32]. We can list: Backhus and Keolian [TA33] Trillium machine [TA34], K. De Blok [TA23] thermoacoustic loop with four thermoacoustic cells, Jensen et al. [TA35] with a piezoelectric transducer.

Acousto mechanic or acousto electric devices are also key factors to consider in the conversion process. Linear alternators, loud speakers [TA36, TA37], bidirectional turbine [TA38] and piezoelectric devices [TA39, TA40] have been developed. The electroacoustic loud speakers are particular devices that tolerate dynamic acoustic pressure of several bars. These systems are performant with more than 80% of acoustoelectric conversion efficiency. However, the price (around 20.000$ for 1kWe), the low power density (near 35W/kg) and the limited power make this technology difficult to integrate in an automotive application. Bidirectional turbines [TA41], proposed in application such as SpaceTRIPS [TA38], can offer many advantages such as a good turbine power density (8kW/kg) and alternator power density (4kWe/kg), a cost effective and scalable device where the turbine can be made from plastic material, presenting a high efficiency of 85% when Argon at 40 bars is used as working fluid.

(a) Linear Alternator   *(b) Loud speaker*   *(c) Bidirectional turbine*

Fig. 1.25: Acousto-mechanical and acousto-electrical devices

Finally, one of the main challenges regarding the operation of thermoacoustic machines, is the streaming phenomenon that appears in the thermoacoustic line, caused by advective heat transport from the hot to the cold side of the stack, induced by acoustic oscillations [TA42]. This issue causes efficiency losses in the machine [TA43, TA44]. Methods and technics to suppress the streaming phenomenon are proposed and investigated in several studies on the literature [TA45-TA50].

1.1.4.2 State-of-the-art of thermoacoustic machines in automotive powertrain applications

Thermoacoustic systems have been largely used for cryogenic applications [TA51]. Today this reversible thermodynamic machine is under investigation in many other domain: cold generation [TA52-TA54], heat pumps [TA55, TA56], electric power generation [TA57-TA61] and waste heat recovery [TA62, TA63].

Backhaus et al. [TA64] designed a 30 bars helium thermoacoustic machine of 710W of acoustic power, which achieved 30% of cycle efficiency when operating with a temperature difference of 725°C. Based on Backhaus model, Mumith et al. [TA65] performed simulation study on a 30 bars thermoacoustic device with hot source at 150°C and cold source at 6°C where a maximum acoustic power of 1029W was calculated with an overall efficiency of 5.4%. Backhaus [TA66] proposed another thermoacoustic generator with 18% efficiency, working with Helium at 55 bars static pressure and delivering 58W electricity with heat input of 400W and maximum hot temperature of 600°C.
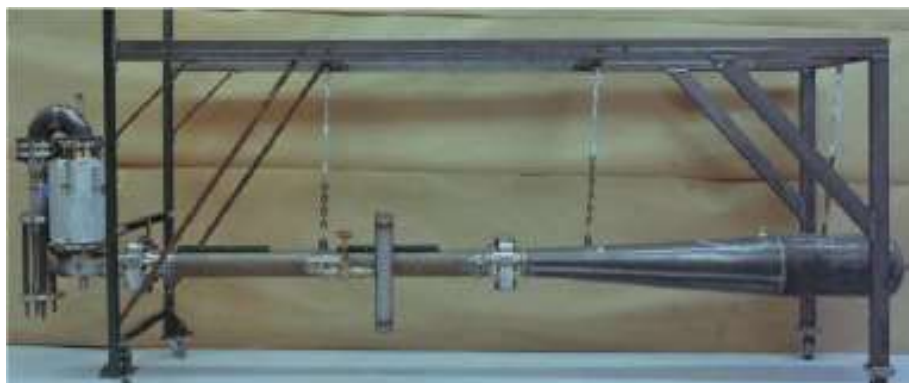
Fig. 1.26: Backhaus et al. thermoacoustic engine [TA64]

Tijani & al. tested a thermoacoustic engine using helium at 40 bars as working fluid. 300W of acoustic power were measured with a thermal to acoustic efficiency conversion of 27% [TA67]. Hekyom company patented a three amplifications cells thermoacoustic engine and is working to advance their technology. Hekyom's Valta project [TA53], aimed to design and build a thermoacoustic engine recovering waste heat from an electric generator set and converting 70kW thermal power to 15 kW electric power. Hekyom developed other prototype with Airbus that delivers 1kWe and works on other projects, such as ESA Project, a 5kWe thermoacoustic machine recovering solar energy [TA68].

(a) 3D scheme of Hekyom's prototype   (b) Hekyom's prototype
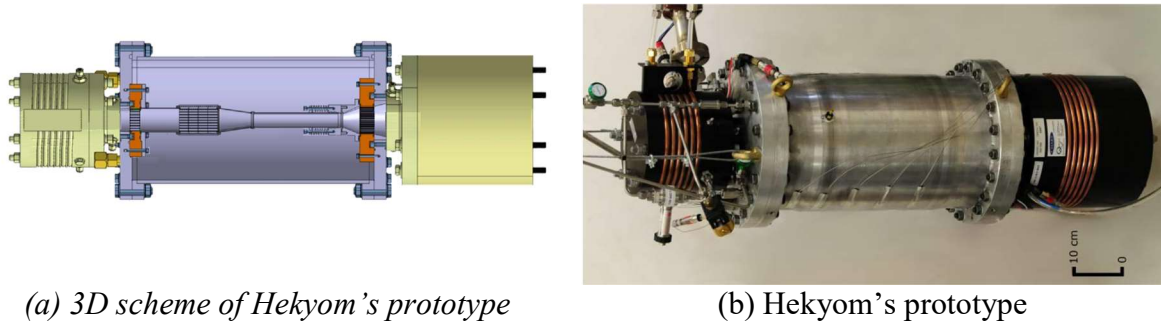
Fig. 1.27: Thermoacoustic prototype [TA53]

Wu et al [TA69] investigated the potential of a double acting thermoacoustic electric generator having the advantages of high power density and efficiency by employing three thermoacoustic engine cells with three alternators in a special configuration, eliminating therefore the resonance and the feedback tubes. Tests done showed maximum electric power of 1.57 kW with 16% thermal to electric conversion efficiency. NASA worked on the Thermoacoustic Stirling Heat Engine (TASHE) project [TA70]. The system operated at 30Hz, 945K at hot HEX and 287K at cold HEX. It achieved an acoustic efficiency of 36.4% equivalent to 52% of Carnot efficiency. Based on TASHE prototype, Nirvana Energy Systems [TA71] is developing a commercialized micro-combined heat and power system for home applications that converts gas up to 4 kW of electrical power and provides 15 to 30 kW of thermal power. The system size is about 42L and the weight is about 30kg.

Since, the sound energy is a simple and reliable energy, thermoacoustic engine are of interest in automotive applications [TA31, TA72] mainly for engine WHR. Gardner & al. [TA73] modeled a trithermal thermoacoustic system that produces both electricity and cold from vehicle exhaust gas as hot source, and using water at ambient air temperature as cold source. Helium was the working fluid, used at 16 bars. The simulation data correspond to a Mitsubishi Magna V6 engine. For 6kW of thermal power recovered from the exhaust line at 700°C, 500W of acoustic power is produced achieving then an overall acoustic efficiency of 8.3%. Backhaus & Keolian tested and patented in 2011 a thermoacoustic machine for trucks and automotive exhaust gas WHR [TA74]. The system uses helium as working fluid at high pressure of 80 bars. The truck's system is composed of 2 recovery stages and 2 thermoacoustic cells and delivers 4kW of electric power using loudspeaker as acousto-electric converter. The light vehicle WHR system uses three acoustic cells and can deliver up to 1kWe with a conversion efficiency of 20%. The thermoacoustic machine has a volume of 30 liter and a mass of 17kg. The total system has then a power to volume ratio and power to mass ratio of 33 W/liter and 65 W/kg respectively. Fritzsche et al. [TA75] proposed an acoustic device system with acoustic diode for automotive and heavy duty applications based on a micro-CHP application. The simulated vehicle is Golf VII 90 kW. The electric power output of the machine was simulated using Dymola. Results show fuel consumption savings of 3 to 5 g CO2/km over WLTP. Karlsson et al. [TA76] studied the applicability of thermoacoustic engines for automotive WHR applications. A thermoacoustic engine based on non-linear model is coupled to ICE and simulated on drive cycle on a typical commercial vehicle. The net gain over a drive cycle is 237W corresponding to a thermal efficiency of 7%.

(a) System for heavy-duty trucks   *(b) System for light vehicles*
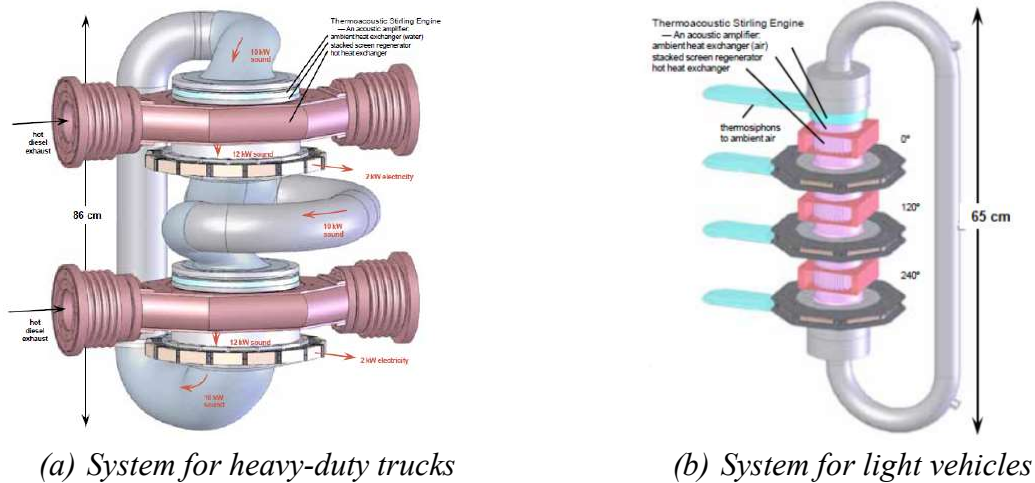
Fig. 1.28: Backhaus & Keolian WHR system [TA74]

Etalim company is working on thermoacoustic for both WHR on truck engines and CHP applications [TA77, TA78]. The WHR system efficiency of 15 to 25% has a price target of 350$/kW compared to 500$/kW for ORC systems and can deliver up to 5kW of electricity. Etalim system with high reliability, no exotic materials or refrigerants, low complexity and simple cooling is considered as competitive technology for WHR. For CHP, the target is to achieve 35% of thermal to electrical efficiency. Fueled with natural gas, but other fuels can be used, the thermoacoustic machine target of 1-2 kWe is to ensure reliability, lifetime, maintenance and startup time better than Stirling and fuel cell systems.
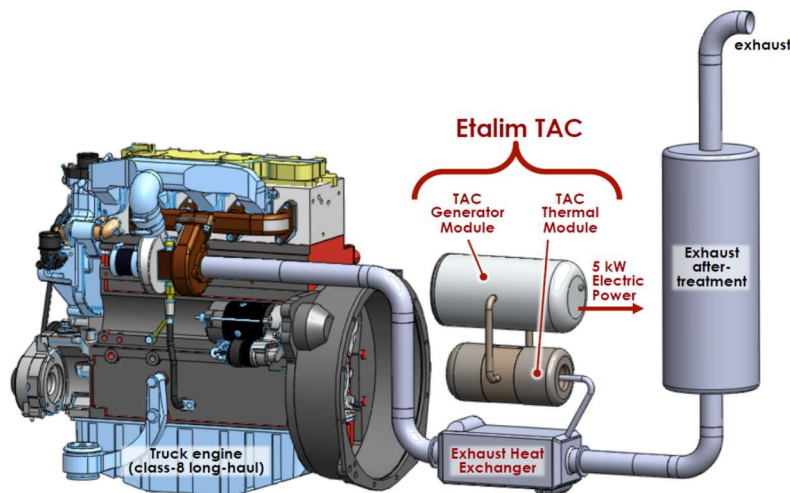
Fig. 1.29: Etalim thermoacoustic WHR system [TA77]

1.1.4.3 Synthesis on thermoacoustic machine

Thermoacoustic machines have been used for many years mainly in cryogenic applications. These simple and reliable devices do not have moving parts and are capable of using multi-fuel and with acceptable achievable efficiency; therefore, they are considered today as disruptive technology in automotive applications, mainly for WHR on conventional powertrain and for

heat pumps applications on electric vehicles. Numerous investigations on the potential of thermoacoustic machines for power and cold production are presented in the literature. These machines with electric output power are only compatible with series hybrid electric powertrain architecture. However, these machines require expertizes in many engineering domain including acoustics, fluid mechanics, heat exchangers, electric conversion among others. Careful selection of the machine thermodynamic configuration must be made in order to optimize the efficiency and the power density. Adding to that, deep understanding for phenomenon such as streaming is also necessary in order to control their operation.

Table 1.14 summarizes the advantages and drawback of thermoacoustic machines observed in the literature and table 1.15 synthesizes the performance assessment.

Table 1.14: Advantages and drawbacks of the thermoacoustic machine for automotive applications.

Advantages	· Good efficiency
	· No-nocif working fluid - No supper alloys material (low material cost)
	· Reduced number of mobile parts – high reliability – Low maintenance
	· Flexible geometry
	· No lubrication required and no components' wear
	· Tri-generation option: electricity, hot and cold
	· Multi-fuel capability
Drawbacks	· Acoustic streaming phenomenon – internal losses
	· Thermoacoustic phenomenon not well mastered for power generation
	· Mass, size and cost of linear alternator (between 3 and 8 liters for 2kWe)
	· Low power to weight ratio and power to size ratio
	· Sealing problematics with high pressure fugitive working fluid

Table 1.15: Summary of thermoacoustic machine performance criteria.

Characteristics	Value and Description
Efficiency range	7% (WHR) and up to 35% (CHP)
Power to weight ratio	65 W/kg (Backhaus & Keol WHR) - 130W/kg
Power to size ratio	33 W/L (Backhaus & Keol WHR) - 100W/L
Fuel	Multi-fuel capability
Combustion process	External combustion
Working fluid	Hydrogen, Helium, Argon, Nitrogen, Air
Emissions	Controlled at source through continuous combustion
Complexity/size	High integration complexity – Bulky system
Noise and vibration	Low noise and vibration aspects
Controllability	Good controllability for stationary power systems
Maintainability	High maintainability machine
Reliability	High reliability machine
Safety	Good safety level
Powertrain compatibility	Compatible only with serial or range extender powertrains
Technical maturity	Low maturity for automotive applications - R&D for cold production

1.1.5 Thermoelectric generators

1.1.5.1 Literature review and performance assessment

Thermoelectric generator is a thermodynamic system that transforms thermal energy directly to electricity and inversely [TE1, TE2]. It consists of semi-conductors with positive charge (p) and negative charge (n) linked together in parallel disposition thermally, and in serial one electrically, in order to ensure a current flow in one direction, as illustrated in figure 1.30.
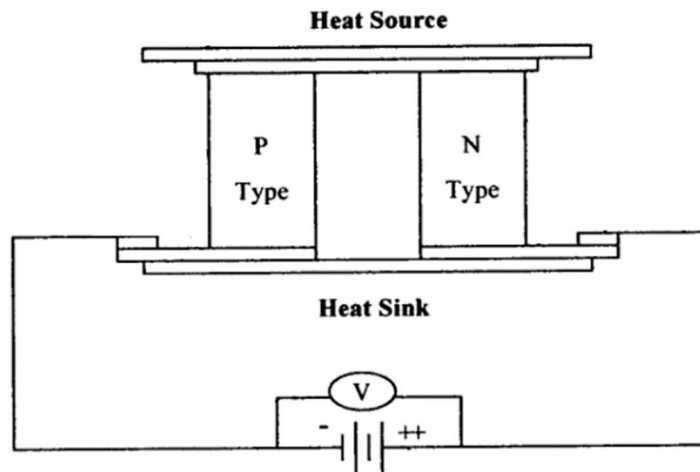
Fig. 1.30: Thermoelectric generator

In 1821, Thomas Johann Seebeck found that a temperature difference between two different metals welded together generates an electric current, and the produced voltage is proportional to the temperature difference between the two junctions [TE3]. In 1834, Peltier proved the reverse phenomenon: an electrical current would flow in a circuit made from two dissimilar metals, with the junctions at different temperatures [TE4]. In 1851, Thomson established the relation between Seebeck and Peltier effects and showed that the thermoelectric phenomenon can occur even in a single homogeneous conductor without the need of a junction [TE5, TE6].

The thermoelectric generator (TEG) operates according to the Seebeck effect, where temperature is imposed and constraint the electric load carriers to move from the hot toward cold zones, generating therefore an electric current [TE7, TE8]. TEG were mostly gas-fired and were used in different countries to run radios, or to charge lead-acid accumulators. They have also been used in industrial applications for a long time, such as aerospace [TE2], cooling systems [TE9-TE11], thermo generation of electricity (TGE) [TE12], temperature measurement [TE13] as well as for mobile phone charging or watches [TE14], and even proposed as WHR on car seats [TE15].

This technology regained interest since the 1990th, mainly to solve environmental and energetic challenges. TEG efficiency depends on Seebeck coefficient, on electric conductivity of thermoelectric materials, on temperature difference as well as on the electric resistance under the closed circuit current flow, which can be expressed in terms of a unidimensional number,

the merit factor ZT, characterizing the thermoelectric materiel. The higher the ZT is, the higher the TEG efficiency will be [TE16].

Today, the main strategic research axes in this field are related to the identification of new materials with good merit factor and to the introduction of small compact systems.

Regarding thermoelectric material, many studies are carried out to assess the impact of physical parameters such as the electric conductivity, the thermoelectric capacity, the thermal conductivity among others, on the merit factor ZT [TE17-TE22].

Scientific and empirical studies [TE23-TE26] showed that a performant thermoelectric material must have a good electric conductivity, a high thermoelectric capacity, and the lowest thermal conductivity [TE27-TE30]. Note that thermoelectric materials operate efficiently in a specific range of temperature [TE17]. For instance, at low temperature, (150-200K), the performant semiconductors are alloys based on Bismuth (Bi) and Antimony (Sb) with a ZT around 0.4 [TE31]. At ambient temperatures, the best materials currently used are alloys of type n, such tellure of bismuth (Bi2Se3) [TE32, TE33]. PbTe alloys are better candidates for temperature ranging between 450 to 800K. However, their stability stays limit due to the volatility of the Pb in a pollutant environment. Therefore, the Mg2Si and the β-FeSi2 where developed and present more advantages in term of temperature stability, price and toxicity [TE34]. For higher temperature, around 1300K, SiGe and high magnesium Silicium (HMS) materials are more used [TE35-TE39]. However, the cost of germanium (Ge) is high for application other than space.

These thermoelectric conventional materials, despite the fact that are used for large temperature range, still present low merit factor (ZT). Therefore, even if this balance between advantages and drawbacks is acceptable for some applications, it is still strongly limited to compete with traditional power and refrigeration systems. Researches on the development of new materials, such as nano-materials [TE40-TE45], are essential for the development of large scale and economically profitable applications such as for automotive powertrains. Many materials with high ZT value can be found in the literature [TE46-TE51]. Some commercial devices have ZT around 0.8 and operate with efficiency between 5 and 6% [TE52-TE54]. According to [TE26], this efficiency can reach 30% if the ZT can be increased up to 4.

It is noteworthy to mention that a good thermoelectric material for industrialization must have a good mechanical behavior, a good thermal stability with no degradation during operation, as well as a mastered production process, which also impacts the cost of the TEG devices.

Among production processes we can list: the Czochralski's method [TE55-TE58], the local fusion process with affordable price equipment for production [TE59, TE60], the compression and extrusion processes with good mechanical properties and reduced cost [TE55], the crystallization in a cavity [TE61], the mechano-chemical synthesis [TE62-TE70], the solvo-thermal and wet reaction methods [TE71-TE73], the wheel quenching method [TE74-TE76],

the spark electro-erosion method [TE77] and the hot compression and Spark Plasma Sintering processes [TE66].
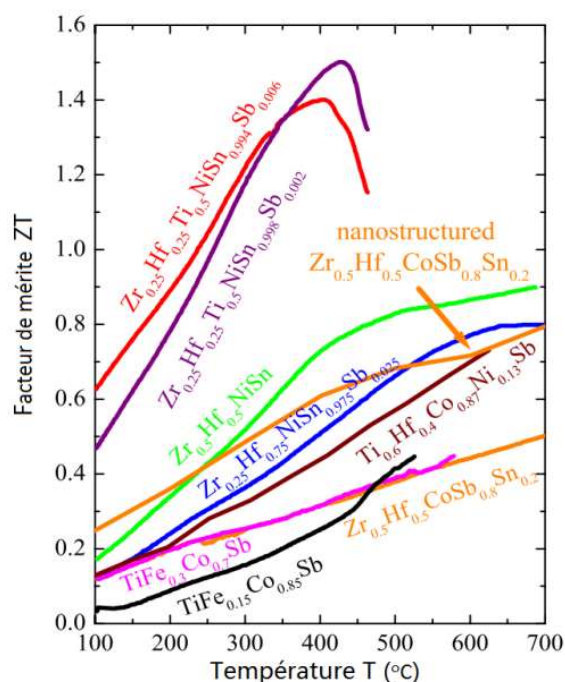
Fig. 1.31: State of art of TEG materials [TE78]

1.1.5.2 State-of-the-art of thermoelectric generators in automotive powertrain applications

The review of the literature shows no specific attempt to use TEG as main energy converter instead of an ICE in automotive applications. However, thermoelectric generators, with silent and free vibration operation, are potentially attractive for WHR on ICE [TE79, TE80] to convert exhaust heat energy directly into electrical energy, thereby reducing fuel consumption. Many numerical modeling [TE81-TE83], parametric evaluation and topological studies [TE84-TE85] based on vehicle TEG prototypes were performed.

The first attempt to apply a thermoelectric generator in cars was developed in the University of Karlsruhe in Germany in 1988 [TE86]. A thermoelectric generator using Bi2Te3 for truck diesel engines was built and tested by Hi-Z Technology Incorporation in the United States in the 1990s, and a 1 kW generator was tested in 1995 [TE87, TE88].

General Motors was committed to develop new thermoelectric materials with high merit factor values under the next generation vehicle program (PNGV) [TE89, TE90]. BMW tested many thermoelectric generators prototypes. In 2003, an experimental prototype produced 80W and the first vehicle prototype was in 2009 producing around 200W, with ZT = 0.4 and 2% efficiency [TE91]. In 2011, BMW tested a WHR TEG capable of producing 750 W of electric power on the 5 series vehicle. During the same year, another prototype on X6 vehicle produced more than 600W of electricity [TE92] and achieved a fuel saving of 5% during motorway use.

Fiat investigates the TEGs on Iveco light duty vehicles [TE93] using 270°C maximum working temperature material. Results show 4% of fuel economy improvement over the WLTP. Honda investigated the TEG technology on F1 vehicle [TE94] and particular vehicles [TE95]. Tests were performed with low and high material and with insulating the exhaust line. A 450W of electric power were produced on an operating point of 14kW, leading to 3% of fuel economy. French government funded partially the Renoter project in 2011 [TE96], which brings together eight partners and three laboratories. The TEG power target for passenger car was 100W on NEDC cycle, 300W at constant speed of 100 km/h and 500W at constant speed of 120 km/h [TE97]. Testing shows that 50We to 100We were recovered with Diesel engine on NEDC and between 80We to 160We on customer cycle. Other investigated the direct coupling of thermoelectric material on exhaust system of gasoline engine such as at the Chair of Combustion Engine Faculty at the Dresden Technical University [TE98].

Fig. 1.32: BMW series 5 with TEG as waste heat recovery system [TE101]

All studies show that improving the ZT of thermoelectric material is a key of success for such devices for automotive applications. Development activities may shift focus towards component integration, such as TEGs and catalytic converters. This is due to the fact that temperature increase yields a TEG power output increase [TE99].

1.1.5.3 Synthesis on thermoelectric generators

Thermoelectric generators can play an important role in reducing energy consumption and protecting the environment. These devices present a particular potential in industrial applications. Despite research that began some time ago, thermoelectric materials still need to be improved and the dimensions of the devices must be reduced for automotive applications.

The TEG system is simple, silent, with cogeneration capability, without moving parts and can be used with different fuel types providing directly a direct current electricity compatible with batteries of series or range extended hybrid electric powertrains.

However, weight and size power densities as well as the efficiency, limited by the merit factor of TEG materials, are still very small compared to the ICE. Moreover, studies on manufacturing cost [TE100] show that TEG are still not cost-beneficial for automotive applications due to high

material costs, such as the Germanium, the Silver, among others. Other challenges are the toxicity of material such as the Lead. Increasing the efficiency can be promising for automotive WHR applications first, due to system integration simplicity.

Table 1.16 summarizes the advantages and drawback of thermoelectric generators observed in the literature and table 1.17 synthesizes the performance assessment.

Table 1.16: Advantages and drawbacks of the thermoelectric generator.

Advantages	• Silent operation • No moving components • Low complexity and integration • DC power generation • No environmental side effects and no toxic gas or materials • Multi-fuel capability
Drawbacks	• Low efficiency due to low merit factor coefficient • Low weight and size power density • System durability and TEG material resistance to temperature • Require specific materials • Price of thermoelectric materials • Processing of electrical signal

Table 1.17: Summary of thermoelectric generator performance criteria.

Characteristics	Value and Description
Efficiency range	3-8% for WHR applications [TE101, TE102] Between 15 and 25% TEG machines [TE15]
Power to weight ratio	20-80W/kg [TE85, TE98, TE103-TE105]
Power to weight ratio	65-140 W/L [TE102, TE104, TE106]
Fuel	Multi-fuel capability
Combustion process	External combustion
Working fluid	No working fluid required. Thermoelectric specific materials are required
Emissions	Controlled at source through continuous combustion
Complexity/size	Low complexity integration – however, bulky system for high net power because of low size to power ratio
Noise and vibration	Low noise and vibration aspects
Controllability	Good controllability for stationary power systems
Maintainability	High maintainability machine
Reliability	Medium reliability machine – depends on TEG material life
Safety	Good safety level
Powertrain compatibility	Compatible only with serial or range extender powertrains
Technical maturity	Emerging technology - no commercial applications for automotive Mature for other applications (aerospace, military, cooling…)

1.6 Electrochemical energy converters

1.6.1 Fuel Cells

1.6.1.1 Literature review and performance assessment

The process of using electricity to decompose water into hydrogen and oxygen, was described in 1800 by the scientists William Nicholson and Anthony Carlisle. In 1839, the first fuel cell (FC) was demonstrated by Sir William R. Grove [FC1, FC2] who found that it may be possible to generate electricity by reversing the electrolysis of water. In 1889, two researchers, Charles LANGER and Ludwig MOND, invented the term "fuel cell" when they were trying to engineer the first practical fuel cell using air and coal gas [FC3]. In the early 1900s, further attempts were made to develop this technology, but the advent of ICE temporarily quashed any hopes of further development.

In 1953, Francis Bacon introduced the first Fuel Cell prototype with a hydrogen–oxygen cell using alkaline electrolytes and nickel electrodes, and in 1959, he demonstrated a practical 5-kW fuel cell system when Harry Karl IHRIG presented in the same year, his now-famous 20-hp fuel-cell-powered tractor [FC4].

General electric (GE) invented the proton exchange membrane fuel cell in the 1950's and during the 1960's, NASA introduce a 1 kWe FC developed with GE for space applications at time where many manufacturers, including major automakers, and various federal agencies have supported ongoing research into the development of this technology for use in vehicles and other applications. Automotive constructers are attracted by the FC environmental benefits [FC5], the longer driving range compared to electric vehicle (EV), the high efficiency compared to ICE vehicles [FC6], the quiet operation [FC7], the few moving parts and the possibility to use it as cogeneration machine for vehicle passenger cabin thermal heating.

These thermochemical devices used to produce mainly electric power can be classed in six major types depending on the electrolyte type: solid or liquid. The Proton Exchange Membrane Fuel Cells (PEMFCs), the Direct Methanol Fuel Cells (DMFCs) and the Solid Oxide Fuel Cells (SOFCs) use solid electrolyte, while the Alkaline Fuel Cells (AFCs), the Phosphoric Acid Fuel Cells (PAFCs) and the Molten Carbonate Fuel Cells (MCFCs) have liquid electrolyte.

The PEMFC is an attractive energy converter for automotive application because of its high efficiency, low-operating temperature between 60 and 100°C, high power density (0.35-0.6 W/cm²), compatibility with renewable energy and modular design [FC8]. In this FC, the chemical energy of the fuel, the hydrogen, is converted directly into electrical energy by means of electrochemical processes. The fuel and the oxidizing agent, oxygen of the ambient air, are continuously supplied in the two electrodes of the cell, where they undergo a reaction emitting waste heat and exhaust gases [FC6]. The heart of this FC, called fuel cell stack, consists of two plates between which a membrane layer and catalyst are compressed. One plate serves as the anode and the other plate as the cathode. The reactant fuels make uniformly contact with the catalyst, through these plates through channels etched in the material. The electro-chemical reaction produces a thermodynamic voltage associated with the energy released given by the

change in Gibbs free energy, and the number of electrons transferred in the reaction. PEMFCs have the ability to start up quickly and to vary rapidly the output electrical power to meet the power demand required by the powertrain. Also, its solid membrane electrolyte is stable and does not move or evaporate as occurring with liquid electrolytes. However, PEMFCs presents some drawbacks such as the cathode reliability and durability, the water management problematic, the humidification of the FC's membrane and the poisoning caused by the Platinum catalyst affinity to carbon monoxide (CO) and sulfur products, which reduce fuel cell performances and lifetime. Adding to that, the cost of membrane and noble metal used as well as the need of hydrogen infrastructure [FC9].
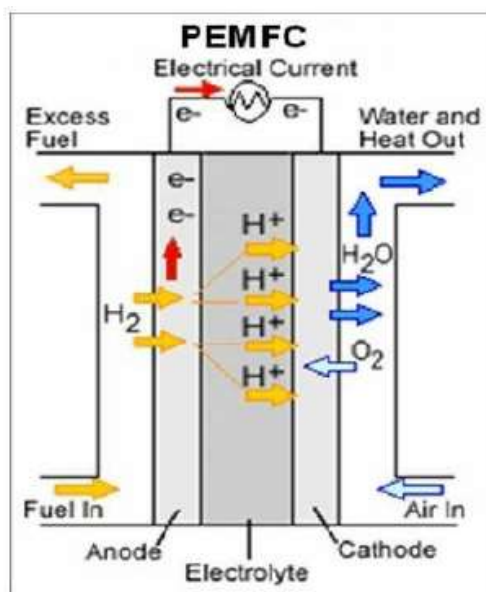
Fig. 1.33: Basic operation of a Fuel Cell [FC10]

The DMFCs with operating temperature around 100°C use methanol, the simplest organic fuel that can be economically and efficiently produced on a large scale from fossil fuel and other processes. This liquid fuel, have the advantage for automotive applications to be easily stored, distributed and marketed. However, compared with PEMFCs, DMFCs have low power density, slow power response time, and low efficiency [FC11, FC12].

SOFCs are mainly suitable for stationary applications. These FCs, with operating high temperature between 1000-1200°C, have exhaust gas outlet between 500-850°C which are attractive for cogeneration applications or coupled to bottoming cycles. However, challenges such as low power density, high operating temperature, fast start up and thermal cycling, inability to respond quickly to a change in power demand and extremely brittle ceramic electrolyte and electrodes are problematic for vehicular applications [FC13, FC14].

In the AFCs, unlike the acidic fuel cells, water is formed on the hydrogen electrode capable of operating over a wide range of temperatures (from 80°C to 230°C) and pressures (from 2.2 to 45 atm). AFCs are capable of achieving very high efficiencies because of the fast kinetics allowed by the hydroxide electrolyte. This fast kinetics allows using silver or nickel as catalysts instead of platinum, reducing therefore the cost of the FC stack. However, durability due to

corrosive electrolyte, water management produced on the fuel electrode and the poisoning by carbon dioxide remain problematic [FC15, FC16].

The PAFCs with operating temperature between 60-200°C is the first fuel cell technology to be marketed in hospitals, hotels and military bases where it acts as cogeneration machine, producing electricity and heat. It relies on cheap acidic electrolyte to conduct hydrogen ions. However, its temperature must be kept above 42°C freezing point to avoid stack's stress. This requires additional components which makes it complex for vehicle applications. On the other hand, the high operating temperature (above 150°C) requires energy consumption associated with warming up the stack, every time the fuel cell is started, and wasted heat, every time the fuel cell is turned off [FC17].

Finally, the MCFCs, reaching efficiency of 55%, have operating temperature between 500 and 800°C. These FCs use an electrolyte composed of a molten-carbonate salt mixture suspended in a ceramic matrix solid electrolyte, capable of using gases derived from coal or carbon oxides fuel. They have also the possibility of internal reforming by converting other fuels to hydrogen directly. They are also more resistant to impurties than other FC types and are not prone to poisoning by CO2 and CO. the high operating temperature allows them to be used in cogeneration applications. However, challenges such as slow start-up time, complex system for CO2 recycling, durability due to corrosive nature of the electrolyte and high temperature are the main issue limiting the commercialization of such devices [FC18].

Table 1.18: Fuel Cell type [FC19, FC20]

Fuel Cell type	Electrolyte	Operating Temperature	Electrical Efficiency	Fuel
PEMFEC	Solid: Proton Exchange membrane	Room temperature to 100°C	45-60%	H2
DMFC	Solid: Proton Exchange Membrane	Room temperature to 120°C	20-30%	CH3OH
SOFC	Solid: Oxide ion conducting ceramic	800-1200°C	50-65%	Natural gas, Bio gas, coal gas, H2
AFC	Liquid: Potassium Hydroxid (KOH) solution	Room temperature to 100°C	55-65%	H2 / O2, air
PAFC	Liquid: Phosphoric Acid	60-220°C	40-50%	Natural gas, Bio gas, H2
MCFC	Liquid: Molten mixture of alkali metal carbonates	500-800°C	45-55%	Natural gas, Bio gas, coal gas, H2

The PEMFC is considered for the rest of this study. To operate normally and continuously, the complete Fuel Cell System (FCS) require a blower to blow the air into the stack, a water circulating pump to remove the heat produced by the exothermic reaction of hydrogen and oxygen, and a fan to evacuate heat outside the system [FC9]. Adding to that a humidification system is required because the humidification of inlet streams is necessary to prevent dehydration of the membranes in the FC stack. Other components such as hydrogen storage system, valves, and regulators are also required. A management control system ensure that all these components work together to deliver and to regulate the electric power load and to ensure thermal management, water management and system safety.

FCS performance depends on the following parameters: temperature, reactant gas stoichiometric flow rates, anode and cathode pressures and humidification [FC7, FC21]. The air pressure is one of the important parameters that affect the efficiency and the power density of the PEMFC. Increasing the oxidizer pressure increase the performance of the stack, however it consumes more power for the blower. Therefore, there is an optimal operating point for an efficient system operation which depends on required specifications [FC22, FC23].
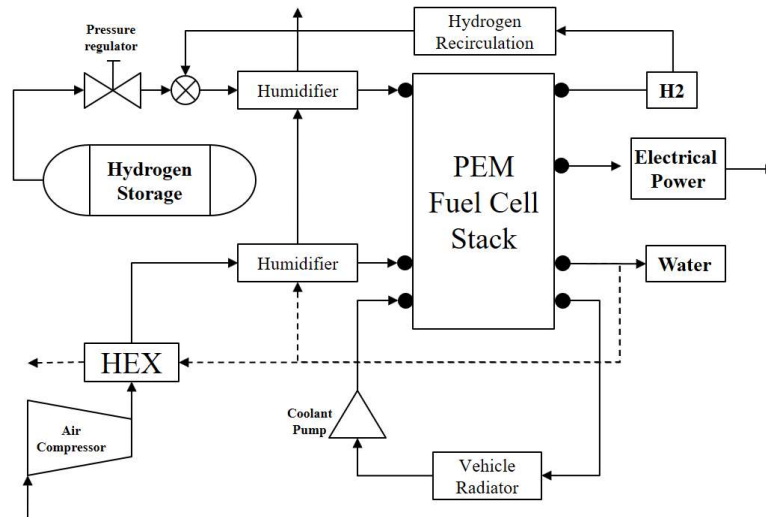
Fig.1.34: PEM Fuel Cell System

Another important point to mention is the fuel supply to the on-board PEM fuel cells, which is a major challenge for FC vehicle applications. Hydrogen gas is awkward to be stored, with a wide range of flammability ranging from 4% to 75% of H2 in the air, fugitive characteristics, a high diffusion coefficient in the air and a very low density, requiring bulky tank.

Today, three different types of hydrogen storage systems are developed. The first one is the cryogenic storage, where hydrogen is maintained in the liquid state with low pressure storage, high density (71 kg/m3) and small size storage tank. This system investigated by BMW [FC24] is complex for automotive because of difficulty to maintain the liquid form. Another way to store this fuel is through a chemical process. Hydrogen can be stored by being absorbed using metallic hydrides material, or on a big surface of carbon nanotubes. The advantage is the simplicity and security; however, the inconvenient is mainly the low weight density. Finally, the third system is compressed gas storage systems, where hydrogen can be stored at 200 bars industrial bottles, or 350 and up to 700 bars for automotive applications. This technology, that equip the Toyota Mirai, offers a good density (42 kg/m3 under 700 bars), but requires specific storage tank with high strength materials [FC25]. Note that other mixt solutions are under investigation such as the cryogenic-compression and hydride pressure.

PEMFC is today a mature technology for many applications [FC26] such as portable power [FC27, FC28], stationary and residential applications [FC19, FC29-FC33], electrolyze [FC34-FC36], naval [FC37, FC38], aerospace [FC39] and transportation [FC40, FC41].

Plenty of engineering and scientific works are present in the literature, treating the PEMFC simulations and parametric studies, dynamic modeling, energetic and exergetic analysis,

technological and exergo-economic analysis, testing, thermal management and vehicle integration and simulations. Table 1.19 below summarizes the work field for different authors working on fuel cell energy converter.

Table 1.19: Scientific work on fuel cell

	Dynamic modeling	Simulations and parametric study	Energetic and exergetic analysis	Technological and exergo-economic	Tests	Thermal management	Vehicle simulations
Baschuk & al [FC42, FC43]		x					
Pukrushkapan [FC44]		x					
Mert et al. [FC45, FC46]		x	x	x			
Wang et al. [FC47, FC48]		x			x		x
Najafi et al. [FC49]		x					
Saeed et al. [FC50]		x					
Yigit et al. [FC51]		x	x				
Springer et al. [FC52]		x					
Dincer & al. [FC53]			x	x			
Abdin & al. [FC54]		x		x			
Nguyen & al. [FC55]	x				x		
Kazim [FC56]			x	x			
Midilli and Dincer [FC57]			x	x			
Barelli [FC58-FC60]	x		x	x			
Barbir and Gomez [FC61]			x	x			
Cownden et al. [FC62]			x				
Ishihara et al. [FC63]			x				
Mueller et al. [FC64]	x						
Andreasen et al. [FC65, FC66]	x				x	x	
Zhang et al. [FC67]	x						
Liso et al. [FC68]	x						
Reddy and Jayanti [FC69]						x	
Supra et al. [FC70]						x	
Li et al [FC71]					x		
Sorensen [FC72		x					x
Liang et al. [FC73]		x					x

1.6.1.2 State-of-the-art of PEMFC in automotive powertrain applications

As discussed in the introduction, automotive applications have specific requirements. Today, among many fuel cell types, the PEMFEC presents the best compromise for vehicle and are commercially available [FC74, FC75] with a power spectrum ranging from 0.1 kW to 500 kW, a FCS weight power density up to 550W/kg, and a size power density higher than 450W/L [FC76, FC77].

The ability of the PEMFC to change power output quickly, especially when operating on pure hydrogen, makes it a suitable technology for series and range extender hybrid electric vehicles. For vehicles applications, the PEMFCs operate at temperatures between 20 and 80°C [FC55]. Note that this low temperature operation requires an input stream almost free of carbon monoxide (CO) and impurities.
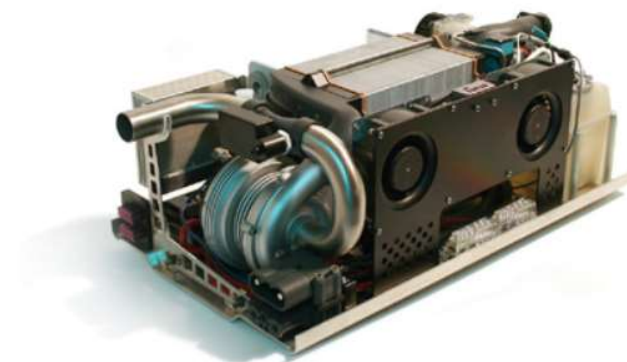
Fig. 1.35: PSA 10kWe PEMFC [FC78]

PSA had an intense activity of FC during the 2000's, with many prototypes and concept cars such the Citroën CZERO, the GENEPAC, the Peugeot 308 Epure, the TESSA concept [FC25, FC79, FC80]. Hyundai – Kia commercializes the ix35 FCell in March 2013 and presented two generations of Hyundai Tucson series hybrid electric vehicle (SHEV), equipped with FCS of 100 kW, a hydrogen storage system (HSS) of 5.6 kg capacity, a battery of 2 kWh and driven by a 100kW electric machine. The vehicle achieve 594 km autonomy on NEDC cycle [FCV-009]. Renault proposed the Kangoo H2 in 2015, a 2 seats commercial range extender FCEV equipped by Symbio FCell, a 5kW FCS and 1.74 kg HSS capacity driven by a 44 kW electric machine and with 22 kWh battery. The vehicle autonomy is about 320 km on NEDC cycle. Toyota commercialized the MIRAI FCV since March 2015. The vehicle equipped with a FCS of 100 kW, a HSS of 5kg capacity, a 1.3 kW.h battery capacity and driven by an electric machine of 113 kW power. Vehicule autonomy is about 500km on NEDC driving cycle [FC81]. Honda commercialized the Honda Clarity vehicle in 2016, a 5 seats 1890 kg vehicle equipped with an FCS of 103 kW, 3.1 kW/L of size power ratio and two HSS of 5 kg total capacity. Driven by a 130 kW electric machine, the vehicle achieves 480 km autonomy on NEDC. Daimler commercializes the FCV starting from 2017, on the GLC vehicle. This plug-in fuel cell powertrain has 500km autonomy including 50km on battery. The HSS has 4kg capacity and the battery capacity is 8.8 kWh [FC82]. Audi, with the engineering support of Ballard, unveiled different FC vehicles [FC83]. The A2H2 equipped with PEMFC has a 66 kW electric motor, a Dynetek 350 bars HSS with total capacity of 3kg where the Audi Q5 HFC is equipped with a 90 kW PEMFC, a 1.3 kWh lithium battery and a 700 bars hydrogen storage tank [FC84]. BMW working on cryogenic HSS [FC85] unveiled the i8 FCV with cryogenic hydrogen cylindrical tank, powered by 115 kW FC and driven by an electric motor of 242 bhp. The series 5 BMW co-developed with Toyota equipped also with a cryogenically pressure vessel tank, containing 7.1 kg of hydrogen at -220°C, has a range of 700 km on real-world driving and a lifetime of around 5.000h equivalent to 200.000 km. Fiat presented the Fiat Panda, a 200km autonomy FCV equipped with 60 kW FC and a 350 bars HSS. Kia presented the Kia Borrego FCEV in 2008. The 426 miles range vehicles, is equipped with a 10,000 psi HSS and an upgraded 115 kW FCS with super capacitor delivering 134 hp at 450 Volt and an electric motor of 109 kW [FC86]. GM with long FCV story since 1966 [FC87, FC88], unveiled in 1996, the EV1 concept car using the methanol powered FC with highway range of around 480 km. Other automotive constructers are also working on concept cars with hydrogen and fuel cell

technologies. We can list: Mazda [FC89], Morgan [FC90], Renault [FC91], Suzuki [FC92], Ford [FC5], Volkswagen [FC93-FC95] and Opel [FC88]. The table 1.20 below presents the technological design choice for different FC powertrains.

Table 1.20: FC powertrains technological choice in automotive applications

	FCS power	HSS Capacity	Electric machine power	Battery capacity	Autonomy
Audi A2H2	x	3 kg	66 kW	x	x
Audi Q5 HFC	90 kW	x	x	1.3 kW.h	x
BMW i8 FCV	115 kW	Cryogenic	242 bhp	x	x
BMW series 5 FCV	x	Cryogenic 7.1kg	199 bhp	1 kW.h	700 km
Daimler GLC	x	4kg	x	8.8 kW.h	500km
Fiat Panda	60 kW	x	x	x	200 km
Honda CLARITY	103 kW	5 kg	130 kW	x	480 km
Hyundai–Kia ix35	100 kW	5.6 kg	100 kW	2 kW.h	594 km
Kia Borrego	115 kW	x	109 kW	x	426 miles
Mitsubishi	68 kW	117L@35 Mpa	65 kW	x	150 km
Morgan	22 kW	x	x	x	250 miles
Nissan X-trail FCV	90 kW	700 bars	90 kW	x	500 km
Peugeot 207 EPure	20 kW	15 L @ 70 MPa	95 bhp	50 kW	350 km
Peugeot H2Origin	10 kW	35 Mpa	x	47 hp	100 km
Renault Kangoo ZE	5 kW	1.74 kg	44 kW	22 kW.h	320 km
Renault Scenic	x	3.7 kg	90 kW	x	320 km
Suzuki	80 kW	70 Mpa	68 kW	X	250 km
Toyota MIRAI	100 kW	5 kg	113 kW	1.3 kW.h	500 km

1.6.1.3 Synthesis on PEMFC

PEMFC are today commercially available for vehicle applications as main energy converter on series hybrid electric vehicle powertrains. Many technological problematics such as water freezing during cold start conditions, operating temperature, unsatisfactory durability, poor transient performance, and cost of catalyst material are being resolved. The mass of platinum electrolyze have been largely reduced. Also, security components are under development to avoid drastic accident and numerous works are done to manage the hydrogen fire risks.

However, other drawbacks remain and today engineers are working to eliminate them. For instance, the drive range still shorter than ICE vehicles and limited by the hydrogen storage energy density and cost. The FCS overall efficiency with peaks near 50% have relatively lower efficiency at low power. The thermal integration of the fuel cell is also problematic. In fact, around 50% of heat generated is rejected at low temperature. This requires big radiator surfaces. PEMFC is also a unidirectional device and cannot receive power back. Therefore, storage devices such battery or ultra-capacitor has to be introduced in order to gain a regenerative capability, which adds additional cost and complexity.

Finally, PEMFC vehicle is a zero carbon vehicle that rejects only water. However, the hydrogen production cost in term of carbon dioxide remains a dilemma and depends mainly, on how hydrogen is produced. Today, around 48% of total hydrogen production is obtained through steam reforming of natural gas, 30% from petroleum oil's cracking, 18% from coal's gasification and 4% from water electrolysis [FC25, FC96]. While water electrolysis offers no

CO2 emissions, electricity provided must be produced from renewable energy such as solar or wind turbines, therefore FCV are potentially important in the long term, if the hydrogen is produced with lower carbon emissions [FC97].

Table 1.21 summarizes the advantages and drawback of PEMFC observed in the literature and table 1.22 synthesized the performance assessment.

Table 1.21: Advantages and drawbacks of the PEM fuel cell in automotive applications

Advantages	- Zero Carbon emissions - Longer driving range without a long battery charging time compared to EV - High efficiency compared to ICE - Quiet operation - Few moving parts - simplicity - Cogeneration capability.
Drawbacks	- Require Hydrogen energy, HSS and specific infrastructure - Thermal integration – cooling system - Heavy and bulky power unit - lower power density compared to ICE - Long start-up time, and slow power response compared to ICE - Drive range is limited by the hydrogen storage energy density and cost. - Water freezing problematic during cold start - Cost compared to ICE

Table 1.22: Summary of PEM fuel cell performance criteria.

Characteristics	Value and Description
Efficiency range	Between 45-50% (FC system)
Power to weight ratio	125-1000W/kg for the system [FC20, FC76, FC77] (without HSS)
Power to size ratio	125-700W/L for the system [FC20] (without HSS)
Fuel	Hydrogen
Combustion process	Electro-chemical reaction
Working fluid	Air
Emissions	Zero emission
Complexity/size	Moderate complexity integration – (storage system and radiator)
Noise and vibration	Low noise and vibration aspects
Controllability	Good controllability for stationary power systems
Maintainability	High maintainability machine
Reliability	Medium reliability machine – depends on stack life
Safety	Moderate safety level (hydrogen problematic)
Powertrain compatibility	Compatible only with series hybrid electric vehicle powertrains
Technical maturity	High maturity - commercially available for vehicle applications

1.7 Synthesis

This section presents the synthesis of the study on the different assessed energy converters. The section summarizes first the status of integrating these converters into vehicle applications.

Second, a cross comparison among the quantitative and qualitative criteria of the different energy converters is presented considering their use as main prime movers in the vehicle. The assessed quantitative criteria are the efficiency range, the weight to power density and the size to power density. The presented qualitative criteria include the compatibility of the converter with the powertrain architecture, the multi-fuel use capability, the cogeneration capability, and the need of specific materials. Additional intrinsic criteria needed in automotive applications are summarized, such as the system packaging, the noise and vibration, the reliability and the maintainability. Finally, technologies are classified as function of their attractiveness to vehicle manufacturers in integrating new-electrified powertrain architectures and their development potential in meeting the consumption and emissions targets post-2025.

Table 1.23 summarizes the status of the studied energy converters in terms of their development and integration in vehicle applications. The only existing substitute to the ICE revealed in the literature is the PEM fuel cell, which was investigated by almost all OEM's as well as many laboratories. The first commercialization of this converter was observed in 2015 on the Toyota Mirai. Other energy converters, such as gas turbines, Stirling engines and vapor cycle machines, have been largely investigated and tested in vehicle prototypes only. However, the literature did not show any potential use of the remaining energy converters, such as Ericsson, thermoacoustic and thermoelectric generators, as main energy converters in vehicle powertrains.

Table 1.23: Status of energy converters in automotive applications.

Energy Converter	Status	OEM's or other companies
Split Cycle	🟡	Scuderi
Gas Turbine	✅	Chrysler, GM, Fiat, Citroën, Peugeot, Fiat, Volvo
Stirling	✅	GM, Ford, Opel, NASA
Vapor Cycle Machine	✅	GM, NASA
Ericsson	❌	-
Thermoacoustic	❌	-
Thermoelectric	❌	-
PEM Fuel Cell	✅	Almost all vehicle manufacturers

✅ Vehicle prototype or commercialized, 🟡 Investigation without vehicle prototype, ❌ No attempt

Figure 1.36 presents the maximum efficiency range of the different energy converters. The ICE maximum efficiency ranges from 35% for a basic gasoline engine up to 42% for diesel or gasoline Atkinson-Miller engines. However, the combination of these ICE to WHR systems allows an additional increase in efficiency of 2 to 4 % [ICE40, ICE41]. Similarly, the efficiency of split cycle engines can reach up to 50% when combined to internal heat recovery systems.

Simple gas turbine systems showed a maximum efficiency of 30% in powertrain applications; however, advanced gas turbine systems with intercooler, regenerative, reheat and water injection systems can reach more than 52%, while using high temperature resilient materials. These high efficiency figures were shown to be lower with external combustion gas turbine

systems (ECGT) since heat is added from an external source. Their efficiency ranged between 25 and 41% [ICE42, GT6].

The review of the literature showed a maximum efficiency of 39% for the MODII Stirling engine, with the capability to reach 42%. However, efficiency of vapor cycle machines was limited to 30% in powertrain applications due to the low expansion ratio and the limited condensing temperature.

The Ericsson external combustion machine, based on the piston-conrod-crankshaft architecture, can achieve realistic overall efficiency between 25% and 35% in automotive applications. These lower efficiency figures compared to other energy converters are due to the losses in the crossover passage between compression and expansion piston on one hand, and on the other hand caused by the low heat extraction efficiency from the external combustion chamber.

The efficiency of thermoacoustic machines reached 35% in micro-cogeneration applications, and they can achieve the same efficiency level if deployed in automotive applications. Regarding the thermoelectric generators, their maximum efficiency is limited to 25% due to the low merit factor. Finally, the PEMFC system have a maximum efficiency ranging between 42% and 50%.
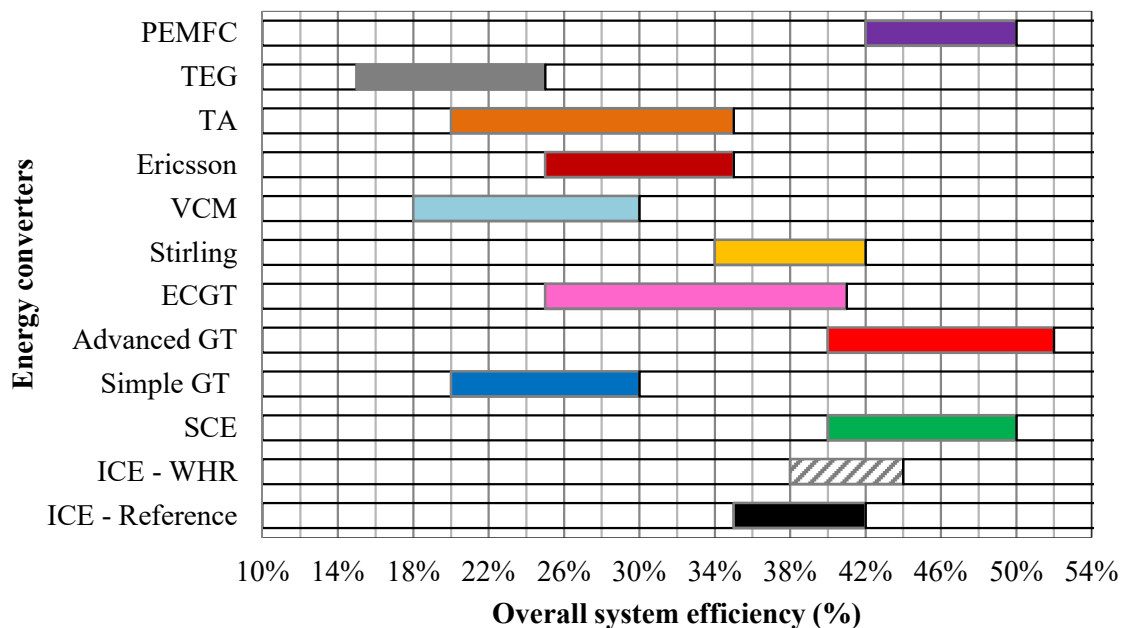
Fig. 1.36: Efficiency range of energy converters in automotive applications.

*ECGT (External combustion Gas turbine) efficiency are estimated from [GT6].

Based on the aforementioned synthesis on maximum efficiency range of the different energy converters, PEMFC, advanced GT, split cycles, advanced ECGT and Stirling machines are the only energy converters that can achieve an efficiency higher than the efficiency of an ICE with today state-of-art of material and components.

Two additional criteria are considered in the selection process of energy converters in vehicle powertrains:

- · The weight of the system which affects directly the total vehicle weight and consequently the vehicle fuel consumption
- · The size of the system which impacts the implementation of the system and the vehicle aerodynamics and consequently the vehicle fuel consumption

Both criteria have impact on the vehicle energy consumption and define the system power density. Figure 1.37 illustrates the power to size range versus the power to weight range of the studied energy converters. The simple and advanced GT systems with high rotational speed have higher power to size and power to weight ratios as compared to the ICE, whereas, the power density of ECGT systems is lower due to the additional required heat exchangers and the lower working fluid operating temperature.

Split cycle engines present lower power densities since they require an additional heat exchanger to recover waste heat internally. Moreover, the lean mixture burning due to temperature limitations causes their lower net specific power.

Advances in PEMFC have enabled this system to achieve high power densities for vehicle powertrains, comparable to the ICE.

Stirling machines have undergone many developments to reduce their weight and size to fit in automotive applications. Their power densities reached comparable figures to the ICE in the 70's and 80's, but this advantage was lost later and the power density gap between Stirling and ICE became larger due to the tremendous developments that followed on the latter. In fact, the high-pressure working fluid of the Stirling engine requires higher engine thickness, and the needed external combustion system increases its weight and size. Similarly, the same conclusions are drawn for the external combustion Ericsson engine, which requires an ICE piston basic architecture with a specific cylinder head and an external combustion chamber.

The thermoacoustic machines use bulky and heavy resonator, hence present low power density. Alike, TEG systems show poor power-to-weight and power-to-size ratios compared to the ICE due to the limited operating temperature and the need for external combustion, which requires large thermoelectric exchange surfaces.

Therefore, the energy converters with improved or comparable power densities to the ICE are the PEMFC for thermo-chemical energy converters, the gas turbine systems and the split cycle machines for internal combustion engines, and the ECGT and the Stirling engines for the external combustion systems.

Table 1.24 classifies the studied energy converters according to the investigated qualitative criteria for automotive applications. Among these criteria the need to specific material, the powertrain architecture's compatibility, the cogeneration and the multi-fuel use capabilities.
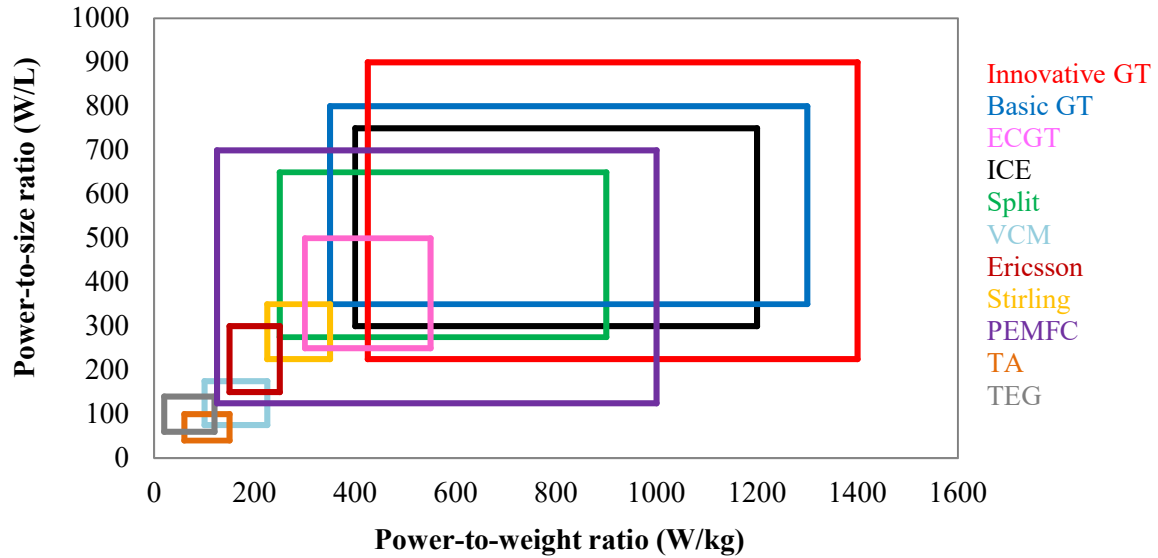
Fig 1.37: Power to size ratio versus power to weight ratio.

The ICE and SCE do not require any heat resistant material due to their advanced cooling systems and controlled combustion. Specific and costly material are only needed in the exhaust after-treatment system. The GT systems materials, including the ECGT materials, depend on the maximum combustion chamber outlet temperature. Specific nickel alloys are required for temperature higher than 950°C and ceramic material for temperature higher than 1250°C. This is similar for the Stirling and Ericsson systems, where the hot heat exchanger requires specific materials depending on the operating temperature. Although, for the VCM, the evaporator material depends on the maximum cycle temperature and pressure, where specific nickel alloys may be required. For the thermoacoustic systems, the hot heat exchanger and the choice of the calorimetric fluid depend on the system maximum temperature. On the other hand, the TEG requires specific materials as described above and the PEMFC requires platinum as catalyst.

Regarding powertrain compatibility, the ICE, SCE and Stirling machine are compatible with all powertrain architectures, both conventional and hybrid electric. GT systems with high rotational speed requires reduction gears in order to be coupled to conventional powertrains. These machines perform poorly under transient operations and consequently are optimized to operate under quasi-steady power range, which make them also more suitable for SHEV powertrains, where the energy converter is decoupled from mechanical load. This is also the case for the Ericsson and the VCM, performing better when operating at constant power in SHEV. Finally, the thermoacoustic machine using acousto-electric devices, the thermoelectric generators and the PEMFC where electric power is the output, are only suitable with both SHEV and EREV powertrains.

As for the cogeneration capability, all of these machines reject waste heat which can be recovered partly to ensure the vehicle cabin heating needs. Therefore, they all present cogeneration capability.

Regarding multi-fuel capability, the different energy converters are classified according to their capability of using multi-fuel, liquid, gas and solid fuels. Internal combustion engines such as the ICE, the SCE and the GT are compatible only with liquid and gas fuels. External combustion engines are compatible with all fuels including solid fuels. Note that PEMFC is only compatible with pure hydrogen.

Table 1.24: Qualitative assessment of energy converters for automotive applications.

Energy Converter	Specific material (*)	Compatibility with powertrain architectures (**)	Cogeneration capability	Multi-fuel capability (including solid fuels)	Liquid and gas fuel capability	Cooling system (***)
ICE	✗	✓	✓	✗	✓	✓
SCE	✗	✓	✓	✗	✓	✓
Simple GT	◉	◉	✓	✗	✓	✗
Advanced GT	◉	◉	✓	✗	✓	◉
ECGT	◉	◉	✓	✓	✓	◉
Stirling	◉	✓	✓	✓	✓	✓
Ericsson	◉	◉	✓	✓	✓	✓
VCM	◉	◉	✓	✓	✓	✓
TA	◉	✗	✓	✓	✓	✓
TEG	✓	✗	✓	✓	✓	✓
PEMFC	✓	✗	✓	✗	✗	✓
*Specific material:	✓ Require specific material, ◉ Required specific material only for high temperature operating cycles ✗ don't require specific material)					
**Powertrain compatibility:	✓ compatible with all powertrains, ◉ can be used for conventional and parallel HEV powertrain because of the mechanical output power generated, but not well suited due to acceleration lag and time response problematics as well as the high fuel consumption due to operating in a low efficiency zone. ✗ compatible only with series powertrain architecture					
***Cooling system:	✓ require vehicle cooling system ◉ Depend on the architecture ✗ Don't require cooling system					

Finally, one of the important vehicle criteria to be considered when selecting energy converter substitute to the ICE, is the cooling system and the required cooling surface area. This criterion affects the vehicle frontal surface area where the heat exchange has to occur with the ambient air. While the ICE and SCE require a radiator to reject heat at temperature between 85 and 105°C, simple GT rejects only heat in the exhaust gases. The only cooling system required is for cooling the electric generator and bearings, which is still considered very small and presents lower constraints than ICE vehicle radiator. On the other hand, depending on the thermodynamic configuration of the advanced GT, the ECGT and the Ericsson open loop systems, they may require an intercooler in order to reduce the compression work. This device has a size that is close or smaller than the intercooler used today on the turbocharged ICE. On the other hand, other converters, namely the Stirling engines, vapor cycle machines, Ericsson

closed loop machines, thermoacoustic and thermoelectric generator systems are closed loop systems requiring a specific cooling system. Their efficiency depends on the cold source temperature and the heat exchanger surface.

Finally, the non-energy benefits of the different energy converters are summarized in table 1.25. Energy converters are classified according to different criteria among them the opportunity for novel integration and packaging, the noise and vibration aspects, the reliability and the maintainability. Regarding the opportunity for novel integration and packaging in powertrains, the SCE based on the piston ICE architecture does not offer any specific advantages, where the same implementation constraints as in ICE are present. On the contrary, this energy converter requires additional components such as crossover passage and heat exchanger. On the other side, GT offer novel packaging opportunity for series hybrid powertrains where the system can be designed and integrated independently of the architecture constraints of the vehicle propulsion system. The Stirling, the Ericsson, the TA and the TEG systems offer no valuable packaging novelty. Their external combustion system remains bulky and cannot be located far from the energy converter itself. On the other hand, VCM can be integrated in different way, because the different system components can be located in different places in the vehicle. Regarding noise and vibration, the Split cycle engines present similar noise and vibration levels compared to the ICE. As for the remaining energy converters, they all present additional benefits in terms of noise and vibrations as compared to the ICE, except the Ericsson which remains with higher noise level due to the valves operation

Table 1.25: Non-energy Benefits of Energy Converter Options

Energy Converter	Opportunity for novel integration & packaging	Noise and vibration reduction	Improved reliability	Improved maintainability
Split Cycle Engine	❌	❌	❌	❌
Gas turbines	✅	✅	✅	✅
ECGT	✅	✅	✅	✅
Stirling	❌	✅	❌	❌
Ericsson	❌	🟡	🟡	🟡
VCM	✅	✅	🟡	🟡
Thermoacoustic	❌	✅	🟡	✅
ThermoElectric	❌	✅	❌	❌
PEMFC	❌	✅	❌	❌
✅ Better compared to ICE, 🟡 no solid data, ❌ can be worse than ICE				

Based on the different results, the different technologies are classified in table 1.26 in term of "most promising", "moderately promising" and "least promising" as main energy converter for future vehicle applications. The advanced GT and the split cycle are among internal combustion machines most promising energy converters. They offer high efficiency and high power densities. The Stirling and the ECGT are among external combustion machines most promising energy converters, offering also high efficiency and power density among others.

Table 1.26: Promising technology as prime mover for automotive applications

Status	Energy converter
Most promising	Advanced GT cycles, PEMFC, Split Cycle, Stirling, ECGT
Moderately promising	Simple GT / Regenerative GT, Vapor cycle machines, Ericsson
Least promising	ThermoElectric, Thermoacoustic

Among internal combustion machines compatible only with some liquid and gas fuels, SCE are compatible with all hybrid electric powertrains and GT systems, despite their investigation in conventional powertrains, are most suitable for SHEV and EREV powertrains. On the other hand, among external combustion systems compatible with all fuels including solid fuels, Stirling machines are compatible with all hybrid electric powertrain and the ECGT systems are more suitable for series and range extended hybrid electric powertrains.

Table 1.27: Promising energy converters compatibility with powertrain and fuels

	Compatible with all hybrid electric powertrains	Compatible with series hybrid electric powertrains
Compatible with all fuels including solid fuels	Stirling	Stirling, ECGT
Compatible with liquid and gas fuels	Stirling, SCE	Stirling, GT

Finally, the different recommendations for the most promising technologies are summarized in the table below.

Table 1.28: Recommended initiatives for the promising technologies

Energy converter	Recommended initiatives
SCE	Development of high strength temperature material, innovative valves systems, high temperature efficient heat exchangers, water injection technology and intercooled and reheat concepts.
Advanced GT and ECGT	Development of high strength temperature material, high temperature efficient heat exchanger and regenerators, water injection technology, high isentropic efficiency turbomachines, isothermal combustion processes, intercooled and reheat processes.
Stirling machines	Development of high strength temperature material, efficient high temperature head, heat exchanger and internal regenerators, innovative sealing system and/or electromagnetic coupling devices
PEMFC	Development of innovative storage systems, reliable membrane and stack, high pressure HHS with high capacity.

1.8 Conclusion

An overview study was performed on different energy converters for automotive applications in an attempt to be considered as a substitute to actual internal combustion engine. Energy converter machines studied can be classified under three different categories: (1) internal combustion machines such as internal combustion engines, split cycle engines and gas turbines,

(2) external combustion machines such as external combustion gas turbines, Stirling, vapor cycle machines, Ericsson, thermoacoustic and thermoelectric generators, and (3) electro-chemical energy converters such as the proton exchange membrane fuel cells.

For each energy converter, a state of the art and a bibliographical study are conducted first, followed by a design analysis. In addition, qualitative and quantitative technological criteria were compared. Qualitative criteria include efficiency, power to weight and power to size ranges. Qualitative criteria include the need of specific materials, the powertrain compatibility, the cogeneration capability and the multi-fuel ability. Advantages and drawbacks for the use of these converters in automotive applications are then presented.

Among the studied energy converters, the split cycle engines, the Stirling, the gas turbines systems and the PEMFC are identified to present a potential for use in automotive powertrains as the fuel energy converter, due to their higher efficiency and power densities as compared to the ICE. Stirling and external gas turbine machines offer the advantages of multi-fuel use capability with good efficiency, where SCE and GT offer high efficiency and power densities. PEMFC requires hydrogen as specific fuel, this energy converter provides high powertrain efficiency, no pollutant emissions and acceptable power densities.

In today's context of high degree of powertrain electrification, the range extended electric powertrains based on series hybrid architecture seems to be the future potential powertrain to be considered. These electric-based powertrains require a compact, low weight and high efficient energy converter to serve as an auxiliary power unit that refills the battery once depleted. This will prevent from the need of implementing large battery capacities. Gas turbine systems offer these benefits in addition to the advantages of multi-fuel use capability.

In addition, gas turbine systems are mature technology applied in different industries, namely the electric power production sector. Hence, GT systems know-how and expertise can be easily transmitted to the automotive industry and do not require the development of a new energy vector such as Hydrogen for PEMFC. Therefore, given all these advantages, this energy converter will be considered in the rest of this study.

Résumé chapitre 2

Des efforts de recherche importants ont été investis dans l'industrie automobile sur les groupes motopropulseurs hybrides afin de réduire la dépendance des voitures particulières au pétrole. L'électrification des groupes motopropulseurs a donné lieu à une large gamme d'architectures de véhicules hybrides. La consommation de carburant de ces groupes motopropulseurs dépend fortement des performances du convertisseur d'énergie, ainsi que de la stratégie de gestion de l'énergie déployée à bord. De plus, les normes de consommation de carburant et d'émissions de dioxyde de carbone sont appliquées dans le monde entier sur la plupart des marchés de véhicules légers. Les cycles de conduite réglementaires, définis comme des modèles temps-vitesse spécifiques, sont utilisés pour mesurer les niveaux de consommation de carburant et d'émissions. Ces mesures devraient refléter de manière réaliste les performances de conduite en situation réelle, mais on s'inquiète de plus en plus de leur adéquation en raison des écarts observés entre les valeurs de consommation et d'émissions certifiées et celles du monde réel. L'une des principales raisons de cet écart est que les protocoles d'essai actuels ne tiennent pas compte des besoins énergétiques non mécaniques des véhicules, tels que les besoins de confort thermique des passagers et l'utilisation d'auxiliaires électriques à bord. Le chauffage et le refroidissement de la cabine peuvent notamment entraîner une augmentation considérable de la consommation d'énergie du véhicule.

Le présent chapitre examine le potentiel d'économies de consommation de carburant d'un véhicule à chaîne de traction électrique hybride série, sur un cycle d'homologation prenant en compte tous les besoins energétiques du véhicule, et utilisant une turbine à gaz comme convertisseur d'énergie au lieu du moteur thermique à combustion interne conventionnel.

Tout d'abord, un modèle de cabine de véhicule est développé et les besoins en énergie de confort thermique sont dérivés pour le refroidissement et le chauffage, en fonction de la température extérieure ambiante sous des climats froids, modérés et chauds. Le cycle d'homologation WLTP est ainsi modifié pour inclure les profils de puissance générés pour le confort thermique et les besoins auxiliaires. Ensuite, une analyse exergétique et technologique explicite est developpée pour identifier la meilleure configuration thermodynamique du système turbine à gas. Un cycle avec refroidissement intermédiaire, récupération et réchauffage intérmédiaire est priorisé, offrant une efficacité et une densité de puissance plus élevées par rapport aux autres systèmes étudiés. Un modèle de véhicule hybride série est développé et les composants du groupe motopropulseur sont dimensionnés en tenant compte des critères de performance du véhicule.

Des simulations de consommation d'énergie sont effectuées sur le cycle de conduite modifié en utilisant la programmation dynamique comme stratégie globale de gestion optimale de l'énergie.

Les résultats montrent une augmentation de la consommation de 20 à 96 % par rapport au WLTP actuellement adopté, selon le climat considéré. De plus, Les résultats montrent une amélioration de la consommation de carburant de 22 à 25 % avec le GT comme groupe auxiliaire de puissance ou prolongateur d'autonomie par rapport au moteur thermique à combustion interne convnetionnel.

Chapter 2: Exergo-Technological Explicit Selection Methodology for Energy Converters for Series Hybrid Electric Vehicles: Case of Gas Turbine Systems*

Gas turbine (GT) systems are among potential energy converters for future vehicle powertrains as discussed and concluded in chapter 1. These systems offer vehicle intrinsic benefits such as good efficiency, multi-fuel and cogeneration capability, low vibration and noise, reduced number of components, compactness as well as reduced weight compared to other energy converters.

GTs are also compatible with series hybrid electric vehicles (SHEV) and range extended hybrid electric vehicles (EREV) powertrains. These powertrains offer, with the adequate battery capacity sizing, a full electric drive wich can be favourable to reduce local emissions, mainly in dense cities. Note that in these powertrains where the mechanical driving power is ensured by an electric motor and the energy converter is cinematically decoupled from the vehicle load, GT can be designed to operate at its maximum efficiency which reduce furthermore the fuel consumption and emissions.

Today, standards for fuel consumption and carbon dioxide emissions are implemented worldwide in most light-duty vehicle markets where regulatory drive cycles are used to measure levels of fuel consumption and emissions. These measurements should realistically reflect real world driving performance. However, there is increasing concern about their adequacy due to the discrepancies observed between certified and real world consumption and emissions values. One of the main reasons for the discrepancy is that current testing protocols do not account for non-mechanical vehicle energy needs, such as passengers' thermal comfort needs and the use of electric auxiliaries on-board, which can lead to considerable increase in vehicle energy consumption.

Therefore, this chapter presents a methodology of choice and optimization of GT energy converter for SHEV powertrains. The study starts with a simulation-based assessment framework to account for the additional fuel consumption related to the cabin thermal energy and auxiliary needs under the worldwide-harmonized light vehicles test cycle (WLTC). The thermal comfort energy needs are derived for cooling and heating, depending on ambient external temperature under cold, moderate temperate and warm climates. A modification to the WLTC is proposed by including the generated power profiles for thermal comfort and auxiliary needs.

Then, an investigation of the potential of fuel consumption savings of an SHEV using a GT as energy converter instead of the conventional internal combustion engine (ICE) is developed. The investigation starts by applying an exergo-technological explicit selection method analysis to identify the best GT-system configuration for SHEV based on exergetic analysis and considering technological constraints. The intercooled regenerative reheat cycle is prioritized, offering higher efficiency and power density compared to other investigated GT-systems. An

SHEV model is developed and powertrain components are sized considering vehicle performance criteria such as acceleration, maximum speed and gradability. Energy consumption simulations on plug-in and self-sustaining SHEVs are performed on the modified WLTC driving cycle using dynamic programing as global optimal energy management strategy.

Results show around 22% of improved fuel consumption with GT as auxiliary power unit (APU) compared to ICE. Consequently, the studied GT-APU presents a potential for implementation on SHEVs.

The same methodology was applied for other energy converters including External Combustion Gas Turbines (ECGT), Stirling machines, Brayton WHR, Vapor Cycle Machines (VCM), Split Cycle Engines (SCE) and Thermoacoustic machines. The prioritized optimal thermodynamic configurations and the fuel consumption simulations results on SHEV are presented in the conclusion paragraph of this chapter (section 2.8).

2.1 Introduction

Different manufacturers have investigated the integration of gas turbines (GT) in conventional powertrains over years as the main energy converter instead of conventional internal combustion engines (ICE). Early GT vehicle models in the 60's and 70's showed poor acceleration response and higher fuel consumption compared to internal combustion engine vehicles (ICEV) [2.1, 2.2]. These drawbacks were mainly due to operating the GT at high speed even at idle conditions, in addition to mechanically coupling the turbine to the vehicle driving load, which resulted in a low efficiency operating range of the GT-system. Despite the many technological advancements and improvements made later on GTs such as variable turbine geometry, water injection for improving the performance, and increase of turbine inlet temperature (TIT), the acceleration lag and the poor fuel efficiency are still the main reasons hindering their deployment in conventional powertrains.

A review of recent research and development programs of automotive manufacturers revealed new interests in GT for automotive applications, demonstrated in several vehicle concept cars. Moreover, the review of the recent literature showed interesting insights on GT consumption and emissions reductions. A study on GT for automotive applications at Chalmers University of Technology, presented an interest in operating GT at optimal efficiency point compared to ICE [2.3]. A complementary study at the University of Rome showed that GT emissions at optimal efficiency operation meet the Euro 6 emissions levels of CO, NOx and soot even without the use of after-treatment systems [2.4]. In addition, GT-systems offer other intrinsic benefits for vehicle powertrains such the reduced number of moving parts, vibration-free operation, low maintenance cost, high durability and the absence of cooling system [2.1].

Based on the aforementioned findings, GT-systems present a forthcoming potential for improving modern vehicle efficiency and emissions, with the benefit of fuel-use flexibility when compared to ICEVs; particularly, in series hybrid electric vehicle (SHEV) and extended

range hybrid electric vehicle (EREV) technologies. These powertrains combine a thermal and an electric powertrain in a series energy-flow arrangement, as illustrated in figure 2.1. The thermal powertrain is constituted of an energy converter and an electric generator, and is referred to as Auxiliary Power Unit (APU). The APU is mainly used to recharge the battery once depleted, and the electric powertrain provides the necessary power to overcome the driving load. Consequently, the APU operating speed is cinematically decoupled from the vehicle velocity, and the energy converter operating point is easily controllable to meet its best efficiency.

On another hand, several GT-system options could be considered for integration in SHEVs, combining a basic GT to regenerative systems and single or multi-stage compressions and expansions. There have been numerous studies published over the past decade in the academic literature covering a multitude of GT-system configurations and performance analysis in different applications, such as industrial [2.5-2.15] and aeronautics [2.16, 2.17]. The survey of these studies confirms that most GT-systems are designed based on efficiency optimization, power density optimization or a compromise between the two criteria. For instance, industrial GT-system studies focused on finding an acceptable compromise between maximizing the system efficiency and the power density, with less concern on reducing the weight [2.7-2.13]. Along these lines, aeronautical GT-system studies focused on maximizing the power density due to the high weight-reduction priority constraint for such applications [2.17]. In both applications, a combination of several measures was required such as the need to increase TIT, to add intercooler, regenerator and reheat systems in order to achieve the needed optimization [2.9, 2.16, 2.17]. However, there have only been a few recent papers on GT-systems suitable for automotive applications [2.18-2.20] due to the lack of competitiveness of GT compared to ICE in conventional powertrains. Other papers date for more than 20 years [2.21-2.24]. The review of these recent and old studies underlines the following two gaps:

- No specific methodology on selecting the best-suited GT-system for automotive applications is adopted. The studies focus is on the performance investigations of some pre-defined GT-systems, without taking into consideration any optimization requirement or technological constraints.
- The overall vehicle consumption under driving conditions is not evaluated and benchmarked against ICEV. These studies did not provide a complete vehicle model integrating the investigated GT-systems into a powertrain model, supervised by an energy management strategy.
- None of the studies consider the vehicle non-mechanical energy need such as the cabin thermal comfort and electric auxiliary needs which can account for significant fuel consumption under certain climates.

Therefore, based on the above synthesis of the insights and gaps in the literature for re-adopting GT in automotive applications, this chapter proposes a comprehensive methodology to identify the potential GT-system options and select the optimal system configuration for SHEV application.

First, a methodology for the modification of the WLTC optimization cycle to include cabin thermal comfort and electric auxiliary needs in addition to vehicle propulsion needs is carried out. The study starts with a framework for redefining the vehicle energy needs in section 2.1. This includes a methodology for defining the heating and cooling power profiles under three different climates: hot, cold and temperature climates. The resulting heating and cooling power profiles, in addition to the auxiliary power needs are used to propose a "modified WLTC" that is more representative of real world conditions under the three climate categories. Then, a methodology for identification and assessment of the different GT-system options applicable to SHEV are carried out in section 2.2, based on exergy analysis and automotive technological constraints. Observed results are used for the prioritization and the selection of the optimal GT-system configuration. The selection criterion is optimizing the system efficiency. Thereafter, the identified GT-system is integrated in an SHEV model in section 2.3, and a comparison between two SHEV models with different APU technologies (GT-APU and ICE-APU) is presented. SHEV models are developed with a backward-modeling approach, and the powertrain components are sized according to automotive performance criteria such as the maximum vehicle speed and acceleration. Finally, energy consumption simulations of both models are compared on the modified WLTC driving cycle. Dynamic Programing (DP) is adopted as Energy Management Strategy (EMS) in section 2.4 in order to provide the global optimal strategy to power ON and OFF the APU [2.25, 2.26].

2.2 Methodology for Optimal Gas Turbine System Selection and Optimization for SHEV

This section presents the methodology adopted to evaluate the potential of GT-systems in an EREV. Figure 2.1 presents this methodology. It starts by defining an optimization cycle based on the WLTC in which we account, in addition to vehicle propulsion mechanical energy need, the vehicle thermal and auxiliary electric energy needs. Therefore, the modified WLTC is the input for the vehicle model. Note that, the study considers three different climates: (1) a cold climate, (2) a temperate climate designed also as moderate climate and (3) a hot climate.

As output, the criteria are minimizing the fuel consumption under vehicle constraints such size, weight, and frontal surface among others, while ensuring the vehicle requirements in terms of acceleration, maximum speed and vehicle gradability. The vehicle powertrain is composed of an energy converter, which can be the GT or the ICE, coupled to an electric generator, both constitute the auxiliary power unit (APU) which role is to feed the SHEV's battery by electric energy.

Regarding the energy converter, an exergo-technological explicit selection (ETES) method is applied for the identification and assessment of the different GT-system options applicable to SHEV and to select the best-suited energy converter, based on exergy analysis and automotive technological constraints. Observed results are then used for the prioritization and the selection of the optimal GT-system configurations. The selection criteria are optimizing the system efficiency and increasing the net specific work.

Thereafter, an SHEV vehicle model is developed, and powertrain components are designed to ensure vehicle requirements in term of acceleration, maximum speed and gradability. The identified most suited GT-system is integrated in the developed vehicle model and a comparison between two SHEV models with different APU technologies is presented: (1) a GT-APU and (2) a reference ICE-APU.

Energy consumption simulations are compared on the modified WLTC. Dynamic Programing (DP) is adopted as Energy Management Strategy (EMS) in order to provide the global optimal strategy to power ON and OFF the APU. Consequently, the analysis considers only the impact of the energy converter systems on consumption and excludes the influence of rule-based EMS.
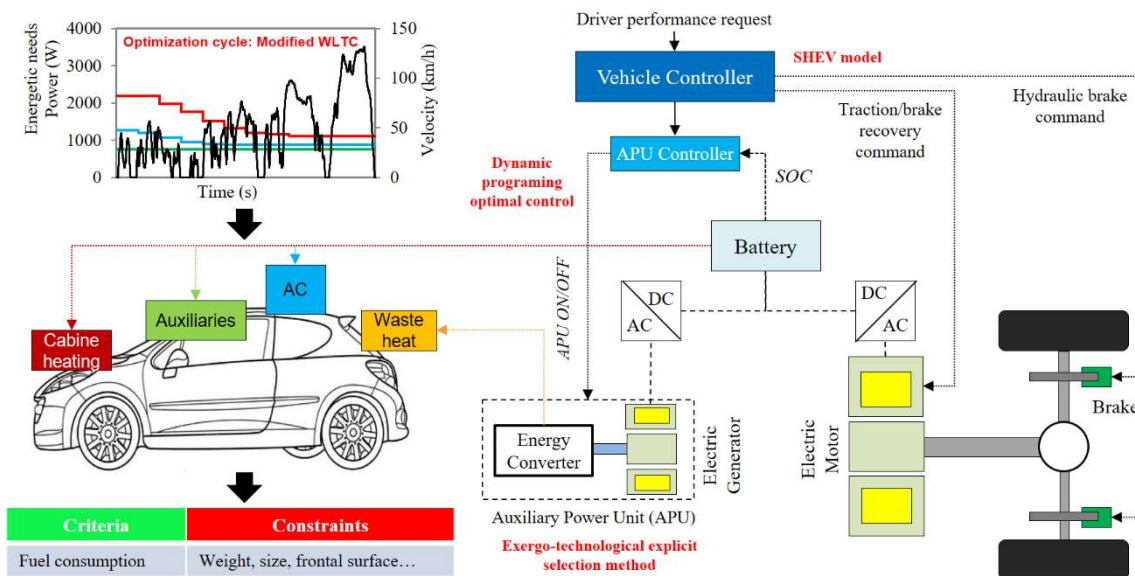

Fig. 2.1: Scheme of the overall methodology of choice and optimization of energy converters for SHEV

2.3 Optimization cycle

Regulatory drive cycles, defined as specific time-speed patterns, are used to measure levels of fuel consumption and emissions for passenger cars. These standards are implemented worldwide in most light-duty vehicle markets in order to reflect real world driving performance.

However, these measurements, which should realistically reflect real consumption and emissions, present discrepancies between certified and real world consumption and emissions values. One of the main reasons for the discrepancy is that current testing protocols do not account for non-mechanical vehicle energy needs, such as passengers' thermal comfort needs and the use of electric auxiliaries on-board. Cabin heating and cooling can especially lead to considerable increase in vehicle energy consumption.

Hence, in order to better inform future assessments of fuel consumption in real world conditions for both GT and ICE, and to reduce the discrepancies observed between certified and real world consumption and emissions values, the following paragraph proposes a modification to the

WLTC that includes cabin thermal comfort and electric auxiliary needs in addition to vehicle propulsion needs.

The resulting amended WLTC will be denoted in the rest of the study as "modified WLTC". The study starts with a framework for redefining the vehicle energy needs. This includes a methodology for defining the heating and cooling power profiles under different climates. To that end, a vehicle cabin thermal model is developed and presented in the thesis in the annex (A.2). The resulting heating and cooling power profiles, in addition to the auxiliary power needs are used to propose a modified WLTC that is more representative of real world conditions under three climate categories (hot, moderate and cold).

2.3.1   Methodolgy for accounting of vehicle thermal cabin and auxiliary power needs on the WLTC

This section presents the framework methodology for developing a modified WLTC that takes into account the vehicle thermal and electrical energy needs that are not currently considered. The framework consists of a two-step method for generating vehicle thermal and electrical power profiles and presented in details in the paper listed in the annex 3. These power profiles would be used in combination with the WLTC velocity profile for a more representative fuel and emissions assessment. The framework is summarized in figure 2.2.
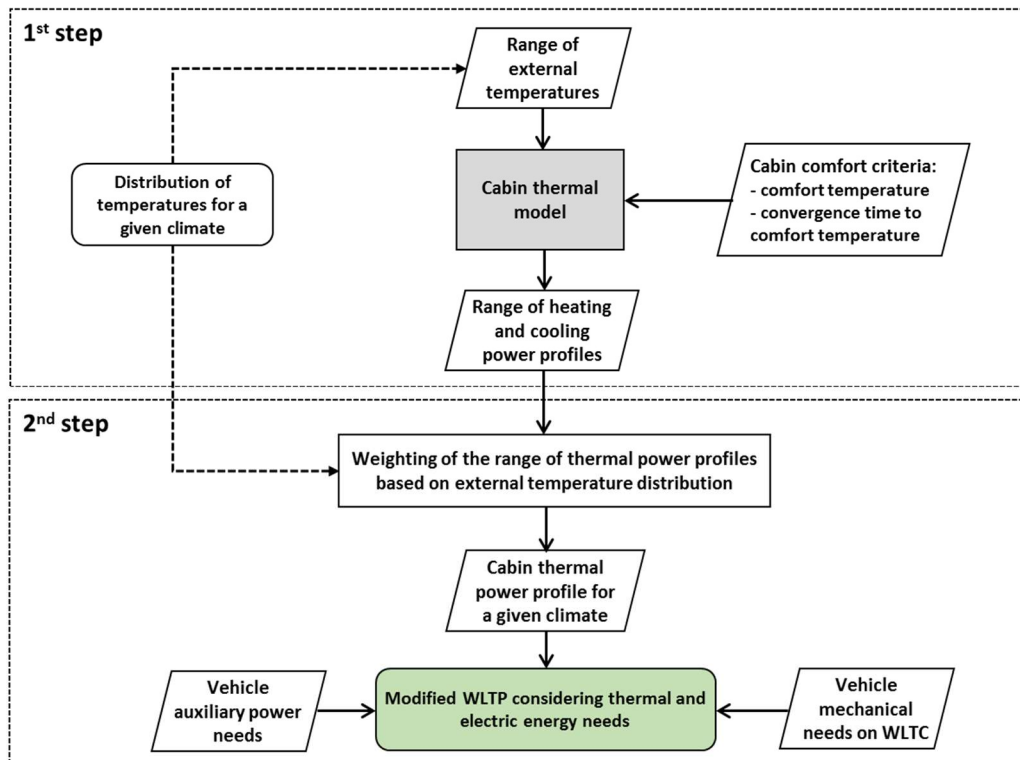

Fig. 2.2: Framework for redefinition of WLTC considering thermal and electrical energy needs.

The first step in the proposed framework is to predict the thermal energy needs. It consists of feeding the cabin thermal model with the range of external temperatures for a given climate, as

well as the cabin comfort criteria consisting of the internal comfort temperature and the corresponding convergence time to this temperature. The outcome is a range of power profiles emulating the cabin thermal energy needs corresponding to the different external temperatures.

Hence, a cabin thermal model is developed for that purpose using the Dymola-Modelica software. The cabin thermal model consists of several sub-models and is described in detail in the paper listed in the annex 3 and in [2.27]. The model calculates both the transitory and steady-state thermal needs in the cabin. First, given a thermal power need, the model computes the dynamic response (i.e. transitory state) of the cabin air temperature, producing the transitory curve from the initial temperature; and, given a target in terms of steady-state thermal comfort, the model determines the thermal power needs, i.e. the evaporator cooling capacity and the radiator heating capacity.

Figure 2.3 illustrates the heating and cooling thermal energy needs of the cabin as a function of external ambient temperature. Two types of curves are shown, for steady state and transient state, respectively. The steady state curves illustrate the thermal power needs to maintain the cabin at the comfort temperature of 23°C. The transient state curves illustrate the thermal power needs to bring the cabin to the comfort temperature, with the convergence time being determined according to the external temperature, as shown in Figure 2.4, which was developed by experimental measurement at the reference temperatures (-15°C, +20°C and +45°C) and linear interpolation in between.
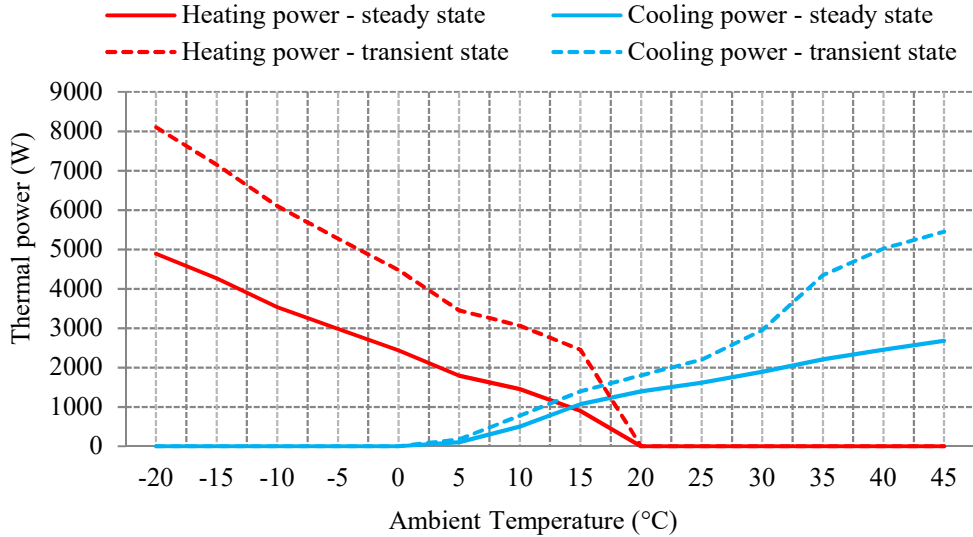
Fig. 2.3: Cabine thermal power function of external temperature.

Note the presence of a zone (between 5 and 20°C) where both heating and cooling are required simultaneously. This is the defogging zone where ambient air must be dehumidified before being heated and flowed into the cabin.
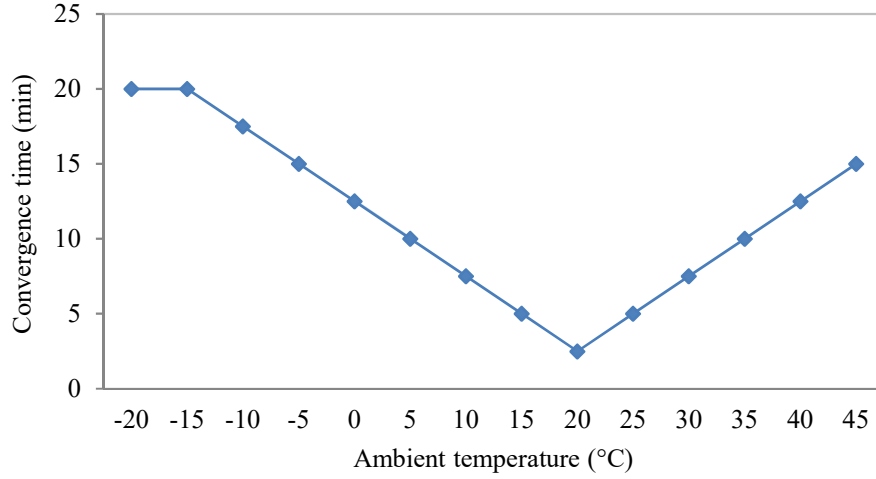
Fig. 2.4: Convergence time as a function of the external temperature (°C).

Finally, for the range of external temperatures considered, the corresponding cabin thermal power curves are derived by combining the transient thermal power required (dashed lines in Figure 2.3) during the convergence time (from Figure 2.4) with the steady state thermal power (solid lines in Figure 2.3). For example, at an external temperature of -5°C, a heating power of 5,200 W is applied during the transient state over a convergence time of 15 minutes, followed by a heating power of 3,000 W during the steady state for the remaining trip duration to ensure thermal comfort of the cabin is maintained.

The range of thermal power load curves are derived by this process for all considered temperature ranges, and presented in Figure 2.5. This concludes the calculations under the first step of the proposed framework.
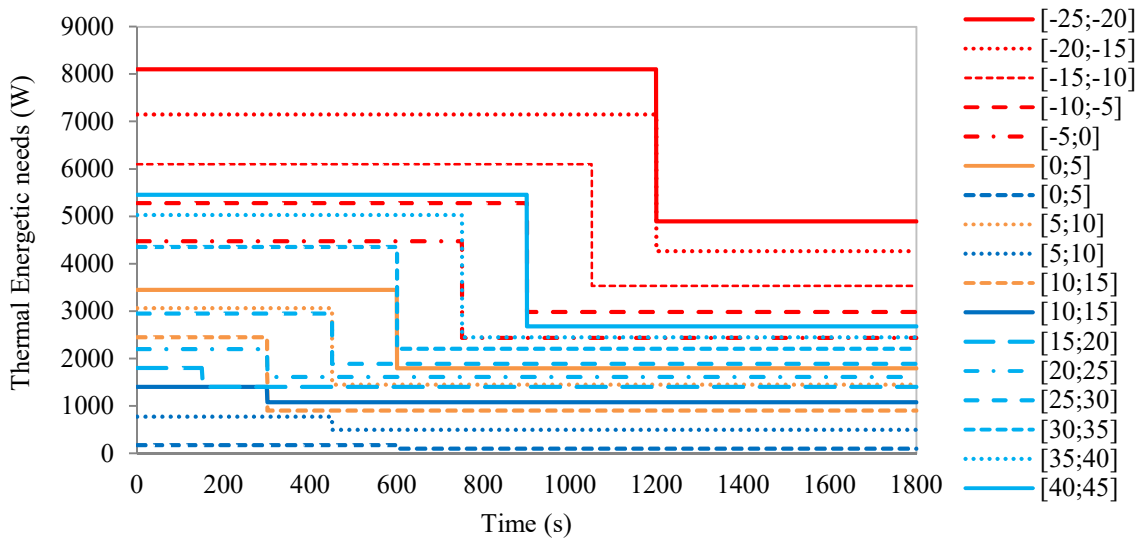

Fig. 2.5: Heating and cooling power needs for different external temperatures.

The second step involves weighting of the range of cabin thermal power curves obtained in step 1, using the frequency of annual temperature occurrences for a given climate. Three different climate conditions were considered corresponding to cold climate (Climate C), moderate climate (Climate M) and hot climate (Climate H), as shown in Figure 2.6 below.

For each defined climate, a weighted-average cabin thermal power is computed for both heating and cooling, using equation 2.1:

$$P = \sum_i x_i \times P_i(T_i)$$

(2.1)

Where x_i is the percent of occurrence of annual temperature T_i, and P_i is the corresponding cabin thermal power at T_i.

Based on a survey of industry best practice, a constant value of 750 W was assumed as an average electric consumption on middle class vehicles [2.28]. Therefore, the modified WLTC consists of combining the WLTC drive cycle with the heating and cooling thermal power curves and the constant electricity consumption, that now considers both mechanical power on wheels required to drive the vehicle at a given speed, and the heating and cooling thermal needs required to ensure the vehicle comfort.
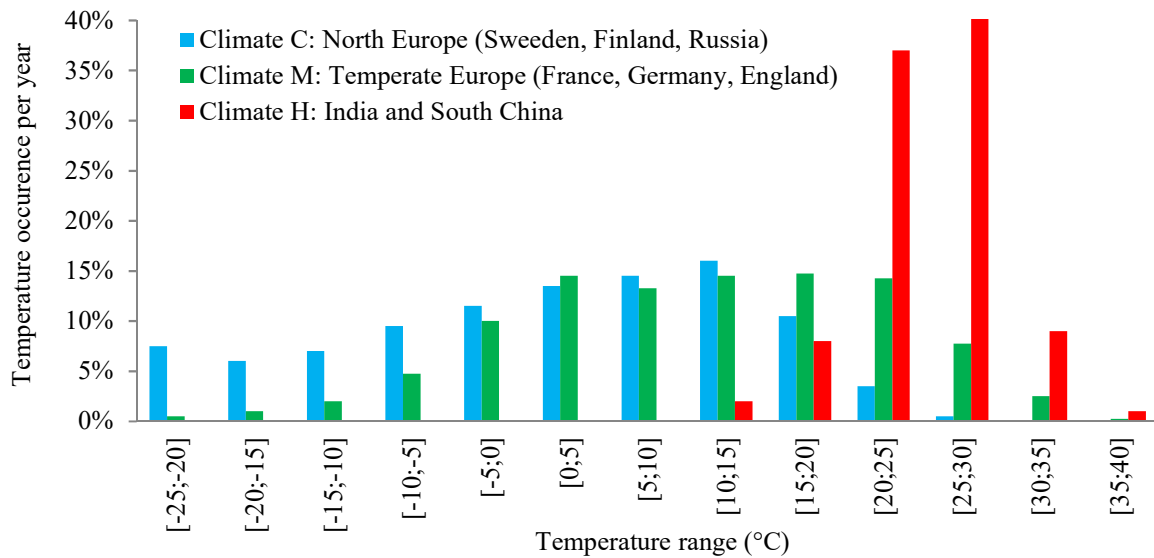

Fig. 2.6: Percentage of temperature occurrence for the investigated cold, moderate and hot climates [2.29].

2.3.2 Modified WTLC results

The final modified WLTC is shown in Figures 2.7 to 2.9 for the three climates defined. Note that this methodology adopted to derive the modified WLTC is generalizable and can be applied for different test procedures for drive cycles, climates, and vehicle classes.
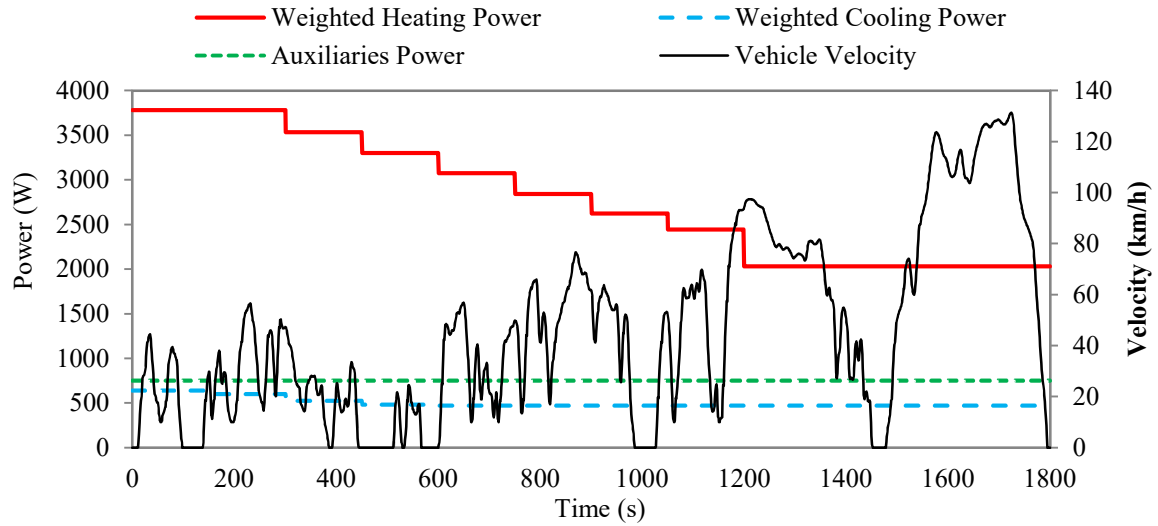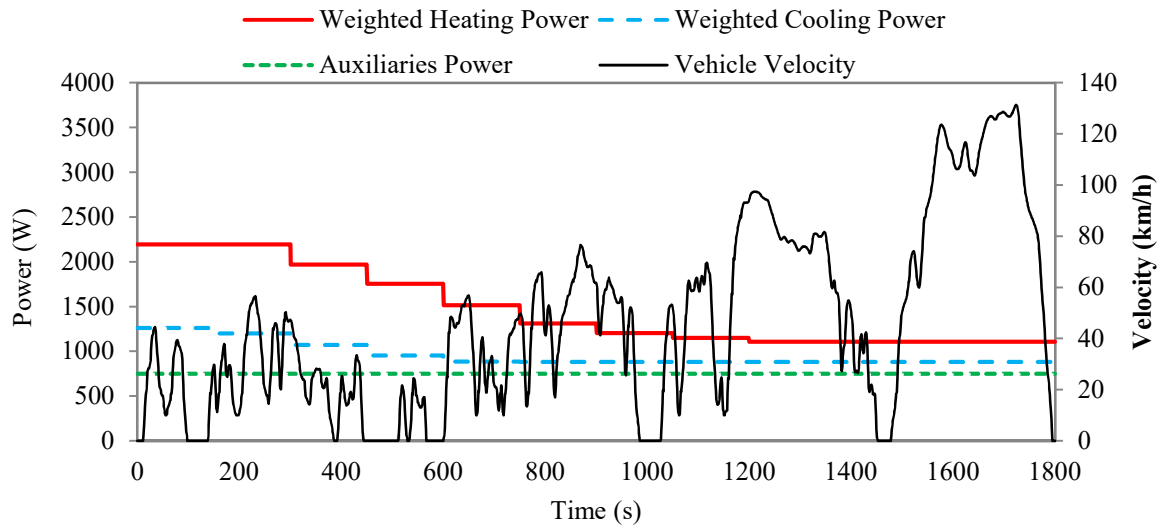
Fig. 2.7: Modified WLTC for cold climate.

Fig. 2.8: Modified WLTC for moderate climate.
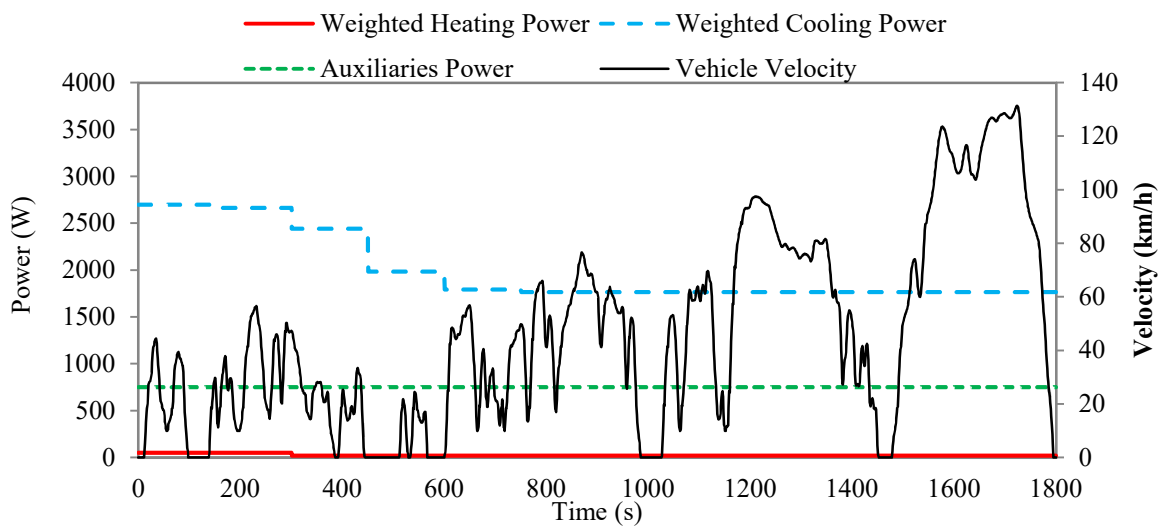

Fig. 2.9: Modified WLTC for hot climate.

2.4   Exergo-Technological Explicit Selection Method

This section presents the methodology adopted to evaluate the potential of GT-systems in SHEVs. It consists of two-steps assessment plan, as described in sections 2.2.1 and 2.2.2, and summarized in figure 2.10. The first assessment step consists of an energy and exergy analysis applied to the basic GT cycle, where the system efficiency, specific work, and exergy are calculated. Based on the resulting exergy destructions in the system, modifications of the basic GT cycle are presented, by considering several measures such as internal heat recovery and multi-stage compressions among others, in order to reduce exergy losses. Accordingly, the list of potential GT-system configurations is identified.

The energy and exergy calculations are then carried out in the second assessment step on all identified configurations. Components technological constraints and automotive design constraints are considered, and the optimal-realistic GT-system configuration for the SHEV application is selected. Components technological constraints such as the maximum TIT, the maximum compression ratio per stage and the maximum components' efficiencies are based on state-of-the-art data of available and newly developed technologies for automotive applications. However, automotive design constraints such as the number of compression and expansion stages, the power density and the number of heat exchangers are applied in order to simplify the system-integration complexity in vehicles.
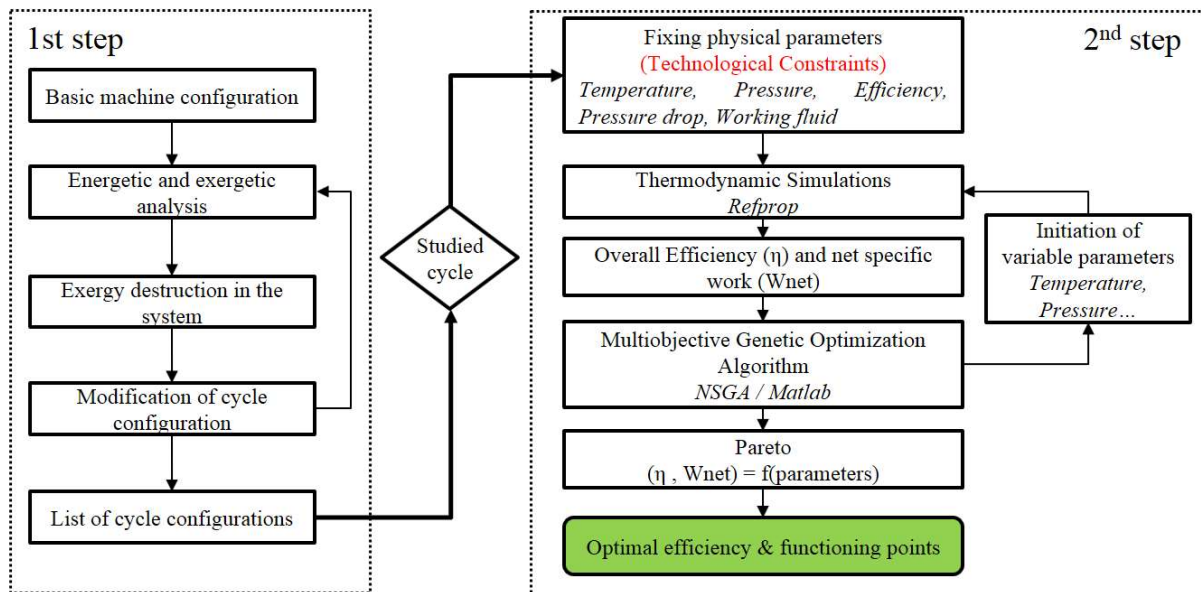
Fig. 2.10: Exergo-technological explicit selection method of the best-suited GT-system for SHEV

2.4.1   Energy and exergy analysis of simple gas-turbine system

In this section, the modeling of the basic Brayton GT cycle, which consists of a compressor, a combustion chamber and a turbine, is presented. First law of thermodynamics is applied to each component in order to deduce the cycle thermal efficiency and power density. The air is considered as the working fluid.

Fig. 2.11: Simple Gas turbine System (SGT)

The compressor and the turbine steady-state work are determined using equations 2.2 and 2.3, by neglecting the heat exchange with the surroundings and the variation in potential and kinetic energy between inlet and outlet of the components.

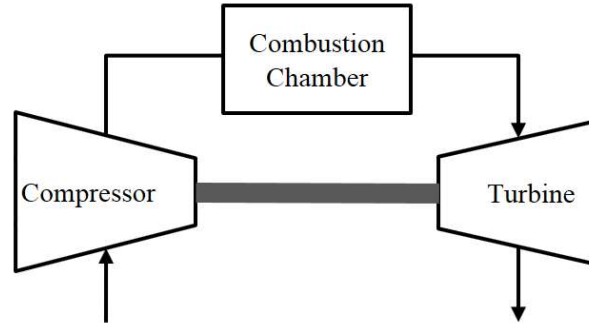$$w_{Compressor} = h_{C_{outlet}} - h_{C_{inlet}} \tag{2.2}$$

$$w_{Turbine} = h_{T_{outlet}} - h_{T_{inlet}} \tag{2.3}$$

With			
	$w_{Compressor}$	:	Compressor specific work in the GT loop (kJ/kg)
	$h_{C_{outlet}}$	:	Specific enthalpy at compressor outlet (kJ/kg)
	$h_{C_{inlet}}$	:	Specific enthalpy at compressor inlet (kJ/kg)
	$w_{Turbine}$	:	Turbine specific work in the GT loop (kJ/kg)
	$h_{T_{outlet}}$	:	Specific enthalpy at turbine outlet (kJ/kg)
	$h_{T_{inlet}}$	:	Specific enthalpy at turbine inlet (kJ/kg)

The heat added in the combustion chamber is computed using equation 2.4, while assuming air as the working fluid.

$$q_{CC} = h_{CC_{outlet}} - h_{CC_{inlet}} \tag{2.4}$$

With			
	q_{CC}	:	Specific heat added in the combustion chamber (kJ/kg)
	$h_{CC_{inlet}}$	:	Specific enthalpy at combustion chamber inlet (kJ/kg)
	$h_{CC_{outlet}}$	:	Specific enthalpy at combustion chamber outlet (kJ/kg)

The system energy efficiency $\left(\eta_{system}\right)$ is computed according to equation 2.5.

$$\eta_{system} = \frac{w_{Turbine} - w_{Compressor}}{q_{CC}} \tag{2.5}$$

Exergy analysis is then carried out in order to trace the work losses in the system, their types and quantities, in order to better inform on the possible options to reduce the inefficiencies. Energy and exergy model equations for each component are available in thermodynamic fundamentals books such as [2.30, 2.31].

$$e_{in} = [w_{CV}]_{in}^{out} + \left(e_{out}^{Q} - e_{in}^{Q}\right) + e_d + e_{out} \tag{2.6}$$

With			
	e_{in}	:	Specific exergy of the entering flow (kJ/kg)
	e_{out}	:	Specific exergy of the leaving flow (kJ/kg)
	$[w_{CV}]_{in}^{out}$	:	Net specific work output (kJ/kg)
	e_{out}^{Q}	:	Exergy of the heat rejected (kJ/kg)
	e_{in}^{Q}	:	Exergy of the heat added (kJ/kg)
	e_d	:	Exergy destruction in the system (kJ/kg)

The exergy destruction in the compressor and the turbine are determined using equations 2.7 and 2.8, assuming no heat exchange with the surroundings.

$$e_{d_{Compressor}} = w_{Compressor} - \left(e_{C_{outlet}} - e_{C_{inlet}}\right) \tag{2.7}$$

$$e_{d_{Turbine}} = \left(e_{T_{inlet}} - e_{T_{outlet}}\right) - w_{Turbine} \tag{2.8}$$

With			
	$e_{d_{Compressor}}$	:	Exergy destruction in the compressor (kJ/kg)
	$e_{C_{outlet}}$	:	Specific exergy at compressor outlet (kJ/kg)
	$e_{C_{intlet}}$	:	Specific exergy at compressor inlet (kJ/kg)
	$e_{d_{Turbine}}$	:	Exergy destruction in the turbine (kJ/kg)
	$e_{T_{inlet}}$	:	Specific exergy at turbine inlet (kJ/kg)
	$e_{T_{outlet}}$	:	Specific exergy at turbine outlet (kJ/kg)

The heat exchanger exergy destruction is determined using equation 2.9:

$$e_{d_{HEX}} = \left[\left(e_{Hot_{inlet}} - e_{Hot_{outlet}}\right) + \left(e_{Cold_{inlet}} - e_{Cold_{outlet}}\right)\right] \tag{2.9}$$

With			
	$e_{d_{HEX}}$	:	Exergy destruction in the heat exchanger (kJ/kg)
	$e_{Hot_{inlet}}$	:	Specific exergy at the inlet of the HEX hot stream (kJ/kg)
	$e_{Hot_{outlet}}$	:	Specific exergy at the outlet of the HEX hot stream (kJ/kg)
	$e_{Cold_{inlet}}$	:	Specific exergy at the inlet of the HEX cold stream (kJ/kg)
	$e_{Cold_{outlet}}$	:	Specific exergy at the outlet of the HEX cold stream (kJ/kg)

Finally, the exergy destruction calculations for the combustion chamber requires the use of Gibbs function value for fuel; however, it was substituted in this study by equation 2.10, where the average temperature in the combustion chamber is estimated from 2.11 [2.32, 2.33].

$$e_{d\_CC} = \frac{T_0}{\check{T}} \cdot \Delta Q_{CC} \tag{2.10}$$

$$\check{T} = \frac{\Delta Q_{CC}}{\Delta S_{CC}} = \frac{h_{CC,outlet} - h_{CC,inlet}}{S_{CC,outlet} - S_{CC,intlet}} \tag{2.11}$$

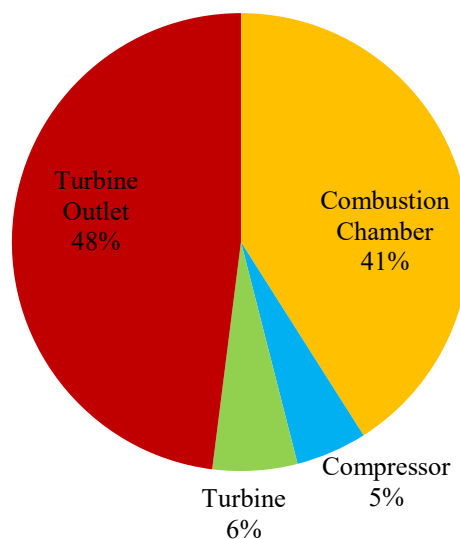| With			
	e_{d_CC}	:	Exergy destruction in the combustion chamber (kJ/kg)
	$\check{T}$	:	Average temperature in the combustion chamber (K)
	ΔQ_{CC}	:	Enthalpy difference in the combustion chamber (kJ/kg)
	ΔS_{CC}	:	Entropy difference in the combustion chamber (kJ/kg.K)
	T_0	:	Reference temperature (K)

Exergy destruction results of the investigated basic GT-system are illustrated in figure 2.12. The figure points out the two highest shares of exergy losses, occurring in the combustion chamber and the exhaust gas at the turbine outlet.

It was demonstrated in several studies [2.34-2.36] that the exergy destruction in the combustion chamber decreases as the average temperature increases. Accordingly, two ways can be considered to decrease these exergy losses: (1) increasing the TIT while respecting metallurgic constraints, and (2) increasing the average combustion temperature through a regenerator upstream of the combustion chamber.

As for the second major source of exergy destruction, losses from the exhaust gases at the turbine outlet to the ambient air can be recovered by adopting waste heat recovery systems. Two recovery options are applicable: (1) an external heat recovery system through a steam Rankine bottoming cycle, and (2) an internal heat recovery system, using a regenerator.

The exergy destruction shares of the compressor and turbine illustrated in figure 2.12 can be reduced by improving the efficiency of these components.

Fig. 2.12: Distribution of exergy destruction in the Brayton gas-turbine system with turbine inlet temperature of 1250°C and maximum cycle pressure of 1.2 MPa.

Based on these findings, the list of the different GT-system options considered in this study is presented below, based on the combination of the suggested techniques for exergy losses reduction as illustrated in figure 2.13. The considered GT-system options are as follow:

1. Regenerative GT (RGT)
2. Intercooled Regenerative GT (IRGT)
3. Intercooled Regenerative Reheat GT (IRReGT)
4. Isothermal Compression Regenerative GT (IcRGT)
5. Isothermal Compression Regenerative Reheat GT (IcRReGT)
6. Isothermal Compression Regenerative Isothermal Expansion GT (IcRIeGT)

Note that the efficiency and power density of the GT-system options 3 and 4 can be further improved if isothermal compression and expansion are considered. In fact, the isothermal compression maximizes the heat recovery process in the regenerator, and the isothermal expansion maximizes the expansion work [2.16, 2.36]. To this end, isothermal compressions are considered in IcRGT, IcRReGT and IcRIeGT and isothermal expansion in IcRIeGT (options 4 to 6). Although isothermal processes are technically difficult to achieve and remain currently theoretical, they are considered in this study for comparison purposes, and to emphasize their additional benefits. Nevertheless, many studies in the literature investigated technical options for getting close to isothermal processes such as reheat cycles [2.8], intercooling compression [2.17], isothermal combustion cycles [2.35] and cooling compression with water or liquid nitrogen [2.36].

Triple stage compressions were also considered in the analysis; however, results did not reflect substantial additional advantage compared to the dual stage compression. Therefore, due to the additional complexity in vehicle integration for little improvements, triple compression cycles were disregarded and only dual stage compressions are considered.

The exergo-technological explicit selection method was also applied for the combined cycle gas turbine (CCGT), the Stirling machines, the vapor cycle machines (VCM), the Brayton system as waste heat recovery system on ICE, and the external combustion gas turbine (ECGT) systems. These studies are presented in the annexes (2 to 7) of this thesis.
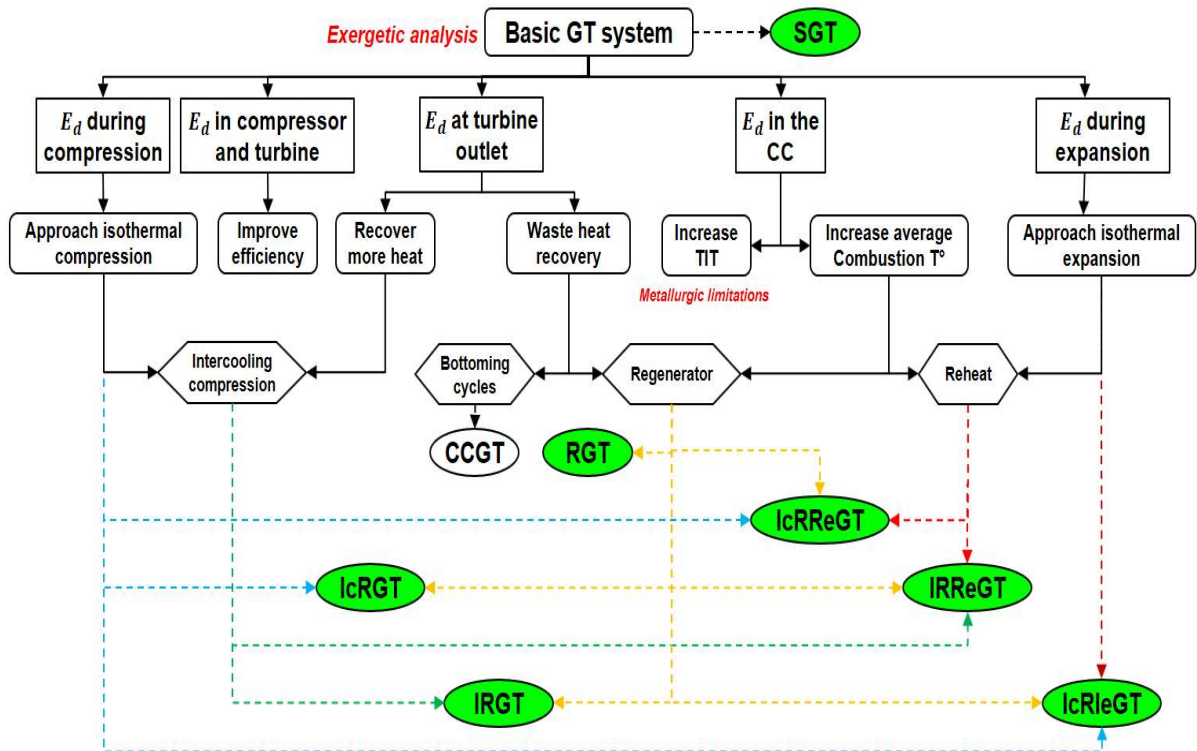

Fig. 2.13: Exergy assessment methodology for the identification of the GT-system options with reduced exergy losses in a basic GT-system.
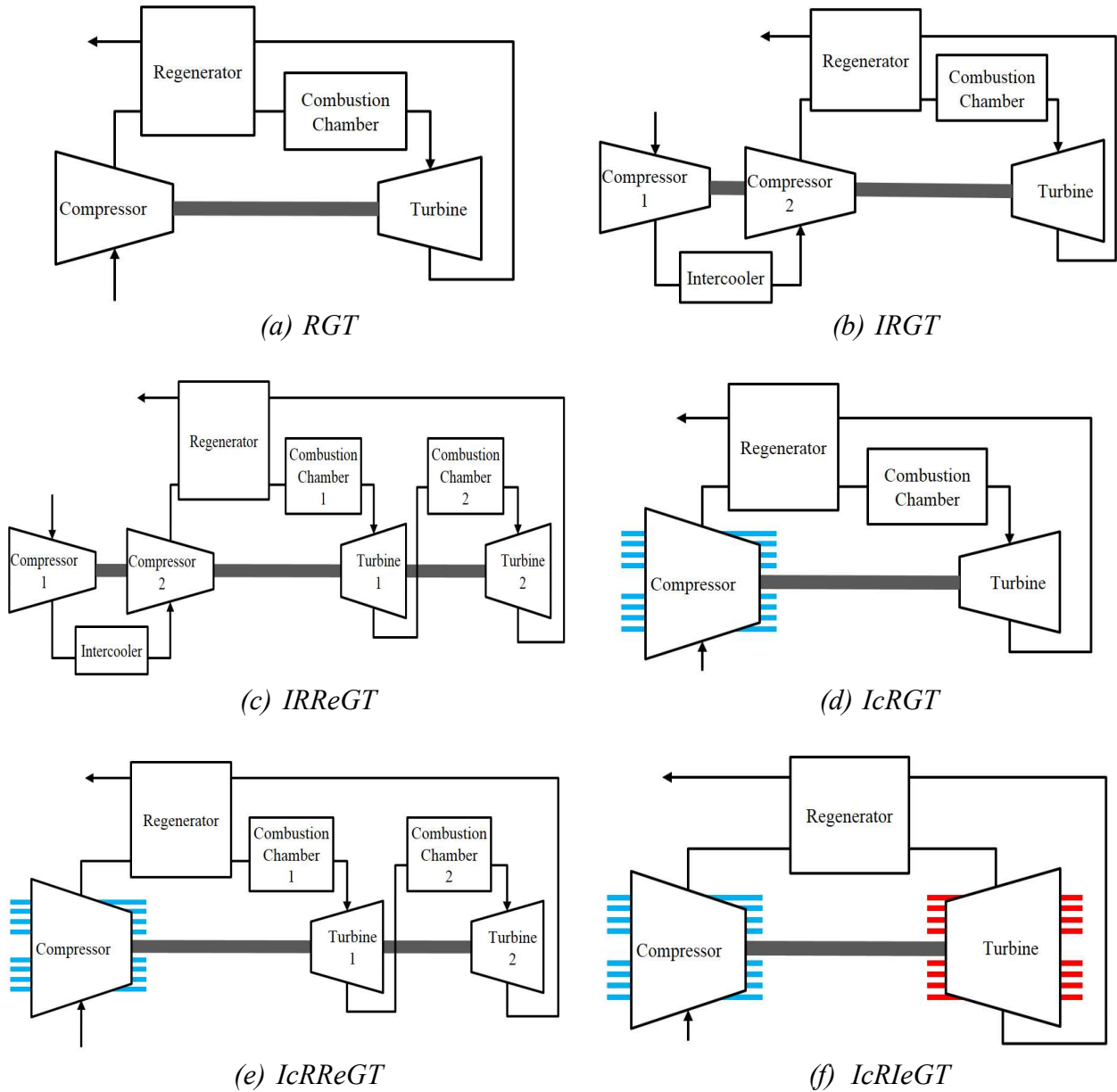
(a) RGT · *(b) IRGT*

(c) IRReGT · *(d) IcRGT*

(e) IcRReGT · *(f) IcRIeGT*

*Fig. 2.14: Thermodynamic configuration of the investigated GT systems*

2.4.2 Energy and exergy analysis of identified potential gas-turbine systems

The identified GT-system options of figure 2.14 are assessed here in order to prioritize these options based on their respective efficiency and net specific work, and select the most suitable configuration. The assessment methodology for each option is illustrated in figure 2.15. Energy and exergy calculations are performed first with Refprop software, using the set of physical parameters such as the TIT, the cycle pressure, the components efficiencies, among others; as summarized in table 2.1. These parameters correspond to the state-of-the-art specifications and limitations of GT component technologies and to automotive design constraints and are explained in details in chapter 3.

The energy and exergy calculations are made as function of two parametric design criteria: the compression ratio (π_i) and the expansion ratio (β_j), with i and j referring to the number of compressors and turbines respectively. Therefore, the second calculation step uses the NSGA multi-objective genetic algorithm to determine the Pareto optimal efficiency and net specific work solutions for the optimal (π_i) and (β_j) [2.37]. For the rest of the study, the comparison between the different GT-systems will be based on the best efficiency points on the Pareto curves. Therefore, the selection of the best-suited GT-system for SHEV will be made with respect to the highest efficiency among the compared systems.

Table 2.1: Simulation parameters based on state-of-the-art component specifications and automotive design constraints.

Parameter	Unit	Value	Parameter	Unit	Value
Compressor technology	-	Radial	Regenerator efficiency	%	85
Max number of compression stages	-	2	Regenerator pressure drop cold side	%	4
Compressor maximum pressure ratio	-	4	Regenerator pressure drop hot side	%	3
Compressors efficiency	%	80	Combustion chamber pressure drop	%	4
Compressor inlet pressure drop	%	0.5	Max number of expansion stages	-	2
Maximum cycle pressure	MPa	1.2	Turbine Inlet Temperature (TIT)	°C	1250
Intercoolers pressure drop	%	5	Turbines isentropic efficiency	%	85
Intercoolers outlet temperature	°C	60	Turbine expansion ratio	-	3.5
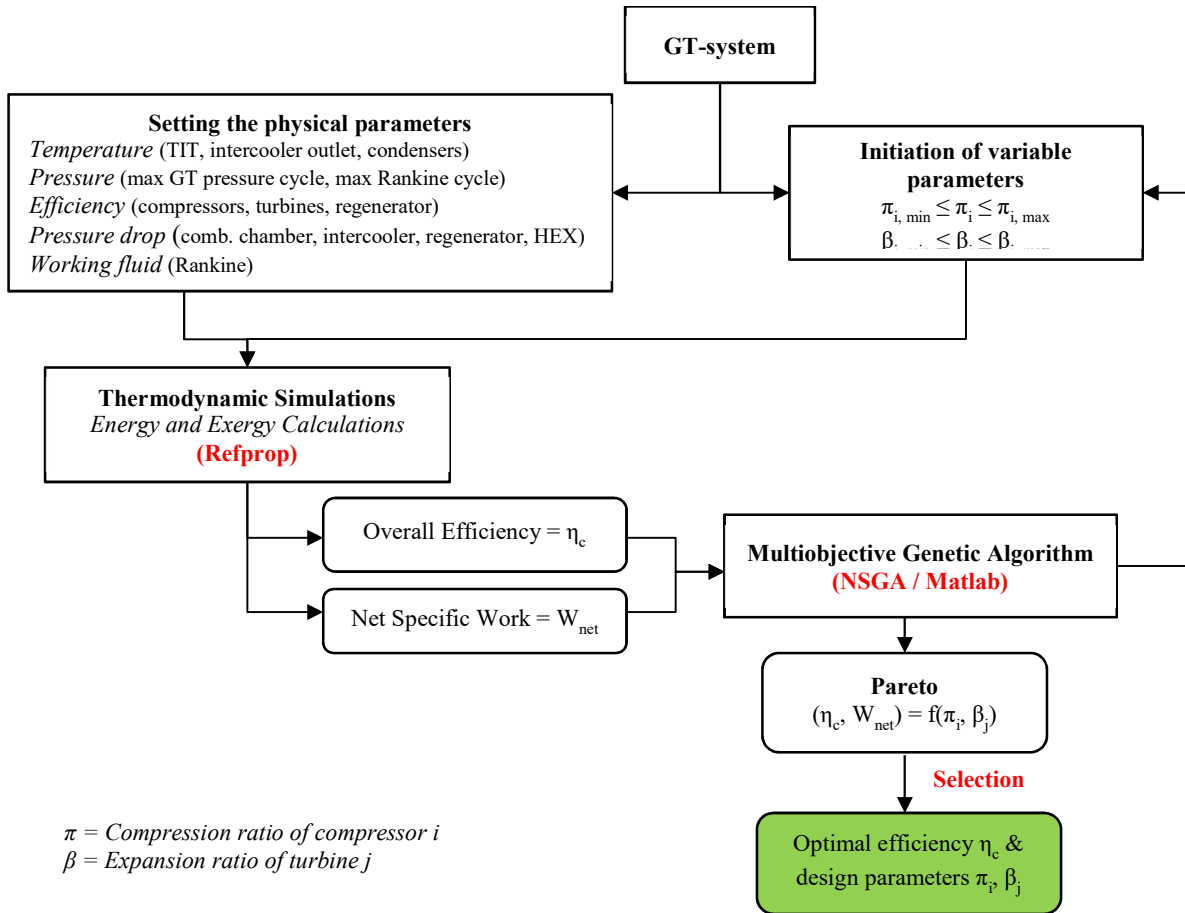
Fig. 2.15: Assessment methodology for the identification of the highest efficiency GT-system and its optimal design parameters.

Figure 2.16 presents the exergy losses for 1 kW of net mechanical power produced from the different considered GT-systems, operating at optimal efficiency.
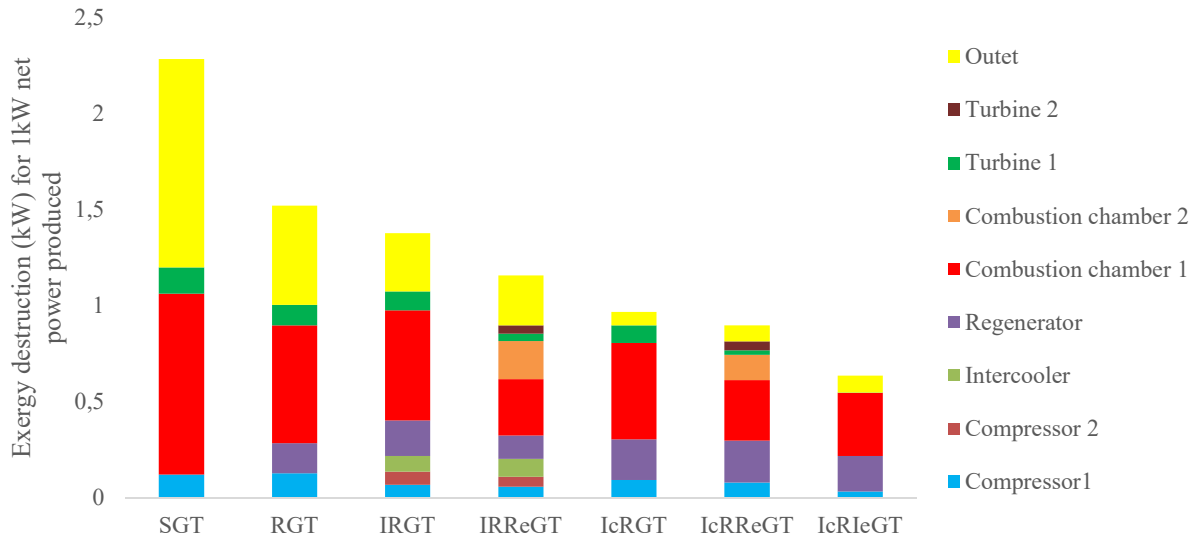

Fig. 2.16: Exergy destruction for 1 kW net power delivered from the different GT-systems.

The results with simple compression and expansion, confirm the results of figure 2.12, where the main exergy destructions of the SGT are in the combustion chamber and at the turbine outlet. Therefore, the RGT configuration considers adding a regenerator heat exchanger on the upstream of the combustion chamber in order to increase the combustion chamber inlet temperature and reduce the combustion chamber exergy destruction as compared to the SGT, since the average combustion chamber temperature has increased.

Also performing an intercooled compression reduce the compression exergy destructions at system outlet since more heat is recovered. For instance, the IRGT compared to RGT shows 41% less exergy destruction at outlet and around 9.5% of less total exergy destruction.

Reheat cycles in which a second combustion chamber is added, such as the IRReGT, allow reducing the total exergy destruction in the combustion chambers. For instance, the IRReGT and the IcRReGT show 14% and 11% less exergy destruction in the combustion chamber compared to IRGT and IcRGT respectively.

Note that the compressors and turbines present low exergy losses compared to the heat exchangers and combustion chambers. Therefore, this illustrates the importance of the proposed explicit methodology and the exergy analysis, since it emphasizes on the importance of improving the system configuration efficiency rather than improving the isentropic efficiency of only the compressors and turbines.

Based on the above exergy assessment findings, the GT-systems showing the lowest exergy destruction per 1 kW of net power produced will present the highest efficiency. This is reflected in the Pareto curves illustrated in figure 2.17, where the theoretical GT-systems using the

isothermal compression and expansion processes (IcRGT, IcRReGT and IcRIeGT) as well as the IRReGT present the highest efficiencies among the compared systems.
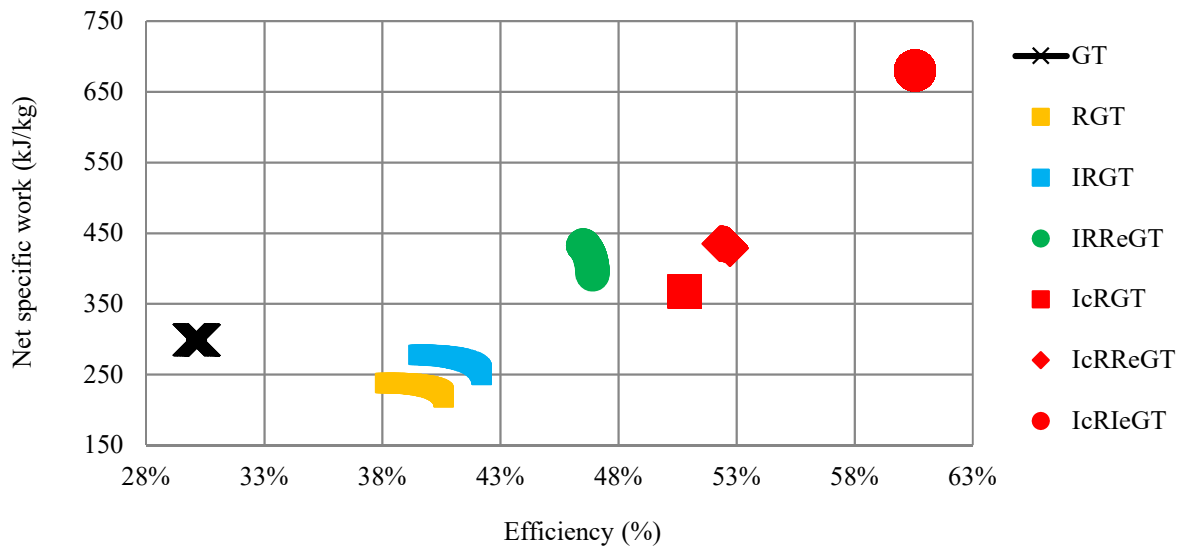

Fig. 2.17: Pareto optimal efficiency and net specific work solutions of the different GT-systems.

Figures 2.18 and 2.19 illustrate the efficiency, net specific work and optimal compression and expansion ratio simulation results of the investigated GT-systems, compared to the ICE. ICRIEGT presents the highest efficiency and net specific work; however, as discussed in the previous section, this cycle is not realistic for implementation in SHEV since it relies on isothermal compression and expansion. Consequently, the IRReGT, figure (2.14c) is the optimal-realistic GT-system considered for the rest of this study, which emulates the isothermal compression and expansion of IcRIeGT through a dual stage compression with an intercooler and a dual-expansion turbine with a reheat system.
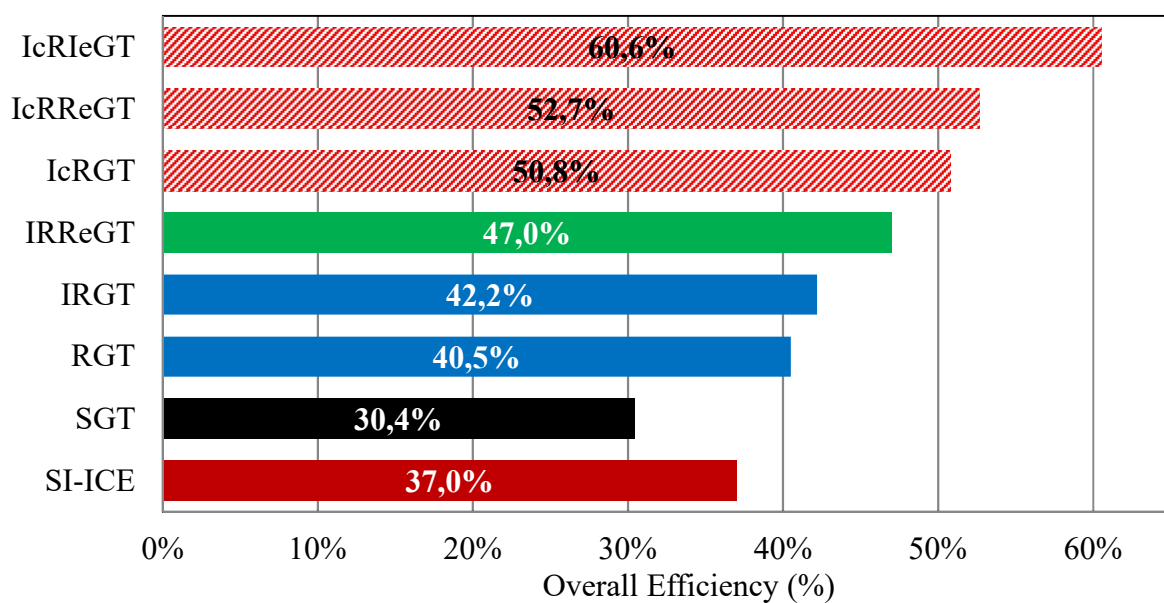

Fig. 2.18: Optimum efficiency comparison of ICE and the investigated GT-system options.
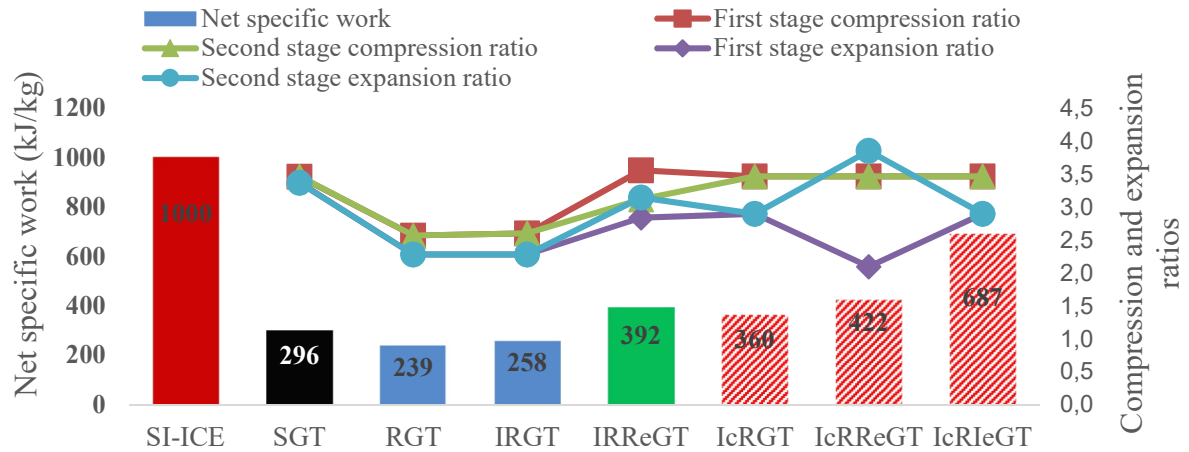
Fig. 2.19: Net specific work of ICE and the investigated GT-system at optimal efficiency.

2.5 Vehicle Model

In order to evaluate the benefits of the IRReGT-system in terms of fuel savings compared to ICE, a medium-class series hybrid vehicle, consisting of an IRReGT-APU and an electric traction system (figure 2.1) is modelled and presented in this section. Series configuration presents the advantage of tackling the two main deficiencies of GT-systems in automotive applications as discussed in the literature: the poor efficiency and the acceleration lag. On one side, the IRReGT operates in an SHEV at steady power corresponding to the optimum efficiency, which is higher than the maximum efficiency of ICE, as illustrated in figure 2.18. On the other side, the vehicle is propelled by an electric motor, powered by a battery and/or the APU, and properly sized to ensure the vehicle acceleration and velocity performance without deficiency. The first paragraph presents the methodology for SHEV powertrain component design and sizing and the second paragraph presents the powertrain components sizing.

2.5.1 Methodology

The powertrain design methodology is illustrated in figure 2.20 below. The vehicle dynamic longitudinal equations are applied on a medium class vehicle with predefined characteristics. The optimization cycle defined in section 2.1, the modified WLTC, is considered, and the average load power on the whole WLTC and on the city driving phase are accounted. Considering the additional energetic needs, which include the electric, heating and cooling needs, the energy converter maximum continuous power is calculated. Note that the thermal power rejected from the intercooler of the IRReGT must be evacuated through the vehicle frontal surface. The electric motor power is found by considering the vehicle performance criteria and by selecting the maximum among the following automotive constraints: (1) the vehicle maximum continuous speed, (2) the acceleration and (3) the gradability. Finally, the battery power is sized according to electric motor power and to the IRReGT power and the battery capacity is selected depending on the energy converter maximum power, as well as on the driving ranges mainly the full electric driving range in cities and on highway.
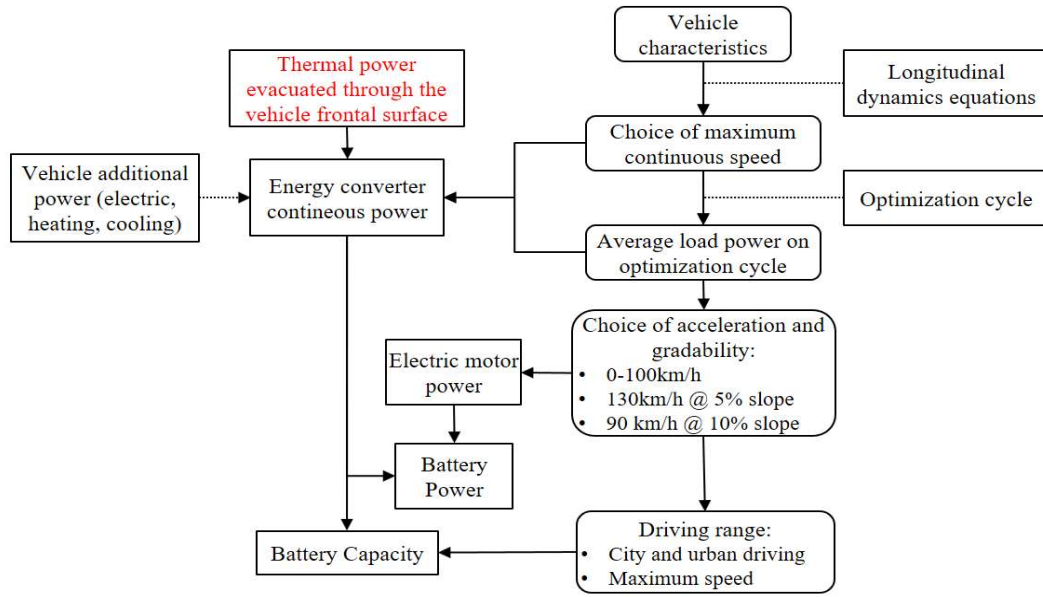
Fig. 2.20: Methodology for component powertrain design

2.5.2   Powertrain setup and components sizing

As described in the methodology section, the electric traction motor is sized in order to ensure similar performance to a medium class hybrid vehicle. The electric motor must ensure the required power to drive the vehicle at 90 km/h on a 10% slope, at 130km/h at 5% slope, to achieve a maximum speed maximum speed of 160 km/h, and to achieve an acceleration from 0-100 km/h in 9.6 s. The first three criteria are calculated using equation 2.13 which provides the required vehicle traction power as a function of aerodynamic parameters, rolling resisting force, inertial force, and vehicle velocity, while the equation 2.14 computes the $P_{m_{acc}}$, the tractive power required to accelerate the vehicle from zero to V_f in t_a seconds. Note that V_b is the vehicle velocity corresponding to the motor base speed.

$$P_{load}(t) = \left(\frac{1}{2}\rho SC_x v(t)^2 + M_t gf_r\big(v(t)\big)\cos(\theta) + M_t gsin(\theta) + (M_t + M_e).\frac{dv(t)}{dt}\right) \times v(t) \qquad (2.13)$$

$$P_{m_{acc}} = \frac{M_t}{2t_a}\left(V_f^2 + V_b^2\right) + \frac{2}{3}M_t gf_r V_f + \frac{1}{5}\rho C_x S V_f^3 \qquad (2.14)$$

With			
	M_v	:	Vehicle weight (kg)
	M_e	:	Equivalent mass of rotational components (kg)
	a_v	:	Vehicle acceleration (m/s²)
	θ	:	Slope angle
	f_r	:	Friction rolling coefficient
	g	:	gravity (m/s²)
	ρ	:	Air density (kg/m3)
	S	:	Vehicle frontal area (m²)
	Cx	:	Vehicle drag coefficient
	v	:	Vehicle velocity (m/s)
	t	:	Time (s)

The APU is used to ensure the battery sustainability under specific driving conditions. Hence, the IRReGT and the electric generator are sized taking into consideration urban stop-and-go patterns and highway-driving patterns. The urban stop-and-go patterns are represented in this study by the WLTC, and the average load power is computed using equation 2.15, where the P_{IRReGT} presents the IRReGT-system average power required to maintain the battery energy sufficiently sustained under stop-and-go urban-driving patterns. Note that t_c corresponds to the driving cycle time length.

$$P_{IRReGT} = \frac{1}{\eta_g}\left(\frac{1}{t_c}\int_0^{t_c}\left(M_t g f_r + \frac{1}{2}\rho_a C_x S V^2\right)V dt + \frac{1}{t_c}\int_0^{t_c}M_t\frac{dV}{dt}dt\right) \qquad (2.15)$$

The highway-driving pattern is emulated as driving for a long distance at the maximum velocity of 160 km/h without the need of the battery support. Equation 2.16 computes the continuous power required from the GT-system in order to maintain the vehicle cruising for long distance at a certain speed V on highway without the support of the battery.

$$P_{IRReGT} = \frac{1}{\eta_g}\left(\frac{V}{\eta_t \eta_m}\cdot(M_t g f_r + \frac{1}{2}\rho_a C_x S V^2)\right) \qquad (2.16)$$
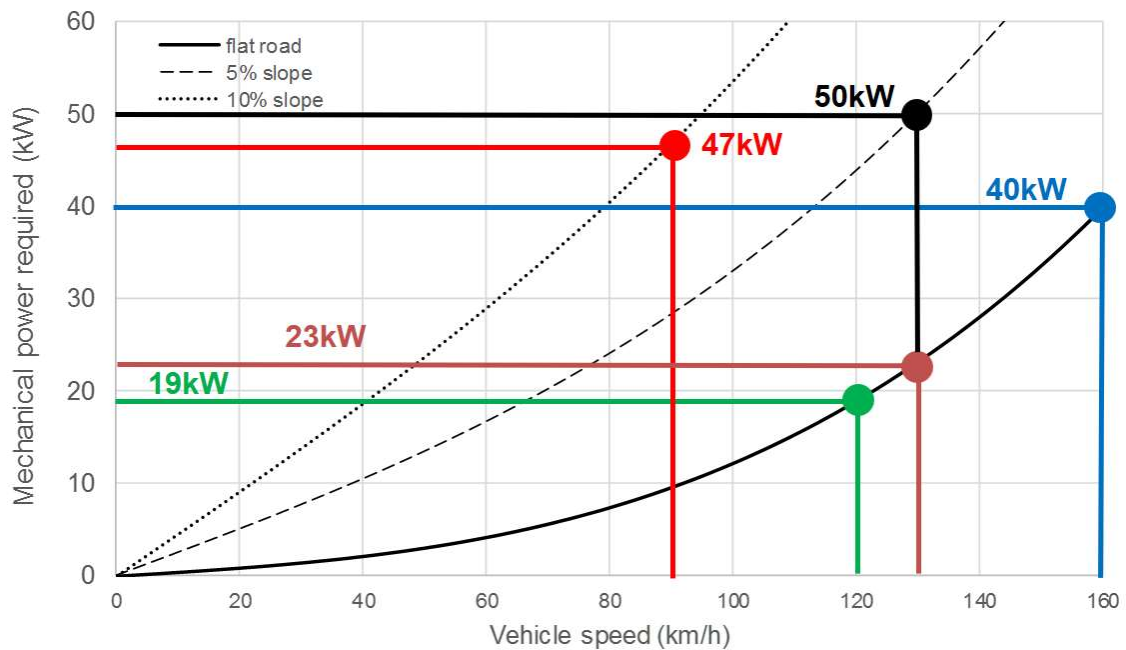

Fig. 2.21: Mechanical power required to drive the vehicle and different constant speed and on slope road of 5% and 10%.

According to equation 2.14, around 80 kW tractive power is needed to accelerate the vehicle from 0 to 100km/h. According to figure 2.21 and equation 2.16, 40 kW is required to maintain the vehicle at a maximum speed of 160 km/h without depleting the battery. Also around 47kW is required to drive the vehicle at 90 km/h on a 10% slope compared to around 50kW at 130km/h at 5% slope. Consequently, the selected electric traction motor power is 80 kW. Note that 23kW

is required to maintain a constant speed of 130km/h on flat road compared to 19kW at 120km/h on flat road. Also, an average power of 10.4 kW is required on the WLTC.
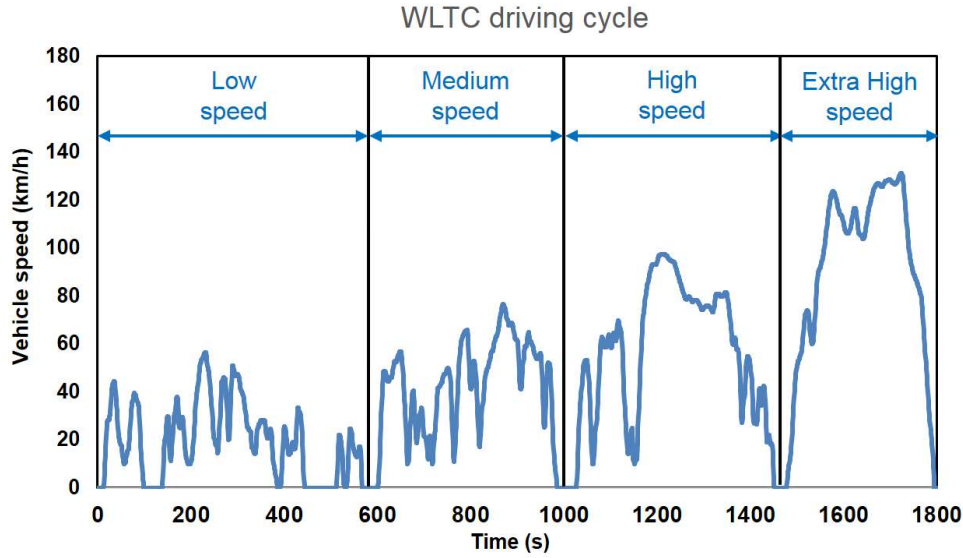

Fig. 2.22: WLTC driving cycle

Considering a continuous auxiliaries electric power of 750W, and a 95% electric generator efficiency, an IRReGT with 25kW net mechanical power is selected. It allows a continuous speed at 130km/h without depleting the battery. It is worthy to mention that for this selected power, around 8kW of thermal power are evacuated from the vehicle frontal surface through the intercooler. This thermal power requires less surface than actual vehicle radiator which rejects an amount of thermal heat almost equal to the net mechanical power produced.

As for sizing the battery, power and capacity have to be considered. Under any driving conditions, the battery must provide sufficient traction power, with the support of the APU under extreme power demand. Consequently, battery maximum power required to propel the vehicle under any driving patterns is sized with respect to the electric motor maximum power and the APU power, using equation 2.17. A 70 kW battery is therefore considered.

$$P_b \geq \frac{P_{m_{max}}}{\eta_m} - P_{GT}\eta_g \tag{2.17}$$

As for the electric driving range, a 50km of autonomy is required for running in cities. Considering the 1.75kW additional vehicle non-mechanical power required (750W electric and 1000W thermal power) and the driving average speed of 25km/h on low speed part of WLTC cycle which require an average of 2.75kW of mechanical power, around 10kWh battery is required when considering an initial battery state of charge (SOC) of 80% and a final SOC of 30%. The additional battery mass is taken into account and values were retrieved from commercialized battery specifications [2.38].

Based on the above, table 2.2 summarizes the vehicle parameters needed for modeling the IRReGT-APU-SHEV and the ICE-APU-SHEV.

Equations (2.13) and (2.18) to (2.26) present the powertrain backward model. The model calculates the power needs for traction, electric consumption and cabin thermal comfort in order to derive the final energy consumption of the vehicle. Equation 2.18 provides the traction and braking power of the electric motor using the efficiencies of the motor and the transmission.

$$P_m(t) = \begin{cases} \dfrac{P_{load}(t)}{\eta_t \times \eta_m}, & \dfrac{dv}{dt} \geq 0 \\[2em] P_{load}(t) \times \eta_t \times \eta_m, & \dfrac{dv}{dt} < 0 \end{cases} \tag{2.18}$$

Table 2.2: Vehicle and components specifications.

Vehicle specifications	Symbol	Unit	Value
Vehicle mass (including driver)	M_v	kg	1210
Frontal area	S	m²	2.17
Drag coefficient	C_x	-	0.29
Wheel friction coefficient	f_r	-	0.0106
Air density	ρ	kg/m3	1.205
Wheel radius	R_w	m	0.307
Acceleration 0-100km/h	ta	s	9.6
Auxiliaries consumption	P_{aux}	W	750
Battery maximum power	$P_{b\ max}$	kW	70
Battery capacity	C_b	kWh	10
Battery mass	M_b	kg	259
IRReGT-system power	P_{GT}	kW	25
IRReGT efficiency	η_{GT}	%	47
ICE maximum power	$P_{ICE,max}$	kW	97
ICE maximum efficiency	$\eta_{ICE,max}$	%	37
Generator maximum power	P_g	kW	45
Generator maximum efficiency	η_g	%	95
Motor maximum power	P_m	kW	80
Motor maximum efficiency[1]	η_m	%	93
Transmission ratio	i	-	5.4
Transmission efficiency	η_t	%	97
Vehicle total mass	M_t	kg	$M_v + M_b$
Fuel heating value	H_v	MJ/kg	42.5
[1] The model includes a torque-speed efficiency map of the electric motor.			

The APU controller monitors the battery state of charge (SOC) by controlling the APU operations in order to maintain the SOC in the desired range. Equation (2.19) calculates the power provided by the IRReGT-APU when the GT is on, where $u(t)$ is the APU on/off control variable (0 for off, 1 for on):

$$P_g(t) = u(t) \times P_{GT} \times \eta_g \tag{2.19}$$

For the ICE, when the APU is turned ON, the APU controller manages the engine speed control variable $u_1(t)$ and the engine torque control variable $u_2(t)$ as presented in equation 2.20 in order to operate the APU at the optimum efficiency. The engine is allowed to operate at any

point of its performance; consequently $u_1(t)$ ranges between 0 and the maximum allowed speed of the engine, while the $u_2(t)$ ranges between 0 and the engine maximum torque.

$$P_{ICE}(t) = u_1(t) \times u_2(t) \tag{2.20}$$

$$P_g(t) = P_{ICE} \times \eta_g \tag{2.21}$$

Equations 2.22 provides the battery power consumption which depends on the power of the electric motor power, the auxiliaries, the electric heater and the air-conditioning, supplemented by the APU power when on.

$$P_b(t) = P_m(t) + P_{aux}(t) + P_{heater}(t) + P_{A/C}(t) - P_g(t) \tag{2.22}$$

$P_{A/C}(t)$ is given by Equation 2.23, where COP is the coefficient of performance of the HVAC cooling system (considered to be equal to 1.5 [2.39, 2.40]) and $\eta_{m,c}$ the electric compressor efficiency (90%).

$$P_{A/C}(t) = \frac{P_{cooling}(t)}{\eta_{m,c} \times COP} \tag{2.23}$$

Note that the auxiliaries draw constant power, and the cooling and heating power are as derived in Section 2. Therefore, the electric consumption can now be calculated by Equation (2.25):

$$I_b(t) = \frac{V_{oc}(SOC(t)) - \sqrt{V_{oc}^2(SOC(t)) - 4P_b(t)R_i(SOC(t))}}{2R_i(SOC(t))} \tag{2.25}$$

Where SOC is given by Equation (2.26):

$$SOC(t) = SOC_i(t) + \frac{1}{C_b} \int_{t_0}^{t} I_b(t)dt \tag{2.26}$$

Finally, the vehicle fuel consumption is found by Equation (2.27) and (2.28) for both GT-APU and ICE-APU respectively:

$$\dot{m}_f(t) = \begin{cases} \dfrac{P_{GT}(t)}{\eta_{GT} \times H_v}, & APU: ON \\ 0, & APU: OFF \end{cases} \tag{2.27}$$

$$\dot{m}_f(t) = \begin{cases} \dfrac{P_{ICE}(t)}{\eta_{ICE} \times H_v}, & APU: ON \\ 0, & APU: OFF \end{cases} \tag{2.28}$$

Note that longitudinal dynamics of the chassis are only considered on flat roads. It is also noteworthy to mention that the mass of the GT-system, the generator and the electric motor are considered equal to the mass of the engine and its accessories. In fact, it was presented in [2.18, 2.23] that the power density of a 75kW GT-system combined to a generator and a 90 kW electric motor is in the range of 375 W/kg, slightly better than the 350 W/kg of the considered ICE in this study.

2.6 Energy Management Strategy

Two distinct controllers are considered in the model as illustrated in figure 2.1: the vehicle controller and the APU controller. The vehicle controller is in charge of meeting the driver request in terms of performance. Hence, its main objective is to control the electric motor power in order to meet the traction and brake energy recovery demand. The APU controller monitors the battery SOC; thus, it controls the APU operations in order to maintain the SOC in the desired range. Therefore, for the GT energy converter, an on/off variable $u(t)$ is considered in equation 2.18 in order to control the APU start operations. $u(t)$ takes the value of 0 for APU-off and 1 for APU-on. For the ICE, two control variables are considered, the engine speed $u_1(t)$ and the engine torque $u_2(t)$ respectively as in equation 2.20.

Dynamic programming (DP) is considered in order to provide the global optimal strategy to control the APU operations. It decides on the optimal strategy $U_{opt} = \{u(1), \dots, u(N)\}_{opt}$ for the scheduled route at each instant t while minimizing the fuel cost function J presented in equation 2.29 for the GT-APU and 2.30 for the ICE-APU. Consequently, DP computes backward in time from the final desired battery state of charge SOC_f to the initial SOC_i the optimal fuel mass flow rate in the discretized state time space as per equations 2.29 and 2.30.

$$J = min\left\{\sum_{t=1}^{N} \dot{m}_f\big(SOC(t), u(t)\big) \times dt_s\right\} \tag{2.29}$$

$$J = min\left\{\sum_{t=1}^{N} \dot{m}_f\big(SOC(t), u_1(t), u_2(t)\big) \times dt_s\right\} \tag{2.30}$$

with	discrete step time:	$dt_s = 1$	(2.31)
	number of time instances:	$N = \frac{n}{dt_s}$ (with n the time length of the driving cycle)	(2.32)
	state variable equation:	$SOC(t+1) = f\big(SOC(t), u(t)\big) + SOC(1)$	(2.33)
	initial SOC:	$SOC(1) = SOC_i$	(2.34)
	final SOC:	$SOC(N) = SOC_f$	(2.35)
	SOC constraint:	$SOC(t) \in [0.2, 0.9]$	(2.36)
	battery power constraint:	$P_{b_{min}} \leq P_b(t) \leq P_{b_{max}}$	(2.37)
	motor torque constraint:	$P_{m_{min}}\big(\omega_m(t)\big) \leq P_m(t) \leq P_{m_{max}}\big(\omega_m(t)\big)$	(2.38)
	motor speed constraint	$0 \leq \omega_m(t) \leq \omega_{m_{max}}(t)$	(2.39)
	generator power constraint:	$P_{g_{min}}\big(\omega_m(t)\big) \leq P_g(t) \leq P_{g_{max}}\big(\omega_m(t)\big)$	(2.40)
	generator speed constraint:	$0 \leq \omega_g(t) \leq \omega_{g_{max}}(t)$	(2.41)

Note that the resulting optimal APU on/off strategy U_{opt} must not cause the components to violate their relevant physical boundary constraints in terms of speed, power or SOC, in order to ensure their proper functioning within the normal operation range. These constraints are included in the DP model and summarized in equations 2.31 to 2.41. It is also noteworthy to mention that using DP as APU energy management strategy excludes the impact of rule-based energy management strategy currently used on hybrid vehicles on the consumption. Consequently, the obtained fuel consumption results with DP are only dependent on the investigated energy converter and its efficiency.

2.7 Results and discussion

Two different SHEV configurations are compared in this section: the suggested IRReGT-APU and a reference ICE-APU. The IRReGT-APU is designed to operate at its optimal operating point and delivers 25 kW of mechanical power. The ICE-APU uses a 1.2 liters spark ignition engine with maximum efficiency of 36%. During APU operations, the ICE is allowed to operate at any point of its torque-speed map. The maximum efficiency zone corresponds to a power between 18 and 26kW as shown in figure 2.23.

The potential of fuel savings of the IRReGT-APU compared to the ICE-APU was simulated over a sequence of one to ten-repeated WLTC driving cycles (23 km each) covering driving distances up to around 230 km. Simulations emulate the behavior of plug-in hybrids EREV with the option of battery charging from the grid and self-sustaining SHEV. For the plug-in, the initial SOC is set at 80% and the final SOC at 30% by the end of the trip. For the self-sustaining, the initial SOC is equal to the final SOC of 60%. Simulations are performed on a baseline scenario similar to current fuel consumption on standard regulatory drive cycles where only propulsion energy needs are accounted, and four additional scenarios accounting for different cooling, heating and electric consumption needs. In all scenarios considered, the electric auxiliaries draw constant energy from the battery, and the cooling needs are ensured by the A/C system driven by the electric compressor using energy from the battery.
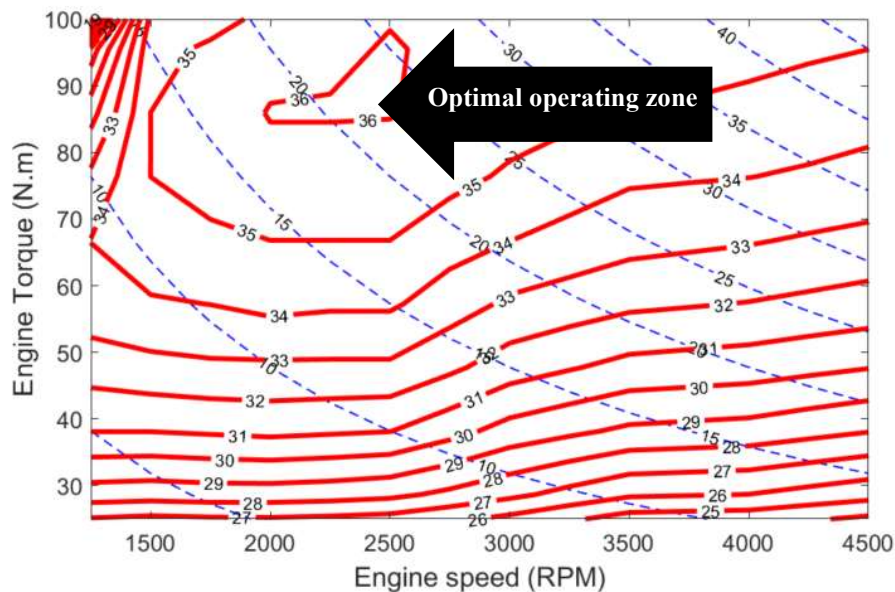

Fig. 2.23: ICE efficiency (red line) and net power (bleu line) function of engine speed (RPM) and engine torque (N.m)

The heating needs are normally ensured by waste heat when the energy converter (EC), the ICE or the IRReGT, is on. When the EC is off, other means are needed to heat the cabin. In the considered scenarios, two options are included: storing excess waste heat when the EC is on, to be used later for heating the cabin when the EC is off; or, an electric heater where electricity from the battery powers a resistance to heat the air:

- Baseline: Only mechanical propulsion needs
- Scenario 1: Baseline + continuous electric auxiliaries needs of 750W
- Scenario 2: Scenario 1 + cabin cooling ensured by A/C + heating ensured by stored waste heat
- Scenario 3: Scenario 1 + cabin cooling ensured by A/C + cabin heating ensured by electric heater when EC is off, or by waste heat when EC is on
- Scenario 4: Scenario 1 + cabin cooling ensured by A/C + cabin heating needs always ensured by electric heater

Figures 2.24 and 2.25 show the fuel consumption as a function of the different considered scenarios for different climates for the plug-in and the self-sustaining configurations. Several conclusions can be drawn from the simulation results.

First, it is clear that the fuel consumption under each of the four scenarios, which consider cabin thermal and vehicle electric needs, is notably higher than the baseline for all climates considered. This means that despite the introduction of the new WLTC, the current industry estimates for fuel consumption still under estimate the real-world driving consumption. Second, it is clear that the fuel consumption of self-sustaining SHEV is higher than the plug-in SHEV. In fact, in the self-sustaining configuration, the electric energy consumed from the battery is zero, and the powertrains rely only on the energy converter, therefore, higher amount of fuel is consumed to ensure the powertrain energetic needs.

In scenario 1, the vehicle electric needs increase the fuel consumption by 31% and to 12.5% on one to 10 repeated WLTC respectively with IRReGT-APU and by 33% to 12.6% on one to 10 repeated WLTC respectively with ICE-APU, regardless of climate condition since the electric consumption is assumed to be constant. The increase in fuel consumption decreases as the travelled distance increases. This shows that the electric consumption of auxiliaries should not be neglected, and it would be beneficial to explore ways to reduce this consumption on-board.

In scenario 2, the cabin cooling needs provided by the AC system have considerable negative effect on fuel consumption especially in hot climates, increasing by about 0.74 L/100km with IRReGT-APU and by 0.95L/km with ICE-APU compared to scenario 1. Therefore, the cooling needs need to be accounted for in consumption assessments.

In scenario 3, the cabin heating needs increase the fuel consumption by about 0.9 to 1 L/100km with GT-APU and 0.6 to 0.9 L/100km with ICE-APU for the cold climates and that despite the use of waste heat recovery from the engine when operating. The moderate climate shows less increase in fuel consumption as well as for the hot climate. This shows that, similar to cooling, the heating needs also need to be considered in consumption assessments.
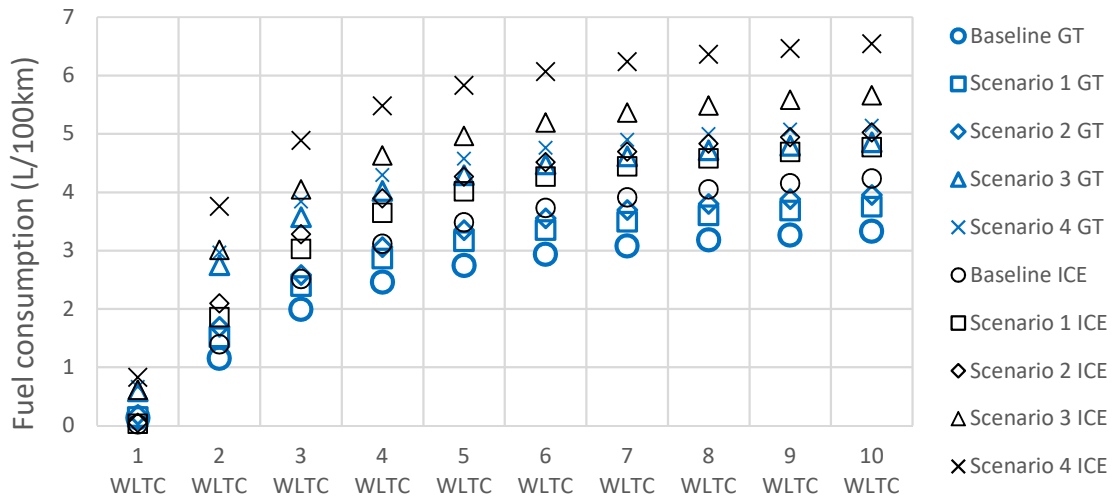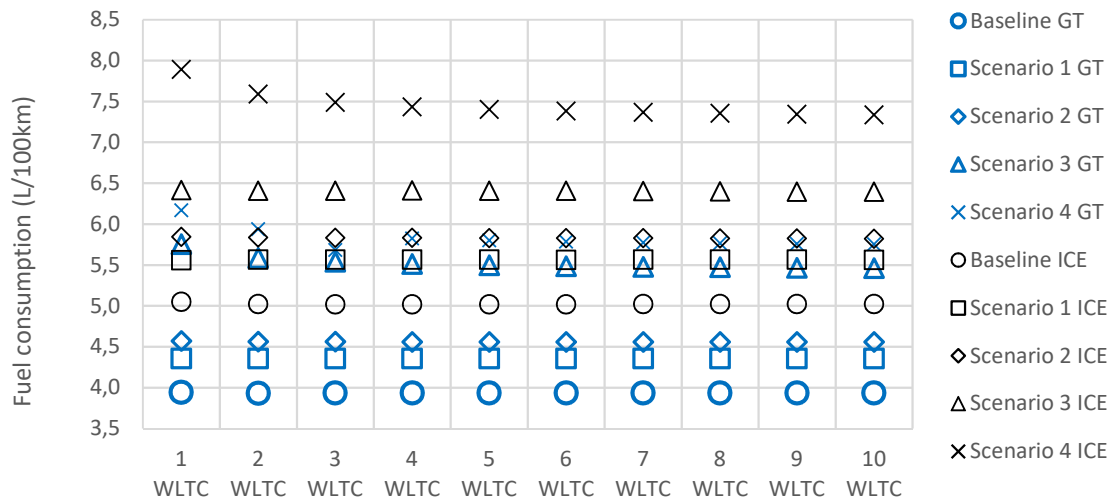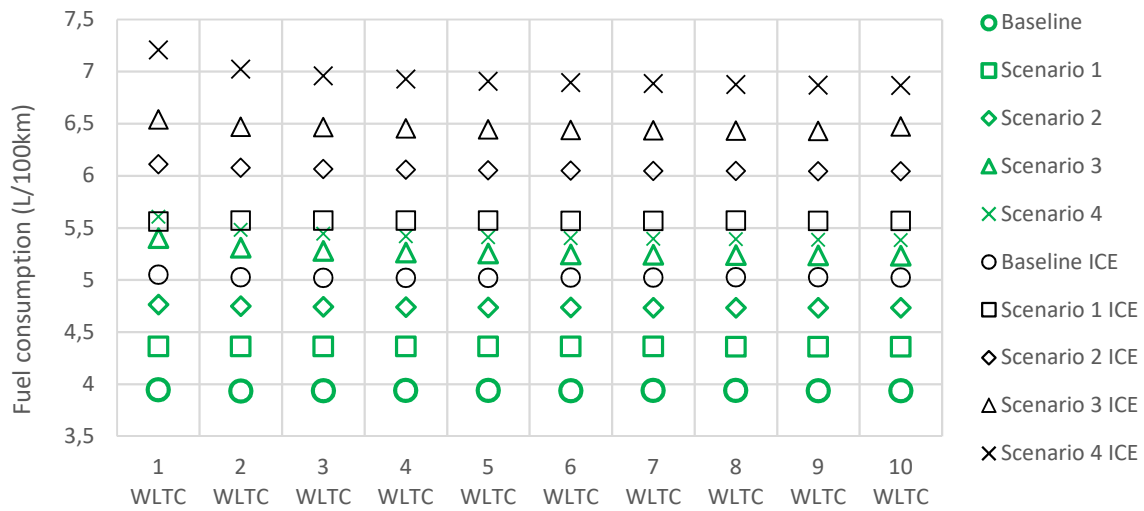
(a) Cold climate
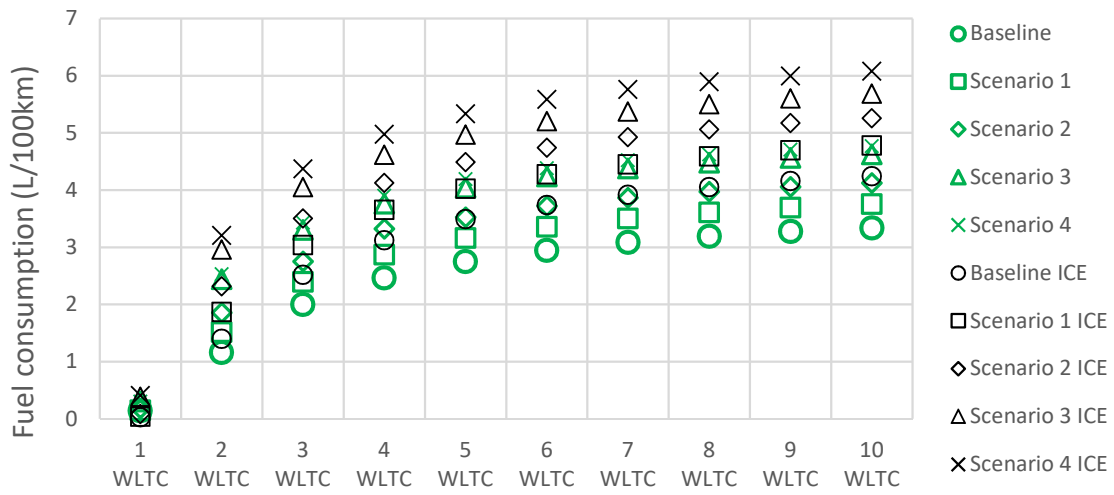
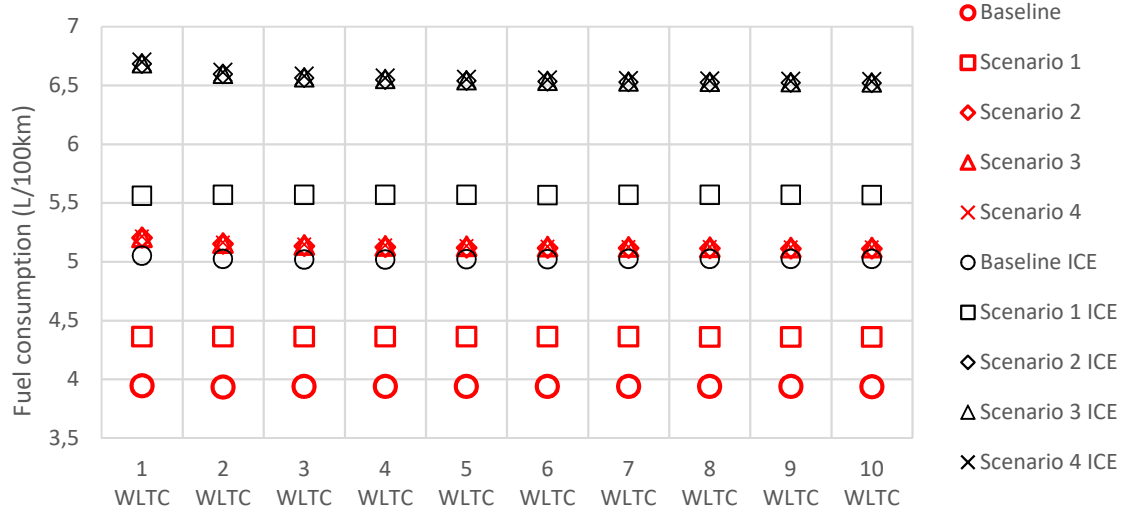*(b) Temperate climate*
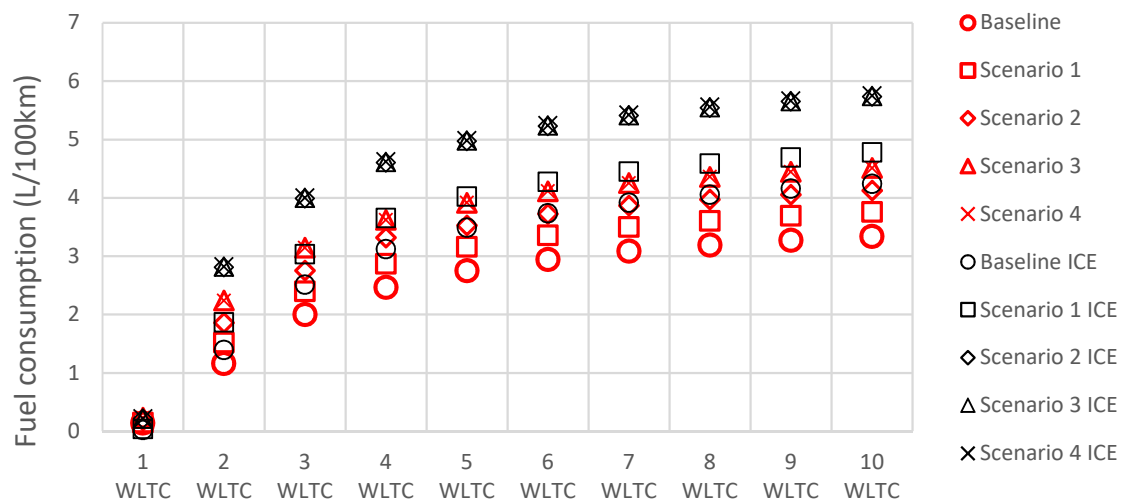
(c) Hot climate

Fig. 2.24: Fuel consumption simulation results of the modelled plug-in EREVs under the three investigated climates.

(a) Cold climate

(b) Temperate climate

(c) Hot climate

Fig. 2.25: Fuel consumption simulation results of the modelled self-sustaining EREVs under the three investigated climates.

In scenario 4, the cabin heating needs significantly affect the fuel consumption, especially in cold climates. This is due to the reliance on the battery to power the heater, which requires the engine to operate longer in order to charge the battery, without any recovery of its waste heat. This highlights, from an energy standpoint, the performance challenges currently faced by electric vehicles in cold climates in terms of range and consumption.

Higher fuel consumption is observed in the ICE-APU SHEV model compared to IRReGT-APU. Assuming the same driving cycle length d, consequently, improving the APU efficiency induces a decrease in fuel consumption, as expressed in 2.42 where $E_{b_{traction}}$ is the battery electric energy consumption to overcome the vehicle traction load, E_{ber} the the vehicle load energy recovered through regenerative braking, E_{fuel} the energy of the consumed fuel and E_{grid} the consumed electric energy from the grid to recharge the battery.

$$\frac{E_{b_{traction}}}{d} = \frac{1}{d}\left(E_{ber} \times \eta_m + E_{fuel} \times \eta_{APU} + E_{grid} \times \eta_{charging}\right) \qquad (2.42)$$

Accordingly, the IRReGT-APU performs more efficiently than the ICE-APU in SHEV.

Comparing between figures 2.24 (a), (b) and (c) and 2.25 (a), (b) and (c), it is noteworthy to mention that the fuel consumption of the plug-in SHEV configuration converges toward the fuel consumption of the self-sustaining model as the driving cycle length d exceeds increases. In fact, when d tends to infinity, the battery energy consumption ($E_{b_{traction}}$) to overcome the traction load in SHEV configuration expressed in equation 2.42 could be simplified by eliminating the term (E_{grid}/d), and therefore, $E_{b_{traction}}$ tends to the battery consumption of the self-sustaining configuration.

Finally, comparing the fuel consumption results between the IRReGT-APU and the ICE-APU, around 22% of fuel savings are observed on SHEV on the different WLTC sequence. As detailed above, these savings are explained by the higher operating efficiency of the IRReGT since it was constrained to operate at its optimal efficiency of 47%. Although the ICE was not constrained to operate at one operating point, results showed that ICE operation was at the optimal operating line (OOL) where the efficiency remains between 35 and 36%, almost at its maximum efficiency of 36%.

2.8   Conclusion and perspectives

This chapter presents the methodology for the choice and optimization of gas turbine energy converter system for series and extended range hybrid electric vehicles.

The study starts by assessing additional sources of consumption not currently accounted for in regulatory drive tests, such as passengers' thermal comfort and auxiliary electric needs in order to reduce the consumption gap between real world driving conditions and regulatory driving tests, and to define an optimization cycle on which GT and ICE fuel consumption are compared. Hence, the chapter starts by presenting a framework for assessing the impact of cabin cooling

and heating, in addition to electric auxiliary needs on vehicle consumption on the WLTC under different climate conditions. To that end, a methodology was presented to generate the average heating and cooling power profiles as function of the ambient external temperature. Three climate conditions were considered (hot, moderate and cold) for that purpose. Constant electric power consumption was assumed representing the average auxiliary consumption in modern vehicles. The outcome from this approach is a modified WLTC combining the generated power profiles with the WLTC drive cycle, thereby combining the vehicle thermal comfort and auxiliary needs with the required mechanical power to drive the vehicle.

Then, an exergo-technological explicit method considering energy and exergy analysis, as well as components and automotive technological constraints was applied to identify the suitable GT-system for series hybrid vehicle applications. The Intercooled Regenerative Reheat Gas Turbine (IRReGT) was prioritized. It offers the best combination of high efficiency and net specific work compared to the investigated realistic GT-systems and to conventional internal combustion engines. A series hybrid electric vehicle was modeled and the IRReGT-APU and ICE-APU energy converters were simulated and compared in term of fuel consumption on the modified WLTC using the DP optimal control as APU management strategy.

Simulation results showed that the electric consumption of auxiliaries should not be neglected since an auxiliary's load of 750 W causes more than 12% increase in fuel consumption on an SHEV depending on the travelled distance. Similarly, cabin thermal comfort needs significantly affect the fuel consumption. Furthermore, when heating is done solely by electric heaters without heat recovery from the engine, the additional consumption almost equals the fuel consumption needed for traction. Therefore, relying on waste heat recovery from the engine to heat the cabin in cold climates can be very beneficial for reducing the fuel consumption. Therefore, it is necessary to account for cabin thermal comfort and auxiliary needs in vehicle consumption estimation under regulatory drive tests, which will allow for closing the gap with real world driving performance. Results also highlighted that the IRReGT-system on SHEV configuration offers about 22% of fuel consumption savings compared to similar ICE on SHEV configuration. This is due to operating the GT at higher efficiency compared to ICE.

In addition to the fuel savings, the IRReGT-system offered other intrinsic automotive advantages such as reduced mass compared to ICE, suitable vehicle integration as well as multi-fuel use capability, which makes it a potential energy converter option for implementation on series hybrid powertrains in the future.

This methodology for identification of potential thermodynamic cycle configuration of GT-systems have been applied also in this thesis work for other energy converters. Among them: (1) the ICE coupled to Brayton waste heat recovery system, (2) the Split Cycle Engine, (3) the Combined Cycle Gas Turbine System, (4) the External Combusiton Gas Turbine System, (5) the Stirling machine, (6) the thermoacoustic machine and (7) the vapor cycle machines.

The different studies have been presented in the papers listed in the annexes 2 to 7. The potential realistic thermodynamic configuration of these different machines, identified through the exergo-technological explicit selection method are presented in figures 2.26 to 2.32.

Figure 2.34 shows the optimal efficiency and the fuel consumption on self-sustaining SHEV on WLTC on basic scenario for the different identified energy converter using DP as global optimal strategy.
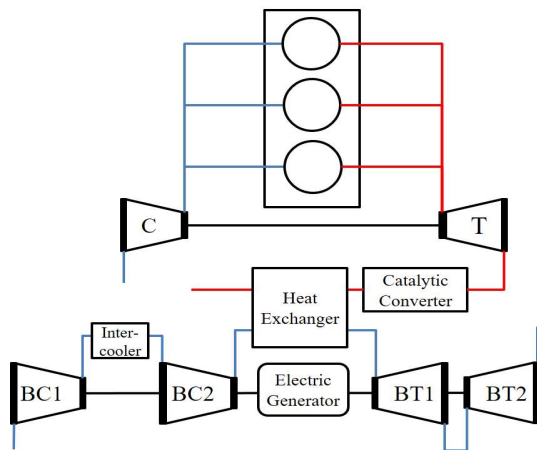

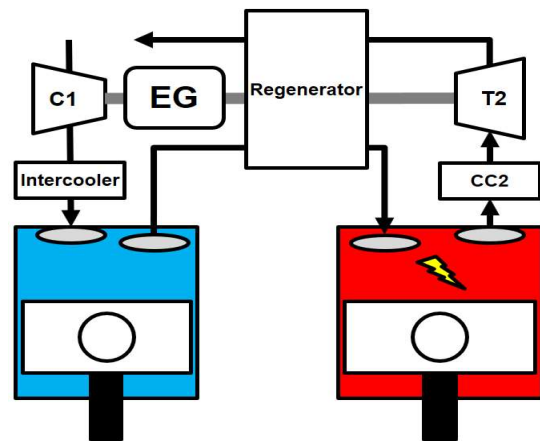Fig. 2.26: ICE coupled to Intercooled Brayton WHR

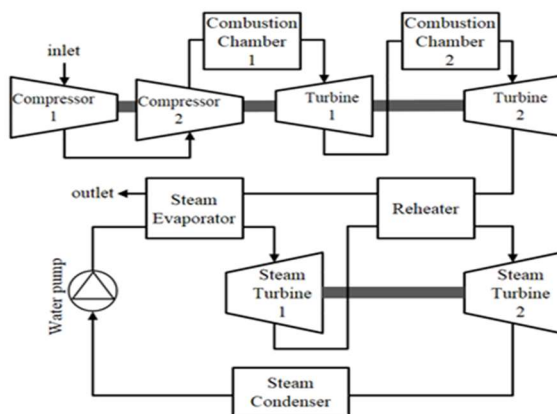Fig 2.27: Regenerative Reheat Split cycle Engine (RRe-SCE)

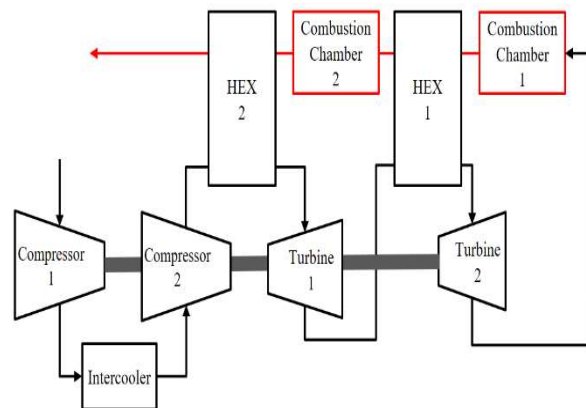Fig. 2.28: Reheat GT with Turbine Reheat Steam Rankine cycle (ReGT-TReSRC)

Fig 2.29: Downstream Intercooled Reheat External Combustion GT (DIRe-ECGT)
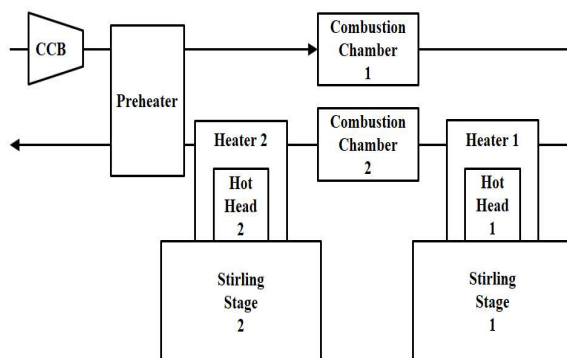

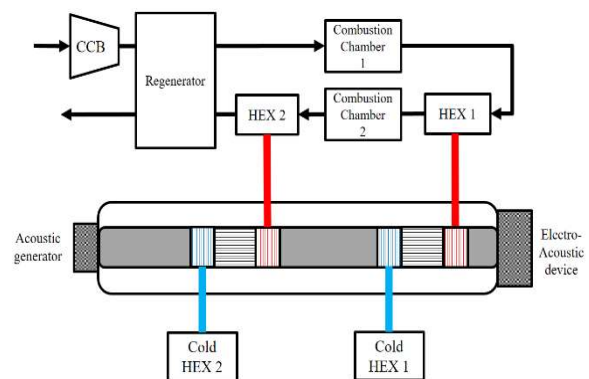Fig. 2.30: Regenerative Reheat Stirling (RRe-Stirling)

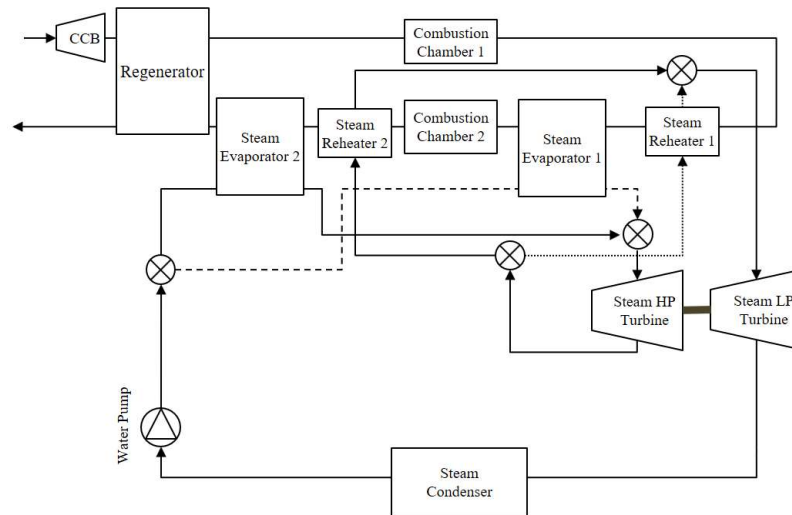Fig 2.31: Regenerative Reheat Thermoacoustic machine (RRe-TA)

Fig. 2.32: Regenerative Reheat Turbine Reheat Steam Rankine Cycle (RReTRe-SRC)

The graph shows that the higher the efficiency, the lower the fuel consumption. However, simulations were performed considering an energy converter weight equal to the ICE one without any pre-design to approach the realistic system weight. Also, the control strategy is optimal and not realistic since the number of switching ON and OFF was not constrained.
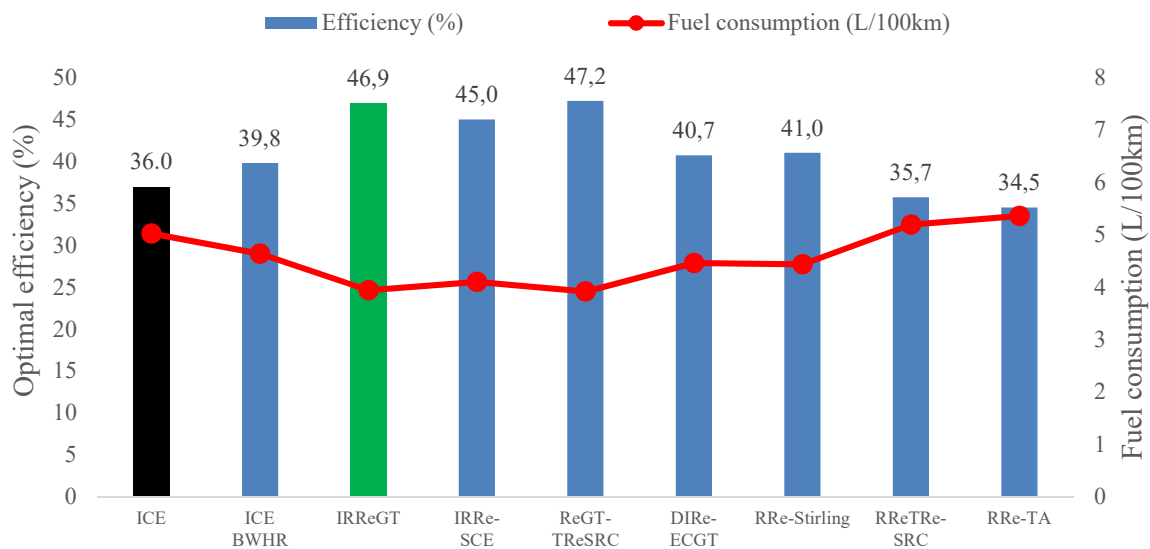
Fig. 2.33: Energy converters efficiency and fuel consumption simulated on SHEV

Therefore, in order to justify the choice of the IRReGT as best suitable GT-system for SHEV, and to approach the real vehicle fuel consumption while considering the weight of the energy converters, the methodology presented in this chapter will be further elaborated in the next one. A technological and pre-design analysis of the different realistic GT-systems (SGT, RGT, IRGT and IRReGT) identified through the exergo-technological explicit selection method will be carried out, and the weight of the different realistic configurations will be accounted for. The fuel consumption will be simulated on the modified WLTC and on all the defined scenarios while considering a bi-level control energy management strategy to approach the real fuel consumption by constraining APUs' number of switching ON and OFF.

Résumé chapitre 3

Les turbines à gaz font partie des convertisseurs d'énergie potentiels pour remplacer le moteur thermique à combustion interne comme groupe auxiliaire de puissance (APU) ou prolongateur d'autonomie dans les futurs véhicle à groupes motopropulseurs électriques hybrides série (SHEV). La consommation de carburant de ces systèmes, dans ces chaînes de traction, dépend fortement du rendement du convertisseur d'énergie, du rapport puissance/poids ainsi que de la stratégie de gestion de l'énergie déployée à bord.

Ce chapitre présente une analyse technologique et examine le potentiel d'économies de consommation de carburant d'un véhicule à chaîne de traction hybride série utilisant différentes configurations thermodynamiques du système turbine à gas. Ces configurations comprennent une turbine à gaz simple (GT), une turbine à gaz régénérative (RGT), une turbine à gaz régénérative à refroidisseur intermédiaire (IRGT) et une turbine à gaz régénérative à refroidissement intermédiaire et réchauffage intermédiaire (IRReGT).

Une analyse énergétique et technologique est effectuée pour identifier l'efficacité et le rapport puissance/poids des systèmes pour différentes températures de fonctionnement. Un modèle de véhicule hybride série est développé et les différentes configurations de systèmes turbines à gas sont intégrées en tant que groupes auxiliaires de puissance. Une méthode d'optimisation à deux niveaux est proposée pour optimiser le groupe motopropulseur. Elle consiste à coupler l'algorithme génétique (NSGA) à la programmation dynamique (DP) afin de minimiser la consommation de carburant et le nombre de démarrages de la machine, ce qui a un impact sur sa durabilité.

Les simulations de consommation de carburant sont réalisées sur le cycle d'homologation (WLTC) tout en considérant les besoins énergétiques additionnels du véhicule tels que le confort thermique et le besoin électrique à bord. Les résultats montrent que l'IRReGT comme prolongateur d'autonomie présente une consommation de carburant améliorée par rapport aux autres systèmes de turbine à gas étudiés et un bon potentiel d'implémentation dans les véhicules à chaîne de traction hybrides séries.

Chapter 3: Technological analysis of different GT-system thermodynamic configurations as auxiliary power unit for automotive powertrain applications*

3.1 Introduction

Gas turbine (GT) systems are among potential energy converters for integration in future hybrid electric vehicle (HEV) powertrains. This thermodynamic machine has been largely investigated by different automotive companies over the years as a main energy converter, substitute to internal combustion engines (ICE) prime mover in conventional powertrains [3.1-3.5]. Automotive manufacturers were attracted by many GT intrinsic benefits, among them the reduced number of engine components and rotating parts compared to ICE, the reduced vibration as well as the multi-fuel capability [3.1].

However, GT-systems in conventional powertrains suffered from two main drawbacks: (1) the high fuel consumption due to operating the GT at low efficiency zone during important portions of the vehicle driving patterns, mainly during city driving, and (2) the acceleration lag problematic due to the coupling of the GT mechanically to the vehicle wheel [3.1]. Today, with the development of range extender hybrid electric vehicles (EREV) and series hybrid electric vehicle (SHEV) powertrains, GT-systems have gained interest. In fact, these two powertrains tackle the two main deficiencies of GT systems in automotive mentioned above [3.6-3.9]. On the one hand, GT-systems can be designed to operate at their optimal efficiency point and drive an electric generator (EG) where both GT and the EG constitute the auxiliary power unit (APU) which role it is to recharge the battery once it is depleted. On the other hand, the vehicle is propelled by an electric motor (EM) designed to achieve the vehicle performances in terms of acceleration, speed and gradability.

From a practical point of view, the integration of a new energy converter in automotive environment is a complex process requiring the respect of many vehicle criteria and constraints such as the cost, the size, the weight, the energy consumption, the emission and the durability among others. Some of these criteria are interdependent. For instance, reducing the EC weight decreases the vehicle fuel consumption [3.10, 3.11] by reducing the mechanical propulsion energy demands. Also, reducing the vehicle frontal surface by reducing the energy converter components size, such as the radiator in the case of the ICE or the proton-exchange membrane fuel cell (PEMFC) [3.12, 3.13], reduces the vehicle fuel consumption by reducing the aerodynamic drag resistance power. Furthermore, it is obvious that increasing the EC efficiency reduces the fuel consumption since less amount of fuel is burnt for the same EC output power required. Finally, increasing the efficiency of GT thermodynamic system can be achieved by increasing the maximal turbine inlet temperature (TIT) [3.14]. This will require the use of specific component materials, leading to higher GT final cost [3.15].

Many gas turbine system configurations can be integrated in EREVs and SHEVs ranging from simple gas turbine (SGT), to regenerative gas turbine (RGT), to intercooled regenerative gas turbine (IRGT) and intercooled regenerative reheat gas turbine (IRReGT) among others [3.16-3.19]. Paper [3.5] shows that for these configurations, the efficiency which impacts the vehicle fuel consumption and the net specific work which impacts the GT components size and weight,

This chapter is written in the form of a scientific paper that will be published later. Therefore some informations are redundant with chapter 2 mainly in the « introduction » section (3.1) and in the « Energetic analysis » section (3.3).

113

and consequently the vehicle fuel consumption, depend on the turbine maximum inlet temperature (TIT) as well as on the components' physical characteristics, among them the component efficiencies and pressure drops. Adding to that, the non-mechanical energetic needs such as the vehicle electric auxiliaries and cabin thermal comfort needs can affect the vehicle total fuel consumption. For instance, it was demonstrated in paper [3.20], that in cold climate conditions, the cabin hot thermal energetic needs can increase the fuel consumption by 40%. Therefore, considering the EC thermal waste heat as a potential source for thermal comfort, is an intelligent way to reduce the real customer fuel consumption.

Based on these findings, and in order to assess the fuel consumption potential of GT-systems in automotive applications, this chapter proposes a pre-design study on the different GT-system realistic configurations identified in chapter 2.

A methodology for assessing the fuel consumption potential of GT-systems in automotive applications is presented in section 2. For each of the identified GT-system configuration, thermodynamic simulations are carried out in order to account for the overall efficiency (η) and the net specific work (W_{net}) while considering state-of-the-art component specifications. The non-dominated sorting genetic algorithm (NSGA) is used to plot the pareto solution for efficiency and net specific work depending on component physical parameters and for three operating TIT: TIT=950°C emulating a machine with low cost materials, TIT=1100°C emulating a machine with specific alloys materials and TIT=1250°C emulating a machine with super-alloys and/or ceramic materials.

In order to account for the power to weight ratio for different operating temperature for the different GT-configurations, different GT net power are selected and the mass flow rate across the different components as well as the components' power is accounted for. A study is carried out on different existing automotive turbochargers in order to establish a relation between component weight, power and mass flow rate. Then a pre-design of the heat exchangers (HEXs), including the intercoolers and the regenerators was carried out in order to account for the HEX weight for each configuration and operating temperature. The total GT weight is calculated and the GT-system power to weight ratio for each configuration is estimated. Then an SHEV powertrain is modelled and the different GT-system configurations are integrated in this powertrain. A bi-level optimization process is proposed and consists of two combined optimization algorithms: a genetic algorithms (GA) and the Dynamic Programming (DP). Dynamic programming (DP) is used as optimal energy management strategy (EMS) in order to find the optimal way to well manage the vehicle power flows while respect component constraints. The bi-level optimization minimizes two objective functions : the fuel consumption vehicle criteria and the number of ON/OFF switching of the APU which impact its durability. Simulations are performed on WLTC optimization cycle and considering the vehicle additional non-mechanical energetic need such as the electric energetic need and the thermal comfort energetic needs.

This study is novel in three ways. First it is the first study to consider the integration of different GT-system configurations in SHEV and to evaluate the fuel consumption while considering different GT operating temperatures and different GT-system power to weight ratio. Second, it is the first study that includes the GT On/Off switching in the APU operation optimization process. Third, it provides a comparative fuel consumption assessment between different

SHEVs using different GT-APU configurations and ICE-APU while considering the vehicle electric energetic needs and the thermal comfort energetic needs.

3.2 Methodology

This section presents the methodology adopted to evaluate the potential fuel consumption savings of different GT-systems in SHEV. The methodology consists of four-step assessment plan as illustrated in figure 3.1 and described in the following subsections.

The first assessment step consists of an energy analysis applied on different realistic GT-system configurations identified in chapter 2, where the system efficiency and the net specific work are calculated. The technological constraints and the automotive design constraints of the components are considered. For instance, the compressors' maximum compression ratio, the turbines' maximum expansion ratio and the components' efficiency are taken into account. These specifications are based on the state-of-the-art data of available systems as well as on newly developed technologies for automotive applications.

In the second assessment step, the different GT components weight are assessed for different GT-systems net mechanical power knowing the net specific work at optimal efficiency operating point for each GT-system configuration. The turbomachines weights, including the compressors and the turbines were estimated by performing an analysis on automotive commercialized turbochargers. Related data were retrieved from the literature and from turbocharger supplier catalogues. As for the heat exchangers, a pre-design was conducted on two types of HEX: a water-air plate-fins HEX for the intercooler and an air-air plate fins HEX for the regenerator. The combustion chamber's weight was estimated based on 3D computer aided-design of an existed GT combustion chamber and by establishing a relation between the gas mass flow rate across the physical existing CC and the different GT-system combustion chambers. The GT motor-generator weight was calculated by considering the power to weight ratio of different existing electric machines found in the literature.

In the third assessment step, a SHEV powertrain is modelled. Powertrain components are designed according to vehicle characteristics and performances as explained in chapter 2. Battery capacity is selected in order to ensure 50km full-electric driving mode range during city driving. Battery weight is estimated based on study performed on different commercialized battery for hybrid and electric vehicles and as presented in chapter 2.

Finally, in the fourth assessment step, the fuel consumption simulations of the different GT-system APU were performed using a bi-level optimization method which consists of coupling the NSGA to DP. The NSGA is responsible for exploring the design space of GT net power and the weighting factor, introduced to have a balanced global control objective, and to generate many parameter combinations. The DP is used to realize the global minimum of two control objectives, the fuel consumption and the switching ON/OFF times, while respecting the component constraints and guaranteeing the SOC levels to the desired values. Fuel consumption is calculated on the modified WLTC described in chapter 2, which accounts for the vehicle non-mechanical energetic needs in addition to the propulsion mechanical needs. Therefore, the same scenarios were considered in this chapter.
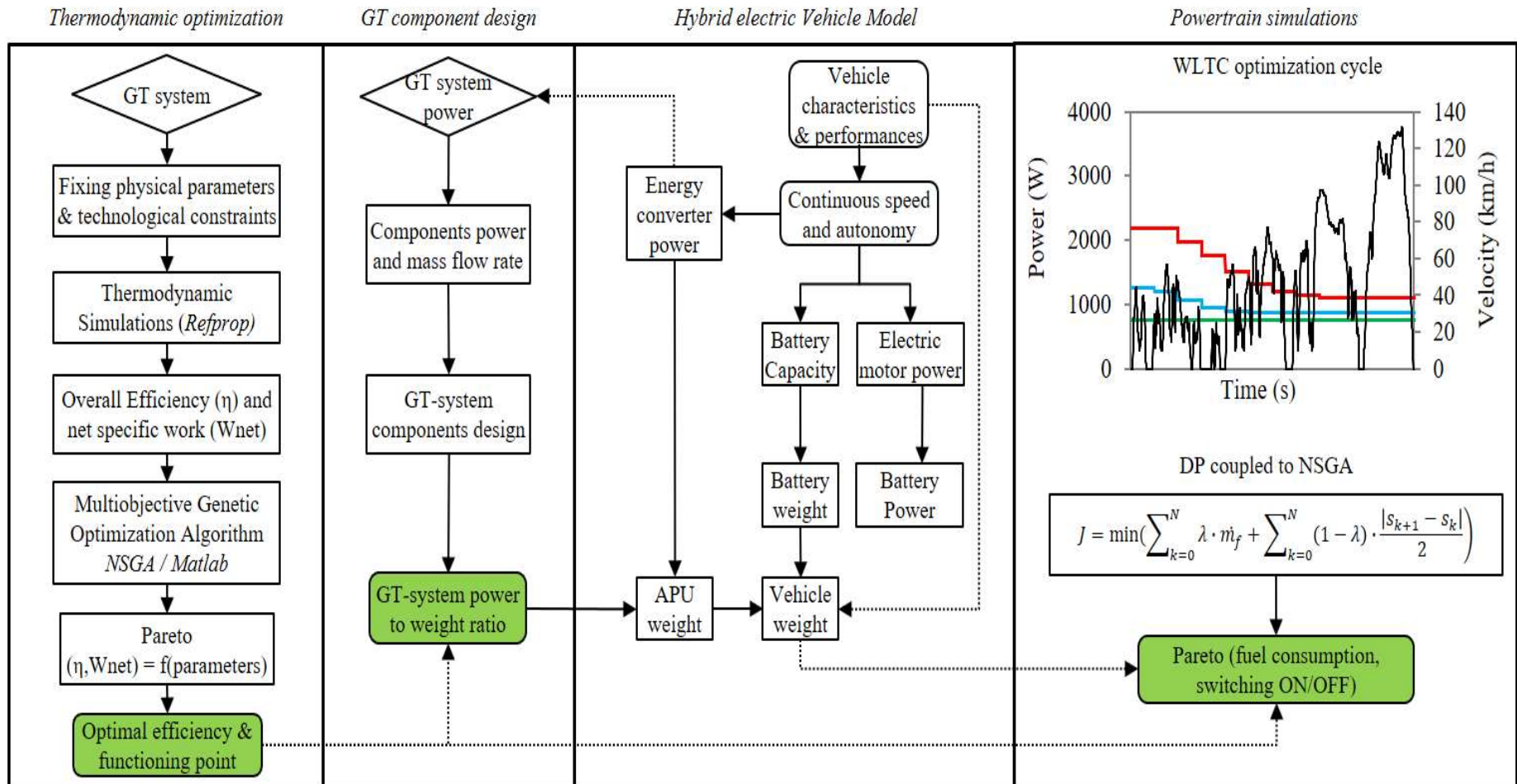
Fig.3.1: Methodology for fuel consumption assessment of different GT-systems on SHEV

## 3.3   Energetic analysis of the different GT-system options

The identified realistic GT-system options of chapter 2, are assessed here in order to account for their respective energy efficiency and net specific work. The assessment methodology for each option is illustrated in figure 3.1. Energy and exergy calculations are performed first with Refprop software [3.21], using the set of physical parameters such as the turbine inlet temperature (TIT), the maximum cycle pressure (Pmax), the components' efficiencies, among others; as summarized in table 3.1. These parameters correspond to the state-of-the-art specifications and limitations of GT component technologies and to automotive design constraints which are presented in the next section. The thermodynamic equations are presented in chapter 2.
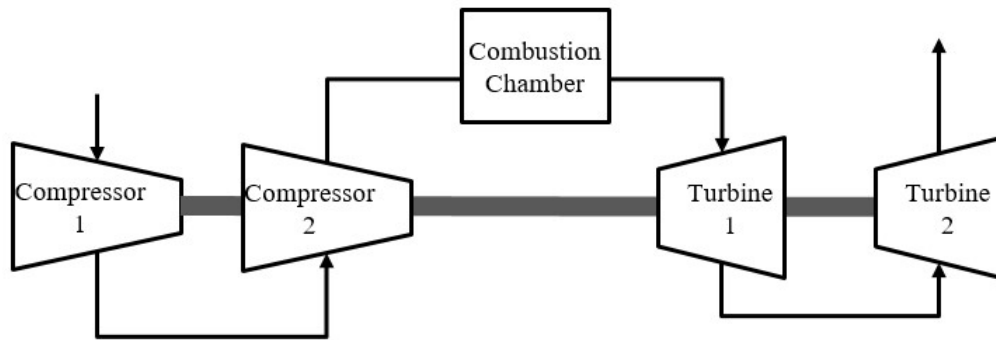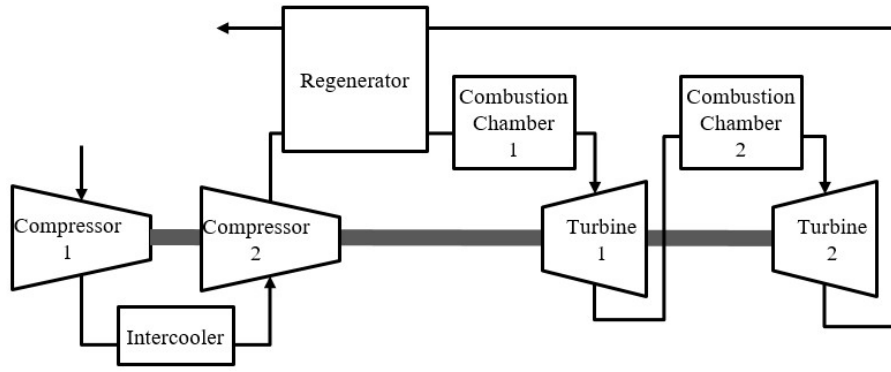

(a) SGT
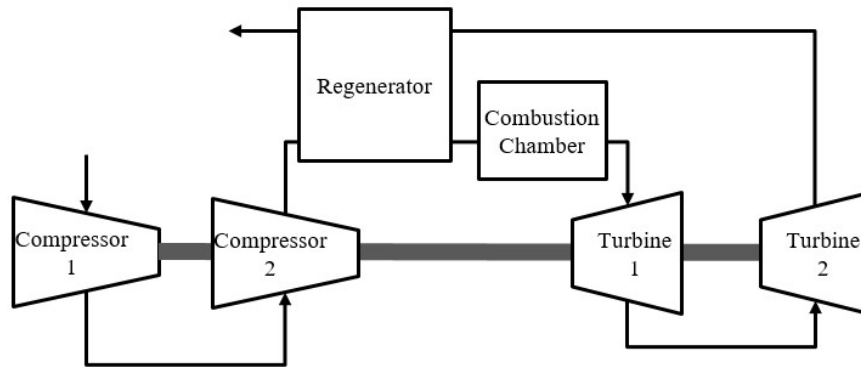
(b) RGT
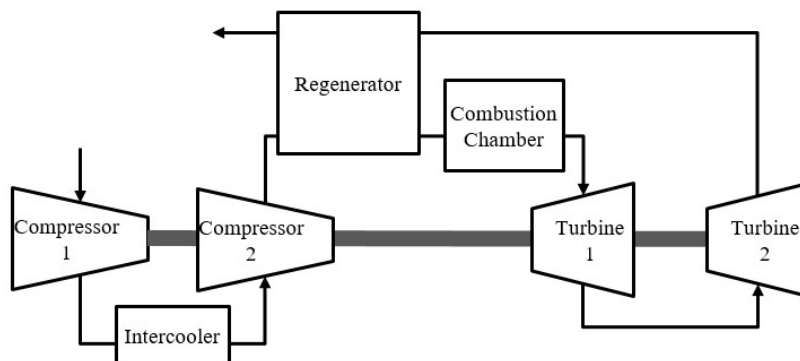
(c) IRGT

(d) IRReGT
Fig 3.2: Thermodynamic configuration of the investigated GT-systems

The energy and exergy calculations are made as function of two parametric design criteria: the compression ratio (π_i) and the expansion ratio (β_j), with i and j referring to the number of compressors and turbines respectively. For each configuration, three different TIT are considered, 950°C, 1100°C and 1250°C emulating three different machines:

- TIT= 950°C: No specific high cost materials are required and components can be manufactured with known alloys
- TIT=1100°C: specific alloys materials but within the know-how of turbocharger and heat exchangers suppliers as well as automotive industry
- TIT=1250°C: ceramic and high cost manufacturing materials are required

The second calculation step uses the NSGA multi-objective genetic algorithm to determine the Pareto optimal efficiency and net specific work solutions for the optimal (π_i) and (β_j) [3.22]. For the rest of the study, the comparison between the different GT-systems will be based on the best efficiency points on the Pareto solution curves. Therefore, the integration of the different GT-system options in SHEV will be made with respect to the highest efficiency among the compared systems.

3.3.1 Components specifications

In this paragraph, the choice of GT-system component technologies and specifications is presented based on state-of-the-art components specifications and automotive design constraints. For automotive applications, many criteria are to be considered such as the mass, the power density, the size, the component efficiencies, as well as the maintenance, the environmental aspects, the security, the technology master, the reliability, the noise and vibration aspects and the cost. In order to evaluate the overall efficiency and power density of each cycle, a component based analysis is done for the major components of the GT-system

3.3.1.1 Compressors

Two technologies of compressors are mainly used in gas turbines: centrifugal and axial compressors with different operating performances, especially in terms of efficiency and pressure ratio [3.23].

Radial centrifugal compressors dominate in small size units where small volume flow are required and mainly when the cost is a priority [3.24]. On the other hand, axial flow compressors dominate in applications where small frontal area, low weight, high flow rate and high efficiency are essential, which make them the only choice for large GT. Radial centrifugal compressors have also other advantages, among them we can list: a shorter length than an equivalent axial compressor, better resistance to foreign object damage, less susceptibility to loss of performance by build-up of deposits on the blade surfaces and the ability to operate over a wider range of mass flow at a particular rotational speed. That's why radial centrifugal compressors have been studied largely in GT for automotive and used today in automotive engines as turbochargers, where low unit cost outweighs a low frontal area and weight. Comparing the pressure ratio, a pressure ratio in a centrifugal compressor of around 4:1 can be obtained from a single-stage compressor made of aluminum alloy [3.25]. For axial flow compressors, 1.1 to 1.4 pressure ratio can be achieved with very high efficiency. Therefore, a radial centrifugal compressor with pressure ratio up to 4 is considered in this study.

The number of compressing stages defines the size of the machine, since the higher the maximum cycle pressure, the more the number of compression and expansion stages [3.23, 3.25]. Compression ratio and isentropic efficiency of $\pi_1 = 4$ and $\eta_{isC} = 80\%$ respectively are selected based on Chrysler Gas Turbine radial compressor [3.1]. Literature shows that the relative inlet and outlet pressure drop for an industrial SGT5-4000F Gas turbine are respectively 0.4% and 1.3% [3.16, 3.26], tests done on 28 kW MGT show a pressure drop at inlet of compressor of 500 Pa at full power [3.6]. Therefore, a 5% pressure drop at the inlet of the first compressor is considered in the simulations. This emulates the operation with air filter.

3.3.1.2 Combustion Chamber

The design of a gas turbine combustion system is a complex process involving, fluid dynamics, combustion and mechanical design especially with today's high cycle temperature GT-systems. High combustion efficiency and low level of visible smoke are achieved with today's combustion chambers, however, after the 1970s, a much more demanding problem has been the reduction of oxides of nitrogen.
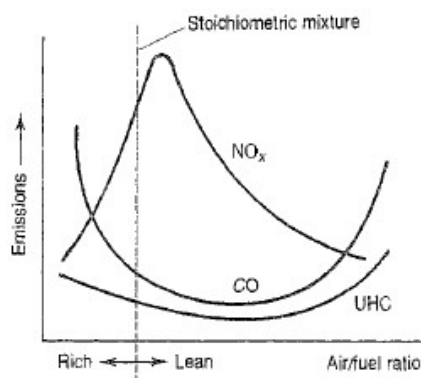

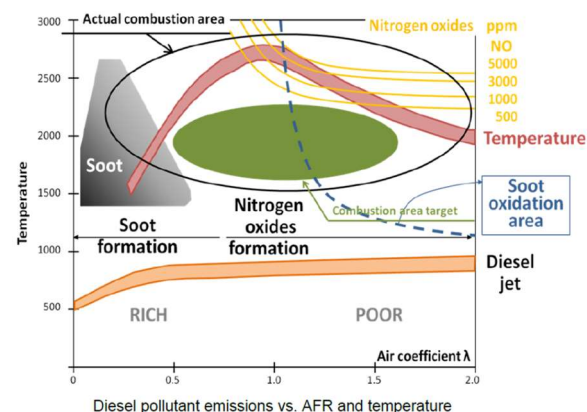Fig. 3.3: Dependence of emissions on fuel/air ratio [3.25]

Fig. 3.4: Effect of flame temperature on NOx and particulate – Pischinger Diagram [3.43]

Therefore, many technologies are under investigation to meet the more stringent pollution limits while maintaining existing levels of reliability and keeping costs affordable [3.25]. Figure 3.3

shows the emission of NOx, CO and UHC depending on air/fuel ratio. The NOx emission is maximum when the air/fuel ratio is lean and close to stoichiometric conditions, because of two main effects as shown in Pischinger diagram of figure 3.4: the excess of oxygen and the high temperature inducing the oxygen to react with the nitrogen. NOx emission can be more than halved by reducing the flame temperature by 100K from 1900 to 1800K [3.25]. Many methods to achieve this goal are used such as water or steam injection [3.27, 3.28], selective catalytic reduction [3.29-3.31], SCONOX [3.32], Dry low NOx [3.32] with lean burning or rich burning in the primary zone of combustion to achieve the necessary reduction in flame temperature.

Another important factor to be considered when modeling GT combustion chambers is the pressure losses across this component. Today, it is estimated to be around 2 to 8 percent of the static pressure and affects the global cycle efficiency [3.32, 3.33]. A value of 4% is taken into account for calculations.

3.3.1.3 Intercooler HEX

The automotive intercooler technology is considered since approximately the same mass flow rate and integration constraints are required. In an internal combustion engine, the intercooler system for turbocharging operates at a maximum outlet temperature of 60°C and the pressure drop is about 3% [3.34, 3.35]. For conservative reasons a pressure drop value of 5% is considered based on test results for the intercooler of a 110 kW 2.0L Diesel engine [3.36].

3.3.1.4 Regenerator HEX

The regenerator is an essential element to increase the efficiency of gas turbine [3.37]. Wrightspeed confirms this, during the development of their IRGT [3.38]. The thermal efficiency of small gas turbines, with a power range between 5-200 kW that can be used for automotive applications, is about 20% or less if no heat-exchanger is used in the system. Today, high heat exchanger effectiveness of more than 90% can be achieved with a pressure drop less than 5% where 3% are just inside the HEX and the remaining in manifolds and piping [3.1, 3.39]. An 85% effectiveness HEX regenerator with 3% pressure drop in hot side and 4% in the cold side is considered for the simulations [3.25, 3.40].

3.3.1.5 Turbines

As for the compressor, there are two basic types of turbine, the radial flow and the axial flow turbines. The radial turbine first used in jet engine flight in the late 1930s [3.23] and used today in the turbochargers for ICE, can handle low mass flows more efficiently than the axial flow machine and has been widely used in the cryogenic industry also as a turbo expander [3.25]. While the axial flow turbine is normally more efficient, the radial turbine mounted with a centrifugal compressor offers the benefit of a short and rigid rotor and used where compactness is more important than low fuel consumption as in the APUs for aircraft [3.41] and for supercharged ICE [3.42].
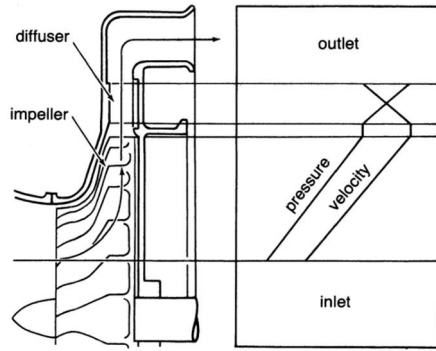
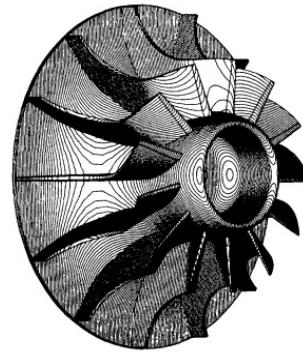Fig. 3.5: Radial compressor – Pressure and velocity variation [3.23]

Fig. 3.6: Radial turbines [3.42]

Radial centrifugal turbine expansion ratio (TER) of around 3.5 can be reached. It is limited by choking because it discharges into the atmosphere at ambient pressure. Also, radial turbine can reach more than 82% of isentropic efficiency in a limited operating region where the isentropic efficiency for axial turbine can reach 90% [3.25]. Based on Chrysler GT results, 85% radial turbine efficiency is considered for the simulations [3.1].

Table 3.1 synthesizes the simulation parameters selected based on state-of-the-art component specifications and automotive design constraints as described in previous paragraph.

Table 3.1: Simulation parameters based on state-of-the-art component specifications and automotive design constraints.

| Parameter	Unit	Value	Parameter	Unit	Value
Compressor technology	-	Radial	Regenerator efficiency	%	85
Max number of compression stages	-	2	Regenerator pressure drop cold side	%	4
Compressor max pressure ratio	-	4	Regenerator pressure drop hot side	%	3
Compressors efficiency	%	80	Combustion chamber pressure drop	%	4
Compressor inlet pressure drop	%	0.5	Max number of expansion stages	-	2
Maximum cycle pressure	MPa	1.2	Turbine Inlet Temperature (TIT)	°C	1250
Intercoolers pressure drop	%	5	Turbines isentropic efficiency	%	85
Intercoolers outlet temperature	°C	60	Turbine expansion ratio	-	3.5

3.3.2 Thermodynamic optimization results

Figure 3.7 presents the pareto front solution for the different GT-systems operating at three different TIT. The Non-dominated Sorting Genetic Algorithm (NSGA) is used for the multi-objective optimization as an effective method to find the optimal solution among the two main objectives: the efficiency and the net specific work. Because these objectives are nonlinear, the global optimal solution of multiple objectives is obtained by Pareto optimal solution set as described in figure 3.7. Therefore, this presented Pareto are a compromise solution of different objectives, and we can make decisions based on Pareto front and requirements of different objectives. Many conclusions can be drawn out from this figure:

1- Increasing the TIT increases the system efficiency. For instance, an increase in efficiency of 12% is obtained from the GT configuration when TIT increases from 950°C up to 1100°C. The efficiency increases by around 20% when TIT increases from 950°C up to 1250°C for the same system configuration. Same conclusions can be drawn when comparing

the impact of increasing the TIT on the efficiency of the RGT, the IRGT and the IRReGT configurations.

2- Increasing the TIT increases the system net specific work resulting in lower air flow for the same system net output power. The increase of TIT from 950°C up to 1100°C increases the net specific work of the GT system by 44% and up to 88% when TIT reaches 1250°C. Same conclusions can be retrieved when comparing the impact of increasing the TIT on the net specific work of the RGT, the IRGT and the IRReGT configurations.

3- Adding a regenerator increases the efficiency of the system since waste heat from the turbine outlet is recovered to heat the air at combustion chamber inlet, resulting in a lower amount of fuel injected to reach the same combustion chamber temperature. However, adding a regenerator reduces the net specific work at optimal efficiency point as shown when comparing the GT to the RGT.

4- Performing an intercooling on the regenerative GT increases both the system efficiency and the net specific work. For instance, the intercooling compression reduces the compression work, resulting in higher net specific work. Also, this results in a decrease in the regenerator inlet temperature which leads a higher amount of heat recovered, resulting in higher system efficiency.

5- Performing turbine reheat increases both the system efficiency and the net specific work. For instance, a turbine reheat allows higher power recovered from the expansion leading to higher net specific work. Also, it allows higher turbine outlet temperature which results in higher regenerator temperature and higher combustion chamber inlet temperature, resulting in lower fuel injected in the first combustion chamber for the same maximum combustion chamber temperature.
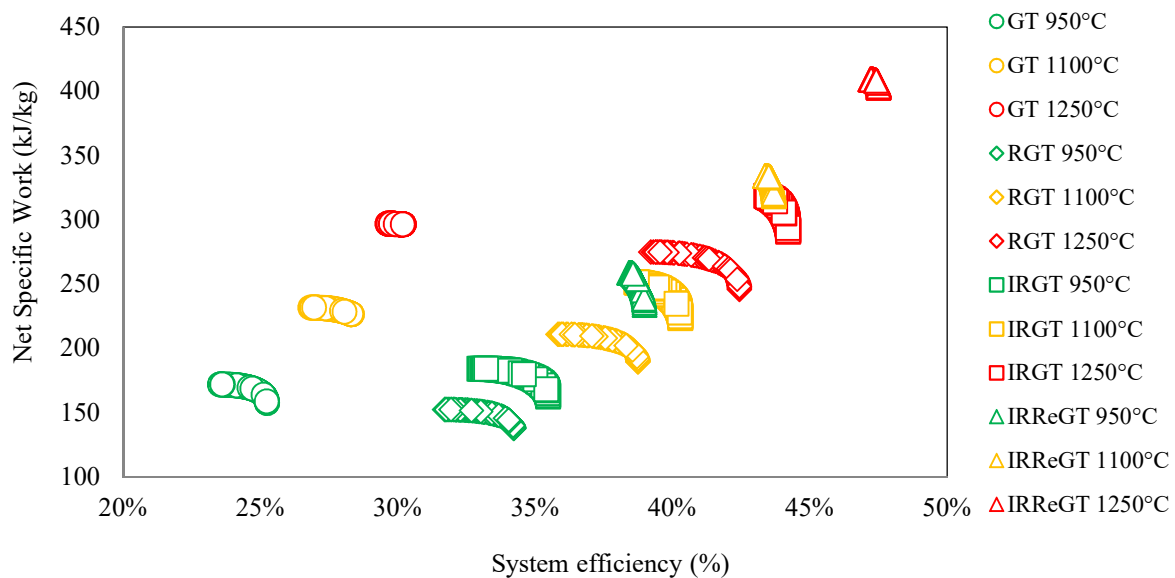
Fig. 3.7: Pareto optimal net specific work and efficiency for the different GT-system configurations for three different TIT
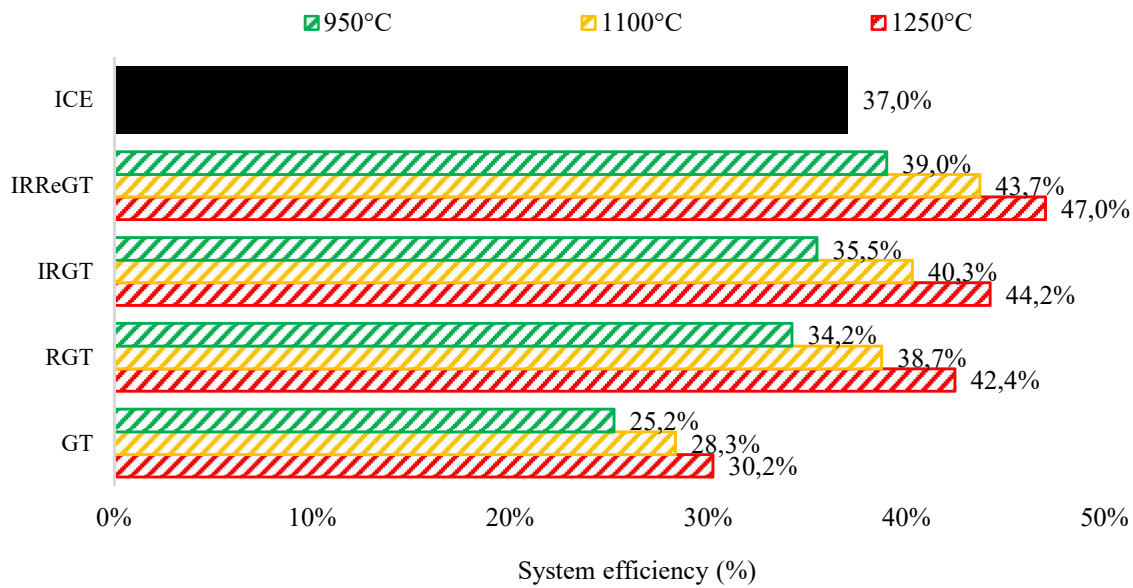
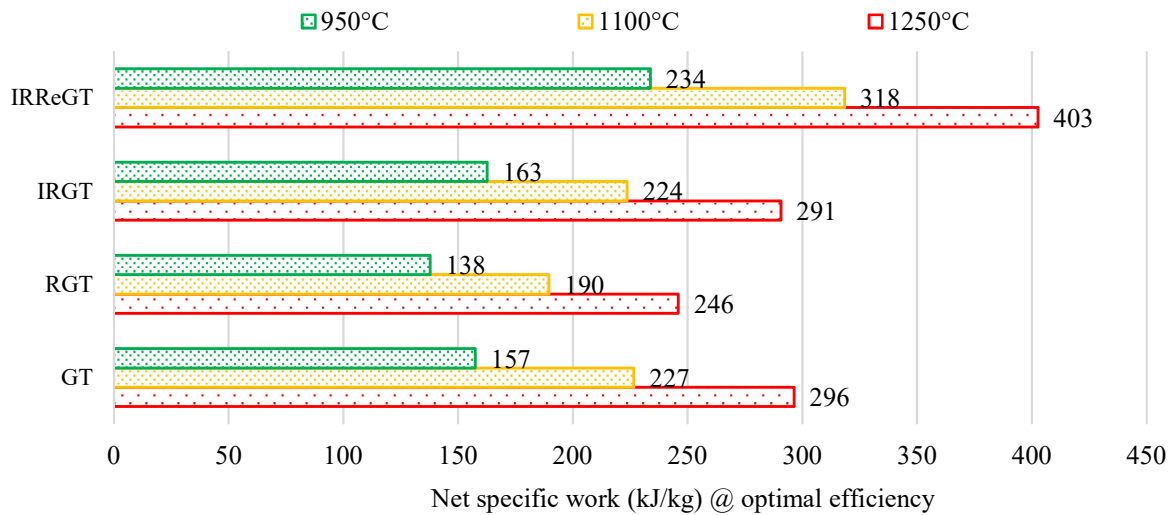*Fig. 3.8: GT-Systems optimal efficiency compared to ICE optimal efficiency*

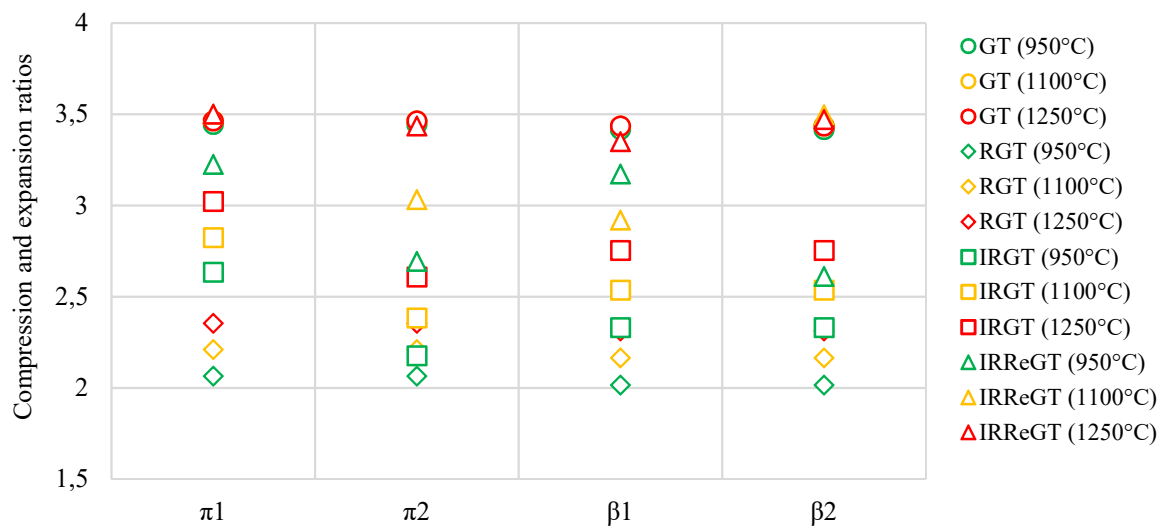*Fig. 3.9: Net specific power at optimal efficiency*

Fig. 3.10: Compression and expansion ratio design criteria at optimal efficiency

3.4 GT-system components design

In this section, a components weight assessment study is carried out on the four different GT-system configurations in order to account for the power to weight ratio for the three different TIT. Each GT-system was divided into different subsystems which are:

- The turbomachines: compressors and turbines
- The heat exchangers: intercooler and regenerator
- The combustion chambers
- The electric motor/generator

For each of these subsystems, a correlation between the components' power and or the mass flow rate across them, and the weight was established. Up to this end, four different GT-system net powers (15kW, 20kW, 25kW and 30kW) were selected. These powers match the energy converter power calculated in the vehicle model section.

The mass flow rate across each GT-system for the different selected net power and for the three TIT is calculated according to equation 3.1 and presented in figure 3.11.

$$P_{GT-system} = \dot{m}_{flow} * W_{net} \tag{3.1}$$

Where:	$P_{GT-system}$	:	GT-system net power (kW)
	$\dot{m}_{flow}$	:	Mass flow rate across the GT-system (kg/s)
	W_{net}	:	System net specific work (kJ/kg)

Two main conclusions can be drawn out from the figure:

1- According to equation 3.1, a linear relation between system net power and mass flow rate is observed. For instance, increasing the power from 15kW to 30kW results in doubling the air mass flow rate across the system.

2- The IRReGT with higher net specific works presents the lower mass flow rate, followed by the GT, the IRGT and the RGT.
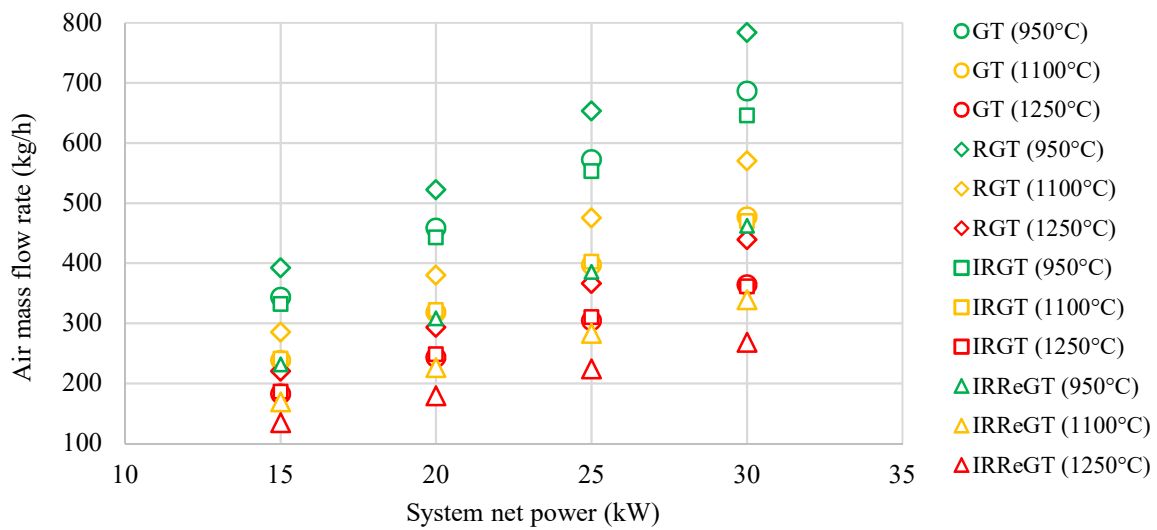

Fig. 3.11: Mass flow rate for the different GT system powers

3.4.1 Turbomachines

A study on different turbomachines has been carried out in order to establish a mathematical relation between the mass flow rate across a turbocharger and power to weight ratio. The study includes a turbocharger from Garett, Borgwarner and MTI designed for automotive and including turbine variable geometry technology as waste gate technology [3.43-3.46].

Automotive turbochargers are radial technology centrifugal machines operating according to a geometric relation between the mass flow rate, the expansion/compression ratio and the machine rotating speed. Hence, for a given defined compressor or wheel geometry, and for a given mass flow rate, the compression or expansion ratio increases as the rotation speed increases.

Therefore, knowing the available map for a turbocharger, and for a given pressure ratio and mass flow rate, the machine power has been evaluated. Then, from the available data on turbocharger weight, a mathematical relation between mass flow rate and power to weight ratio has been established for each turbomachinery speed. The different points are presented in the figure 3.12 below. For mass flow rate ranging between 100 and 800kg/h and a turbocompressor rotational speed around 90.000 RPM, the mathematical relation between the mass flow rate and the system power to weight ratio can be described as follow:

$$\dot{m}_{TC} = -275 * \left(\frac{P_{TC}}{M_{TC}}\right)^2 + 645 * \left(\frac{P_{TC}}{M_{TC}}\right) + 122 \tag{3.2}$$

Where:	$\dot{m}_{TC}$	:	Mass flow rate across the turbomachine
	P_{TC}	:	Turbocharger mechanical power (kW)
	M_{TC}	:	Turbocharger weight (kg)
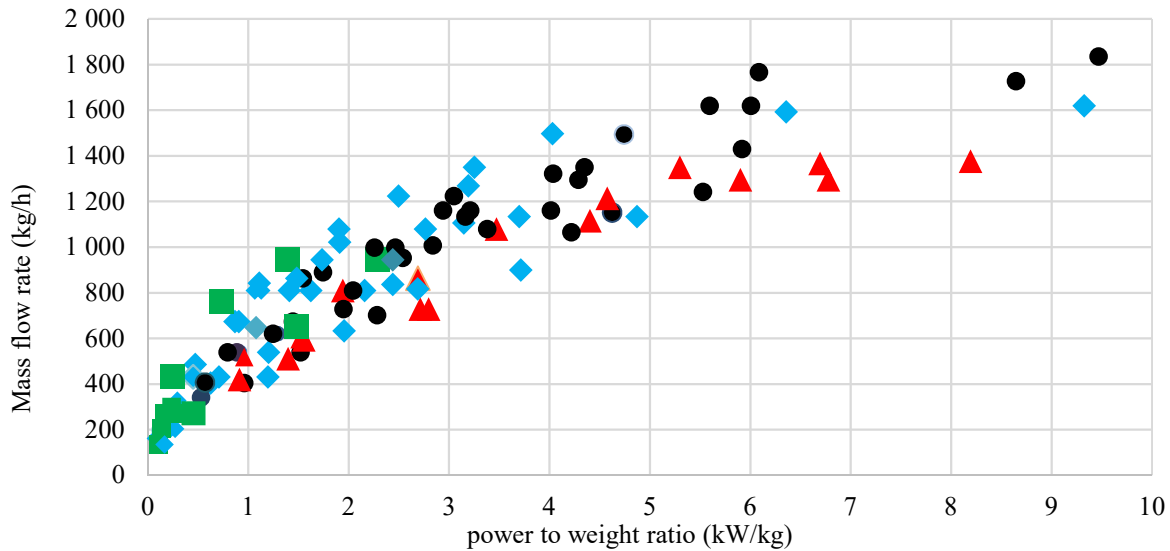
Fig. 3.12: Mass flow rate function of power to weight ratio for different rotational speeds for different turbochargers studied. (green square=60kRPM, Bleu rhombus = 90kRPM, black round = 120kRPM, red triangle = 150kRPM)

The turbocompressor is composed of a compressor housing and a compressor wheel, a turbine housing and a turbine wheel, a shaft and an oil bearing system, and depending on the technology, a mechanism for turbine variable geometry or a waste gate system. Weight assessment shows

that about 30% of the total turbomachine weight is from the compressor side weight and about 70% is from the turbine side weight. Based on these findings, the weights of the different turbomachinery components have been accounted for knowing the component power, the operating rotational speed as well as the air mass flow rate across the component.

3.4.2   Heat Exchangers

Recovering GT waste heat and reducing the compression energy are two efficient ways to increase the overall efficiency of a GT-system [3.5, 3.16-3.18]. Regarding the waste heat at turbine outlet, this thermal power can be recovered internally by using a regenerator, a recuperator that preheat the combustor inlet air using the exhaust gases at turbine outlet. As for the compression work, it was demonstrated that the use of an intercooler to reject heat during the compression phase is technically feasible and induces an increase in efficiency and net specific work of the system [3.5, 3.16-3.18].

Different types of HEX are used for regenerator in microturbines. Among them, the Shell-and-tube, the plate-fin, the primary surface and the rotary [3.47]. While the rotary HEX presents high efficiency, this technology is complex since it requires specific mechanical design and kinematic to rotate the HEX. Also, leakage can occur across the rotary system. On the other hand, the shell-and-tube regenerators are typically bulky and weighty compared to plate-fin and primary surface HEX. In recent years, many research program have been conducted in order to improve the efficiency and to reduce the cost of plate-fin HEX. On the scientific level, many works have been carried out to find correlations for modeling these components with different fin types. For instance, Manglik et al. [3.48] presented correclations for the Colburn number (j) and the friction factor (f) for rectangular offset strip fin with laminar, transition and turbulent flow regimes. Others such as Chang et al. [3.49, 3.50] proposed correlations for the friction factor for louver fin geometry. Others such as Traverso and Mussardo [3.51] were interested in the techno-economical optimization of plate-fin and primary surface regenerators while Qiuwang et al. [3.52] used a genetic algorithm to optimize a primary surface regenerator used in a GT. Wen et al. [3.53] optimized the configuration parameters of serrated fin in plate-finned HEX using a genetic algorithm and entropy generation equations. Peng and Ling [3.54] used neural networks coupled to Genetic algorithms for optimization of a crossflow plate-fin HEX. Other thermo-economic optimizations of plate-fin HEX using multi-objective genetic algorithm were mentioned in literature [3.55-3.57].

As for the intercooler, air-air plate-fin HEX is used today in ICE to cool the air and to increase the power density. In this study, the compressed air is considered to be cooled down through a specific loop, using water as fluid. This will allow to use the waste heat from the intercooler to heat the vehicle cabin when hot thermal power is required.

Therefore, and in order to account for the weight and size of the different selected GT-systems, two different plate-fin HEX with offset strip fin are modeled in this section: (1) a regenerator and (2) an intercooler. The study starts by presenting the general equations for designing the HEX and the system modeling including the pressure drop calculations. Then the estimated weight for the different configurations are calculated and are used later to estimate the total weight of each GT-system.

3.4.2.1 Geometric and thermohydraulic characteristics of the plate-fin HEX

The different correlations for the calculation of the friction factor and the heat transfer characteristics, including the Nusselt number and the Colburn number are presented in this section. The HEX consists of a counter flow plate-fin as presented in figure 3.13 below. The offset strip fin is selected for this study, where the main geometry parameters are the fin pitch (c), the fin height (b), the fin length (X), and the fin thickness (tr) [3.58].
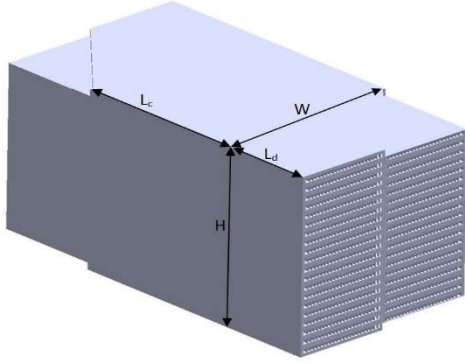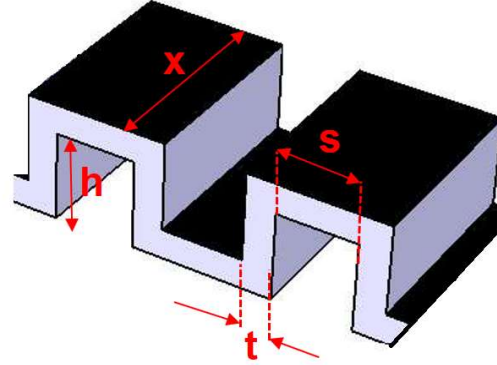

Fig. 3.13: Counter flow plate fin HEX   *Fig. 3.14: Schematic view of the offset strip fin*

Many researchers have investigated the heat transfer coefficient and the friction factor of plate-fin HEX [3.49, 3.59]. Correlations for calculation of Colburn number and friction factor of the offset strip fin for the regenerator are obtained from the following equations 3.3 and 3.4 below [3.48, 3.49]. It is worth mentioning that for uninterrupted fins, the error on the heat exchanger's efficiency is negligible when considering constant wall temperature correlations on friction factor and Nusselt number. Also, for compact HEXs used for the range of Reynolds number between 500 and 1500, it is assumed that the flow is in fully developed region, therefore $\left(\frac{L}{D_h}\right) >$ 100. According to paper [3.60], the f correlations for air can also be applied to the offset-strip fins when water is the working fluid. However, the j values vary according to Prandtl number. Therefore, the j correlations for the intercooler is presented in equation 3.9.

$$j = 0.6522Re^{-0.5403}\alpha^{-0.1541}\delta^{0.1499}\gamma^{-0.0678} \qquad (3.3)$$
$$* [1 + (5.269 * 10^{-5}Re^{1.34}\alpha^{0.504}\delta^{0.456}\gamma^{-1.055})]^{0.1}$$

$$f = 9.6243Re^{-0.7422}\alpha^{-0.1856}\delta^{0.3053}\gamma^{-0.2659} \qquad (3.4)$$
$$* [1 + (7.669 * 10^{-8}Re^{4.429}\alpha^{0.92}\delta^{3.767}\gamma^{0.236})]^{0.1}$$

$$120 < \text{Re} < 10^4 \qquad (3.5)$$

$$0.134 < \alpha = \frac{s}{h} < 0.9997 \qquad (3.6)$$

$$0.012 < \delta = \frac{t}{x} < 0.048 \qquad (3.7)$$

$$0.041 < \gamma = \frac{t}{s} < 0.121 \qquad (3.8)$$

$$j = \exp(1.3)(\alpha)^{0.004}(\delta)^{0.251}(\gamma)^{0.031}(Re)^{(0.0507lnRe-1.07)}(Pr)^{0.051} \qquad (3.9)$$

3.4.2.2 HEX modeling

In this section, the efficiency and pressure drop equations are presented. The mass flow rate, the inlet pressures and temperatures are determined for each GT-system configuration. Also, the simulations consider only the steady-state operation, therefore the physical parameters at inlet

and outlet of the HEXs are considered constant. The outlet conditions are considered by fixing the pinch for each HEX. In addition, the pressure drops were considered during calculations.

The efficiency for counter-flow HEX is obtained from equation 3.10 below where the number of transfer units (NTU) and the ratio of heat capacity rate (c^*) are calculated according to equations 3.10 and 3.11 [3.61, 3.62]. The heat transfer coefficient (UA) according to equation (3.13).

$$\varepsilon = \frac{1 - \exp[-NTU(1 - c^*)]}{1 - c^*\exp[-NTU(1 - c^*)]} \tag{3.10}$$

$$NTU = \frac{UA}{C_{min}}, \qquad C_{min} = \min\{m_c Cp_c, m_h Cp_h\} \tag{3.11}$$

$$c^* = \frac{C_{min}}{C_{max}}, \qquad C_{max} = \max\{m_c Cp_c, m_h Cp_h\} \tag{3.12}$$

$$UA = \frac{1}{[\frac{1}{h_c \eta_{s,c} A_c} + \frac{1}{h_h \eta_{s,h} A_h} + \frac{a}{A_w k_w} + \frac{R_{f,c}}{A_c} + \frac{R_{f,h}}{A_h}]} \tag{3.13}$$

$$\eta_s = 1 - \frac{A_{fin}}{A}(1 - \eta_{fin}) \tag{3.14}$$

$$\eta_{fin} = \frac{tgh(M * L)}{M * L} \tag{3.15}$$

$$M = \sqrt{\frac{2h}{k_{fin}t}} \tag{3.16}$$

$$L = 0.5b - t \tag{3.17}$$

Where ε :   Recuperative effectiveness (%)
          R_f :   The fouling factor
          η_s :   The overall surface efficiency (%)
          η_{fin} :   Single fin efficiency (%)

As for the pressure drop (ΔP), it was calculated by considering the total pressure drops in the HEX, including the entrance effect ΔP, the momentum effect ΔP, the core friction ΔP, and the exit effect ΔP according to the following equation 3.18 [3.61]:

$$\frac{\Delta P}{P_i} = \frac{G^2}{2g_c \rho_i p_i}[(1 - \sigma^2 + K_c) + 2\left(\frac{\rho_i}{\rho_0} - 1\right) + f\frac{L}{r_h}\frac{\rho_i}{\rho_0} - (1 - \sigma^2 - K_e)\frac{\rho_i}{\rho_0}] \tag{3.18}$$

Where σ :   Ratio of minimum free flow area to frontal area
          K_c :   The entrance pressure loss coefficient
          K_e :   The exit pressure drop coefficient

The flowchart of the recuperator and the intercooler thermo-hydraulic design is presented in figure 3.15. it shows the calculation steps realized to find the HEXs design.

The estimated weight of the intercooler and the regenerator depending on the thermal power are presented in figures 3.16 and 3.17. Many conclusions can be drawn out from these two figures:

1- First, the intercooler weighs less than the regenerator. On the one hand, less thermal power is exchanged in the intercooler compared to the regenerator and on the other hand, the intercooler used aluminum material with around one third of the steel density used for the regenerator. Therefore, comparing both figures, the regenerator weight seems to be ten times the intercooler weight for the same GT-system.

2- Increasing the net power of the GT-system increases the weight of both the intercooler and the regenerator. In fact, for the same machine, meaning the same efficiency and net specific work, an increase in the net mechanical power leads to an increase in the air mass flow rate across the HEXs, leading therefore to bigger exchanger surface.

3- The IRReGT-system with higher net specific work presents lower HEXs weight compared to the other investigated regenerative GT-systems.

Table 3.2: Heat exchangers technology

Component	Intercooler	Regenerator
Material	Aluminum	Steel
Type	Plate-fin	Plate-fin
Fins type	Offset strip fin	Offset strip fin
Working fluid	Air / Water	Air / Air

Table 3.3: Geometric dimensions of the offset fins for the plate fin HEX

Fins dimensions (mm)			
s	b	x	t
1.27	4	3.18	0.2

For each GT-system operating at specific TIT with same net specific work, a linear mathematical relation between the HEX weight and the thermal power exchanged can be drawn out from both figures. This relation will serve to define the power to weight ratio of each GT-system at the end of this section.
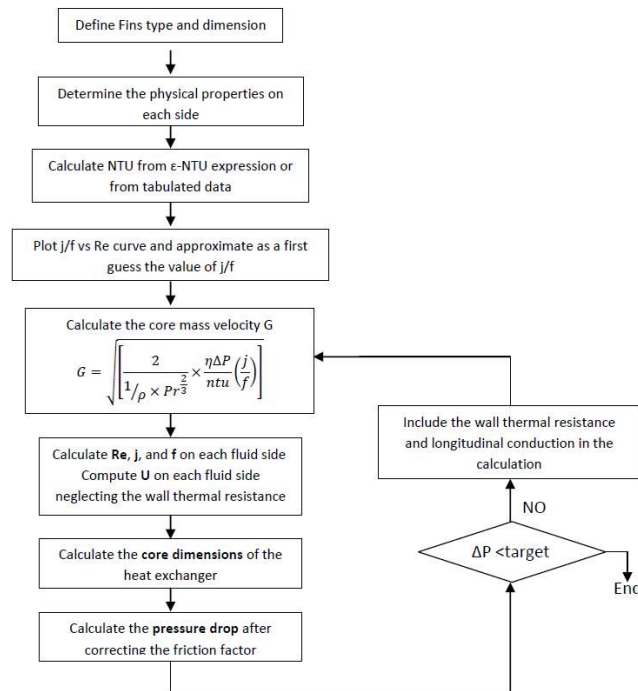
Fig. 3.15: Sizing steps of the core of the HEXs
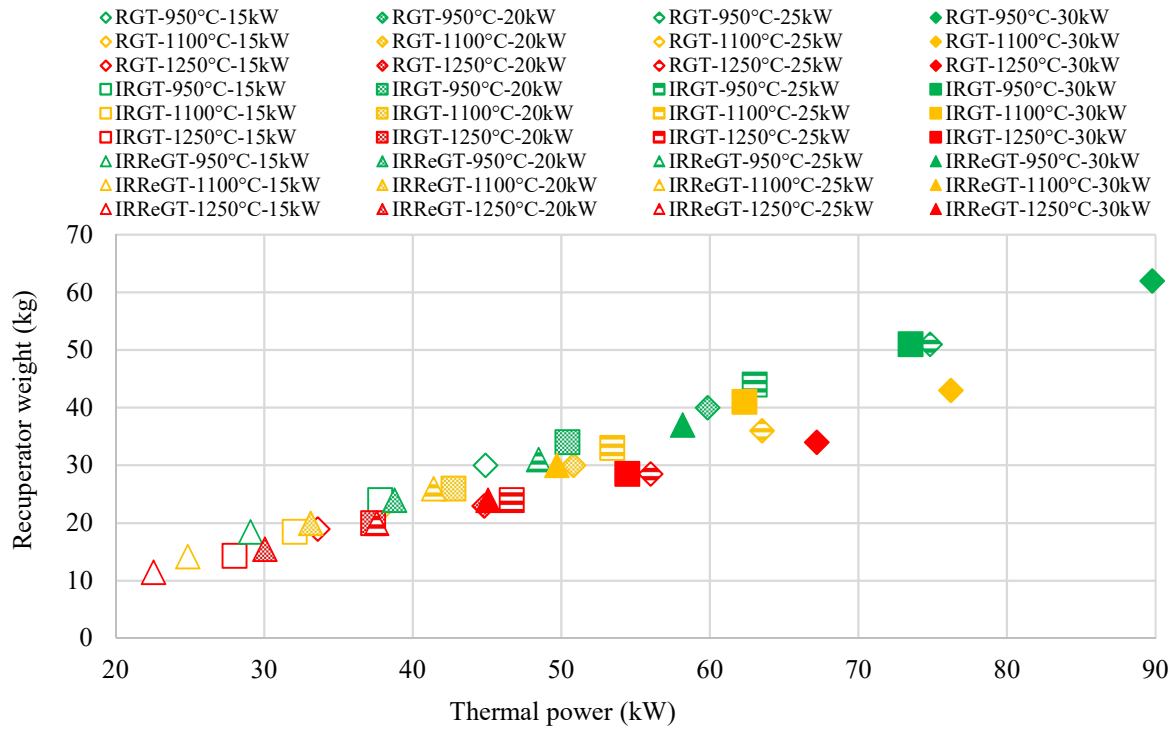
Fig. 3.16: Regenerators calculated weight
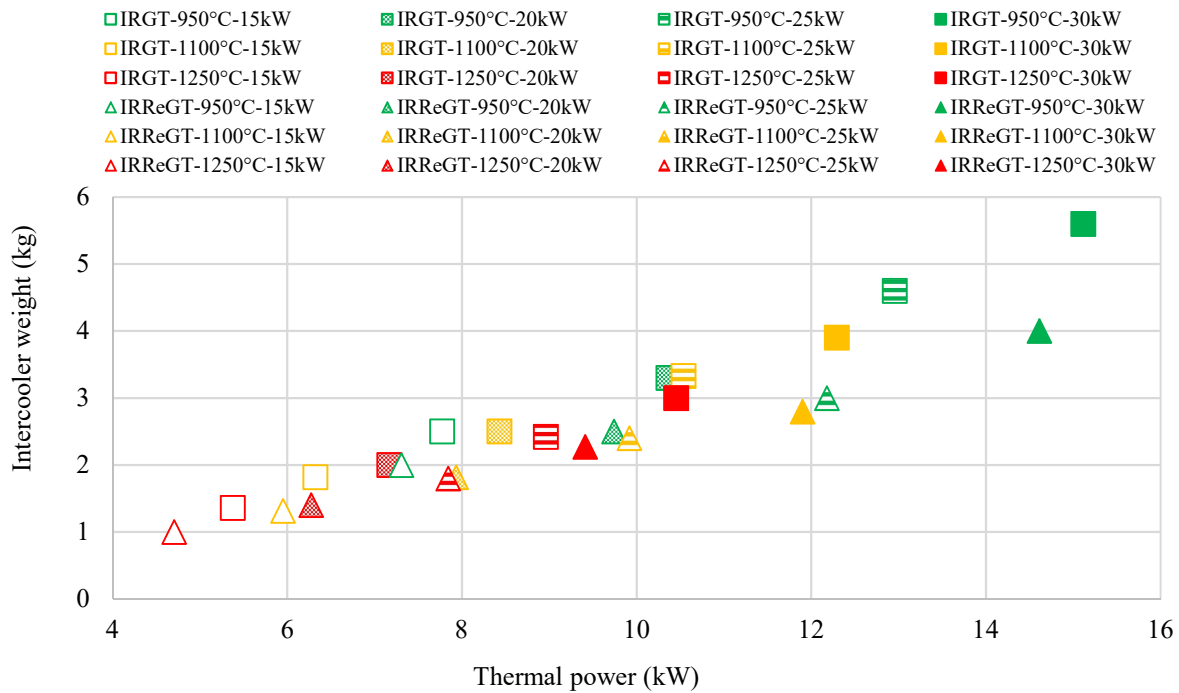
Fig. 3.17: Intercooler calculated weight

3.4.3 Conclusions

The total system weight of the different GT-configurations is the sum of the weight of the different components that constitute the system (compressors, turbines, combustion chambers, heat exchangers, electric motor/generator, fuel system, accessories…). It is worthy to mention that a 3kW/kg electric generator power density is considered in the study according to data on

generator power densities found from literature regarding high speed rotating machines [3.63-3.65] As for the combustion chambers, the weight estimation was done by establishing a relation between the weight, the mass flow rate and the thermal power of a pre-existing combustion chamber presented in figure 3.18 according to equation 3.19. Consequently, the same combustion chamber material was considered for all the combustion chambers. Also a package of 10kg is considered for all GT-systems. This includes the accessories, the controlled valves, the injectors as well as the electric invertor required.

Fig. 3.18: Reference GT combustion chamber

$$M_{CC} = M_0 * \left(\frac{\dot{m}_{cc}}{\dot{m}_0}\right) * \left(\frac{Q_{cc}}{Q_0}\right) \tag{3.19}$$

Where	M_{CC}	:	Weight of the combustion chamber (kg)
	M_0	:	Weight of the reference combustion chamber (kg)
	$\dot{m}_{cc}$	:	Mass flow rate across the combustion chamber (kg/s)
	$\dot{m}_0$	:	Mass flow rate of the reference combustion chamber (kg/s)
	Q_{cc}	:	Thermal power of the combustion chamber (kW)
	Q_0	:	Thermal power of the reference combustion chamber (kW)

The total system weight of the different GT-configurations for the different TIT is presented in figure 3.19 below. Many conclusions can be drawn out from this figure:

1- An increase of TIT is shown to reduce the weight of the system for all the thermodynamic configurations. Considering the same material density as explained before, the increase in temperature reduces the air mass flow, reducing therefore the system weight and size. For instance, increasing the TIT from 950°C up to 1100°C for the SGT, shows a decrease in weight by an average of 21%. On the other hand, 32.5% of weight reduction is observed when the TIT increases from 950°C up to 1250°C for the same GT-system configuration. Same conclusions can be underlined when comparing the total system weight for different TIT for the RGT, the IRGT and the IRReGT.

2- Comparing the different configurations, the SGT configuration presents the lowest weight among other configurations. Firstly, the high net specific work of this configuration leads to small air mass flow, as shown in figure 3.11, resulting in small turbomachines size according

to equation 3.2. Secondly, the absence of a regenerator presenting a high share of total weight of the system as shown in figure 3.20, has a positive impact on the total SGT weight.

3- The worst configuration is the RGT, with low net specific work. On one hand, the air mass flow is high, according to figure 3.11, resulting in bulky components mainly the regenerator. In fact, it is proven according to figure 3.20 that the regenerator constitutes around 42% of the RGT weight when TIT is 950°C, and 35% when TIT increases to 1250°C.

4- The IRGT configuration has reduced weight compared to the RGT operating at the same TIT. This can be explained also by the IRGT lower air mass flow rate leading to smaller component size, mainly the regenerator. For instance, the regenerator of a RGT 20kW net power machine operating at 950°C TIT has an estimated weight of 40kg compared to 34kg for an IRGT 20kW net power machine functioning at the same TIT.

5- The IRReGT configuration has reduced weight compared to both RGT and IRGT operating at the same TIT. Since the net specific work is high, the air mass flow is low and the different components such as compressors, turbines and regenerator are small compared to RGT and IRGT configurations. For instance, a 20kW net power IRReGT machine operating at 950°C TIT has an estimated regenerator weight of 24kg, 40% lighter than the RGT one and 29.5% lighter than the IRGT one.

6- Increasing the system's net power results in an increase of the system's weight as shown in figure 3.19. This increase is shown to be quasi-linear for all studied configurations.

Finally, the average power to weight ratio of the different GT-system configurations is presented in figure 3.21. The following conclusions can be drawn out from this figure:

1- The higher the TIT, the higher the power to weight ratio for all studied configurations.

2- The GT presents the better power to weight ratio while the RGT presents the worst power to weight ratio

The IRReGT presents high power to weight ratio compared to other regenerative configurations.
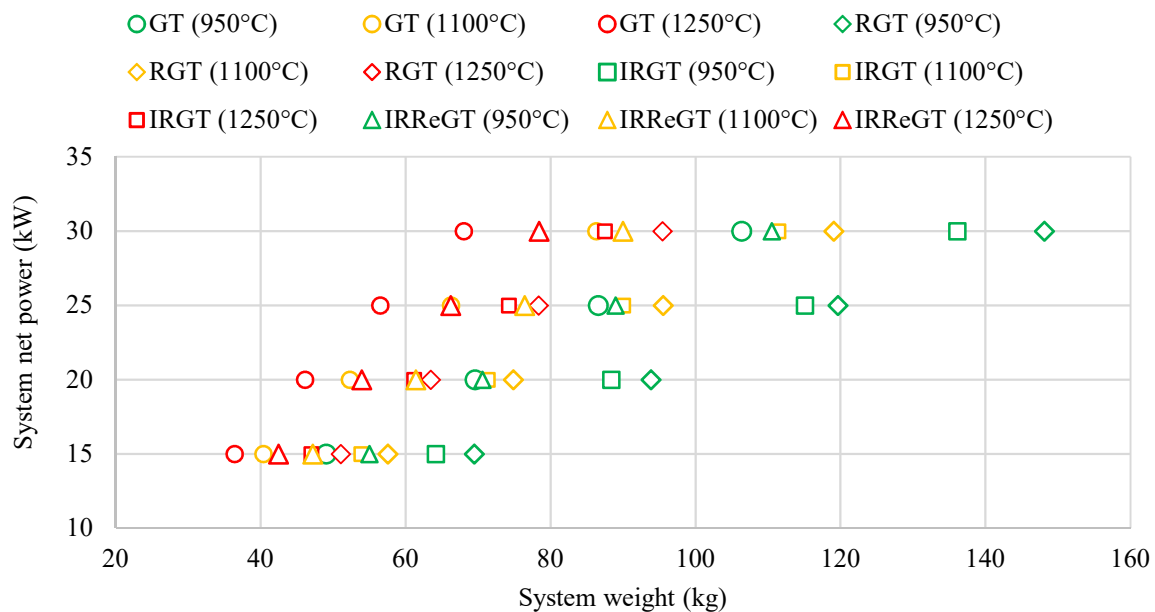

Fig. 3.19: Power versus weight for the different GT-systems
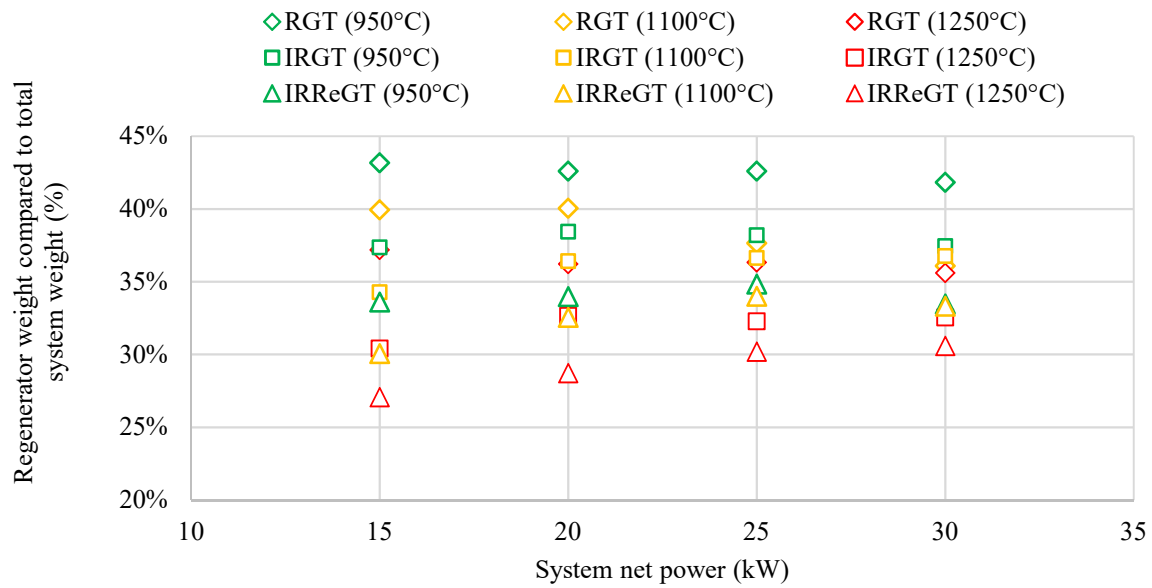
Fig. 3.20: Regenerator weight compared to total system weight for the RGT, IRGT and IRReGT configurations
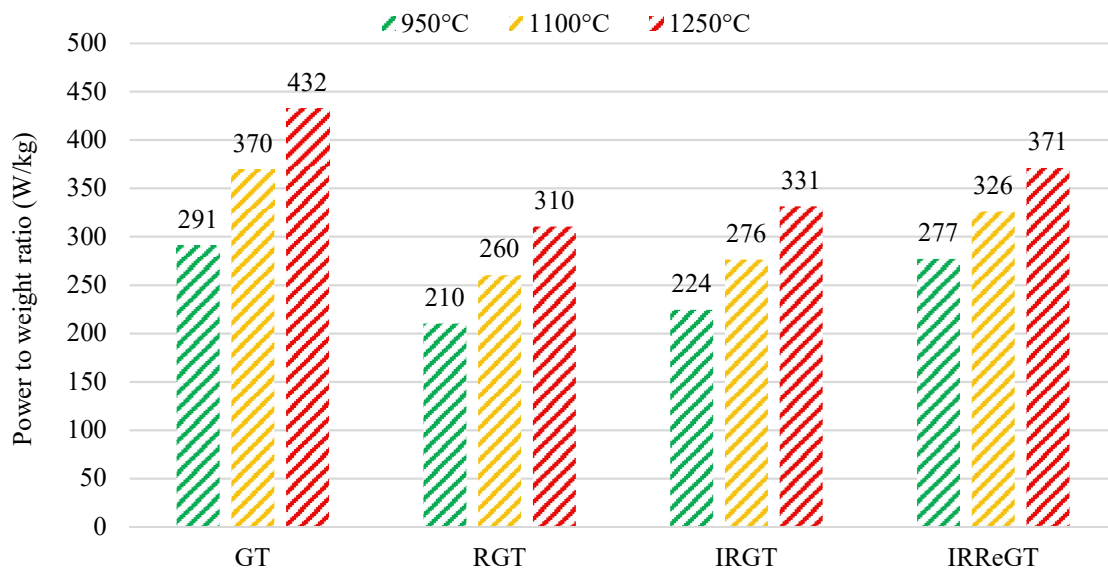
Fig. 3.20: Power to weight ratio for each GT-system at different TIT.

Note that these resulting power to weight ratios will be used during the simulations in the next section to evaluate the potential of fuel consumption saving for each GT-APU on SHEV.

3.5 Series Hybrid Electric vehicle model

In order to evaluate the benefits of the different GT-systems in terms of fuel savings compared to ICE, a medium-class series hybrid vehicle, is considered and presented in this section. It consists of a GT-APU and an electric traction system as illustrated in figure 2.1, and developed in chapter 2.

As described in many papers [3.5, 3.66, 3.67], series configuration presents the advantage of operating the APU at steady power corresponding to the optimum efficiency, which, for some GT-configurations, is higher than the maximum efficiency of ICE, as illustrated in figure 3.8. The vehicle is propelled by an electric motor, powered by a battery and/or the APU, and properly sized to ensure the vehicle acceleration and velocity performance without deficiency.

The powertrain design methodology is presented in chapter 2. The first section presents a quick reminder on the vehicle characteristics used for simulations and the second section presents the bi-level optimization method used for fuel consumption simulations.

3.5.1 Powertrain setup

The SHEV vehicle model was developed in details in chapter 2. The same vehicle model, with characteristics presented in table 2.2, is used in this chapter with the different GT-systems as APU. The different systems efficiency and power to weight ratio function of the different turbine inlet temperature (TIT) are presented in table 3.4 below. The GT-system power was allowed to vary between 15 and up to 30kW. The different GT-systems efficiencies are retrieved from figure 3.8 and the GT-systems power to weight ratio from figure 3.20.

Table 3.4: GT-APU characteristics.

	Symbol	Unit	TIT=950°C	TIT=1100°C	TIT=1250°C
SGT-system power	P_{SGT}	kW	15 to 30		
SGT efficiency	η_{SGT}	%	25.2	28.3	30.2
SGT power to weight ratio	PWR_{SGT}	W/kg	291	370	432
RGT-system power	P_{RGT}	kW	15 to 30		
RGT efficiency	η_{RGT}	%	34.2	38.7	42.4
RGT power to weight ratio	PWR_{SGT}	W/kg	210	260	310
IRGT-system power	P_{IRGT}	kW	15 to 30		
IRGT efficiency	η_{IRGT}	%	35.5	40.3	44.2
IRGT power to weight ratio	PWR_{IRGT}	W/kg	224	276	331
IRReGT-system power	P_{IRReGT}	kW	15 to 30		
IRReGT efficiency	η_{IRReGT}	%	39	43.7	47
IRReGT power to weight ratio	PWR_{IRReGT}	W/kg	277	326	371

3.5.2 Energy Management Strategy

As discussed in chapter 2 and during the introduction of this chapter, the DP simulation results are optimal but not realistic, since the switching On/Off number of the APU is not constrained. This is not coherent with rule based controlled defined in real hybrid vehicles where the APU operation is constrained according to different automotive technological criteria.

In this chapter, the EMS role is to manage the vehicle power flows in order to minimize both the fuel consumption and the switching ON/OFF times of the APU. This is done while also satisfying the driving and thermal power demands and while respecting the components constraints, the ON/OFF switching times of the APU and the SOC constraints. These constraints are listed in Table 3.5.

Table 3.5: Battery constrained

discrete step time:	$dt_s = 1$	(3.20)
number of time instances:	$N = \dfrac{n}{dt_s}$ (with n the time length of the driving cycle)	(3.21)
SOC evolution:	$SOC(t+1) = f\big(SOC(t), u(t)\big) + SOC(1)$	(3.22)
initial SOC:	$SOC_0 = 0.6$	(3.23)
final SOC:	$SOC_f = 0.6$	(3.24)
SOC limits:	$SOC(t) \in [0.2, 0.9]$	(3.25)
battery power constraint:	$P_{b_{min}} \le P_b(t) \le P_{b_{max}}$	(3.26)
battery current constraint:	$I_{b_{min}}(SOC) \le I_b(t) \le I_{b_{max}}(SOC)$	(3.27)
motor torque constraint:	$P_{m_{min}}\big(\omega_m(t)\big) \le P_m(t) \le P_{m_{max}}\big(\omega_m(t)\big)$	(3.28)
motor speed constraint	$0 \le \omega_m(t) \le \omega_{m_{max}}(t)$	(3.29)
generator power constraint:	$P_{g_{min}}\big(\omega_m(t)\big) \le P_g(t) \le P_{g_{max}}\big(\omega_m(t)\big)$	(3.30)
generator speed constraint:	$0 \le \omega_g(t) \le \omega_{g_{max}}(t)$	(3.30)

In fact, a compromise must be made for the two control objectives: minimization of both total fuel consumption and the switching ON/OFF times of APU. Indeed, a frequent ON/OFF operation could reduce greatly the fuel consumption, but obviously, it's not possible to operate the APU in such a way for technical reasons, mainly to avoid thermomechanical fatigue stress due to temperature variation for the different components of the GT. Therefore, since the DP has a mono-objective cost function, a weighting factor $\boldsymbol{\lambda}$, which varies from 0 to 1, is introduced to have a balanced global control objective as illustrated in the equation 3.31.

$$J^* = \min\left(\sum_{k=0}^{N} \lambda \cdot \dot{m}_f + \sum_{k=0}^{N} (1-\lambda) \cdot \frac{|s_{k+1} - s_k|}{2}\right) \qquad (3.31)$$

Where, $\boldsymbol{N}$ is the total duration of the given driving cycle, which is discretized into many time stages $\boldsymbol{k}$, $\dot{\boldsymbol{m}}_f$ the engine's instantaneous fuel consumption rate at time stage $\boldsymbol{k}$, $\boldsymbol{s_k}$ the engine's state (ON or OFF) at the current time stage. The choice of parameter $\boldsymbol{\lambda}$ has an important impact on the results. As we could see from equation 3.31, if $\boldsymbol{\lambda}$ is close to 1, it means that fuel consumption is more important than the engine ON/OFF state changes and it should be reduced as much as possible. Otherwise, the engine ON/OFF state change is more sensitive, and the fuel consumption is less important. Therefore, the choice of $\boldsymbol{\lambda}$ should be decided in an optimal way in order to achieve a balanced global minimization. Another important parameter that should be optimized is the power of the GT system ($\boldsymbol{P_{GT}}$). For our application, the GT-system will be operated at one fixed working point with constant operating power and efficiency.

As illustrated in figure 3.21, a bi-level optimization process is proposed as the Energy Management Strategy (EMS) in this study, which consists of two combined optimization algorithms: a genetic algorithms (GA) and the Dynamic Programming (DP). Inspired by natural selection and evolution, GA is an adaptive heuristic search algorithm and is commonly used to generate high-quality solutions to optimization and search problems [3.68]. In our optimization

process, as an upper level optimization, GA is responsible for exploring the design space of P_{GT} and λ and to generate many parameter combinations or individuals (a set of parameter combination of P_{GT} and λ) by relying on GA operators as selection, reproduction, crossover, mutation, etc.
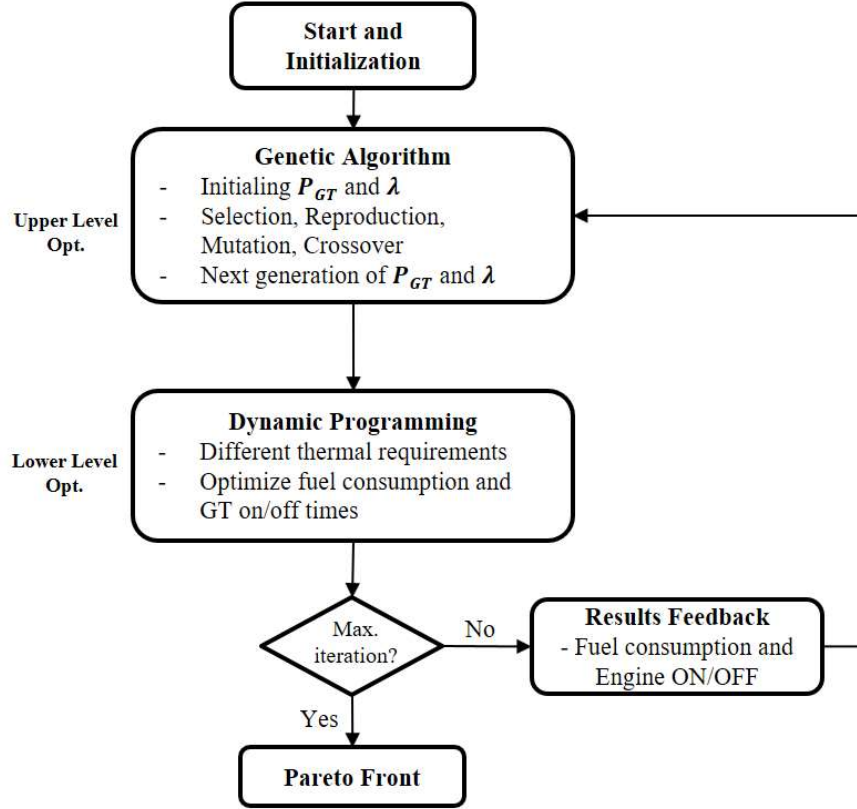

Fig. 3.21: Bi-level Optimization process of EMS

In the lower level, after receiving a generation of individuals from upper level, the DP algorithm is used to realize the global minimum of the objective function while respecting the component constraints and guaranteeing the *SOC* levels equal to the settings at the beginning SOC_0 and at the end SOC_f. Based on the Bellman principle, DP is a well known benchmarking technique to solve the optimal control issue of hybrid electric vehicles (HEVs) for given hybrid architecture, component sizings, and the driving cycle [3.69]. It allows the HEV controller to make a sequence of decisions in order to minimize the cost function in equation 3.31. In order to calculate the total switching ON/OFF times, the engine's ON/OFF state must be chosen as the second state variable besides the battery SOC as the first state variable. As an SHEV, the only degree of freedom for controlling the APU is the engine's ON/OFF command. The lower level in the optimization process will generate not only the optimal objective function, but also the optimal controls such as when and how long to start/stop the GT-system.

With the feedbacks from the lower level, the GA will decide the next generation of individuals for lower level to evaluate. This optimization loop will continue until the end of iterations. Finally, the combined GA and DP algorithms will find the optimal solutions and the associated control sequences.

3.6 Simulation results

The potential of fuel savings of the GT-systems-APU compared to the ICE-APU was simulated on three consecutive WLTC driving cycles (23 km each) covering driving distance up to around 70 km. Simulations emulate the behavior of self-sustaining SHEV, with no use of electric energy from the grid. The initial SOC is set at 60% and the final SOC at 60% by the end of the trip. As in chapter 2, simulations are performed on a baseline scenario similar to current fuel consumption on standard regulatory drive cycles where only propulsion energy needs are accounted, and four additional scenarios accounting for different cooling, heating and electric consumption needs. These scenarios are explained in details in chapter 2. They are the followings:

- Baseline (S0): Only mechanical propulsion needs
- Scenario 1 (S1): Baseline + continuous electric auxiliary need of 750W
- Scenario 2 (S2): Scenario 1 + cabin cooling ensured by A/C + heating ensured by stored waste heat
- Scenario 3 (S3): Scenario 1 + cabin cooling ensured by A/C + cabin heating ensured by electric heater when EC is off, or by waste heat when EC is on
- Scenario 4 (S4): Scenario 1 + cabin cooling ensured by A/C + cabin heating needs always ensured by electric heater

Figures A.3.1 to A.3.12 show the switching ON/OFF results versus fuel consumption for the different GT-system and the ICE using the bi-level optimization process. Several conclusions can be drawn from the simulation results:

1- In fact, compared to results in chapter 2 where the number of switching ON/OFF was not controlled, reducing the switching ON/OFF number increases the fuel consumption of the powertrain in all configurations by about 4 to 5%.

2- Comparing the fuel consumption between the different GT-configurations, around 26% of reduced fuel consumption is observed when comparing the RGT operating at 950°C to the SGT operating at 950°C on all other scenario on all climates. Same percentage of fuel consumption reduction is observed when the TIT increases to 1100°C and 1250°C. On the other hand, up to 30% of fuel consumption reduction is observed when comparing the IRGT to the SGT on all scenarios on all climates and for all the TIT and up to 36% when comparing the IRReGT to the SGT on all scenarios on all climates and for all the TIT. These results confirm the importance of the right selection of the GT thermodynamic configuration to be implemented in a SHEV.

3- Comparing the fuel consumption between the same GT configurations operating at different TIT, around 10% less fuel consumption is observed for the SGT when increasing the TIT from 950°C up to 1100°C and up to 15% when increasing the TIT from 950°C to 1250°C on all scenarios and for all the climates. For the RGT configuration, increasing the TIT from 950°C to 1100°C shows a reduction in fuel consumption by 12% on all scenarios and for all the climates. Also, increasing the TIT of the RGT from 950°C up to 1250°C results in a reduction of fuel consumption by 20% on all scenarios and for all the climates. These results

highlight the importance of increasing the TIT of GT systems and its results in terms of fuel consumption saving.

4- Comparing the different scenarios, around 10% of additional fuel consumption is observed when considering the 750W additional electric auxiliary need. Around 5% of additional fuel consumption is observed when considering the air conditioning cooling needs in cold climate, between 8% and 10% in the temperate climate and up to 20% in the hot climate. When hot thermal needs are ensured from EC waste heat when the engine is ON and from the use of electric heater when it is OFF as in scenario 3, the fuel consumption increases by around 21% in cold climate, by around 18% in temperate climate and by less than 0.05% in hot climate. When hot thermal needs are ensured always using electric heater as in scenario 4, the fuel consumption is shown to increase by 30% on cold climate, by 15% on temperate climate and by less than 0.1% in hot climate. These results confirm the impact of considering the vehicle non-mechanical energetic needs described in details in chapter 2 on fuel consumption. They highlight also the importance of using the EC waste heat to ensure the hot thermal needs since the fuel consumption can be reduced by 12% in cold climate on SHEV and by 6% in temperate climate on the same powertrain architecture.

5- Finally, comparing the different climates, it is obvious that the base line scenario and the scenario 1 show no difference in fuel consumption results. However, the cold climate shows between 3 to 6% less fuel consumption compared to temperate climate in scenario 2. This can be explained by lower thermal power required to ensure the cooling of the vehicle's cabin. On the other hand, the hot climate compared to the temperate climate shows an increase in fuel consumption by 7% and 10%. This can be explained by the additional thermal power required to cool the vehicle's cabin in hot climate. These results highlight the importance of considering the different climates during vehicle fuel consumption. These results show also the importance to consider innovative technologies to reduce the non-negligible additional fuel consumption resulting from considering the vehicle's non-mechanical energetic needs. Among these technologies, we can list the ejector and other tri-thermal systems recovering hot waste thermal heat and transforming a fraction of them to cooling thermal power which can be used to ensure the air conditioning functions for free. These technologies are not considered in this thesis work but will be envisaged in futur research works.

The fuel consumption results' for the lower switching ON/OFF number of the APU for the different climates are presented in figure 3.22 to 3.30 below. For the rest of the study, only scenario 3 will be considered since it accounts for all vehicle energetic needs and uses the GT-system wasted heat when it is ON to heat the vehicle's cabin.
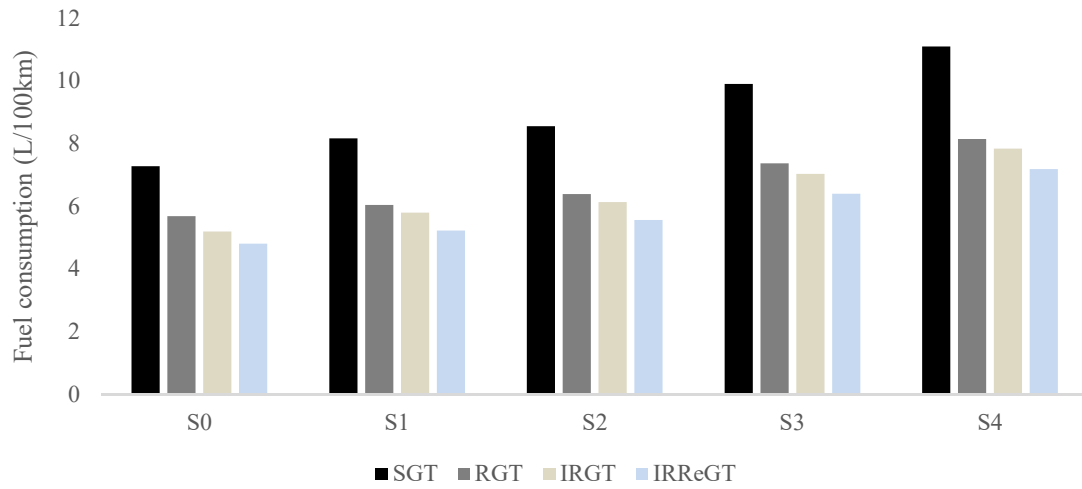
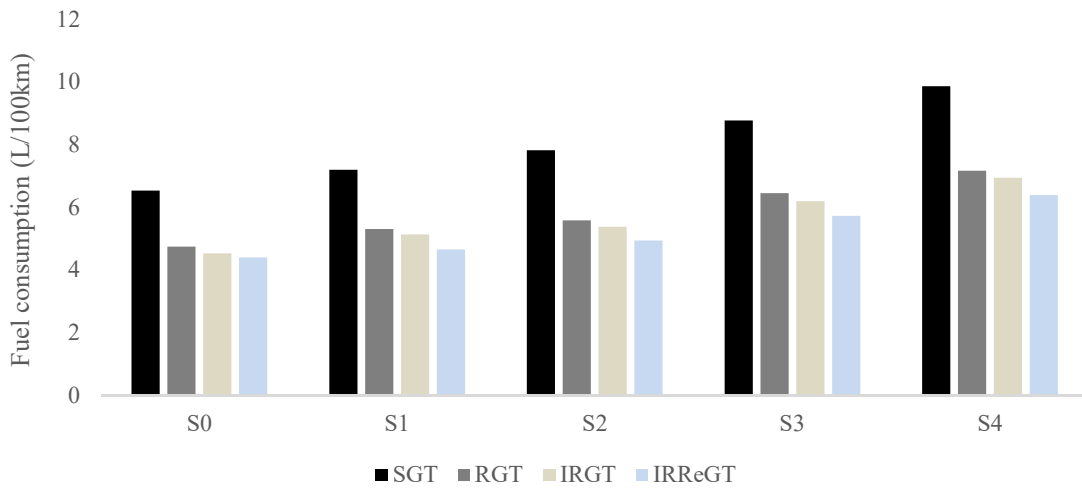*Fig. 3.22: Fuel consumption for the four GT-systems operating at TIT=950°C for cold climate*

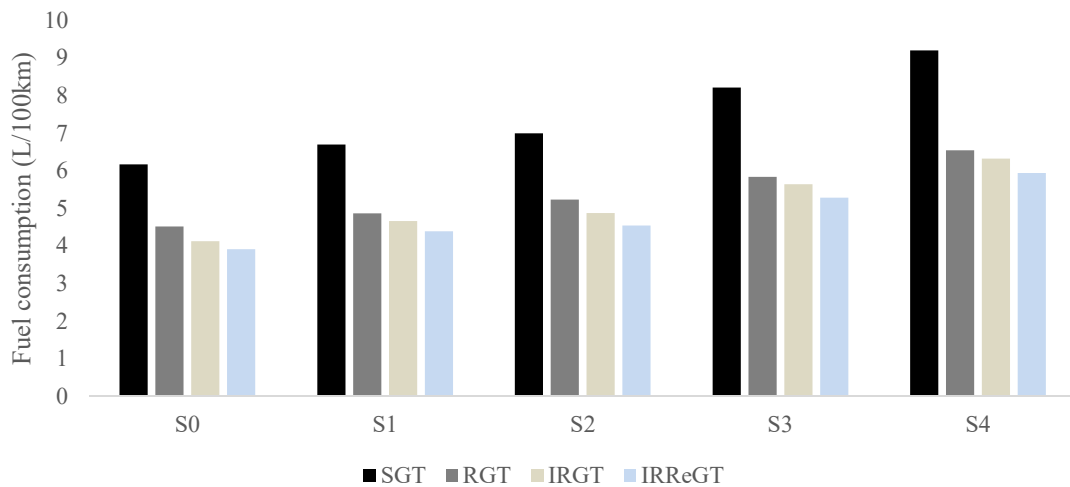*Fig. 3.23: Fuel consumption for the four GT-systems operating at TIT=1100°C for cold climate*

Fig. 3.24: Fuel consumption for the four GT-systems operating at TIT=1250°C for cold climate

Fig. 3.25: Fuel consumption for the four GT-systems operating at TIT=950°C for temperate climate

Fig.3.26: Fuel consumption for the four GT-systems operating at TIT=1100°C for temperate climate
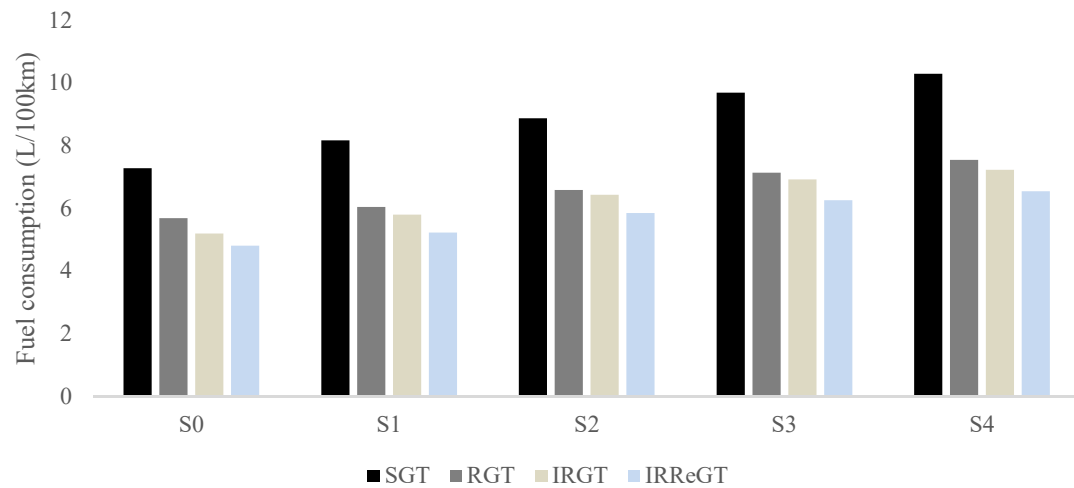

Fig.3.27: Fuel consumption for the four GT-systems operating at TIT=1250°C for temperate climate

Fig.3.28: Fuel consumption for the four GT-systems operating at TIT=950°C for hot climate

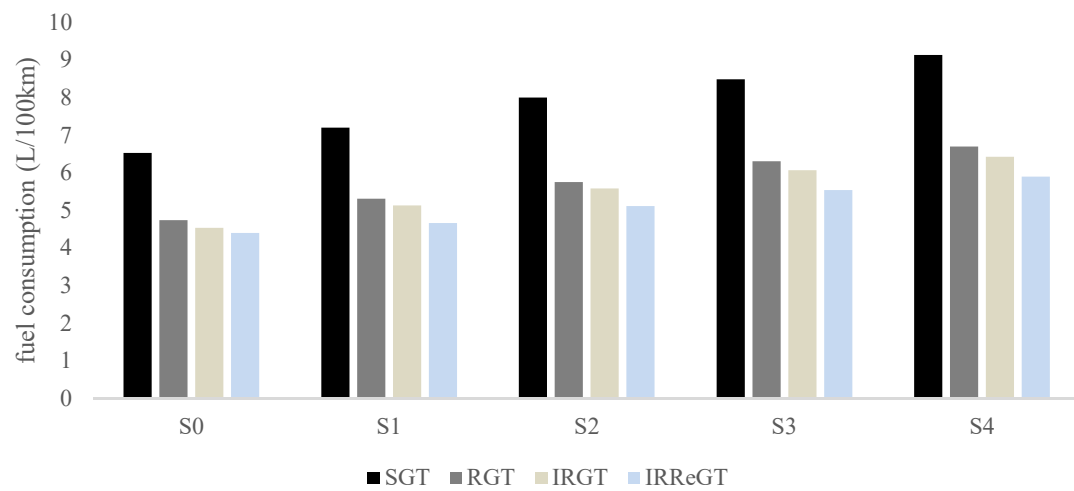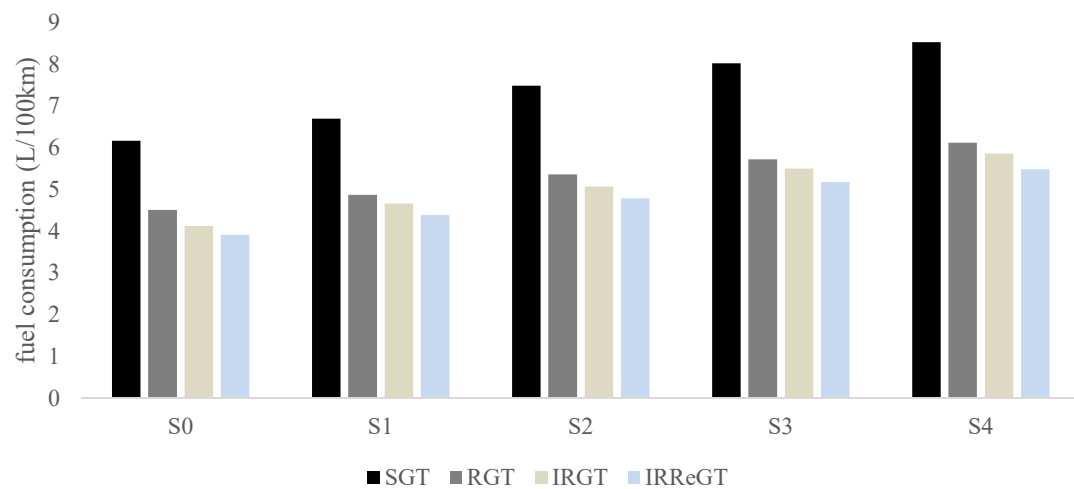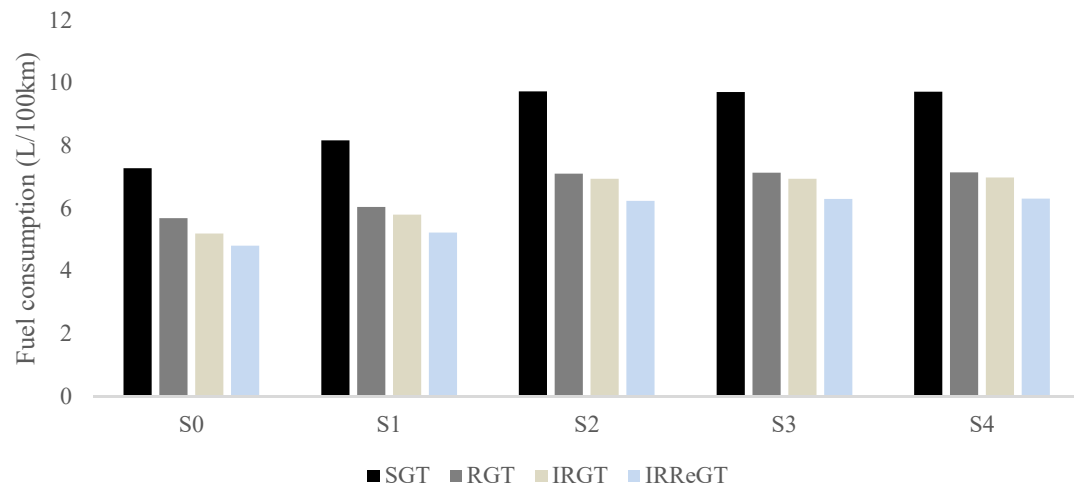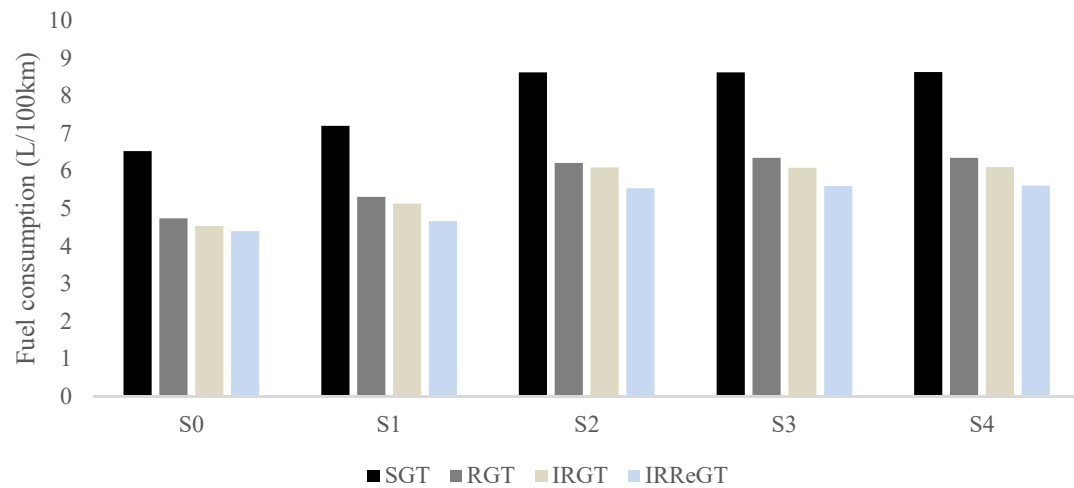*Fig.3.29: Fuel consumption for the four GT-systems operating at TIT=1100°C for hot climate*
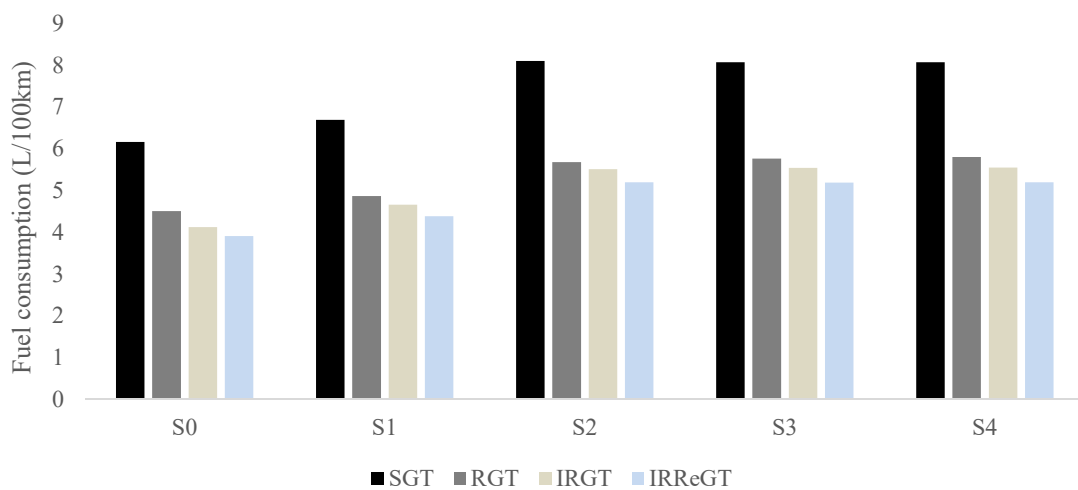

Fig.3.30: Fuel consumption for the four GT-systems operating at TIT=1250°C for hot climate

3.7 Conclusion and perspectives

A pre-design analysis was carried out in this chapter on the four identified realistic gas turbine configurations identified through the exergo-technological explicit selection method developed in chapter 2. The different configuration are: the simple gas turbine (SGT), the regenerative gas turbine (RGT) and intercooled regenerative gas turbine (IRGT) and the intercooled regenerative reheat gas turbine (IRReGT).

The study starts by an energetic analysis and a thermodynamic optimization for the different GT-system configurations for three different operating temperatures in order to identify the optimal operating point of the system. The two main objectives to maximize are the efficiency and the net specific work. The Non-dominated Sorting Genetic algorithm (NSGA) was used to find the optimal solution for maximizing these two objectives. The final operating point choice was made according to the best efficiency point found from the optimization. Therefore, the net specific work resulting was considered to calculate the mass flow rate for the different configurations under the different operating temperatures.

Then a predesign was carried out based on the optimization results. It consists to find a relation between the air mass flow rate and the different components' weight. Up to this end, the turbomachines weight was estimated by establishing a mathematical relation between the mass flow rate and the power for a given rotation speed of different commercialized automotive turbochargers. As for the heat exchangers, a design was carried out for both intercooler and regenerator and the weight of these components for the different configurations and the different operating temperature was calculated. The combustion chambers' weight was calculated based on an already existed combustion chamber for gas turbine application and by applying a correlation between the air mass flow rate across it and its thermal power. As for the electric generators, the weight was estimated using data retrieved from literature. Finally, the power to weight ratio was accounted for.

Then the different GT-systems were integrated in the SHEV model developed on chapter 2. Fuel consumptions were simulated using a bi-level optimization method developed in this chapter in order to find a compromise between two control objectives: (1) the minimization of the total fuel consumption and (2) the minimization of switching ON/OFF times of APU. Simulation results show an increase in fuel consumption by 5% compared to fuel consumption results of chapter 2 where the number of switching On/Off of the APU was not constrained. Results highlights also the impact of considering the vehicle additional non-energetic needs such the electric and thermal needs as well as the impact of climates on vehicle fuel consumption. It highlights also the beneficial impact of increasing the GT-systems operating temperature and proves again that the IRReGT is among the best suitable gas turbine configurations in terms of fuel consumption reduction.

Annex 3.A : Simulation results

Fig. A.3.1: Number of switching ON/OFF versus fuel consumption for SGT operating at three different TIT on the WLTC considering cold climate

Fig. A.3.2: Number of switching ON/OFF versus fuel consumption for RGT operating at three different TIT on the WLTC considering cold climate

Fig. A.3.3: Number of switching ON/OFF versus fuel consumption for IRGT operating at three different TIT on the WLTC considering cold climate

Fig. A.3.4: Number of switching ON/OFF versus fuel consumption for IRReGT operating at three different TIT on the WLTC considering cold climate

Fig. A.3.5: Number of switching ON/OFF versus fuel consumption for SGT operating at three different TIT on the WLTC considering temperate climate

Fig. A.3.6: Number of switching ON/OFF versus fuel consumption for RGT operating at three different TIT on the WLTC considering temperate climate

Fig. A.3.7: Number of switching ON/OFF versus fuel consumption for IRGT operating at three different TIT on the WLTC considering temperate climate

Fig. A.3.8: Number of switching ON/OFF versus fuel consumption for IRReGT operating at three different TIT on the WLTC considering temperate climate
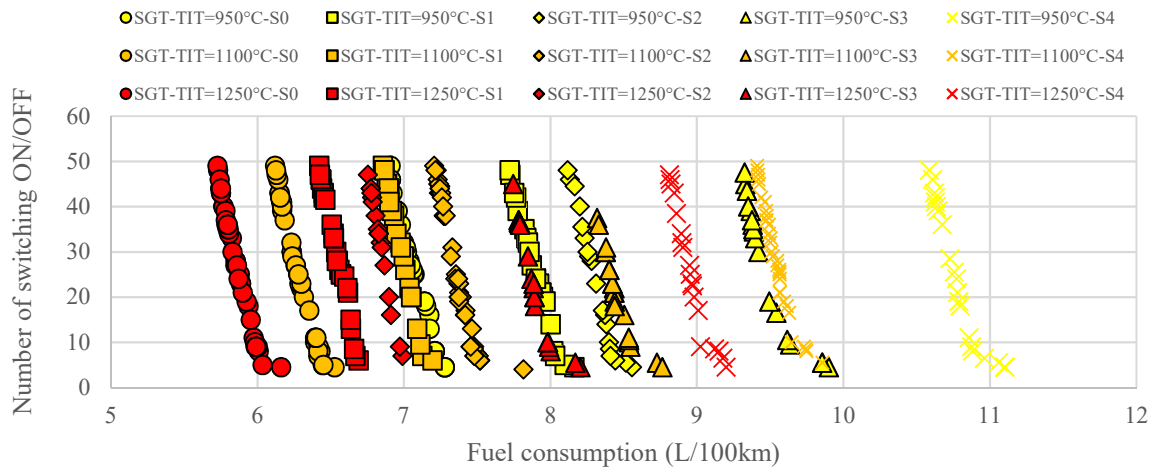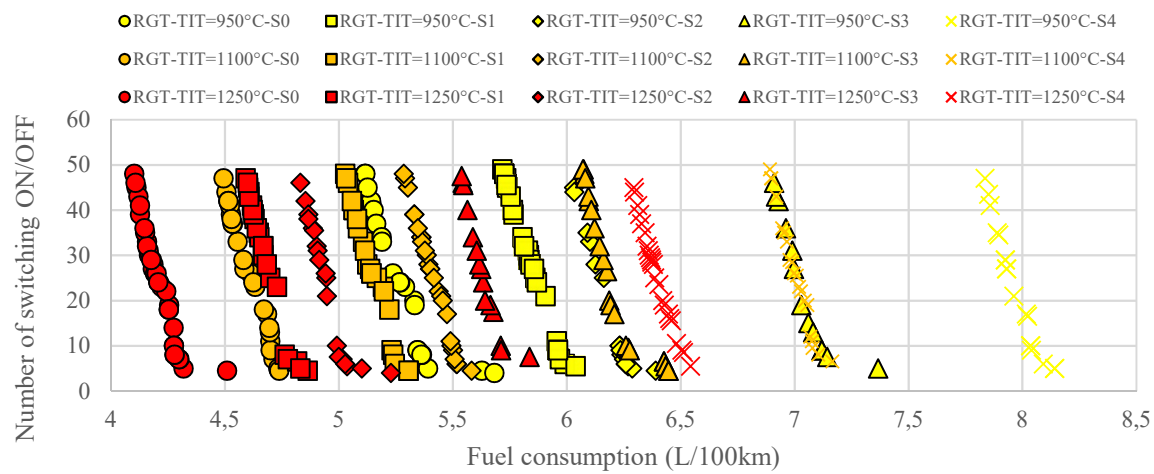

Fig. A.3.9: Number of switching ON/OFF versus fuel consumption for SGT operating at three different TIT on the WLTC considering hot climate

Fig. A.3.10: Number of switching ON/OFF versus fuel consumption for RGT operating at three different TIT on the WLTC considering hot climate
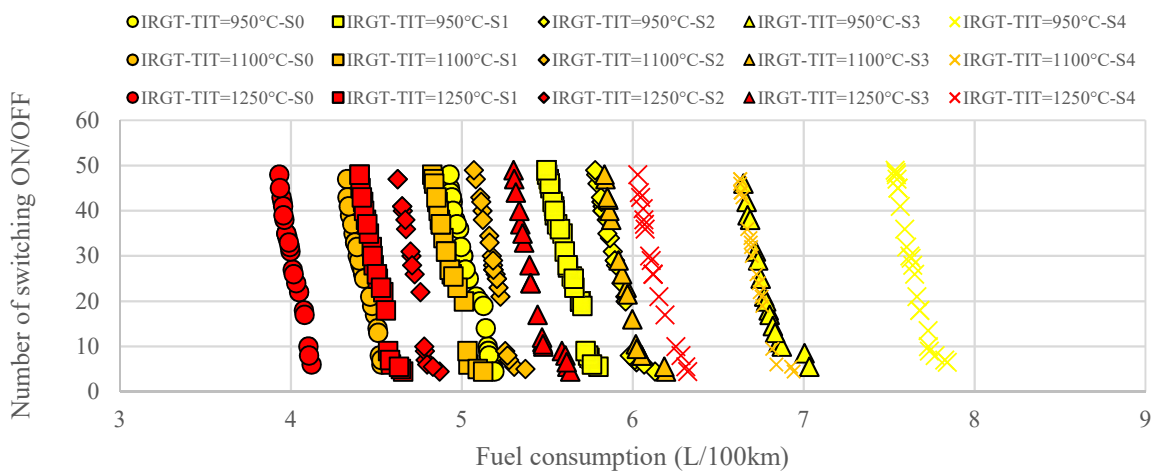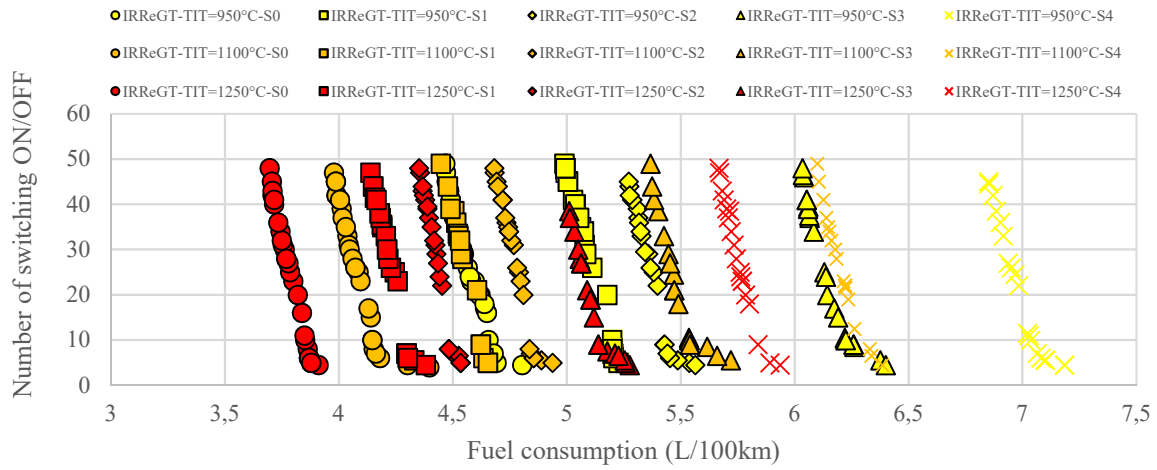

Fig. A.3.11: Number of switching ON/OFF versus fuel consumption for IRGT operating at three different TIT on the WLTC considering hot climate
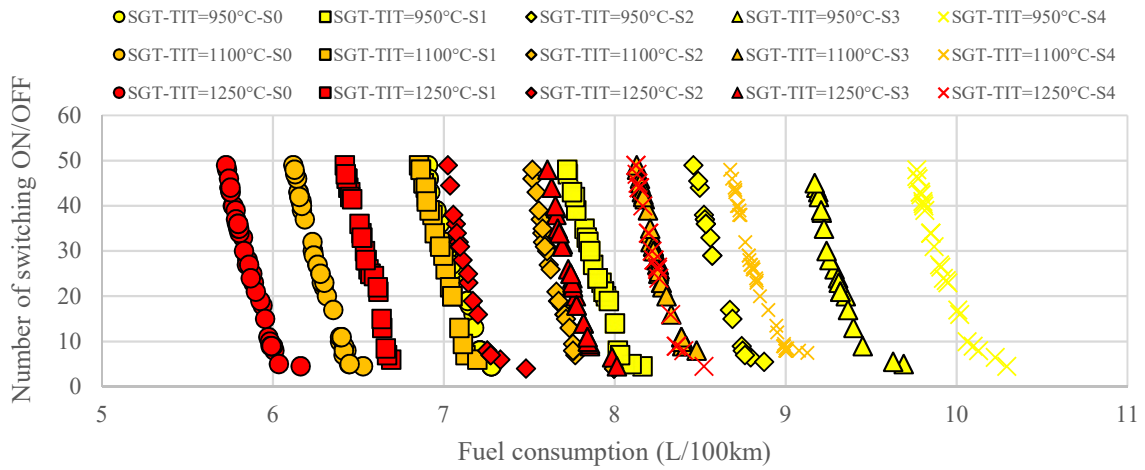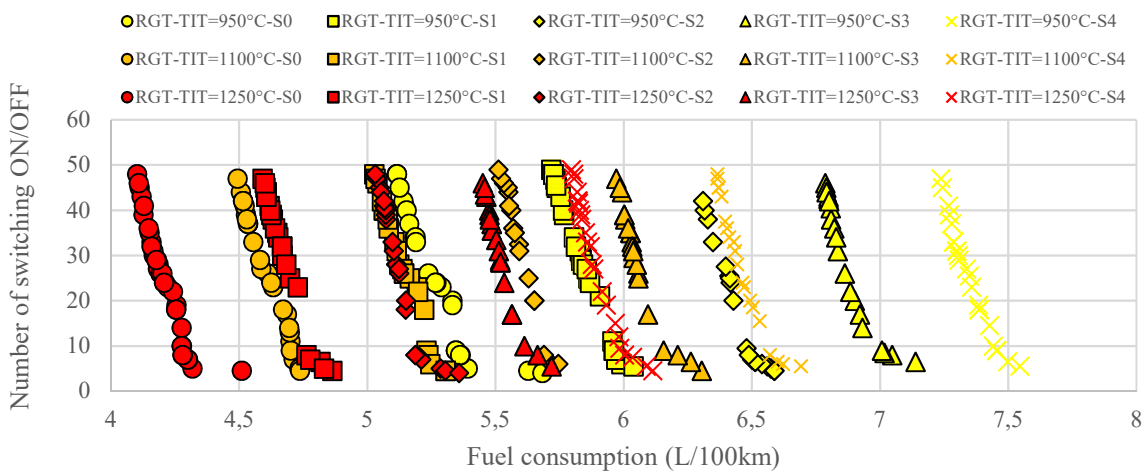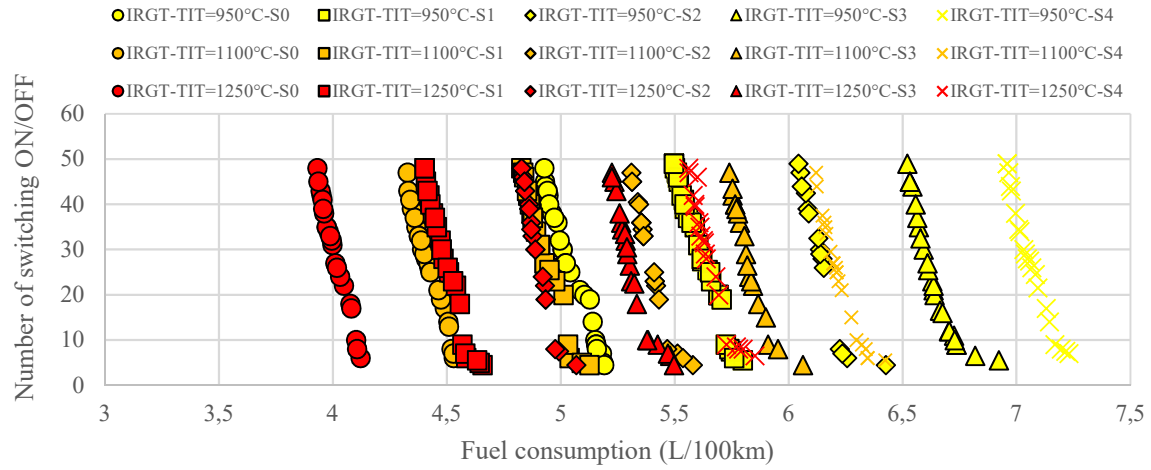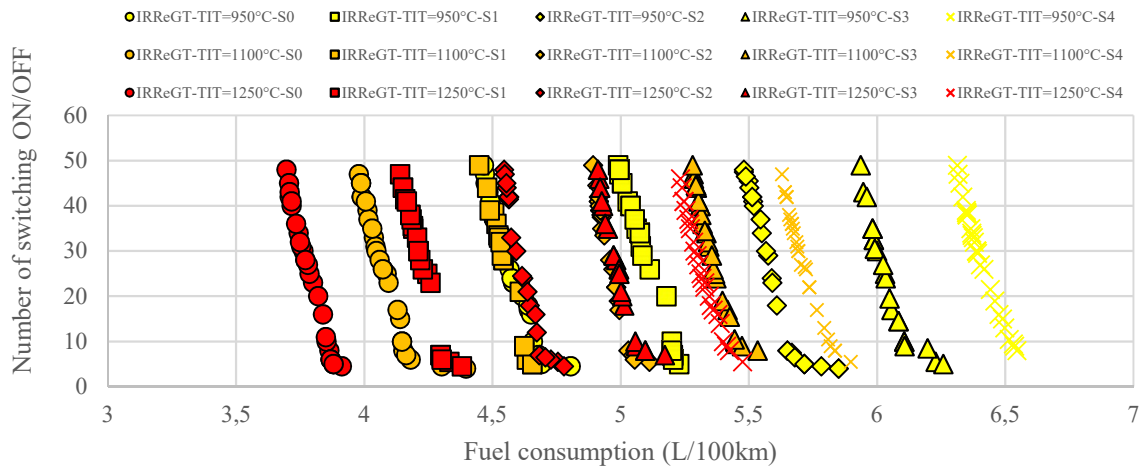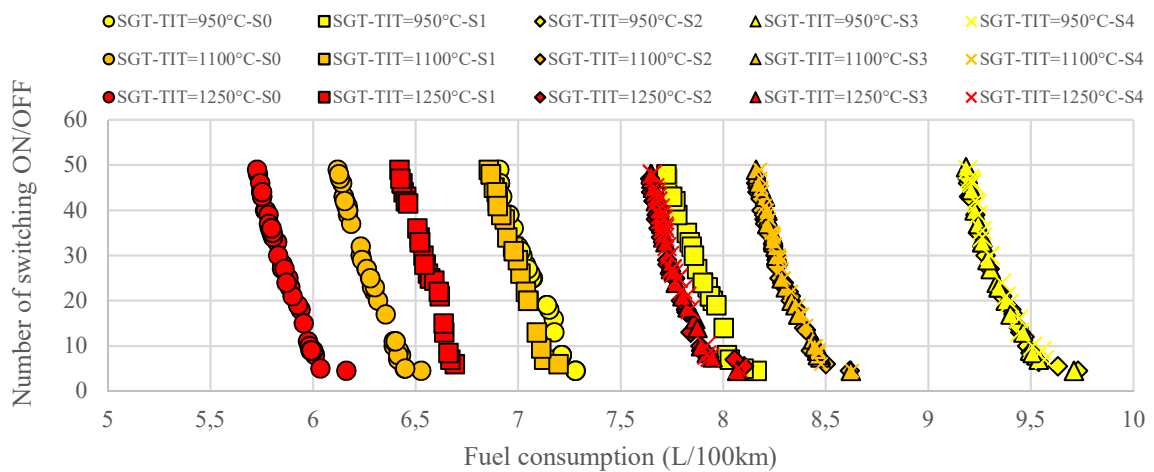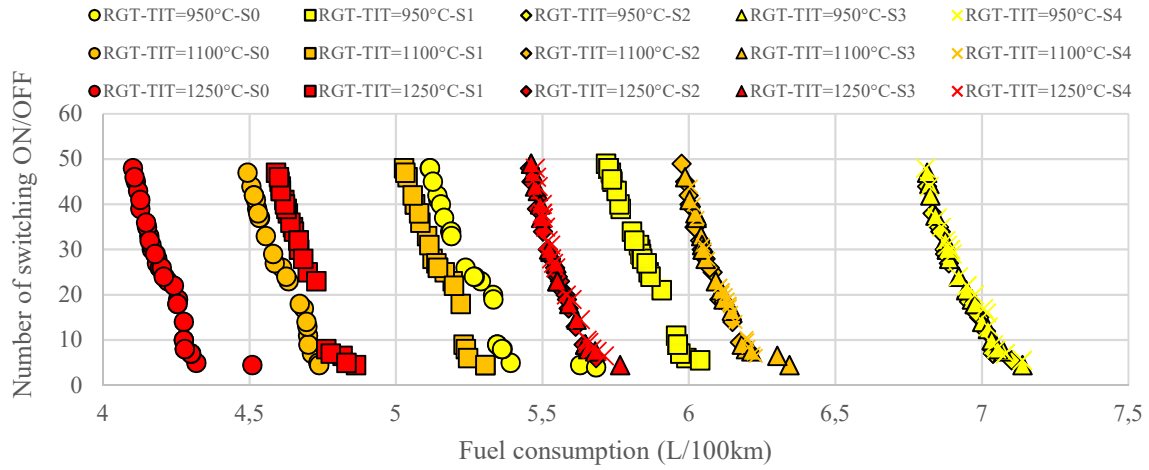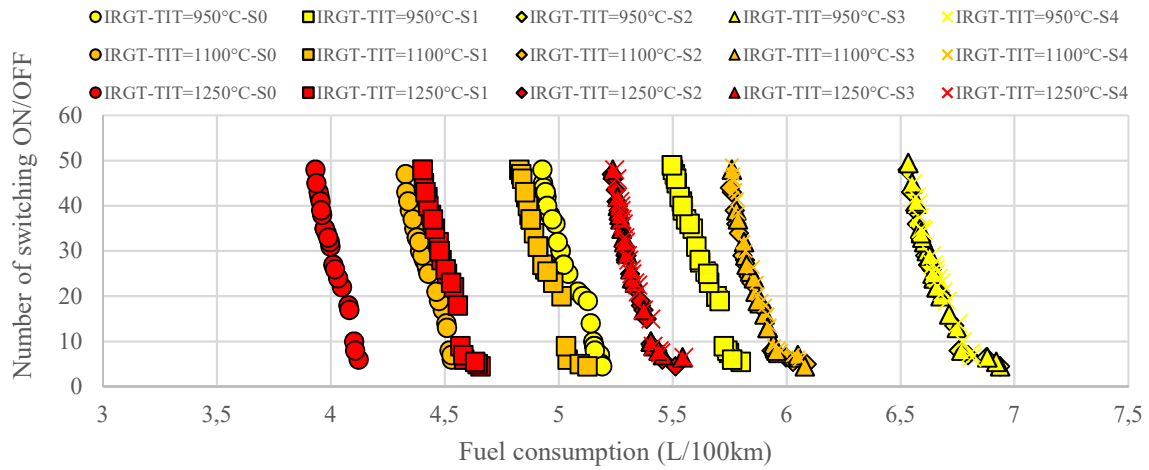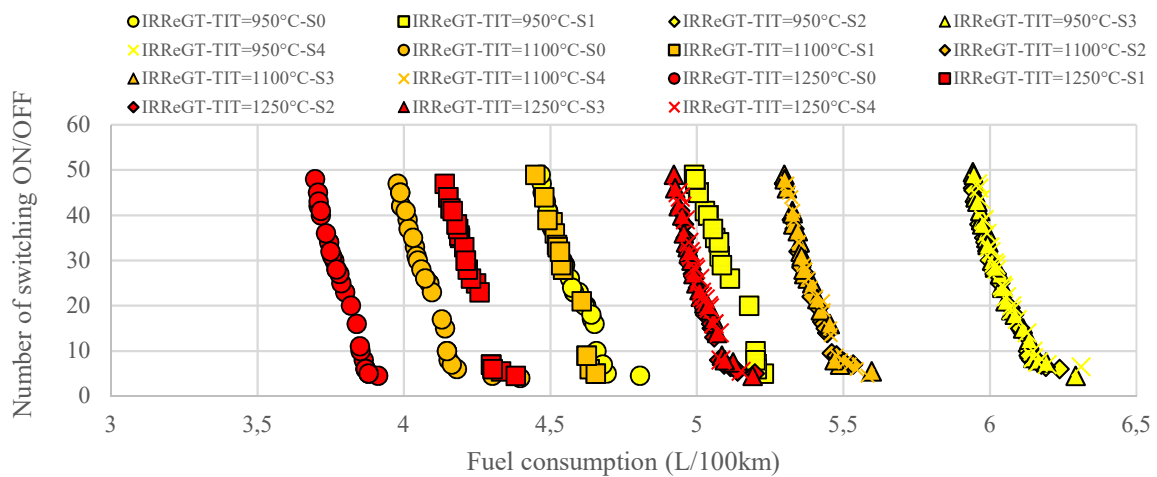

Fig. A.3.12: Number of switching ON/OFF versus fuel consumption for IRReGT operating at three different TIT on the WLTC considering hot climate

Résumé chapitre 4

Les systèmes de turbine à gaz font partie des convertisseurs d'énergie potentiels pour remplacer le moteur à combustion interne dans les futurs véhicules à chaîne de traction hybrides électriques séries. La consommation de carburant de ces groupes motopropulseurs dépend fortement du rendement du convertisseur d'énergie, de la stratégie de gestion de l'énergie déployée à bord ainsi que du fonctionnement transitoire pendant la phase de démarrage.

Ce chapitre présente une modélisation dynamique et le calcul de la consommation de carburant d'un système de turbine à gaz à refroidissement intermédiaire avec récupérateur et réchauffage intermédiaire utilisé comme groupe auxiliaire de puissance sur un véhicule électrique hybride en série. Un modèle de véhicule est développé et une méthode d'optimisation est proposée pour optimiser le fonctionnement du groupe motopropulseur. Cette méthode consiste à utiliser la programmation dynamique comme stratégie de gestion de l'énergie afin de minimiser la consommation de carburant et le nombre de démarrages. Les simulations de consommation de carburant sont réalisées sur le cycle d'homologation WLTP tout en considérant les besoins énergétiques additionnelle du véhicule tels que le besoin électrique et les besoins thermique de chaud et de froid.

Ensuite, un modèle dynamique de turbine à gaz est développé, dans lequel les différents composants, tels que la turbomachine et les échangeurs de chaleur, sont modélisés en tenant compte de leurs inerties dynamiques. Le rendement, la puissance et la consommation de carburant sont calculés en régime transitoire. Sur la base des résultats d'optimisation du nombre de démarrage du système, les résultats de la simulation dynamique de la consommation de carburant sont pris en compte à la place des résultats de la programmation dynamique. Deux stratégies de démarrages ont été investigués, une stratégie de démarrage à puissance constante et une stratégie de démarrage à quantité de carburant injectée constante.

Les résultats montrent une augmentation de la consommation de carburant entre 2,4 % et 3,8 % avec le premier scénario de démarrage et entre 5,7 % et 6,4 % avec le second scénario, par rapport au modèle statique développé dans le chapitre 3.

Chapter 4: Dynamic modelling of an Intercooled Regenerative Reheat Gas Turbine for auxiliary power unit on series hybrid electric vehicle*

4.1 Introduction

Gas turbine (GT) machine presents a forthcoming potential for integration as main energy converter as replacement of internal combustion engine (ICE) in hybrid electrified powertrains [4.1]. Despite the fact that this system suffered from high fuel consumption and acceleration lag in conventional vehicles, GT regains interest today in series hybrid electric vehicle (SHEV). In fact, in this newly advanced powertrain shown in figure 4.1, the GT drives an electric motor generator (EMG) at constant speed and power while operating at its maximal efficiency. The GT and the EG constitute the auxiliary power unit (APU) which operates to recharge the vehicle battery once depleted. On the other hand, the vehicle propulsion is ensured by an electric motor (EM), designed to ensure the vehicle's performance in terms of speed, acceleration and gradability.

GT-systems as main energy converter for automotive applications, offer many benefits compared to ICE [4.2, 4.3]. Among these benefits, we can mention the reduced number of the energy converter components and rotating parts, the reduced vibration and the multi-fuel capability. Adding to that, the GT is a thermodynamic machine operating according to Brayton open cycle, where the amount of heat not transformed to noble mechanical power, is rejected outside the thermodynamic cycle to the ambient. Therefore, this wasted heat can be used to ensure vehicle thermal hot needs, increasing therefore the overall powertrain efficiency by avoiding the use of cabin electric heaters [4.4].

Different GT thermodynamic configurations can be considered for integration in SHEV, ranging from simple GT, to regenerative GT (RGT), to intercooled GT, to reheat GT among others [4.1, 4.5]. The review of literature shows that RGT using a regenerator heat exchanger (HEX) that recovers heat from turbine outlet to heat the air upstream the combustion chamber has been largely investigated over the years [4.2, 4.6, 4.7]. However, this thermodynamic configuration with good optimal efficiency, suffers from low net specific work leading to high air mass flow rate [4.1, 4.2] which consequently increases the size and weight of the machine, leading to higher vehicle integration complexities. Moreover, recent papers published show that the intercooled regenerative reheat gas turbine (IRReGT) configuration presents higher efficiency than RGT which leads to better fuel consumption in SHEV [4.1, 4.8]. Adding to that, with intercooled compression and turbine reheat processes, higher net specific work can be achieved compared to RGT configuration, leading to reduced air flow rate for the same power output and consequently a reduced weight and size of the system which leads to lower integration complexity. Powertrain simulations of an IRReGT-APU-SHEV with dynamic programing (DP) as energy management strategy (EMS) show up to 22% of fuel consumption saving compared to ICE-APU-SHEV. The IRReGT operates at a maximum turbines inlet temperature (TIT) of 1250°C. Moreover, the heat rejected from the intercooled can be recovered for cabin heating to ensure hot thermal comfort energetic needs. The choice of intercooler for waste thermal heat compared to heat rejected from GT exhaust gases was made for three main

This chapter is written in the form of a scientific paper that will be published later. Therefore some informations are redundant with chapter 2 and 3 mainly in the « introduction » section (4.1) and in the « SHEV model » section (4.4).

149

reasons: First, the heat rejected from the intercooler is sufficient to ensure cabin heating when the IRReGT is ON even under most severe conditions. Second, the maximum air temperatures reached in the intercooler allow the use of an aluminum heat exchanger (HEX) instead of steel HEX as in the case of exhaust gases, reducing therefore the weight and the cost of the heating system. Finally, recovering thermal waste heat from the intercooler prevents the use of an additional HEXs on the GT exhaust line which adds more back pressure and reduces therefore the GT-system thermal efficiency.

However, the powertrain control strategy in these studies [4.1, 4.8] used the dynamic programing as energy management strategy (EMS) in order to provide the global optimal strategy to power the APU ON and OFF. Consequently, the results consider only the impact of IRReGT-system on the consumption and exclude the influence of the rule-based energy management strategy found in vehicle controller [4.9, 4.10]. For instance, during the transient phase during the switching ON of the system, the efficiency, the power and the operating temperature are considered to be the same as during established permanent steady state operation, which is not realistic. Also the number of switching ON/OFF of the system during the operation is not restrained when DP is considered as EMS. In fact, in order to respect some thermomechanical constraints regarding GT-system material and emissions mainly during transient operation, the number of IRReGT-system startups must be limited.

Furthermore, according to Newton second law, some amount of energy is required to drive the system from rest to its steady state operating regime. This amount of energy depends on IRReGT rotating components inertia among them the compressors (C), the turbines (T), the electric motor generator (EMG) and the common shaft, on the system friction, as well as on the compression and the expansion phases. This amount of energy must be consumed from vehicle battery during starting and was not considered in previous studies. Adding to that, the regenerator presents a thermal inertia which worsens the efficiency during the transient starting phase. For instance, when the regenerator is relatively cold, the IRReGT first combustion chamber inlet temperature is low and a higher amount of fuel is required to achieve the desired TIT temperature, which increases the fuel consumption and reduces as result the startup system efficiency.

The review of literature shows interesting insight in modeling dynamically gas-turbine systems or turbomachinery systems. For instance, Mazloum et al [4.11, 4.12] developed dynamic model components for an adiabatic compressed air energy storage system using Dymola software. Their model, validated through testing, considers the inertial rotation transient operation for centrifugal turbomachines as well as the heat exchanger thermal transient behavior. Camporeale et al [4.13] developed a Matlab-Simulink code for singe-shaft heavy-duty GT and double-shaft aeroderivative industrial GT. Others such as Hussain et al [4.14], Turie et al [4.15], Thirunavukarasu [4.16] worked on dynamic modeling for different GT configurations. Kim et al [4.17] developed a simulation program for transient analysis of the start-up procedure of heavy duty GT for power generation. Others such as Botros et al. [4.18] have developed numerical techniques to resolve the dynamics equations describing the GT unit and compressors transient behavior. Some software were developed to understand the dynamic behavior of GT engines. For instance, GETRAN was developed to simulate the nonlinear dynamic behavior of single and multi-spool power generation gas turbine engines under different dynamic operating

conditions [4.19]. None of these studies have considered the transient operation of a IRReGT-thermodynamic configuration system and its impact on vehicle fuel consumption.
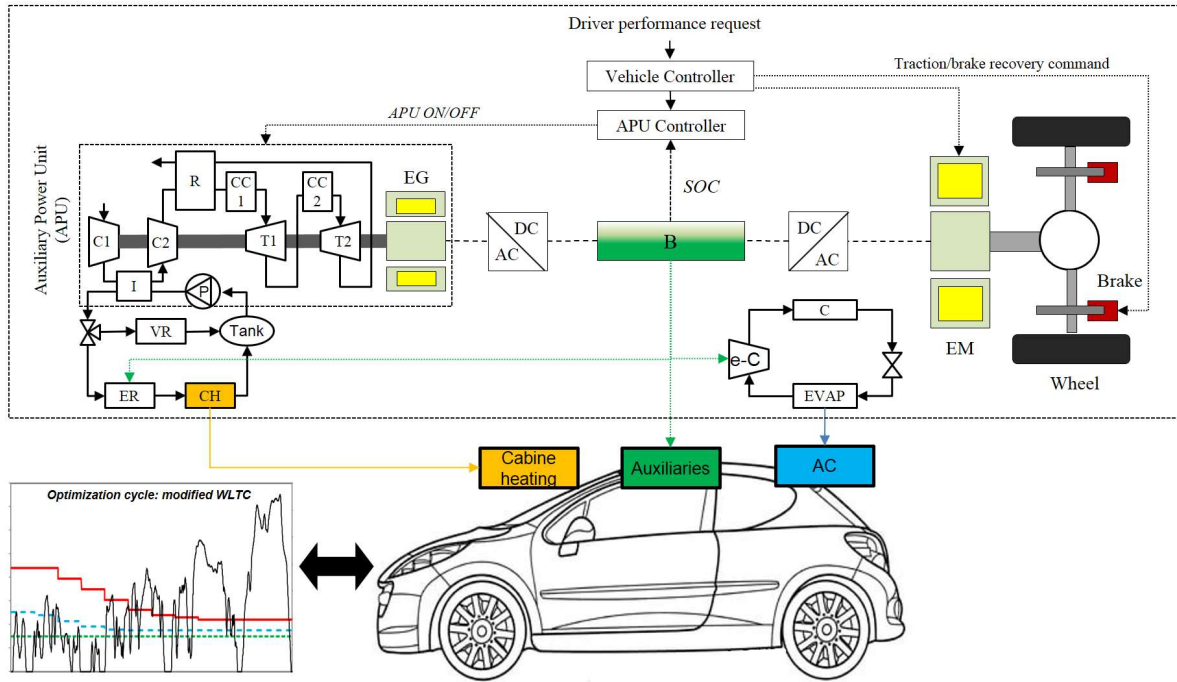

Fig. 4.1: SHEV powertrain with IRReGT as main energy converter

Based on these findings, and in order to approach the real fuel consumption of an IRReGT-APU-SHEV, while accounting for the penalty imposed by the transient operating phases, a dynamic IRReGT model is developed in this study. A methodology for assessing the fuel consumption potential of IRReGT while considering dynamic operation is presented in section 2 of this study. First, a SHEV model is developed and a bi-level optimization process is proposed as the energy management strategy (EMS) in order to find the optimal decision for switching ON and OFF the APU. The bi-level optimization consists of two combined optimization algorithms: a Genetic Algorithms (GA) and Dynamic Programming (DP) as presented in chapter 3. Dynamic programming (DP) is used as optimal energy management strategy (EMS) in order to find the optimal way to well manage the vehicle power flows and respect component constraints to minimize two control objectives: the fuel consumption vehicle criteria and the switching ON/OFF times of APU which impacts its durability. The GA is responsible for exploring the design space of GT power and the weighting factor introduced to have a balanced global control objective. Simulations are performed on WLTC optimization cycle by considering the vehicle additional non-mechanical energetic needs, among them the electric energetic need and the thermal comfort energetic needs. Then an IRReGT dynamic model is developed where turbomachinery and heat exchanger components are modeled using dynamic equations. The efficiency, the electric power, the thermal heat power and the temperature are calculated during transient operation. Based on bi-level optimization results of switching ON and OFF the APU and of defining the IRReGT optimal power, the dynamic simulation results are considered instead of DP results. Two different startups strategies were considered: (1) a constant power startup strategy where additional fuel is injected to maintain the desired IRReGT output power and (2) a constant fuel strategy where the same amount of fuel is injected during

the startup phase as during the permanent operation. The gap in terms of fuel consumption between DP optimal results and dynamic model results is obtained and the impact of considering the dynamic transient phases on fuel consumption is highlighted.

This study is novel in three ways. First, it is the first study to use a bi-level optimization results to serve as ON/OFF starting decision and to optimize the IRReGT net power for dynamic simulations. Second, it presents a comprehensive methodology for dynamic transient modeling of an IRReGT configuration for automotive application by considering the rotating machine's inertia and the heat exchanger thermal inertia impacts on fuel consumption, system efficiency, power and temperatures during transient phases. Third, it is the first study to highlight the impact of transient phases on the fuel consumption of a SHEV with IRReGT-APU.

4.2 IRReGT-System overview

The Intercooled Regenerative Reheat Gas Turbine (IRReGT) system is presented in figure 4.1. The system consists of two-stage intercooled (I) centrifugal compressors (C1, C2), a regenerator (R), a two-stage reheat centrifugal turbines (T1, T2) and two combustion chambers (CC1, CC2). The system can be divided into subsystems: the compression, the expansion, the combustion and the thermal heat regeneration subsystems. The GT-system is designed to operate at constant power and speed. The compression is performed in the two-stage intercooled compressors and the air working fluid is pressurized up to 12 bar. The intercooler is installed between the compressors in order to reduce the compression work and to cool down the air entering the regenerator. The regenerator recovers heat at the outlet of the second turbine in order to increase the temperature of the air entering the first combustion chamber. A second combustion chamber is installed downstream the first turbine in order to reheat the exhaust gases, increasing therefore the system efficiency and the net specific work [4.20-4.22]. An electric motor generator (EMG) is installed on the same shaft coupling the compressors to the turbines. During steady operation, it acts as an electric generator and recovers the net power produced by the machine, the turbines' power minus the compressors' power. During the starting phase, it acts as an electric motor, and drives the GT to its nominal operating speed.

Since thermal heat must be rejected outside the cycle during the intercooling compression phase, and knowing that thermal heat is required for vehicle cabin heating in order to ensure the thermal comfort [4.4], it is smart to consider the intercooler waste thermal heat, which dispenses the need for an electric heater or heat pump to ensure the cabin heating function. Therefore, the proposed architecture consists of the use of a working fluid that circulates in a closed-loop. This loop consists of a circulating pump (P), a controlled three-way valve, an electric resistance (ER), the vehicle cabin heater (CH), the vehicle radiator (VR) and a tank. The cabin heater, a heat exchanger, serves to heat the vehicle cabin and to ensure vehicle hot thermal energetic needs by exchanging with the cabin air when the GT-system in switched ON. During this phase, the vehicle radiator rejects the excess heat not used for cabin heating to the outside. The electric resistance serves as heater when the GT-system is off. It uses the electricity directly from the battery.

4.3 Methodology

This section presents the method adopted to evaluate the impact of the IRReGT's startup transient phases on the fuel consumption of a SHEV. The method consists of a three-step assessment plan as presented in figure 4.2.

In the first assessment step, an IRReGT-APU is integrated in a series hybrid electric vehicle (SHEV), and fuel consumption was simulated on a self-sustaining hybrid powertrain configuration where the fuel consumption depends only on the energy converter efficiency without using the electric energy from the grid to recharge the battery [4.23, 4.24]. Fuel consumption is simulated using a bi-level optimization process as the energy management strategy (EMS). It consists of two combined optimization algorithms: a genetic algorithm (GA) and Dynamic Programming (DP). DP is used as optimal energy management strategy (EMS) in order to find the optimal way to well manage the vehicle power flows and respect component constraints to minimize two control objectives: the fuel consumption vehicle criteria and the switching ON/OFF times of APU. The GA is responsible for exploring the design space of GT power and the weighting factor introduced to have a balanced global control objective. Simulations are performed on a sequence of three WLTC optimization cycles covering a total distance of around 70km, by considering the vehicle additional non-mechanical energetic needs: the electric energetic need and the thermal comfort energetic needs. The fuel consumption results are accounted considering an IRReGT constant power and efficiency during the startup phase, which leads to a biased fuel consumption results.

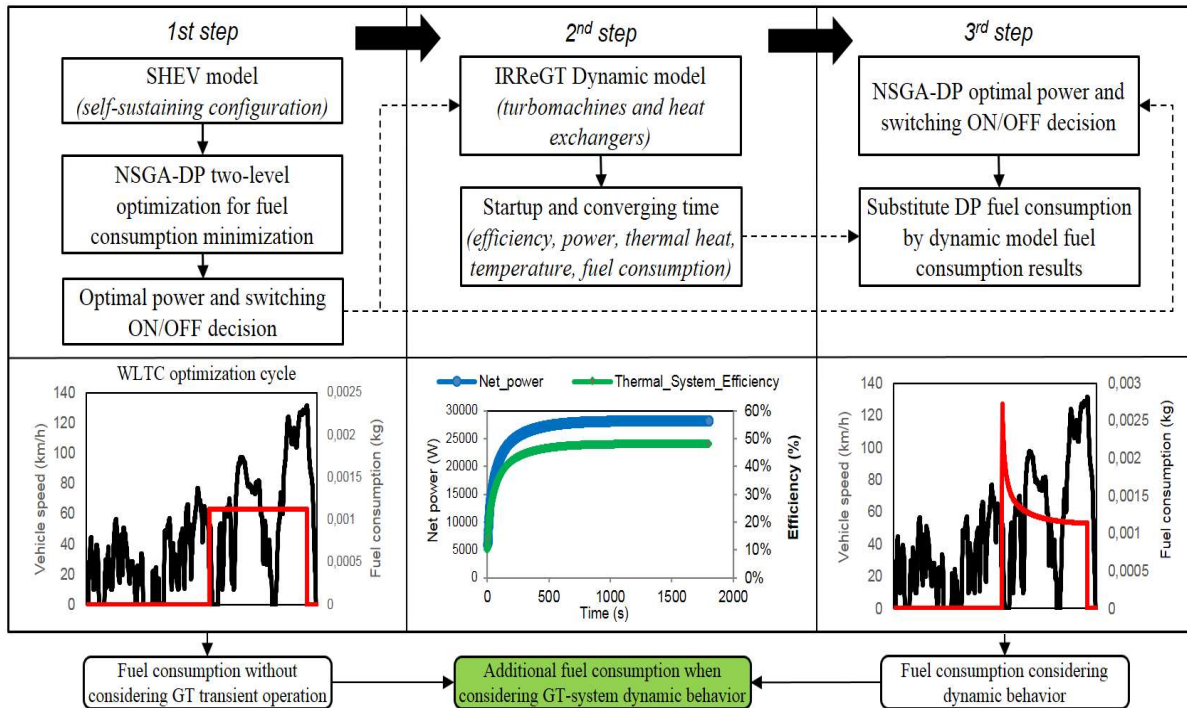*Fig.4.2: Methodology for estimating the overconsumption of the IRReGT-APU-SHEV when considering the transient startup*

In the second assessment step, a dynamic model of the IRReGT is developed and the different system components are modelled. This includes the turbomachines (compressors and turbines coupled to the electric generator/motor), and the heat exchangers (intercooler and regenerator).

The impact of considering the dynamic model on the efficiency, temperature, net power and thermal heat during the IRReGT start-up phase, is evaluated by considering two startup strategies: (1) a constant startup power strategy where higher fuel consumption is injected during the startup in order to maintain the same GT output power. This strategy leads to a quick increase in the temperatures, and (2) a constant fuel injection startup strategy where the same amount of fuel is injected during the transient phase as during permanent operation. This strategy leads to a longer convergence time to reach the nominal GT operation since the GT-system and mainly the regenerator takes more time to reach its permanent temperature.

Finally, in the third assessment step, the first step optimization results, "the instantaneous fuel consumption", are replaced by the dynamic fuel consumption results of the second step. The additional fuel consumptions are then accounted for and compared between the non-realistic NSGA-DP decisions. Also a comparison in terms of fuel consumption is done between the two-different considered startup strategies.

4.4 SHEV model

In order to account for the vehicle fuel consumption with IRReGT-system as main energy converter and to account later for the additional fuel consumption when considering the GT start-up transient operation, a medium-class SHEV, consisting of a IRReGT-APU and an electric traction system (as illustrated in figure 4.1) is modelled and presented in this section.

As described in many published papers [4.1, 4.8, 4.25], SHEV configuration presents the advantage of operating the APU at steady power corresponding to the optimum efficiency. On the other hand, the vehicle is propelled by an electric motor, powered by a battery and/or the APU, and properly sized to ensure the vehicle acceleration and velocity performance without deficiency.

In this section, we present a brief reminder since the powertrain design methodology was presented in chapter 2. First, the vehicle propulsion power needs are modelled using the vehicle dynamic longitudinal equations and the vehicle characteristics defined in the specifications. The vehicle maximum continuous speed is selected and the average load power on the selected optimization cycle, the Worldwide-harmonized Light Vehicles Test Cycle Cycle (WLTC), was accounted for, considering the vehicle mechanical propulsion energetic needs as well as the non-mechanical needs such as the electric needs and the thermal comfort needs.

The energy converter's continuous power depends on the vehicle autonomy on a given driven pattern and on the battery capacity. The vehicle autonomy criterion is defined as the time that the vehicle can be driven at maximum continuous speed, while ensuring the electric auxiliaries and thermal comfort needs and maintaining the battery's state of charge (SOC) within a defined range. As for the battery capacity, it was calculated by choosing the driving distance on the city part, the low speed part, of the WLTC without the need to switch ON the energy converter, for pollutant problematic in cities. Consequently, this corresponds to a full-electric driving mode. Finally, the electric motor power is accounted by considering the vehicle performance in terms of acceleration, maximum speed and gradability. The battery maximum power is then selected.

4.4.1 Powertrain setup

The same SHEV model presented in chapter 2 and chapter 3 is used in this chapter. The vehicle characteristics have been presented and are summarized in tables 2.2 and 3.4 respectively. Three different IRReGT machines were considered in this chapter. The first one corresponds to a low temperature-low cost material IRReGT where the maximum combustion temperature achieved is 950°C. The second one corresponds to a machine with a combustion chamber temperature of 1100°C, using specific alloys. The third machine achieves a combustion chamber temperature of 1250°C and uses specific materials and super-alloys [4.26]. The corresponding efficiencies and power to weight ratios of these three machines are also presented in table 3.4. Also the IRReGT were allowed to operate at constant power which will be decided by the optimization algorithm. This power was set between 15kW and 30kW. According to equations 4.1 and 4.2, with a 10kWh battery capacity allowing for a full-electric mode for about 50km as discrbed in chapter 2, an electric auxiliary consumption of 750W, a 1kW thermal power need for thermal comfort, a battery maximum state of charge (SOC) of 80% and minimum SOC of 30% and a maximum continuous speed of 120km/h on flat-road, the SHEV autonomy varies between 46 minutes for a 15kW net power IRReGT machine and up to around 600 min for a 22kW. When driving at constant speed of 130km/h on flat road, the autonomy will decrease to around 27min with a 15kW net power IRReGT machine and about 67 min for a 22kW net power IRReGT machine as shown in figure 4.3 below. It is worthy to mention that a 23kW net mechanical power IRReGT machine is required to drive the SHEV at 120km/h continuously without consuming electricity from the battery compared to 27kW IRReGT machine when the speed increases to 130km/h.

$$P_{Load} * T = P_{Electric} * T + E_{Bat_{available}} \tag{4.1}$$

$$(P_{mechanical} + P_{aux} + P_{Hot_{thermal}} + P_{Cold_{thermal}}) * T$$
$$= P_{IRReGT} * \eta_{EMG} * T + (SOC_{max} - SOC_{min}) * C_{bat} \tag{4.2}$$

| With	T	:	Time autonomy (h)
	$P_{Electric}$	:	Electric power charging the battery (kW)
	$E_{Bat_{available}}$	:	The energy available in the battery (kWh)
	$P_{mechanical}$	:	Mechanical power required to drive the vehicle (kW)
	P_{aux}	:	Electric auxiliaries power (kW)
	$P_{Hot_{thermal}}$	:	Electric power required to ensure hot thermal needs (kW)
	$P_{Cold_{thermal}}$	:	Electric power required to ensure cold thermal needs (kW)
	P_{IRReGT}	:	IRReGT system power (kW)
	η_{EMG}	:	Electric motor Generator efficiency (%)
	SOC_{max}	:	Battery maximum state of charge (%)
	SOC_{min}	:	Battery minimum state of charge (%)
	C_{bat}	:	Battery capacity (kWh)
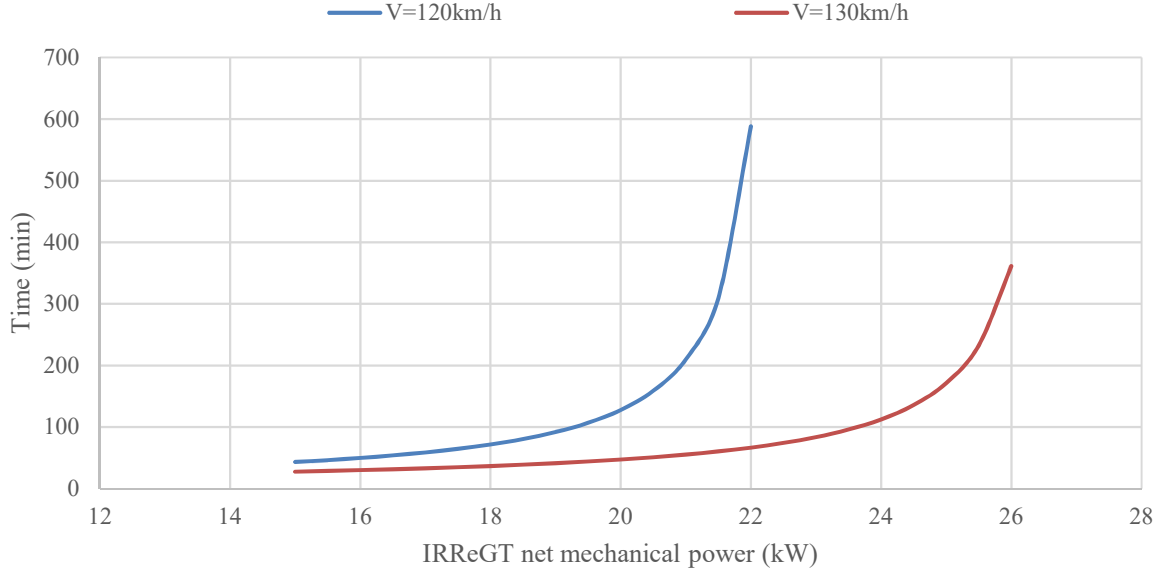
Fig. 4.3: SHEV autonomy (minutes) function of IRReGT net mechanical power (kW) for constant vehicle speed of 120km/h and 130km/h on flat-road

4.4.2 Energy Management Strategy

In order to assess the fuel consumption when considering the IRReGT-APU, an energy management strategy (EMS) must be developed in order to control the operation of the APU. The EMS was presented in details in chapter 3 and reiterated in this chapter. It mission is to satisfy the driving request and on-board thermal power needs as described in figure 2.1. Also it should find an optimal way to well manage the vehicle power flows and respect component constraints to minimize both the fuel consumption and the switching ON/OFF times of APU. As discussed in details in chapter 3, a compromise must be made for the two control objectives: minimization of both total fuel consumption and the switching ON/OFF times of APU. Therefore, a weighting factor λ, which varies from 0 to 1, was introduced to have a balanced global control objective as illustrated in the equation 3.31. Up to this end, a bi-level optimization process is proposed as the Energy Management Strategy (EMS), which consists of two combined optimization algorithms: a genetic algorithms (GA) and the Dynamic Programming (DP). This combined GA and DP algorithms are used to find the optimal solutions and the associated control sequences. GA is responsible to explore the design space of the IRReGT net power ($\boldsymbol{P_{IRReGT}}$) and λ and to generate many parameter combinations or individuals by relying on GA operators as selection, reproduction, crossover, mutation, etc. The DP algorithm is used to realize the global minimum of two control objectives while respecting the component constraints and guaranteeing the SOC levels equal to the settings at the beginning SOC_0 and at the end SOC_f.

4.4.3 Powertrain simulation results

This section presents the optimization results using the bi-level optimization method described in the EMS section. For the fuel consumption simulation, the WLTC accounting for auxiliaries and thermal comfort needs described in chapter 2 was considered. The three climates were considered: the cold climate, the temperate moderate climate and the hot climate.

As shown in figure 4.1, the auxiliary electric need is provided directly from the battery. As for the cold thermal need, an electrified air conditioning loop, with an electrified compressor (e-C) is selected to ensure the cold thermal comfort as used today in hybrid electric vehicles [4.29]. Regarding the hot thermal needs, this power is ensured by the waste heat from the IRReGT intercooler when the machine is switched ON as described before. When the machine is OFF, an electric resistance is used to satisfy the hot thermal needs. Therefore, the general equation describing the power needed from the battery is presented is 4.3, where u is the control variable that takes value of 0 when the IRReGT is OFF and the value of 1 when the IRReGT is ON.

$$P_{bat} = P_{EM} + P_{aux} + P_{Cold_{thermal}} + P_{Hot_{thermal}} * (1 - u) \hspace{2cm} (4.3)$$

| Where | P_{bat} | : | Battery power consumption (kW) |
| | P_{EM} | : | Electric machine power consumption (kW) |

Fuel consumption simulation results using the combined bi-level optimization method is presented in figure 4.4 below. Simulations were carried out on self-sustaining SHEV where the initial SOC is set equal to the final SOC (60%). Many important conclusions can be drawn out from this figure:

1- First, the higher the turbine inlet temperature (TIT) or the max combustion temperature, the lower the fuel consumption, since the GT-system efficiency is higher when TIT is higher and the power to weight ratio is also higher. For instance, 11% less fuel consumption is observed when comparing the 1100°C TIT with the 950°C TIT on all the climates, cold, moderate and hot, and up to around 17% when comparing the 1250°C with 950°C also for all the considered climates.

2- Despite the use of waste heat from the GT-system when it is switched ON to ensure cabin hot thermal needs, the cold climate remains with the higher fuel consumption with up to 3.4% more consumption yearly compared to temperate climate. Hot climate increases the fuel consumption by 1.1% compared to temperate climate.

3- Fuel consumption depends on the number of switching ON/OFF the GT-system. Reducing the number of ON/OFF increases the fuel consumption since it constrains the operation of the GT-system to a reduced number of starting. Also increasing the number of ON/OFF shows lower fuel consumption. In fact, the GT-system net power can meet the vehicle power demand for higher percentage of time, which avoids losses from the battery. It is worthy to mention that the curves present a changing slope for all the configurations and the climates at about 10 switching ON/OFF. This could be explained by the battery size selected. In fact, for 10kWh battery, the powertrain number of starting cannot be reduced less than 3 times because the energy demand to ensure three consecutive WLTC is higher than the useful amount of energy from the battery. This will constrain the GT-system to operate more than one time.
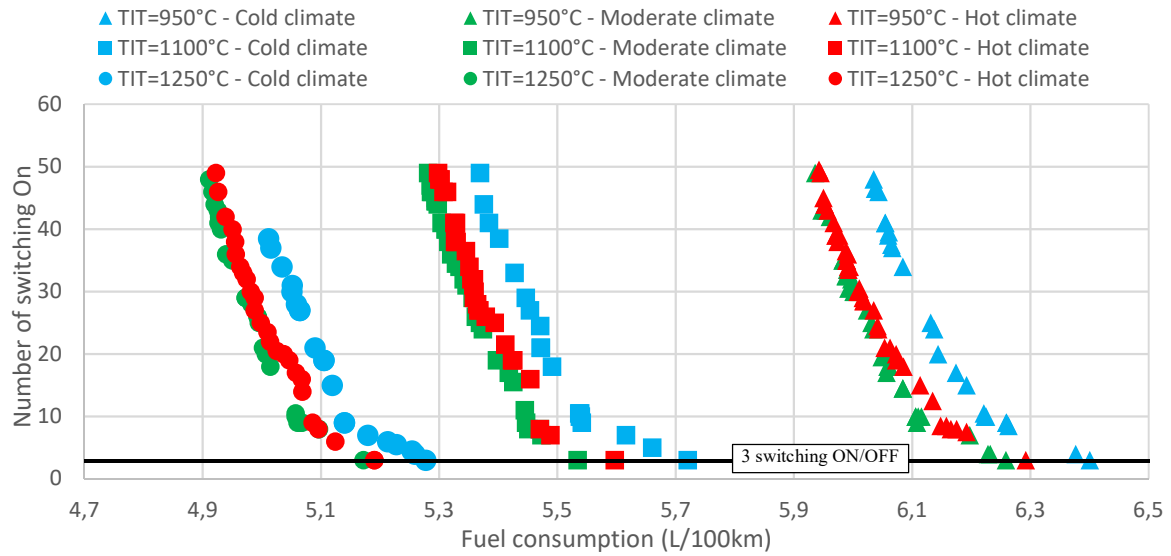
Fig. 4.4: Pareto Fuel consumption function of switching ON/OFF time

For the rest of the study, the operating parameters corresponding to the lower number of switching ON/OFF the APU is considered in order to reduce the thermo-mechanical fatigue stress mainly on the turbine housing and the regenerator. This number corresponds to three switching ON/OFF on the three consecutive WLTC. The resulting fuel consumption is presented in figure 4.5 below. Same conclusions can be figured out as discussed above.

The APU optimal operating powers corresponding to fuel consumption results in figure 4.5 are presented in figure 4.6. The operating power varies between 18.4kW for GT with TIT=950°C in the cold climate and up to 24kW for the same GT operating temperature in the hot climate. The results are obvious. In the cold climate, since the cabin hot thermal heat can be ensured for free from the waste heat rejected from the intercooler of the GT-system, the optimal strategy was to operate the GT-system at a lower power for a longer duration as shown in figure 4.7 which presents the GT-system percentage of operating time. In the hot climate, where the hot thermal need is very low, the GT operate at higher power for shorter duration.
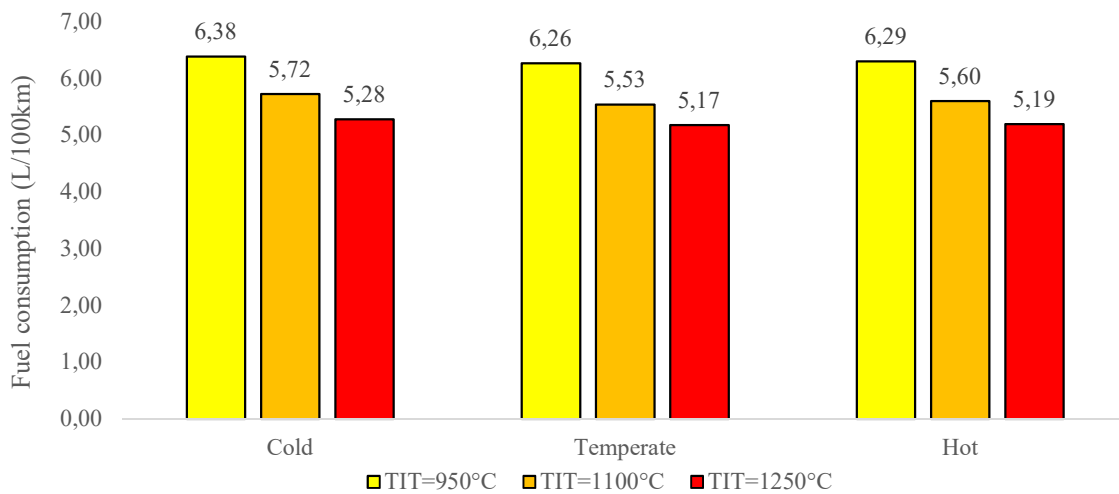

Fig. 4.5: IRReGT-APU-SHEV fuel consumption for the three different TIT and for the three different climates (Case corresponding to three switching ON/OFF of the APU)
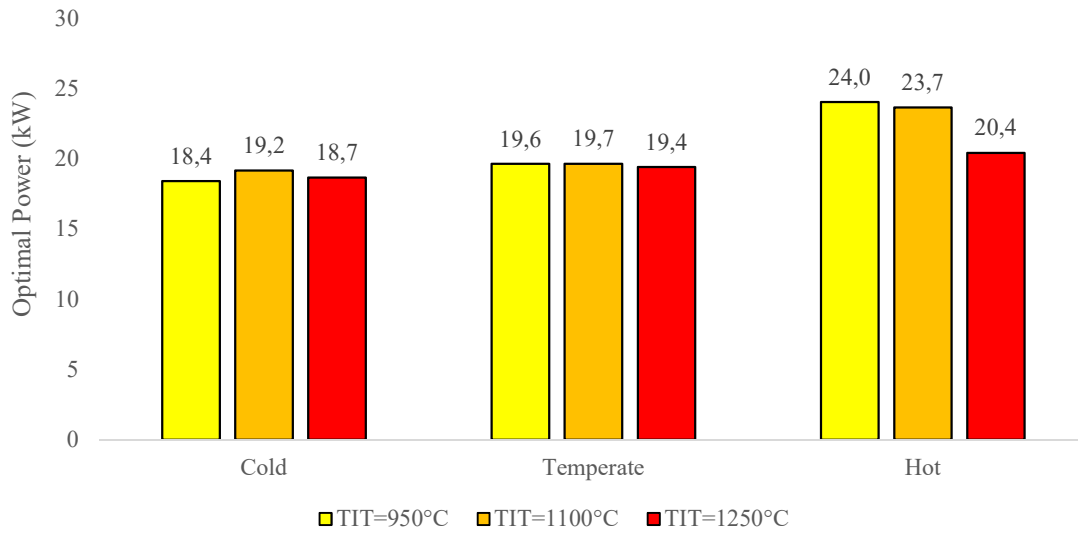
Fig. 4.6: IRReGT-APU-SHEV optimal net power for the three different TIT and for the three different climates (Case corresponding to three switching ON/OFF of the APU)
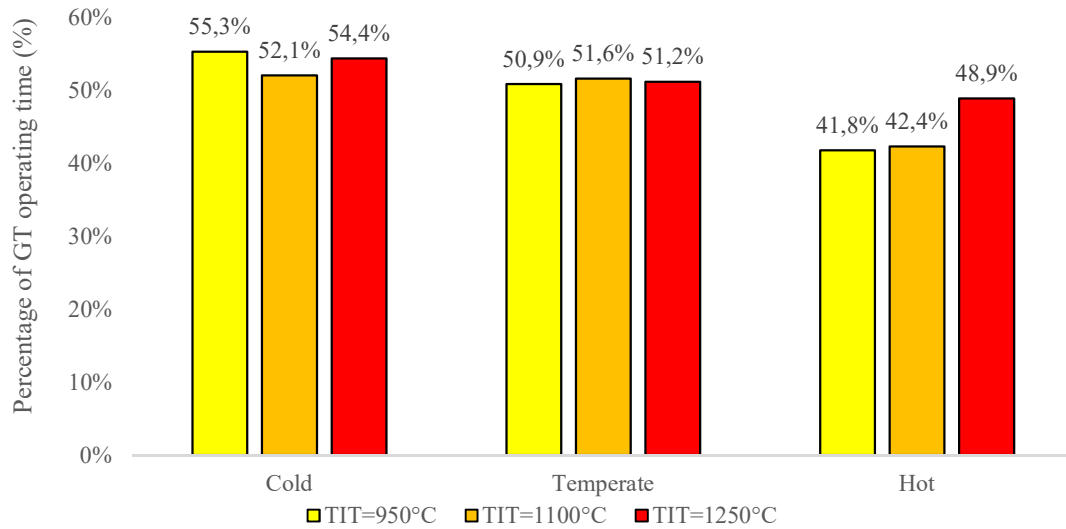
Fig. 4.7: IRReGT-APU-SHEV operating time' percentage for the three different TIT and for the three different climates (Case corresponding to three switching ON/OFF of the APU)

4.5 IRReGT dynamic modeling

This section presents the dynamic model of the IRReGT-system. The dynamic model is divided into two subsystems representing the main parts of the IRReGT system: the turbomachines (compressors and turbines) and the heat exchangers (HEX) (intercooler and regenerator). Each subsystem encloses the mass and the energy conservation laws. A controller is also included to control the system operation in order to reach the set point target in terms of mass flow rates, pressure ratios and temperatures.

Some assumptions are considered in this study. First, the thermal inertia of the turbomachines is neglected compared to the thermal inertia of the heat exchangers. Also, the combustion chambers' thermal inertia is not considered in this study. The combustion is considered to occur

instantly and adiabatically without losses to the outside and without heat exchange with the combustion chamber walls.

This section is divided into three main parts. In the first part, the turbomachines' transient model is elaborated and the different equations are presented. In the second part, the heat exchangers' dynamic model is presented and finally in the third last part, the transient operation results are presented.

4.5.1 Turbomachines

This section presents the turbomachines' dynamic model. As for the configuration setup, the compressors and turbines are considered mounted on the same shaft with the electric motor/generator as presented in figure 4.1.

Starting and shutting down the centrifugal machines affects the performance of the IRReGT in terms of efficiency and consequently the vehicle fuel consumption. In fact, the time characteristic of these machines depends mainly on their kinetic inertia, thermal inertia and technical criteria among them the friction and the compression and expansion ratios [4.11, 4.12]. The dynamic model of the turbocharger takes into account in each stage the mechanical inertia and the different efficiencies. This allows assessing the changes in pressure and temperature of the working fluid. The transient starting phase of the turbocompressor is modeled considering mechanical data available from automotive turbochargers, among these data, the inertia of the different compressors and turbines wheel.

According to Newton second law for rotation, the sum of the external torques acting on a shaft is equal to the total moment of inertia times the angular acceleration (equations 4.4 and 4.5):

$$J * \frac{d\omega}{dt} = \sum C_i \tag{4.4}$$

$$J * \frac{d\omega}{dt} = C_m + C_{C_1} + C_{C_2} + C_{T_1} + C_{T_2} + C_{friction} \tag{4.5}$$

Where	J	:	System inertia including Compressors, turbines, motor/generator and shaft inertia (kg.m²)
	$\frac{d\omega}{dt}$	:	Angular acceleration (rad/s²)
	$\sum C_i$	:	Sum of the torque (N.m)
	C_m	:	The motor torque during starting (N.m)
	C_{C_1}	:	First compressor torque (N.m)
	C_{C_2}	:	Second compressor torque (N.m)
	C_{T_1}	:	First turbine torque (N.m)
	C_{T_2}	:	Second turbine torque (N.m)
	$C_{friction}$	:	Friction torque resistance (N.m)

The turbomachine is assumed to accelerate from rest to its optimal nominal speed, before starting the combustion. During this transient phase, the compression and expansion in the compressors and turbines is assumed to be adiabatic. Since radial centrifugal machines are used, a relation between air mass flow rate across the turbomachine and its speed is considered according to equation 4.6. Data such as mass flow rate, pressure ratio, efficiency and rotation

speed are retrieved from automotive turbochargers. Note that the compressor pressure during transient phase depends on the turbine flow permeability discussed later.

$$\dot{m}_{i_{TM}} = f(C_{PR_{TM}}, C_{RPM_{TM}}) \tag{4.6}$$

$$\eta_{C_{TM}} = f(\dot{m}_{C_{TM}}, C_{PR_{TM}}, C_{RPM_{TM}}) \tag{4.7}$$

Where	$\dot{m}_{C_{TM}}$	:	Mass flow rate of the turbomachine
	$C_{PR_{TM}}$	:	Pressure ratio of the turbomachine
	$C_{RPM_{TM}}$	:	Rotation speed of the turbomachine
	$\eta_{C_{TM}}$	:	Efficiency of the turbomachine

The turbomachines torque is accounted according to equation 4.8 which gives the power as function of the torque and the rotational speed. The power is calculated from equation 4.9 by considering the mass flow rate and the difference of enthalpy between the inlet and outlet of the component. This equation results from the law of conservation of energy by considering that no heat transfer occurs between the component and the surrounding and by neglecting the variation of kinetic and potential energy across the components. Note that the outlet enthalpy is calculated by considering the isentropic efficiency of the component where values are retrieved from literature. Formula for compressors and turbines are presented in 4.10 and 4.11.

$$P_{TM}(t) = C_{TM}(t) * w_{TM}(t) \tag{4.8}$$

$$P_{TM}(t) = \dot{m}_{TM} * (h_{inlet_{TM}} - h_{outlet_{TM}}) \tag{4.9}$$

$$\eta_{is_{C_i}} = \frac{h_{outlet\ is_{C_i}} - h_{inlet_{C_i}}}{h_{outlet_{C_i}} - h_{inlet_{C_i}}} \tag{4.10}$$

$$\eta_{is_{T_i}} = \frac{h_{inlet_{T_i}} - h_{outlet_{T_i}}}{h_{inlet_{T_i}} - h_{outlet\ is_{T_i}}} \tag{4.11}$$

Where	P_{TM}	:	Turbomachine power (kW)
	C_{TM}	:	Turbomachine torque (N.m)
	w_{TM}	:	Turbomachine rotation speed (rad/s)
	$\dot{m}_{TM}$	:	Mass flow rate across the turbomachine (kg/s)
	$h_{inlet_{TM}}$	:	Enthalpy at turbomachine inlet (kJ/kg)
	$h_{outlet_{TM}}$	:	Enthalpy at turbomachine outlet (kJ/kg)
	$\eta_{is_{C_i}}$	:	Isentropic efficiency of compressor i (%)
	$h_{outlet\ is_C}$	:	Isentropic enthalpy at compressor outlet
	h_{inlet_C}	:	Enthalpy at compressor inlet (kJ/kg)
	h_{outlet_C}	:	Enthalpy at compressor outlet (kJ/kg)
	$\eta_{is_{T_i}}$	:	Isentropic efficiency of turbine i (%)
	h_{inlet_T}	:	Enthalpy at turbine inlet (kJ/kg)
	h_{outlet_T}	:	Enthalpy at turbine outlet (kJ/kg)
	$h_{outlet\ is_T}$	:	Isentropic enthalpy at turbine outlet (kJ/kg)

Expansion process is assumed to be adiabatic and the isentropic efficiency is assessed using empirical polynomial equation specific for each expansion stage. The equation considers both the variation of the air mass flow rate as well as the angular velocity of the rotating machine. The efficiency equations are calculated using data for turbomachines found from the literature

for different turbines [4.2]. In order to find the system pressure ratio during the transient operation, the Stodola equation [4.15, 4.30] which defines the mass flow rate as function of the turbine pressure ratio according to equation 4.12 below is used. K values are extracted from turbine's data [4.31-4.33] and for a given mass flow ($\dot{m}$) rate and turbine inlet temperature (T_{in}), the pressure ratio is found therefore according to equation 4.13.

$$\dot{m}_T = k_T * \frac{P_{in}}{\sqrt{T_{in}}} * \sqrt{1 - (\frac{P_{out}}{P_{in}})^2} \qquad (4.12)$$

$$\frac{P_{out}}{P_{in}} = \sqrt{1 - \frac{\dot{m}^2 T_{in}}{K_T{}^2 P_{in}{}^2}} \qquad (4.13)$$

Where
$\dot{m}_T$: Turbine mass flow rate (kg/s)
k_T : Turbine characteristic (m.s.√k)
P_{in} : Turbine inlet pressure (Pa)
P_{out} : Turbine outlet pressure (Pa)
T_{in} : Turbine inlet temperature (K)

Note that the compressors and the turbines models include a control system which serves to adjust the mass flow rate and the pressure ratio by mean of a PID through an electronic system that controls the electric machine in order to control the rated speed of the turbomachine. The combustion chamber outlet temperature is also controlled through a PID that controls the fuel mass flow rate.

4.5.2   Heat Exchanger
The HEX used in the IRReGT, the intercooler and the regenerator are counter flow heat exchangers as presented in figure 4.8. These components are essential to reject heat during the compression and to recover the heat from turbine exhaust respectively. The thermal inertia of both heat exchangers, mainly the regenerator, increases the transient state duration. This leads to reduced efficiency during transient mode since a higher quantity of fuel must be injected to achieve the desired net power or longer convergence time is required to achieve the steady state operation. Therefore, a dynamic model of HEXs is required to account for the system efficiency during startups.

Many papers in the literature treat the design and optimization of plate-fin HEX for micro-GT systems and for other applications [4.34-4.36]. This HEX dynamic model consists of modeling the heat transfer between the two fluids in a plate-fin HEX. Therefore, the HEX is divided into several elementary volumes (Δx , as shown in figure 4.9, in order to define the partial differential equations that govern the heat transfer.
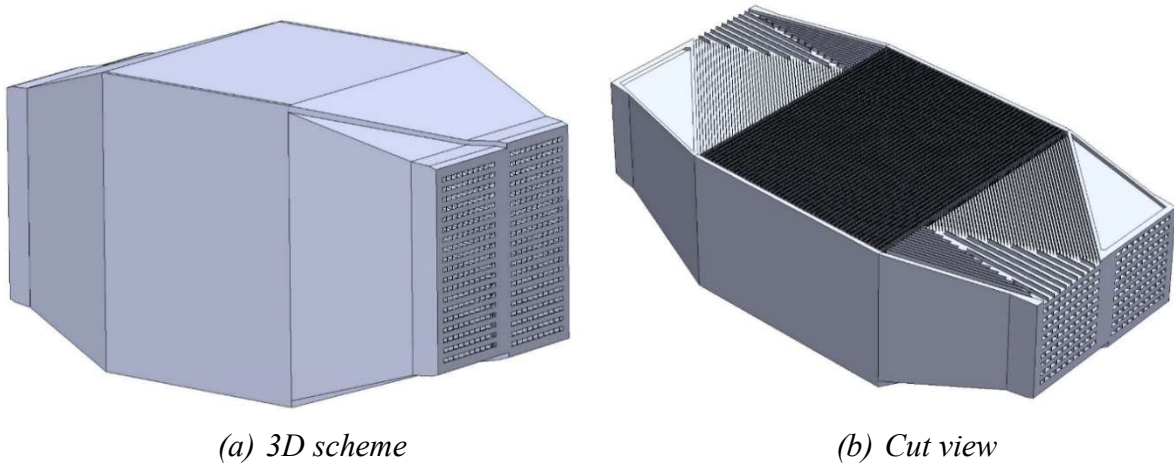
(a) 3D scheme   *(b) Cut view*

Fig. 4.8: Counter-flow plate-fin HEX

The temperature of each elementary volume is evaluated according to the conservation of energy law using equations 4.14 to 4.17. These formula accounts for the convection and axial conduction phenomenon. The conduction phenomenon allows to calculate the temperature homogenization during the transient operation.
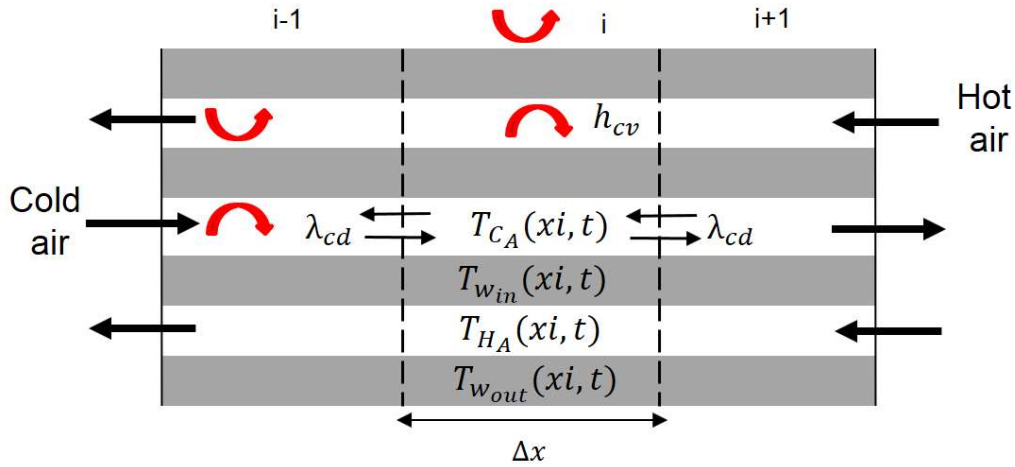

Fig. 4.9: HEX elementary volumes

$$M_{C_A,i} \frac{\partial u_{C_A,i}}{\partial t} = \dot{m}_{C_A}\left(h_{C_A,i-1} - h_{C_A,i}\right) + h_{cv,i}A\left(T_{w_{in},i} - T_{C_A,i}\right)$$
$$+ \frac{\lambda_{C_A,i}S}{\Delta x}\left[\left(T_{C_A,i-1} - T_{C_A,i}\right) + \left(T_{C_A,i+1} - T_{C_A,i}\right)\right] \quad (4.14)$$

$$M_w Cp_w \frac{\partial T_{w,i}}{\partial t} = h_{cv_{in},i}A_{in}\left(T_{C_A,i} - T_{w,i}\right) + h_{cv_{out},i}A_{out}\left(T_{H_A,i} - T_{w,i}\right)$$
$$+ \frac{\lambda_w S}{\Delta x}\left[\left(T_{w,i-1} - T_{w,i}\right) + \left(T_{w,i+1} - T_{w,i}\right)\right] \quad (4.15)$$

$$M_{H_A,i} \frac{\partial u_{H_A,i}}{\partial t} = \dot{m}_{H_A}\left(h_{H_A,i+1} - h_{H_A,i}\right) + h_{cv_{in},i}A_{in}\left(T_{w_{in},i} - T_{H_A,i}\right)$$
$$+ h_{cv_{out},i}A_{out}\left(T_{w_{out},i} - T_{H_A,i}\right)$$
$$+ \frac{\lambda_{H_A}S}{\Delta x}\left[\left(T_{H_A,i-1} - T_{H_A,i}\right) + \left(T_{H_A,i+1} - T_{H_A,i}\right)\right] \quad (4.16)$$

$$M_w Cp_w \frac{\partial T_{w,i}}{\partial t} = h_{cv_{in},i} A_{in} \left(T_{H_A,i} - T_{w_{out},i} \right) + h_{cv_{out},i} A_{out} \left(T_a - T_{w,i} \right)$$
$$+ \frac{\lambda_w S}{\Delta x} [\left(T_{w,i-1} - T_{w,i} \right) + (T_{w,i+1} - T_{w,i})] \tag{4.17}$$

Where A :   The longitudinal heat transfer area

              S :   The cross-sectional area

              T_w :   Wall material temperature (°C)

              T_a :   Ambient temperature (°C)

The convective heat transfer coefficients between both fluids and the tube are calculated, as function of the geometric characteristics of the heat exchanger, by using correlations based on the Reynolds, the Prandtl and the Nusselt numbers as stated in [4.34-4.38] and presented in chapter 3. The pressure drop is evaluated by [4.39] as described in chapter 3.

4.5.3   Dynamic model results

In order to understand the impact of the GT startup on the fuel consumption, a GT model is developed using Dymola [4.40], a plug and drop software designed to model complex systems with mechanical, hydraulic and thermal subsystems among others. The Dymola's simulation language, Modelica, an object-oriented language uses a simulator which allows solving the system equations at each time step. A library of several fluids, including the air and water libraries is integrated in the Dymola software [4.41, 4.42].

The IRReGT-system modeled on Dymola is presented in figure 4.10 below. A proportional-integral-derivative (PID) controller is used to control the mass flow rate, the pressure ratio and the combustion chamber outlet temperature. Nine different configurations have been simulated corresponding to the nine different optimal machines found in the SHEV model section: three different TIT (950°C, 1100°C and 1250°) for three different climates (cold, temperate and hot).
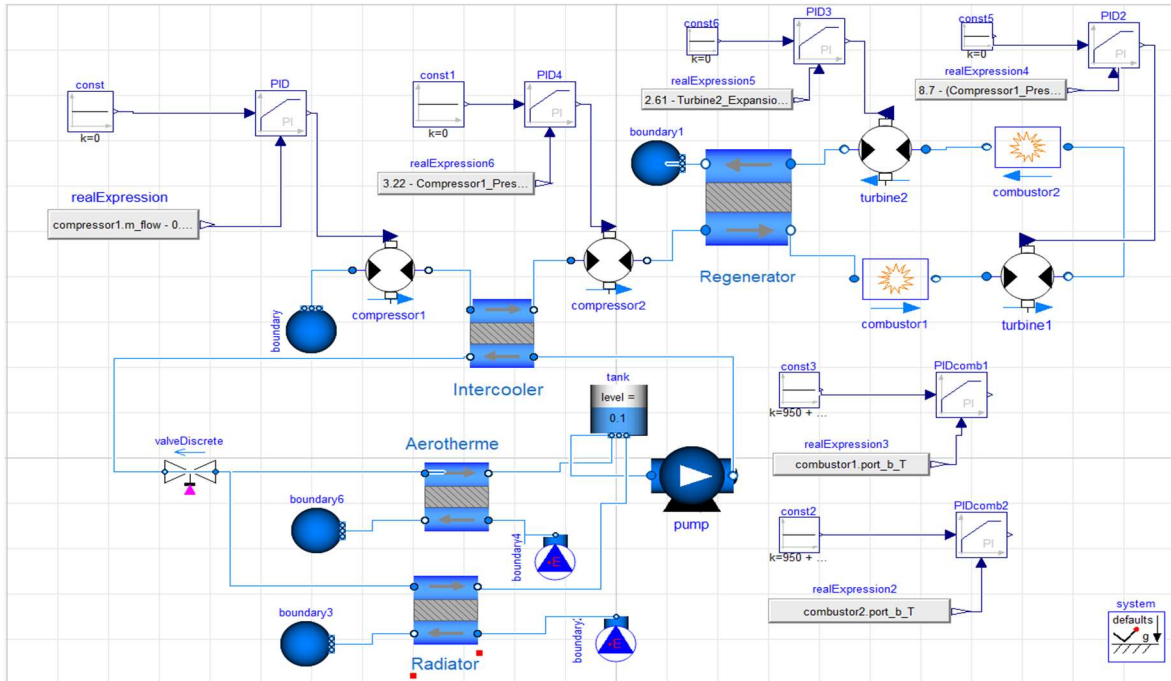

Fig. 4.10: IRReGT Dynamic simulation on Dymola

Table 4.1 lists the technical specifications used to model the launching phase of the IRReGT-system from rest to the nominal speed. The moments of inertia considered are retrieved from automotive turbocharger suppliers. The nominal rotation speed selected is 90.000 RPM. It corresponds to the state-of-the-art of actual micro GT-machines developed as APU for different applications [4.43-4.45]. The compressors and turbines' maps corresponding to automotive turbochargers are presented in figure 4.11 to 4.14. They were used to account for the resistant torque during the startup of the machine.

Figure 4.15 presents the turbomachinery shaft mechanical power during the system startup. The plotted curve can be divided in two different zones: (1) startup from 0s to 1s where turbomachinery's speed accelerates from rest up to 90.000 RPM, (2) steady state rotational speed, following the accelerating phase.

Table 4.1: Turbomachinery technical specifications

Compressor 1 moment of inertia	J_{C_1}	Kg.m²	2.75e-6
Compressor 2 moment of inertia	J_{C_2}	Kg.m²	2.75e-6
Turbine 1 moment of inertia	J_{T_1}	Kg.m²	4.56e-6
Turbine 2 moment of inertia	J_{T_2}	Kg.m²	4.56e-6
Motor/Generator moment of inertia	$J_{M/G}$	Kg.m²	1e-5
Friction torque	f	Kg.m²/s	3.2e-6
IRReGT nominal rotational speed	RPM_{GT}	RPM	90.000
IRReGT startup to nominal speed	t_s	s	1

In the first zone, the mechanical shaft power increases as the rotation speed increases and reaches its maximum of around 2.4 kW at 1s. During this phase, the main power required to accelerate the machine is mainly due to the inertial power of the rotating parts rather than the resistance torque due to the compression according to equation 4.5. In fact, on one hand, during the startup, the turbine expansion ratio remains low according to equation 4.13, since the turbine inlet temperature is low leading therefore to lower compression ratio. This can be explained by the fact that the air working fluid remains at low temperature since no combustion occurs yet, therefore the turbine permeability is high leading to smaller backpressure in the system and consequently, a lower pressure ratio. On the other hand, the compression required power is quasi-recovered by the turbine expansion power produced, therefore the important share of the mechanical power required to startup the machine is due to the inertial power of the rotating components.
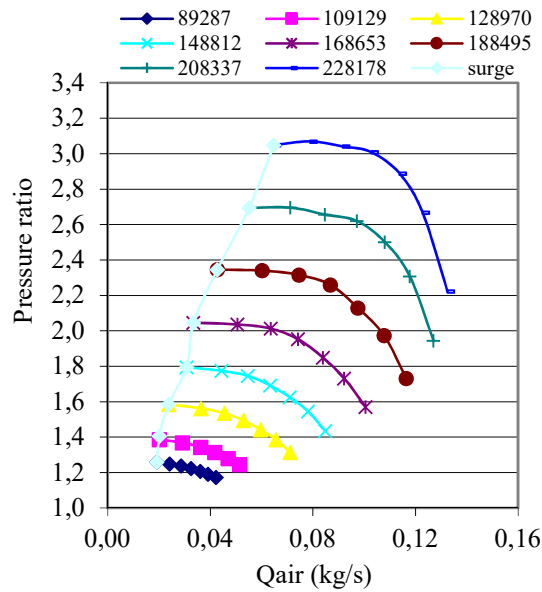
Fig. 4.11: Compressor pressure ratio function of the mass flow rate for different compressor speeds
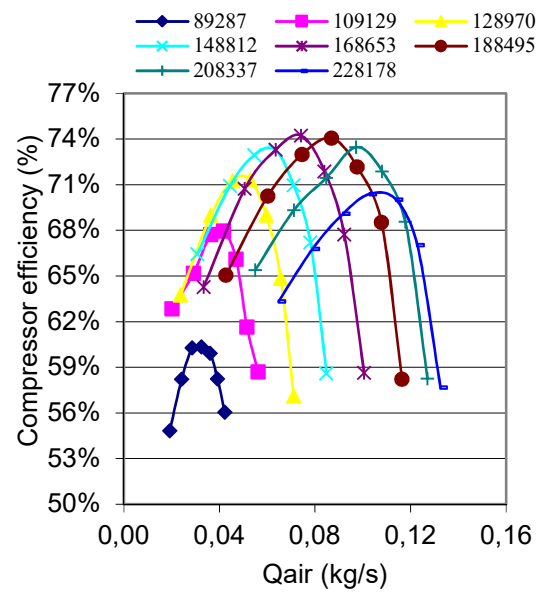

Fig. 4.12: Compressor efficiency function of the mass flow rate for different compressor speeds
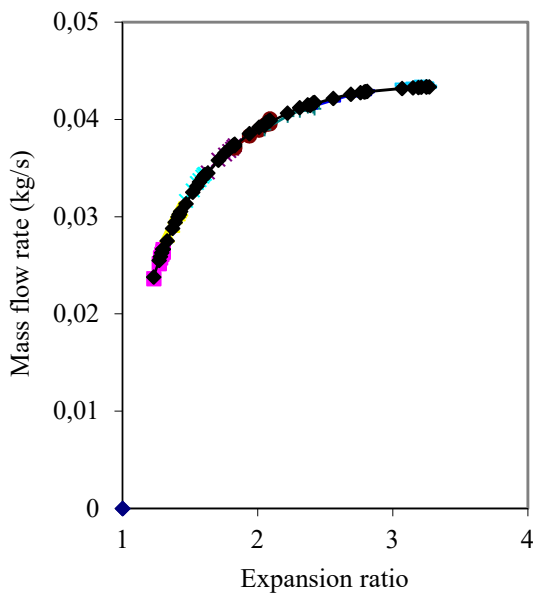

Fig. 4.13: Turbine mass flow rate function of the expansion ratio for different turbine speeds
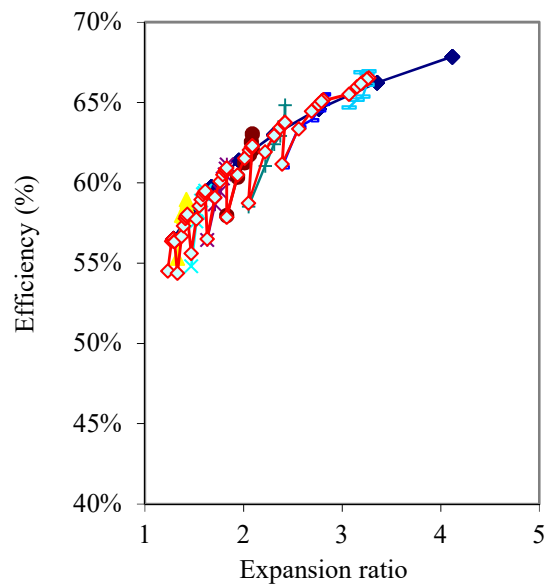
Fig. 4.14: Turbine efficiency function of the expansion ratio for different turbine speeds

In the second zone, when the nominal rotational speed is reached, the mechanical power shaft decreases to around 0.2 kW. In this zone, only the shaft frictions and the net power from the compression/expansion processes persists.

Finally, the electric energy consumed from battery to accelerate the machine from rest to nominal speed is presented in figure 4.16 below. Around 1.2 kJ is required to accelerate the turbomachine from rest to nominal speed. It is worthy to mention that for a 20kW net power machine, this amount of energy consumed during the startup phase can be recovered in about 0.06 second when the machine operates at this power. Therefore, based on these findings, this

launching phase from rest speed to GT nominal speed has been neglected for the rest of this study, where it was demonstrated that the thermal inertia of the regenerator has more impact on the GT fuel consumption than the inertial forces during startup phase.
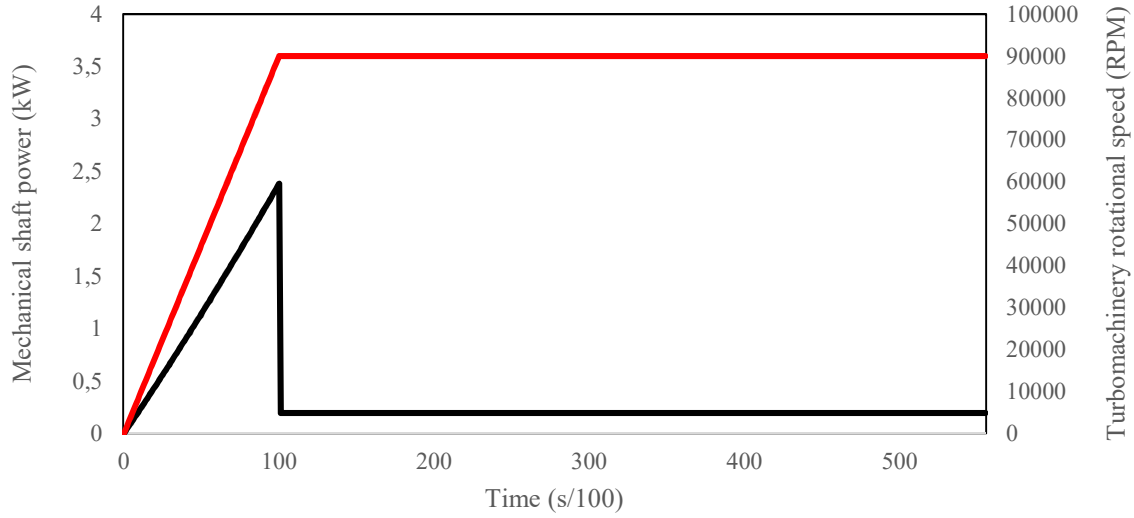
Fig. 4.15: Turbomachinery requested shaft power during startup phase
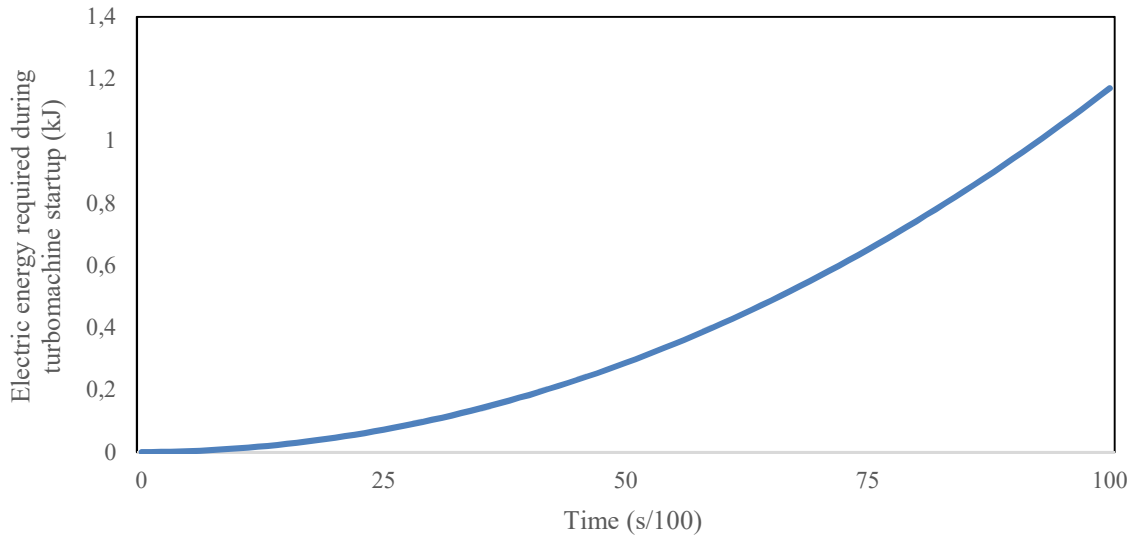
Fig. 4.16: Energy required to startup the turbomachine

As for the regenerator thermal inertia simulations, two different strategies have been considered in this study. The first one, considers operating the IRReGT at its nominal power from the time where it reaches its nominal speed after 1s of launching. This means that since the regenerator is not warm yet, an additional quantity of fuel is injected in order to reach the desired combustion chamber outlet temperature. This leads to an overconsumption of fuel during the startup time. Simulations were performed by controlling the fuel quantity injected in the combustion chambers through the PID controller to respect the set up net power desired. The second strategy considers the burning of the same fuel quantity during the startup phase and the steady state operating. Therefore, the combustion chamber outlet temperature remains low during the startup phase and consequently the output power reaches its nominal value after attaining the steady state operation. In this case, the energy deficit from the startup phase can be covered by

operating the machine for a longer duration which can be accounted for, knowing the nominal machine operating power.

The following figures 4.17 and 4.18 present the regenerator working fluid temperature for the two different strategies for a machine with of 20 kW net power operating at a combustion chamber outlet temperature of 1250°C. The analysis of the two figures leads to the following conclusions:

1- The first strategy compared to the second one, leads to faster increase in the regenerator cold side outlet temperature since higher quantity of fuel is injected in order to maintain the desired net power during the transient phase. This can be seen when comparing the fuel injected curves for both strategies that shows a higher quantity of fuel injected at the startup phase in strategy one compared to the second strategy. Note that in the first strategy, the regenerator cold side outlet temperature reaches 95% of the steady state temperature at around 100 seconds compared to around 500 seconds in the second strategy.

2- The mass of fuel injected when achieving the steady state operation is the same in both strategies. This is obvious, since during permanent regime, the IRReGT-system operates under the same conditions of efficiency.

As consequence of the regenerator transient operation, the first strategy allows achieving the system efficiency quicker than the second strategy. This is shown in figure 4.19 in which we plotted the efficiency of a 20kW net power IRReGT machine operated at three different turbine inlet temperatures.
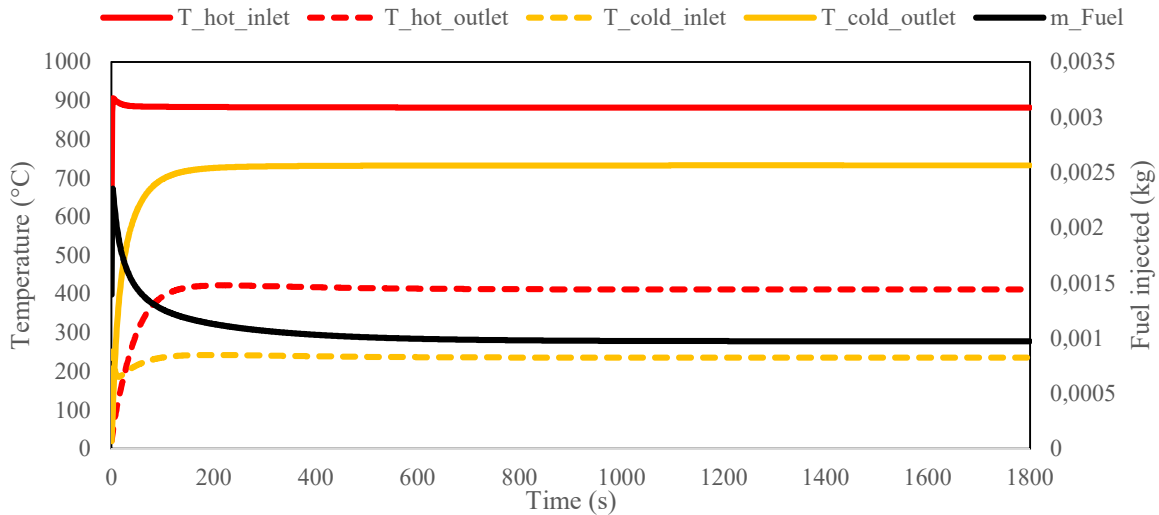
Fig. 4.17: Regenerator temperatures – TIT=1250°C – net power = 20kW – strategy 1: constant power
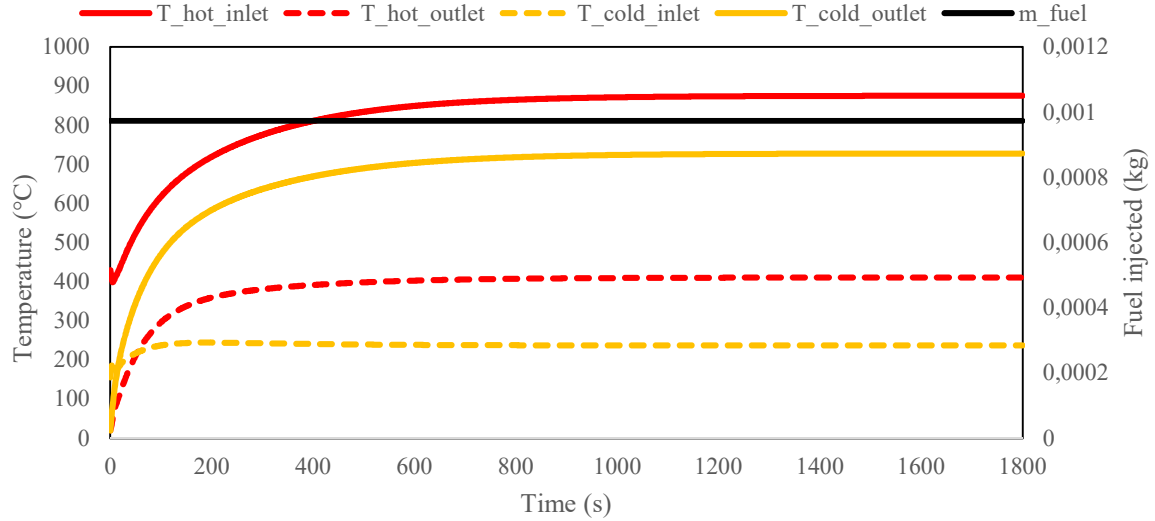
Fig. 4.18: Regenerator temperatures – 1250°C TIT – net power = 20kW – strategy 2: constant fuel

It is worthy to mention that while the first strategy seems to give better results in terms of fuel consumption since the system maximal efficiency is achieved faster, it presents higher thermomechanical constraints since the increasing temperature slope is higher. However, this strategy was envisaged in order to show the upper limits in terms of fuel consumption savings when considering the system transient behavior.

In the next section, the fuel consumption for the nine different IRReGT found in section 1 are simulated during transient operation. Simulation results are used instead of optimal control results found in section 1. This allows to account for the additional fuel consumption when IRReGT transient operation is considered.
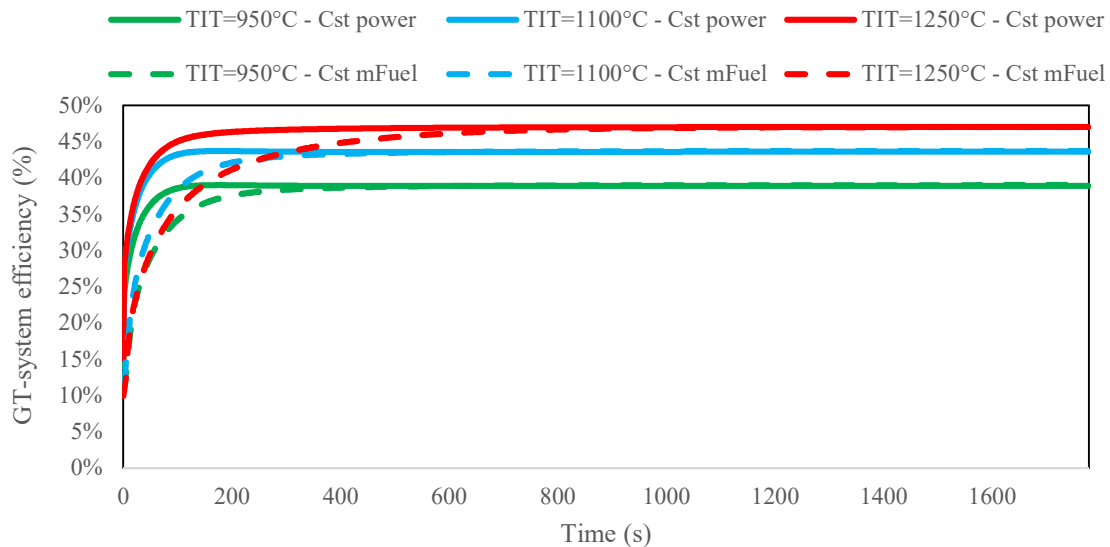
Fig. 4.19: GT-systems efficiency for 20kW net power and for the three different TIT temperatures

4.6 IRReGT-SHEV Fuel consumption dynamic simulation results

In this section, the IRReGT-system fuel consumption results during transient operation in section 2 are used instead of NSGA-DP fuel consumption results in section 1 in order to approach the real vehicle fuel consumption on the three consecutive WLTC cycles while accounting for IRReGT-system dynamic operation. Up to this end, the IRReGT switching ON/OFF decisions found in section 1 are considered for the nine different cases presented in figure 4.4. The operating power corresponding to switching ON /OFF the APU three times are presented in figure 4.6.

Therefore, for each case, the NSGA-DP resulting fuel consumptions are replaced by the dynamic results. Both strategies described in the last section (constant power and constant fuel injected) are simulated. It is worthy to mention that since the regenerator transient load impacts largely the fuel consumption, different regenerators corresponding to the optimal IRReGT-system power were designed and integrated in the Dymola dynamic simulation. The regenerators weight and size for the corresponding optimal power shown in figure 4.6, are presented in figure 4.21 below. The mathematical equations defining the relations between the system net mechanical power and the regenerator's weight and the system net mechanical power and the regenerator's size are shown in figure 4.20. The equations leading to sizing the regenerator were presented in chapter 3.

As for the simulation method, for the first strategy, since the system net power is controlled to a constant set point value corresponding to the optimal power found in figure 4.6, the IRReGT operating time is equal to the same time as in NSGA-DP optimization results since the same amount of electric energy is produced to refuel the battery. As for the second strategy, since the IRReGT net power increases as the combustion chamber inlet temperature increases as shown in figure 4.22, a deficit of energy for the battery must be recovered.
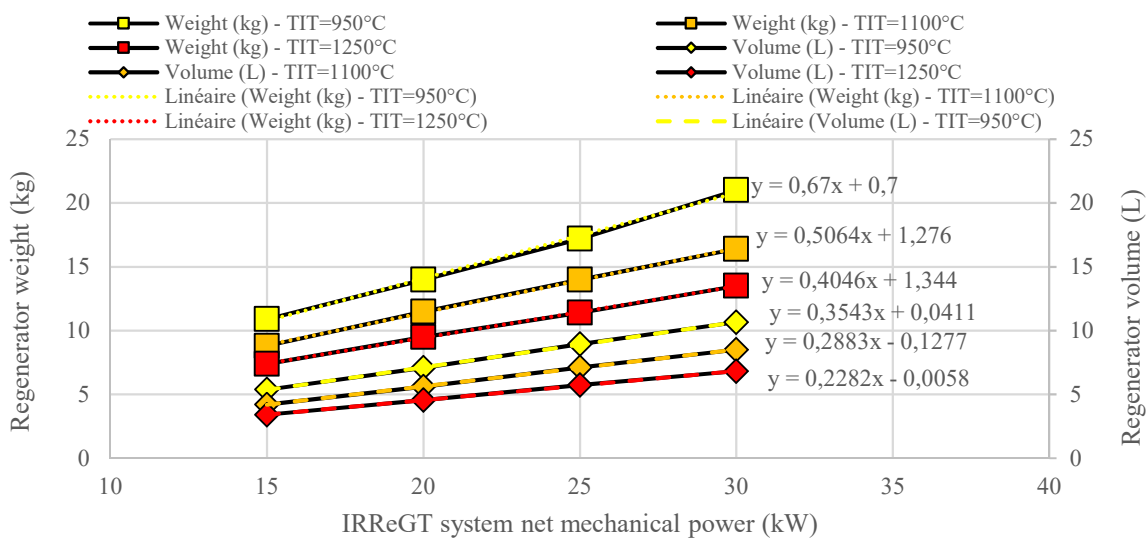
Fig. 4.20: Regenerator weight and volume function of the IRReGT system net mechanical power
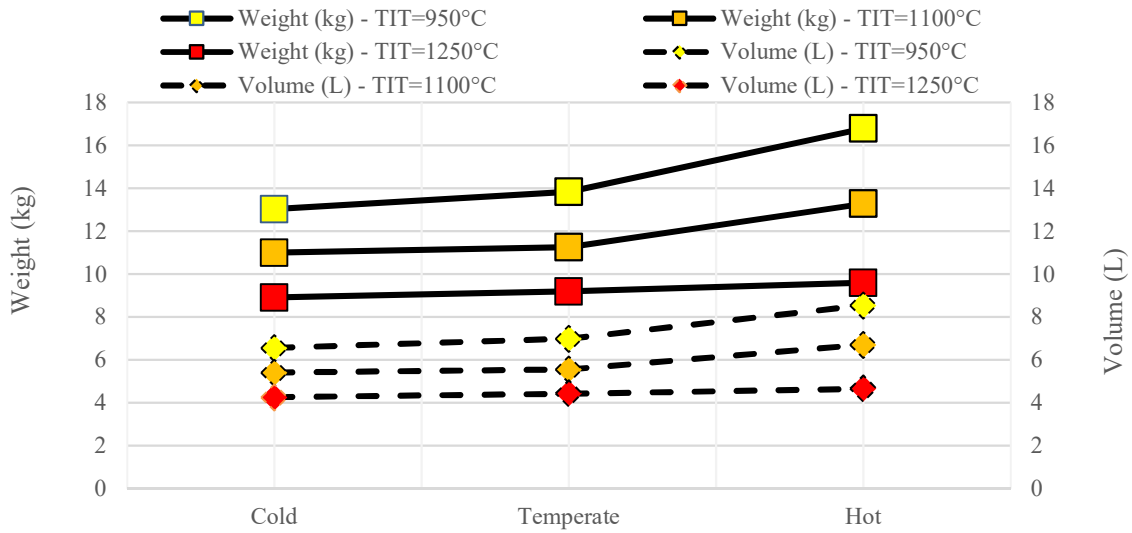
Fig. 4.21: Regenerator weight (kg) and volume (L) for the corresponding optimal power for the different climates

Therefore, the IRReGT additional operating time (T_{add}) was considered using equation 4.18 which presents the ratio between the electric energy deficit due to the transient net power and the APU power during steady state. The electric energy delivered by the APU during transient phase was accounted using equation 4.19.

Note that during simulations, a constant electric motor generator efficiency (η_{EMG}) was considered. In fact, as discussed during the turbomachine dynamic model, the combustion is initiated after accelerating the APU from rest to its nominal speed. Therefore, during the transient thermal phase, the EMG operates already at constant speed where the torque increases from zero to its nominal value. In this operating region, constant EMG efficiency is considered.

Fig. 4.22: Total energy and energy deficit during APU transient startup

$$T_{add} = \frac{E_{Deficit}}{P_{APU_{Steady}}} = \frac{E_{constant\ power} - E_{bat}}{P_{APU_{Steady}}} \qquad (4.18)$$

$$E_{Bat} = \int \eta_{EMG} * P_{IRReGT_{transient}} * dt \qquad (4.19)$$

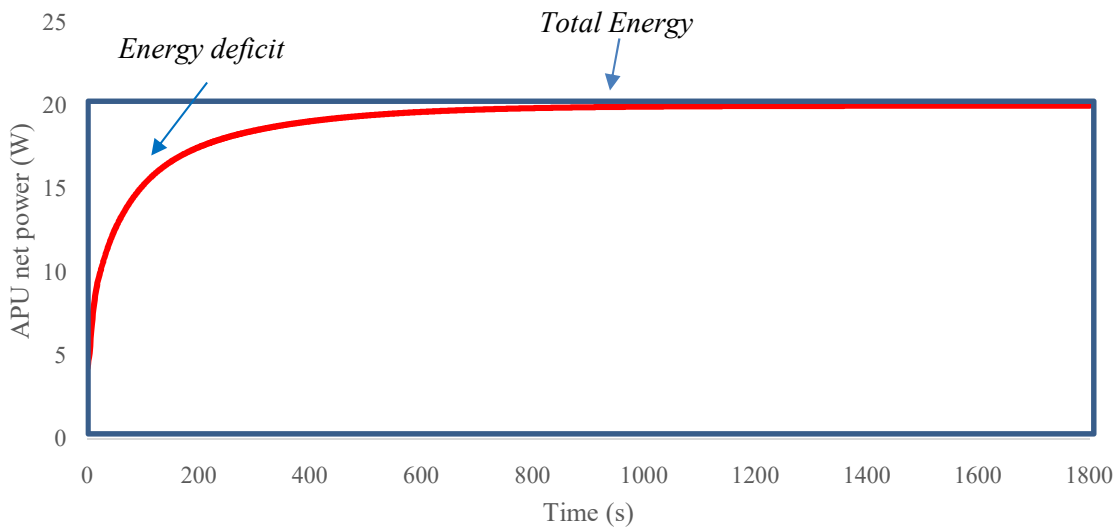| Where			
	T_{add}	:	Additional operating time (s)
	$E_{Deficit}$	:	Electric energy deficit during transient phase
	$E_{constant\ power}$	:	Cumulated energy at constant power (kJ)
	E_{bat}	:	Cumulated energy stored in the battery (kJ)
	$P_{APU_{Steady}}$	:	APU delivered power at steady state (kW)
	η_{EMG}	:	Electric motor generator efficiency (%)
	$P_{IRReGT_{transient}}$	:	IRReGT power during transient state (kW)

The instantaneous fuel consumption over the three consecutive WLTC cycles, for the three different TIT, for the three different climates and for both strategies are presented in annex A.2 and A.3 respectively. Figures 4.23 and 4.24 present the fuel consumption in liter per 100km for both strategies. Many conclusions can be drawn out from these figures:

1- Strategy one (constant power) shows reduced fuel consumption compared to strategy two (constant fuel injected), despite the higher instantaneous fuel consumption during the startup phase. For instance, according to figures 4.25 and 4.26, an increase in fuel consumption of around 2.4% is shown in strategy one for the cold climate compared to about 5.7% in strategy 2 for the same climate. For temperate climate, an average additional fuel consumption of 2.6% is shown in the first strategy compared to around 5.8% in the second strategy. Also, for the hot climate, an average increase in fuel consumption of 3% in the first strategy compared to about 6% in the second strategy. This can be explained in two ways. First, the IRReGT-system operating at around 50% of the time according to figure 4.7, reaches it efficiency in about 100s with the first strategy compared to about 500s in the second strategy. Second, since the APU was constrained to switch ON/OFF only three times, the impact of transient phase on the fuel consumption was reduced on the whole travelled distance.

2- The increase in fuel consumption compared to NSGA-DP seems lower with cold climate. In fact, in this climate, the APU operates for a longer time, therefore the impact of transient phase on the fuel consumption is lower since the nominal high efficiency operating accounts for a longer portion of time. For instance, in the first startup strategy, the increase in fuel consumption is about 2.4% on average in the cold climate, compared to 2.6% on average in temperate climate and up to 3.5% on average in the hot climate according to figure 4.25. The corresponding operating times are respectively 54%, 51% and 43%. In the second startup strategy the increase in fuel consumption is about 5.7% in cold climate on average, 5.8% in temperate climate on average and about 6.3% in hot climate on average according to figure 4.26.

3- Comparing the fuel consumptions between the different climates, the cold climate shows the higher fuel consumption in both scenarios, followed by the hot climate, then by the

temperate climate. For instance, an additional fuel consumption between 1.5% and 3.5% is observed with both strategies when comparing the fuel consumption of cold climate to the temperate one. These results are coherent with the ones found during NSGA-DP simulations. Despite the use of free thermal waste heat to ensure the cabin hot thermal comfort when the APU in ON, the energetic needs remain high in this climate leading to higher fuel consumption.

4- Comparing the fuel consumption between the different machines, it is obvious that the higher the TIT, the lower the fuel consumption on the three consecutive WLTC since the efficiency is higher. For instance, a decrease in fuel consumption between 10 to 11% is seen in the three climates in both startup strategies, when increasing the TIT from 950°C up to 1100°C and between 17 and 18.3% when increasing the TIT from 950°C up to 1250°C.
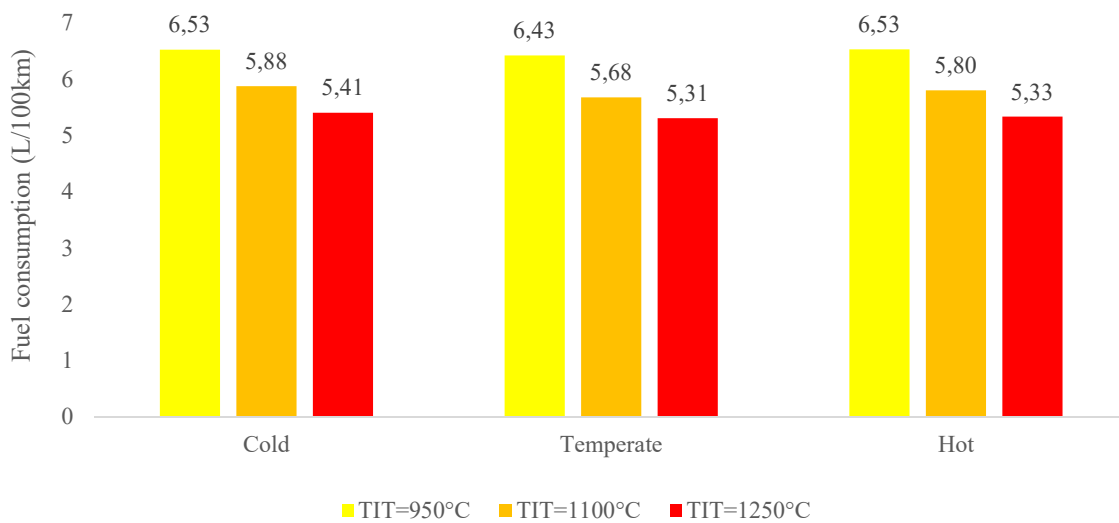
Fig. 4.23: Fuel consumption results considering GT dynamic operation – Scenario 1
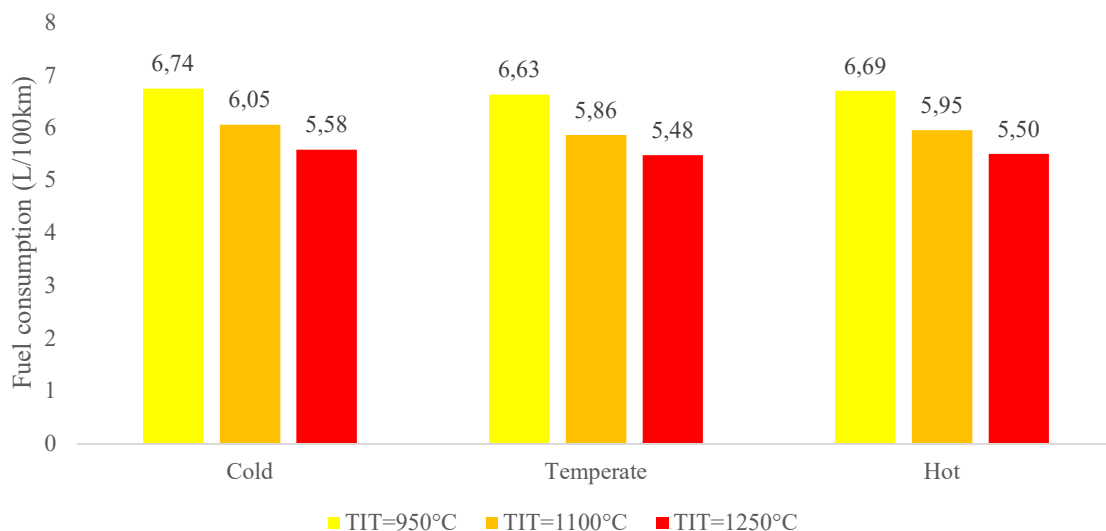
Fig. 4.24: Fuel consumption results considering GT dynamic operation – Scenario 2
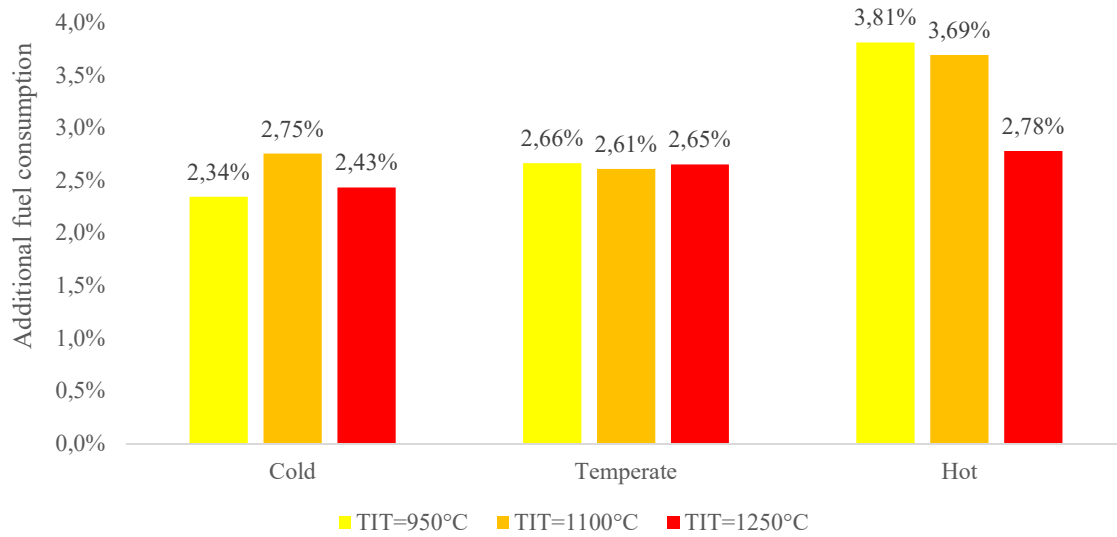
Fig. 4.25: additional fuel consumption compared to NSGA-DP results with first startup strategy
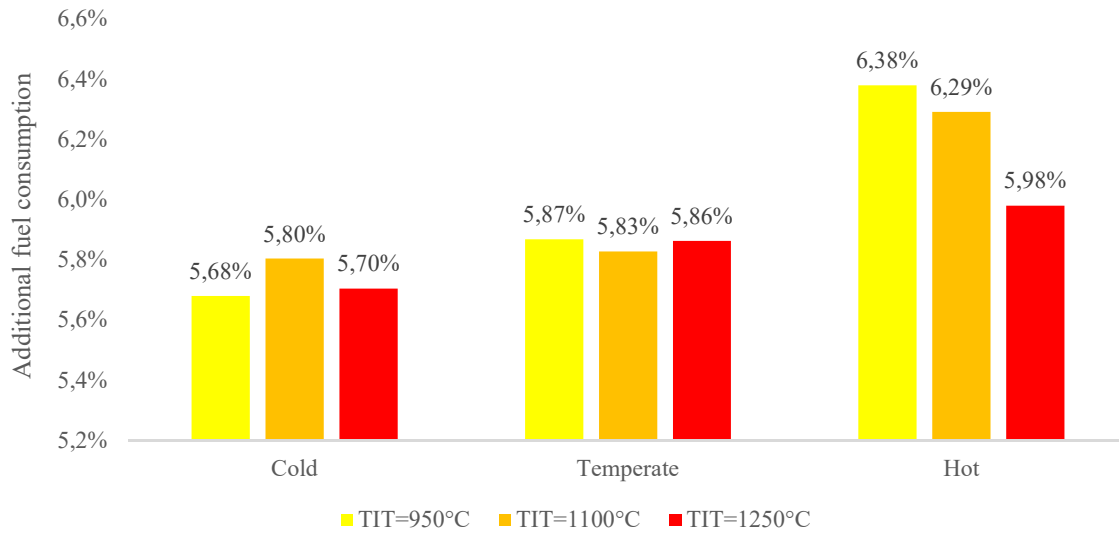
Fig. 4.26: additional fuel consumption compared to NSGA-DP results with second startup strategy

4.7 Conclusions

A bi-level optimization method was proposed in this chapter to simulate the fuel consumption of a series hybrid electric vehicle (SHEV) with an intercooled regenerative reheat gas turbine (IRReGT) energy converter as auxiliary power unit (APU). The optimization method consists of coupling the non-dominated sorting genetic algorithm (NSGA) to the dynamic programing (DP) in order to find the APU optimal power while minimizing the switching ON/OFF number for technical constraint reasons. Simulations were performed on three consecutive WLTC while considering three different turbine inlet temperatures (TIT) and three different climates: cold, temperate and hot. The NSGA-DP optimization results inform on the impact of TIT as well as the impact of the climate, implicitly the thermal comfort needs, on the fuel consumption.

However, these optimization results remain biased since the IRReGT-system startup transient phase impact on the fuel consumption is not considered.

Therefore, up to this end, and in order to evaluate the impact of startup transient phase on the vehicle fuel consumption, an IRReGT dynamic model machine was developed on Dymola software. The model accounts for the turbomachinery inertial transient operation as well as the heat exchangers' (HEX) transient operation. Then, two startup strategies were considered for the evaluation of the IRReGT efficiency, temperature, fuel consumption and convergence time during startup phase. The first strategy is a constant power startup strategy where the PID controls the amount of fuel injected during startup phase in order to maintain the desired IRReGT-system net power to its set point value. This strategy leads to a quick increase in the regenerator temperature and therefore a rapid attaining of the maximal system efficiency. The second strategy is a constant mass fuel injected strategy where the same amount of fuel is injected during the startup phase. In this strategy, the IRReGT net power and efficiency increase as the combustion chamber outlet temperatures, the TIT, increase with the increasing of the regenerator cold side outlet temperature. The convergence time to achieve the desired optimal efficiency and the desired net power is therefore longer. Simulations showed also that the turbomachines' startup from rest to nominal speed have negligible impact on fuel consumption and electric consumption from the battery compared to the regenerator transient operation.

Finally, the NSGA-DP switching ON/OFF decision results are used to evaluate the fuel consumption with dynamic results. Therefore, the instantaneous fuel consumption results from the NSGA-DP are replaced by the instantaneous fuel consumption resulting from the dynamic modeling. For the first startup scenario, since the APU output power is controlled to the set point value by regulating the fuel quantity injected, the operating time is the same as for the NSGA-DP. However, for the second startup scenario, where the startup power is lower and converges toward the nominal value, an additional operating time is considered to account for the energy deficit during startup time.

An increase in fuel consumption between 2.4% and 3.8% is observed with first scenario startup depending on the considered climate and the IRReGT maximum combustion chamber temperature and between 5.7% and 6.4% with the second scenario. Results show also that the impact of transient operation is reduced on the cold climate, since the APU is constrained to operate for longer time. Note that the final choice of the startup strategy depends on technological constraints, among them the thermomechanical fatigue stress on the regenerator and turbine housing and are not discussed in this scientific study. These damage modes require specific testing and validation which must be undertaken during the integration-validation plan before the commercialization of the machine.

Annex 4.1: Fuel consumption results
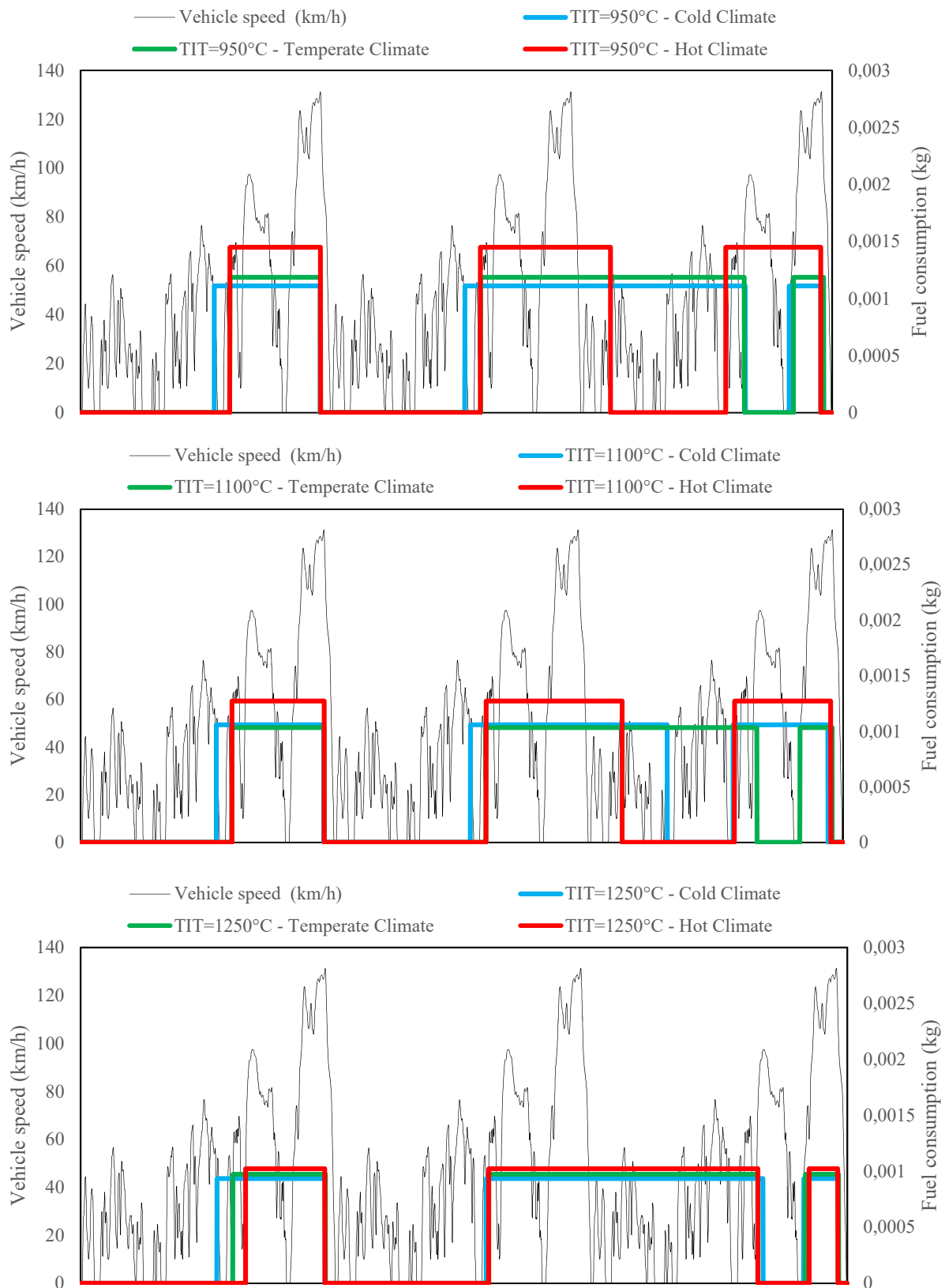
Fig. A.4.1 fuel consumption for the different GT-system configurations on the optimal operating point corresponding to three switching ON/OFF on the three consecutive WLTCs

Annex 4.2: Scenario 1 strategy
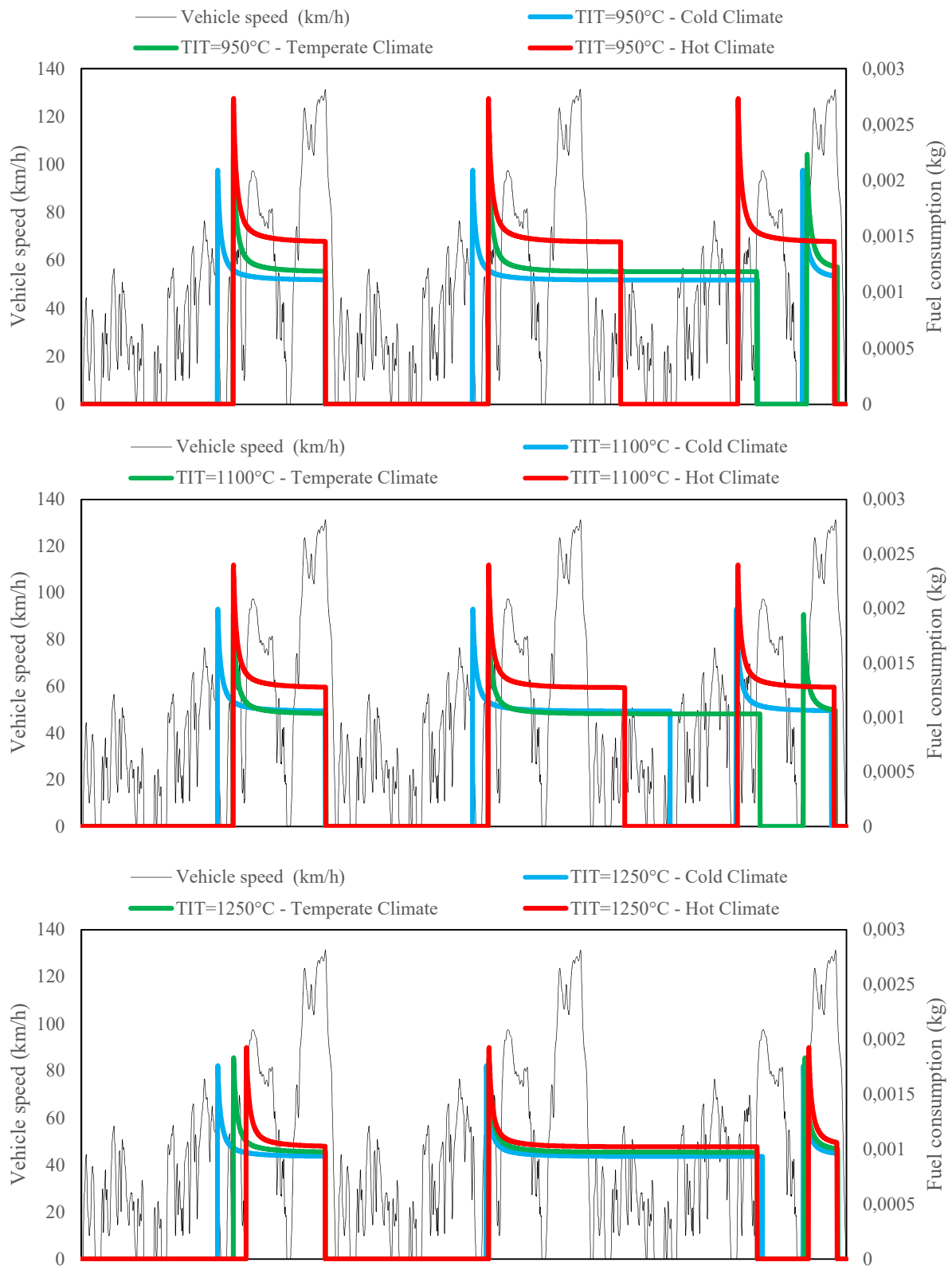
Fig. A.4.2 fuel consumption for the three different GT-system turbine inlet temperature with the scenario1 strategy on the three consecutive WLTC

Annex 4.3: Scenario 2 strategy
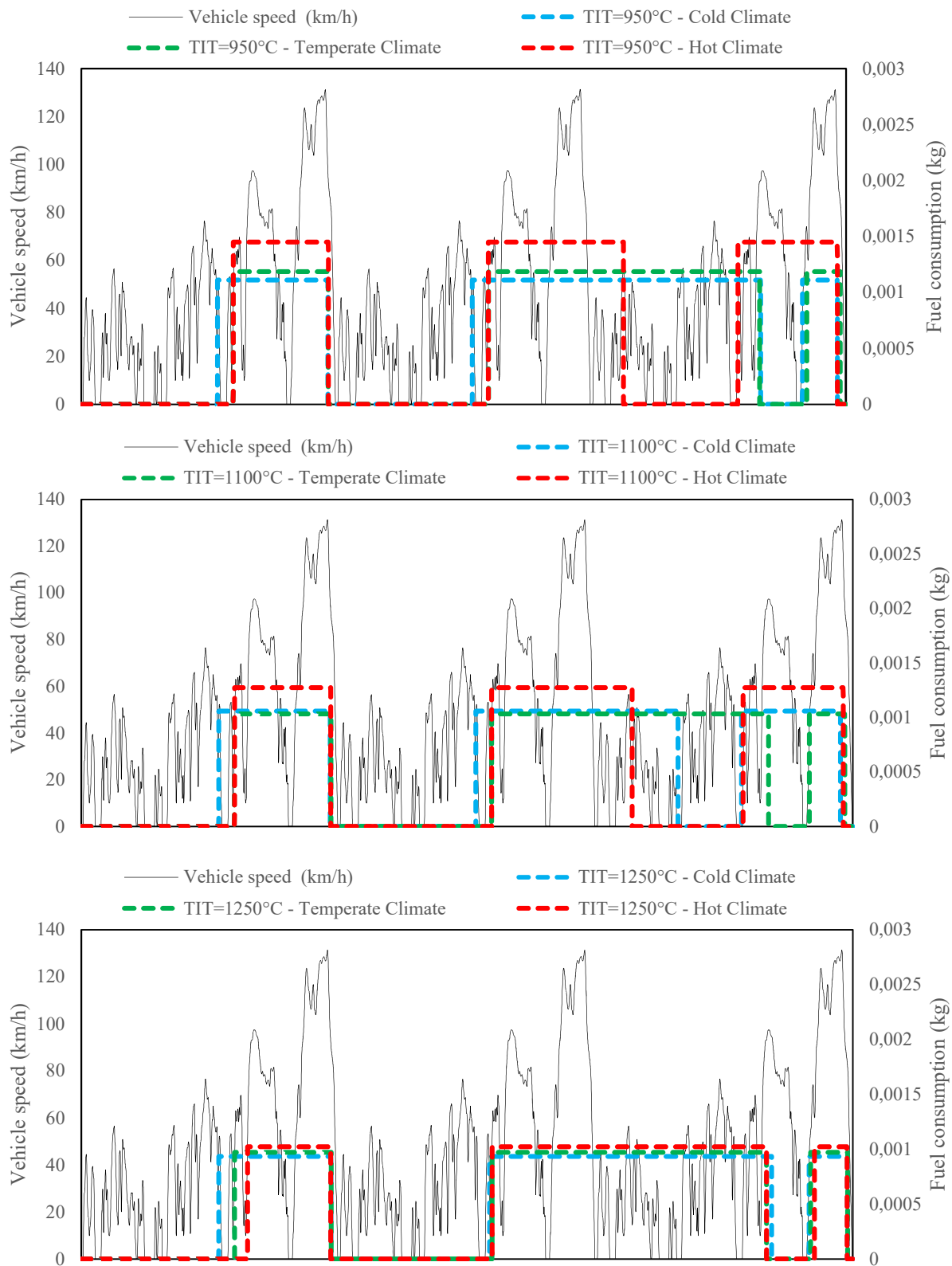
Fig. A.4.3 fuel consumption for the three different GT-system turbine inlet temperature with the scenario2 strategy on the three consecutive WLTC

Résumé chapitre 5

Les systèmes à turbine à gaz présentent un potentiel pour remplacer le moteur thermique à combustion interne comme groupe auxiliaire de puissance ou prolongateur d'autonomie dans les futures véhicules à chaînes de traction hybride électriques en série comme présenté dans les chapitres 2 et 3.

Différentes configurations thermodynamiques de turbine à gaz peuvent être envisagées pour être intégrées comme prolongateur d'autonomie, parmi elles, le cycle thermodynamique de turbine à gaz à refroidissement intérmédiaire, récupération et réchauffage intérmédiaire, offre un travail spécifique net élevé et un rendement élevé. Cela se traduit par une réduction du poids, de la taille, de la complexité d'intégration du système, ainsi que par une amélioration de la consommation de carburant du véhicule.

Ce chapitre présente une étude expérimentale de l'impact du processus de réchauffage intérmédiaire durant la phase de détente sur le rendement du système de turbine à gaz. Tout d'abord, deux cycles de turbine à gaz sont considérés: une turbine à gaz simple et une turbine à gaz avec réchauffage intérmédiaire. L'effet du processus de réchauffage sur le travail net de la turbine est simulé.

Ensuite, une technologie de turbocompresseur à géométrie variable est sélectionnée et testée sur un banc d'essai. L'effet du processus de réchauffage intérmédiaire est évalué en mesurant le travail du compresseur du turbocompresseur dans trois configurations différentes émulant à la fois une expansion avec et sans réchauffage.

Les essais ont été effectués à différentes températures d'entrée de la turbine, à différents débits massiques d'air et à différentes pressions d'entrée de la turbine. Les résultats des essais montrent une cohérence avec les simulations thermodynamiques et prouvent l'importance du processus de réchauffage intérmédiaire et son impact positif sur l'augmentation du travail de détente de la turbine.

Les résultats soulignent également la nécessité de considérer une conception aérodynamique spécifique principalement pour le premier étage de détente, l'étage turbine haute pression, ainsi que l'importance de réduire les pertes thermique de la turbine, principalement l'énergie thermique évacuée vers le système de lubrification.

Chapter 5: Experimental study on gas turbine subsystems: Evaluation of the turbine's reheat process effect on the system performances

This chapter describes the tests performed on one of the main subsystem of the Intercooled Regenerative Reheat Gas Turbine (IRReGT) selected configuration presented in figure 5.1. This gas turbine (GT) system has been divided into four subsystems:

1- The intercooled compression subsystem: consists of the first compressor, the intercooler and the second compressor
2- The thermal heat recuperator subsystem: the regenerator heat exchanger
3- The combustion chambers subsystem: the combustion chamber 1 upstream the turbine 1 and the combustion chamber 2, upstream the turbine 2
4- The turbines expansion subsystem: consists of the first and second turbines.

In this study, we have focused on the turbine expansion subsystem. In fact, this subsystem is considered as the innovative part in our works compared to other gas turbine systems studied for automotive applications where no turbine reheat process have been proposed yet.
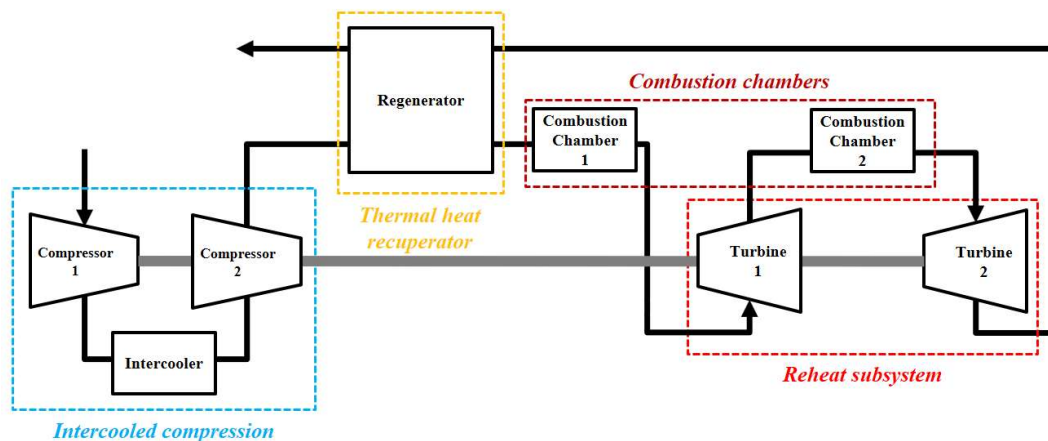
Fig. 5.1: IRReGT configuration and its different subsystems

The chapter starts by presenting the objectives of the tests which are understanding and evaluating the impact of reheat during expansion on the net specific work. It is worthy to mention that since the study focuses on the turbine reheat subsystem, it was not possible to evaluate the reheat impact on the GT system efficiency, an issue discussed later in this chapter. Then, a theoretical analysis is performed in the second paragraph in order to understand the impact of physical parameters such as the turbine inlet temperature (TIT), the components efficiency and the cycle pressure on the net specific work main objective. The bench cell including the test setup are described in the third paragraph, and the tested turbocharger is presented in paragraph four. Note that an automotive turbocharger was selected to perform the experimentation. Testing methodology is presented in the fifth paragraph, and the test results are commented in the sixth paragraph. Finally, this chapter concludes on the importance of the turbine reheat process and delivers scientific recommendations for future engineering development works on this thermodynamic configuration.

5.1 Test objectives

In order to evaluate the importance of the reheat on the efficiency and power density of the IRReGT machine, tests were performed on an ordinary automotive series turbocharged. The objectives are to understand the operating principle of turbochargers and to assess the importance of the reheat on system net specific work using low cost and easily found components. In this section, we start by reminding from the theoretical point of view the importance of turbine reheat configuration on the performance of gas turbine machines.

The simple gas turbine machine is presented in figure 5.2. The compression occurs in two compressors mounted in serial arrangement since the maximum cycle pressure in our case cannot be realized with only one stage with radial wheels centrifugal machines technology, as discussed in chapter 2. Same for the expansion side, where the system requires two radial centrifugal turbines in order to expand from the maximum cycle pressure to the atmosphere pressure.
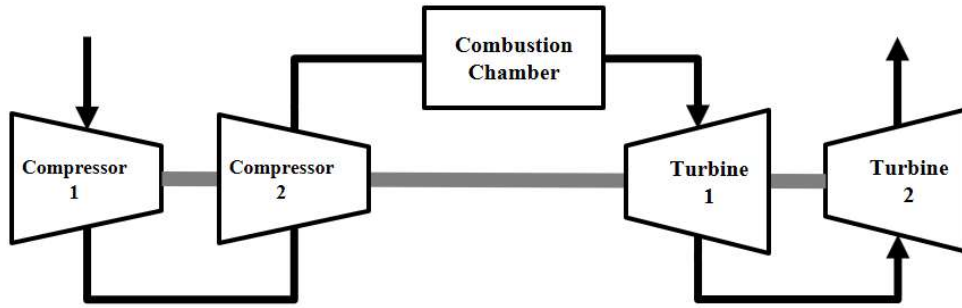
Fig. 5.2: Simple gas turbine cycle

The machine thermodynamic cycle in the P-V diagram is presented in figure 5.3. The simple gas turbine cycle, the black line consists of:

- Polytropic compression (process 1-2) that occurs during compression in the compressors
- Constant heat addition (process 2-3) that occurs in the combustion chamber
- Polytropic expansion (process 3-4) that occurs during expansion in the turbines
- Constant heat rejection (process 4-1) that occurs at turbine outlet

The efficiency of a simple GT machine can be written as:

$$\eta_{GT} = \frac{W_{net}}{Q_{CC}} = \frac{W_{T_1} + W_{T_2} - W_{C_1} - W_{C_2}}{Q_{cc}} \tag{5.1}$$

With
- η_{GT} : Simple GT efficiency (%)
- W_{net} : Net specific work (k/kg)
- Q_{cc} : Heat added in the combustion chamber (kJ/kg)
- W_{T_1} : Turbine 1 specific work (kJ/kg)
- W_{T_2} : Turbine 2 specific work (kJ/kg)
- W_{C_1} : Compressor 1 specific work (kJ/kg)
- W_{C_2} : Compressor 2 specific work (kJ/kg)

From a thermodynamic point of view, the net specific work of the cycle is equal to the cycle loop surface in the P-V diagram. Splitting the expansion process by expanding the burned gas to an intermediate pressure (process 3-3'), then reheating through a second combustion chamber (process 3'-3'') downstream the turbine, before expanding again to the atmosphere (process 3''-4'), increases the cycle net specific work since the cycle surface increases as presented in red color in the P-V diagram of figure 5.3.
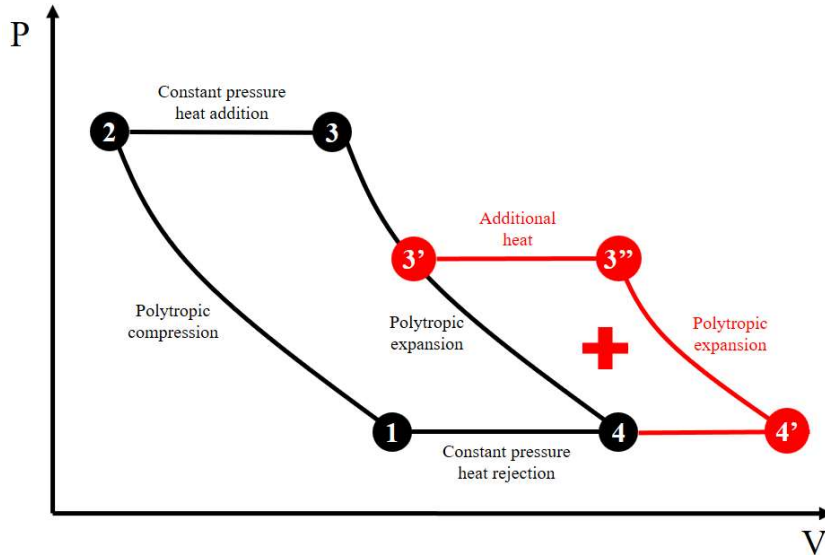
Fig. 5.3: P-V diagram for the simple and reheat gas turbine cycle

Therefore, the efficiency of a reheat machine, described in figure 5.4 can be written according to the equation 5.2:

$$\eta_{Reheat} = \frac{W_{net} + W_+}{Q_{cc_1} + Q_{cc_2}} = \frac{W_{T_1} + W_{T_{2R}} - W_{C_1} - W_{C_2}}{Q_{cc_1} + Q_{cc_2}} \tag{5.2}$$

$$W_{T_{2R}} = W_{T_2} + W_+ \tag{5.3}$$

With	η_{Reheat}	:	Reheat cycle efficiency (%)
	$W_{T_{2R}}$	:	Turbine 2 specific work with reheat (kJ/kg)
	W_+	:	Additional net work (kJ/kg)
	Q_{cc_1}	:	Heat added in the combustion chamber 1 ($=Q_{CC}$) (kJ/kg)
	Q_{cc_2}	:	Heat added in the combustion chamber 2 (kJ/kg)
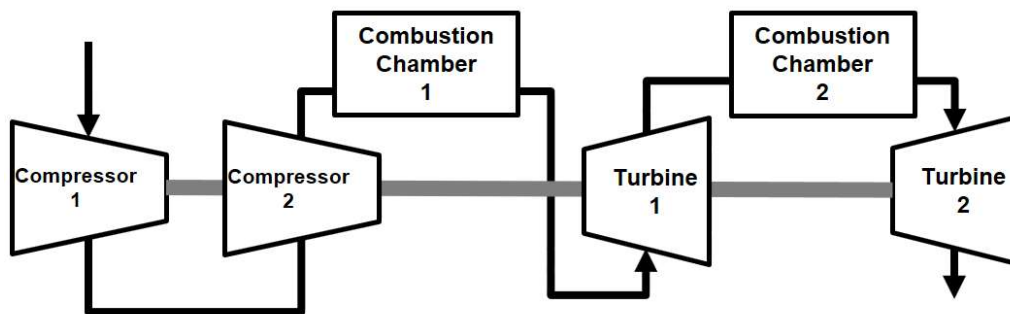
Fig. 5.4: Reheat gas turbine cycle

From the efficiency formula 5.1 and 5.2, it is obvious that to compute for the cycle efficiency, we need to account for the compressors' work. However, when testing the turbine reheat subsystem, only the turbines' work can be accounted for, by measuring the work of turbine 1 and turbine 2 in both configurations: with and without reheat.

Therefore, in this experimental study, we focused on the understanding of the impact of reheat on the turbines' specific work by accounting for the additional power recovered (W_+) when reheat is performed. Note that when considering the whole GT machine, the impact of reheat on cycle efficiency is evaluated by accounting for the ratio of additional power over the additional heat added ($\frac{W_+}{Q_{cc_2}}$) that should be higher than ($\frac{W_{net}}{Q_{cc}}$).

5.2 Theoretical power

In this paragraph, the turbines' theoretical expansion work has been calculated depending on turbine efficiency and the turbine inlet pressure. Turbines' net work has been accounted by applying the first law of thermodynamic as described in equation 5.4.

$$\frac{dE_{cv}}{dt} = \dot{Q} - \dot{W} + \dot{m}_i\left(u_i + \frac{V_i^2}{2} + gz_i + P_i v_i\right) - \dot{m}_e(u_e + \frac{V_e^2}{2} \tag{5.4}$$
$$+ gz_e + P_e v_e)$$

| With			
	E_{cv}	:	Total mechanical power (kJ/kg)
	$\dot{Q}$	:	Heat exchanger to the surroundings (kW)
	$\dot{W}$	:	Turbine power excluding the power flow (kW)
	$\dot{m}_i$	:	Mass flow at turbine inlet (kg/s)
	$\dot{m}_e$	:	Mass flow at turbine outlet (kg/s)
	u_i	:	Internal energy at inlet (kJ/kg)
	u_e	:	Internal energy at outlet (kJ/kg)
	P_i	:	Pressure at turbine inlet (Pa)
	P_e	:	Pressure at turbine outlet (Pa)
	v_i	:	Specific volume at turbine inlet (m³)
	v_e	:	Specific volume at turbine outlet (m³)
	V_i	:	Velocity at turbine inlet (m/s)
	V_e	:	Velocity at turbine outlet (m/s)
	gz_i	:	Potential energy at turbine inlet (kJ/kg)
	gz_e	:	Potential energy at turbine outlet (kJ/kg)

The following assumptions have been considered in order to simplify the equation:

- Steady state operation: $\frac{dE_{cv}}{d} = 0$
- Conservation of the mass: $\dot{m}_i = \dot{m}_e = \dot{m}$
- No change in kinetic and potential energy: $\dot{m}_i\left(\frac{V_i^2}{2} + gz_i\right) - \dot{m}_e\left(\frac{V_e^2}{2} + gz_e\right) = 0$
- No heat exchange to the outside: $\dot{Q} = 0$

Therefore, the turbine specific work is calculated according to equation 5.5 and 5.7, where the turbine outlet enthalpy is accounted by considering the turbine isentropic efficiency according to the equation 5.8.

$$\dot{W} = \dot{m} * (u_i + P_i v_i - u_e - P_e v_e) \tag{5.5}$$

$$h = u + pv \tag{5.6}$$

$$\frac{\dot{W}}{\dot{m}} = (h_i - h_e) \tag{5.7}$$

$$\eta_{Turbine} = \frac{h_i - h_e}{h_i - h_{es}} \tag{5.8}$$

With
$\eta_{Turbine}$: Turbine isentropic efficiency
h_i : Enthalpy at turbine inlet (kJ/kg)
h_i : Enthalpy at turbine outlet (kJ/kg)
h_{es} : Turbine isentropic outlet enthalpy (kJ/kg)

Simulation were performed by varying the turbine isentropic efficiency and the first turbine inlet pressure for each TIT, and by calculating the total expansion work wich is the sum of the first turbine expansion work and the second turbine expansion work according to equation 5.9:

$$W_T = W_{T_1} + W_{T_2} \tag{5.9}$$

With
W_T : Turbines total specific work (kJ/kg)
W_{T_1} : Turbine 1 specific work (kJ/kg)
W_{T_2} : Turbine 2 specific work (kJ/kg)

During the simulations, two TIT have been considered: 400°C and 500°C. The first turbine outlet pressure is regulated to a value equal the root square of its inlet pressure. Therefore, the expansion ratio is considered to be equal in both turbines. First turbine inlet pressure varies between 3 and 4.5 bars. As for the turbine efficiency, the same isentropic efficiency is considered for both turbines during simulations with values ranging from 40% up to 75%.
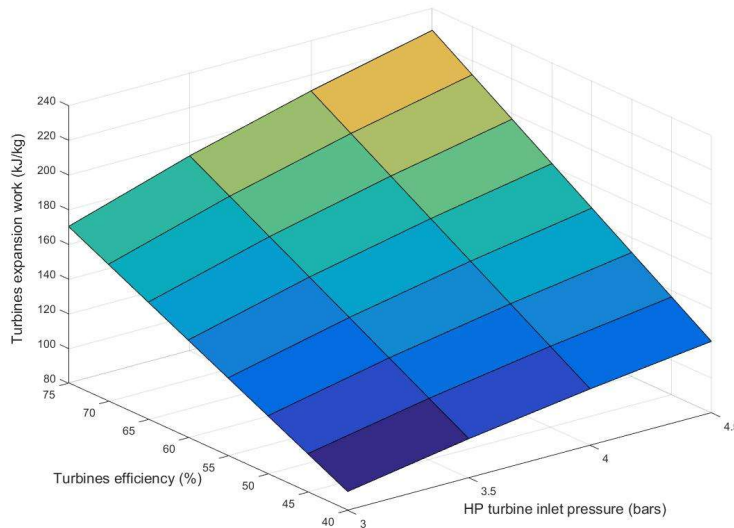

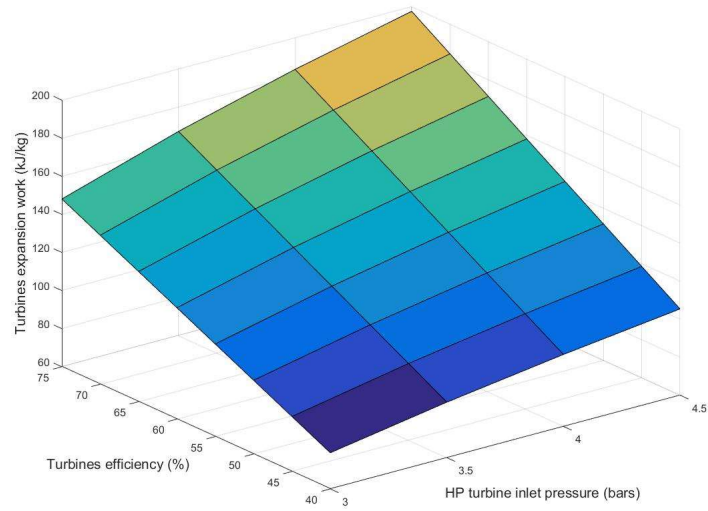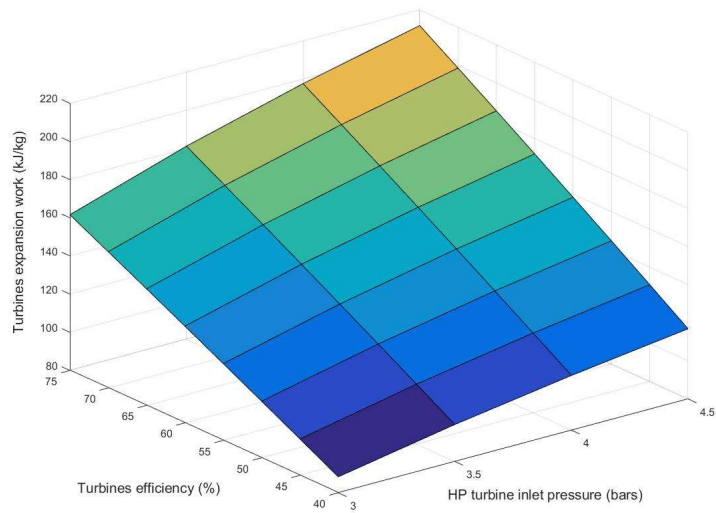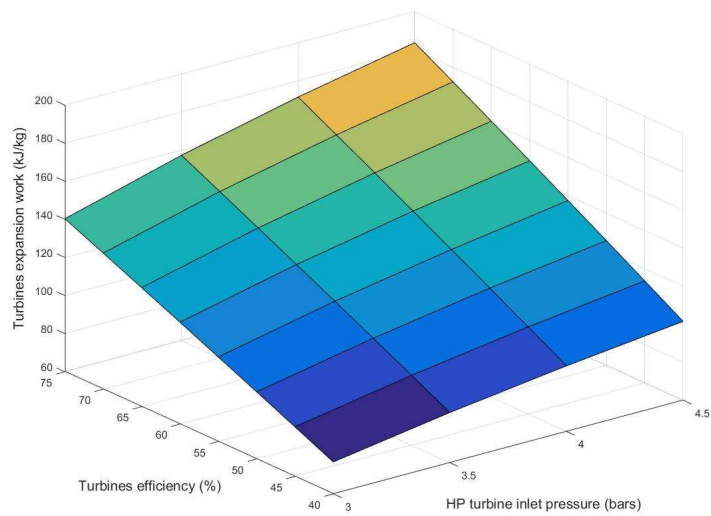*Fig. 5.5: Turbines expansion work with reheat – TIT=500°C*

Fig. 5.6: Turbines expansion work with reheat – TIT=400°C

Fig. 5.7: Turbines expansion work without reheat – TIT=500°C

Fig. 5.8: Turbines expansion work without reheat – TIT=400°C

Many conclusions can be drawn from these figures:

1- The turbines' expansion work increase as the turbines' efficiency increase and the high pressure (HP) turbine inlet pressure increases. In fact, higher turbine efficiency implies lower enthalpy at turbine outlet, where higher inlet pressure leads to higher expansion ratio and consequently to lower enthalpy at turbine outlet. Increasing both physical parameters, the isentropic efficiency and the expansion ratio, lead therefore for higher enthalpy variation across turbines and consequently to higher turbines work according to equation 5.7.

2- The increase in turbine inlet temperature (TIT) leads to higher expansion work. Comparing both reheat and no reheat configurations, around 15% of additional work is recovered when increasing the TIT from 400°C up to 500°C. This can be explained by the higher enthalpy at turbine inlet, and accordingly higher enthalpy variation across it.

3- Finally, comparing the turbines expansion work between reheat and non reheat cycles, we conclude that reheat configuration increases the turbines' expansion work. This increase is more important as the turbines' efficiency increases and the high pressure turbine inlet increases. For instance, for TIT=500°C, only 2.8% of additional work is found when turbine efficiency is 40% and HP turbine inlet pressure is equal to 3 bars, compared to 5.4% when turbines' efficiency increases to 75% at the same inlet pressure, and up to 7.5% when inlet pressure increases up to 4.5 bars with 75% turbines' isentropic efficiency.

5.3 Test bench description

This section presents the test bench in which the experimentations have been performed. The section starts by describing the test bench cell and all testing setup used for the experimentation.

Fig. 5.9: PSA turbocharger test bench

The test cell is located in the Groupe PSA - Technical center of Vélizy. The testing means were designed to test turbocharger for automotive applications in order to study these machines from engineering and scientific point of view, in order to enhance later their performances.

The bench is equipped by an air tank of 2m^3 of volume. Compressed air is stored inside at a pressure up to 10 bars. A Brooks flowmeter is installed downstream the air tank in order to measure the airflow rate which can go up to 750 kg/h. This circuit is connected to the inlet of the turbine of the tested turbocharger.

Fig. 5.10: Air tank

Fig. 5.11: Brooks flowmeter

Two valves are installed in parallel arrangement in the airflow circuit downstream the air flow meter, and are used to control the air mass flow rate.

Fig. 5.12: Air flow control valves

The air flow is then heated through an electric heater of 144kW electric power. This device increases the air temperature from ambient and up to 600°C.
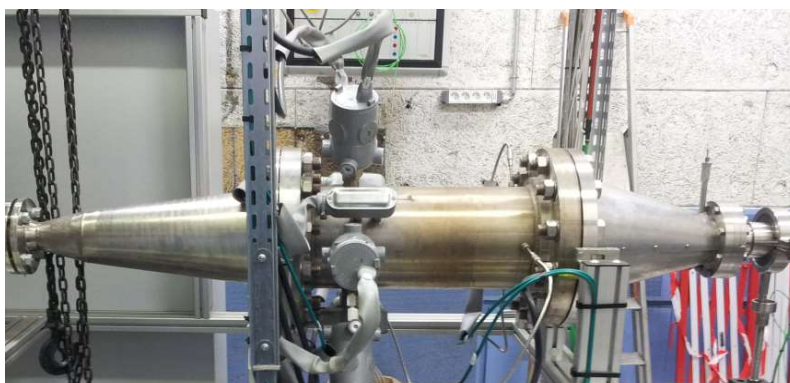
Fig. 5.13: Electric heater

This heated air enters the tested component which can be a heat exchanger, an electrified turbine, a turbocharger or other system. In case of turbocharger, the hot air expands and turns a

turbine coupled to a compressor that compress the air. The compressor air is sucked from the cabin, and passes through a flowmeter before it enters the compressor.
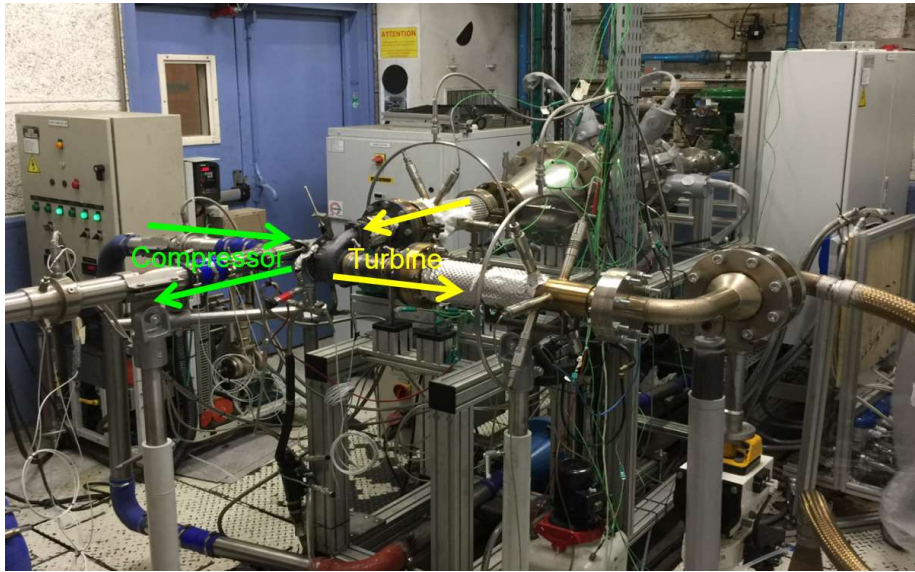
Fig. 5.14: Turbocharger setup

The turbine expansion ratio is controlled through an expansion valve control system while the compressor compression ratio is controlled through a compressor back pressure control system.

Fig. 5.15: Compressor back pressure control system
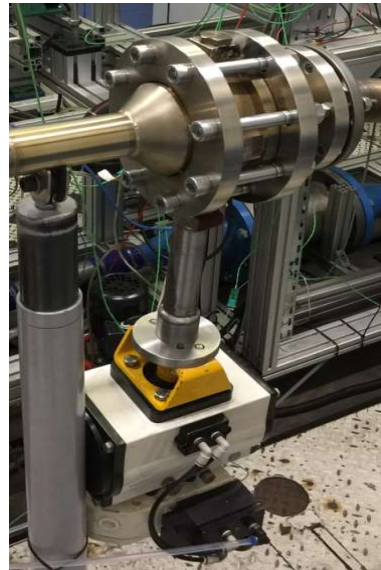
Fig. 5.16: Turbine expansion valve control system

Compared to automotive applications where the lubrication of the turbocharger is ensured by the pressurized engine oil through an oil pressure, the bench is equipped with an oil conditioning system which controls the oil pressure and temperature in order to ensure the lubricating and the cooling of the turbocharger bearings.

The setup is equipped with different thermocouples and pressure sensors, in order to measure the air flow temperature and the pressure respectively at different locations in the system, mainly upstream and downstream the compressor and the turbine.

Fig. 5.17: Oil conditioning system
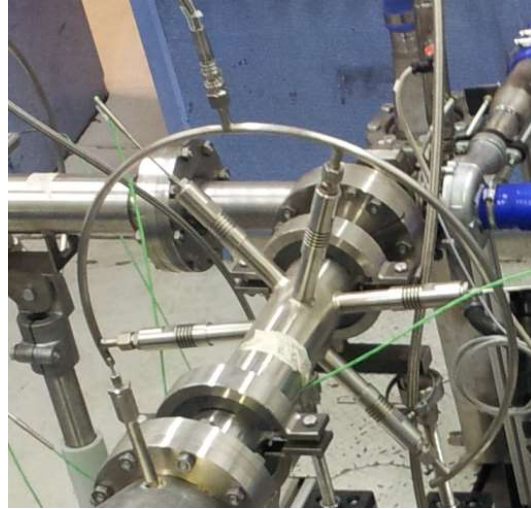
Fig. 5.18: Thermocouples and pressure sensors

Finally, the bench is equipped with an acquisition system that provides all required information in terms of temperature, pressure, upstream and downstream the compressor and the turbine. The acquisition provides also the mass flow rate of the compressor and the turbine, as well as the turbine operating speed of the turbocharger measured using an optic sensor that counts the number of reflected signal on the compressor blades during the turbocharger operation.
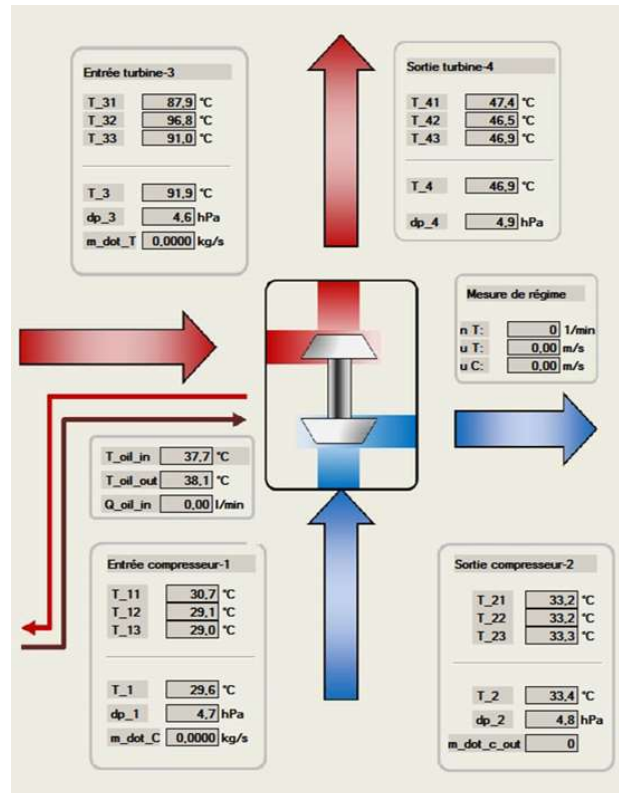
Fig. 5.19: Test bench acquisition system

5.3.1 Turbocharger description

The turbocharger used for testing is a turbine variable geometry turbocharger developed and commercialized on Diesel internal combustion engines with the technical characteristics presented in table 5.1.
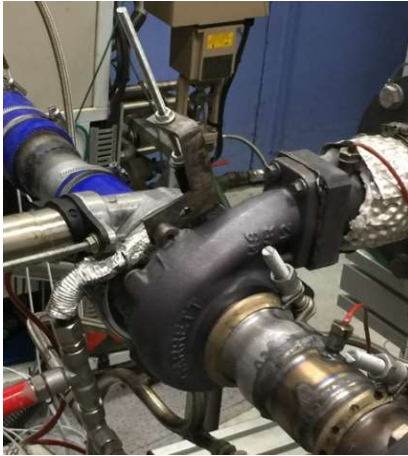
Fig. 5.20: tested turbocharger
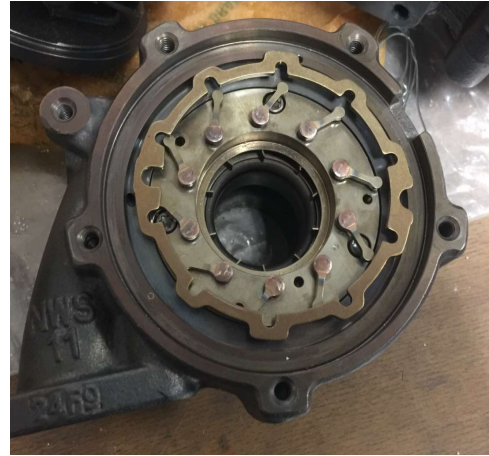
Fig. 5.21: Turbine variable geometry

Table 5.1: Tested turbocharger characteristics

Garett Turbocharger	Compressor	Turbine
Wheel bigger diameter (mm)	44 mm	39 mm
Wheel smaller diam (mm)	31	19,5 mm
Trim (mm)	50	72
Inertia (kg.m²)	2,75e-06	4,56e-06
Maximum speed (RPM)	243.000	

It consists of a compressor and a turbine coupled on the same shaft and turning at the same rotation speed. The shaft bearings are normally lubricated by the engine oil which is ensured in our tests by the oil conditioning system.
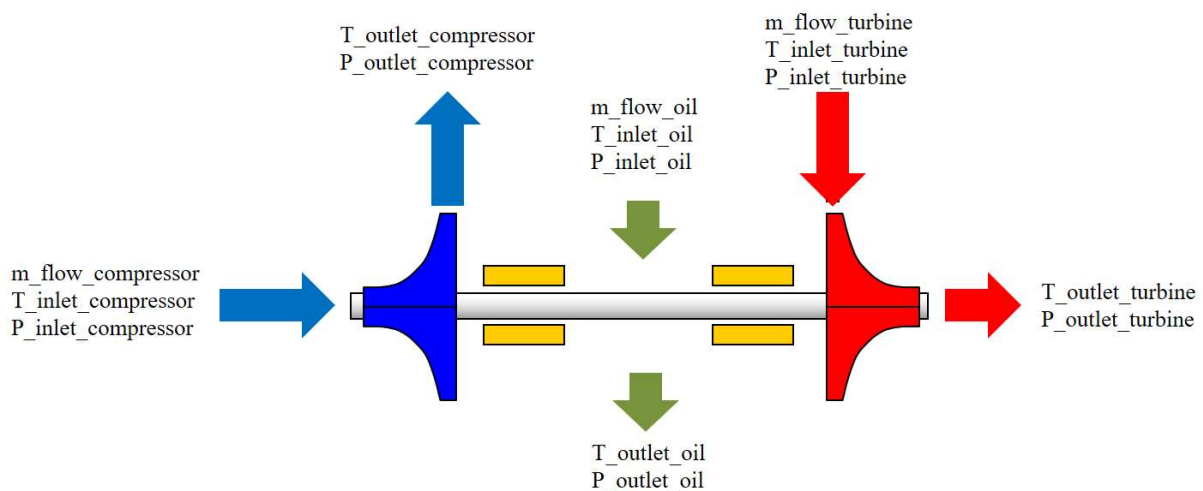
Fig. 5.22: Turbocharger configuration

The compressor and turbine maps are presented in figures 5.23, 5.24 and 5.25 below. The maximum compressor efficiency is attainable with mass flow rate between 220 kg/h and 315 kg/h and pressure ratio between 1.8 and 2.4, and reach about 74%.

As for the turbine, the efficiency depends on the position of the variable geometry as well as on the mass flow rate, the operating speed, the expansion ratio and the inlet temperature. Therefore, for each operating temperature and variable geometry position, a turbine efficiency map can be definied as presented in the figures 5.24 and 5.25 below. Note that the maximum efficiency of the selected turbine approaches 68% when gas inlet temperature is about 800°C.
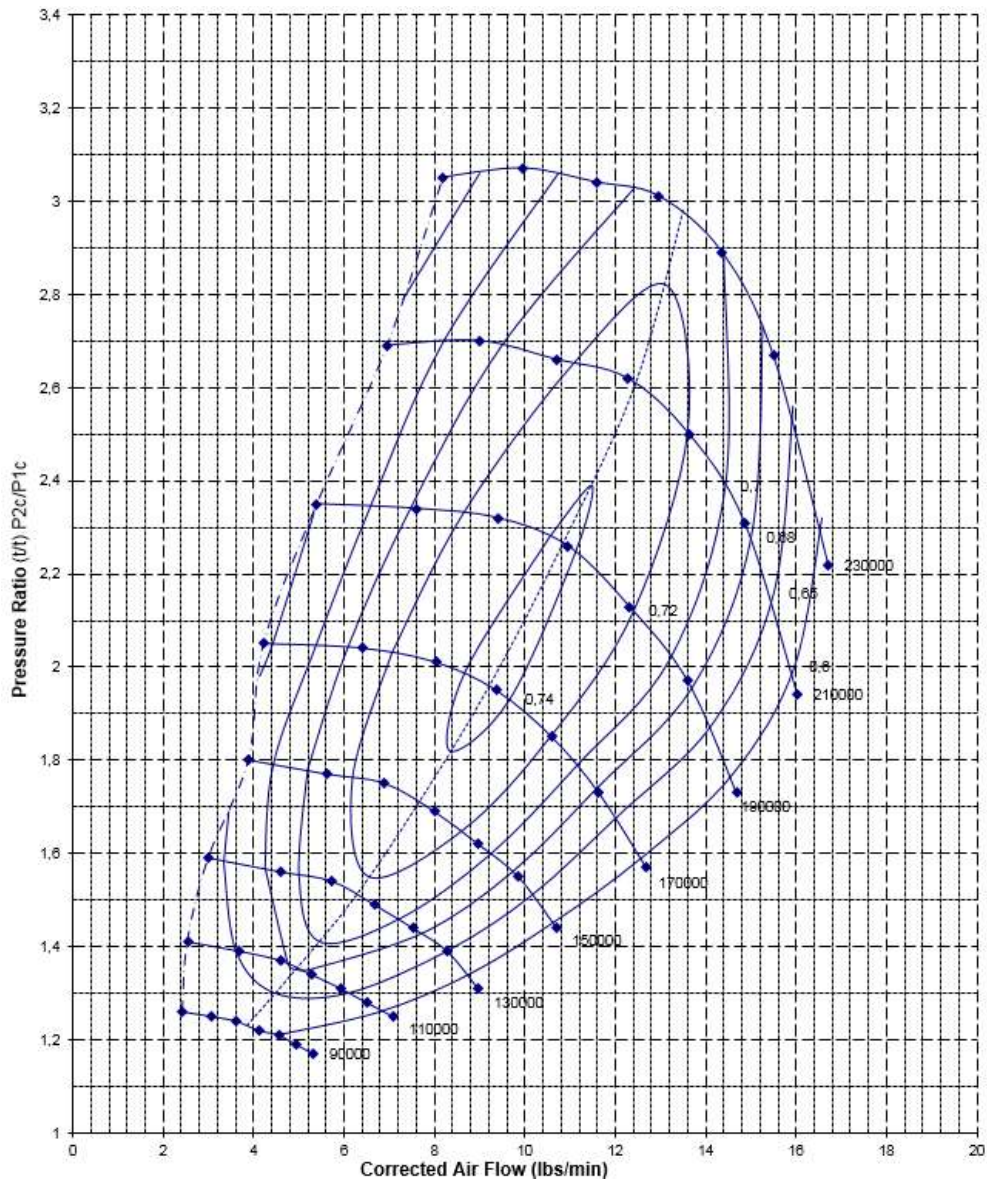
Fig. 5.23: turbocharger compressor MAP
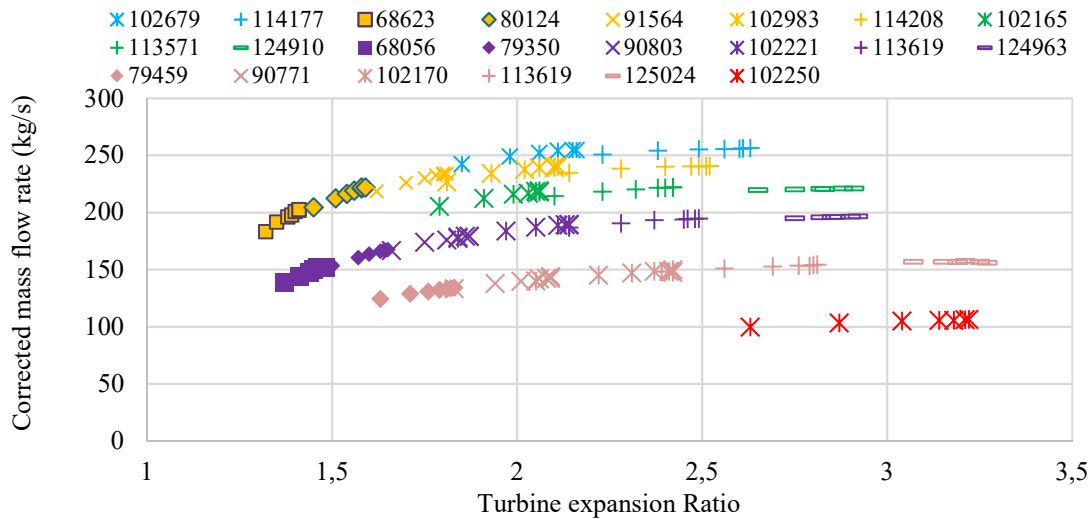
Fig. 5.24: Turbine corrected mass flow rate (kg/s) function of turbine expansion ratio for different rotation speed (RPM)
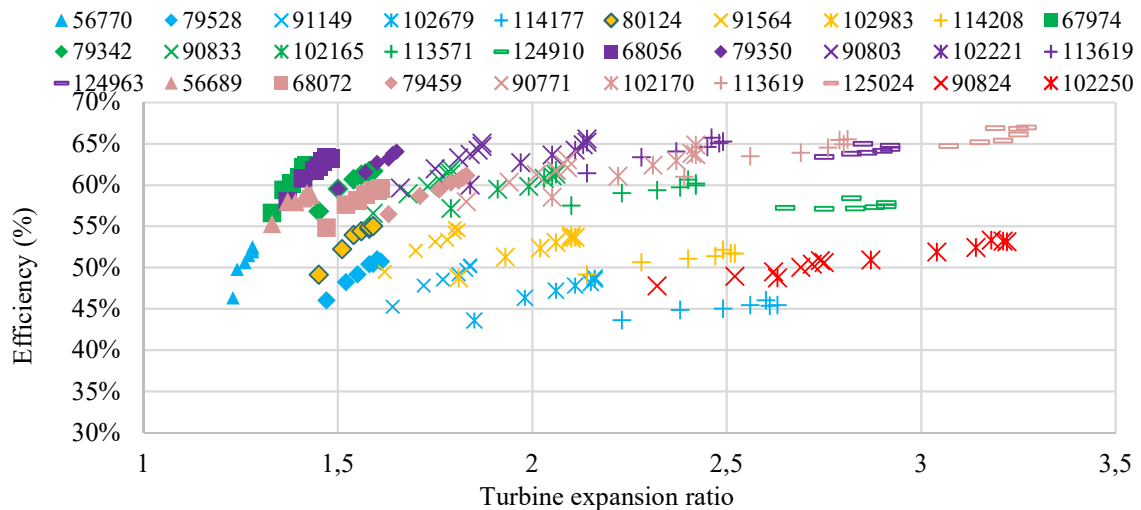
Fig. 5.25: Turbine efficiency (%) function of expansion ratio for different rotation speed (RPM)

5.4 Testing Method

This section presents the methodology adopted to evaluate the impact of reheat process on the net specific work of gas turbine systems using the testing setup described before. The method presented in figure 5.26 consists of three testing steps. Note that only one turbocharger with the specific turbine and compressor maps described before has been used during the experimentation, and during the three test steps.

In the first step, tests are performed by regulating the air temperature at turbine inlet at a given value using the electric heater. The turbine inlet pressure depends on the expansion ratio and the turbine mass flow rate. Therefore a calibration of the variable geometry position and the expansion valve position is realized for each operating point in order to regulate both the turbine inlet and the outlet pressure. The turbine outlet temperature and pressure are measured using a thermometer and a pressure sensor at the turbine outlet. The compressor work is calculated

knowing the inlet and outlet conditions (temperature and pressure) as well as the compressor mass flow rate. The compressor work value is validated knowing the compressor map. The thermal power released to the oil lubricating system was accounted knowing the lubricating oil inlet and outlet temperature as well as the oil specific heat and the oil mass flow rate.
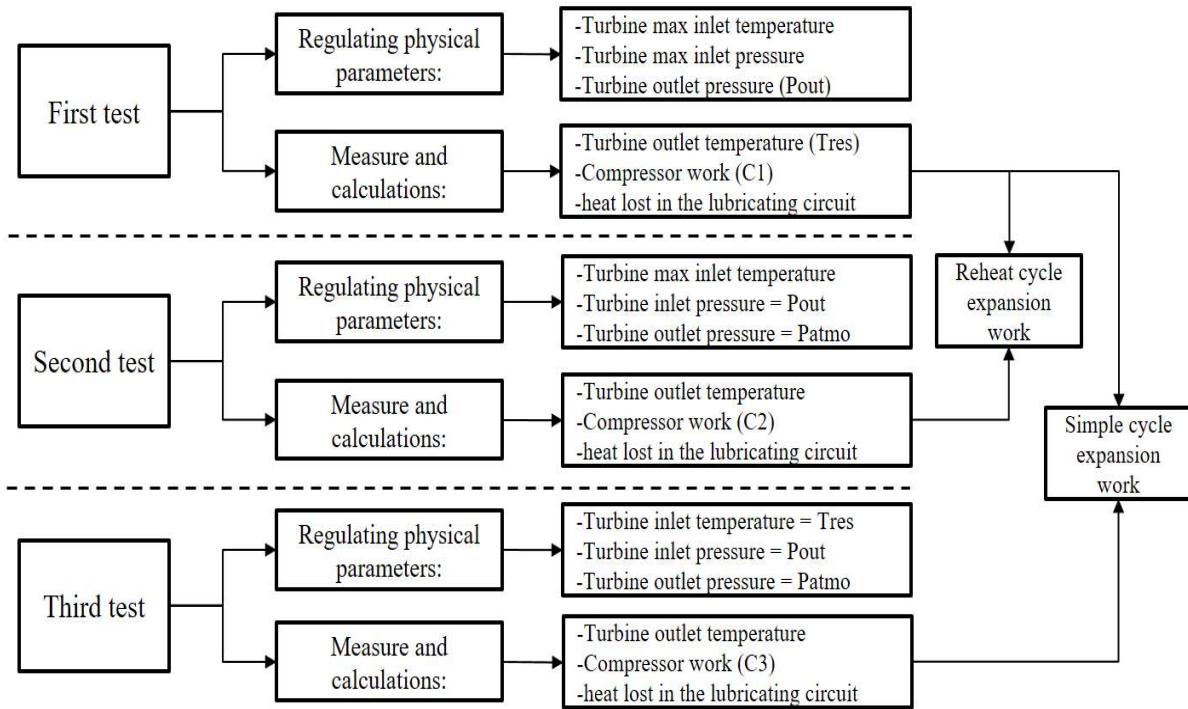
Fig. 5.26: Method to evaluate the impact of reheat on system performance

In the second step, experimentations were carried out on the same turbocharger, by adjusting the turbine inlet temperature and pressure to values equal to the turbine inlet temperature and turbine outlet pressure of the first step tests respectively. The turbine expands to the ambient pressure. This test step allows us to evaluate the impact of the reheat on the turbine work, measured by standing out the compressor work. The turbine efficiency is accounted knowing the compressor power and the thermodynamic conditions at the inlet and the outlet of this component. The heat losses to the oil circuit are accounted as in tests step 1 and the additional heat input is also accounted, knowing the turbine outlet temperature (Tres) and the mass flow rate.

Finally, in the third testing step, tests were done with Tres and Pout as turbine inlet parameters. As in step two, the turbine outlet pressure is the ambient pressure. The compressor work and the thermal losses in the oil lubricating circuit are accounted as in step one and two.

The expansion work with reheat is therefore accounted by summing the compressor work from the first test step (C1) and the compressor work from the second test step (C2). The expansion work without reheat is accounted by summing the (C1) with the expansion work from the third test step (C3). These expansion work values are then compared to the theoretical value by accounting for the turbine efficiency at each operating point.

5.5 Tests results

The tests' operating conditions are presented in table 5.2 below. Tests were performed at two different turbine inlet temperature (TIT): 500°C and 400°C. For each TIT, three different turbine mass flow rates (150, 200 and 250 kg/h) and four different high-pressure (HP) turbine inlet pressures (3, 3.5, 4 and 4.5 bars) were investigated.

Table 5.2: Tests' physical operating conditions

N°	TIT (°C)	Turbine mass flow rate (kg/h)	HP Turbine inlet pressure (bars)	N°	TIT (°C)	Turbine mass flow rate (kg/h)	HP Turbine inlet pressure (bars)
1	500	150	3	13	400	150	3
2	500	150	3.5	14	400	150	3.5
3	500	150	4	15	400	150	4
4	500	150	4.5	16	400	150	4.5
5	500	200	3	17	400	200	3
6	500	200	3.5	18	400	200	3.5
7	500	200	4	19	400	200	4
8	500	200	4.5	20	400	200	4.5
9	500	250	3	21	400	250	3
10	500	250	3.5	22	400	250	3.5
11	500	250	4	23	400	250	4
12	500	250	4.5	24	400	250	4.5

For each operating condition, the three steps of the tests described in the method section were realized and compressors' mass flow rate has been regulated to a value equal to turbine flow rate by acting on the compressor backpressure valve. This was done in order to simulate the operation of gas turbine systems and internal combustion engines where the compressor flow rate is equal to the turbine flow rate minus the fuel quantity injected wich represents a small fraction. The different operating points are plotted on the compressor map below.
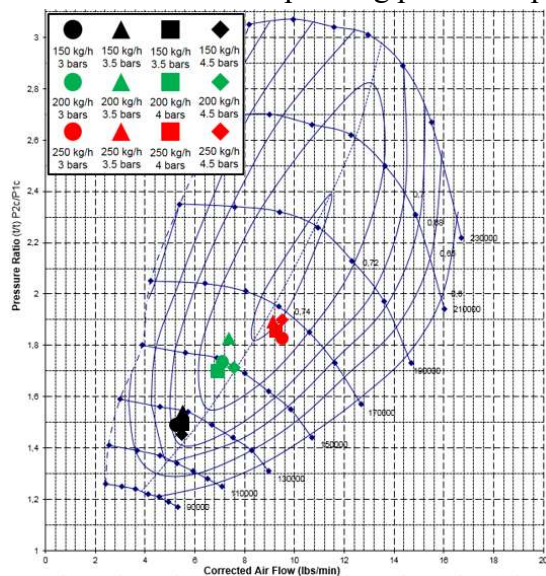
Fig. 5.27: Compressor operating points - Tests step 1 - results for TIT=500°C
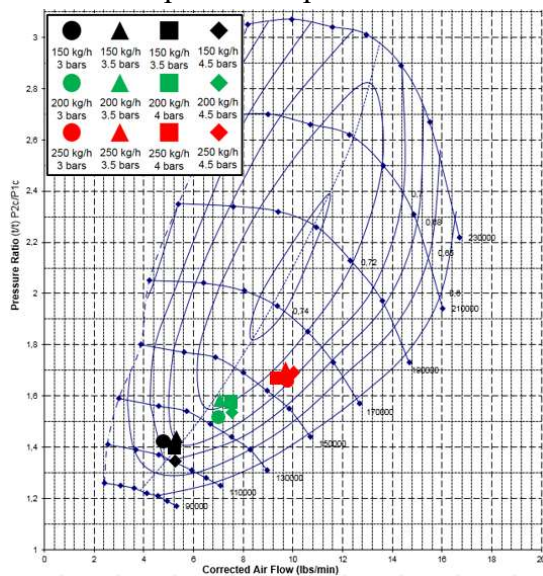
Fig. 5.28: Compressor operating points - Tests step 1 - results for TIT=400°C
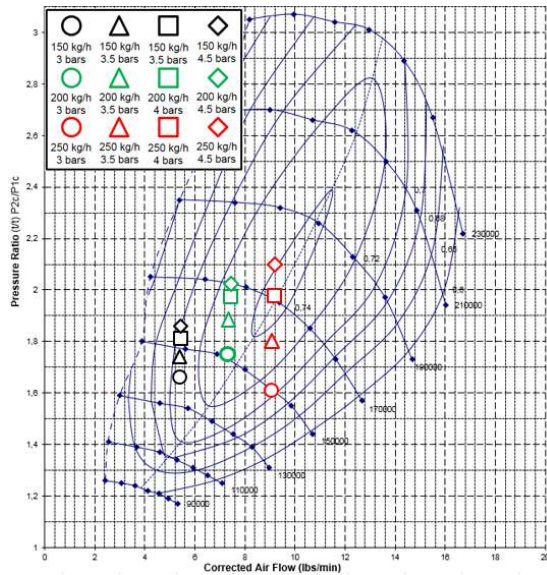
*Fig. 5.29: Compressor operating points -
Tests step 2 - results for TIT=500°C*
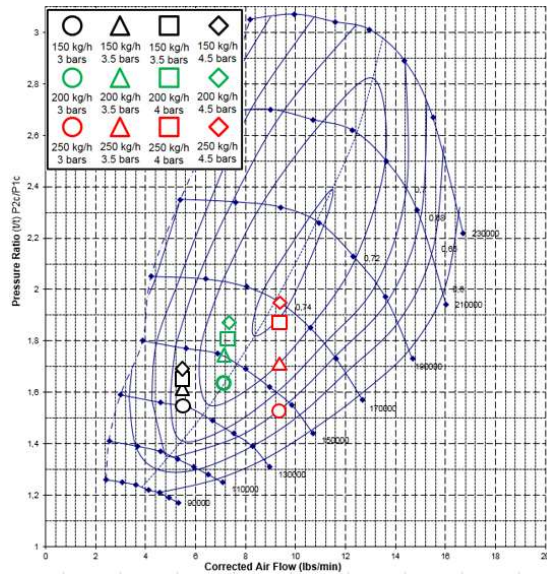
*Fig. 5.30: Compressor operating points -
Tests step 2 - results for TIT=400°C*
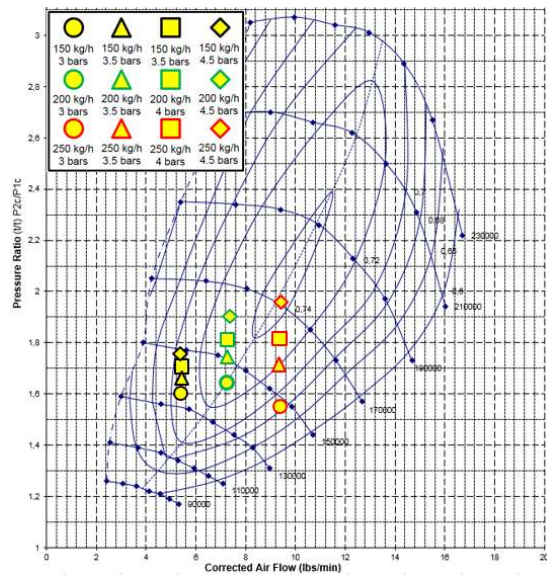
*Fig. 5.31: Compressor operating points -
Tests step 3 - results for TIT=500°C*
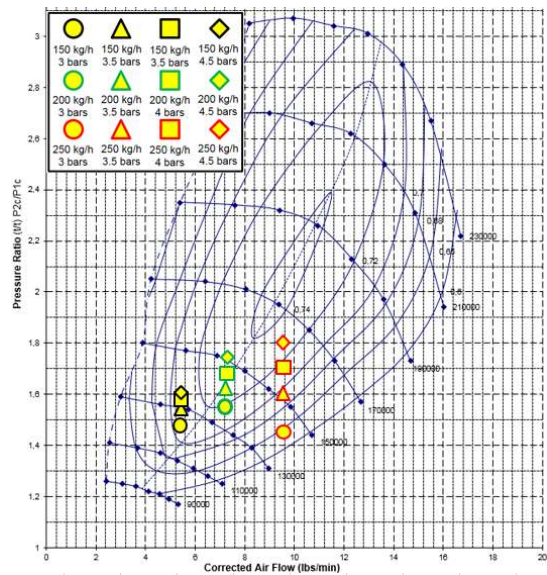
*Fig. 5.32: Compressor operating points -
Tests step 3 - results for TIT=400°C*

As for the compressor, its power at different operating points is calculated by measuring the temperature and the pressure at the inlet and the outlet of the compressor, knowing the inlet mass flow rate. The values for both TIT = 500°C and TIT=400°C are presented in figures 5.33 and 5.34. Many conclusions can be drawn out from these figures:

1- The compressor's power when turbine operates at TIT = 500°C is higher than when the TIT=400°C. In fact, we can see from the plotting points on the compressor map, that while the air flow is the same between tests done at 400°C and 500°C TIT, the pressure ratio for tests at TIT=500°C are higher, and the turbocharger operating speed is also higher. This implies higher turbine power delivered when TIT increases.

2- For the same high cycle pressure, the compressor power increases as the turbine flow rate increases since the turbine power increases.

3- For the same mass flow rate, the compressor power increases as the HP turbine inlet pressure increases.
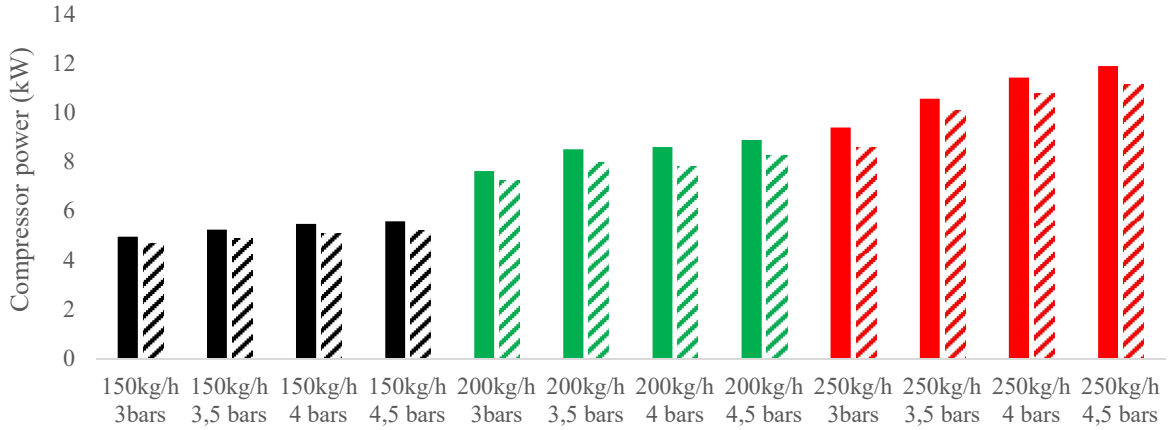
Fig.5.33: Compressor power with reheat (full filling) and without reheat (dashed filling) for TIT=500°C
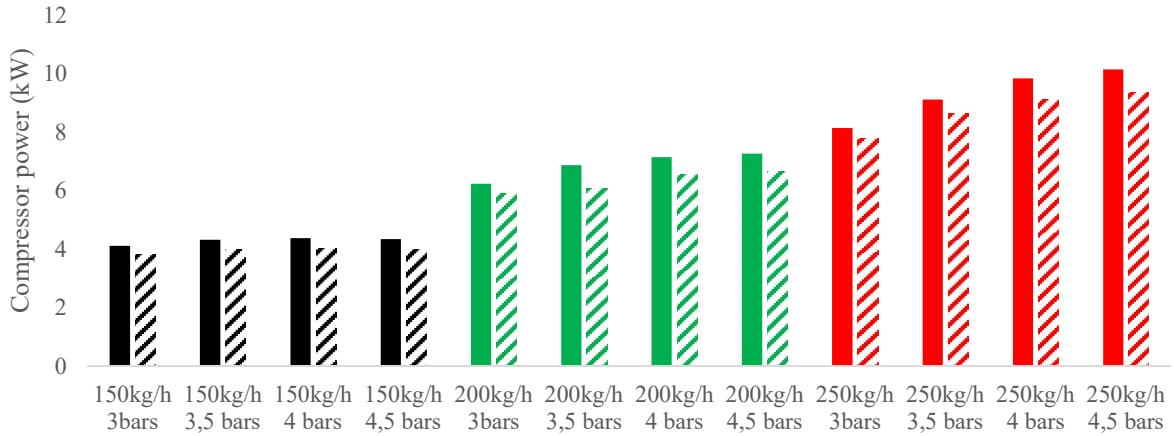
Fig.5.34: Compressor power with reheat (full filling) and without reheat (dashed filling) for TIT=400°C

The compressor efficiencies figured out from the compressor map in figures 5.27 to 5.32 are then compared to the compressor isentropic efficiency calculated knowing the compressor operating parameters according to equation 5.10 and the relative errors between testing and calculations are plotted in figure 5.35 and 5.36.

$$\eta_{Compressor} = \frac{h_{2S_C} - h_{1_C}}{h_{2_C} - h_{1_C}} \qquad (5.10)$$

With $\eta_{Compressor}$: Compressor isentropic efficiency
h_{2S_C} : Isentropic enthalpy at compressor outlet (kJ/kg)
h_{1_C} : Enthalpy at compressor inlet (kJ/kg)
h_{2_C} : Enthalpy at compressor outlet (kJ/kg)

These figures show a coherence between testing and theoretical efficiency where the relative error for both tests at 400°C and 500°C TIT remains lower than 10%, and with maximum deviation of 3.5% as shown in figures 5.36 and 5.37.
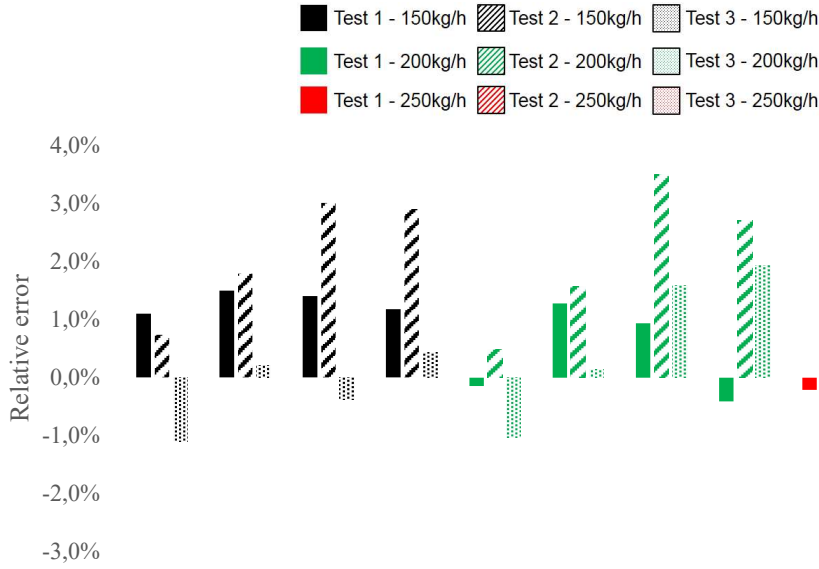
Fig. 5.35: Compressor relative error @ TIT=500°C
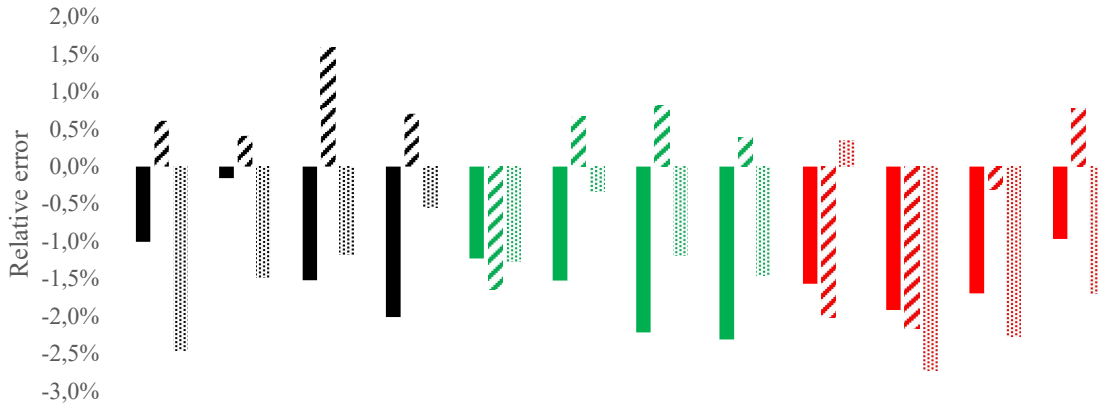
Fig. 5.36: Compressor relative error @ TIT=400°C

As for the turbine, its efficiency is calculated by comparing the compressor power to the isentropic power according to equation 5.11 since the power delivered by the turbine serves to drive the compressor and to outwit the turbocharger frictions losses.

$$\eta_{Turbine} = \frac{\dot{W}_{Compressor}}{\dot{m}_{flow_T} * (h_{1_T} - h_{2S_T})} \tag{5.11}$$

With
	$\eta_{Turbine}$	:	Turbine efficiency
	$\dot{W}_{Compressor}$	:	Compressor power (kW)
	$\dot{m}_{flow_T}$	:	Turbines mass flow rate (kg/s)
	h_{1_T}	:	Enthalpy at turbine inlet (kJ/kg)
	h_{2S_T}	:	Isentropic enthalpy at turbine outlet (kJ/kg)

Turbine efficiency for TIT = 400°C and TIT = 500°C with different mass flow rates and turbine inlet pressure are presented in figure 5.37 and 5.38 respectively. Many conclusions can be deduced from these figures:

1- For the first test step, the turbine efficiency decreases as the inlet pressure increases. In fact, the selected automotive turbocharger is not designed to be considered as a high pressure stage turbine. The turbine is designed for maximum pressure of about 3 bars and discharge to atmosphere pressure, therefore it seems unsuited as a high pressure turbine. Therefore, the operating pressure is not adapted and increasing the mass flow rate has negative impact both at TIT=500°C and at TIT=400°C TIT.

2- For both test 2 and test 3, the turbine functions at normal designed point since the discharge pressure is atmospheric and the max pressure is 2.12 bars ($\sqrt{4.5}$). Therefore, the turbine efficiency is close to the one found in automotive turbochargers. This efficiency range varies between 50% and 68%.

3- The turbine performs better at high mass flow rate. In fact, the selected turbocharger is designed for Diesel engine with high mass flow rate, therefore the efficiency at 200kg/h and 250kg/h is found to be higher than that at 150kg/h for both 400°C and 500°C TIT.
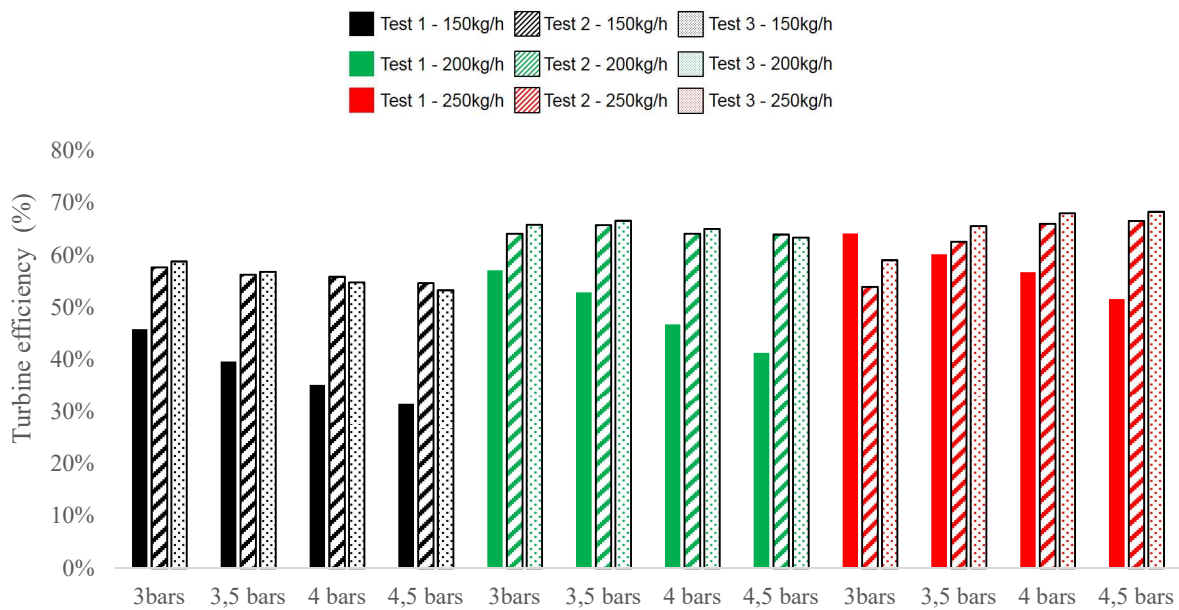
Fig. 5.37: Turbine efficiency @ 500°C TIT
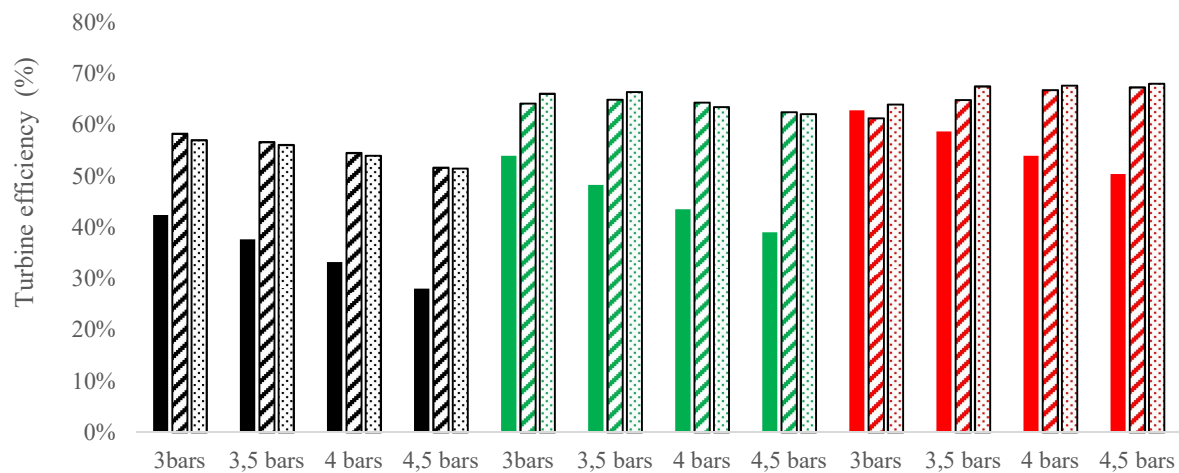
Fig. 5.38: Turbine efficiency @ 400°C TIT

As for the compressor, the relative error between testing and calculations is evaluated by comparing the turbine work between testing (compressor work) and the theoretical value according to equation 5.10. Note that the relative error was only calculated for step one and step two tests, since we cannot evaluate the theoretical turbine net specific work from step 3 tests, as its value depends on the turbine efficiency of step 1 tests.

Figures 5.39 and 5.40 show a coherence between turbine testing and theoretical efficiency calculated where the relative error for both tests at 500°C and 400°C TIT remains low (less than 5%) except for some operating points. The maximum error calculated is about 11%.
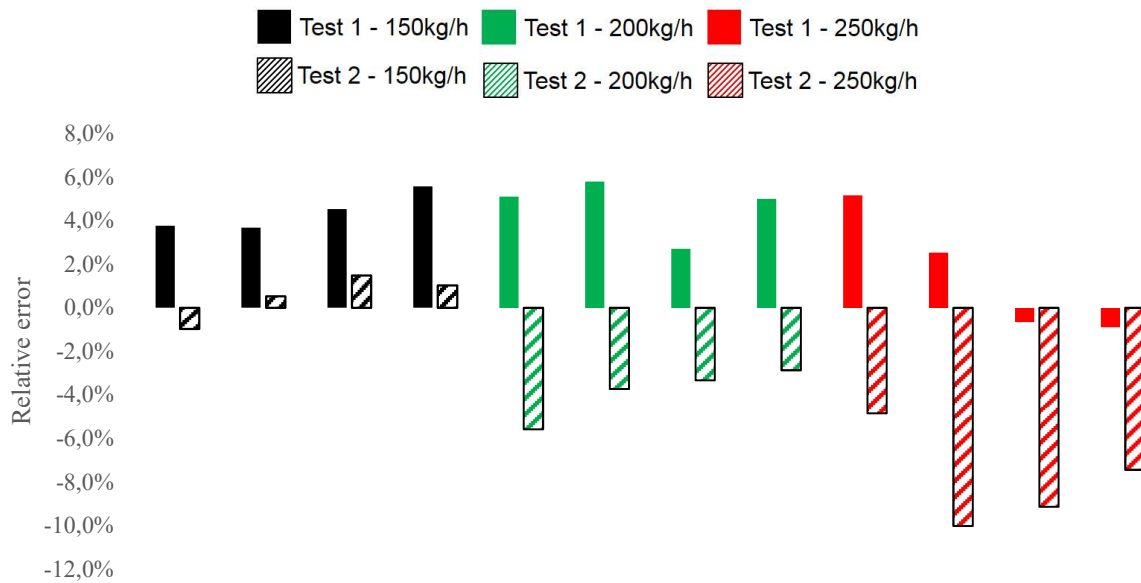
Fig. 5.39: Turbine relative error @ TIT=500°C
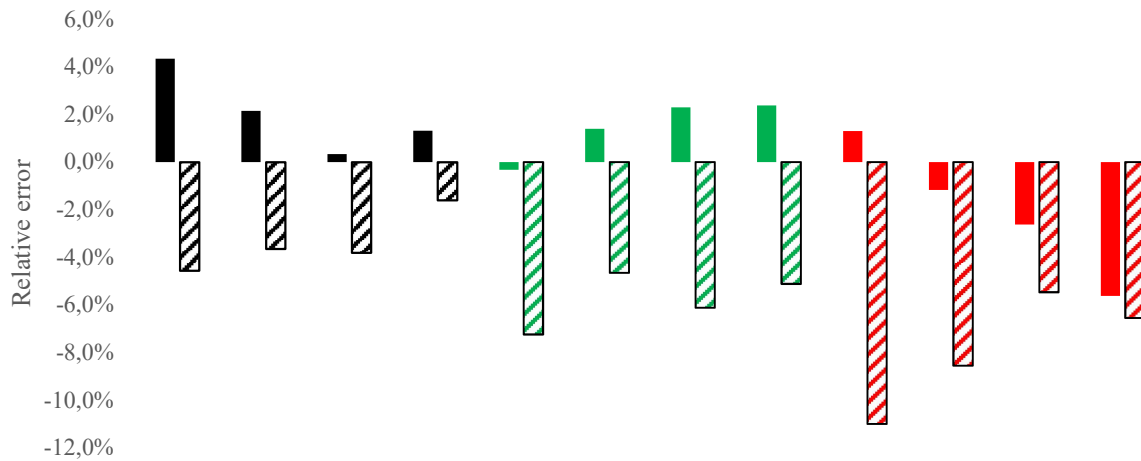
Fig. 5.40: Turbine relative error @ TIT=400°C

Finally, the thermal heat evacuated to the oil circuit for both TIT=500°C and TIT=400°C are presented in figures 5.41 and 5.42 below. The figures show that the thermal power evacuated from the oil circuit increases as the TIT and the turbine mass flow rate increase. This is explained according to different physical phenomena occurring at the same time:

1. Increasing the TIT increases the turbine housing temperature, and a higher amount of heat is evacuated to the oil circuit through the turbocharger bearings housing system.
2. Increasing the turbine mass flow rate for the same turbine expansion ratio increases the turbocharger rotation speed, and therefore more friction occurs between lubricating oil and turbocharger main shaft, leading to higher oil temperature.
3. For test step 2 and 3 where the turbine discharges to the atmospheric pressure, increasing the inlet pressure for the same mass flow rate increases the turbine speed. This increases the oil temperature for the same reasons as explained in point 2.

It is worth mentioning that the amount of thermal heat evacuated to the oil is not negligible compared to the turbine work. This explains the low turbine efficiency presented in figures 5.38 and 5.39. A well-designed turbine with low heat losses is required in order to achieve high efficiency.
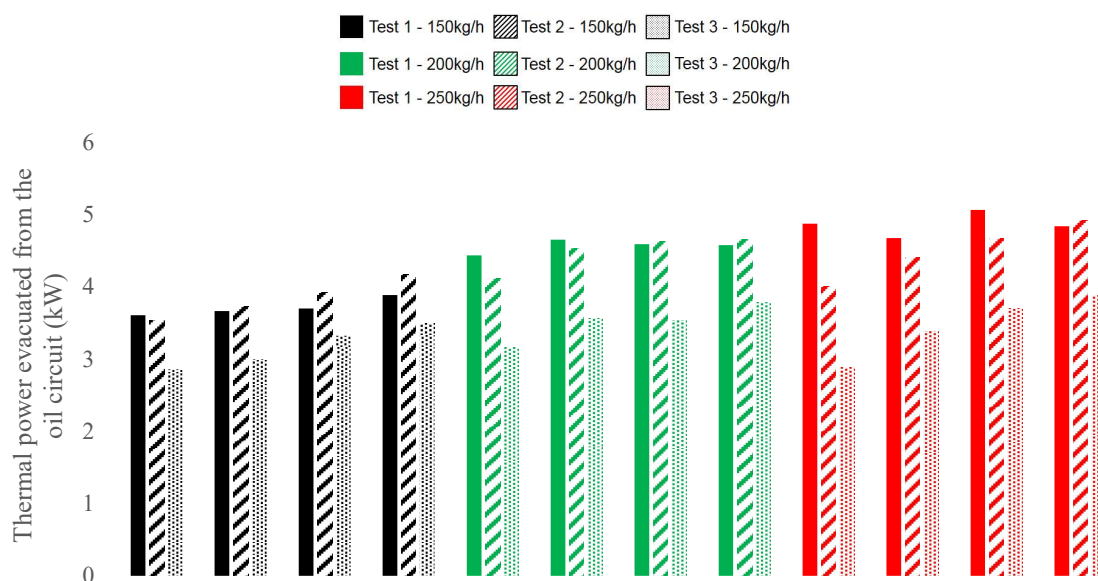
Fig. 5.41: Thermal power (kW) evacuated from the oil circuit at TIT=500°C
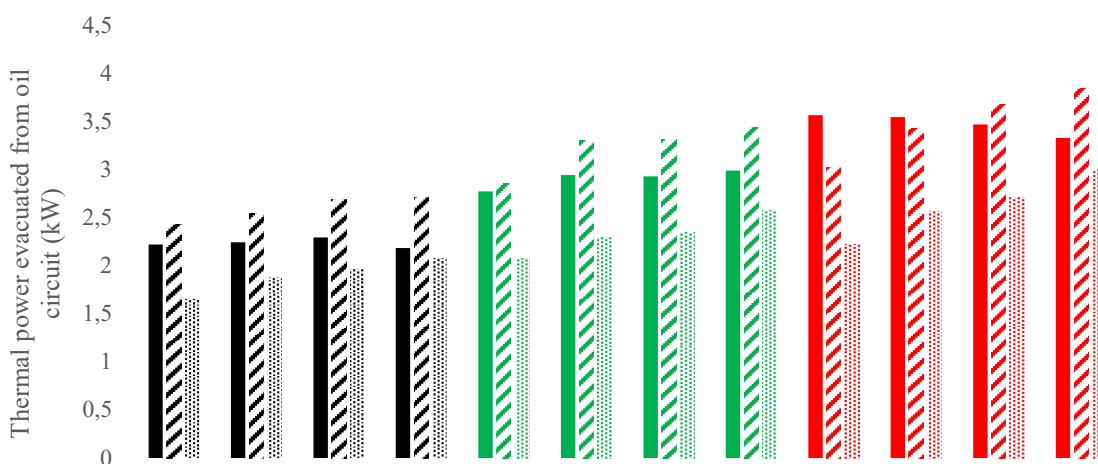
Fig. 5.42: Thermal power (kW) evacuated from the oil circuit at TIT=400°C

5.6 Conclusions

Test bench experimentations were performed in the PSA technical center of Vélizy on a commercialized turbine variable geometry turbocharger developed for Diesel engines. The goal of the test was to understand the effect of turbine's reheat on the turbines' specific power of an intercooled regenerative reheat gas turbine system.

Compared to free floating and waste gate turbocharger technologies, the variable geometry turbocharger has the advantage of controlling the turbine inlet and outlet pressure by adjusting the position of the variable geometry mechanism and by using a backpressure valve system at turbine outlet. This enables us to characterize the turbocharger at different inlet and outlet pressures.

Tests were performed on the same turbocharger at two different turbine inlet temperatures, three different mass flow rates and four different turbine inlet pressures. The testing method consists of three step tests in which the turbine inlet temperature and pressure as well as the turbine outlet pressure are adjusted in order to simulate both the reheat and the non-reheat configurations and to account for the increase in turbine specific work when reheat is performed.

From a thermodynamic point of view, the test results show a coherence between theoretical calculation and real testing conditions for both 400°C and 500°C TIT and prove that the reheat configuration allows to increase the turbine specific work. Although, the automotive turbocharger is known to have a low efficiency turbine and to operate at limited inlet pressure, experimentation results highlight the importance of increasing the turbine efficiency and the turbine inlet pressure in order to recover more work and to increase therefore the machine net specific work.

From a turbomachinery design point of view, test results show that a specific turbine aerodynamic design must be considered mainly for the first turbine which operates at high inlet pressure and discharges to an intermediate pressure higher than ambient pressure. Furthermore, turbine design must consider the thermal heat losses to the bearings system, the lubricating system and to the ambient which have a negative impact on turbine efficiency. This means, a specific bearings system and lubricating system must be envisaged when considering high efficiency turbocharger machines, as well as a performant isolating system.

Finally, note that the tests performed are not sufficient to conclude on the effect of the turbine reheat on system efficiency. In fact, as described in the equations presented in the first section, a complete gas turbine system consisting of a compression subsystem, a regenerator subsystem, a combustion chambers subsystem and a turbine reheat subsystem is required in order to assess the importance of reheat on gas turbine system efficiency.

Additional tests will be performed later to understand the impact of the intercooling compression, the regenerator effectiveness and the water injection in different system's location, on the system's efficiency and net specific power.

General Conclusion and perspectives

Due to the current global environment problems, governments around the world are implementing policies to reduce oil consumption, climate-related emissions, and local air pollution. These new regulations are pushing the road transportation sector and mainly the automotive manufacturers to find solutions for reducing CO2 and polutant emissions.

Improving the ICE efficiency and introducing new hybrid electric powertrains is a short to medium term solution, since the pontential of fuel consumption reduction is limited due to the ICE energy converter efficiency limitation. As for the long term, the battery electric vehicle (BEV) with zero-emission is subject of controversity. While these vehicles offer the advantage of zero-polutant, well-to-wheel CO2 emissions of a BEV are not advantageous compared to conventional ICE powered vehicles, mainly in markets where the electricity production relies on dirty fossil fuels. Adding to that, these vehicles require huge battery capacity and open questions on the battery and electric machines materiel resources availability, as well as other questions such as geopolitical impacts. Today, there is no clear study on the long term impact of this technological choice.

Based on these findings, Groupe PSA is conducting a prospective project named "Low Environmental and Social Impact Vehicle" in order to propose solution for post 2030. The project includes the identification of potential alternative powertrain using alternative zero-carbon fuels. These fuels are not always compatible with todays' ICE and thus, new energy converters must be studied as a substitute to ICE in future powertrains.

The objective of this thesis is to therefore investigate the potential of new energy converters in order to replace the ICE and develop a methodology of choice and optimization of new energy converters for automotive powertrain applications while considering the energy converter compatibility with non-conventional fuels and new electrified powertrains, the vehicle additional non-mechanical energetic needs including the cabin heating and cooling energetic needs and the electric auxiliary needs, as well as the vehicle integration and performance in terms of weight, size and fuel consumption among others.

A review on different energy converters for automotive powertrain applications have been conducted in the first chapter of this work. Different energy converters have been investigated including internal and external combustion machines as well as electro-chemical machines. For each energy converter, a literature review and performance assessment have been done. The literature study showed that the only existing substitute to the ICE in todays' automotive commercialized vehicles is the PEM fuel cell. This energy converter which was investigated by almost all OEM's is only commercialized today on Toyota Mirai vehicles. Other energy converters, such as gas turbines, Stirling engines and vapor cycle machines, have been largely investigated and tested in vehicle prototypes only. However, the literature did not show any potential use of the remaining energy converters, such as Ericsson, thermoacoustic and thermoelectric generators, as main energy converters in vehicle powertrains. Regarding the performances, while the ICE maximum efficiency ranges from 35% for a basic gasoline engine up to 42% for diesel or gasoline Atkinson-Miller engines, the combination of these ICE to WHR

systems allows an additional increase of 2 to 4 efficiency points. Moreover, the efficiency of split cycle engines (SCE) can reach more than 45% when using regenerator internal heat recovery system and water injection technologies. In internal combustion engines, the simple gas turbine systems always showed a maximum efficiency of 30% in powertrain applications; however, advanced gas turbine systems with intercooler, regenerative, reheat and water injection systems can reach up to 52%, when using high temperature resilient super alloys materials. These high efficiency figures were shown to be lower with external combustion gas turbine system, and their efficiency ranges between 25 and 41%. For Stirling external combustion machines, the literature review also showed a maximum efficiency of 39% with a 42% capability potential. However, the efficiency of vapor cycle machines was limited to 35% in powertrain applications. For the other external combustion machines, the Ericsson can achieve a realistic overall efficiency ranging between 25% and 35% and the thermoacoustic machines can reach 35% if deployed in automotive applications. As for the thermoelectric generators, the maximum efficiency is limited to 25% due to the low merit factor (ZT). Finally, the PEMFC system has maximum efficiency ranging between 42% and 50%. Therefore, the PEMFC, the advanced GT, the split cycles, the advanced ECGT and the Stirling machines are the only energy converters which have the potential to achieve a higher efficiency than the ICE's one. As for the weight to power and size to power ratios, the PEMFC, the split cycle and the Gas turbine systems, achieve good power densities compared to the ICE. Regarding qualitative criteria, mainly the powertrain compatibility, the ICE, SCE and Stirling machine are compatible with all powertrain architectures. On the other hand, the GT systems, the Ericsson, the VCM, the thermoacoustic, the thermoelectric generators and the PEMFC are suitable with series hybrid electric and range extender hybrid electric powertrains. Note that all considered energy converters can be used as cogeneration machines to ensure cabin heating energetic needs. The GT-system has been selected for further investigation in the study. It presents many vehicle intrinsic benefits such as multi-fuel capability, compactness, reduced weight, cogeneration capability and reduced number of moving parts compared to today ICE.

On the other hand, many GT-systems thermodynamic configurations can be considered, ranging from simple gas turbine (SGT) cycles, to regenerative gas turbine (RGT) cycles, to intercooled regenerative gas turbine (IRGT) cycles and to intercooled regenerative reheat gas turbine (IRReGT) cycles. Therefore, an exergo-technological explicit selection method considering energy and exergy analysis, as well as components and automotive technological constraints was applied in chapter 2 and different realistic GT-systems configurations were identified. The Intercooled Regenerative Reheat Gas Turbine (IRReGT) was selected as the best suitable configuration for series hybrid electric vehicle application (SHEV). It offered the best combination of high efficiency and power density compared to the investigated realistic GT-systems and to conventional internal combustion engines. A SHEV model was developed and the powertrain components were designed according to the vehicle technical specifications and performances in terms of acceleration, maximum speed and gradability. The identified IRReGT was integrated in the SHEV and was coupled to an electric generator to constitute the powertrain's auxiliary power unit (APU) which role is to recharge the battery of the vehicle once depleted. A methodology for accounting for the additional vehicle non-mechanical energetic needs on the WLTC is also developed in this work. Three modified WLTC cycles

were created for cold, temperate and hot climates. The fuel consumption simulations were performed on these three modified WLTCs while using the dynamic programming optimal control strategy. These first results show that IRReGT operating at 1250°C offers up to 22% of fuel consumption saving compared to the reference ICE.

The SHEV fuel consumption depends on many parameters among them the energy converter efficiency, the vehicle energy demands but also the powertrain energy management strategy. A low fuel consumption requires a high energy converter efficiency, a low vehicle energetic demands and a control management strategy which approaches an optimal control. Since the real weight of the GT system which impacts directly the vehicle energetic needs was not accounted for in chapter 2 and the energy management strategy was the dynamic programming, a non realistic optimal control, a pre-design of the different realistic gas turbine systems identified is performed in chapter 3 ; the fuel consumption was simulated using a bi-level optimization method to approach the APU operation in real situations by reducing the number of On/Off toggling of the APU. Based on the thermodynamic optimization of efficiency and net specific work for different GT-systems configurations and for three different operating temperatures, the power to weight ratio of each gas turbine configuration is calculated by accounting for the weight of the different components that constitute the system. Up to this end, the turbomachines' weight was estimated by establishing a mathematical relation between the mass flow rate and the power for a given rotational speed of different commercialized automotive turbochargers. As for the heat exchangers, a design was carried out for both the intercooler and the regenerator, the weight of these components for different configurations and different operating temperature was calculated. The combustion chambers' weight was calculated based on an already existing combustion chamber for gas turbine application and then by applying a correlation between the air mass flow rate across it and its thermal power. As for the electric generators, the weight was estimated using data retrieved from literature. Then each GT-system was integrated in the SHEV vehicle developed in chapter 2 and simulations were performed using a bi-level optimization method to find a compromise between two control objectives: (1) the minimization of the total fuel consumption and (2) the minimization of the On/Off toggling of the APU. The optimization uses the non-sorting genetic algorithm (NSGA) and the dynamic programming (DP) global optimal strategy. Simulation results show an increase in fuel consumption by 5% compared to fuel consumption results of chapter 2 where the number of the On/Off toggling of the APU was not constrained. Results also highlight the impact of considering the vehicle additional non-energetic needs such the electric and thermal needs as well as the impact of climates on vehicle fuel consumption. It highlights also the beneficial impact of increasing the GT-systems operating temperature and proves again that the IRReGT is the best suitable gas turbine configurations in terms of fuel consumption reduction.

In order to evaluate the impact of the startup transient phase on the vehicle fuel consumption, a dynamic model for the selected IRReGT machine was developed on Dymola software in chapter 4. The model accounts for the turbomachinery inertial transient operation as well as the heat exchangers' (HEX) transient operation. Two startup strategies were considered for the evaluation of the IRReGT efficiency, temperature, fuel consumption and convergence time

during the startup phase. The first strategy is a constant power startup strategy where an implemented PID controls the amount of fuel injected during startup phase in order to maintain the desired IRReGT-system net power to its set point value. This strategy leads to a quick increase in the regenerator temperature and therefore a rapid attaining of the maximal system efficiency. The second strategy is a constant mass fuel injected strategy where the same amount of fuel is injected during the startup phase. In this strategy, the IRReGT net power and efficiency increase as the combustion chamber outlet temperature increases with the increasing of the regenerator cold side outlet temperature. The convergence time to achieve the desired optimal efficiency and the desired net power is therefore longer. The NSGA-DP switching ON/OFF decision results from chapter 3 are used to evaluate the fuel consumption with dynamic results. Therefore, the instantaneous fuel consumption results from the NSGA-DP are replaced by the instantaneous fuel consumption resulting from the dynamic modeling. An increase in fuel consumption ranging between 2.4% and 3.8% is observed with the first scenario startup depending on the considered climate and the IRReGT maximum combustion chamber temperature and ranging between 5.7% and 6.4% in the second scenario. Results also show that the impact of transient operation is reduced on the cold climate, since the APU operates for longer time. The final startup strategy would be a compromise between fuel consumption and thermomechanical fatigue and stress on the GT components.

Finally, in chapter 5, Test bench experimentations were performed in the PSA technical center of Vélizy on a commercialized turbine variable geometry turbocharger. The test's goal was to understand the effect of turbine reheat on the turbines' specific power of an intercooled regenerative reheat gas turbine system. Up to this end, a variable geometry turbocharger was selected and the turbine inlet and outlet pressure was controlled by adjusting the position of the variable geometry mechanism using a backpressure valve system at the turbine outlet. This enables to characterize the turbocharger at different inlet and outlet pressures. The test results performed at 400°C and 500°C turbine inlet temperature show a coherence with theoretical calculations and prove that the reheat configuration allows the increase of the turbine specific work. Experimentation results also highlight the importance of increasing the turbine efficiency and the turbine inlet pressure in order to recover more work and to therefore increase the machine net specific work. Test results show that a specific turbine aerodynamic design must be considered mainly for the first turbine which operates at high inlet pressure and discharges to an intermediate pressure higher than ambient pressure. Furthermore, turbine design must consider the thermal heat losses to the bearings system, to the lubricating system and to the ambient which have a negative impact on the turbine efficiency. This means, a specific bearings system and lubricating system must be taken into account when considering high efficiency turbocharger machines, as well as a performant isolating system.

Finally, following the investigations described in this thesis, there are many arising future perspectives that should be pursued as follows:
- The dynamic model must be further developed, it must be able to include the thermal cabin heating ensured from the intercooler, it also has to be able to integrate it in an overall SHEV model.

- Additional tests are scheduled on the intercooler compression subsystem, on the regenerator as well as on a two-stage reheat turbine. These tests results must be conformed with performances of the different subsystems and improvements must be undertaken to reach higher system efficiency.

- Water injection at different locations in the system including upstream and downstream the compressors as well as in the combustion chamber and upstream the turbines must be investigated.

- Pre-design and Techno-economic analysis of an IRReGT operating at high temperatures (> 1250°C) and using ceramic materials is to be also researched.

- This work focuses more on the thermodynamic configuration and optimization, it doesn't investigate the combustion chamber aspects, additional studies must be undertaken to fully understand the functioning of gas turbine combustion chamber with reheat process.

- Finally, an interesting system is yet to be investigated, offering a very high efficiency. This system consists of a gas turbine coupled to a solid oxide fuel cell (SOFC) where the SOFC replaces the combustion chamber. Thermodynamic system configurations and feasibility must be envisaged in future studies.

References

Introduction and synthesis

[IC1] John B. Heywood, Internal Combustion Engine Fundamentals, McGraw-Hill Co, 1998

[IC2] Michael J. Denny, Potential Future Engine Cycles for Improved Thermal Efficiency, Chalmers University of Technology, 2014

[IC3] M. WITTLER, P. GLUSK, A. NASE, M. DANIEL « Future Engine Strategies – Survival of the ICE Beyond 2025? », 24th Aachen Colloquium Automobile and Engine Technology 2015.

[IC4] EUROPEAN UNION / EUROPEAN COMMISSION A Roadmap for moving to a competitive low carbon economy in 2050 European Union, European Commission, Brussels, 2011

[IC5] EUROPEAN UNION / EUROPEAN COMMISSION White Paper — Roadmap to a Single European Transport Area — Towards a competitive and resource efficient transport system European Union, European Commission, Brussels, 2011

[IC6] Ichiro HIROSE, Mitsuo HITOMI, SKYACTIV Engine Efficiency Improvement and Monotsukuri Innovation to Be Applied to Next Generation SKYACTIV, Mazda Motor Corporation, 24th Aachen Colloquium Automobile and Engine Technology 2015.

[IC7] EUROPEAN UNION / EUROPEAN COMMISSION Regulation (EU) No. 333/2014 of the European Parliament and of the Council of 11 March 2014 amending Regulation (EC) No. 443/2009 to define the modalities for reaching the 2020 target to reduce CO2 emissions from new passenger cars European Union, European Commission, Brussels, 2014

[IC8] EUROPEAN ENVIRONMENTAL AGENCY (EEA) Monitoring CO2 emissions from passenger cars and vans Copenhagen, Denmark, 2015

[IC9] M. KRÜGER, R. MAIER, D. NABER, S. SCHERER, H. SCHUMACHER, M. STROBEL, Robert Bosch GmbH Diesel Systems, Stuttgart, Germany, « Emission Optimization of Diesel Passenger Cars to Fulfill ''Real Driving Emission (RDE)

[IC10] ERNST, C.-S., OLSCHEWSKI, I., ECKSTEIN, L. CO2 reduction potential for passenger cars until 2020 Study commissioned by the Federal Ministry for Economic Affairs and Technology to the Institute of Automotive Engineering of RWTH Aachen University, Aachen, Germany 2012.

[IC11] Gouzonnat F, DA SILVA V, "New PSA PEUGEOT CITROËN 3-Cylinder Engine: Friction Losses Optimization and CO2 Impact Calculation", SIA - R-2011-08-11

[IC12] Gouzonnat F, REGENT L "Realizing Fuel Saving Potential By Taking Advantage Of New Technology For Friction Reduction", Integrated Powertrain Engineering – Fuel Economy Congress 2012

[IC13] N. CHAMPAGNE, D. LAURENT, Total M&S. Solaize, France « Improving Fuel Economy and Durability of New Engines with Innovative Lubricants », 24th Aachen Colloquium Automobile and Engine Technology 2015.

[IC14] M. SEEMANN, F. LAUTERWASSER, D J. SMOLENSKI, B. LIU, « Megatrend Fuel Economy : How to Optimize Viscosity with VI Improvers », 24th Aachen Colloquium Automobile and Engine Technology 2015.

[IC15] Tomar S., Mishra R., Bisht S., Kumar S., Balyan A., Saxena G., Optimisation of Connecting Rod Design to Achieve VC, Journal of Engineering Research and Applications, 2013

[IC16] Asthana S., Bansal S., Jaggi S., Kumar N., A comparative Study of Recent Advancements in the Field of Variable Compression Ratio Engine Technology, SAE International, 2016

[IC17] Doric J., Klinar J. I., Efficiency of a new internal combustion engine concept with variable piston motion, Thermal Science, January 2014.

[IC18] Junichi HATANO, Hiroyuki FUKUSHIMA, Yuji SASAKI, Ken NISHIMORI, Taro TABUCHI, Yoshinori ISHIHARA, « The New 1,6L 2-Stage Turbo Diesel Engine for HONDA CR-V », Honda R&D CO., Ltd., Tochigi, Japan, 24th Aachen Colloquium Automobile and Engine Technology 2015.

[IC19] M. BASSETT, B. HIBBERD, J. HALL, MAHLE Powertrain Limited, Northampton, UK, « Dynamic Downsizing for Gasoline Engines », 24th Aachen Colloquium Automobile and Engine Technology 2015.

[IC20] C. LANDERL, M. RUELICKE, B. DURST, W. MATTES, « The New BMW Inline 6-Cylinder Gasoline Engine with TwinPower Turbo, Direct Injection, and VALVETRONIC in the New BMW 7 Series », 24th Aachen Colloquium Automobile and Engine Technology 2015.

[IC21] Oropeza, A., and Orozco, F., "A Different Combustion Engine", ICES 2005-1007, ASME Conference, Chicago, USA, Apr. 2005.

[IC22] SCHEIDT, M., BRANDS, C., LANG, M., KUHL, J., GÜNTHER, M., MEDICKE, M., VOGLER; C. Statische und dynamische Zylinderabschaltung an 4- und 3-Zylindermotoren Internationaler Motorenkongress 2015 Proceedings Springer Verlag, Wiesbaden, Deutschland, 2015

[IC23] AUDI AG Audi Technology Portal: "cylinder on demand" http://www.audi-technology-portal.de/de/antrieb/fsi-tfsi-motoren/cylinder-on-demand, Accessed: 11.05.2015

[IC24] Hussaini Y. S., Lahane S., Patil G. N., Analysis of Performance and Emission Characteristics of a Homogeneous Charge Compression Ignition (HCCI) Engine, Global Colloquium in Recent Advancement and Effectual Researches in Engineering, Science and Technology (RAEREST), 2016

[IC25] A review of Homogeneous charge compression ignition (HCCI) engine, International Journal of Scientific & Engineering Research, January 2015.

[IC26] R. BUDACK, M. KUHN, R. WURMS, T. HEIDUK, « Optimization of the Combustion Process as Demonstrated on the New Audi 2.0L TFSI », 24th Aachen Colloquium Automobile and Engine Technology 2015.

[IC27] M. HOUBEN, A. SOMMERMANN, D. WWEBERSKIRCH, J. WENGERT, "Two Stage Turbo Charging as Fuel Consumption Concept for Long Haulage Applications", MAN Truck & Bus AG, Nuremberg, Germany, 24th Aachen Colloquium Automobile and Engine Technology 2015

[IC28] A. KAWAGUCHI et al. « Toyota's Innovative Termal Management Approches – Thermo Swing Wall Insulation Technology », 24th Aachen Colloquium Automobile and Engine Technology 2015

[IC29] S. JURASCHEK, R. VACHENAUER, K. LORENZ, T. MARSCHALL, A. STEPHAN, J. TACHTLER, « The Efficient Plug-In Hybrid Drive in the New BMW 2 Series Active Tourer eDrive », BWM Group, Munich, Germany, 24th Aachen Colloquium Automobile and Engine Technology 2015.

[IC30] Mike RICHARDSON, Omar MUSTUFVI, Ranbir NOTA, Ciprian ANTALOA, Alex MICHAELIDES, Mark McNALLY « Evoque_e Meeting the CO2 Chalenge Through Novel Propulsion System Technologies Incorporating Low Rare-Earth Material Electric Motors », Jaguar Land Rover, Warwickshire, UK, 24th Aachen Colloquium Automobile and Engine Technology 2015.

[IC31] H. PAFFRATH, F. SEIFERT, S. DEWENTER, B. HERRMANN, S. ROTHGANG, Pierburg GmbH, Neuss, Germany, « The Electrical Air Charger Implemented in a Multi Stage Charging System – Technical

Challenges and Application of the eAC », 24th Aachen Colloquium Automobile and Engine Technology 2015.

[IC32] A. HUBERT, P. BLOORE, "Benefits of a Switched-Reluctance E-Motor for Mild Hybrid 48V Applications", Controlled Power Technologies Ltd., Laindon, Essex, Great Britain, 24th Aachen Colloquium Automobile and Engine Technology 2015

[IC33] H. SORGER, W. SCHÖFFMANN, A. ENNEMOSER, G. FUCKAR, M. GRÖGER, Dr PETUTSCHNIG, G. TEUSCHL, J. HOOD, AVL List GmbH, Graz, Austria, « The Ideal Base Engine for 48 Volts – Chances for Efficiency Improvement and Optimization of the Overall System Complexity », 24th Aachen Colloquium Automobile and Engine Technology 2015.

[IC34] I. STEINBERG, M. DANIEL, K. WOLFF, P. GLUSK, « Conventional Powertrain including Automatic Transmission for Entry Level Vehicle Segment », 24th Aachen Colloquium Automobile and Engine Technology 2015.

[IC35] M. HÖCK, "ECO2 TWINSTER a Modular Axle Concept to Improve Efficiency and Vehicle Performance", GKN Driveline, Lohmar, Germany, 24th Aachen Colloquium Automobile and Engine Technology 2015.

[IC36] C. Mansour, W. Bou Nader, F. Breque, M. Haddad and M. Nemer, Assessing additional fuel consumption from cabin thermal comfort and auxiliary needs on the worldwide harmonized light vehicles test cycle, Transportation Research Part D, 2018

[IC37] F. MOHAMMADKHANI, S. KHALILARYA, I. MIRZAEE, "Exergy and exergoeconomic analysis and optimization of Diesel engine based combined heat and power (CHP) system using genetic algorithm", Int. J. Exergy, Vol. 12, No. 2, 2013

[IC38] [M. ÖZKAN, "A Comparative Study on energy and exergy Analyses of a CI Engine Performed with Different Multiple Injection Strategies at Part Load - Effect of Injection Pressure". Entropy 2015, 17, 244-263, ISSN 1099-4300

[IC39] T. J. WALLINGTON, E. W. KAISER, J. T. FARRELL, "Automotive fuels and internal combustion engines: a chemical perspective", Chemical Society Reviews, DOI: 10.1039/b410469m

[IC40] Wissam Bou Nader, Charbel Mansour, Clément Dumand and Maroun Nemer, "Brayton cycles as waste heat recovery systems on series hybrid electric vehicles", Energy Conversion and Management, 168 (2018) 200-2014

[IC41] Charbel Mansour, Wissam Bou Nader, Clément Dumand and Maroun Nemer, Waste heat recovery from engine coolant on mild hybrid vehicle using organic Rankine cycle, Journal of Automobile Engineering, 2018

[IC42] Wissam Bou Nader , Charbel Mansour, Maroun Nemer and Olivier Guezet, exergo-technological explicit methodology for gas-turbine system optimization of series hybrid electric vehicles, Journal of Automobile Engineering, 2017

Split cycle

[SC1] Sudeer Gowd PATIL, Martin A.J., Ananthesha, "Study on Performance Characteristics of Scuderi – Split Cycle Engine".

[SC2] John ZAJAC, Joseph MORAN, Split Cycle Engine and Method with Increased Power Density, US 20110303185 A1

[SC3] Dattu Balu GHANE, "Scuderi Split Cycle Engine : Revolutionary technology & evolutionary design review", International Journal of Innovation in Engineering, Research and Technology, IJIERT

[SC4] D. Branyon, D. Simpson. (2012). "Miller Cycle Application to the Scuderi Split Cycle Engine (by Downsizing the Compressor Cylinder)." SAE International. (Online article). DOI: 10.4271/2012-01-0419.

[SC5] Ricardo and Univ. of Brighton working on advanced combustion system for heavy-duty vehicles; CoolR features recuperated split-cycle with isothermal compression using cryogenic injection, 23 June 2011, Green Car Congress.

[SC6] Ricardo advancing with two novel heavy-duty vehicle technologies: cryogenic split-cycle engine and microwave fuel reforming, 4 September 2013.

[SC7] The Scuderi Engine – Strength in Pairs, http://www.autoevolution.com/news/the-scuderi-engine-strength-in-pairs-15457.html

[SC8] Split Cycle Engine – History, http://www.liquisearch.com/split_cycle_engine/history

[SC9] Collier, G., "Hydrocarbon Motor," U.S. Patent 1,130,148, March 2, 1915.

[SC10] DeFrancisco, R., "Internal Combustion Engine of Positive Displacement Expansion Chambers with Multiple Separate Combustion Chambers of Variable Volume, Separate Compressor of Variable Capacity and Pneumatic Accumulator", U.S. Patent 4,696,158, September 29, 1987.

[SC11] Thring, R., "Regenerative Internal Combustion Engine", U.S. Patent 5,499,605, March 19, 1996.

[SC12] Ruiz, F., "Thermodynamic Modeling of the Two-Cylinder Regenerative Internal Combustion Engine," SAE Technical Paper 910346, 1991, doi: 10.4271/910346.

[SC13] Scuderi Group LLC, Exhaust valve timing for split cycle engine, WO 2012/050910 A1 at www.ScuderiGroup.Com, 19 April 2012

[SC14] Scuderi Group LLC (2009), Split Cycle Four Stroke Engine, EP Patent No. 1639247B9, available at www.Freepatentsonline.com , 14th January 2009.

[SC15] Ford PHILLIPS, Ian GILBERT, Jean-Pierre PIRAULT and Marc MEGEL, "Scuderi Split Cycle Research Engine : Overview, Architecture and Operation", Southwest Research Institute, SAE International, 20111-01-0403

[SC16] Scuderi Group LLC, "Split Cycle Engine With helical Crossover Passage", WO 2009/020491 A1 at www.ScuderiGroup.com , 12th Feb 2009.

[SC17] Ashwini S. GAIKWAD, Rajendra M. SHINDE, "Review on Scuderi Split Cycle Engine", International Journal of Emerging Technologies in Computational and Applied Sciences (IJETCAS)

[SC18] Scuderi Group LLC, "Part Load Control in Split Cycle Engine", WO 2010/120499 A1, at www.ScuderiGroup.com, 21st October 2010.

[SC19] Riccardo MELDOLESI, George BAILEY, Clive LACY, Ian GILBERT, Jean-Pierre PIRAULT and Anthiny PERKINS, "Scuderi Split Cycle Fast Acting Valvetrain : Architecture and Development", Southwest Research Institute, SAE International 2011-01-0404

[SC20] Nhut LAM, Martin TUNER, Per TUNESTAL, Arne ANDERSSON, Staffan LUNDGREN, Bengt JOHANSSON, "Double Compression Expansion Engine Concepts : A Path to High Efficiency", SAE International, doi : 10.4271/2015-01-1260

[SC21] Scuderi Group LLC (2011), Split cycle Air-hybrid engine with air tank valve, EP Patent No. WO2011/115873 A1, at www.Scuderi Group.com, 22 September 2011.

[SC22] Riccardo MELDOLESI, "Scuderi Split Cycle Engine Development Overview", Southwest Research Institute, 17 February 2012

[SC23] Ford PHILLIPS, Riccardo MELDOLESI and Ian GILBERT, "The Scuderi Split Cycle Engine – Technical Update", July 5th 2011.

[SC24] Scuderi Group LLC, "Air supply for components of a split –cycle engine", WO 2010/129872A1, at www.ScuderiGroup.com, 11 November 2010.

[SC25] Scuderi Group LLC, "Variable volume crossover passage for a split-cycle engine", WO2010/120856A1, at www.ScuderiGroup.com, 21 October 2010.

[SC26] SwRI simulations indicate Scuderi split-cycle engine consumes 25% less fuel than comparable conventional engine in Cavalier; 36% reduction with hybrid configuration, Green Car Congress, 2011

[SC27] R. Hanson. "First Scuderi split-cycle engine prototype completed." Motor Authority. 2009

[SC28] Guangyu DONG, Robert MORGAN, Morgan HEIKAL, "A Novel split cycle internal combustion engine with integral waste heat recovery", Elsevier, Applied Energy, 2015

[SC29] Iain CAMERON, Asndrzej SOBIESLAK, "Combustion characteristics of a spark-ignited split cycle engine fuelled with methane", Combustion Engines. 2015, 161(2), 33-41, ISSN 2300-9896

[SC30] New split-cycle concept to control diesel HCCI combustion, Green Car Congress, 25 October 2010

[SC31] Keshav SUD, Transient Modeling and Control of Split Cycle Clean Combustion Diesel Engine, Thesis, University of Illinois at Chicago, 2013

[SC32] "Tour Engine moves its opposed-cylinder split cycle engine to beta prototype; coupling a compression ratio of 8:1 with expansion ratio of 16:1 for increased efficiency", Green Car Congress, 12 October 2011

[SC33] Benjamin TOUR, "Double Piston Cycle Engine", Patent WO2006/099106A2

[SC34] Benjamin TOUR, "Steam enhanced double piston cycle Engine", Patent WO2006/113635A2

[SC35] Tour Engine has Prototype II split-cycle engine running, Green Car Congress, 21 April 2012

[SC36] Motiv Engines introduces 2nd-generation split cycle concept; MkII Clarke-Brayton heavy-duty engine being designed for LNG, Green Car Congress, 8 May 2014

[SC37] Neville Stuart JACKSON, Andrew Farquhar ATKINS, "Split cycle Reciprocating Piston Engine", Patent US 2012/0103314 A1, May 2012

[SC38] Claus LINNEMANN and Mike W. CONEY "The isoengine : realisation of a high efficiency power cycle based on isothermal compression", International Journal of Energy Technology and Policy, Vol. 3, 2005.

[SC39] N. JACKSON, A. ATKINS and R. MORGAN, "An Alternative Thermodynamic Cycle for Reciprocating Piston Engines", In: 36th International Vienna Motor Symposium 2015, Viennna, 7-8 May 2015.

[SC40] Ricardo investigating potential for its split-cycle engine in large engine market, Green Car Congress, 23 June 2016

[SC41] Adam Gurr (2016) "The 60% Efficiency Reciprocating Engine: A Modular Alternative to Large Scale Combined Cycle Power" CIMAC 2016 paper Nº 267

Gas Turbine

[GT1] History of Chrysler Corporation Gas Turbine Vehicles, Chrysler Corporation, January 1979

[GT2] Jan P. NORBYE - Volkswagen develops a gas-turbine car - https://books.google.fr/books?id=j989VTOlPwMC&pg=PA77&lpg=PA77&dq=volkswagen+gas+turbine+vehicle&source

[GT3] Jay Leno Builds a Turbine-Powered Biodiesel Supercar. Jay Leno's Garage, Feb. 2010. url: http://www.jaylenosgarage.com/extras/articles/jay-leno-builds-a-turbine-powered-biodiesel-supercar/.

[GT4] Christophe COTTARD, Peugeot 406 Hybrid, PSA PEUGEOT CITROËN

[GT5] John Excell, "This Week in 1965 – The Rover-BRM gas turbine car", 2013

[GT6] Wissam BOU NADER, Charbel MANSOUR, Maroun NEMER, Optimization of a Brayton external combustion gas-turbine system for extended range electric vehicles, Energy, 2018.

[GT7] Meherwan P. BOYCE, "Gas Turbine Engineering Handbook", Second Edition, Butterworth-Heinemann, 2002

[GT8] H. COHEN, GFC. ROGERS, HIH. SARAVANAMUTTOO, "Gas Turbine Theory", 4th Edition, Longman Group Limited, 1996

[GT9] Joseph LAWTON, "Gas Turbine Engine R&D for Shipboard Applications", NSWCCD 824

[GT10] Bogdan POJAWA, Malgorzata HOLDOWSKA, "Determination of Operating Characteristics of Naval Gas Turbines LM2500", 2011

[GT11] R. ANDRIANI, F. GAMMA, U. GHEZZI, "Main Effects of Intercooling and Regeneration On Aeronautical Gas Turbine Engines", 46th AIAA/ASME/SAE/ASEE Joint Propulsion Conference & Exhibit 25 - 28 July 2010, Nashville, TN.

[GT12] H. CUNHA, "Investigation of the Potential of Gas Turbines for Vehicular Applications", Chalmers, Department of Applied Mechanics, Division of Fluid Dynamics, CHALMERS UNIVERSITY OF TECHNOLOGY Gothenburg, Sweden 2011, Master's thesis 2011:43

[GT13] Moran M and Shapiro H. Fundamentals of engineering thermodynamics. 5th Edition – 2006, p.388-390.

[GT14] R. T. Sawyer, "The Modern Gas Turbine", Prentice-Hall, New York, 19454

[GT15] L. E. Baklen, K. Jordal, E. Syverud, and T. Veer, "Centenary of the first gas turbine to net power output: A tribute to AEgidius Elling", ASME Paper No. GT2004-53211, 2004

[GT16] H. Lukas, "Survey of alternative gas turbine engine and cycle design", EPRI Report, AP-4450, Research Project 2620-2, February 1986

[GT17] Darian Unger and Howard Herzog, "Comparative Study on Energy R&D Performance: Gas Turbine Case Study", Massachusetts Institute of Technology, 1998

[GT18] E. Jeffs, "Franz Stolze: Gas turbine engineer ahead of his time", Gas Turbine World, 1986

[GT19] D. Eckardt a,d P. Rufli, "Advanced gas turbine technology – ABB/BCC historical firsts", ASME Paper No. 2001-GT-0395, 2001

[GT20] Hans Holzwarth, "The Gas Turbine: Theory, Construction, and Records of the Results Obtained from Two Actual Machines", 1912

[GT21] The world's first industrial gas turbine set at Neuchatel (1939)-An international historic mechanical engineering landmark, ASME publication, September 2, 1988.

[GT22] R. K. Bhargava, M. Bianchi, A. De Pascale, G. Negri di Montenegro and A. Peretto, "Gas turbine Based Power Cycles – A State-of-the-Art Review", International Conference on Power Engineering, Hangzhou, China, 2007.

[GT23] D. G. Evans and T. J. Miller, "An Overview of Aerospace Gas turbine Technology of Relevance to the Development of the Automotive Gas Turbine Engine", National Aeronautics and Space Administration, Lewis Research Center, SAE, 1978.

[GT24] A. J. Scalzo, R. L. Bannister, M. DeCorso, and G. S. Howard, "Evolution of heavy-duty power generation and industrial combustion turbines in the United States," ASME Paper No. 94-GT-488, 1994

[GT25] G. A. Cincotta, "The testing of GE's MS7001F gas turbine," Diesel & Gas Turbine Worldwide, January-February 1991

[GT26] R. L. Bannister, N. S. Cheruvu, D. A. Little, and G. McQuiggan, "Development requirements for an advanced gas turbine system," ASME Paper No. 94-GT-388, 1994

[GT27] S. A. Ali and H. A. Webb, "Advanced turbine systems program requirements and an approach to implementation," ASME Paper No. 94-GT-411, 1994

[GT28] J. C. Corman, "Gas turbine power generation evolutionary advances for the future," ASME Paper No.95-GT-271, 1995

[GT29] A. W. Layne, "Developing the next generation gas turbine systems – A national partnership," ASME Paper No. 2000-GT-176, June 2000

[GT30] I. S. Diakunchak, G. R. Gaul, G. McQuiggan, and L. R. Southall, "Siemens Westinghouse advanced turbine systems program final summary," ASME Paper No. GT-2002-30654, 2002

[GT31] G. A. Kool, Current and future materials in advanced gas turbine engines, Journal of Thermal Spray Technology, March 1996

[GT32] M. YURI, J. MASADA, K. TSUKAGOSHI, E. ITO, S. HADA, Development of 1600°C C-Class High efficiency Gas Turbine for Power Generation Applying J-Type Technology, Mitsubishi Heavy Industries Technical Review Vol. 50 No. 3 (September 2013)

[GT33] Key Technologies for 1700°C Class Ultra High Temperature Gas Turbine, Mitsubishi Heavy Industries Technical Review, September 2017

[GT34] F. WHITTLE, "The early history of Whittle jet propulsion gas turbines", Proceedings of the Institution of Mechanical Engineers, 152, 1945, 419-35.

[GT35] L J. CHESHIRE, "The design and development of centrifugal compressors for aircraft gas turbines", Proceedings of the Institution of Mechanical Engineers, 153, 1945, 426-40.

[GT36] P. Walsh and P. Fletcher. Gas Turbine Performance. Blackwell Publishing, 2004. isbn: 0-632-06434-X.

[GT37] R. GORLA, A. KHAN, "Turbomachinery Design and Theory", Marcel Dekker, Inc. New York. Basel

[GT38] Y. RIBAUD, C. MISCHEL, "Study and Experiments of a Small Radial Turbine for Auxiliary Power Units", The American Society of Mechanical Engineers, 1986, 86-GT-23.

[GT39] D. G. AINLEY, G. C. R. MATHIESON, "A Method of Performance Estimation for Axial-Flow Turbines", Ministry of Supply, Aeronautical Research Council Reports and Memoranda, 1957

[GT40] Q. H. NAGPURWALA "Design of Gas Turbine Combustors", M.S. Ramaiah School of Advanced Studies, Bengaluru

[GT41] R.C. HENDRICKS, D.T. SHOUSE, W.M. ROQUEMORE, "Water Injected Turbomachinery", NASA/TM – 2005-212632, ISROMAC10-2004-039

[GT42] R. PAVRI, G. D. MOORE, « Gas Turbine Emissions and Control », GE Energy Services, Atlanta, GA

[GT43] "Alternative Control Techniques Document - NOx Emissions from Stationary Gas Turbines", U.S Environmental Protection Agency, Emission Standards Division

[GT44] K. SUNDSBO ALNE, "Reduction of Nox Emissions from the Gas Turbines for Skarv Idun", Master of Science in Energy and Environment, NTNY Innovation and Creativity, June 2007

[GT45] M. SCHORR, J. CHALFIN, "Gas Turbine Nox Emissions Approaching Zero – Is it worth the price?", General Electric Power Systems, Schenectady, New York

[GT46] J. W BURNS, D. J. COOPER, "Active NOX Control of Cogen Gas Turbine Exhaust using a Nonlinear Feed Forward with Cascade Architecture", University of Connecticut, Storrs, CT 06269

[GT47] "Power Generation Handbook", Chapter 12: Gas Turbine Combustors.

[GT48] P. SRAVAN KUMAR, P. PUNA RAO, "Design and Analysis of Gas Turbine Combustion Chamber", International Journal Of Computational Engineering Research (ijceronline.com) Vol. 03 Issue. 12

[GT49] R.K. Shah, "Compact Heat Exchangers for Microturbines", Compact Heat Exchangers for Microturbines, Compact Heat Exchangers for Microturbines

[GT50] M. A. El-Masri, "Thermodynamics and performance projections for intercooled / reheat / recuperated gas turbine systems," ASME Paper No. 87-GT-108

[GT51] S. SULLIVAN, X. ZHANG, A. A. AYON, J. BRISSON, « Demonstration of a microscale heat exchanger for a silicon micro gas turbine engine », The 11th International Conference on Solid-State Sensors and Actuators, (2001)

[GT52] S. SULLIVAN, "Development and Testing of Microscale Silicon Heat Exchangers for the MIT Micro Gas-Turbine Engine", B.S. Mechanical Engineering (1998), Renseelaer Polytechnic Institute.

[GT53] Helms, H. E., et. al., "Ceramic Applications in Turbine Engines", DOE/NASA/0017-6, Allison Gas Turbines, Indianapolis, IN 46206, October 1984.

[GT54] K.A.B. PATHIRANTHNA, "Gas Turbine Thermodynamic and Performance Analysis Methods using available catalog data", University of Gävle, Faculty of engineering and sustainable development, 2013.

[GT55] T. NADA, "Performance Characterization of different configurations of gas turbine engines", Propulsion and Power Research, September 2014

[GT56] R.M.R.A. SHAH, A. Mc GORDON, M. AMOR-SEGAN, P. JENNINGS. "Micro Gas Turbine Range Extender – Validation Techniques for Automotive Applications", University of Warwick, United Kingdom.

[GT57] J.H. HORLOCK, "Advanced Gas Turbine Cycles", ISBN 0-08-044273-0, Pergamon, 2003

[GT58] T. AI, J. MASADA, E. ITO, "Development of High Efficiency and Flexible Gas turbine M701F5 by Applying J Class Gas Turbine Technologies", Mitsubishi Heavy Industries Technical Review Vol. 51 No. 1 (March 2014)

[GT59] S. HADA, K. TAKATA, Y. IWASAKI, M. YURI, J. MASADA, "High-efficiency Gas Turbine Development applying 1600°C class "J" Technology", Mitsubishi Heavy Industries Technical Review Vol. 52 No. 2 (June 2015)

[GT60] Davidson, B.J. and Keeley, K.R. (1991). "The thermodynamics of practical combined cycles, Proc. Instn. Mech. Engrs". Conference on Combined Cycle Gas Turbines, 28-50.

[GT61] Briesch, M.S., Bannister, R.L., Dinkunchak, 1.S. and Huber, D.J. (1995), "A combined cycle designed to achieve greater than 60% efficiency", ASME J. Engng Gas Turbines Power 117(1), 734-741.

[GT62] Wunsch, A. (1978), Combined gas/steam turbine power stations- the present state of progress and future developments, Brown Boveri Review 65(10), 646-655

[GT63] H. Termuehlen, "Forty years of combined cycle power plants," Energy-Tech, ASME Publication, October 2002

[GT64] D. L. Chase, "Combined Cycle development evolution and future," GE Power Systems, GER-4206, April 2001

[GT65] H. Lukas, "Cycles Revisited," IGTI News Letter, August 1994

[GT66] R. K. Bhargava, "Gas turbine inlet air cooling technologies," Invited Lecture at National Institute of Technology, Jamshedpur, India, January 2007

[GT67] M. J. Reale, "New High Efficiency Simple Cycle Gas Turbine-GE's LMS100™", GE Power Systems GER - 4222A, 2004

[GT68] C. Jones and J. A. Jacobs III, "Economical and technical considerations for combined-cycle performance - enhancement options," GE Power Systems, GER 4200, October 2000

[GT69] M. A. El-Masri, "A modified high efficiency recuperated gas turbine cycle," J. of Eng. for Gas Turbines and Power, Vol. 110, pp 233-242, 1988

[GT70] M. S. PATIL, D. B. PAWASE, E. R. DEORE, "Thermal Performance of Reheat Regenerative Intercooled Gas turbine Cycle", IJRMET Vol. 5, May – October 2015

[GT71] S. B. Shepard, T. L. Bowen, and J. M. Chiprich, "Design and development of the WR-21 intercooled recuperated (ICR) marine gas turbine," ASME Paper No. 94-GT-79, 1994

[GT72] I. G. Rice, "Thermodynamic evaluation of gas turbine cogeneration cycles: part II. Complex cycle analysis", J.of Eng. for Gas Turbines and Power, Vol. 109, 1987

[GT73] W. A. SIRIGNANO, F. LIU, "Performance Increase for Gas-Turbine Engines Through Combustion Inside the Turbine", Journal of Propulsion and Power, Vol.15, No. 1, January – February 1999

[GT74] E. D. Larson and R. H. Williams, "Steam injected gas turbines", J. of Eng. for Gas Turbines and Power, 1997, Vol. 109, pp. 55-63

[GT75] D. Y. Cheng, and A. L. C. Nelson, "The chronological development of the Cheng cycle steam injected gas turbine during the past 25 years," ASME Paper No. GT-2002-30119, 2002

[GT76] J. Tuzson, "Status of steam-injected gas turbines," J. of Eng. for Gas Turbines and Power, Vol. 114, pp 682-686, 1992

[GT77] H. Abdallah, and S. Harvey, "Thermodynamic analysis of chemically recuperated gas turbines," Int. J. Therm. Sci. Vol. 40, pp372-384, Elsevier, 2001

[GT78] P. A. Dellenback, "Improved gas turbine efficiency through alternative regenerator configuration," J. of Eng. for Gas Turbines and Power, Vol. 124, pp 441-446, 2002

[GT79] K. F. Kesser, J. F. Hoffman, and J. W. Baughn, "Analysis of a basic chemically recuperated gas turbine power plant," J. of Eng. for Gas Turbines and Power, Vol. 116, pp 277-284, 1994

[GT80] K. K. Botros, M. J. de Boer, and H. G. Fletcher, "Thermodynamics, environmental economic assessment of CRGT for exhaust heat recovery in remote compressor station applications," ASME Paper No 97-GT-510, 1997

[GT81] R. D. Brdar and R. M. J ones, "GE IGCC technology and experience with advanced gas turbines," GE Power Systems, GER-4207, Oct. 2000

[GT82] J. H. Horlock, "The evaporative gas turbine (ECT) cycle," ASME Paper No. 97-GT-408, 1997

[GT83] A. Lazzaretto, and F. Segato, Thermodynamic optimization of the HAT cycle plant structure-Part I: Optimization of the Basic plant configuration, J. of Eng. for Gas Turbines and Power, Vol. 123, 2001

[GT84] M. Nakhamkin, and J. R. Schiebel, CHAT technology: an alternative approach to achieve advanced turbine systems efficiencies with present combustion turbine technology, ASME Paper No. 98-GT-143, 1998

[GT85] S. E. Veyo, S. D. Vora, K. P. Litzinger, and W. L. Lundberg., "Status of pressurized SOFC/Gas turbine development at Siemens Westinghouse," ASME Paper No. GT-2002-30670, 2002

[GT86] A. D. Rao, G. S. Samuelsen, F. L. Robson, and R. A. Geisbrecht, "Power plant system configurations for the 21st century," ASME Paper 2002-GT-30671, 2002

[GT87] A. J. JUHASZ, "Automotive Gas Turbine Power System - Performance Analysis Code", the 1997 International Congress and Exposition, Lewis Research Center, NASA Technical Memorandum 107386

[GT88] Italy's Gas turbine Car, June 1995, http://blog.modernmechanix.com/italys-gas-turbine-car/#mmGal

[GT89] A. GEORGE, "The Turbine-Powered Lotus That Was So Good It Got Banned", 2014. http://www.wired.com/2014/10/lotus-turbine-racecar/

[GT90] B. Senefsky. Chevrolet Turbo-Titan III Concept Vehicle - Space Truckin'. Sport Truck, 2003. url:http://www.sporttruck.com/featuredvehicles/chevy/0309st_chevrolet_turbo_titan_3_concept_vehicle/index.html.

[GT91] J. Norbye. Turbine Drives Chevy Truck. Popular Science, Oct. 1965.

[GT92] J. G. Ingersoll. "Natural Gas Vehicles". The Fairmont Press, 1995. isbn: 0-88173-218-4.

[GT93] "EV1 Electric: Series Hybrid". National Automobile Bankers Associates / Vehicle Information Services, 2001.

[GT94] Capstone CMT-380 electric hybrid supercar with microturbines - http://www.gizmag.com/capstone-cmt-380-an-electric-hybrid-featuring-wind-turbines/13517/

[GT95] ETV Motors - Electric Technology for Vehicles, 2011. url: http://etvmotors.com/

[GT96] Simon BICKERSTAFFE, "Taking the Long VieW"; Development Electric Vehicles, Geneva Motor Show

[GT97] Capata R, Coccia A and Lora M. A Poposal for CO2 abatement in urban areas: the UDR1 - Lethe Turbo-Hybrid Vehicle. University of Roma 1 "La Sapienza", Italy, *Energies* ISSN 1996-1073.

[GT98] J-L. MOREAU "Ca turbine en coulisses" Auto Moto Avril 2016

[GT99] ECT and FL6 Hybrid. Volvo Trucks. url: http://www.volvotrucks.com/trucks/global/en-gb/company/history/1990s/Pages/ECT_and_FL6_Hybrid.aspx.

[GT100] "Wrightspeed unveils new turbine range extender for medium- and heavy-duty electric powertrains; 30% more efficient than current microturbine generators", Green Car Congress, 4 May 2015

[GT101] "Walmart showcases WAVE tractor-trailer at MATS; micro-turbine range extended electric vehicle with 45.5 kWh Li-ion pack", Green Congress Car, 28 March 2014

Stirling

[ST1] Benjamin Cheverton, "On the use of heated air as a motive power". Journal of the Franklin Institute, 55(6) :365_368, June 1853.

[ST2] Hargreaves C.M. The Philips Stirling Engine. Elsevier Science Pub. Co., 1991

[ST3] Graham Thomas READER, Charles HOOPER, "Stirling Engines", 1983

[ST4] William R. Martini, "Stirling Engine Design Manual", 2nd Edition, NASA-CR-158-088, January, 1983

[ST5] Parlak N., Wagner A., Elsner M., Soyhan, H.S. Thermodynamic analysis of a gamma type Stirling Engine in non-ideal adiabatic conditions. Int. J. Renew. Energy 2009, 34, 266–273.

[ST6] Godett, T., Meijer, R., Verhey, R., Pearson, C. et al., "STM4-120 Stirling Engine Test Development," SAE Technical Paper 890149, 1989, doi:10.4271/890149

[ST7] D.G. Thombare, S.K. Verma, "Technological development in the Stirling cycle engines", Renewable and Sustainable Energy Reviews, 12 (2008)

[ST8] http://www.stirlinginternational.org/docs/presentations/history.asp

[ST9] William John Viacqiiorn Rankine. On the means of realizing the advantages of the air engine: By , civil engineer, f. r. SS. long. and edin., &c. Journal of the Franklin Institute, 30(5) :330_339, November 1840.

[ST10] Andy ROSS, "Stirling Cycle Engines", 1977

[ST11] Alexander R. P. Walker. Stirling Alternative: Power Systems, Refrigerants and Heat Pumps. CRC Press, 1 edition, August 1994.

[ST12] Kirkley, D., "A Thermodynamic Analysis of the Stirling Cycle and a Comparison with Experiment," SAE Technical Paper 650078, 1965, https://doi.org/10.4271/650078.

[ST13] West, C. D., "Theoretical basis for the Beale number". Proceedings of the 16th Intersociety Energy Conversion Engineering Conference. Atlanta: American Society of Mechanical Engineers; 1981 [Paper 819787]

[ST14] Droher, JJ., SE. Squier. Performance of the Vanguard Solar Dish-Stirling Engine Module. EPRI AP- 4608. Palo Alto, CA: Electrical Power Research Insti- tute. 1986.

[ST15] Washam, BJ., T. Hagen, D. Wells, W. Wilcox. Vanguard I Solar Parabolic Dish-Stirling Engine Module, Final Report, May 28, 1982 - September 30, 1984. Advanco Report DOE-AL-16333-2. Advanco Corp., El Segundo, CA. 1984.

[ST16] PAUL R. FRASER, "Stirling Dish System Performance Prediction Model", University of Wisconsin-Madison, 2008.

[ST17] Shaltens, R., Schreiber, J., and Wong, W., "Update on the Advanced Stirling Conversion System Project for 25 kW Dish Stirling Applications," SAE Technical Paper 929184, 1992, https://doi.org/10.4271/929184.

[ST18] F. Nepveu, Alain Ferriere, Françoise Daumas-Bataille, Isabelle Verdier, Philippe Lefevre, « Modélisation énergétique du système Parabole / Stirling EURODISH de production d'électricité », Congrès Français de Thermique, SFT 2007.

[ST19] Bratt, C., Holgersson, S., Nelving, H., and Percival, W., "The Stirling Engine - A Ready Candidate for Solar Thermal Power," SAE Technical Paper 810456, 1981, https://doi.org/10.4271/810456.

[ST20] R. Mangion, M. Muscat, T. Sant, J. Rizzo, R. Ghirlando, J. Cilia, J. Mizzi, S. Vural, « Challenges in developing a solar powered Stirling engine for domestic electricity generation », 9 th International Conference on Heat Transfer, Fluid Mechanics and Thermodynamics, Malta, July 2012

[ST21] D. Thimsen, "Stirling Engine Assessment", EPRI, Final Report, October 2002

[ST22] H. Nilsson, "Submarine Power Systems Using the V4-275R Stirling Engine", United Stirling AB, Malmo, Sweden

[ST23] N. Schnebelen, F. Nepveu, A. Ferriere, "Le système parabole-Stirling Eurodish appliqué à la cogeneration électricité / eau chaude sanitaire", PROMES, Journée Microcogénération – Paris CNAM – Janvier 2008.

[ST24] Hugo Ljunggren Falk, Sandra Berg, "Implementation of a Stirling engine generation system for residential use in rural areas of Beni department of Bolivia", KTH School of Industrial Engineering and Management, Stockholm, 2014

[ST25] Mario L. Ferrari, Matteo Pascenti, Alberto Traverso, Massimo Rivarolo, "Smart polygeneration grid: a new experimental facility", Proceedings of ASME Turbo Expo, Copenhagen, Denmark 2012.

[ST26] Thiers, S., Aoun, B., Peuportier, B., ''Experimental characterization, modeling and simulation of a wood pellet micro-combined heat and power unit used as a heat source for a residential building', Energy and Buildings 42 (2010) 896–903

[ST27] Franco Cotana, Antonio Messineo, Alessandro Petrozzi, Valentina Coccia, Gianluca Cavalaglioand Adrea Aquino, "Comparison of ORC Turbine and Stirling Engine to Produce Electricity from Gasified Poultry Waste", sustainability, 2014, ISSN 2071-1050

[ST28] Carlsen, H., Ammundsen, N., Trerup, J., "40 kW STIRLING ENGINE FOR SOLID FUEL", Energy Conversion Engineering Conference, Proceedings of the 31st Intersociety, DOI: 10.1109/IECEC 1996.553904

[ST29] [STR-08] G. J. HANE, R. A. HUTCHINSON, "Stirling Engine Research at National and University Laboratories in Japan", September 1987

[ST30] Saxena, S. and Ahmed, M., "Automobile Exhaust Gas Heat Energy Recovery Using Stirling Engine: Thermodynamic Model," SAE Technical Paper 2017-26-0029, 2017, https://doi.org/10.4271/2017-26-0029.

[ST31] Sigma 3kWe Stirling engine, http://www.microchap.info/sigma_3kwe_stirling_engine.htm

[ST32] D.G. Thombare, S.K. Verma, "Technological development in the Stirling cycle engines", Renewable and Sustainable Energy Reviews, 12 (2008)

[ST33] R.H. TITRAN, J. R. STEPHENS, Advanced high temperature materials for the energy efficient automotive Stirling engine, NASA Lewis, 1984

[ST34] Costea, M.; Feidt, M. The effect of the overall heat transfer coefficient variation on the optimal distribution of the heat transfer surface conductance or area in a Stirling engine. Energy Convers. Manag. 1998, 39, 1753–1761.

[ST35] L. G. Thieme. Low-power baseline test results for the GPU 3 stirling engine. DOE/NASA, 1040-79(6), Avril 1979.

[ST36] Gheith, R.; Aloui, F.; Tazerout, M.; Ben Nasrallah, S. Experimental investigations of a Gamma Stirling engine. Energy Res. 2012, 36, 1175–1182.

[ST37] Gheith, R.; Aloui, F.; Ben Nasrallah, S. Study of regenerator constituting material influence on a Gamma type Stirling engine. J. Mech. Sci. Technol. 2012, 26, 1251–1255.

[ST38] Gheith, R.; Aloui, F.; Ben Nasrallah, S. Determination of adequate regenerator for a Gamma-type Stirling engine. Appl. Energy 2015, 139, 272–280.

[ST39] Gheith, R.; Aloui, F.; Ben Nasrallah, S. Optimization of Stirling engine performance based on an experimental design approach. Int. J. Energy Res. 2013, 37, 1519–1528.

[ST40] Donald Murray Clucas, Development of a Stirling Engine battery charger based on a low cost wobble mechanism, 1993.

[ST41] Mounir Ibrahim, Terry Simon, David Gedeon, Roy Tew, "Improving Performance of the Stirling Converter: Redesign of the Regenerator with Experiments, Computation and Modern Fabrication Techniques", Cleveland State University, October 2001

[ST42] Gheith, R.; Aloui, F.; Ben Nasrallah, S. Study of regenerator constituting material influence on a Gamma type Stirling engine. J. Mech. Sci. Technol. 2012, 26, 1251–1255.

[ST43] Hachem, H.; Gheith, R.; Aloui, F.; Ben Nasrallah, S.; Dincer, I. Energetic and Exergetic Performance Assessments of an Experimental Beta Type Stirling Engine. In Proceedings of the 7th International Ege Energy Symposium & Exhibition (IEESE 2014), Usak, Turkey, 18–20 June 2014.

[ST44] Gheith, R.; Aloui, F.; Ben Nasrallah, S. Determination of adequate regenerator for a Gamma-type Stirling engine. Appl. Energy 2015, 139, 272–280.

[ST45] Theodor Finkelstein, Allan J. Organ, Air Engines - The History, Science, and Reality of the Perfect Engine, 2001

[ST46] R.A. FARREL, Mod II Stirling Engine Overview, SAE 880539, 1988

[ST47] Drogosz P., Nitkiewicz S. and Andrzej Pietak., The selection of Stirling engines applied to cogeneration systems, J. of Kones, Powertrain and Transports, 19, 2, 2012.

[ST48] Parlak N., Wagner A., Elsner M., Soyhan, H.S. Thermodynamic analysis of a gamma type Stirling Engine in non-ideal adiabatic conditions. Int. J. Renew. Energy 2009, 34, 266–273.

[ST49] Comiskey P. et al., Stirling Engine Microgrid Generator, Milwaukee School of Engineering, 2013.

[ST50] Walker, G., Weiss, M., Fauvel, R., Reader, G. et al., "Simulation Program for Multiple Expansion Stirling Machines," SAE Technical Paper 929036, 1992, https://doi.org/10.4271/929036.

[ST51] Bennethum, J., Laymac, T., Johansson, L., and Godett, T., "Commercial Stirling Engine Development and Applications," SAE Technical Paper 911649,

[ST52] Thorsen, J.E, Bovin, J.K., and Carlsen, H., "3 kW Stirling Engine for Power and Heat Production", Energy Conversion Engineering Conference, 1996.

[ST53] Smith, L., Nuel, B., Weaver, S., Berkower, S., Weaver, S. and Gross, B., '25 kW Low-Temperature Stirling Engine for Heat Recovery, Solar and Biomass Applications', Cool Energy, ISEC 2016.

[ST54] Dioguardi, F., "Use of Stirling Cryogenerators for on-site bio-LNG production", Nordic Biogas Conference, August 2013.

[ST55] Godett, T., Meijer, R., Verhey, R., Pearson, C. et al., "STM4-120 Stirling Engine Test Development," SAE Technical Paper 890149, 1989, doi:10.4271/890149

[ST56] Nilsson, H., The United Stirling 4-95 and 4-275 Engines for underwater use. Intersociety Energy Conversion Engineering Conference, Orlando, FL, USA, 21 August 1983, pp.102-107.

[ST57] Noel P. NIGHTINGALE, Automotive Stirling Engine – Mod II Design Report, National Aeronautics and Space Administration, Lewis Research Center, DOE/NASA/0032-28, 1986

[ST58] Nilsson H, Submarine Power Systems Using the V4-275R Stirling Engine, Proceedings of the Institution of Mechanical Engineers, Part A: Journal of Power and Energy, 1998.

[ST59] Nomaguchi, Y., M. Suganami, M. Fujiwara, M. Sakai, Y. Kazumoto, H. Koseki, K. Kawajiri, Y. Hisamori, K. Taketa, T. Yoshida, T. Koda and K. Kashiwamura. 1986 (English). "Progress on 3 kW Class Stirling Engine and Heat-Pump System." Presented at the 21st Intersoci ety Energy Conversion Engineering Conference, 1986.

[ST60] Nomaguchi, T., T. Suganami, M. Fujiwara, M. Sakai, Y. Kazumoto, H. Koseki, K. Kaswajiri, K. Taketa, T. Yoshida, T. Koda and K. Kashiwamura. 1986 (English). "3 kW Class Stirling Engine and Heat Pump System." Presented at the 3rd International Stirling Engine Conference, Rome, 1986.

[ST61] Kagawa, N., S. Nagatomo, M. Sakamoto, T. Komakine, L. Hongo and T. Sakuma. 1986 (English). "Performance Analysis and Improvement of a 3 kW Stirling Engine." Presented at the 21st lntersociety Energy Conversion Engineering Conference, 1986.

[ST62] Watanabe, T., K. Yamaguchi andY. Momose. 1985 (English). "30 kW Stirling Engine." Presented at the 20th Intersociety Energy Conversion Engineering Conference, 1985.

[ST63] Momose, Y., and T. Watanabe. 1986 (English). Stirling Engine NS30A." Presented at the 3rd Engine Conference, Rome, 1986.

[ST64] Matsue, J., R. Katona, H. Sekiya, M. Takamatsu and H. Kurita. (Japanese). Development of a Compact 30 kW Stirling Engine. Technical Review. Vol. 18, No.1.

[ST65] Lampert William., V160 stirling Engine for a Total Energy System, the 5th International Symposium on Automotive Propulsion Systems, 1980

[ST66] Godett T., Meijer R., Verhey R., Pearson C. "STM4-120 Stirling Engine Test Development", SAE Technical Paper

[ST67] Khalili K., Godett T., Meijer R., Verhey R., "Design and Testing of a heat pipe gas combustion system for the STM4-120 Stirling engine", Energy Conversion Engineering Conference, 1989. IECEC-89

[ST68] Takamoto Saito, Heat Pumps: Solving Energy and Environmental Challenges, Proceedings of the 3rd International Energy Agency Heat Pump Conference, Tokyo, Japan, 1990

[ST69] Rosenqvist, K., Lia, T., and Goldwater, B., "The Stirling Engine for the Automotive Application,SAE Technical Paper 790329, 1979, https://doi.org/10.4271/790329.

[ST70] Koichi HIRATA, Masakuni KAWADA, "Development of a multi-cylinder Stirling engine, Proceedings of 12th International Stirling Engine Conference, p.315-324, Sept. 2005.

[ST71] Graham Walker, Stirling Engines Oxford University Press. 1980 - ISBN 0-19-856209-8

[ST72] Agarwal, P., Mooney, R., and Toepel, R., Stir-Lec I, A Stirling Electric Hybrid Car, SAE Technical Paper 690074, 1969, https://doi.org/10.4271/690074.

[ST73] Postma, N., Van Giessel, R., and Reinink, F., The Stirling Engine for Passenger Car Application, SAE Technical Paper 730648, 1973, https://doi.org/10.4271/730648.

[ST74] Grandin, A. and Ernst, W., Alternative Fuel Capabilities of the Mod II Stirling Vehicle, SAE Technical Paper 880543, 1988, https://doi.org/10.4271/880543.

[ST75] Allan J Organ, Striling Cycle Engine – Inner Working and Design, Wiley

[ST76] Graham Thomas READER, Charles HOOPER, "Stirling Engines", 1983

[ST77] Meijer R.J, The Philips Stirling thermal engine analysis of the rhombic drive mechanism and efficiency measurements, Philips research reports supplements, 1961.

[ST78] J. E. Cairelli, L. G. Thieme, and R. J. Walter, "Initial test results with a single-cylinder rhombic-drive stirling engine, 1978.

[ST79] van Giessel, R. and Reinink, F., "Design of the 4-215 D.A. Automotive Stirling Engine," SAE Technical Paper 770082, 1977, https://doi.org/10.4271/770082.

[ST80] William R. MARTINI, "Stirling Engine Design Manual", University Press of the Pacific, September 2004.

[ST81] Dowdy, M. and Nightingale, N., "Mod I Automotive Stirling Engine System Performance," SAE Technical Paper 820353, 1982, https://doi.org/10.4271/820353.

[ST82] Richey, A., "Mod I Automotive Stirling Engine Performance Development," SAE Technical Paper 840461, 1984, https://doi.org/10.4271/840461.

[ST83] Farrell, R., "Mod II Stirling Engine Overview," SAE Technical Paper 880539, 1988, https://doi.org/10.4271/880539.

[ST84] A. E. RICHEY, "Mod II Automotive Stirling engine – Design Description and Performance Projections", SAE Technical Paper 860059, 1986, https://doi.org/10.4271/860059.

[ST85] Allan J. Organ, "Thermodynamics and Gas Dynamics of the Stirling Cycle Machine". Cam- bridge University Press, 2010.

[ST86] Youssef Timoumi, Iskander Tlili, Sassi Ben Nasrallah, Design and performance optimization of GPU-3 Stirling engines, Energy, Volume 33, Issue 7, July 2008, Pages 1100–1114

[ST87] W. ERNST, Automotive Stirling Engine Development Project, NASA Lewis, 1997

[ST88] AUTOMOTIVE STIRLING ENGINE DEVELOPMENT PROGRAM, Ford Motor Company, 1977

[ST89] Donald G. Beremand, Stirling Engines for Automobiles, International Conference on Energy Use Management, Los Angeles, California, 1979

[ST90] Gunnar Lundholm, "The Experimental V4X Stirling Engine – A Pioneering Development", Department of Heat & Power Engineering Lund University

[ST91] A.E. RICHEY, S.C HUANG, Mod II Automotive Stirling Engine, Design Description and Performance Projections, SAE 860059

[ST92] Ernst, W., Stirling Engines for Hybrid Electric Vehicle Applications, SAE Technical Paper 929137, 1992, https://doi.org/10.4271/929137.

[ST93] Ernst, W., Meacher, J., and Bascom, R., Status and Emissions Results for Natural-Gas-Fired Stirling Engine, SAE Technical Paper 920383, 1992, https://doi.org/10.4271/920383.

[ST94] Lienesch, J. and Wade, W., Stirling Engine Progress Report: Smoke, Odor, Noise and Exhaust Emissions, SAE Technical Paper 680081, 1968, https://doi.org/10.4271/680081.

[ST95] Davis, S., Henein, N., and Lundstrom, R., "Combustion and Emission Formation in the Stirling Engine with Exhaust Gas Recirculation," SAE Technical Paper 710824, 1971, https://doi.org/10.4271/710824.

Vapor cycle machine

[VM1] Andrew JAMIESON, "Steam and Steam Engines", Fifth Edition, 1889

[VM2] Jorgen Lovland, "A History of Steam Power", NTNU, Norway 2007

[VM3] William C. Strack, "Condensers and Boilers for Steam-powered Cars: A Parametric Analysis of their Size, Weight, and Required Fan Power", NASA Technical Note, TN D-5813, Lewis Research Center, Cleveland, Ohio 4413

[VM4] Tadashi Tanuma, "Advances in Steam Turbines for Advanced Power Plants", 2017

[VM5] Sonntag R and Borgnakke R. Fundamentals of Thermodynamics, Sixth Edition, 2003, p.384-410.

[VM6] Moran M and Shapiro H. Fundamentals of engineering thermodynamics. 5th Edition – 2006, p.325-365.

[VM7] Cha W, Kim K, Choi K, et al. « Optimum Working Fluid Selection for Automotive Cogeneration System". World Academy of Science, Engineering and Technology, 2010

[VM8] Fujio Abe, « Research and Development of Heat-Resistant Materials for Advanced USC Power Plants with Steam Temperatures of 700°C and Above", Engineering, 2015

[VM9] F. Starr, "High temperature materials issues in the design and operation of coal-fired steam turbines and plant", Structural alloys for Power Plants, 2014

[VM10] Lemort, V." Contribution to the characterization of scroll machines in compressor and expander modes", thesis, 2008.

[VM11] Seher D, Lengenfelder T, Gerhardt J, et al. Waste heat recovery for commercial vehicles with a Rankine process. In: 21st Aachen Colloquium on Automobile and Engine Technology, Aachen, Germany, 2012

[VM12] Daccord, R., Darmedru, A., and Melis, J., "Oil-Free Axial Piston Expander for Waste Heat Recovery," SAE Technical Paper 2014-01-0675, 2014, doi:10.4271/2014-01-0675.

[VM13] Badr O, O'Callaghan PW, et al. Multi-vane expanders as prime movers for low-grade organic Rankine cycle engines. Appl Energ 1984;16(2):129–46.

[VM14] Badr O, O'Callaghan PW, et al. Multi-vane expanders: geometry and vane kinematics. Appl Energ 1985;19(3):159–82.

[VM15] Badr O, O'Callaghan PW, et al. Performances of Rankine cycle engines as functions of their expanders' efficiencies. Appl Energ 1984;18(1):15–27.

[VM16] Leduc P, Smague P, Rankine System for Heat Recovery: an Interesting Way to Reduce Fuel Consumption, SIA 2013

[VM17] O. Badr, S. Naik, P.W. O'Callaghan, S.D. Probert "Expansion machine for a low power-output steam Rankine-cycle engine" Appl. Energy, 39 (1991), pp. 93–116

[VM18] Kang S H. Design and experimental study of ORC (organic Rankine cycle) and radial turbine using R245fa working fluid. Energy 2012; 41(1): 514-524.

[VM19] Eckoldt, C.: Kraftmaschinen I: Muskelkraft,Wasserkraft, Windkraft, Dampfkraft, Deutsches Museum, München, 1996.

[VM20] Jackson Nyamwange, Monica Nyamwange, "Major Innovation in Transportation: Evolution of Automobiles", International Journal of Humanities and Social Science, Vol. 4, No. 5(1); March 2014

[VM21] Brinkley, Douglas. Wheels for the World. New York: Viking, 2003

[VM22] Rayner, D.: Traction Engines and other steam road engines, Shire Album 404, 2002.

[VM23] Sebastian ANTHONY, « Are steam cars poised for an epic comeback?", 2013, http://www.extremetech.com/extreme/148416-are-steam-cars-poised-for-an-epic-comeback

[VM24] https://en.wikipedia.org/wiki/Doble_steam_car

[VM25] Gouse, S. W. Jr. Steam Powered Automobile Should Come Back. Engineer, May-June 1968, pp. 22-26.

[VM26] Gouse, S. William, Jr. "Automotive Vehicle Propulsion". ,Part **I:** The Steam Engine and Part 11: Total Energy Ecology Implications. Advances in Energy Conversion Engineering. ASME, 1967, pp. 917-926.

[VM27] Bjerklie, J. W. ; and Sternlicht, B. "Critical Comparison of Low-Emission Otto and Rankine Engine for Automotive Use". Paper 690044, SAE, 1969.

[VM28] Ayres, Robert U. Alternative Nonpolluting Power Sources. SAE J., vol. 76, no. 12, Dec. 1968, pp. 40-80.

[VM29] Sprouse, C., Depcik, C., "Review of organic Rankine cycle for internal combustion engine exhaust waste heat recovery," Applied Thermal Engineering, vol 51, pp 711-722, 2013

[VM30] Abbe Horst T, Tegethoff W, Eilts P and Koehler J, "Prediction of Dynamic Rankine Cycle waste heat recovery performance and fuel saving potential in passenger car applications considering interactions with vehicles energy management". Energy Conversion and Management 78 (2014) 438-451

[VM31] Armstead J R and Miers S A. "Review of waste heat recovery mechanisms for internal combustion engines". Journal of Thermal Science and Engineering Applications 2013.

[VM32] V. Maizza, A. Maizza, "Working fluids in non-steady flows for waste energy recovery systems", Applied Thermal Engineering 16 (7) (1996) 579–590.

[VM33] V. Maizza, A. Maizza, "Unconventional working fluids in organic Rankine-cycles for waste energy recovery systems", Applied Thermal Engineering 21 (3) (2001) 381–390.

[VM34] S. Vijayaraghavan, D.Y. Goswami, "Organic working fluids for a combined power and cooling cycle", ASME Journal of Energy Resources Technology 127 (2005) 125–130.

[VM35] Mago J P, Chamra L, Srinivasan K, Somayaji C "An examination of regenerative organic Rankine cycles using dry fluids" Applied Thermal Engineering 28 (2008) 998–1007

[VM36] Badr O, Probert SD, O'Callaghan PW. Selecting a working fluid for a Rankine cycle engine. Appl Energ 1985;21:1–42.

[VM37] Cha W, Kim K, Choi K, et al. « Optimum Working Fluid Selection for Automotive Cogeneration System". Tc 2010;374(240.7):132.2.

[VM38] R Haller, B Nicolas, S Hammi et al. "Comparison of High and Low Temperature Working Fluids for Automotive Rankine Waste Heat Recovery Systems".

[VM39] Tahani M, Javan S, Biglari M. "A comprehensive study on waste heat recovery from internal combustion engines using organic Rankine cycle". Therm Sci 2013; 17(2):611-624.

[VM40] Mago P J, Chamra L M, Srinivasan K, et al. An examination of regenerative organic Rankine cycles using dry fluids. Appl Therm Eng 2008;28(8):998-1007.

[VM41] T.C. Hung, "Waste heat recovery of organic Rankine cycle using dry fluids", Energy Conversion & Management 42 (2001) 539–553.

[VM42] Endo T, Kawarjiri S, Kojima Y, Takahashi K, Baba T, Ibaraki S, Takahashi T, Shinohara M, Study on Maximizing Exergy in Automotive Engines. SAE Technical Paper 2007-01-0257

[VM43] Ibaraki, S.; Endo, T.; Kojima, Y.; Takahashi, K.; Baba, T. & Kawajiri, S: "Study of efficiency onboard waste heat recovery system using Rankine cycle", Review of Automotive Engineers, 28, 307-313, 2007.

[VM44] Freymann R, Ringler J, Seifert M, Horst T, The second generation Turbosteamer. MTZ Worlidwide 2012;73:18-23

[VM45] Freymann, R.; Strobl, W. & Obieglo, A.: "The Turbosteamer: a system introducing the principle of cogeneration in automotive applications", MTZ, 69, 20-27, 2008.

[VM46] Smague P, Leduc P « Integrated Waste Heat Recovery System with Rankine Cycle » 22nd Aachen Colloquium Automobile and Engine Technology 2013

[VM47] E. F. Doyle, L. DiNanno, S. K, Installation of a Diesel-Organic Rankine Compound Engine in a class 8 Truck for a Single-Vehicle Test, Society of Automotive Engineers, 790646, 1979.

[VM48] Espinosa N, Tilman L, Lemort V, Quoilin S, Lombard B "Rankine cycle for waste heat recovery on commercial trucks: approach, constraints and modeling", Volvo Powertrain France, University of Liège

[VM49] Dumand C, Bou Nader W, Coma G, Smague P, Enjeux et évaluation de solutions de récupération d'énergie à l'échappement : une analyse du Groupement Scientifique Moteur, regroupant PSA, Renault et IFPEN, Pôle Mov'eo, Décembre 2014

[VM50] Furukaa T, Nakamura M, Machida K, Shimokawa K, "A study of the Rankine Cycle Generating System for Heavy Duty HV Trucks." Hino Motors, Ltd. SAE Technical Paper 2014-01-0678, 2014, doi:10.4271/2014-01-0678

[VM51] Ringler, J., Seifert, M., Guyotot, V., and Hübner, W., Rankine Cycle for Waste Heat Recovery of IC Engines, SAE Int. J. Engines 2(1):67-76, 2009, doi:10.4271/2009-01-0174.

[VM52] Nelson, C., Waste Heat Recovery, DEER Conference, 2008.

[VM53] Stanton D, Charlton S, Vajapeyazula P, Cummins Inc Diesel Engine Technologies Enabling Powertrain Optimization to Meet U.S Greenhouse Gas Emissions. SAE International 2013-24-0094

[VM54] Teng, H., Klaver, J., Park, T., Hunter, G. et al., A Rankine Cycle System for Recovering Waste Heat from HD Diesel Engines - WHR System Development, SAE Technical Paper 2011-01-0311, 2011, doi:10.4271/2011-01-0311

[VM55] Park, T., Teng, H., Hunter, G., van der Velde, B. et al., A Rankine Cycle System for Recovering Waste Heat from HD Diesel Engines - Experimental Results, SAE Technical Paper 2011-01-1337, 2011, doi:10.4271/2011-01-1337

Ericsson

[ER1] I. Kolin. Stirling motor: history, theory, practice. University Publications Ltd, Zagreb, 1991.

[ER2] Th. Finkelstein, A.J. Organ, Air engines, Professional Engineering Publishing Ltd, London 2001.

[ER3] A.J. Organ. "The regenerator and the Stirling engine", Mechanical Engineering Publications, London (1997).

[ER4] I. Kolin, "The Evolution of the Heat Engine", Reprint. Moriya Pr, 1998.

[ER5] Appleton's mechanics' magazine and engineers' journal. New York: D. Appleton & Co., 1851.

[ER6] J. Dejust, « Machines à vapeur et machines thermiques diverses », Dunod 1899

[ER7] William Johnson, « The Imperial Cyclopaedia of Machinery", 1853

[ER8] G. Descombes, J.L. MAGNET, Moteurs non conventionnels, traité de Génie mécanique, Techniques de l'Ingénieur, BM 2593-3. 11

[ER9] A. Touré, "Etude théorique et expérimentale d'un moteur Ericsson à cycle de Joule pour conversion thermodynamique de l'énergie solaire ou pour micro-cogénération", Thèse, Université de Pau et des Pays de l'Adour, Novembre 2010.

[ER10] A. Fula, P. Stouffs, F. Sierra, In-cylinder heat transfer in an Ericsson engine prototype, International Conference on Renewable Energies and Power Quality, Bilbao, Espagne, 20-22 mars 2013.

[ER11] A. Touré, P. Stouffs, Modélisation du moteur Ericsson, Actes de la septième édition du colloque francophone en énergie, environnement, économie et thermodynamique COFRET'14, Paris, France, 2014.

[ER12] Marie Cryex, "Etude théorique et expérimentale d'une unité de micro-cogénération biomasse avec moteur Ericsson", Thèse, Université de Valenciennes et du Hainaut-Cambresis, 2014.

[ER13] Angelino, G.; Invernizzi, C. Real gas effects in Stirling engines. In Proceedings of the Energy Conversion Engineering Conference and Exhibit (IECEC) 35th Intersociety, Las Vegas, NV, USA, 24–28 July 2000.

[ER14] M. Creyx, E. Delacourt, C. Morin, B. Desmet, P. Peultier, "Energetic Optimization of the Performances of a Hot Air Engine for Micro-CHP systems working with a Joule or an Ericsson cycle", Energy, 49, 229-239, 2013

[ER15] P. Stouffs, Le moteur d'Ericsson, un moyen de valorisation de l'énergie thermique à réhabiliter?, Entropie, Vol. 241, p. 26-32 (2002).

[ER16] M.A.F. ROJAS, « Modélisation Thermique, Thermodynamique et Expérimentation d'un moteur Ericsson à air chaud à cycle de Joule », Thèse, Université de Pau et des Pays de l'Adour, 2015.

[ER17] H. Kim, W. Kim, H. Kim, et S. Kim, « Applicability of scroll expander and compressor to an external power engine: Conceptual design and performance analysis », Int. J. Energy Res., vol. 36, no 3, p. 385-396, mars 2012.

[ER18] D. Mikielewicsz, J. Mikielewicz, et J. Wajs, « Experiences from operation of different expansion devices for application in domestic micro CHP », Arch. Thermodyn., vol. 31, no 4, p. 3–13, 2010.

[ER19] J. W. Bjerklie, « A Free Piston Brayton Cycle Engine for Low Power », SAE International, Warrendale, PA, SAE Technical Paper 719109, févr. 1971.

[ER20] Sorin Rajiu, "The History of The Internal Combustion Engine", Annals of the faculty of engineering hunedoara, 2003

[ER21] Proeschel, R., Afterburning Ericsson Cycle Engine, SAE Technical Paper 1999-01-2880, 1999,

[ER22] D.A. Blank and C. Wu, "Power limit of an endoreversible Ericsson cycle with regeneration", Energy Convers. Mgmt Vol, 37, No. I, pp. 59-66, 1996.

[ER23] M. Golub, Power and efficiency of Ericsson motor, compared to modern engines, ISEC97065, 8th International Stirling Engine Conference and Exhibition, May 27-30, 1997 Ancona, Italy.

[ER24] Delameter, "Ericsson's New Hot Air Pumping Engine", Delameter Iron Works, New York 1890.

[ER25] J. Chen, J.A. Schouten, "The comprehensive influence of several major irreversibilities on the performance of an Ericsson heat engine", Applied Thermal Engineering 19 (1999) 555-564.

[ER26] B. C. Fryer, « Design, construction, and testing of a new valved, hot-gas engine. », Thesis, Massachusetts Institute of Technology, 1973.

[ER27] G. A. Tsongas et T. J. White, « A Parametric Analysis Microcomputer Model for Evaluating the Thermodynamic Performance of a Reciprocating Brayton Cycle Engine », J. Eng. Gas Turbines Power USA, vol. 111:1, janv. 1989.

[ER28] K. K. Craven et N. N. Clark, « Ideal Computer Analysis of a Novel Engine Concept », SAE International, Warrendale, PA, 960080, févr. 1996.

[ER29] F. Lontsi, « Modélisation dynamique des moteurs thermiques alternatifs à apport de chaleur externe à cycle de Joule (Moteurs Ericsson », thèse, UPPA, Pau France, 2010.

[ER30] D.A. Blank and C. Wu, "Finite-time power limit for solar-radiant Ericsson engines in space applications", Applied Thermal Engineering 18 (1998) 1347-1357.

[ER31] M. Alaphilippe, Recherche d'un nouveau procédé de conversion thermodynamique de l'énergie solaire, en vue de son application à la cogeneration de petite puissance, Thèse de Doctorat, Université de Pau et des pays de l'Adour, 2007.

[ER32] S. Bonnet, M. Alaphilippe, P. Stouffs, "Energy, exergy and cost analysis of a micro-cogeneration system based on an Ericsson engine", International Journal of Thermal Sciences 44 (2005) 1161-1168.

[ER33] P. Stouffs, Machines thermiques non conventionnelles : état de l'art, applications, problèmes à résoudre. Journées SFT, pp 1-15, Paris 1999.

[ER34] P. Stouffs, « Pré-dimensionnement d'un moteur Ericsson pour production d'énergie électrique pour station télécom ».

[ER35] P. Stouffs, « Dimensionnement d'un moteur Ericsson pour production d'énergie électrique pour station télécom en vue de la réalisation d'un prototype ».

[ER36] W. G. le Roux, T. Bello-Ochende, et J. P. Meyer, « Thermodynamic optimisation of the integrated design of a small-scale solar thermal Brayton cycle », Int. J. Energy Res., vol. 36, no 11, p. 1088–1104, 2012.

[ER37] Marie Creyx, "Développement d'un prototype de micro-cogénération bois incluant un moteur Ericsson à cycle de Joule ouvert", Laboratoire TEMPO, Journée micro cogénération CNAM, 2014

[ER38] Durcansky P., Papucik S., Jandacka J., Holubcik M., Nosek R., Design of Heat exchanger for Ericsson-Brayton Piston Engine, The Scientific World Journal, 2014

[ER39] A. Traverso, A. F. Massardo, R. Scarpellini, Externally Fired micro-gas Turbine: Modelling and experimental performance, Applied Thermal Engineering 26 (2006) 1935-1941. 18

[ER40] R.W. Moss, A.P. Roskilly, S.K. Nanda, Reciprocating Joule-cycle engine for domestic CHP systems, Applied Energy 80 (2005) 169-185

[ER41] J. Wojewoda, Z. kazimierski, "Numerical model and investigations of the externally heated valve Joule engine", Energy 35 (2010) 2099-2108.

[ER42] M.A. Bell, T. Partridge, Thermodynamic design of a reciprocating Joule cycle engine, Proc. Instn Mech. Engrs Vol. 217, N_3 Part A: Journal of Power and Energy, pp 239-246, 2003.

[ER43] J.C. Schlatter, Ultralow NOx via Catalytic Combustion, IMechE Seminar on 'Turbulent Combustion of Gases and Liquids-Leading Edge Technologies',15-16 December 1998, Lincoln, UK.

[ER44] G. B. Warren et J. W. Bjerklie, « Proposed Reciprocating Internal Combustion Engine with Constant Pressure Combustion - Combustion Chamber Separated from Cylinders (Modified Brayton Cycle) », SAE International, Warrendale, PA, SAE Technical Paper 690045, 1969.

[ER45] M. Doubs et F. LANZETTA, « Experimental study of the use of metal bellows as an Ericsson Engine Expansion Chamber », PROCEEDINGS OF ECOS 2015 - THE 28TH INTERNATIONAL CONFERENCE ON EFFICIENCY, COST, OPTIMIZATION, SIMULATION AND ENVIRONMENTAL IMPACT OF ENERGY SYSTEMS, PAU, FRANCE, 2015.

[ER46] T. Cartigny, M. Mille, M. Doubs, « Projet INDEHO: Système de micro-cogénération à cylindrée variable », Assystem, Journée micro cogénération CNAM, 2015

[ER47] T. Cartigny, M. Doubs, P. Ranc, « ENERGINE: Système de micro-cogénération à cylindrée variable », Assystem, Journée micro cogénération CNAM, 2016

Thermoacoustic

[TA1] K. Sondhauss, "Über die Schallschwingungen der Lufit in erhitzen Glasrohren und in gedeckten Pfeifen von ungleicher Weite", Annalen der Physik und Chemie, Vol 79, 1-34, 1850

[TA2] B. Higgins, Journal of Natural Philosophy and Chemical Arts, vol. 129, p. 22, 1802

[TA3] K. T. Feldman. Review of the literature on Rijke thermoacoustic phenomena. J. Sound Vib., 1968

[TA4] P. L. Rijke, "On the vibration of the air in a tube open at both ends", Philisophical Magazine, vol. 17, pp. 419-422, 1859.

[TA5] K. T. Feldman. Review of the literature on Sondhauss thermoacoustic phenomena. J. Sound Vib., 7:71—82, 1968.

[TA6] Lord Rayleigh. "The explanation of certain acoustical phenomena". Nature, 1878.

[TA7] Maurice-Xavier FRANCOIS, « Valorisation des Rejets Thermiques par le procédé Thermoacoustique », 16ième Cycle de Conférence CNAM/SIA, 2015.

[TA8] Greg Swift, "What is thermoacoustics? A brief description, with technical details and citations", Condensed Matter and Thermal Physics Group, Los Alamos National Laboratory

[TA9] B. Zinn. Pulsating combustion. In F. J. Weinberg, editor, Advanced Combustion Methods, pages 113—181. Academic, London, 1986.

[TA10] T. Hofler, J. C. Wheatley, G. W. Swift, and A. Migliori. Acoustic cooling engine, 1988. US Patent No. 4,722,201.

[TA11] W. E. Gifford and R. C. Longsworth. Pulse tube refrigeration progress. Adv. Cryogenic Eng., 10B:69—79, 1965.

[TA12] P. S. Spoor and G. W. Swift. Thermoacoustic separation of a He—Ar mixture. Phys. Rev. Lett.,85:1646—1649, 2000.

[TA13] D. A. Geller and G. W. Swift. Thermoacoustic enrichment of the isotopes of neon. J. Acoust. Soc. Am., 115:2059—2070, 2004.

[TA14] N. Rott. Damped and thermally driven acoustic oscillations in wide and narrow tubes. Z. Angew. Math. Phys., 20:230—243, 1969.

[TA15] N. Rott. Thermally driven acoustic oscillations, part III: Second-order heat flux. Z. Angew. Math. Phys., 26:43—49, 1975.

[TA16] N. Rott. Thermoacoustics. Adv. Appl. Mech., 20:135—175, 1980.

[TA17] Donald Fahey, "Thermoacoustic Oscillations", Wave Motion & Optics, Spring 2006

[TA18] Backhaus, S., Swift, G.W., 2000. "A thermoacoustic-Stirling heat engine: Detailed study." The Journal of the Acoustical Society of America 107, 3148 (June 2000)

[TA19] E. L. Mikulin, A. A. Tarasov, and M. P. Shkrebyonock. Low-temperature expansion pulse tubes. Adv. Cryogenic Eng., 29:629—637, 1984

[TA20] R. Radebaugh. A review of pulse tube refrigeration. Adv. Cryogenic Eng., 35:1191—1205, 1990

[TA21] I. Urieli and D. M. Berchowitz. Stirling Cycle Engine Analysis. Adam Hilger, Bristol UK, 1984.

[TA22] T. Yazaki, A. Iwata, T. Maekawa, and A. Tominaga. Traveling wave thermoacoustic engine in a looped tube. Phys. Rev. Lett., 81:3128—3131, 1998.

[TA23] C. M. de Blok. Thermoacoustic system, 1998. Dutch Patent: International Application Number PCT/NL98/00515. US Patent 6,314,740, November 13, 2001.

[TA24] S. Backhaus and G. W. Swift. A thermoacoustic-Stirling heat engine. Nature, 399:335—338, 1999

[TA25] Mathew SKARIA, K. K. Abdul Rasheed, K. A. Shafi, S. Kasthurirengan and Upendra Behera, "Simulation stuies on the performance of thermoacoustic prime movers and refrigerator", Computers & Fluids 111 (2015) 127-136, Elsevier

[TA26] Mostafa A. Nouh, Nadim M. Arafa, Ehab Abdel-Rahman, "Stack Parameters Effect on the Performance of Anharmonic Resonator Thermoacoustic Heat Engine", 2014

[TA27] Esmatullah Maiwand Sharify, Shun Takahashi, Shinya Hasegawa, "CFD Study of Oscillatory Flow around Parallel Plates in a Travelling-Wave Thermoacoustic Engine", Thermoacoustic systems & applications, Proceedings of the 3rd International Workshop on Thermoacoustic, October 2015, The Netherlands

[TA28] Mohd Zubir Bin Yahaya, "Evaluation of Heat Exchanger on Thermoacoustic Performance", Master of Engineering, Iniversiti Tun Hussein Onn Malaysia, June 2013

[TA29] Castro, Nelson C., "Experimental heat exchanger performance in a thermoacoustic prime mover", 1993

[TA30] K. TOURKOV, F. ZINK, L. SCHAEFER, "Thermoacoustic sound generation under the influence of resonator curvature", International Journal of Thermal Sciences, 88 (2015) 158 – 163

[TA31] Cynthia Haddad, Christell Périlhon, Amélie Danlos, Maurice-Xavier François and Georges Descombes, "Some Efficient Solutions to Recover Low and Medium Waste Heat : Competitiveness of the Thermoacoustic Technology", The International Conference on Technologies and Materials for Renewable Energy, Envieonment and Systainability, TMREES 14, Energy Procedia 50 (2014) 1056-1069

[TA32] J.G.B. Jacobs, "Design, construction and experimental observation of a thermoacoustic prime mover", Master of Science, Delft University of Technology, 2014.

[TA33] Backhaus, S.N., KEOLIAN, R.M., 2011. In-line stirling energy system. US7908856 B2, 2007

[TA34] R.M. KEOLIAN, M.E. POESE, R.W.M. SMITH, E.C. MITCHELL, C.M. ROBERTS, S.L. GARRETT, « TRILLIUM : An Inline Thermoacoustic-Stirling Refrigerator », Thermoacoustic systems & applications, Proceedings of the 3rd International Workshop on Thermoacoustic, 2015

[TA35] Jensen, C., Raspet, R., 2010. Thermoacoustic power conversion using a piezoelectric transducer. The Journal of the Acoustical Society of America 128, 98-103.

[TA36] Thiele, A., 1971. Loudspeakers in Vented Boxes : Parts I and II. J. Audio Eng. Soc., 19(5) 382-392.

[TA37] Small, R.H., 1973. Vented-Box Loudspeaker Systems–Part 1 : Small-Signal Analysis. JAES 21, 363-372.

[TA38] K. KANEUCHI, K. NISHIMURA, « Evaluation of Bi-Directional Turbines Using the Two-Sensor Method », Proceedings of the 3rd International Workshop on Thermoacoustic, 2015

[TA39] J. Lin, C. Scalo and L. Hesselink, "High-fidelity simulations of a standing-wave thermoacoustic-piezoelectric engine", Thermoacoustic systems & applications, Proceedings of the 3rd International Workshop on Thermoacoustic, October 2015, The Netherlands

[TA40] Smoker, J., Nouh, M., Aldraihem, O., and Baz, A. "Energy harvesting from a standing wave thermoacoustic piezoelectric resonator". Journal of Applied Physics, 111, (2012), 104901.

[TA41] Kees De Blok, Pawel Owczarek, Maurice-Xavier Francois, "Bi-directional turbines for converting acoustic wave power into electricity »

[TA42] C. Olivier, G. Poignand, G. Pénelet, « Do it yourself: make your own thermoacoustic engine with steel wool or rice », European Journal of Physics, 2016.

[TA43] J. R. Olson and G. W. Swift. Acoustic streaming in pulse tube refrigerators: Tapered pulse tubes. Cryogenics, 37:769—776, 1997.

[TA44] N. Rott. The influence of heat conduction on acoustic streaming. Z. Angew. Math. Phys., 25:417—421, 1974.

[TA45] C. Olivier, G. Poignand, G. Penelet and P. Lotton, « Simplified Modeling of a Thermo-Acousto-Electric Engine Forced by An External Sound Source », Thermoacoustic systems & applications, Proceedings of the 3rd International Workshop on Thermoacoustic, October 2015, The Netherlands

[TA46] N. Sugimoto, "On General Expressions of Temporal Means of Mass Flux, Shear Stress and Heat Flux due to Thermoacoustic Waves", Thermoacoustic systems & applications, Proceedings of the 3rd International Workshop on Thermoacoustic, October 2015, The Netherlands

[TA47] R. Paridaens, S. Kouidri, F. Jebali-Jerbi, « Experimental investigations of acoustic streaming in a thermoacoustic traveling wave engine using Laser Doppler Velocimetry », The Journal of the Acoustical Society of America, 2014

[TA48] J.A. Lycklama, M. E. H. Tijani and N. B. Siccama, "CFE Modelling of the Effect of Oscillating Jets on Streaming Heat Losses in a Torus-shaped Thermoacoustic Engine", Proceedings of the 3rd International Workshop on Thermoacoustic, October 2015, The Netherlands

[TA49] G. Q. Lu, P. Cheng, "Thermoacoustic streaming in a tube with isothermal outer surface", International Journal of Heat and Mass Transfer 48 (2005) 1599-1607

[TA50] A. Gopinath, N.L. Tait, "Thermoacoustic streaming in a resonant channel: the time-averaged temperature distribution", Journal of Acoustic. Soc. Am. 103 (1998) 1388–1405.

[TA51] Timothy S. RYAN, « Design and Control of a Standing-Wave Thermoacoustic Refrigerator ». B.S. in Mechanical Engineering, University of Pittsburgh, 2006.

[TA52] K. De Blok, « Low Operating Temperature Integral Thermo Acoustic Devices for Solar Cooling and Waste Heat Recovery », Aster Thermoakoestische Systemen, Sfa acoustics08, Patis, 2008

[TA53] M-X FRANCOIS, K. DE BLOK, P. BOUAKHAO, M. NIPHON, J. P THERMEAU, B. GUESTIN, L. COURTES, D. CLODIC, « The VALTA project : Full scale conversion of CHP engine flue gas heat into electricity », Thermoacoustic systems & applications, Proceedings of the 3rd International Workshop on Thermoacoustic, 2015

[TA54] Jay A. Adeff, Thomas J. Hofler, "Design and construction of a solar powered, themoacoustically driven, thermoacoustic refrigerator", 2000

[TA55] R. BESSIS, G. POIGNAND, H. BAILLIET, H. LAZURE, J-C VALIERE, E. BOUDARD, « Dual Thermoacoustic Core Compact Heat-Pump for Automotive Application », Thermoacoustic systems & applications, Proceedings of the 3rd International Workshop on Thermoacoustic, 2015

[TA56] T. Jin, R. Yang, Y.L. Liu, K. Tang and B. M. Chen, « Study on a looped 2-stage thermoacoustic engine », Thermoacoustic systems & applications, Proceedings of the 3rd International Workshop on Thermoacoustic, October 2015, The Netherlands

[TA57] Olivier, C.,Penelet, G., Poignand, G., and Lotton, P., 2014. Active control of thermoacoustic amplification in a thermo-acousto-electric engine. J. Appl. Phys. 115(17), 174905.

[TA58] Poignand, G., Olivier, C., Penelet, G., Lotton, P., 2014. Active tuning of acoustic oscillation in a thermo-acoustic power generator. 2nd International Workshop on Thermoacoustics, Sendai, Japon.

[TA59] P. Lotton, G. Poignard, G. Penelet and C. Olivier, "Thermoacoustic Electric Generation", Laboratoire d'Acoustique de l'Université du Maine (LAUME), June 2014

[TA60] Michael Petach, Emanuel Tward and Scott Backhaus, Design of a High Efficiency Power Source (HEPS) Based On Thermoacoustic Technology, NASA, 2004

[TA61] Yu, Z., Jaworski, A.J., Backhaus, S., 2010. A low-cost electricity generator for rural areas using a travelling-wave looped-tube thermoacoustic engine. Proceedings of the Institution of Mechanical Engineers, Part A: Journal of Power and Energy 224, 787-795.

[TA62] Normah MG, Irfan AR, Koh KS, Manet A, Zaki Ab M. "Investigation of a portable standing wave thermoacoustic heat engine". Procedia Engineering 2013 (56); pp. 829-834.

[TA63] Baiman Chen, Abdalla A. Yousif, Paul H. Riley, David B. Hann, « Development and Assessment of Thermoacoustic Generators Operating by Waste Heat from Cooking Stove », Scientific Research, Engineering, 2012, 4, 894-902

[TA64] S. Backhaus and G. Swift, "A thermoacoustic-Stirling heat engine : detailed study," Journal of Acoustical Society of America, vol. 107, pp. 3148–3166, 2000.

[TA65] J.-A. Mumith, C. Makatsoris, and T. Karayiannis, "Design of a thermoacoustic heat engine for low temperature waste heat recovery in food manufacturing," Applied Thermal Engineering, vol. 65, pp. 588–596, 2014.

[TA66] Backhaus, S., Tward, E., Petach, M., 2004. Traveling-wave thermoacoustic electric generator. Appl. Phys. Lett. 85, 1085.

[TA67] M. Tijani and S. Spoelstra, "A hot air driven thermoacoustic-Stirling engine," Applied Thermal Engineering, vol. 61, pp. 866–870, 2013.

[TA68] Didier Alary, Cyrille Tourneur, Jaime Reed, Bruno Rechain and Maurice François, "Thermo-Acoustic Generators for Space Missions"

[TA69] Zhanghua Wu, Guoyao Yu, Limin Zhang, Wei Dai and Ercang Luo, "Development of a 3 kW double-acting thermoacoustic Stirling electric generator", Applied Energy 2014.

[TA70] Mark Haberbusch, "Thermoacoustic Stirling Heat Engine (TASHE) for Space Power and Cooling", Sierra Lobo, NASA, 2015

[TA71] "Startup commercializing thermo-acoustic Stirling technology for combined heat and power for homes". Green Car Congress, 27 December 20013.

[TA72] Yu G, Wang X, Dai W, Luo E. Study on energy conversion characteristics of a high frequency standing-wave thermoacoustic heat engine. Applied energy 2013 (111); pp. 1147-1151.

[TA73] D. Gardner and C. Howard, "Waste-heat-driven thermoacoustic engine and refrigerator," conf. Acoustics, 2009.

[TA74] I. line stirling energy system, "S. backhaus and r. keolian," US patent number 7908856 B2, 2011.

[TA75] J. FRITZSCHE, J. DRÜCKHAMMER, C. KÄPPNER, E. HASSEL, T.W. STEINER, « Thermoacoustics as an Alternative Technology for Waste Heat Recovery in Automotive and (Heavy) Duty Applications », 24th Aachen Colloquium Automobile and Engine Technology 2015

[TA76] Karlsson, M., Abom, M., Lalit, M., and Glav, R., "A Note on the Applicability of Thermo-Acoustic Engines for Automotive Waste Heat Recovery," SAE Int. J. Mater. Manf. 9(2):286-293, 2016, doi:10.4271/2016-01-0223.

[TA77] Etalim Inc, Breakthrough micro-generation technology

[TA78] Etalim Inc, NRCan ecoENERGY Innovation Initiative, Stakeholder Report, May 2014

Thermoelectric

[TE1] D.M. Rowe, CRC Handbook of thermoelectrics. 1995: CRC Press.

[TE2] D.M. Rowe, Thermoelctrics Handbook: macro to nano. 2006: CRC/Taylow & Francis.

[TE3] T.J. Seebeck, Abhandlungen der Deutschen Akademi der Wissenschaften. 1823. 265.

[TE4] D.D. Allred, An overview of thermoelectrics in "Short course on thermoelectrics". Edited by the international thermoelectric society, 1993.

[TE5] W. Thomson, proceedings of the Royal Society of Edinburgh. 1851. 91.

[TE6] L. Onsager, Reciprocal relations in irreversible processes II. PHYSICAL REVIEW, 1931. 38: p. 2265.

[TE7] Nowotny, H., The chemistry of extended defects in non-metallic solid. North holland, Amsterdam ed. 1970.

TE8] Gottlieb, U., et al., Magnetic properties of single crystalline Mn4Si7. Journal of Alloys and Compounds, 2003. 361(1-2): p. 13-18.

[TE9] L. Onsager, Reciprocal relations in irreversible processes I. PHYSICAL REVIEW 1931. 37: p. 405.

[TE10] Nishihata, H.K., O. Ueno, T. PELTIER cooling system utilizing liquid heat exchanger combined with pump. in Proceedings of the 21st International Conference on Thermoelectrics. 2002.

[TE11] Davis, M.W., R. Clarke, P. CPU cooling using high efficiency liquid flow heat exchangers. in Proceedings of the 23rd International Conference on Thermoelectrics. 2004.

[TE12] Snyder, G.J. and E.S. Toberer, Complex thermoelectric materials. Nature Materials, 2008. p. 105-114

[TE13] http://energiein.e-monsite.com/pages/p1-et-moi.html

[TE14] Kishi, M.N., H. Hamao, T. Yamamoto, M. Sudou, S. Mandai M. Yamamoto, S. Micro thermoelectric modules and their application to wristwatches as an energy source. in In Proceedings of the 18th International Conference on Thermoelectrics. 1999.

[TE15] John W. FAIRBANKS, « Thermoelectric Developments for Vehicular Applications », FreedomCar & Vehicle Technologies Program, U.S Department of Energy, Energy Efficiency and Renewable Energy, August 2006.

[TE16] Bertrand LENOIR, Jean-Pierre MICHENAUD, Anne DAUSCHER, « Thermoélectricité : des principes aux applications », 2010

[TE17] Zebarjadi, M., et al., Perspectives on thermoelectrics: from fundamentals to device applications. Energy & Environmental Science, 2012. 5(1): p. 5147-5162.

[TE18] N.F.Mott, H.J., The theory of the properties of metals and alloys.Dover Publications. 1958

[TE19] Mahan, G.D. and J.O. Sofo, The best thermoelectric. Proceedings of the National Academy of Sciences of the United States of America, 1996. 93(15): p. 7436-7439.

[TE20] T.K. Reynolds, J.G.B., R.F.Kelley, F.J.Disalvo, Chemistry, physics, materials science of thermoelectric materials, beyond bismuth telluride. 2002: Kluwer Academic/Plenum

[TE21] Goldsmid, H.J., Thermoelectric Refrigeration. 1964: Plenum Press, New York.

[TE22] [TEG-19] B. Lenoir, J.P. Michenaud, A. Dauscher, Conversion d'énergie par effets thermoélectriques: théorie, matériaux et application 3ed. 2009.

[TE23] Ioffe, A., Semiconductors, Thermoelements and Thermoelectric cooling. 1957.

[TE24] Goodman, C.H.L., The prediction of semiconducting properties in inorganic compounds. Journal Of Physics And Chemistry Of Solids, 1958. 6: p. 305.

[TE25] Goldsmid, H.J.D., R. W, The use of semiconductors in thermoelectric refrigeration. British journal of applied physics, 1954. 5: p. 386.

[TE26] G.A. Slack, "New material and performance limits for thermoelectric cooling" in CRC Handbook of thermoelctrics, ed. D.M. Rowe. 1995: CRC Press, Boca Raton. 407.

[TE27] G.D. Mahan, B.C.S., J. Sharp, Thermoelectric materials: new approaches to an old problem. Physics Today, 1997. 50: p. 42.

[TE28] B. Lenoir, H.S.T. Caillat, "An overview of recent developpements for BiSb alloys," in Recent Trends in Thermoelectric Materials. Academic Press, San Diego ed. Vol. 69. 2001.

[TE29] Graf, T., S.S.P. Parkin, and C. Felser, HEUSLER Compounds-A Material Class With Exceptional Properties. Ieee Transactions on Magnetics, 2011. 47(2): p. 367-373.

[TE30] Graf, T., et al., Phase separation in the quaternary HEUSLER compound CoTi(1-x)MnxSb - A reduction in the thermal conductivity for thermoelectric applications. Scripta Materialia, 2010. p. 1216-1219.

[TE31] W.M. Yim, A.A., Bi-Sb alloys for magneto-thermoelectric and thermomagnetic cooling. Solid-State Electronics, 1972. 15: p. 1141.

[TE32] Yamashita, O. and S. Tomiyoshi, Effect of annealing on thermoelectric properties of bismuth telluride compounds. Japanese Journal of Applied Physics Part 1-Regular Papers Short Notes & Review Papers, 2003. 42(2A): p. 492-500.

[TE33] Simmard, J.M.V., D. Turenne, S. Influence of composition and texture on the thermoelectric and mechanical properties of extruded (Bi1-xSbx)2(Te1-ySey)3 alloys. in In Proc. 22th Int. Conf. on Thermoelectrics. 2003. La Grande Motte, France.

[TE34] Sharp, J., Some properties of Ge-Te based thermoelectric materials, in International Conference on Thermoelctrics. 2003: La Grande Motte, France. p. 267.

[TE35] Kawasumi, I., et al., Crystal-Growth of Manganese Silicide, Mnsi Approximately 1.73 and Semiconducting Properties of Mn15si26. Journal of Materials Science, 1981. 16(2): p. 355-366.

[TE36] Toberer, E.S., et al., Traversing the Metal-Insulator Transition in a Zintl Phase: Rational Enhancement of Thermoelectric Efficiency in Yb14Mn1-xAlxSb11. Advanced Functional Materials, 2008. p. 2795-2800.

[TE37] Toberer, E.S., A.F. May, G.J. Snyder, Zintl Chemistry for Designing High Efficiency Thermoelectric Materials. Chemistry Of Materials, 2010. 22(3): p. 624-634.

[TE38] Cox, C.A., et al., Structure, Heat Capacity, and High-Temperature Thermal Properties of Yb14Mn1-xAlxSb11. Chemistry Of Materials, 2009. 21(7): p. 1354-1360.

[TE39] Brown, S.R., et al., Yb14MnSb11: New high efficiency thermoelectric material for power generation. Chemistry Of Materials, 2006. 18(7): p. 1873-1877.

[TE40] Hicks, L.D., M.S. Dresselhaus, Thermoelectric Figure of Merit of a One-Dimensional Conductor. Physical Review B, 1993. 47(24): p. 16631-16634.

[TE41] Hicks, L.D. M.S. Dresselhaus, Effect of Quantum-Well Structures on the Thermoelectric Figure of Merit. Physical Review B, 1993. 47(19): p. 12727-12731.

[TE42] Harman, T.C., D.L. Spears, and M.P. Walsh, PbTe/Te superlattice structures with enhanced thermoelectric figures of merit. Journal of Electronic Materials, 1999. 28(1): p. L1-L4.

[TE43] Venkatasubramanian, R., et al., Thin-film thermoelectric devices with high room-temperature figures of merit. Nature, 2001. 413(6856): p. 597-602.

[TE44] Winkler, M., et al., Current Status in Fabrication, Structural and Transport Property Characterization, and Theoretical Understanding of Bi2Te3/Sb2Te3 Superlattice Systems. Zeitschrift Fur Anorganische Und Allgemeine Chemie, 2012. 638(15): p. 2441-2454.

[TE45] Yan, X.A., et al., Enhanced Thermoelectric Figure of Merit of p-Type Half-HEUSLERs. Nano Letters, 2011. 11(2): p. 556-560.

[TE46] Puyet, M., et al., Beneficial effect of Ni substitution on the thermoelectric properties in partially filled CayCo4-xNixSb12 skutterudites. Journal Of Applied Physics, 2005. 97(8).

[TE47] Kuznetsov, V.L., et al., Preparation and thermoelectric properties of A(8)(II)B(16)(III)B(30)(IV) clathrate compounds. Journal Of Applied Physics, 2000. 87(11): p. 7871-7875.

[TE48] Snyder, G.J., et al., Disordered zinc in Zn4Sb3 with phonon-glass and electron-crystal thermoelectric properties. Nature Materials, 2004. 3(7): p. 458-463.

[TE49] Akrap, A., et al., High-pressure resistivity and thermoelectric power in Yb14MnSb11. Physical Review B, 2007. 76(8).

[TE50] He, Y., et al., High Thermoelectric Performance in Non-Toxic Earth-Abundant Copper Sulfide. Advanced Materials, 2014. 26(23): p. 3974-3978.

[TE51] Zhao, L.D., et al., Ultralow thermal conductivity and high thermoelectric figure of merit in SnSe crystals. Nature, 2014. 508(7496): p. 373-+.

[TE52] Hogan, T.P., et al., Nanostructured thermoelectric materials and high-efficiency power-generation modules. Journal Of Electronic Materials, 2007. 36(7): p. 704-710.

[TE53] Uher, C., et al., Transport properties of pure and doped MNiSn (M=Zr, Hf). Physical Review B, 1999. 59(13): p. 8615-8621.

[TE54] Bhattacharya, S., et al., Effect of Sb doping on the thermoelectric properties of Ti-based half-HEUSLER compounds, TiNiSn1-xSbx. Applied Physics Letters, 2000. 77(16): p. 2476-2478.

[TE55] Drabkin, I.A., ed. Thermoelectric cooling text of lectures. 2002: Stpsultft, in Russian.

[TE56] Abrikosov, N.K.B., V.F. Fedorova, G.A, Metallurgy and Physics of Semiconductors. J. N.Ch, 1957.

[TE57] Svechnikova, T.E., et al., The Homogeneity of Czochralski-Grown Bi2te2.85se0.15 Single-Crystals. Inorganic Materials, 1995. 31(1): p. 20-28.

[TE58] Lenoir, B., et al., Transport properties of Bi-rich Bi-Sb alloys. Journal of Physics and Chemistry of Solids, 1996. 57(1): p. 89-99.

[TE59] Shcherbachev, K.D., V.T. Bublik, O.E. Daricheva, The Study of Microdefects in Gaas Single-Crystals Doped with Si by X-Ray Diffuse-Scattering. Kristallografiya, 1995. 40(5): p. 868-876.

[TE60] Ufimtsev, V.B., et al., Structure, homogeneity and properties of thermoelectric materials based on ternary solid solutions of bismuth and antimony chalcogenides. Advanced Performance Materials, 1997. 4(2): p. 189-197.

[TE61] Katano, N.M.M., Ingot plate made of thermoelectric material, rectangular bar cut from the ingot plate, and process of fabricating the ingot plate. 1998: U.S.A.

[TE62] Koch, C.C., Materials Synthesis by Mechanical Alloying. Annual Review of Materials Science, 1989. 19: p. 121-143.

[TE63] Maurice, D.R., T.H. Courtney, The Physics of Mechanical Alloying - a 1st Report. Metallurgical Transactions a-Physical Metallurgy and Materials Science, 1990. 21(2): p. 289-303.

[TE64] Han, S.H., K.A. Gschneidner, B.J. Beaudry, Preparation of a Metastable High-Temperature Phase (Gamma-Dy2s3) and a Metastable High-Pressure Phase (Gamma-Y2s3) by Mechanical Alloying and Mechanical Milling. Scripta Metallurgica Et Materialia, 1991. 25(2): p. 295-298.

[TE65] Martin-Lopez, R., et al., Mechanical alloying of BiSb semiconducting alloys. Materials Science and Engineering a-Structural Materials Properties Microstructure and Processing, 1998. 248(1-2): p. 147-152.

[TE66] Bouad, N., R.M. Marin-Ayral, and J.C. Tedenac, Mechanical alloying and sintering of lead telluride. Journal of Alloys and Compounds, 2000. 297(1-2): p. 312-318.

[TE67] Bouad, N., et al., Mechanical alloying of a thermoelectric alloy: Pb0.65Sn0.35Te. Journal of Solid State Chemistry, 2004. 177(1): p. 221-226.

[TE68] Nagai, H., et al., Effect of Si/C ratio on thermoelectric properties of beta-FeSi2 mechanically alloyed with (Si plus C) additions. Materials Transactions Jim, 2000. 41(2): p. 287-292.

[TE69] Yang, J.Y., et al., Synthesis of CoSb3 skutterudite by mechanical alloying. Journal of Alloys and Compounds, 2004. 375(1-2): p. 229-232.

[TE70] Izard, V., M.C. Record, and J.C. Tedenac, Mechanical alloying of a new promising thermoelectric material, Sb3Zn4. Journal of Alloys and Compounds, 2002. 345(1-2): p. 257-264.

[TE71] Zhang, Y.C., et al., Silver-Based Intermetallic Heterostructures in Sb2Te3 Thick Films with Enhanced Thermoelectric Power Factors. Nano Letters, 2012. 12(2): p. 1075-1080.

[TE72] Ji, X.H., et al., Improved thermoelectric performance in polycrystalline p-type Bi(2)Te(3) via an alkali metal salt hydrothermal nanocoating treatment approach. Journal of Applied Physics, 2008. 104(3).

[TE73] Zhou, W.W., et al., Binary-Phased Nanoparticles for Enhanced Thermoelectric Properties. Advanced Materials, 2009. 21(31): p. 3196-+.

[TE74] Xie, W.J., et al., Identifying the Specific Nanostructures Responsible for the High Thermoelectric Performance of (Bi,Sb)(2)Te-3 Nanocomposites. Nano Letters, 2010. 10(9): p. 3283-3289.

[TE75] Xie, W.J., et al., High thermoelectric performance BiSbTe alloy with unique low-dimensional structure. Journal of Applied Physics, 2009. 105(11).

[TE76] Xie, W.J., et al., Unique nanostructures and enhanced thermoelectric performance of melt-spun BiSbTe alloys. Applied Physics Letters, 2009. 94(10).

[TE77] Carrey, J., H.B. Radousky, A.E. Berkowitz, Spark-eroded particles: Influence of processing parameters. Journal of Applied Physics, 2004. 95(3): p. 823-829.

[TE78] Casper, F., et al., Half-HEUSLER compounds: novel materials for energy and spintronic applications. Semiconductor Science and Technology, 2012. 27(6).

[TE79] Kakuei MATSUBARA, « Thermoelectric Generator to Utilize Waste Exhaust Heat Energy of Vehicles », Yamaguchi TOKYO University of Science, May 2005

[TE80] J. LaGrandeur, D. Crane, A. Eder, « Vehicle Fuel Economy Improvement through Thermoelectric Waste Heat Recovery, DEER Conference, Chicago, IL, August 24, 2005

[TE81] Sumeet Kumar, Stephen D. Heister, Xianfan Xu, James R. Salvador and Gregory P. Meinsner, "Thermoelectric Generators for Automotive Waste Heat Recovery Systems Part I: Numerical Modeling and Baseline Model Analysis", Journal of Electronic Materials, DOI: 10.1007/s11664-013-2471-9, 2013.

[TE82] N. Espinosa, M. Lazard, L. Aixala, H. Scherrer, "Modeling a Thermoelectric Generator Applied to Diesel Automotive Heat Recovery", Journal of ELECTRONIC MATERIALS, Vol. 39, No. 9, 2010

[TE83] Doug Crane, John Lagrandeur, Vladimir Jovovic, Marco Ranalli, Martin Adldinger, Eric Poliquin, Joe Dean, Dmitri Kossakovski, Boris Mazar and Clay Maranville, "TEG On-Vehicle Performance and Model Validation and What It Means for Further TEG Development", Journal of Electronic Materials, Vol. 42, No. 7, 2013

[TE84] Sumeet Kumar, Stephen D. Heister, Xianfan Xu, James R. Salvador and Gregory P. Meinsner, "Thermoelectric Generators for Automotive Waste Heat Recovery Systems Part II: Parametric Evaluation and Topological Studies", Journal of Electronic Materials, DOI: 10.1007/s11664-013-2472-8, 2013.

[TE85] Horst FRIEDRICH, Michael SCHIER, Christian HAFELE, Tobias WEILER, "Electricity from exhausts – Development of thermoelectric generators for use in vehicles", Research Thermal Management, 2010

[TE86] Birkholz, U.G., E. Stohrer, U. Voss, K. Conversion of waste exhaust heat in automobiles using FeSi2 thermoelements. in In Proceedings of the 7th International Conference on Thermoelectric Energy Conversion. 1988.

[TE87] Bass, J.E., N.B. Leavitt, A. Performance of the 1 kW thermoelectric generator for diesel engines. In proceeding of the 13th Inthernational Conference on Thermoelectrics. 1995. AIP Conf. Proc. New York.

[TE88] John C. Bass, Aleksandr S. Kushch, Norbert B. Elsner, "Thermoelectric Generator (TEG) for Heavy Diesel Trucks", Hi-Z Technology, International Thermoelectric Society, 2006

[TE89] Morelli, D.T. Potential applications of advanced thermoelectrics in the automobile industry. in In proceedings of the 15th International Conference on Thermoelectrics. 1996.

[TE90] Morelli, D.T., Advanced thermoelectric materials and systems for automotive applications in the next millennium, in Material Research Society Symposium Proceedings. 1997: Pittsburgh, PA. p. 297.

[TE91] Liebl, J.; et al.: Der thermoelektrische Generator von BMW macht Abwärme nutzbar. In: MTZ 70 (2009), Nr. 3, S. 272-281

[TE92] Boris MAZAR, « State of the Art Prototype Vehicle with a Thermoelectric Generator », BMW Group, TE Application Workshop, Baltimore, March 21st 2012.

[TE93] Will Hornick, "Case Study Fiat: The First Light Commercial Vehicle Equipped with a Thermo-Electric Generator", 2013

[TE94] Richard Stobart, Dan Milner, "The Potential for Thermo-Electric Regeneration of Energy in Vehicles", SAE International, 2009-01-1333

[TE95] Masayoshi Mori, Takeshi Yamagami, Mitsumasa Sorazawa, Takatoshi Miyabe, Shunji Takahashi and Tomohide Haraguchi, "Simulation of Fuel Economy Effectiveness of Exhaust Heat Recovery System Using Thermoelectric Generator in a Series Hybrid", Honda R&D Co., SAE International 2011-01-1335

[TE96] R. YU, L. AIXALA, C. DE VAULX, « Waste Heat Recovery by Thermoelectricity on passenger car and heavy-duty truck diesel engine : The RENOTER project », 2012

[TE97] Renoter Project, Renault Trucks, 3rd Thermoelectric Applications Workshop : 20-22 March 2012 in Baltimore

[TE98] Silvio RISSE, Hans ZELLBECK, « Close-Coupled Exhaust Gas Energy Recovery in a Gasoline Engine », Thermal Management, MTZ 01/2013 Volume 74

[TE99] Marco RANALLI, Martin ADLDINGER, Dmitri KOSSAKOVSKI, Marcel WOMANN, "Thermoelectric generators : From Aerospace to Automotive", ATZ worldwide, Development Thermal Management, 2013.

[TE100] Saniya LEBLANC, Shannon K. YEE, Matthew L. SCULLIN, Chris DAMES, « Material and Manufacturing Cost Considerations for Thermoelectrics », Renewable and Sustainable Energy Reviews, 32 (2014) 313-327

[TE101] J. LIEBL, S. NEUGEBAUER, A. EDER, M. LINDE, B. MAZAR, W. STÜTZ, « The Thermoelectric Generator from BMW is Making Use of waste Heat", Thermo Management, MTZ 04/2009 Volume 70

[TE102] Orr B., Akbarzadeh A., Mochizuki M. Singh R., A revie of Car Waste Heat Recovery Systems Utilising Thermoelectric Generators and Heat Pipes", Applied Thermal Engineering, 2015

[TE103] Quazi E. HUSSAIN, David R. BRIGHAM, Clay W. MARANVILLE, « Thermoelectric Exhaust Heat Recovery for Hybrid Vehicles", Ford Motor Company, SAE Int. J. Engines, Volume 2, Issue 1, 2009-01-1327

[TE104] Axiala Luc, Renoter Project, Renault Trucks, 2nd Thermoelectric Applications Workshop, San Diego, 2011

[TE105] Vehicular Thermoelectrics: A New Green Technology, Thermoelectrci Applications Workshop, Coronado, California, 2011

[TE106] Axiala Luc, Renoter Project, Renault Trucks, 3rd Thermoelectric Applications Workshop, San Diego, 2012

Fuel cell

[FC1] Larminie J, Dicks A. Fuel cell systems explained. New York: Wiley; 2003.

[FC2] Bard AJ, Faulkner LR. Electrochemical methods. New York: Wiley; 1980.

[FC3] Fuel Cell Technology Showcase, History of Fuel Cells, SAE International

[FC4] The History of Hydrogen, www.eere.energy.gov/hydrogenandfuelcells/

[FC5] FORD SUSTAINABILITY REPORT 2013/14, http://corporate.ford.com/microsites/sustainability-report-2013-14/environment-products-plan-migration-fcv.html

[FC6] Mehrdad EHSANI, Yimin GAO, Ali EMADI, « Modern Electric, Hybrid Electric, and Fuel Cell Vehicles » – Fundamentals, Therory, and Design – Second Edition.

[FC7] Chris MI, M. ABDUL MASRUR, David WENZHONG GAO, « Hybrid Electric Vehicles » - Principles and Applications with Practical Perspectives, WILEY, 2011

[FC8] Junghwan BANG, Han-Sang KIM, Dong-Hun LEE, Kyoungdoug MIN, « Study on Operating Characteristics of fuel cell powered electric vehicle with different air feeding systems », Journal of Mechanical Science and Technology, 22 (2008) 1602-1611

[FC9] Ibrahim DINCER, Marc A. ROSEN, « Exergy » - Energy Environment and Sustainable Development, Second Edition, 2013, p363-381.

[FC10] A.K.M. Mohiuddin, Ataur Rahman, Mohamed Fadhil Chemani and Mohb Baihaqi Zakaria, Investigation of PEM fuel cell for automotive use, IIUM Engineering Journal, 2015.

[FC11] Sajgure M., Kachare B., Gawhale P., Waghmare S., Jagadale G., Direct Methanol Fuel Cell: A Review, International Journal of Current Engineering and Technology, 2016

[FC12] Cameron S. D.,Hards A. G., Harrison B. Potter J. R., Direct Methanol Fuel Cells : Recent Developments in the Search for Improved Performance, Johnson Matthey Technology Centre, 1987.

[FC13] Rajashekara K., MacBain A. J., Grieve J., Evaluation of SOFC Hybrid Systems for Automotive Propulsion Applications, Industry Applications Conference, 41th IAS Annual Meeting, 2006.

[FC14] Singhal S.C., Solid Oxide Fuel Cells for Stationary, mobile, and military applications, Solid State Ionics, 2002.

[FC15] Kordescha K., Gsellmanna J., Cifraina M., Vossa S., Hackera V., Aronsonb R. R., Fabjanc C., Hejzec T., Daniel-Ivadd J., Intermittent use of a low-cost alkaline ful cell-hybrid system for electric vehicles, Journal of Power Sources, 1999.

[FC16] De Geeter E., Mangan M., Spaepen S., Stinissen W., Vennekens G., Alkaline Fuel Cells for Road Traction, Journal of Power Sources, 1999.

[FC17] Pathak S., Narayana Das., Rangarajan J., Choudhury R S., Prakash R., Development of Prototype Phosphoric Acid Fuel Cell Pick-Up Electric Vehicle, Electric and Hybrid Vehicles, IEEE Conference, 2006

[FC18] Mekhilef S., Saidur R., Safari A., Comparative study of different fuel cell technologies, Renewable and Sustainable Energy Reviews, 2012

[FC19] John M. Nail, Gary Anderson, Gerald Ceasar, Christopher J. Hansen, "The Role of the U.S. National Innovation System in the Development of the PEM Stationary Fuel Cell", February 2005

[FC20] Lejda K., Fuel Cells as Alternative for Power Transmission of Automotive Vehicles, Journal of KONES Internal Combustion Engines 2005.

[FC21] T. Hottinen, M. Noponen, T. Mennola, O. Himanen, M. Mikkola and P. Lund, "Effect of ambient conditions on performance and current distribution of a polymer electrolyte membrane fuel cell", Journal of Applied Electrochemistry, 33, 265-271, 2003

[FC22] Mahesh Murthy, Manuel Esayian, Woo-kum Lee, J. W. Van Zee, "The Effects of Temperature and Pressure on the Performance of a PEMFC Exposed to Transient CO Concentrations", Journal of the Electrochemical Society, 150 (1) A29-A34, 2003

[FC23] Bhaskar Balasubramanian, Frano Barbir and Jay Neutzler, "Optimal Operating Temperature and Pressure of PEM Fuel Cell Systems in Automotive Applications", Energy Partners.

[FC24] BMW Group, « Cryo-Compressed Hydrogen Storage », Oxford, 2012

[FC25] Christian Maugy, "Hydrogène, Pile à Combustible: Applications automobiles et Autres", Intervention ENSTA Paristech, 2016

[FC26] Laurencelle F, Chahine R, Hamelin J, Agbossou K, Fournier M, Bose T, et al. Characterization of a Ballard MK5-E proton exchange membrane fuel cell stack. Fuel Cells 2001.

[FC27] Ahmad Mayyas, Max Wei, Shuk Han Chan and Tim Lipman, Fuel Cell Forklift Deployment in the U.S, University of California Berkeley, DOI: 10.1002/9783527693924, Fuel Cells : Data, Facts and Figures, pp.334-342

[FC28] Fuel Cell Forklift Truck Development Status, Toyota Industries Corporation, 2015

[FC29] Pasdag O, Kvasnicka A, Steffen M, Heinzel A. "Highly integrated steam reforming fuel processor with condensing burner technology for maximised electrical efficiency of CHP-PEMFC systems". Energy Procedia 2012;28:57e65.

[FC30] Gandiglio M, Lanzini A, Santarelli M, Leone P. Design and optimization of a proton exchange membrane fuel cell CHP system for residential use. Energy Build 2014;69:381e93.

[FC31] Jung UH, Kim W, Koo KY, Yoon WL. "Genuine design of compact natural gas fuel processor for 1-kWe class residential proton exchange membrane fuel cell systems". Fuel Process Technol 2014;121:32e7.

[FC32] Naja B, Haghighat Mamaghani A, Baricci A, Rinaldi F, Casalegno A. Mathematical modelling and parametric study on a 30 kWel high temperature PEM fuel cell based residential micro cogeneration plant. Int J Hydrogen Energy 2015;40(3):1569e83.

[FC33] Li Zhao, Jacob Brouwer, Sean James, John Siegler, Eric Peterson, Aman Kansai and Jie Liu, "Servers Powered by a 10 kW In-Rack Proton Membrane Fuell Cell System", Proceedings of the ASME 2014 8th International Conference on Energy Sustainability & 12th Fuel Cell Science, Engineering and Technology Conference ESFuelCell2014, Boston 2014

[FC34] Jérôme Gosset, "Hydrogen Technology for Integration of Renewables", Areva

[FC35] Jérôme Gosset, "The Myrte Project: Implementating Hydrogen Energy Storage Through the GreEnergy Box", Areva, 2012

[FC36] Christophe Bidault, Serge Besse, Thomas Nietsch and Valéry Chaudron, "Electrolyser Development at Hélion/Areva", Fuell Cell Seminar & Exposition, Arizona, 2008

[FC37] José J. de Troya, Carlos Alvarez, Carlos Fernandez-Garrido, Luis Carral, "Analysing the Possibilities of Using Fuel Cells in Ships", Spain

[FC38] Christian Topete, Chen Tiankai, Tang Yu Jun, Sam Xie, "Fuel Cell Submarine"

[FC39] Franck Masset, Hycarus: Hydrogen Powered Fuel Cell Systems for non-essential cabin applications, Workshop on aeronautical applications of fuel cells and hydrogen technologies, Lampoldshausen, 2015

[FC40] James Ayre, "Daimler Bringing Electric & Hydrogen Fuel-Cell Buses to Production by 2018", March 2016

[FC41] Demonstration of 1st European Solide Oxide Fuel Cell Truck APU on a Vehicle, DESTA, June 2015

[FC42] Hussain MM, Baschuk JJ, Li X, Dincer I. "Thermodynamic analysis of A PEM fuel cell power system". International Journal of Thermal Sciences 2005;44:903e11.

[FC43] J.J. BASCHUK, Xianguo LI, « A comprehensive, consistent and systematic mathematical model of PEM fuel cells », Applied Energy 86 (2009) 181-193

[FC44] Pukrushkapan JT, Stefenopoulou AG, Peng H. 2002. "Modelling and Control for PEM Fuel cell stack system", American Control Conference, Alaska, USA, TP09e2.

[FC45] S.O. MERT, I. DINCER, Z. OZCELIK, « Performance investigation of a transportation PEM fuel cell system », International Journal of Hydrogen Energy, 37 (2012) 623-633

[FC46] Mert S. O, Dincer I, Ozcelik Z. "Exergoeconomic analysis of a vehicular PEM fuel cell system". Journal of Power Sources 2007;165(1):244e52.

[FC47] Wang L, Husar A, Zhou T, Liu H. "A parametric study of PEM fuel cell performances". International Journal of Hydrogen Energy 2003;28:1263e72.

[FC48] Ya-Xiong WANG, Kai OU, Young-Bae KIM, « Modeling and experimental validation of hybrid proton exchange membrane fuel cell-battery system for power management control", International Journal of Hydrogen Energy 40 (2015) 11713-11721

[FC49] Behzad NAJAFI, Alireza HAGHIGHAT MAMAGHANI, Andrea BARICCI, Fabio RINALDI, Andrea CASALEGNO, Mathematical modelling and parametric study on a 30 kWel high temperature PEM fuel cell based residential micro cogeneration plant, International Journal of Hydrogen Energy 40 (2015)

[FC50] Waseem SAEED, Ghaith WARKOZEK, « Modeling and Analysis of Renewable PEM Fuel Cell System », International Conference on Technologies and Materials for Renewable Energy, Environment and Sustainability, TMREES15, Energy Procedua 74 (2015) 87 – 101

[FC51] Tevfik YIGIT, Omer Faruk SELAMET, « Mathematical modeling and dynamic Simulink simuation of high-pressure PEM electrolyzer system », International Journal of Hydrogen Energy 41 (2016)

[FC52] T. T. Springer, T. A. ZAWODINSKI, S. GOTTESFELD, « Polymer Electrolyte Fuel Cell Model », Los Alamos National Laboratory, J. Electrochem. Soc., Vol. 138, No. 8, 1991

[FC53] Ay M, Midilli A, Dincer I. "Thermodynamic modelling of a proton exchange membrane fuel cell ». International Journal of Exergy 2006a; 3(1):16e44.

[FC54] Z. ABDIN, C.J. WEBB, E. MacA. GRAY, « Modelling and simulation of a proton exchange membrane (PEM) electrolyser cell », International Journal of Hydrogen Energy 40 (2015) 13243-13257

[FC55] Gia NGUYEN, Simon SAHLIN, Soren Juhl ANDREASEN, Brendan SHAFFER, Jack BROUWER, «Dynamic modeling and experimental investigation of a high temperature PEM fuel cell stack", International Journal of Hydrogen Energy 41 (2016) 4729-4739

[FC56] Kazim A. "Exergy analysis of a PEM fuel cell at variable operating conditions". Energy Conversion and Management 2004;45:1949e61.

[FC57] Adnan MIDILLI, Ibrahim DINCER, Development of some exergetic parameters for PEM fuel cells for measuring environmental impact and sustainability, International Journal of Hydrogen Energy 34 (2009)

[FC58] L. BARELLI, G. BIDINI, F. GALLORINI, A. OTTAVIANO, An energetic-exergetic comparison between PEMFC and SOFC-based micro-CHP systems, International Journal of Hydrogen Energy 36 (2011)

[FC59] L. BARELLI, G. BIDINI, F. GALLORINI, A. OTTAVIANO, « An energetic-exergetic analysis of a residential CHP system based on PEM fuel cell », Applied Energy 88 (2011) 4334-4342

[FC60] Barelli L, Bidini G, Gallorini F, Ottaviano A. "Dynamic analysis of PEMFC-based CHP systems for domestic application". Applied Energy 2012;91(1):13e28.

[FC61] Barbir F, Gomez T. "Efficiency and economics of proton exchange membrane fuel cells". International Journal of Hydrogen Energy 1997;22(10/11):121e96.

[FC62] Cownden R, Nahon M, Rosen M. "Exergy analysis of a fuel cell power system for transportation applications". Exergy An International Journal 2001;1:112e21.

[FC63] Ishihara A, Mitsushima S, Kamiyab N, Ota K. "Exergy analysis of polymer electrolyte fuel cell systems using methanol". Journal of Power Sources 2004;126:34e40.

[FC64] Mueller F, Brouwer J, Kang S, Kim H-S, Min K. Quasi-three dimensional dynamic model of a proton exchange membrane fuel cell for system and controls development. J Power Sources 2007;163(2):814e29.

[FC65] Andreasen SJ, Kær SK, "Dynamic Model of the High Temperature Proton Exchange Membrane Fuel Cell Stack Temperature". J Fuel Cell Sci Technol 2009;6(4):41006.

[FC66] Andreasen SJ, Kær SK. "Modelling and evaluation of heating strategies for high temperature polymer electrolyte membrane fuel cell stacks". Int J Hydrogen Energy 2008;33(17):4655e64.

[FC67] Zhang Y-y, Zhang Y, Li X, Cao G-y. Control design of 60 kW PEMFC generation system for residential applications. J Zhejiang Univ Sci A 2013;14(9):679e85.

[FC68] Liso V, Nielsen MP, Kær SK, Mortensen HH. Thermal modeling and temperature control of a PEM fuel cell system for forklift applications. Int J Hydrogen Energy 2014;39(16):8410e20.

[FC69] Harikishan Reddy E, Jayanti S. "Thermal management strategies for a 1 kWe stack of a high temperature proton exchange membrane fuel cell". Appl Therm Eng 2012;48:465e75.

[FC70] Supra J, Janßen H, Lehnert W, Stolten D. "Design and experimental investigation of a heat pipe supported external cooling system for HT-PEFC stacks". 2013;10(5):051002.

[FC71] Li Q, Jensen JO, Savinell RF, Bjerrum NJ. High temperature proton exchange membranes based on polybenzimidazoles for fuel cells. Prog Polym Sci 2009;34(5):449e77.

[FC72] Bent SORENSEN, « On the road performance simulation of hydrogen and hybrid cars», International Journal of Hydrogen Energy, 32 (2007) 683-686

[FC73] Jingming LIANG, Zefeng WU, "A Study of the Performance of PEMFC Hybrid Vehicle Using ADVISOR", Department of Automotive Engineerung, Guangdong Polytechnic Institute, Guangzhou, 510091, China, International Symposium on Knowledge Acquisition and Modeling (KAM 2015)

[FC74] Hydrogen Fuel Cars 1990-1998, http://www.hydrogencarsnow.com/index.php/1990-1998/

[FC75] Michael F. HORDESKI, Hydrogen & Fuel Cells : Advances in Transportation and Power, 2008

[FC76] Dr. Jesse Wainright, "Light-weight, low cost PEM Fuel Cell Stacks", Case Western Reserve University, Endura Plastics Inc, June 2008

[FC77] Olivier J. Murphy, Alan Cisar, Eric Clarke, "Low-cost light weight high power density PEM fuel cell stack", Electrochimica Acta, Volume 43, Issue 24, August 1998, Pages 3829-3840

[FC78] Intelligent Energy To Provide Fuel Cell For Peugeot Electric Cars, 2006, http://evworld.com/news.cfm?newsid=10681

[FC79] Peugeot 207 Epure, Hydrogen Cars Now, Hydrogen Cars, Vehicles and Infrastructure, http://www.hydrogencarsnow.com/index.php/peugeot-207-epure/

[FC80] Peugeot Citroen H2Origin Fuel Cell Delivery Van, Hydrogen Cars Now, Hydrogen Cars, Vehicles and Infrastructure, http://www.hydrogencarsnow.com/index.php/peugeot-h2origin/

[FC81] Toyota FCHV Hydrogen Hybrid Vehicle, http://www.hydrogencarsnow.com/index.php/toyota-fchv/

[FC82] Mercedes-Benz GLC plug-in hydrogen fuel-cell coming in 2017, Daimler worked with Ford to shrink the size of the fuel-cell stack. http://www.autoblog.com/2016/06/13/mercedes-benz-glc-plug-in-hydrogen-fuel-cell-coming-in-2017/

[FC83] Sarah SHELTON, « Audi Is Ready To Produce Fuel Cell Vehicles », HybridCARS Auto alternatives for the 21th century, November 2015

[FC84] Audi developing a hybrid fuel cell drivetrain on a Q5-based prototype that combines a hydrogen-powered car with a hybrid set up that includes a 1.3 kWh lithium-ion battery, 2011

[FC85] BMW 5 Series GT Fuel Cell concept review, http://www.autocar.co.uk/car-review/bmw/5-series-gran-turismo/first-drives/bmw-5-series-gt-fuel-cell-concept-review

[FC86] [Kia Borrego FCEV, Hydrogen Cars Now, Hydrogen Cars, Vehicles and Infrastructure, http://www.hydrogencarsnow.com/index.php/kia-borrego-fcev/

[FC87] GM selects Quantum Fuel Systems to produce H2 storage for Equinox Fuel-Cell Fleet, http://www.autoblog.com/2006/11/06/gm-selects-quantum-fuel-systems-to-produce-h2-storage-for-equino, Nov 6th 2006

[FC88] Dean SLAVNICH, « General Motors is standing firm on its fuel cell investments, as seen during a rececent trip to the company's advanced R&D site in Germany », Fuel Cells, Electric & Hybrid Vehicle technology International, July 2011

[FC89] Mazda 5 / Premacy Hydrogen RE Hybrid Minivan, Hydrogen Cars Now, Hydrogen Cars, Vehicles and Infrastructure, http://www.hydrogencarsnow.com/index.php/mazda-5-premacy/

[FC90] Morgan LIFECar Geneva Concept, http://www.motorauthority.com/news/1025002_new-details-morgan-lifecar-geneva-concept#image=100215297

[FC91] Renault Scenic ZEV H2, Hydrogen Cars Now, Hydrogen Cars, Vehicles and Infrastructure, http://www.hydrogencarsnow.com/index.php/renault-scenic-zev-h2/

[FC92] Suzuki SX4 Fuel-Cell Vehicle Concept, http://www.caranddriver.com/news/suzuki-sx4-fuel-cell-vehicle-concept-auto-shows

[FC93] VW Golf SportWagen, HyMotion Concept FCV, http://www.hydrogencarsnow.com/index.php/vw-golf-hymotion/

[FC94] Volkswagen Touran HyMotion, http://www.hydrogencarsnow.com/index.php/vw-touran-hymotion/

[FC95] Volkswagen Tiguan HyMotion, http://www.hydrogencarsnow.com/index.php/vw-tiguan-hymotion/

[FC96] M. Ahman, Primary energy efficiency of alternative powertrains in vehicles, Energy, 26 (11) (2001)

[FC97] A. Schafer, J. B. Heywood, and M. A. Weiss, "Future fuel cell and internal combustion engine automobile technologies: A 25-year life cycle and fleet impact assessment", Energy, 31 (12) (2006) 2064- 2087.

Chapter 2

[2.1] History of Chrysler Corporation Gas Turbine Vehicles, Chrysler Corporation, January 1979.

[2.2] Huebner G Jr. The Chrysler regenerative turbine-powered passenger car. Society of Automotive Engineers, In: *Automotive Engineering Congress and Exposition*, Detroit, January 13-17, 1964.

[2.3] Cunha H. Investigation of the Potential of Gas Turbines for Vehicular Applications. Chalmers University of Technology, Gothenburg, Sweden, Master's thesis 2011.

[2.4] Capata R, Coccia A and Lora M. A Poposal for CO_2 abatement in urban areas: the UDR1 - Lethe Turbo-Hybrid Vehicle. University of Roma 1 "La Sapienza", Italy, *Energies* ISSN 1996-1073.

[2.5] Davidson J and Keeley R. The thermodynamics of practical combined cycles. In: *Proc. Instn. Mech. Engrs*. Conference on Combined Cycle Gas Turbines, 28-50, 1991.

[2.6] Briesch S, Bannister L, Dinkunchak S. and Huber J. A combined cycle designed to achieve greater than 60% efficiency. ASME J. Eng Gas Turbines Power 117(1), 734-741, 1995.

[2.7] Nada T. Performance Characterization of different configurations of gas turbine engines. Propulsion and Power Research, September 2014.

[2.8] Patil M, Pawase D and Deore E. Thermal performance of reheat regenerative intercooled gas turbine cycle. IJRMET Vol. 5, May-October 2015.

[2.9] Bhargava R, Bianchi M, De Pascale A et al. Gas turbine based power cycles – A state-of-the-art review. In: *International Conference on Power Engineering*. Hangzhou, China, 2007.

[2.10] Dellenback P. Improved gas turbine efficiency through alternative regenerator configuration. In: *J. of Eng. for Gas Turbines and Power*, Vol. 124, pp 441-446, 2002.

[2.11] Pathiranthna K. Gas turbine thermodynamic and performance analysis methods using available catalog data. University of Gävle, Faculty of engineering and sustainable development, October 2013.

[2.12] El-Masri M. A modified high efficiency recuperated gas turbine cycle. In: *Journal of Eng for Gas Turbines and Power.* Vol. 110, pp 233-242, 1988.

[2.13] El-Masri M. Thermodynamics and performance projections for intercooled / reheat / recuperated gas turbine systems. ASME Paper No. 87-GT-108, 1987.

[2.14] Cheng D and Nelson A. The chronological development of the Cheng cycle steam injected gas turbine during the past 25 years. ASME Paper No. GT-2002-30119, 2002.

[2.15] Kulshreshtha D and Mehta S. Exergy Analysis of a Regenerative Micro Gas Turbine Engine. In: *Proceedings of ICFD 10: Tenth International Congress of Fluid Dynamics.* December 16-19, 2010.

[2.16] Sirignano W and Liu F. Performance increase for gas-turbine engines through combustion inside the turbine. In: *Journal of Propulsion and Power.* Vol.15, No. 1, January - February 1999.

[2.17] Andriani R, Gamma F and Ghezzi U. Main effects of intercooling and regeneration on aeronautical gas turbine engines. In: *46th AIAA/ASME/SAE/ASEE Joint Propulsion Conference & Exhibit.* Nashville, TN, 25 - 28 July 2010.

[2.18] Christodoulou F, Giannakakis P and Kalfas A. Performance benefits of a portable hybrid micro-gas-turbine power system for automotive applications. In: *Proceedings of ASME Turbo Expo 2010: Power for Land, Sea, and Air*. GT2010-23248, 2010.

[2.19] Capata R, Sciubba E and Toro C. The gas turbine hybrid vehicle LETHE at UDR1: The on-board innovative ORC energy recovery system – feasibility analysis. In: *Proceedings of the International Mechanical Engineering Conference & Exposition,* Houston, Texas, 2012.

[2.20] Shah B, Mazuir R, McGordon et al. Micro gas turbine range extender – validation techniques for automotive applications. In: *4th Hybrid Electric Vehicle Conference*, London, United Kingdom, 2013.

[2.21] Mackay R. Development of a 24 kW gas turbine-driven generator set for hybrid vehicles. In: *International congress and exposition,* Detroit, Michigan*,* SAE technical paper series, 940510, 1994.

[2.22] Leontopoulos C, Etemad M, Pullen R and Lamperth M. Hybrid Vehicle simulation for a turbogenerator based power-train. *Proceedings of the Institution of Mechanical Engineers*. Part D: *Journal of Automobile Engineering*, Vol 212, pp 357-368, 1998.

[2.23] Lampérth U, Pullen K and Mueller K. Turbogenerator based hybrid versus dieselelectric hybrid-A parametric optimization simulation study. In: *2000 Future Transportation Technology Conference*, Costa Mesa, California, SAE Paper No. 2000-01-3100, 2000.

[2.24] Juhasz A. Automotive gas turbine power system - Performance analysis code. *In: the 1997 International Congress and Exposition.* Lewis Research Center, NASA Technical Memorandum 107386, 1997.

[2.25] Mansour C. Trip-based optimization methodology for a rule-based energy management strategy using a global optimization routine: the case of the Prius plug-in hybrid electric vehicle. In: *Proceedings of the Institution of Mechanical Engineers*. Part D: *Journal of Automobile Engineering*, Vol 230, Issue 11, pp. 1529 – 1545, 2015.

[2.26] Mansour C. Optimized energy management control for the Toyota Hybrid system using dynamic programming on a predicted route with short computation time. *In: International Journal of Automotive Technology.* Paper N° 220100321, vol.13, No. 2, 2012.

[2.27] Breque, F., 2017. Cabin Thermal Needs : Modeling and Assumption Analysis, in: International Modelica Conference. Prague, Czech Republic.

[2.28] Johannes Liebl, Stephan Neugebauer, Andreas Eder, Matthhias Linde, Boris Mazar, Wolfgang Stütz, "The Thermoelectric Generator from BMW is Making Use of Waste Heat", MTZ 01/2009, Volume 70

[2.29] Weather data. Retrieved from National Renewable Energy Laboratory: https://sam.nrel.gov/weather

[2.30] Sonntag R and Borgnakke R. Fundamentals of Thermodynamics, Sixth Edition, 2003, p.411-423.

[2.31] Moran M and Shapiro H. Fundamentals of engineering thermodynamics. 5th Edition – 2006, p.303-308.

[2.32] Hadid Z and Zoughaib A. Exergy recovery during LNG gasification using ambient air as heat source, In: *Proceedings of Ecos 2016 – The 29th international conference on efficiency, cost, optimization, simulation and environmental impact of energy systems.* Portoroz, Slovenia, June 19-23, 2016.

[2.33] Dev N and Attri R. Exergetic analysis of a combustion chamber of a combined heat and power system. In: *Proceedings of the National Conference on Trends and Advances in Mechanical Engineering.* YMCA University of Science & Technology, Faridabad, Haryana, Oct 19-20, 2012.

[2.34] Datta A and Som S. Energy and exergy balance in a gas turbine combustor. J Power Energy - Proc Inst Mech Eng, 213:23–32, 1999.

[2.35] Jubleh N. Exergy analysis and second law efficiency of a regenerative brayton cycle with isothermal Heat Addition. Entropy ISSN 1099-4300, 2005.

[2.36] Linnemann C and CONEY M. The isoengine: realization of a high efficiency power cycle based on isothermal compression. In: *International Journal of Energy Technology and Policy*, Vol. 3, 2005.

[2.37] Deb K, Pratap A, Agarwal S et al. A fast and elitist multiobjective Genetic Algorithm: NSGA-II. In: *IEEE Transactions on evolutionary computation*, Vol. 6, No. 2, APRIL 2002.

[2.38] Wissam Bou Nader, Charbel Mansour, Olivier Guezet and Maroun Nemer, « exergo-technological explicit methodology for gas-turbine system optimization for series hybrid electric vehicles », Journal of Automobile Engineering, Part D, JAUTO-17-0072.

[2.39] Charbel Mansour, Wissam Bou Nader, Florent Breque, Marc Haddad and Maroun Nemer, Assessing additional fuel consumption from cabin thermal comfort and auxiliary needs on the worldwide harmonized light vehicles test cycle, Transportation Research Part D, 2018

[2.40] Wang, Shu Jun, Gu, Jun Jie, 2004. Experimental analysis of an automotive air conditioning system with two-phase flow measurements. In: International Refrigeration and Air Conditioning Conference.

Chapter 3

[3.1] Technical Information Engineering office. History of Chrysler Corporation gas turbine vehicles. Report, Chrysler Corporation, Auburn Mills, Michigan, USA,January 1979.

[3.2] Huebner GJ Jr. The Chrysler regenerative turbine powered passenger car. SAE paper 640414, 1964.

[3.3] Cunha HE. Investigation of the potential of gas turbines for vehicular applications. Master's Thesis, Chalmers University of Technology, Gothenburg, Sweden, 2011.

[3.4] Capata R, Coccia A and Lora M. A proposal for CO2 abatement in urban areas: the UDR1–Lethe_ turbohybrid vehicle. Energies 2011; 4(3): 368–388.

[3.5] Wissam Bou Nader, Charbel Mansour, Maroun Nemer and Olivier Guezet, Exergo-technological explicit methodology for gas-turbine system optimization of series hybrid electric vehicles, Journal of automobile Engineering, 2017.

[3.6] Shah RMRA, McGordon A, Amor-Segan M and JenningsP. Micro gas turbine range extender – validation techniques for automotive applications. In: 4th hybrid and electric vehicles conference, London, UK, 6–7 November 2013, pp. 1–6. Stevenage, Hertfordshire: IET.

[3.7] Leontopoulos C, Etemad MR, Pullen KR and Lamperth MU. Hybrid vehicle simulation for a turbogenerator based power-train. Proc IMechE Part D: J Automobile Engineering 1998; 212(5): 357–368.

[3.8] Lampe´ rth MU, Pullen KR and Mueller KG. Turbogenerator based hybrid versus dieselelectric hybrid – a parametric optimization simulation study. SAE paper 2000-01-3100, 2000.

[3.9] Mackay R. Development of a 24 kW gas turbine-driven generator set for hybrid vehicles. SAE paper 940510, 1994.

[3.10] Anrico Casadei and Richard Broda, Impact of Vehicle Weight Reduction on Fuel Economy for Various Vehicle Architectures, Ricardo, Research Report, 2008.

[3.11] Richard B. Carlson and Jim Francfort, Vehicle Mass Impact on Vehicle Losses and Fuel Economy, U.S. Department of Energy, Energy Efficiency and Renewable Energy, 2012.

[3.12] Wamei lin and Bengt Sunden, Vehicle Cooling Systems for Reducing Fuel Consumption and Carbon Dioxide : Literature Survey, SAE International, SAE Technical Paper, 2010.

[3.13] Samuel Swedenborg, Modeling and Simuation of Cooling System for Fuel Cell Vehicle, Uppsala Universitet, 2017.

[3.14] W. A. Sirignano and F. Liu, Performance Increases for Gas-Turbine Engines Through Combustion Inside the Turbine, Journal Of Propulsion and Power, Vol. 15, no. 1 (1999), pp. 111-118.

[3.15] R. Sivakumar, B. L. Mordike, High temperature coatings for gas turbine blades : A review, Surface and Coatings Technology, Volume 37, Issue 2, April 1989, Pages 139-160.

[3.16] Nada T. Performance characterization of different configurations of gas turbine engines. Propulsion and Power Research 2014; 3(3): 121–132.

[3.17] Patil MS, Pawase DB and Deore ER. Thermal performance of reheat, regenerative, intercooled gas turbine cycle. IJRMET 2015; 5 (2).

[3.18] Bhargava RK, Bianchi M, De Pascale A et al. Gas turbine based power cycles – a state-of-the-art review. In: Challenges of power engineering and environment, International conference on power engineering, angzhou, People's Republic of China, October 2007, pp. 23–27. Berlin: Springer.

[3.19] Dellenback PA. Improved gas turbine efficiency through alternative regenerator configuration. Trans ASME, J Eng Gas Turbines Power 2002; 124(3): 441–446.

[3.20] Charbel Mansour, Wissam Bou Nader, Florent Breque, Marc Haddad and Maroun Nemer, Assessing additional fuel consumption from cabin thermal comfort and auxiliary needs on the worldwide harmonized light vehicles test cycle, Transportation research Part D, 2018.

[3.21] G. Morrison and J.S. Gallagher, Refprop : A Thermodynamic Properties Software Program for Refrigerants and Their Mixtures, International Refrigeration and Air Conditioning Conference, Purdue University, 1990.

[3.22] Deb K, Pratap A, Agarwal S and Meyarivan T. A fast and elitist multiobjective genetic algorithm: NSGA-II. IEEE Trans Evolution Comput 2002; 6(2): 182–197.

[3.23] Meherwan P. BOYCE, "Gas Turbine Engineering Handbook", Second Edition, Butterworth-Heinemann, 2002

[3.24] P. Walsh and P. Fletcher. Gas Turbine Performance. Blackwell Publishing, 2004. isbn: 0-632-06434-X.

[3.25] H. COHEN, GFC. ROGERS, HIH. SARAVANAMUTTOO, "Gas Turbine Theory", 4th Edition, Longman Group Limited, 1996

[3.26] K.A.B. PATHIRANTHNA, "Gas Turbine Thermodynamic and Performance Analysis Methods using available catalog data", October 2013, University of Gävle, Faculty of engineering and sustainable development.

[3.27] R.C. HENDRICKS, D.T. SHOUSE, W.M. ROQUEMORE, "Water Injected Turbomachinery", NASA/TM – 2005-212632, ISROMAC10-2004-039

[3.28] R. PAVRI, G. D. MOORE, « Gas Turbine Emissions and Control », GE Energy Services, Atlanta, GA

[3.29] Alternative Control Techniques Document - NOx Emissions from Stationary Gas Turbines, U.S Environmental Protection Agency, Emission Standards Division

[3.30] K. SUNDSBO ALNE, Reduction of Nox Emissions from the Gas Turbines for Skarv Idun, Master of Science in Energy and Environment, NTNY Innovation and Creativity, June 2007

[3.31] J. W BURNS, D. J. COOPER, Active NOX Control of Cogen Gas Turbine Exhaust using a Nonlinear Feed Forward with Cascade Architecture, University of Connecticut, Storrs, CT 06269

[3.32] M. SCHORR, J. CHALFIN, Gas Turbine Nox Emissions Approaching Zero – Is it worth the price ?, General Electric Power Systems, Schenectady, New York

[3.33] Philip Kiameh, Power Generation Handbook, Second Edition, Chapter 12 : Gas Turbine Combustors, 2012.

[3.34] E. CANLI, S. DARICI, M. OZGOREN, « Intercooler Effect on Conventional Supercharging Systems », International Scientific Conference, 19-20 November 2010, GABROVO

[3.35] K. BILEN, « Intercooler Design for a Diesel Engine with Turbocharger », Kirikkale University, Turkey, 1998

[3.36] Tubocharger Technology and IC Engines Boosting, IFP Course for Energy and Engine Program

[3.37] S. SULLIVAN, X. ZHANG, A. A. AYON, J. BRISSON, « Demonstration of a microscale heat exchanger for a silicon micro gas turbine engine », The 11th International Conference on Solid-State Sensors and Actuators, (2001)

[3.38] Wrightspeed unveils new turbine range extender for medium- and heavy-duty electric powertrains; 30% more efficient than current microturbine generators, Green Car Congress, 4 May 2015

[3.39] R.K. Shah, Compact Heat Exchangers for Microturbines, Proceedings of Fifth International Conference on enhanced, Compact and Ultra-Compact Heat Exchangers: Science, Engineering and Technology, USA, 2005

[3.40] S. SULLIVAN, "Development and Testing of Microscale Silicon Heat Exchangers for the MIT Micro Gas-Turbine Engine", B.S. Mechanical Engineering (1998), Renseelaer Polytechnic Institute.

[3.41] Y. RIBAUD, C. MISCHEL, "Study and Experiments of a Small Radial Turbine for Auxiliary Power Units", The American Society of Mechanical Engineers, 1986, 86-GT-23.

[3.42] H. HIERETH, P. PRENNINGER, "Charging the Internal Combustion Engine", Springer-Verlag, 2007

[3.43] ML CMD IR 2013 – Dépollution Diesel – G. Ballesteros – IFPEN

[3.43] Garett Turbocharger Guide, Volume 4

[3.44] http://www.turbos.bwauto.com/aftermarket/downloads.aspx?doctype=16

[3.45] https://www.garrettmotion.com/turbocharger-technology/gasoline-turbochargers/

[3.46] http://www.mtiracing.com/air-fuel-delivery/superchargers-turbo.html

[3.47] McDonald, C. F., 2003, "Recuperator Considerations for Future Higher Efficiency Microturbines," Appl. Therm. Eng., 23(12), pp. 1463–1487.

[3.48] Manglik, R. M., and Bergles, A. E., 1995, "Heat Transfer and Pressure Drop Correlations for the Rectangular Offset Strip Fin Compact Heat Exchanger," Exp. Therm. Fluid Sci., 10(2), pp. 171–180.

[3.49] Chang, Y., and Wang, C. A., 1997, "Generalized Heat Transfer Correlation for Louver Fin Geometry," Int. J. Heat Mass Transfer, 40(3), pp. 533–544.

[3.50] Chang, Y., Hsu, K., Lin, Y., and Wang, C., 2000, "A Generalized Friction Correlation for Louver Fin Geometry," Int. J. Heat Mass Transfer, 43(12), pp. 2237–2243.

[3.51] Traverso, A., and Massardo, A. F., 2005, "Optimal Design of Compact Recuperators for Microturbine Application," Appl. Therm. Eng., 25(14), pp. 2054–2071.

[3.52] Qiuwang, W., Hongxia, L., Gongnan, X., Min, Z., Laiqin, L., and ZhenPing, F., 2007, "Genetic Algorithm Optimization for Primary Surfaces Recuperator of Microturbine," ASME J. Eng. Gas Turbines Power, 129(2), pp. 436–442.

[3.53] Wen, J., Yang, H., Tong, X., Li, K., Wang, S., and Li, Y., 2016, "Optimization Investigation on Configuration Parameters of Serrated Fin in Plate-Fin Heat Exchanger Using Genetic Algorithm," Int. J. Therm. Sci., 101, pp. 116–125.

[3.54] Peng, H., and Ling, X., 2008, "Optimal Design Approach for the Plate-Fin Heat Exchangers Using Neural Networks Cooperated With Genetic Algorithms," Appl. Therm. Eng., 28(5), pp. 642–650.

[3.55] Sanaye, S., and Hajabdollahi, H., 2010, "Thermal-Economic Multi-Objective Optimization of Plate Fin Heat Exchanger Using Genetic Algorithm," Appl. Energy, 87(6), pp. 1893–1902.

[3.56] Ahmadi, P., Hajabdollahi, H., and Dincer, I., 2011, "Cost and Entropy Generation Minimization of a Cross-Flow Plate Fin Heat Exchanger Using Multi-Objective Genetic Algorithm," ASME J. Heat Transfer, 133(2), p. 021801.

[3.57] Zhang, L., Yang, C., and Zhou, J., 2010, "A Distributed Parameter Model and its Application in Optimizing the Plate-Fin Heat Exchanger Based on the Minimum Entropy Generation," Int. J. Therm. Sci., 49(8), pp. 1427–1436.

[3.58] Dong, J., Chen, J., Chen, Z., Zhang, W., and Zhou, Y., 2007, "Heat Transfer and Pressure Drop Correlations for the Multi-Louvered Fin Compact Heat Exchangers," Energy Convers. Manage., 48(5), pp. 1506–1515.

[3.59] K V Ramana Murthy, C Ranganayakulu and T P Ashok Babu, Development of Heat Transfer Coefficient and Friction Factor Correlations for Serrated Fins in Water Medium using CFD, Journla of Physical Science and Application, 2015, doi: 10.17265/2159-5348/2015.03.010

[3.60] Min-Soo Kim, Jonghyeok Lee, Se-Jin Yook and Kwan-Soo Lee, Correlations and optimization of a heat exchanger with offset-strip fins, International Journal of Heat and Mass Transfer, 2011

[3.61] Ramesh K. Shah and Dusan P. Sekulic, Fundamentals of Heat Exchanger Design, John Wiley & Sons, Inc, 2003

[3.62] Frank P. Incropera, David P. Dewitt, Theodore L. Bergman and Adrienne S. Lavine, Fundamentals of Heat and Mass Transfer, Sixth Edition, 2007

[3.63] L. Austrin, M. Torabzadeh-Tari and G. Engdahl, A New High Power Density Generation System, 25th International Congress of the Aeronautical Sciences, ICAS 2006

[3.64] James Borg Bartolo, He Zhang, David Gerada and L. De Lillo, High Speed Electrical Generators, Applications, Materials and Design, Electrical Machines Design Control and Diagnosis, IEEE, 2013

[3.65] Martin Van der Geest, Henk Polinder, Jan Abraham Ferreira and Markus Christmann, Power Density Limits and Design Trends of High-Speed Permanent Magnet Synchronous Machines, IEEE Transactions on Transportation Electrification, 2015

[3.66] Wissam Bou Nader, Charbel Mansour; Maroun Nemer, Optimization of a Brayton External Combustion Gas-Turbine system for Extended Range Electric Vehicles, Energy, 2018

[3.67] Wissam Bou Nader, Charbel Mansour, Clément Dumand and Maroun Nemer, Brayton Cycles as Waste Heat Recovery Systems on Series Hybrid Electric Vehicles, Energy conversion and Management, 2018.

[3.68] Deb K, Pratap A, Agarwal S et al. A fast and elitist multiobjective Genetic Algorithm: NSGA-II. In: IEEE Transactions on evolutionary computation, Vol. 6, No. 2, APRIL 2002.

[3.69] Sundstrom O and Guzzella L. A generic dynamic programming Matlab function. In: 2009 IEEE control applications & intelligent control, St Petersburg, Russia, 8–10 July 2009, pp. 1625–1630. New York: IEEE.

Chapter 4

[4.1] Wissam Bou Nader, Charbel Mansour, Maroun Nemer and Olivier Guezet, Exergo-technological explicit methodology for gas-turbine system optimization of series hybrid electric vehicles, Journal of Automobile Engineering, 2017

[4.2] History of Chrysler Corporation Gas Turbine Vehicles, Chrysler Corporation, January 1979

[4.3] H. CUNHA, "Investigation of the Potential of Gas Turbines for Vehicular Applications", Chalmers, Department of Applied Mechanics, Division of Fluid Dynamics, CHALMERS UNIVERSITY OF TECHNOLOGY Gothenburg, Sweden 2011, Master's thesis 2011:43

[4.4] Charbel Mansour, Wissam Bou Nader, Florent Breque, Marc Haddad and Maroun Nemer, Assessing additional fuel consumption from cabin thermal comfort and auxiliary needs on the worldwide harmonized light vehicles test cycle, Transportation Research Part D, 2018

[4.5] R. K. Bhargava, M. Bianchi, A. De Pascale, G. Negri di Montenegro and A. Peretto, "Gas turbine Based Power Cycles – A State-of-the-Art Review", International Conference on Power Engineering, Hangzhou, China, 2007.

[4.6] Christophe COTTARD, Peugeot 406 Hybrid, PSA PEUGEOT CITROËN

[4.7] John Excell, "This Week in 1965 – The Rover-BRM gas turbine car", 2013

[4.8] Wissam Bou Nader, Charbel Mansour and Maroun Nemer, Optimization of Brayton external combustion gas-turbine system for extended range electric vehicles, Energy, 2018

[4.9] Mansour C. Trip-based optimization methodology for a rule-based energy management strategy using a global optimization routine: the case of the Prius plug-in hybrid electric vehicle. In: *Proceedings of the Institution of Mechanical Engineers*. Part D: *Journal of Automobile Engineering*, Vol 230, Issue 11, pp. 1529 – 1545, 2015.

[4.10] Mansour C. Optimized energy management control for the Toyota Hybrid system using dynamic programming on a predicted route with short computation time. In: International Journal of Automotive Technology. Paper N° 220100321, vol.13, No. 2, 2012.

[4.11] Youssef Mazloum, Haytham Sayah and Maroun Nemer, Static and Dynamic Modeling Comparison of an Adiabatic Compressed Air Energy Storage System, Journal of Energy Resources Technology, November 2016.

[4.12] Youssef Mazloum, Haytham Sayah and Maroun Nemer, Dynamic modelling and simulation of an Isobaric Adiabatic Compressed Air Energy Storage (IA-CAES) system, Journal of Energy Storage, 2017

[4.13] S. M. Camporeale, B. Fortunato and M. Mastrovito, A Modular Code for Real Time Dynamic Simulation of Gas Turbines in Simulink, Journal of Engineering for Gas turbine and Power, Volume 128, 2002

[4.14] A. Hussain and H. Seifi, Dynamic Modeling of a Single Shaft Gas Turbine, IFAC Control of Power Plants and Power Systems, Munich, Germany, 1992

[4.15] Samson Endale Turie, Gas Turbine Plant Modeling for Dynamic Simulation, Master of Science Thesis, KTH School of Industrial Engineering and Management, October 2011

[4.16] Eshwarprasad Thirunavukarasu, Modeling and Simulation Study of a Dynamic Gas Turbine System in a Virtual Test Bed Environment, Master's thesis, University of South Carolina, 2013

[4.17] J. H. Kim, T. W. Song, T. S. Kim and S. T. Ro, Dynamic Simulation of Full Start-Up Procedure of Heavy Duty Gas Turbines, ASME Proceedings, Controls, Diagnostics and Instrumentation, 2001

[4.18] K. K. Botros, P. J. Campbell and D. B. MAH, Dynamic Simulation of Compressor Station Operation Including Centrifugal Compressor & Gas turbine, The American Society of Mechanical Engineers (ASME), 1990

[4.19] M. T. Schobeiri, M. Attia and C. Lippke, GETRAN: A Generic, Modularly Structured Computer Code for Simulation of Dynamic Behavior of Aero and Poer Generation Gas Turbine Engines, Journal of Engineering for Gas Turbine and Power, 2008

[4.20] Cengel Y and Boles M, Thermodynamics: an engineering Approach, 5th Edition p.517-521

[4.21] Sonntag R and Borgnakke R. Fundamentals of Thermodynamics, Sixth Edition, 2003, p.411-423.

[4.22] Moran M and Shapiro H. Fundamentals of engineering thermodynamics. 5th Edition – 2006, p.404-414.

[4.23] Mehrdad EHSANI, Yimin GAO, Ali EMADI, « Modern Electric, Hybrid Electric, and Fuel Cell Vehicles » – Fundamentals, Therory, and Design – Second Edition.

[4.24] Chris MI, M. ABDUL MASRUR, David WENZHONG GAO, « Hybrid Electric Vehicles » - Principles and Applications with Practical Perspectives, WILEY, 2011

[4.25] Wissam Bou Nader, Charbel Mansour, Clément Dumand and Maroun Nemer, Brayton cycles as waste heat recovery systems on series hybrid electric vehicles, Energy Conversion and Management, 2018

[4.26] Ernesto Benini and Nageswara Rao Muktinutalapati, Advances in Gas Turbine Technology, chapter 13: Materials for Gas Turbines – An Overview, 2011

[4.27] Deb K, Pratap A, Agarwal S et al. A fast and elitist multiobjective Genetic Algorithm: NSGA-II. In: IEEE Transactions on evolutionary computation, Vol. 6, No. 2, APRIL 2002.7

[4.28] Sundstrom O and Guzzella L. A generic dynamic programming Matlab function. In: 2009 IEEE control applications & intelligent control, St Petersburg, Russia, 8–10 July 2009, pp. 1625–1630. New York: IEEE.

[4.29] Y.P.B. Yeung, K.W.E. Cheng, W.W.Chan, .Y.Lam, W.F.Choi and T.W.Ng, Automobile Hybrid Air Conditioning Technology, 3rd International Conference on Power Electronics Systems and Applications, 2009

[4.30] J.H. Kim, T.W. Song, T.S. kim, S.T. Ro, Model Development and Simulation of Transient Behavior of Heavy Duty Gas Turbines, Journal of Engineering for Gas Turbines and Power, July 2001, Vol. 123/589

[4.31] Jin Eun Chung, Jae Woo Chung, Nam Ho Kim, Sang Woom Lee and Gi Yong Kim, An Investigation on the Efficiency Correction Method of the Turbocharger at Low Speed, energies, 2018

[4.32] Schorn, N.A. The Radial Turbine for Small Turbocharger Applications: Evoluation and Analytical Methods for Twin-Entry Turbine Turbochargers; SAE Technical Paper No. 2014-01-1647; SAE International: Warrendale, PA, USA, 2014.

[4.33] Serrano, J.R.; Guardiola, C.; Dolz, V.; Tiseira, A.; Cervelló, C. Experimental Study of the Turbine Inlet Gas Temperature Influence on Turbocharger Performance; SAE International: Warrendale, PA, USA, 2013.

[4.34] Peyman Maghsoudi, Sadegh Sadeghi and Pedram Hanafizadeh, Thermoeconomic Optimization and Comparison of Plate-Fin Heat Exchangers Using Louver, Offset Strip, Triangular and Rectangular Fins Applied in 200kW Microturbines, Journal of Heat Transfer, 2017.

[4.35] Qi Li, Gilles Flamant, Xigang Yuan, Pierre Neveu and Lingai Luo, Compact heat exchangers: A review and future applications for a new generation of high temperature solar receivers, Renewable and Sustainable Energy Reviews, 2011

[4.36] Yinhai Zhu and Yanzhong Li, Three-Dimensional Numerical Simulation on the Laminar Flow and Heat Transfer in Four Basic Fins of Plate-Fin Heat Exchangers, Journal of Heat Transfer, 2008.

[4.37] F. INCROPERA, D. Dewitt, Fundamentals of Heat and Mass Transfer, vol. 886, School of mechanical engineering, Perdue University, 1996, pp. 420–515.

[4.38] R.K. Shah, M. Ishizuka, T.M. Rudy and V.V. Wadekar, Compact Heat Exchangers for Microturbines, Proceedings of Fifth International Conference on Enhanced, Compact and Ultra-Compat Heat Exchangers: Science, Engineering and Technology, 2005.

[4.39] I.E. IDELCHIK, 3rd edition, Handbook of Hydraulic Resistance, vol. 788(1993) , pp. 75–87.

[4.40] Dassault systems, the Official Web Site of Dymola. http://www.3ds.com/ products-services/catia/capabilities/modelica-systems-simulation-info/ dymola.

[4.41] Cooper, J. R., and Dooley, R. B., 2007, "Release on the Ionization Constant of H2O," The International Association for the Properties of Water and Steam, Lucerne, Switzerland.

[4.42] McBride, B. J., Zehe, M. J., and Gordon, S., 2002, "NASA Glenn Coefficients for Calculating Thermodynamic Properties of Individual Species," NASA Glenn Research Center, Cleveland, OH, Report No. TP-2002-211556.

[4.43] Micro Gas turbine Technology, Research and Development for European Collaboration, https://etn.global/wp-content/uploads/2018/02/MGT-Technology-Summary-final-for-the-website.pdf

[4.44] T. Bayar, "Microturbines take on the market," Cogeneration & on-site power production, pp. 21-24, October 2015.

[4.45] Wrightspeed unveils new turbine range extender for medium- and heavy-duty electric powertrains; 30% more efficient than current microturbine generators, Green Car Congress, 2015

Annex 1

[A.1.1] Nikhil DEV, Rajesh ATTRI, Exergetic Analysis of Combustion Chamber of a Combined Heat and Power System, YMCA University of Science & Technology, Faridabad, Haryana, India

[A.1.2] Michael J. MORAN, Howard N. SHAPIRO, Fundamentals of Engineering Thermodynamics – 2006

[A.1.3] S. HADA, K. TAKATA, Y. IWASAKI, M. YURI, J. MASADA, High-efficiency Gas Turbine Development applying 1600°C class "J" Technology, Mitsubishi Heavy Industries Technical Review Vol. 52 No. 2 (June 2015)

Annex 1: Evaluation of fuel availability

In order to study the different energy converters, and to position them in terms of effiency relative to fuel availability, it is mandatory to perform exergetic calculation to evaluate the maximum potential of work when fuel is oxidized, and to evaluate the exergy losses depending on combustion parameters such as the temperature and the air-fuel ratio among others [A.1.1]. The study starts by presenting the calculation's method as shown in the figure A.1.1. Then, the different exergy equations are described and are used to evaluate the adiabatic flame temperature, the thermo mechanical exergy, the chemical exergy and the total exergy for two selected fuel: (1) the methane and (2) the octane.
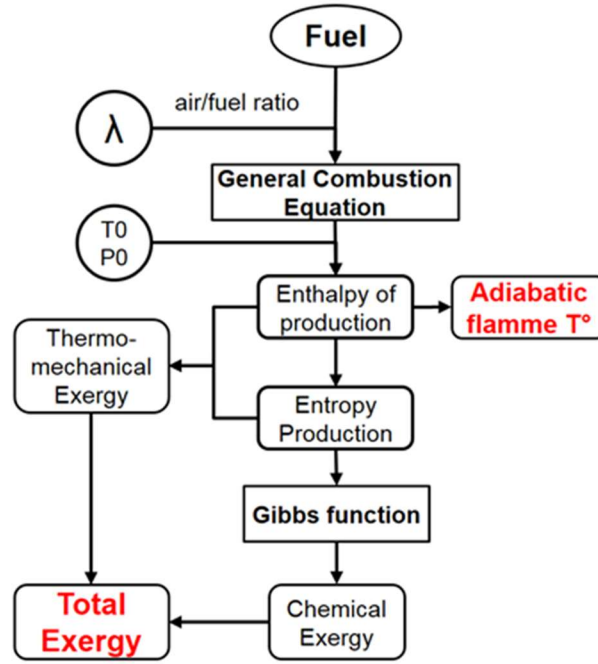
Fig A.1.1 : Method for calculating the adiabatic flame temperature, the thermo-mechanical Exergy, the chemical exergy and the total Exergy

For a given fuel with air as oxidizer, the general combustion equation can be written knowing the chemical composition of fuel and the air fuel ratio, as well as the air composition which is supposed to be with the following ratios: 3.76 moles of Nitrogen for each 1 mole of Oxygen.

$$C_aH_b + \lambda\left(a + \frac{b}{4}\right)(O_2 + 3.76N_2)$$
$$\Longrightarrow aCO_2 + \frac{b}{2}H_2O + (\lambda - 1)(a + \frac{b}{4})O_2 + \lambda\left(a + \frac{b}{4}\right)3.76N_2 \tag{A.1.1}$$
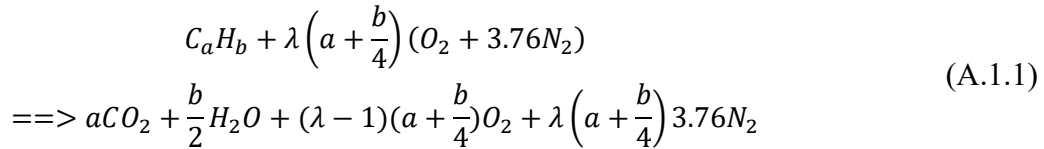
Where the excess of air coefficient λ is defined as:

$$\lambda = \frac{(\frac{moles\ of\ air}{moles\ of\ fuel})_{real}}{(\frac{moles\ of\ air}{moles\ of\ fuel})_{theoretical}} \tag{A.1.2}$$

When reference environmental temperature and pressure are defined (T0, P0), the enthalpy of production is calculated by applying the 1st law of thermodynamic for a control volume by considering that no heat transfer occurs, no work is done and by neglecting the kinetic and the potential energy. Using thermodynamic tables [A.1.2] and iteration calculations, we can estimate therefore the adiabatic flame temperature. Applying the 2nd law of thermodynamic for the same control volume, we can calculate the entropy production, and we can find the thermo mechanical exergy. Knowing the different species, we can calculate then, using the Gibbs function, the chemical Exergy and then the total exergy defined as the sum of thermo mechanical exergy contribution and chemical exergy contribution.

Exergy equation

The exergy of a closed system can be defined as in equation A.1.3:

$$E = (E_t - U_0) + p_0(V - V_0) - T_0(S - S_0) \qquad (A.1.3)$$

With
E	:	Exergy (kJ/kg)
E_t	:	Total Energy (kJ/kg)
U_0	:	Internal Energy of the environment
p_0	:	Environment pressure (Pa)
T_0	:	Environment temperature (K)
S_0	:	Entropy of the environment (kJ/kg.K)
V_0	:	Environment volume (m3/kg)
V	:	Volume of the system (m3/kg)

The total energy when no electric or nuclear reaction occurs, can be written as [TD-01]:

$$E_t = U + KE + PE \qquad (A.1.4)$$

With
U	:	Internal Energy (kJ/kg)
KE	:	Kinetic Energy (kJ/kg)
PE	:	Potential Energy (kJ/kg)

The maximum theoretical work can be written then as:

$$W_c = (E - U_0) + p_0(V - V_0) - T_0(S - S_0) - T_0\sigma_c \qquad (A.1.5)$$

With $T_0\sigma_c$: Irreversibilities in the system (kJ/kg)

And when mass flows across a control volume boundary, there is an exergy transfer accompanying the flow, given by:

$$e_{f1} - e_{f2} = (h_1 - h_2) - T_0(s_1 - s_2) + \frac{V_1^2 - V_2^2}{2} + g(z_1 - z_2) \qquad (A.1.6)$$

Adiabatic flame temperature

Figure A.1.2 shows a steady state reactor in which a fuel is burned with air producing therefore the combustion products. The combustion equation when reaction occurs at stoichiometric conditions ($\lambda=1$), with no formation of other species such as CO, UHC and NOx can be written as:

$$C_aH_b + \left(a + \frac{b}{4}\right)(O_2 + 3.76N_2) ==> aCO_2 + \frac{b}{2}H_2O + \left(a + \frac{b}{4}\right)3.76N_2 \qquad \text{(A.1.7)}$$
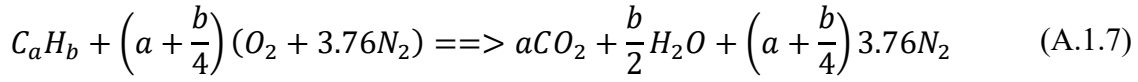

Reactor at steady state
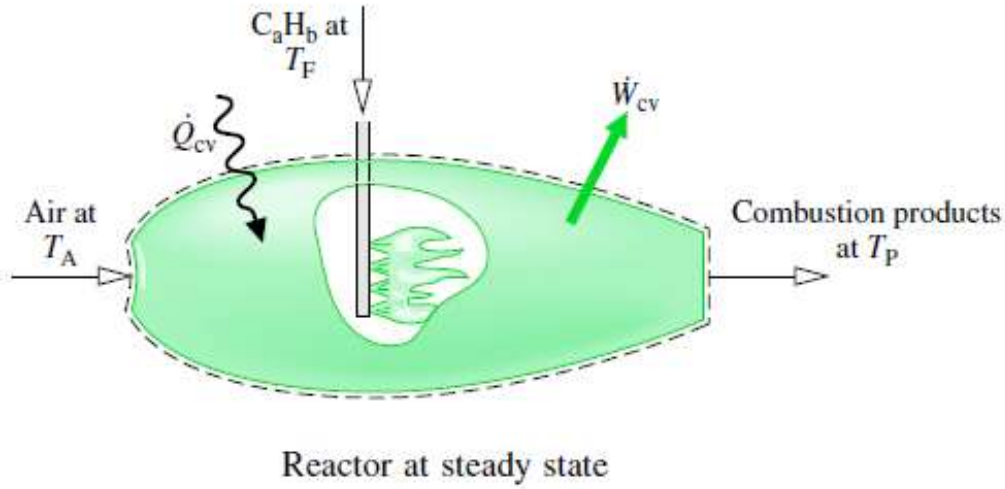
Fig. A.1.2: Reactor at steady state [A.1.2]

The law of conservation of energy, when kinetic and potential energy effects are ignored can be written as:

$$\frac{\dot{Q}_{cv}}{\dot{n}_f} - \frac{\dot{W}_{cv}}{\dot{n}_f} = \left[a\bar{h}_{CO2} + \frac{b}{2}\bar{h}_{H2O} + \left(a + \frac{b}{4}\right)3.76\bar{h}_{N2}\right] - \bar{h}_F - [\left(a + \frac{b}{4}\right)\bar{h}_{O2}$$
$$+ \left(a + \frac{b}{4}\right)3.76\bar{h}_{N2}] \qquad \text{(A.1.8)}$$

The specific enthalpy of a compound at a state other than the standard state is found by adding the specific enthalpy change $\Delta\bar{h}$ between the standard state and the state of interest to the enthalpy of formation [A.1.2].

$$\bar{h}(T,P) = \bar{h}_f^0 + \left[\bar{h}(T,P) - \bar{h}\left(T_{ref}, P_{ref}\right)\right] = \bar{h}_f^0 + \Delta\bar{h} \qquad \text{(A.1.9)}$$

With	$\bar{h}_f^0$	:	Enthalpy of formation at environmental state (kJ/kmol)
	$\Delta\bar{h}$	:	Change of state at constant composition (kJ/kg)

So equation (8) can be written as in A.1.10 or as in A.1.11 in more general form:

$$\frac{\dot{Q}_{cv}}{\dot{n}_f} - \frac{\dot{W}_{cv}}{\dot{n}_f} = \bar{h}_P - \bar{h}_R \qquad \text{(A.1.10)}$$

$$\frac{\dot{Q}_{cv}}{\dot{n}_f} - \frac{\dot{W}_{cv}}{\dot{n}_f} = \sum_P n_e(\bar{h}_f^0 + \Delta\bar{h})_e - \sum_R n_i(\bar{h}_f^0 + \Delta\bar{h})_i \qquad \text{(A.1.11)}$$

With	$\bar{h}_P$	:	The enthalpies of the products per mole of fuel (kJ/kmol)
	$\bar{h}_R$	:	The enthalpies of the reactants per mole of fuel
	n_i	:	Number of mole for each reactant
	n_e	:	Number of mole for each product

The enthalpy of combustion is then defined as:

$$\bar{h}_{RP} = \sum_P n_e \bar{h}_e - \sum_R n_i \bar{h}_i \tag{A.1.12}$$

When no heat transfer occurs and no work is done, we can define the adiabatic flame temperature by writing the following equations:

$$\sum_P n_e \bar{h}_e = \sum_R n_i \bar{h}_i \tag{A.1.13}$$

$$\sum_P n_e (\Delta \bar{h})_e = \sum_R n_i (\Delta \bar{h})_i + \sum_R n_i (\bar{h}_f^0)_i - \sum_P n_e (\bar{h}_f^0)_e \tag{A.1.14}$$

The unknown temperature appears in each term of the sum on the left side of the equation, determination of the adiabatic flame temperature requires iteration: A temperature for the products is assumed and used to evaluate the left side equation.

Entropy production and thermo-mechanical exergy

In order to evaluate the exergy destruction for a reaction occurring with different excess of air coefficients, we need to calculate the entropy production associated with the combustion process. The absolute entropy is defined as in equation A.1.15:

$$\bar{s}(T,p) = \bar{s}(T, p_{ref}) + [\bar{s}(T,p) - \bar{s}(T, p_{ref})] \tag{A.1.15}$$

For ideal gas mixture with temperature T and pressure $p_i = y_i p$ (partial pressure - y_i is the mole fraction) of components i and p is the mixture pressure.

$$\bar{s}_i(T, p_i) = \bar{s}_i^0(T) - \bar{R} \ln \frac{p_i}{p_{ref}} = \bar{s}_i^0(T) - \bar{R} \ln \frac{y_i p}{p_{ref}} \tag{A.1.16}$$

Where	$\bar{s}_i^0(T)$:	Absolute entropy of component i at temperature T and pressure p_{ref}

Applying the energy balance for control volume t steady state, the entropy rate balances for reacting systems with no work done is expressed on a per mole of fuel basis is:

$$0 = \sum_j \frac{\dot{Q}_j / T_j}{\dot{n}_F} + \bar{s}_F + \left[\left(a + \frac{b}{4} \right) \bar{s}_{O2} + \left(a + \frac{b}{4} \right) 3.76 \bar{s}_{N2} \right]$$
$$- \left[a\bar{s}_{CO2} + \frac{b}{2} \bar{s}_{H2O} + \left(a + \frac{b}{4} \right) 3.76 \bar{s}_{N2} \right] + \frac{\dot{\sigma}_{cv}}{\dot{n}_F} \tag{A.1.17}$$

Where	$\dot{n}_F$:	The molar flow rate of the fuel (moles/s)

$\frac{\dot{Q}_j / T_j}{\dot{n}_F} = 0$ when no heat transfer occurs through the combustion chamber walls. This allows calculating the rate of entropy production for a given reaction and to evaluate the exergy from equation (6).

The thermo-mechanical contribution to the flow exergy for an ideal gas is then:

$$\bar{h} - \bar{h}_0 - T_0(\bar{s} - s_0)$$
$$= a[\bar{h}(T) - \bar{h}(T_0)$$
$$- T_0(\bar{s}^0(T) - \bar{s}^0(T_0) - \bar{R}\ln(^{y_{CO2}p}/_{y_{CO2}p_0}))]_{CO2}$$
$$+ \frac{b}{2}[\bar{h}(T) - \bar{h}(T_0)$$
$$- T_0(\bar{s}^0(T) - \bar{s}^0(T_0) - \bar{R}\ln(^{y_{H2O}p}/_{y_{H2O}p_0}))]_{H2O}$$
$$+ (\lambda - 1)\left(a + \frac{b}{4}\right)[\bar{h}(T) - \bar{h}(T_0)$$
$$- T_0(\bar{s}^0(T) - \bar{s}^0(T_0) - \bar{R}\ln(^{y_{O2}p}/_{y_{O2}p_0}))]_{O2}$$
$$+ \lambda\left(a + \frac{b}{4}\right) * 3.76[\bar{h}(T) - \bar{h}(T_0) - T_0(\bar{s}^0(T) - \bar{s}^0(T_0)$$
$$- \bar{R}\ln(^{y_{N2}p}/_{y_{N2}p_0}))]_{N2}$$

(A.1.18)

Chemical Exergy

When chemical reaction occurs between reactants and products, a chemical exergy is added to thermo-mechanical exergy defined as the potential of chemical species to do work when an interaction occurs with the environment. One way to calculate the chemical exergy is by using the specific Gibbs function $\bar{g}$ defined as:

$$\bar{g} = \bar{h} - T\bar{s}$$

(A.1.19)

The Gibbs function of formation $\bar{g}_f^0$ of a compound equals the change in the Gibbs function for the reaction in which the compound is formed from its elements, the compound and the elements all being at T_{ref} and P_{ref}. The Gibbs function at a state other than the standard state is found by adding to the Gibbs function of formation the change in the specific Gibbs function $\Delta\bar{g}$ between the standard state and the state of interest.

$$\bar{g}(T,p) = \bar{g}_f^0 + [\bar{g}(T,p) - \bar{g}(T_{ref},p_{ref})] = \bar{g}_f^0 + \Delta\bar{g}$$

(A.1.20)

$$\Delta\bar{g} = [\bar{h}(T,p) - \bar{h}(T_{ref},p_{ref})] - [T\bar{s}(T,p) - T_{ref}\bar{s}(T_{ref},p_{ref})]$$

(A.1.21)

And finally we can write the chemical exergy as:

$$\bar{e}^{ch} = \left[\bar{g}_F + \left(a + \frac{b}{4}\right)\bar{g}_{O2} - a\bar{g}_{CO2} - \frac{b}{2}\bar{g}_{H2O} - \right](T_0,p_0)$$
$$+ \bar{R}T_0\ln[\frac{(y_{O2}^e)^{(x+\frac{y}{4})}}{(y_{CO2}^e)^{(x)}(y_{H2O}^e)^{(\frac{y}{2})}}]$$

(A.1.22)

Where y_i^e : The mole fraction of component i

For a reaction:

$$C_aH_b + \lambda\left(a + \frac{b}{4}\right)(O_2 + 3.76N_2) ==$$

$$> aCO_2 + \frac{b}{2}H_2O + (\lambda - 1)(a + \frac{b}{4})O_2 + \lambda\left(a + \frac{b}{4}\right)3.76N_2$$
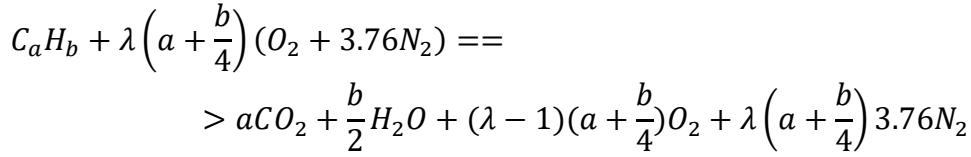
The chemical contribution, per mole of fuel is:

$$\bar{e}^{ch} = \bar{R}T_0 \sum_i y_i \ln\left(\frac{y_i}{y_i^e}\right) \tag{A.1.23}$$

Total exergy

The total exergy is the sum of the thermo-mechanical exergy (value of maximum work) and the chemical exergy associated with a given system at a specified state relative to a specified exergy reference environment. The object is to evaluate the work obtainable by allowing the fuel to react with oxygen from the environment to produce the environmental components carbon dioxide and water each at its respective state in the environment.

For control volume, the specific flow exergy is then the sum of thermo mechanical and chemical exergy:

$$e = (h - h_0) - T_0(s - s_0) + \frac{V^2}{2} + gz + e^{ch} \tag{A.1.24}$$

Where	$(h - h_0) - T_0(s - s_0) + \frac{V^2}{2} + gz$	The thermo-mechanical contribution to the flow exergy
	e^{ch}	The chemical contribution to the flow exergy

Synthesis

Figure A.1.3 shows the adiabatic flame temperature for the methane and the liquid octane function of air-fuel ratio for two air oxidizer temperatures, ambient at 298K and heated air at 400K.

The graph shows that when the amount of the air is increased for the same fuel quantity, the adiabatic flame temperature decreases, and that is explained by the fact that an amount of oxygen and nitrogen are in excess during the combustion and absorb the heat generated. Therefore, the final temperature reached is lower. The graph shows also a comparable adiabatic flame temperature for both Octane and Methane, and a little increase in adiabatic flame temperature when air is preheated from 298K to 400K before combustion.

Figure A.1.4 shows the rate of entropy production when air enters the combustion chamber at 25°C, 1 atm. The entropy production increases when excess of air increases in the combustion chamber, referring to equation A.1.17, since there are more oxygen and nitrogen in the combustion chamber. While the entropy production means a loss of potential of work, we conclude that the thermo-mechanical exergy decreases also with increasing the excess of air in the combustion chamber.

The total Exergy sum of thermo mechanical and chemical exergy is plotted in figure A.1.5. It shows a higher potential for Methane to do work than liquid Octane when burned with air at different excess of air coefficient. The chemical exergy contribution for both fuels is lower compared to thermo mechanical contribution. The figure A.1.5 shows also a decrease in total exergy when λ increases.

Figure A.1.6 shows the total exergy compared to LHV for both Octane and Methane function of air fuel ratio. While the potential of work is around 75% for Octane (81% for Methane) when AF = 1, it is around 68% (69% respectively) when AF = 1.5, and then a potential of work is lost.

Therefore, we conclude that increasing the adiabatic flame temperature allows higher potential of work of the thermodynamic machine considered. However, metallurgic limitation may limit the maximum flame temperature [A.1.3].
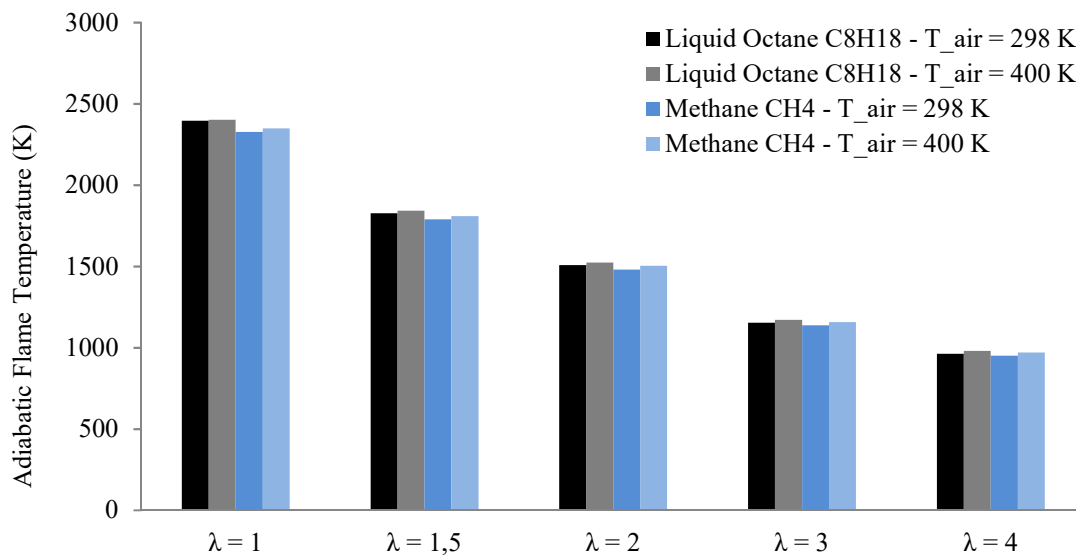
Fig. A.1.3: Adiabatic flame temperature function of excess of air coefficient λ
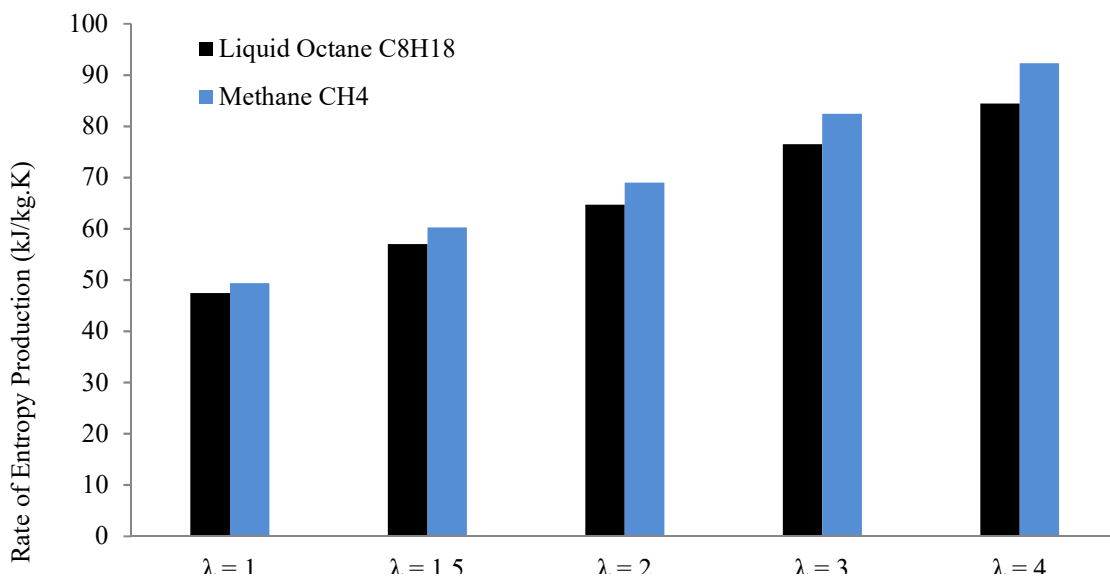
Fig. A.1.4: Rate of Entropy production function of excess of air coefficient
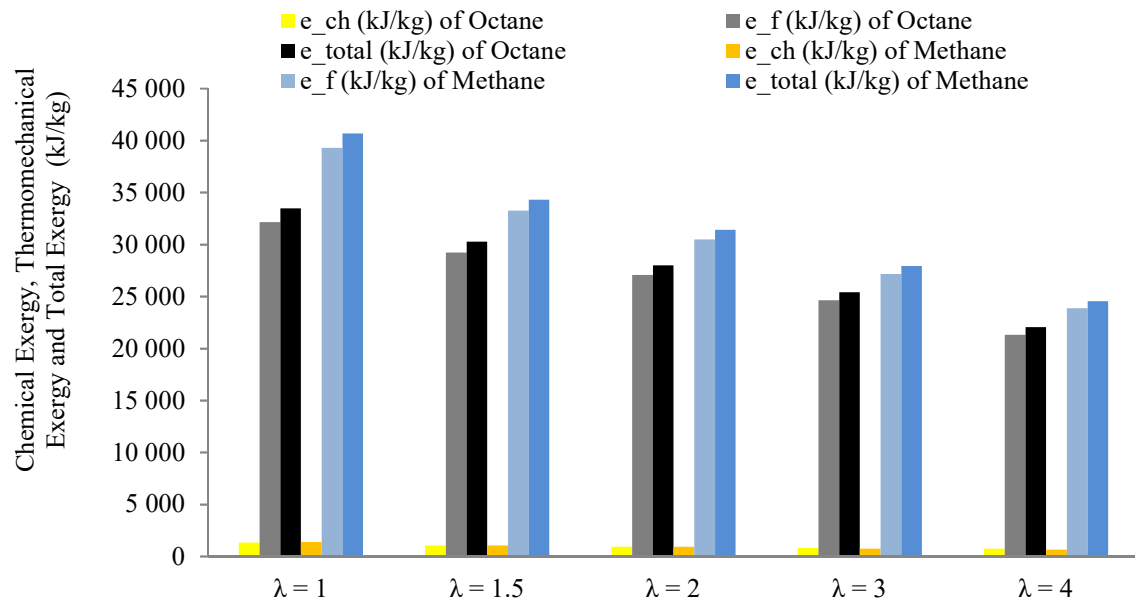
Fig. A.1.5: Chemical exergy, thermo-mechanical exergy and total exergy function of excess air coefficient for Octane and Methane
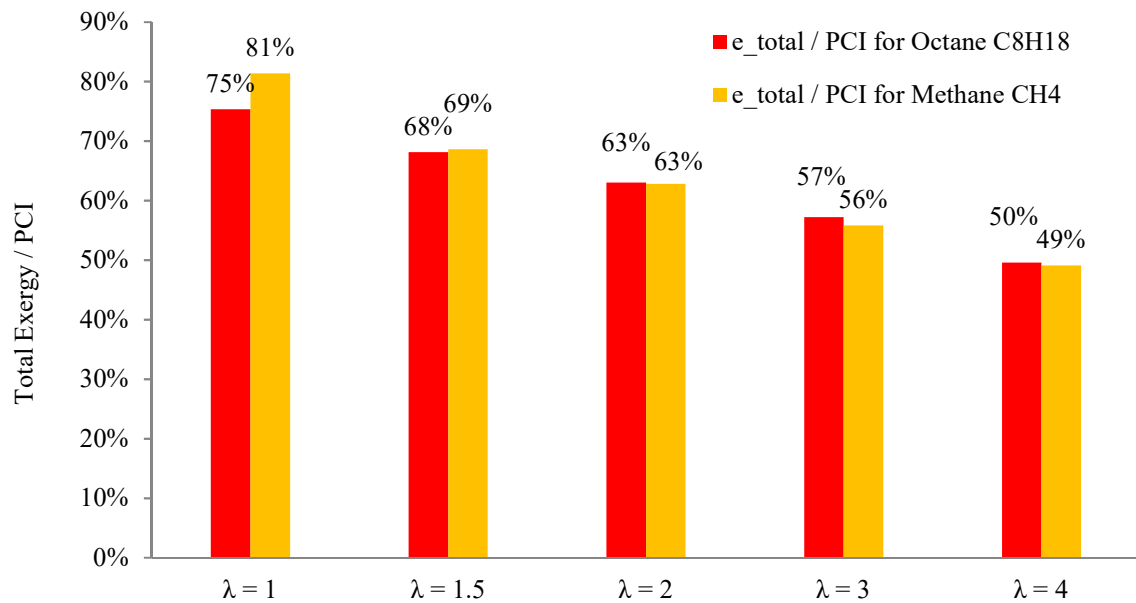
Fig. A.1.6: Total Exergy compared to low heating value function of air/fuel ratio

Annex 2: Exergo-technological explicit methodology for gas- turbine system optimization of series hybrid electric vehicles

Original Article

Exergo-technological explicit methodology for gas-turbine system optimization of series hybrid electric vehicles

Wissam S Bou Nader[1,3], Charbel J Mansour[2], Maroun G Nemer[1] and Olivier M Guezet[3]

Abstract

Significant research efforts have been invested in the automotive industry on hybrid electrified powertrains in order to reduce the dependence of passenger cars on oil. Electrification of powertrains resulted in a wide range of hybrid vehicle architectures. The fuel consumption of these powertrains strongly relies on the energy converter performance, as well as on the energy management strategy deployed on board. This paper investigates the potential of fuel consumption sav-ings of a series hybrid electric vehicle using a gas turbine as an energy converter instead of the conventional internal-combustion engine. An exergo-technological explicit analysis is conducted to identify the best configuration of the gas-turbine system. An intercooled regenerative reheat cycle is prioritized, offering higher efficiency and higher power den-sity than those of other investigated gas-turbine systems. A series hybrid electric vehicle model is developed and power-train components are sized by considering the vehicle performance criteria. Energy consumption simulations are performed over the Worldwide Harmonized Light Vehicles Test Procedure driving cycle using dynamic programming as the global optimal energy management strategy. A sensitivity analysis is also carried out in order to evaluate the impact of the battery size on the fuel consumption, for self-sustaining and plug-in series hybrid electric vehicle configurations. The results show an improvement in the fuel consumption of 22–25% with the gas turbine as the auxiliary power unit in comparison with that of the internal-combustion engine. Consequently, the studied auxiliary power unit for the gas tur-bine presents a potential for implementation on series hybrid electric vehicles.

Corresponding author:

Wissam S Bou Nader, PSA Group, Technical Center of Vélizy, Route de Gizy, 78943 Vélizy Villacoublay Cedex, PO Box VV1415, France.
Centre Efficacite´ Energétique des Systèmes, Ecole des Mines de Paris, 5 rue Léon Blum, 91120 Palaiseau, France.

Emails: wissam.bounader@mpsa.com; wissam.bou_nader@mines-paristech.fr

Annex 3 : Assessing additional fuel consumption from cabin thermal comfort and auxiliary needs on the worldwide harmonized light vehicles test cycle
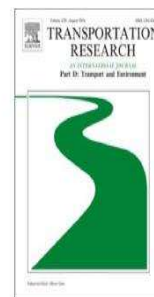
Assessing additional fuel consumption from cabin thermal comfort and auxiliary needs on the worldwide harmonized light vehicles test cycle

Charbel Mansour[a], , Wissam Bou Nader[b], Florent Breque[c], Marc Haddad[a], Maroun Nemer[c]

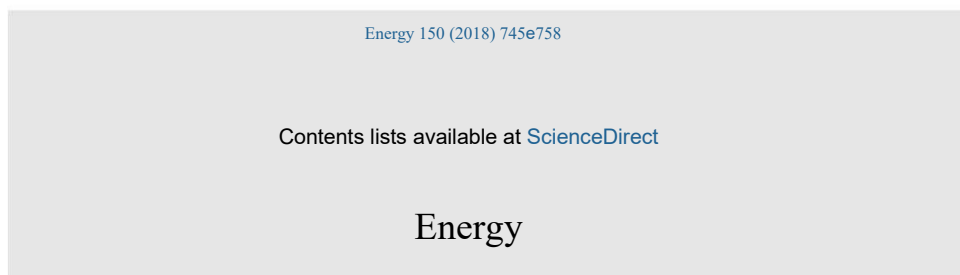[a] Lebanese American University, Industrial and Mechanical Engineering Department, New York, United States

[b] PSA Group, Centre technique de Vélizy, Vélizy, France

[c] Ecole des Mines de Paris, Center for Energy Efficiency of Systems, Palaiseau, France

Abstract

Standards for fuel consumption and carbon dioxide emissions are implemented worldwide in most light-duty vehicle markets. Regulatory drive cycles, defined as specific time-speed patterns, are used to measure levels of fuel consumption and emissions. These measurements should realistically reflect real world driving performance, however there is increasing concern about their adequacy due to the discrepancies observed between certified and real world consumption and emissions values. One of the main reasons for the discrepancy is that current testing pro-tocols do not account for non-mechanical vehicle energy needs, such as passengers' thermal comfort needs and the use of electric auxiliaries on-board. Cabin heating and cooling can espe-cially lead to considerable increase in vehicle energy consumption. This paper presents a simu-lation-based assessment framework to account for the additional fuel consumption related to the cabin thermal energy and auxiliary needs under the worldwide-harmonized light vehicles test procedure (WLTP). A vehicle cabin model is developed and the thermal comfort energy needs are derived for cooling and heating, depending on ambient external temperature under cold, mod-erate and warm climates. A modification to the WLTP is proposed by including the generated power profiles for thermal comfort and auxiliary needs. Dynamic programming is used to com-pute the fuel consumption on the modified WLTP for a rechargeable series hybrid electric vehicle (SHEV) architecture. Results show consumption increases of 20% to 96% compared to the cur-rently adopted WLTP, depending on the considered climate.

Annex 4 : Optimization of a Brayton external combustion gas-turbine system for extended range electric vehicles

Optimization of a Brayton external combustion gas-turbine system for extended range electric vehicles

Wissam S. Bou Nader [a, c], Charbel J. Mansour [b, *], Maroun G. Nemer [a]

[d] Ecole des Mines de Paris, Center for Energy Efficiency of Systems, Palaiseau, France

[e] Lebanese American University, Industrial and Mechanical Engineering Department, New York, USA

[f] PSA Group, Centre Technique de Velizy, Velizy, France

Abstract

Significant research efforts are considered in the automotive industry on the use of low-carbon fuels in order to reduce the emissions and improve the fuel economy of vehicles. Some of these fuels, such as the solid fuels for example, are only compatible with external combustion machines. These machines are only suitable for electrified powertrains relying on electric propulsion, in particular the extended-range-electric-vehicles with series hybrid powertrain configuration where fuel consumption strongly relies on the energy converter efficiency and power density. This paper investigates the fuel savings potential of these vehicles using a Brayton external combustion gas-turbine system as energy converter substitute to the conventional internal combustion engine. An exergo-technological explicit analysis is conducted to identify the best system configuration. A downstream-intercooled reheat external combustion gas-turbine (DIRe-ECGT) system is prioritized, offering the highest efficiency among the investigated sys-tems. An extended-range-electric-vehicle model is developed and energy consumption simulations are performed on the worldwide-harmonized light vehicles test cycle. Fuel consumption simulation results are compared to a reference extended-range-electric-vehicle using an engine auxiliary-power-unit. Re-sults show 6%e11.5% of fuel savings with the prioritized DIRe-ECGT auxiliary-power-unit as compared to the reference model, depending on the battery capacity and the trip distance.

262

Annex 5 : Fuel consumption saving potential of Stirling machine on series parallel hybrid electric vehicle : Case of the Toyota Prius

Technical paper

Fuel Consumption Saving Potential of Stirling Machine on Series Parallel Hybrid Electric Vehicle: Case of the Toyota Prius **2018-01-0421**

Investigations on alternative fuels and new hybrid powertrain architectures have recently undergone significant efforts in the automotive industry, in attempt to reduce carbon emissions from passenger cars. The use of these fuels presents a potential for re-emerging the deployment of external combustion non-conventional engines in automotive applications, such as the Stirling engines, especially under the current development context of powertrain electrification. This paper investigates the potential of fuel consumption savings of a series-parallel hybrid electric vehicle (SPHEV) using a Stirling machine as fuel converter. An exergo-technological explicit analysis is conducted to identify the Stirling system configuration presenting the best compromise between high efficiency and automotive implementation constraints. The Stirling engine with combustion chamber preheater is prioritized. A SPHEV model is developed based on the Prius power-split hybrid electric architecture. Energy consumption simulations are performed on the worldwide-harmonized light vehicles test cycle (WLTC) using dynamic programing as global optimal energy management strategy. Results show improved fuel consumption performance of the Stirling machine compared to the ICE. In addition, the Stirling offers other intrinsic advantages such as low noise and vibration operation and mainly multi-fuel use capability. Consequently, the studied Stirling presents a potential for implementation on SPHEVs.

DOI: https://doi.org/10.4271/2018-01-0421

Author(s): Wissam Bou Nader, Charbel Mansour, Maroun Nemer, Clement Dumand

Affiliated: Ecole des Mines de Paris / PSA Groupe, Lebanese American University

Annex 6 : Brayton cycles as waste heat recovery systems on series hybrid electric vehicles
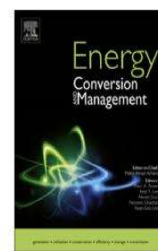
Brayton cycles as waste heat recovery systems on series hybrid electric vehicles

Wissam Bou Nader[a,c,] , Charbel Mansour[b], Clément Dumand[c], Maroun Nemer[a]

[g] Ecole des Mines de Paris, Centre Efficacité Energétique des Systèmes CES, Palaiseau, France

[h] Industrial and Mechanical Engineering department, Lebanese American University, New York, United States

[i] Groupe PSA, Centre technique de Vélizy, Vélizy, France

Abstract

In the global attempt to increase the powertrain overall efficiency of hybrid vehicles while reducing the battery size, engine waste heat recovery (WHR) systems are nowadays promising technologies. This is in particular interesting for series hybrid electric vehicles (SHEV), as the engine operates at a relative high load and under steady conditions. Therefore, the resulting high exhaust gas temperature presents the advantage of increased WHR efficiency. The Brayton cycle offers a relatively reduced weight compared to other WHR systems and presents a low complexity for integration in vehicles since it relies on an open system architecture with air as the working fluid, which consequently avoids the need for a condenser compared to the Rankine cycle. This paper investigates the potential of fuel consumption savings of a SHEV using the Brayton cycle as a WHR system from the internal combustion engine (ICE) exhaust gases. An exergy analysis is conducted on the simple Brayton cycle and several Brayton waste heat recovery (BWHR) systems were identified. A SHEV with ICE-BWHR systems is modeled, where the recovered engine waste heat is converted into electricity using an electric generator and stored in the vehicle battery. The energy consumption simulations is performed on the worldwide-harmonized light-vehicles test cycle (WLTC) while considering the additional weight of the BWHR systems. The intercooled Brayton cycle (IBC) architecture is identified as the most promising for automotive applications as it offers the most convenient compromise between high efficiency and low integration complexity. Results show that 5.5% and 7.0% improved fuel economy on plug-in and self-sustaining SHEV configurations respectively when com-pared to similar vehicle configurations with ICE auxiliary power units. In addition to the fuel economy im-provements, the IBC-WHR system offers other intrinsic advantages such as low noise, low vibration, high dur-ability which makes it a potential heat recovery system for integration in SHEV.

Annex 7 : Exergo-technological explicit selection methodology for vapor cycle systems optimization for series hybrid electric vehicles

Exergo-Technological Explicit Selection Methodology for Vapor Cycle Systems Optimization for Series Hybrid Electric Vehicles

Wissam Bou Nader[a,c], Charbel Mansour[b], Clément Dumand[c] and Maroun Nemer[d]

[a] *Ecole des Mines de Paris, Centre Efficacité Energétique des Systèmes CES, Palaiseau, France,*
wissam.bou_nader@mines-paristech.fr
[b] *Lebanese American University, Industrial and Mechanical Engineering department, New York, United-States, charbel.mansour@lau.edu.lb*
[c] *Groupe PSA, Centre technique de Vélizy, Vélizy, France,*
wissam.bounader@mpsa.com, clement.dumand@mpsa.com
[d] *Ecole des Mines de Paris, Centre Efficacité Energétique des Systèmes CES, Palaiseau, France,*
maroun.nemer@mines-paristech.fr

Abstract

Significant research efforts are considered in the automotive industry on the use of low carbon alternative fuels in order to reduce the carbon dioxide emissions and to improve the fuel economy of future vehicles. Some of these fuels, such as the solid fuels for example, are only compatible with external combustion machines. These machines are only suitable for electrified powertrains relying on electric propulsion, in particular series hybrid electric vehicles (SHEV) where fuel consumption strongly relies on the energy converter performance in terms of efficiency and power density, as well as on the deployed energy management strategy. This paper investigates the potential of fuel savings of a SHEV using a vapor cycle machine (VCM) system as energy converter substitute to the conventional internal combustion engine (ICE). An exergo-technological explicit analysis is conducted to identify the best VCM-system configuration. A Regenerative Reheat Steam Rankine Cycle with condenser reheat and turbine reheat (RReCRTRe-SRC) system is prioritized, offering high efficiency, high power density and low vehicle integration constraints among the investigated systems. A plug-in SHEV model is developed and energy consumption simulations are performed on a worldwide-harmonized light vehicles test cycle (WLTC). Dynamic programing is used as global optimal energy management strategy. A sensitivity analysis is also carried out in order to evaluate the impact of the battery size on the fuel consumption. Fuel consumption simulation results are compared to ICE on same vehicle powertrain. Results show +2% to +3.5% additional fuel consumption, on self-sustaining SHEV, with the RReCRTRe-SRC as auxiliary power unit (APU) compared to ICE. Consequently, the selected VCM-APU presents a potential for implementation on SHEVs with zero carbon alternative fuel.
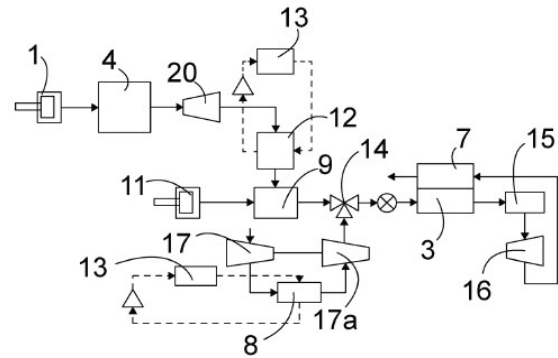
Annex 8: high Efficiency Internal Combustion Engine with Splited Expansion

This patent has been filed as part of this thesis work

Inventor: Wissam BOU NADER

The invention concerns a so-called distributed or separate cycle internal combustion engine with at least two cylinders specifically dedicated to combustion and expansion. Such an engine has the advantages of reducing NOx emissions, as well as improved efficiency and power density. The internal combustion engine of this invention may be used preferably for a vehicle application.
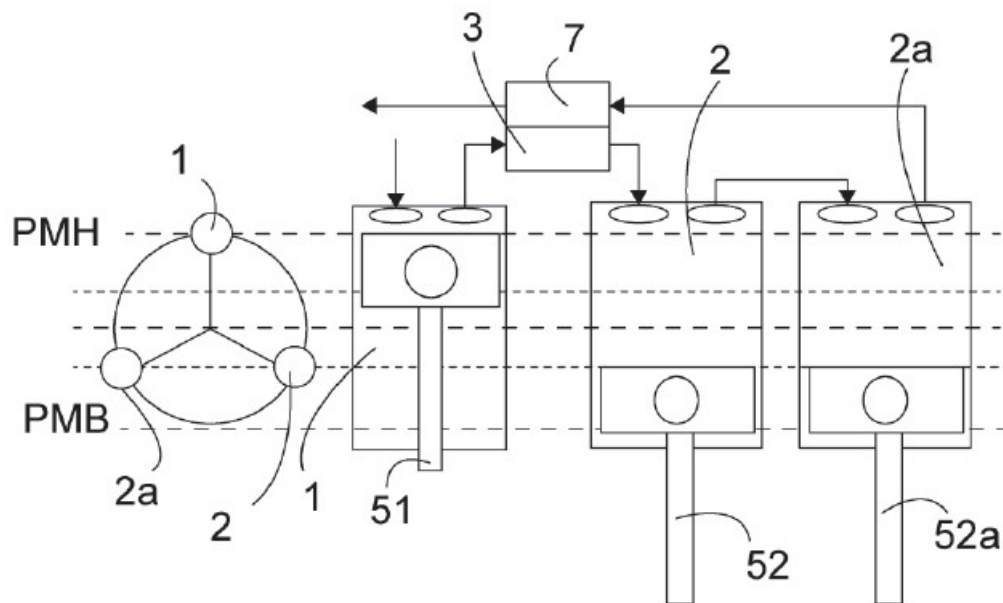
Compression piston (1)
Recuperator cold side (3)
First expansion piston (2)
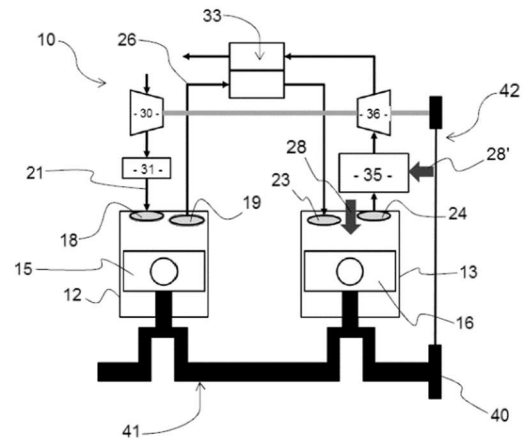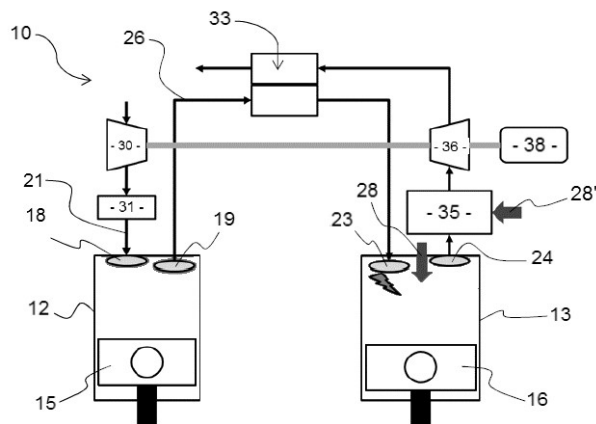Second expansion piston (2a)
Recuperator hot side (7)

Annex 9: Internal combustion engine with high pressure isothermal compression of an intake air flow

This patent has been filed as part of this thesis work

Inventor: Wissam BOU NADER

The invention concerns a split cycle engine or gas turbine internal combustion engine with high pressure isothermal compression of part of an air flow admitted to the system. Such an engine has the advantage of reducing overall emissions, an improvement in efficiency as well as high power density. This internal combustion engine of the present invention may be used preferentially for a vehicle automobile.
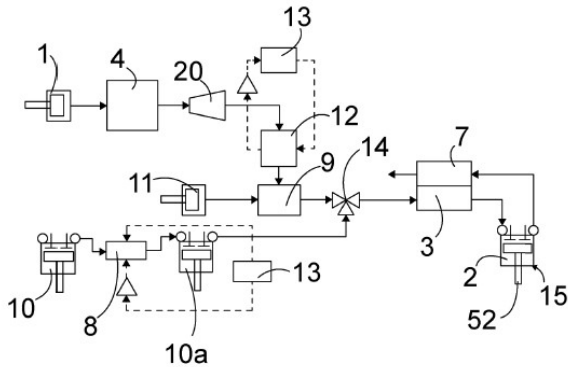
Piston Split cycle engine   *Gas turbine system (centrifugal machine)*

High pressure compressor: (1)

Expansion Piston (2) or centrifugal compression machine (17)

Recuperator cold side (3) – Recuperator hot side (7)

High pressur tank (4)

Expansion turbine (16)

Combustion chamber (15)

Cold expansion turbine (20)

Vehicle cabine cooler or heater (13)

Heat exchanger (12)

Secondary compression piston (11)

Intercooler (8)

Annex 10: Internal combustion engine with high pressure isothermal compression of an intake air flow

This patent has been filed as part of this thesis work

Inventor: Wissam BOU NADER

This invention concerns a split-cycle internal combustion engine with an afterburner combustion chamber. The invention has a particularly advantageous, but not exclusive, application in the field of automotive vehicles.

Compression piston (15)
Expansion piston (13)
Intercooler (31)
Air compressor (30)
Recupérator (33)
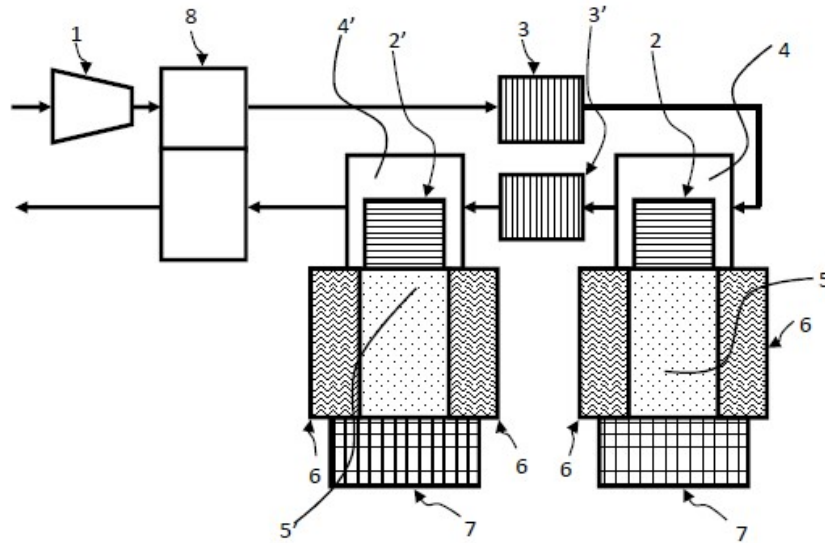Post combustion chamber (35)
Expansion turbine (36)
Electric generator (38)

Annex 11: Regenerative Reheat Stirling machine

This patent has been filed as part of this thesis work

Inventor: Wissam BOU NADER

The invention concerns, in general, appliances with an external combustion chamber to generate electrical energy and heat, and to transfer the heat to an external combustion engine, in particular a Stirling engine. The invention concerns in particular a thermal afterburner combustion chamber device coupled in series with the initial combustion chamber of the Stirling machine, where said device being adapted to a Stirling engine, with a specific goal to improve its efficiency and its net specific power.

Air blower (1)
Recuperator (8)
First combustion chamber (3)
Post combustion chamber (3')
Hot heat exchanger (4)
Stirling hot heat (2, 2')
Stirling cold heat exchanger (7)
Stirling internal regenerator (6)

Annex 12: Innovative thermoacoustic machine for range extender vehicle application

This patent has been filed as part of this thesis work

Inventor: Wissam BOU NADER

The invention concerns the conversion of energy by applying the thermoacoustic effect. More specifically, the invention relates to a thermoacoustic machine, in particular for energy cogeneration systems in hybrid vehicles. The invention also concerns vehicles, in particular motor vehicles, including a thermoacoustic machine, in particular in its traction chain.
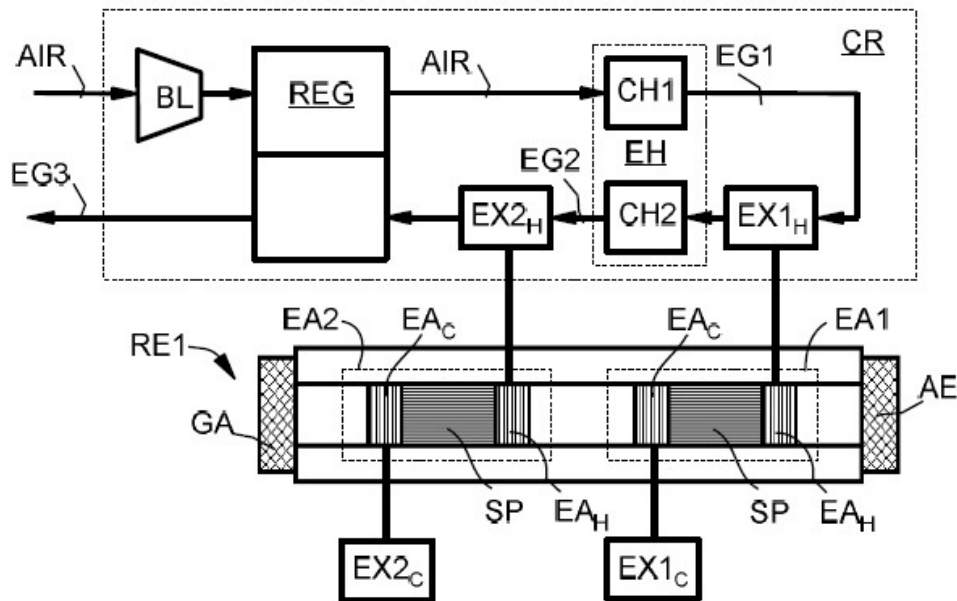
Air blower (BL)
Regeneraotr (REG)
Combustion chamber (CH1, CH2)
Hot heat exchangers (EX1$_h$, EX2$_h$)
Cold heat exchangers (EX1$_c$, EX2$_c$)
Acoustic generator (GA)
Acousto-Electric Generator (AE)
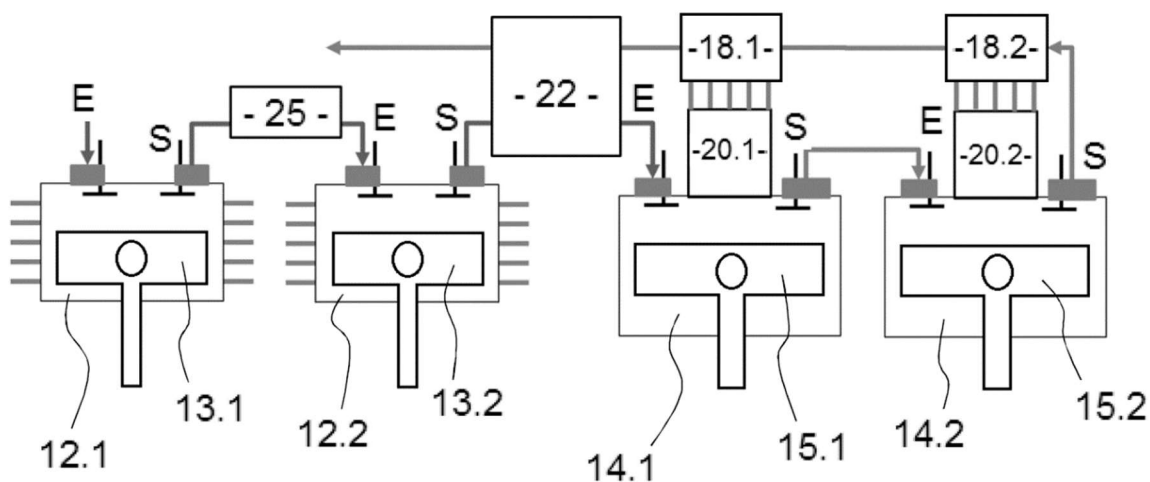Thermoacoustic stack (SP)

Annex 13: External combustion Ericsson Split Cycle Engine for Powertrain Automotive Applications

This patent has been filed as part of this thesis work

Inventor: Wissam BOU NADER

This invention concerns a split-cycle external combustion engine known also as Ericsson engine. The invention has a particularly advantageous, but not exclusive, application in the field of motor vehicles. The engine comprises a compression cylinder for carrying out an air intake and compression phase and an expansion cylinder for carrying out a relaxation and air evacuation. The expansion cylinder is associated with a chamber of external combustion and an air heater to allow air expansion inside of the cylinder. The phases of the engine cycle can then be executed simultaneously with an adequate phasing. These two cylinders perform two cycles in two engine revolutions, as much as a four-stroke twin cylinder of the same displacement.

Compression piston (13.1, 13.2)
Intercooler (25)
Recuperator (22)
Expansion pistons (15.1, 15.2)
Hot heads (20.1, 20.2)
Hot heat exchangers (18.1, 18.2)

Annex 14: External combustion Ericsson Split Cycle Engine for Powertrain Automotive Applications

This patent has been filed as part of this thesis work

Inventor: Wissam BOU NADER

The invention generally concerns the generation of electricity from heat by applying the thermoelectric effect known as the Seebeck effect. More particularly, the invention relates to a thermoelectric machine for the primary conversion of energy in particular for applications in vehicles and, in particular, vehicles hybrid electric vehicles with extended range. The invention also concerns a vehicle including a thermoelectric machine, particularly in its powertrain.
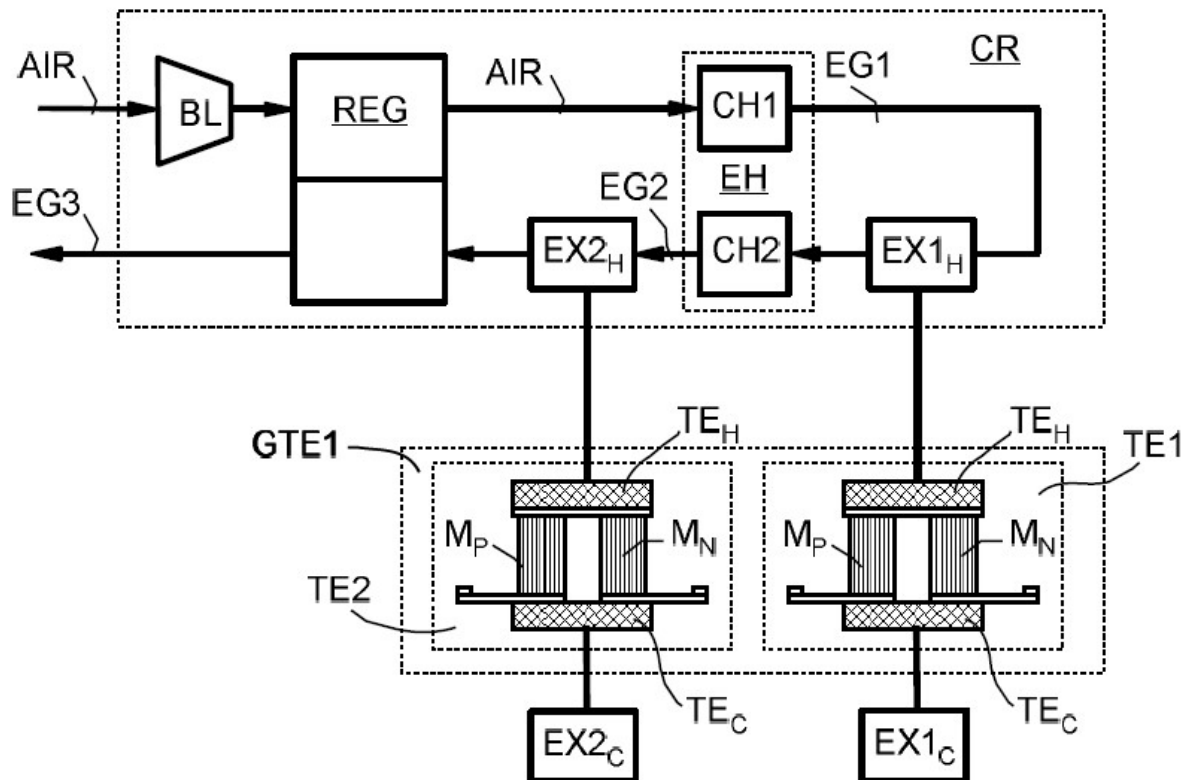
Air blower (BL)
Regeneraotr (REG)
Combustion chambers (CH1, CH2)
Hot heat exchangers (EX1$_h$, EX2$_h$)
Cold heat exchangers (EX1$_c$, EX2$_c$)
Thermoelectric modules (TE1, TE2)

Annex 15: Innovative Combined Cycle Gas Turbine System for Extended Range Hybrid Electric Vehicles

This patent has been filed as part of this thesis work

Inventor: Wissam BOU NADER

The present invention relates to the field of thermodynamic machines. The invention concerns more particularly an assembly combining a gas turbine and a heat transfer fluid cycle known as Rankine cycle.
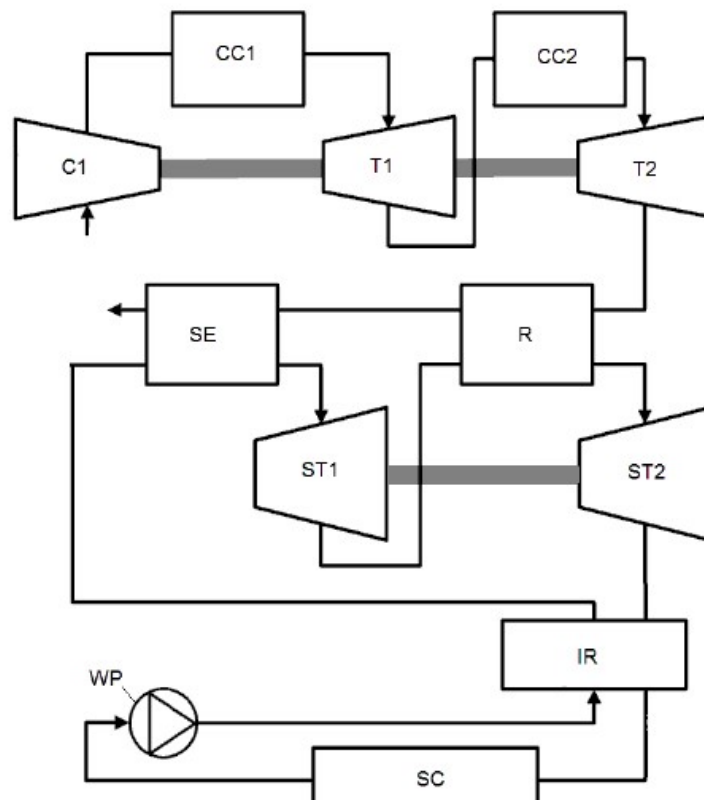
GT compressor (C1)
Combustion chambers (CC1, CC2)
GT Turbines (T1, T2)
Reheater (R)
Steam evaporator (SE)
Steam turbines (ST1, ST2)
Condenser internal heat recuperator (IR)
Water pump (WP)
Steam condenser (SC)

RÉSUMÉ

D'importants efforts de recherche ont été investis dans l'industrie automobile sur les nouveaux carburants et les nouvelles chaînes de traction hybride électrique afin de réduire les émissions de carbone des véhicules. La consommation de carburant de ces groupes motopropulseurs hybrides dépend des performances du convertisseur d'énergie utilisé, des besoins énergétiques du véhicule, ainsi que de la stratégie de gestion énergétique déployée à bord. Cette thèse examine le potentiel de nouveaux convertisseurs d'énergie comme substitut du moteur thermique à combustion interne (ICE). Les systèmes de turbines à gaz sont considérés comme des convertisseurs d'énergie potentiel pour les chaînes de traction hybride série (SHEV), car ils offrent de nombreux avantages intrinsèques à l'automobile, tels que la capacité de fonctionner avec plusieurs carburants, la compacité, la réduction du nombre de pièces mobiles, la réduction du bruit et des vibrations. Une analyse exergo-technologique explicite est proposée pour identifier les configurations thermodynamiques réalistes. Une étude préconceptionnelle a été réalisée pour déterminer les rapports puissance/poids de ces systèmes. Un modèle SHEV est développé et les composants du groupe motopropulseur sont dimensionnés en fonction des critères de performance du véhicule. Des simulations de consommation sont effectuées sur le cycle d'homologation WLTC, en prenant en compte les besoins en énergie électrique et thermique du véhicule en plus des besoins en énergie mécanique, et en utilisant une méthode innovante d'optimisation comme stratégie de gestion de l'énergie. Le cycle turbine à gaz (avec compression refroidie, régénérateur et réchauffe durant la détente (IRReGT)) est priorisé car il offre un rendement et une densité de puissance plus élevés ainsi qu'une consommation de carburant réduite par rapport aux autres systèmes investigués. De plus, un modèle dynamique a été développé et des simulations ont été effectuées pour tenir compte de la surconsommation de carburant pendant les phases transitoires du démarrage. Des essais ont également été mis en œuvre sur certains sous-systèmes du cycle IRReGT identifié. Les résultats montrent une amélioration de la consommation de carburant avec l'IRReGT comme groupe auxiliaire de puissance par rapport à l'ICE. Par conséquent, le système IRReGT sélectionné présente un potentiel, non négligeable, qui remplacerait le moteur thermique à combustion interne dans les futures chaînes de traction hybride électriques.

MOTS CLÉS

ABSTRACT

Significant research efforts have been invested in the automotive industry on alternative fuels and new hybrid electric powertrain in attempt to reduce carbon emissions from passenger cars. Fuel consumption of these hybrid powertrains strongly relies on the energy converter performance, the vehicle energetic needs, as well as on the energy management strategy deployed on-board. This thesis investigates the potential of new energy converters as substitute of actual internal combustion engine in automotive powertrain applications. Gas turbine systems is identified as potential energy converter for series hybrid electric vehicle (SHEV), as it offers many automotive intrinsic benefits such as multi-fuel capability, compactness, reduced number of moving parts, reduced noise and vibrations among others. An exergo-technological explicit analysis is conducted to identify the realistic GT-system thermodynamic configurations. A pre-design study have been carried out to identify the power to weight ratios of those systems. A SHEV model is developed and powertrain components are sized considering vehicle performance criteria. Energy consumption simulations are performed on the worldwide-harmonized light vehicles test cycle (WLTC), which account for the vehicle electric and thermal energy needs in addition to mechanical energy needs, using an innovative bi-level optimization method as energy management strategy. The intercooled regenerative reheat gas turbine (IRReGT) cycle is prioritized, offering higher efficiency and power density as well as reduced fuel consumption compared to the other investigated GT-systems. Also a dynamic model was developed and simulations were performed to account for the over fuel consumption during start-up transitory phases. Tests were also performed on some subsystems of the identified IRReGT-system. Results show improved fuel consumption with the IRReGT as auxiliary power unit (APU) compared to ICE. Consequently, the selected IRReGT-system presents a potential for implementation on futur SHEVs.

KEYWORDS